

Unclassified

SECURITY CLASSIFICATION OF THIS PAGE (When Data Entered)

ADA196290

2

REPORT DOCUMENTATION PAGE		READ INSTRUCTIONS BEFORE COMPLETING FORM
1. REPORT NUMBER	2. GOVT ACCESSION NO.	3. RECIPIENT'S CATALOG NUMBER
4. TITLE (and Subtitle) Final Report for Contract N00014-79-C-0419 on Model Investigations of Lithospheric Propagation		5. TYPE OF REPORT & PERIOD COVERED Final Report April 1, 1979 - March 31, 1988
7. AUTHOR(s) Tai T. Wu, Ronold W. P. King, and Michael F. Brown		6. PERFORMING ORG. REPORT NUMBER
9. PERFORMING ORGANIZATION NAME AND ADDRESS Gordon McKay Laboratory, Harvard University Division of Applied Sciences Cambridge, MA 02138		8. CONTRACT OR GRANT NUMBER(s) N00014-79-C-0419
11. CONTROLLING OFFICE NAME AND ADDRESS Office of Naval Research, Department of the Navy Geology & Geophysics Program (Code 1125GG) Arlington, VA 22217		10. PROGRAM ELEMENT, PROJECT, TASK AREA & WORK UNIT NUMBERS
14. MONITORING AGENCY NAME & ADDRESS (if different from Controlling Office)		12. REPORT DATE May 1988
		13. NUMBER OF PAGES 291
		15. SECURITY CLASS. (of this report) Unclassified
		15a. SEC. CLASSIFICATION/DOWNGRADING SCHEDULE
16. DISTRIBUTION STATEMENT (of this Report) Approved for public release; distribution unlimited.		
17. DISTRIBUTION STATEMENT (of the abstract entered in Block 20, if different from Report)		
18. SUPPLEMENTARY NOTES		
19. KEY WORDS (Continue on reverse side if necessary and identify by block number) lateral electromagnetic waves and pulses measurements in a model tank derivation of new, simple and accurate formulas design of source antennas geophysical applications		
20. ABSTRACT (Continue on reverse side if necessary and identify by block number) Research on the "Model Investigations of Lithospheric Propagation" has been conducted at Harvard University for nine years under the sponsorship of the Office of Naval Research. This "Final Report" summarizes the scientific accomplishments achieved under ONR Contract N00014-79-C-0419 during the period April 1, 1979 through March 31, 1988. The program of research has provided geophysicists with new, quantitatively accurate, and practically useful knowledge for the exploration of the oceanic crust by way of its electrical properties. The results are described in 25 technical papers, (see Appendix).		

DD FORM 1 JAN 73 1473

EDITION OF 1 NOV 65 IS OBSOLETE
S/N 0102-014-6601

Unclassified

SECURITY CLASSIFICATION OF THIS PAGE (When Data Entered)

Model Investigations of Lithospheric Propagation

Table of Contents

1. Introduction	1
2. Basic Principles Underlying the Research Program.....	1
3. Brief Review of Completed Researches	2
A. Building the Theoretical and Experimental Foundations	2
B. Practical Applications of Lateral Electromagnetic Waves	3
C. A New and Complete Understanding of the Properties of Lateral Waves ..	4
D. Sources for the Generation of Lateral Waves	5
E. Lateral-Wave Pulses: A Diagnostic Tool for the Future	5
4. Conclusion	7
5. List of Equipment Purchased on Contract N00014-79-C-0419	8
6. References	9
7. Papers Presented at Scientific Meetings	11
8. Final Report Appendix.....	12



A-1

1. Introduction

The program of research under Contract N00014-79-C-0419 has been directed to acquiring fundamental understanding in an accurate quantitative sense of the generation, propagation, and reception of electromagnetic signals—both continuous waves and pulses—in and near the sea floor. Of primary interest are the determination of the conductivity (resistivity) and permittivity since these are related to basic mechanical-acoustical properties. Definitive advances have been made on (1) the design of sources (horizontal and vertical antennas) for use on and near the sea floor over a wide range of frequencies; (2) the derivation of simple and accurate new formulas for the complete continuous-wave electromagnetic fields both in the sea and in the oceanic crust when this is isotropic or one dimensionally anisotropic, and when there is a layer of sediment with arbitrary thickness; (3) the determination of the effect of irregularities in the form of vertical discontinuities along the boundary surface; (4) the direct application of the new formulas to measurements in a model tank and to data measured on the sea floor as reported by geophysicists; and (5) the derivation of new formulas for the propagation of single electromagnetic pulses along boundary surfaces.

2. Basic Principles Underlying the Research Program

The investigation of the properties of electromagnetic waves propagating in the presence of the sea floor has been three-pronged: (1) The exact integrals for the components of the electromagnetic field have been evaluated by numerical methods with the computer in their general form. The low-frequency forms used by geophysicists in which $\omega\epsilon$ is assumed to be small compared with σ are contained as a special case. This allows the correct inclusion of the air-sea boundary whenever this is also involved. (2) The general integrals have been integrated analytically subject to simple conditions that are fully satisfied in virtually all practical applications. The quite simple integrated expressions have been compared with the numerical calculations and with experiment. They have then been applied to reveal the basic properties of the surface waves, their depth of penetration, and their independence of frequency

and skin depth. (3) A systematic series of measurements has been carried out in a model tank to obtain direct information on the generation, propagation, scattering and detection of surface waves. Since both the theory and the measurements deal with the general formulas—not restricted by the usual geophysical limitation to very low frequencies—a complete, generally significant, and quantitatively accurate picture has been obtained of the properties of electromagnetic waves in the presence of a boundary.

3. Brief Review of Completed Researches

A. Building the Theoretical and Experimental Foundations

The work began with a systematic numerical evaluation of the general integrals for the dominant radial component of the electric field excited by a horizontal electric dipole in the sea close to the sea floor for a wide range of parameters [1]. These exhibited in graphical form the important characteristics of the field as a function of distance, frequency, conductivity and permittivity.

A highly significant advance was contained in a series of three papers [2]-[4] which provided new simple formulas for the complete electromagnetic field generated by a horizontal electric dipole near a plane boundary. This was supplemented by a parallel derivation [5] of the complete field of a vertical electric dipole near a plane boundary. It was shown for the first time that the interaction of the surface wave with the direct wave generates a startling interference pattern [2].

The first report on extensive experimental results obtained with the newly developed apparatus in the model tank is in [6]. This describes the apparatus, the newly designed traveling-wave antennas, measured field patterns, and a comparison of theoretical and measured amplitudes of the radial electric field. Also presented are detailed studies of the effects on the propagation of lateral waves of variously shaped and sized obstacles.

Detailed theoretical and experimental investigations of the reflection of lateral electromagnetic waves at discontinuities and boundaries along the surfaces are contained in [7] and [8]. These show that reflections are surprisingly small when the

obstacle is lower than about a sixth of a wavelength. A study of the significance of atmospheric noise in relation to lateral electromagnetic waves is in [9].

B. Practical Applications of Lateral Electromagnetic Waves

A detailed summary of the properties of lateral electromagnetic waves as revealed by the new, explicit and general formulas is contained in [10] together with a quantitative representation of their application to the important problem of communication with submerged submarines using electrically short vertical dipoles in air (Cutler, ME antenna) and a directive array of horizontal insulated traveling-wave antennas in the sea. Optimum frequencies are determined as a function of the depth of the submarine.

A second important application of lateral electromagnetic waves generated by a horizontal dipole on the air-earth or air-sea surface is the detection and locating of buried or submerged objects by measuring the scattered field from the object when it is excited by an incident lateral wave. A complete quantitative analysis of this problem is contained in [11] and [12].

A study of major significance to geophysicists is the use of the lateral electromagnetic waves excited by a horizontal antenna on the sea floor to determine the electrical properties of the sea floor. The new analytical foundations for the solution of this problem are outlined in [13], and applied directly to measurements by Young and Cox [14]. The new formulas for a simple sea-rock model suggested that the observed field might well be due to an anisotropic upper layer and not to 8 layers to a depth of 33 km as concluded by Young and Cox. This possibility required a rigorous analysis of the lateral-wave field on the sea-oceanic crust boundary when the latter is one-dimensionally anisotropic in conductivity. It was found [15] that the anisotropic two-half-space model yields a better fit with the measured fields than the best-fit, 8-layer model. It also provides a physically meaningful explanation for the significant difference between the behavior as functions of the frequency of the radial and transverse components of the measured electric field.

A summary paper [16] containing a complete set of formulas for all the com-

ponents of the electromagnetic field generated by horizontal and vertical sources on a plane boundary between electrically different half-spaces has been published. A review of applications is also included. A more detailed study of theoretical and experimental aspects of measurements on the sea floor is in [17].

C. A New and Complete Understanding of the Properties of Lateral Waves

The new integrated formulas for the electromagnetic fields generated by horizontal and vertical dipoles near a boundary between electrically different half-spaces apply to the field in the ocean and along the boundary with air or the oceanic crust. In order to really understand the nature of the surface wave that travels near the boundary in the air or oceanic crust, it is necessary to determine the complete field in the air and the oceanic crust at significant distances from the boundary. This analysis is carried out in [18] for the horizontal dipole. By tracing the path of the Poynting vector, a description is obtained for the path of the lateral wave in the air when the source is near the air-sea or air-earth boundary and in the lithosphere when the dipole is near the sea floor. In the low-frequency range for the oceanic crust, the depth of penetration turns out to be *independent of the frequency and skin depth* and to *depend primarily on the distance between the source and the receiver*. The greater the distance, the deeper the penetration into the oceanic crust. Specifically, the maximum depth of penetration is $z_m = \rho_m \sqrt{\sigma_l / \sigma_s}$, where σ_l is the conductivity of the lithosphere, σ_s the conductivity of the sea, and ρ_m is the radial distance between the horizontal-dipole source and the receiver. This indicates that *lateral waves are uniquely adapted to study the properties of the shallow oceanic crust*. It is also shown in [18] that the field observed at any given radial distance from the source is determined largely by the lateral wave that travels in a thin upper layer and only in a small degree by possible reflections from layers at arbitrary depths below the surface. This is of great importance in constructing layered models of the lithosphere. Clearly, the major contribution to the field by the lateral wave cannot be omitted and the entire field assumed to be due to reflections from the layers.

The analysis of the electromagnetic field in the air or oceanic crust due to a vertical electric dipole in the sea is carried out in [19]. The path indicated by the Poynting vector is somewhat different from that for the field generated by the horizontal dipole with a greater—but still relatively small—depth of penetration. Direct application of this basic contribution to the theory of lateral waves was made in terms of the measured data of Edwards et al. [20]. The comparison [19] clearly indicates that complete consideration of the lateral wave and reflected waves from both the air surface and a rock layer below the sediment on the sea floor lead to highly satisfactory results.

The extension of the new approach to the three-layer problem of ocean, sediment, rock has been completed both theoretically [21] and experimentally [22].

D. Sources for the Generation of Lateral Waves

Lateral electromagnetic waves cannot be generated by plane waves incident on a plane boundary between electrically different half-spaces. They can be generated by an incident spherical wave. The best sources are vertical dipoles in the air over the sea or earth (e.g., the Cutler, ME antenna) and horizontal antennas in the sea near the air surface or near the sea floor. Vertical dipoles in the sea are not as effective, but can be used. The extensive study of the properties of lateral waves has included a corresponding study of the design of source antennas over the very wide frequency range in which lateral waves have useful applications. This study is summarized in [23] and [24]. Specifically included are the quite different designs for antennas on the sea floor at $f = 1$ kHz and at very low frequencies of the order of 1 Hz.

E. Lateral-Wave Pulses: A Diagnostic Tool for the Future

The complete continuous-wave properties of lateral electromagnetic waves have been determined analytically in a new, simple and practically accessible form. These have been verified both numerically [2], [3], and experimentally [10], and applied to geophysically significant problems [10]–[13], [15], [17]–[19]. Single electromagnetic pulses have very different properties from continuous waves. This is true both

of direct-wave pulses and lateral-wave pulses. The electrical characteristics of the medium in which they propagate affect the amplitude, width and shape of the pulse and determine the velocity with which it propagates. It follows that these characteristics can be deduced from the observed changes in the pulse as it progresses and from its time of travel from source to observer. A single current pulse on a horizontal dipole in the sea near the sea floor generates a lateral-wave pulse in the oceanic crust, a direct pulse in the sea. There is also a pulse with a spherical wave front that travels downward into the oceanic crust. This can be reflected successively from the boundaries of layers if these exist. The reflected pulses and the lateral-wave pulse all arrive at different times at a point of observation and can be analyzed individually. When combined with continuous-wave observations, the structure of the crust can be determined in an unambiguous manner. A very narrow pulse may propagate deep into the lithosphere because it does not involve the losses associated with the relaxation of water.

A systematic start has been made in the experimental and theoretical study of the generation and propagation of lateral electromagnetic pulses along boundaries between electrically different media. A terminated insulated antenna has been designed and tested for launching a lateral electromagnetic-field pulse. The propagation of such a pulse along an air-water boundary has been studied in detail in the model tank with various concentrations of salt in the water to adjust its conductivity over a wide range. With low conductivities, reflected pulses from the floor of the tank are observed and readily separated from the lateral-wave pulse that travels in the air. Theoretically an exact solution has been obtained from the general integrals for the field generated by a single current pulse in a vertical dipole on the boundary between two dielectric half-spaces. This field is described in [25]. It consists of two pulses that travel with different velocities--the lateral-wave pulse along the boundary in air, the direct-field pulse in the dielectric. A complete set of approximate formulas for the field generated by a single current pulse--delta-function and Gaussian--in both vertical and horizontal dipoles has been obtained

by Fourier transforming the approximate continuous-wave formulas [26]. A theoretical and experimental study of the field generated by a pulsed vertical monopole over salt water is in [27]. These studies lay the foundation for theoretical and experimental studies of the generation and propagation of pulses along two media like salt water over the sea floor.

4. Conclusion

The extensive research completed under Contract N00014-79-C-0419 has provided geophysicists with new, quantitatively accurate, and practically useful knowledge for the exploration of the oceanic crust by way of its electrical properties. The unusual properties of lateral electromagnetic waves and their relation to space waves reflected from layers in the lithosphere provide insights and tools that remain to be explored and applied. With the completion of basic research on the continuous-wave properties of electromagnetic waves near and along boundaries like the sea floor, exciting new research on the properties and applications of lateral-wave and space-wave electromagnetic pulses has opened new and challenging possibilities for geophysical exploration of the oceanic crust.

5. List of Equipment Purchased on Contract N00014-79-C-0419

The following pieces of equipment were purchased with funds provided by ONR Contract N00014-79-C-0419 during its nine years of activity. In accordance with the terms of Contract N00014-79-C-0419, title to these items of equipment is vested in Harvard University.

1 - Wavetek Model 184 5-MHz Sweep Generator	\$784.53
1 - Digital Video Terminal VT100 & Printer Terminal LA120	\$3,500.00
2 - Data Precision Corp. Digital Voltmeters	\$1,497.05
1 - Hewlett Packard Model 7225A Graphic Plotter	\$2,208.50
1 - Epson Model MX-80 F/T Printer with IEEE488 Interface	\$655.00
1 - Tektronix Model WP2110 Digitizer with Option 2	\$51,186.19
1 - AvTech Electrosystems Model AVL-2 Pulse Generator	\$1,718.00
1 - Hewlett Packard Model 8447F RF Amplifier	\$1,875.00

6. References*

- [1] R. W. P. King, J. T. deBettencourt, and B. H. Sandler, "Lateral-wave propagation of electromagnetic waves in the lithosphere," *IEEE Trans. Geosci. Elect.* **GE-17**, 86-92 (1979).
- [2]* T. T. Wu and R. W. P. King, "Lateral waves: A new formula and interference patterns," *Radio Sci.* **17**, 521-531 (1982).
- [3]* T. T. Wu and R. W. P. King, "Lateral waves: New formulas for $E_{1\phi}$ and E_{1z} ," *Radio Sci.* **17**, 532-538 (1982); "Correction," **19**, 1422 (1984).
- [4]* R. W. P. King and T. T. Wu, "Lateral waves: Formulas for the magnetic field," *J. Appl. Phys.* **54**, 507-514 (1983); "Erratum," **56**, 3365-3366 (1984).
- [5]* R. W. P. King, "New formulas for the electromagnetic field of a vertical electric dipole in a dielectric or conducting half-space near its horizontal interface," *J. Appl. Phys.* **53**, 8476-8482 (1982); "Erratum," **56**, 3366 (1984).
- [6]* M. F. Brown, R. W. P. King, and T. T. Wu, "Lateral-wave studies in a model lithosphere," *J. Appl. Phys.* **53**, 3387-3396 (1982).
- [7]* R. W. P. King, "On the reflection of lateral electromagnetic waves from perpendicular boundaries," *J. Appl. Phys.* **55**, 3916-3926 (1984).
- [8]* M. F. Brown, R. W. P. King, and T. T. Wu, "Experiments on the reflection of lateral electromagnetic waves," *J. Appl. Phys.* **55**, 3927-3933 (1984).
- [9]* J. T. deBettencourt, "Lateral waves near the air-sea boundary and atmospheric noise," *Proc. of the IEEE* **72**, 1219-1221 (1984).
- [10]* R. W. P. King and M. F. Brown, "Lateral electromagnetic waves along plane boundaries: A summarizing approach," *Proc. of the IEEE* **72**, 595-611 (1984).
- [11] R. W. P. King, "Scattering of lateral waves by buried or submerged objects. I. The incident lateral-wave field," *J. Appl. Phys.* **57**, 1453-1459 (1985).
- [12] R. W. P. King, "Scattering of lateral waves by buried or submerged objects. II. The electric field on the surface above a buried insulated wire," *J. Appl. Phys.* **57**, 1460-1472 (1985).
- [13]* R. W. P. King, "Electromagnetic surface waves: New formulas and their application to determine the electrical properties of the sea bottom," *J. Appl. Phys.* **58**, 3612-3624 (1985).
- [14] P. D. Young and C. S. Cox, "Electromagnetic active source sounding near the East Pacific Rise," *Geophys. Res. Lett.* **8**, 1043-1046 (1981).

* Asterisk indicates support in part from ONR Contract N00014-79-C-0419.

- [15] W.-Y. Pan, "Surface-wave propagation along the boundary between sea water and one-dimensionally anisotropic rock," *J. Appl. Phys.* **58**, 3963-3974 (1985).
- [16]* R. W. P. King, "Electromagnetic surface waves: New formulas and applications," *IEEE Trans. Antennas Propagat.* **AP-33**, 1204-1212 (1985).
- [17]* M. F. Brown and R. W. P. King, "Shallow sounding of crustal regions using electromagnetic surface waves," *Radio Sci.* **21**, 831-844 (1986).
- [18] R. W. P. King, M. Owens, and T. T. Wu, "Properties of lateral electromagnetic fields and their application," *Radio Sci.* **21**, 13-23 (1986).
- [19] R. W. P. King, "Properties of the lateral electromagnetic field of a vertical dipole and their applications," *IEEE Trans. Geosci. & Remote Sensing* **GE-24**, 813-825 (1986).
- [20] R. N. Edwards, L. K. Law, P. A. Wolfram, D. C. Nobes, M. N. Bone, D. F. Triggs, and J. M. DeLaurier, "First results of Moses experiment: Sea-sediment conductivity and thickness determination, Bute Inlet, British Columbia, by magnetometric offshore electrical sounding," *Geophysics* **50**, 153-160 (1985).
- [21] R. W. P. King, "The three-layer problem for sediment on the oceanic crust," to be submitted for publication.
- [22] W.-Y. Pan, "Measurement of lateral waves along a three-layered medium," *IEEE Trans. Antennas Propagat.* **AP-34**, 267-271 (1986).
- [23] R. W. P. King, "Antennas in material media near boundaries with application to communication and geophysical exploration, Part I: The bare metal dipole," *IEEE Trans. Antennas Propagat.*, **AP-34**, 483-489 (1986).
- [24] R. W. P. King, "Antennas in material media near boundaries with application to communication and geophysical exploration, Part II: The terminated insulated antenna," *IEEE Trans. Antennas Propagat.*, **AP-34**, 490-496 (1986).
- [25] T. T. Wu and R. W. P. King, "Lateral electromagnetic pulses generated by a vertical dipole on the boundary between two dielectrics," *J. Appl. Phys.* **62**, 4345-4355 (1987).
- [26] R. W. P. King, "Lateral electromagnetic pulses generated by a vertical dipole on a plane boundary between dielectrics," *J. Electrom. Waves & Applications*, accepted for publication.
- [27]* M. F. Brown, "Wave packets of lateral waves due to a vertical monopole: Experiment and theory," *Radio Sci.* **22**, 833-846 (1987).

7. Papers Presented at Scientific Meetings*

- *M. F. Brown, R. W. P. King, L. C. Shen, and T. T. Wu, "Experimental and theoretical studies of lateral-wave propagation," presented at the 1980 North American Radio Science Meeting, Québec, Canada, June 1980.
- *M. F. Brown, R. W. P. King, and T. T. Wu, "The propagation and reflection of lateral waves," presented at the 1983 International IEEE/AP-S Symposium, Houston, TX, May 1983.
- *R. W. P. King, "Electromagnetic surface waves: New formulas and applications," presented at the 1984 International IEEE/AP-S Symposium, Boston, MA, June 1984.
- *M. F. Brown, "Scattering of a lateral electromagnetic wave by a metal cylinder," presented at the National Radio Science Meeting, Boston, MA, June 1984.
- *M. F. Brown, "The pulsed lateral-wave field of a vertical monopole in air," presented at the 1985 USNC/URSI Commission F Meeting, Amherst, MA, October 1985.
- R. W. P. King, M. Owens, and T. T. Wu, "Properties of lateral electromagnetic fields and their application," presented at the 1985 USNC/URSI Commission F Meeting, Amherst, MA, October 1985.
- W.-Y. Pan and R. W. P. King, "Surface waves along boundary in anisotropic half-space," presented at the 1985 USNC/URSI Commission F Meeting, Amherst, MA, October 1985.
- R. W. P. King, "Lateral electromagnetic surface waves and pulses," presented at the Heinrich Hertz Symposium, Karlsruhe, FRG, March 1988.

* Asterisk indicates support in part from ONR Contract N00014-79-C-0419.

3. Final Report Appendix

Table of Contents

R. W. P. King, J. T. deBettencourt, and B. H. Sandler, "Lateral-wave propagation of electromagnetic waves in the lithosphere," <i>IEEE Trans. Geosci. Elect. GE-17</i> , 86-92 (1979)	15
T. T. Wu and R. W. P. King, "Lateral waves: A new formula and interference patterns," <i>Radio Sci.</i> 17 , 521-531 (1982)	22
T. T. Wu and R. W. P. King, "Lateral waves: New formulas for $E_{1\phi}$ and E_{1z} ," <i>Radio Sci.</i> 17 , 532-538 (1982); "Correction," 19 , 1422 (1984)	33
R. W. P. King, "New formulas for the electromagnetic field of a vertical electric dipole in a dielectric or conducting half-space near its horizontal interface," <i>J. Appl. Phys.</i> 53 , 8476-8482 (1982); "Erratum," 56 , 3366 (1984)	41
M. F. Brown, R. W. P. King, and T. T. Wu, "Lateral-wave studies in a model lithosphere," <i>J. Appl. Phys.</i> 53 , 3387-3396 (1982)	49
R. W. P. King and T. T. Wu, "Lateral waves: Formulas for the magnetic field," <i>J. Appl. Phys.</i> 54 , 507-514 (1983); "Erratum," 56 , 3365-3366 (1984)	59
R. W. P. King, "On the reflection of lateral electromagnetic waves from perpendicular boundaries," <i>J. Appl. Phys.</i> 56 , 3916-3926 (1984)	69
M. F. Brown, R. W. P. King, and T. T. Wu, "Experiments on the reflection of lateral electromagnetic waves," <i>J. Appl. Phys.</i> 55 , 3927-3933 (1984)	80
J. T. deBettencourt, "Lateral waves near the air-sea boundary and atmospheric noise," <i>Proc. of the IEEE</i> 72 , 1219-1221 (1984)	87
R. W. P. King and M. F. Brown, "Lateral electromagnetic waves along plane boundaries: A summarizing approach," <i>Proc. of the IEEE</i> 72 , 595-611 (1984)	90

- R. W. P. King, "Scattering of lateral waves by buried or submerged objects. I. The incident lateral-wave field," *J. Appl. Phys.* **57**, 1453-1459 (1985) 107
- R. W. P. King, "Scattering of lateral waves by buried or submerged objects. II. The electric field on the surface above a buried insulated wire," *J. Appl. Phys.* **57**, 1460-1472 (1985) 114
- R. W. P. King, "Electromagnetic surface waves: New formulas and their application to determine the electrical properties of the sea bottom," *J. Appl. Phys.* **58**, 3612-3624 (1985) 127
- W.-Y. Pan, "Surface-wave propagation along the boundary between sea water and one-dimensionally anisotropic rock," *J. Appl. Phys.* **58**, 3963-3974 (1985) 140
- R. W. P. King, "Electromagnetic surface waves: New formulas and applications," *IEEE Trans. Antennas Propagat.* **AP-33**, 1204-1212 (1985) 152
- M. F. Brown and R. W. P. King, "Shallow sounding of crustal regions using electromagnetic surface waves," *Radio Sci.* **21**, 831-844 (1986) 161
- R. W. P. King, M. Owens, and T. T. Wu, "Properties of lateral electromagnetic fields and their application," *Radio Sci.* **21**, 13-23 (1986) 175
- R. W. P. King, "Properties of the lateral electromagnetic field of a vertical dipole and their applications," *IEEE Trans. Geosci. & Remote Sensing* **GE-24**, 813-825 (1986) 186
- W.-Y. Pan, "Measurement of lateral waves along a three-layered medium," *IEEE Trans. Antennas Propagat.* **AP-34**, 267-271 (1986) 199
- R. W. P. King, "Antennas in material media near boundaries with application to communication and geophysical exploration, Part I: The bare metal dipole," *IEEE Trans. Antennas Propagat.*, **AP-34**, 483-489 (1986) 204
- R. W. P. King, "Antennas in material media near boundaries with application to communication and geophysical exploration, Part II: The terminated insulated antenna," *IEEE Trans. Antennas Propagat.*, **AP-34**, 490-496 (1986) 211

- T. T. Wu and R. W. P. King, "Lateral electromagnetic pulses generated by a vertical dipole on the boundary between two dielectrics," *J. Appl. Phys.* **62**, 4345-4355 (1987) 218
- M. F. Brown, "Wave packets of lateral waves due to a vertical monopole: Experiment and theory," *Radio Sci.* **22**, 833-846 (1987) 229
- R. W. P. King, "Lateral electromagnetic surface waves and pulses," presented at the Heinrich Hertz Symposium, Karlsruhe, FRG, March 14-15 (1988) 243
- R. W. P. King, "Lateral electromagnetic pulses generated by a vertical dipole on a plane boundary between dielectrics," *J. Electrom. Waves & Applications*, accepted for publication 263

Lateral-Wave Propagation of Electromagnetic Waves in the Lithosphere

RONOLD W. P. KING, FELLOW, IEEE, JOSEPH T. DEBETTENCOURT, FELLOW, IEEE,
AND BARBARA H. SANDLER

Abstract—The possibility of lateral-wave propagation of electromagnetic waves between horizontal electric dipoles near the floor of the ocean is reviewed. The general exact integrals for the radial electric field, which is the most useful component for lateral-wave transmission, are evaluated numerically for a range of possible conductivities of the lithospheric rock. Graphs and contour diagrams are shown and discussed for frequencies from 10 Hz to 1 GHz and radial distances from 0.1 to 100 km. Conditions under which very low frequencies provide the greatest range are defined, and also conditions under which a high-frequency window is available that offers by far the greatest radial range.

I. INTRODUCTION

THE possibility of a waveguide-like propagation of electromagnetic waves in the earth's lithosphere has been studied extensively [1]–[7] in terms of theoretical models that are idealizations of the earth's crust, as represented for example, by Levin [3], and shown in Fig. 1. Such idealizations usually consist of (1) a planar slab of a dielectric with low conductivity to represent a granitic or basaltic lithosphere (2) an upper, more highly conducting layer to correspond to the overburden or the ocean, and (3) a lower, also highly conducting region to represent the mantle. Refinements include the air and the ionosphere above the overburden and ocean, as shown in Fig. 2, but their inclusion usually has an insignificant effect.

The excitation of electromagnetic waves in the slab of dielectric and their reception at distant points have taken several forms. The most commonly used source is a vertical antenna in a borehole that extends close to or into the rock layer. Wait [5] states that if the vertical antenna does not extend into the rock or very close to it, adequate excitation does not occur. He suggests ([5], p. 923) that "every effort should be made to locate both the vertical source dipole and the point of observation within the waveguide. Otherwise, some other mechanism of excitation should be used, such as a horizontal electric dipole." The importance of this suggestion was confirmed theoretically by Frieman and Kroll [8] who studied

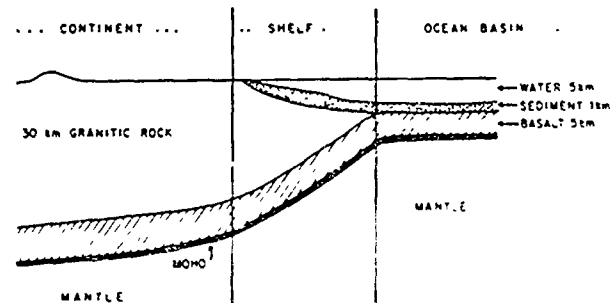


Fig. 1. Profile of earth's crust according to S. B. Levin

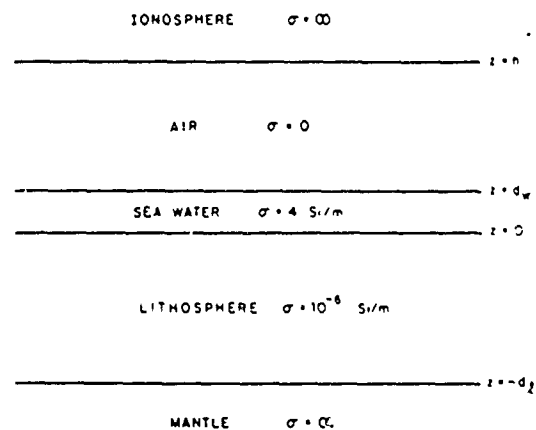


Fig. 2. Model used by Frieman and Kroll

excitation by both vertical and horizontal electric dipoles on the ocean floor using the model shown in Fig. 2. Their conclusion is that "the horizontal electric dipole proves to be more interesting," and "permits the utilization of much larger antennas and hence more efficient antenna design." They suggest that "a horizontal electric dipole is far superior to a vertical electric dipole."

The method of analysis used by Frieman and Kroll [8] resembles that of Wait [5] and others in that the relevant waveguide modes are determined. Their study of the propagation characteristics of the several modes indicates that for horizontal transmitting and receiving antennas on the ocean floor, the field "should be very similar to that of horizontal dipole excitation near the plane boundary of two semi-infinite conducting media." It is well known from the work of Baños [9], King and Sandler [10], and others, that transmission

Manuscript received April 13, 1979. This work was supported in major part by the Office of Naval Research under Contract N00014-78-C-0668 with J. T. deBettencourt, and in minor part by the Joint Services Electronics Program under Contract N00014-75-C-0648 with Harvard University, Cambridge, MA.

R. W. P. King and B. H. Sandler are with the Gordon McKay Laboratory, Harvard University, Cambridge, MA 02138.

J. T. deBettencourt is at 18 Sterling Street, West Newton, MA 02165.

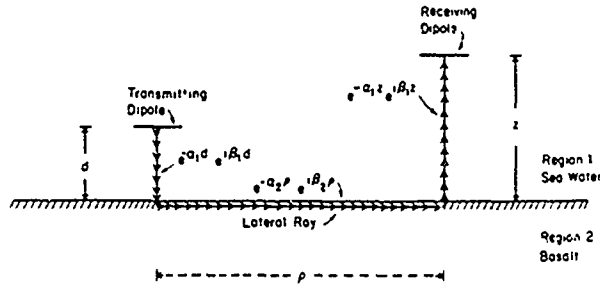


Fig. 3. Schematic diagram of a ray in lateral-wave transmission and its relation to the mathematical representation $\exp\{-[\alpha_2 \rho + \alpha_1(d+z)]\} \exp\{i[\beta_2 \rho + \beta_1(d+z)]\}$.

along an air-sea interface is primarily by so-called lateral waves. This conclusion is confirmed by Bubenik and Fawcett-Smith's [11] analysis of the field of a vertical magnetic dipole located in sea water midway between the air above and the sea floor below. Their comparison of the contributions to the total field by direct transmission through the sea as if this were unbounded with those by air-surface and sea-floor lateral-wave modes shows that for a dipole near the air surface, the air-surface mode dominates, for a dipole near the sea floor, the sea-floor mode dominates. This latter is illustrated schematically in Fig. 3 where a lateral ray is traced. Since a vertical magnetic dipole is equivalent to four horizontal electric dipoles arranged in a square, its field is a superposition of the fields of the four dipoles, each like the field of a single horizontal electric dipole. The superimposed fields of the very closely spaced dipoles suffer from a large reduction due to cancellation, but the essential nature of the field with respect to its modal structure is not changed. Therefore, when the sea-floor lateral-wave mode dominates for a vertical magnetic dipole, it also does for a horizontal electric dipole at the same location.

II. LATERAL-WAVE PROPAGATION ALONG THE LITHOSPHERE-OCEAN BOUNDARY

Comprehensive studies of subsurface communication between horizontal electric dipoles in a dissipative half-space (region 1) near its boundary with air (region 2) [9], [10], [12] have shown that the only generally useful component of the electric field for lateral-wave propagation is the radial one, i.e., $E_{1\rho}$. It may be assumed that this is also true when the air is replaced by rock with conductivities in the range from 4×10^{-8} to 4×10^{-3} Si/m. Thus a quantitative study of lateral-wave transmission along the ocean-lithosphere boundary, shown in Fig. 4, requires the determination of $E_{1\rho}$ at an arbitrary point $P(\rho, \phi, z)$ in the sea water. The source is a horizontal electric dipole with unit moment ($|\Delta| = 1$) located in the sea at a distance d above the origin of coordinates on the boundary surface. The exact expression for $E_{1\rho}$ is given explicitly in King and Smith [13], or it can be obtained from the general formulas given by Baños [9]. It is assumed that $\mu_1 = \mu_2 = \mu_0$, the time dependence is $e^{-i\omega t}$. When $z = d$,

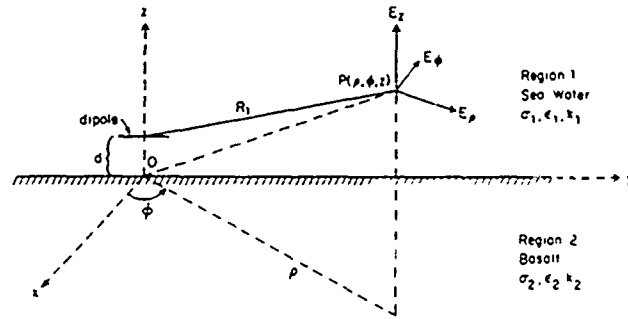


Fig. 4. Two-half-space model for lateral-wave transmission.

$$E_{1\rho} = -\frac{\omega\mu_0}{4\pi k_1^2} \cos \phi \left(\int_0^\infty \{k_1^2 J_0(\lambda \rho) - (\lambda^2/2)[J_0(\lambda \rho) - J_2(\lambda \rho)]\} \gamma_1^{-1} \lambda d\lambda + \int_0^\infty \left\{ \frac{\gamma_1(k_1^2 \gamma_2 - k_2^2 \gamma_1)}{2(k_1^2 \gamma_2 + k_2^2 \gamma_1)} \cdot [J_0(\lambda \rho) - J_2(\lambda \rho)] - \frac{k_1^2(\gamma_2 - \gamma_1)}{2\gamma_1(\gamma_2 + \gamma_1)} \cdot [J_0(\lambda \rho) + J_2(\lambda \rho)] \right\} e^{i2\gamma_1 d} \lambda d\lambda \right) \quad (1)$$

where, with $j = 1, 2$,

$$\gamma_j = (k_j^2 - \lambda^2)^{1/2} \quad (2)$$

and the wavenumbers are

$$k_j = \beta_j + i\alpha_j = (\omega^2 \mu_0 \epsilon_{ej} + i\omega \mu_0 \sigma_{ej})^{1/2}. \quad (3)$$

In (3), ϵ_{ej} is the real effective permittivity and σ_{ej} is the real effective conductivity of the material in region j .

The numerical evaluation of $E_{1\rho}$ from (1) has been carried out by King and Sandler [10] and by King *et al.* [12] when region 2 is air and region 1 is a half-space characterized by conductivities and permittivities in wide ranges. The complicated dependence of $E_{1\rho}$ on the frequency and radial distance as well as on the electrical properties of the material half space that is revealed in the computed graphs in [10] and [12] is interpreted there with the help of a set of simple approximate formulas due to Baños [9]. Since these have been derived specifically when region 2 is a perfect dielectric (air) with a real wavenumber $k_2 = \beta_2$, $\alpha_2 = 0$, it is noteworthy that they are quantitatively fairly good approximations even when region 2 is an imperfect dielectric (lithosphere of rock) that has the properties of a conductor at low frequencies. The following is a general form of the approximate formulas:

$$E_{1\rho} \sim A \cos \phi f(\rho) \exp\{i[k_2 \rho + k_1(z+d)]\} \quad (4)$$

where $f(\rho) \sim 1/\rho^3$ for the near field, $f(\rho) \sim 1/\rho$ for the intermediate field, and $f(\rho) \sim 1/\rho^2$ for the asymptotic or far field. The amplitude A is a different function of k_1 and k_2 in each of these ranges. Formula (4) discloses the lateral-wave nature of the field in the exponential term which can be written in the

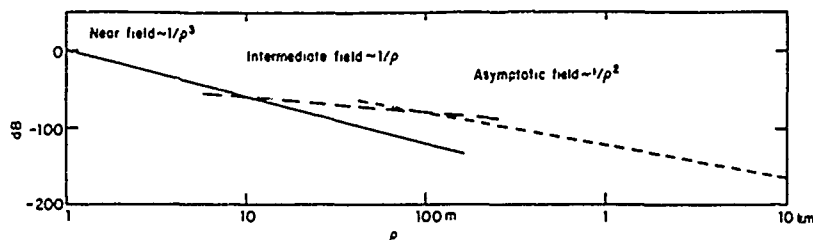


Fig. 5. Schematic example of near, intermediate, and asymptotic fields.

form $\exp\{-[\alpha_2\rho + \alpha_1(z+d)]\}\exp\{i[\beta_2\rho + i\beta_1(z+d)]\}$. A schematic representation of the down-over-up path of a ray and its relation to this expression is shown in Fig. 3. The radial dependence of the amplitude $|E_{1\rho}|$ is seen to be approximated by $f(\rho)\exp\{-[\alpha_2\rho + \alpha_1(z+d)]\}$ which consists of three principal parts, viz., the exponential dependence on the total vertical distance $z+d$, the exponential dependence on the radial distance ρ , and the inverse power dependence on the radial distance. This last consists of three segments beginning with $1/\rho^3$ at low frequencies and electrically short radial distances, $1/\rho$ at intermediate frequencies and electrical distances, and $1/\rho^2$ at high frequencies and large electrical distances. Graphs of $20\log_{10}[f(\rho)/f(1)]$ are shown in Fig. 5 for the three ranges. These have the forms $-60\log_{10}\rho$, $-20\log_{10}\rho$, and $-40\log_{10}\rho$, respectively, for $f(\rho) = 1/\rho^3$, $1/\rho$, and $1/\rho^2$.

III. GRAPHICAL REPRESENTATION AND INTERPRETATION OF $E_{1\rho}$ IN LITHOSPHERIC PROPAGATION

The numerical evaluation of $|E_{1\rho}|$ at $P(\rho, \phi, z)$ from (1) for the disposition of dipole and materials, shown in Fig. 4, has been carried out when region 1 is sea water ($\epsilon_{er1} = 80$, $\sigma_{e1} = 4$ Si/m) and region 2 is rock ($\epsilon_{er2} = 16$, $\sigma_{e2} = 4 \times 10^{-8}$ to 4×10^{-3} Si/m). For convenience in the graphical representation, the quantity $20\log_{10}|E_{1\rho}|$ is used as the dependent variable with the reference amplitude $|E_{1\rho}| = 1$ V/m. The actual magnitude $|E_{1\rho}|$ in volts per meter due to a dipole with unit moment ($I\Delta l = 1$ A m) can be obtained by dividing the values in the graph by 20 and evaluating the antilogarithm. In the computations of $|E_{1\rho}|$, the dipole and point of observation are initially assumed to be the same, and two values, $z = d = 0.15$ m and 1.5 m, are investigated in detail. Subsequently, the results are extended to arbitrary and different values of z and d . The radial distance ρ between the dipole and the point of observation is varied from 0.1 to 100 km with frequencies in the range from 10 to 10^9 Hz.

Graphs of $|E_{1\rho}|$ as a function of the radial distance with $\phi = 0$ and the frequency as the parameter are shown in Fig. 6 for $\sigma_{e2} = 4 \times 10^{-8}$ Si/m and 4×10^{-7} Si/m, and in Fig. 7 for $\sigma_{e2} = 4 \times 10^{-6}$, 4×10^{-5} , 4×10^{-4} , and 4×10^{-3} Si/m. In both figures, $z = d = 0.15$ m. The general validity of the approximate form (4) is readily verified from these graphs and the contributions from the several factors identified. Thus with $\sigma_{e2} = 4 \times 10^{-8}$ Si/m in the upper half of Fig. 6, $\alpha_2\rho$ is sufficiently small over the entire radial range to make $e^{-\alpha_2\rho} \sim 1$, so that the entire dependence on ρ is in $f(\rho)$. A comparison

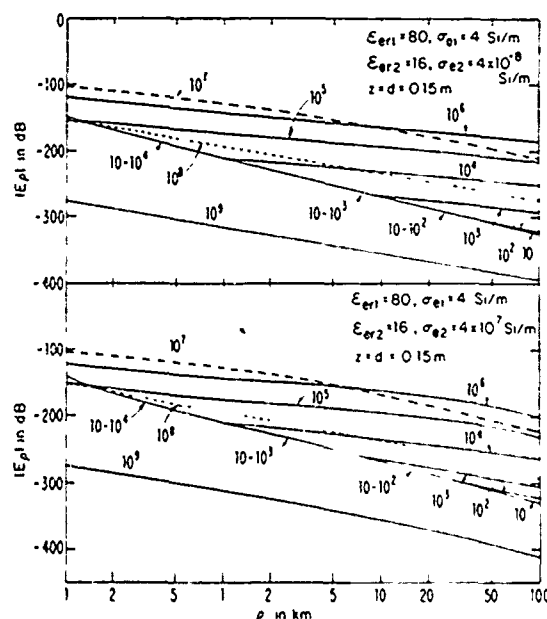


Fig. 6. Magnitude of E_{ρ} in sea water bounded by lithosphere; $z = d = 0.15$ m.

with Fig. 5 shows that at $f = 10$ and 100 Hz, the graphs of $|E_{1\rho}|$ have the near-field form $C - 60\log_{10}\rho$, where C is a constant. The graph for $f = 10^3$ Hz has the near-field form $C - 60\log_{10}\rho$ up to about $\rho = 9$ km, then it changes to the intermediate-field form $C - 20\log_{10}\rho$. The graph for $f = 10^4$ Hz is similar but the change from the near-field to the intermediate-field form occurs near $\rho = 1.2$ km. The graphs for $f = 10^5$ and 10^6 Hz are entirely in the intermediate-field range given by $C - 20\log_{10}\rho$. The graph for $f = 10^7$ has the intermediate-field form occurs near $\rho = 1.2$ km. The graphs for changes to the asymptotic-field form $C - 40\log_{10}\rho$. The graphs for $f = 10^8$ and 10^9 Hz are entirely in the asymptotic field range. The factor C (which is independent of ρ) is given by $C = 20\log_{10}|A|\exp[-\alpha_1(z+d)]$, where A involves $k_1 = \beta_1 + i\alpha_1$ and $k_2 = \beta_2 + i\alpha_2$. With $z + d = 0.30$ m, $\alpha_1(z+d)$ is sufficiently small when $f \leq 10^7$ Hz, so that $\exp[-\alpha_1(z+d)] \sim 1$, and the actual value of C is determined by A . When f is increased above 10^7 Hz, α_1 grows and $e^{-\alpha_1(z+d)}$ decreases rapidly from near 1. This accounts for the sharply reduced values of $|E_{1\rho}|$ in the graphs for $f = 10^8$ and 10^9 Hz. Note that the largest values of $|E_{1\rho}|$ occur with $f = 10^7$ Hz, $\rho \leq 8$ km, $f = 10^6$ Hz, and $\rho > 8$ km.

When the conductivity of the lithosphere is $\sigma_{e2} = 4 \times 10^{-7}$ Si/m, the graphs in the lower half of Fig. 6 apply. These

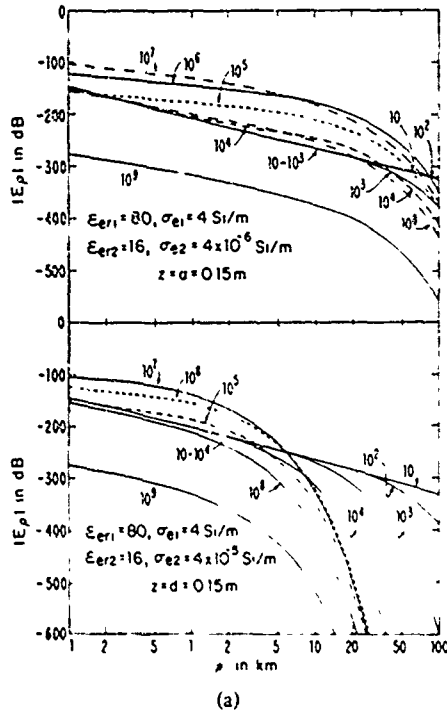


Fig. 7. Magnitude of E_ρ in sea water bounded by lithosphere;
 $z = d = 0.15$ m.

resemble those in the upper half, but at the higher frequencies and the larger radial distances they bend downward. This is because at the higher conductivity α_2 is larger, and at the greater values of ρ , $\alpha_2 \rho$ is large enough to make $e^{-\alpha_2 \rho}$ noticeably smaller than 1. This effect increases as σ_{e2} is raised in steps as shown in the four diagrams in Fig. 7. As σ_{e2} is increased, the greatest values of $|E_{1\rho}|$ shift from $f = 10^7$ and 10^6 Hz to lower frequencies, so that with $\sigma_{e2} = 4 \times 10^{-5}$ Si/m, the $|E_{1\rho}|$ at $f \leq 10$ Hz is greater than at $f = 10^7$ Hz, $\rho > 6$ km,

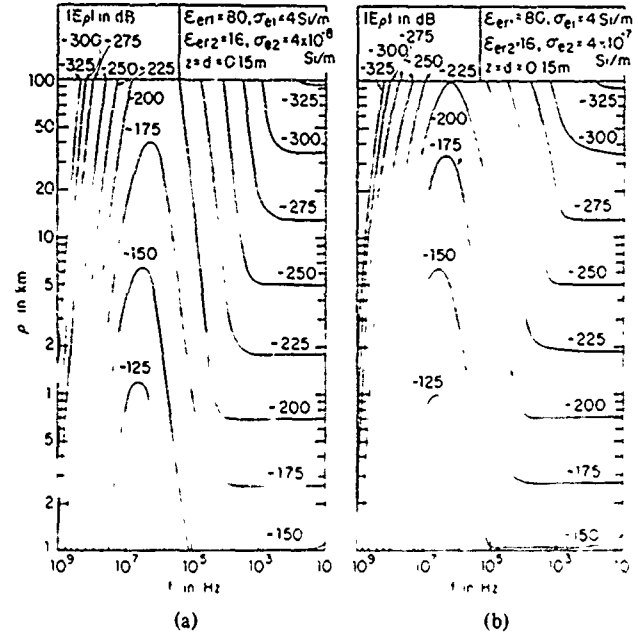


Fig. 8. Contours of constant $|E_\rho|$ in sea water bounded by lithosphere,
 $z = d = 0.15$ m.

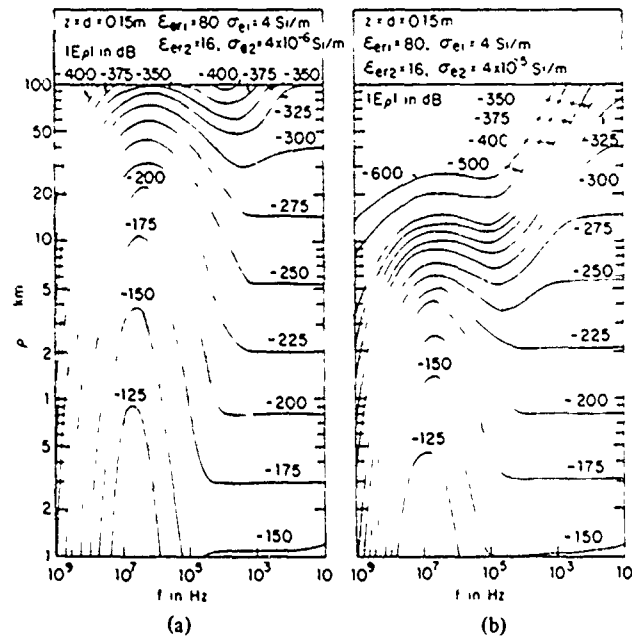


Fig. 9. Contours of constant $|E_\rho|$ in sea water bounded by lithosphere,
 $z = d = 0.15$ m.

with $\sigma_{e2} = 4 \times 10^{-4}$ Si/m, $|E_{1\rho}|$ at $f \leq 10^4$ Hz is greater than at $f = 10^7$ Hz when $\rho > 0.4$ km.

The information contained in Figs 6 and 7 is shown in a different manner in Figs 8-10, in which contours of constant $|E_{1\rho}|$ are drawn as functions of the radial distance ρ and the frequency f . The scale for the frequency is arranged to increase from right to left so that the wavelength $\lambda(\text{km}) = 3 \times 10^5/f$ (Hz) increases from left to right. In the graphs in Fig 8 for $\sigma_{e2} = 4 \times 10^{-8}$ and 4×10^{-7} Si/m, the short ranges ρ for a given $|E_{1\rho}|$ at the low frequencies are a consequence of the rapid $1/\rho^3$ decrease in the near-field range, the sharp reduction

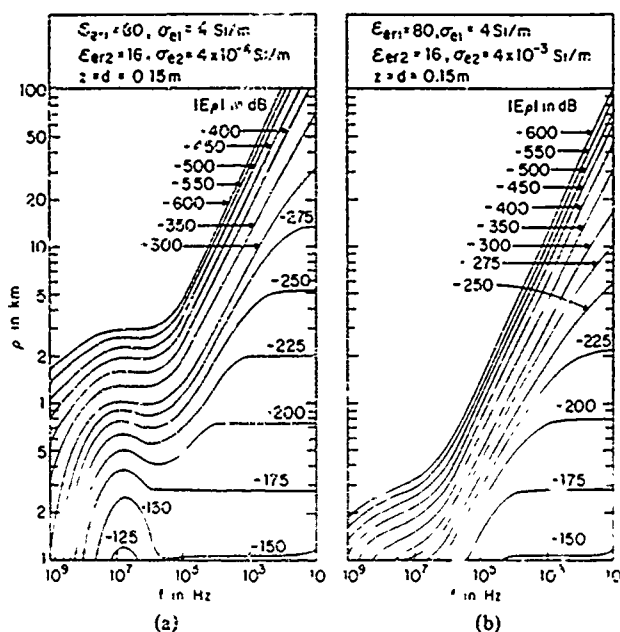


Fig. 10. Contours of constant $|E_\rho|$ in sea water bounded by lithosphere, $z = d = 0.15$ m.

in radial range at the high frequencies on the left are due to the combined effects of the factors in $e^{-\alpha_1(z+d)}/\rho^2$. The large peak in radial range which occurs when the frequency is between $f = 10^6$ and 10^7 Hz is possible because the exponential terms are near unity and the intermediate range value $f(\rho) \sim 1/\rho$ applies. Note, for example, that the value $|E_{1\rho}| = -175$ dB occurs at a radial distance of nearly 40 km with f near 10^7 Hz and near $\rho = 0.25$ km at $f \leq 10^3$ Hz. As the conductivity of the lithosphere is increased, the effect of $e^{-\alpha_1\rho}$ makes itself felt beginning at the higher frequencies and larger values of ρ , as shown in Fig. 9(a) for $\sigma_{e2} = 4 \times 10^{-6}$ Si/m and Fig. 9(b) for $\sigma_{e2} = 4 \times 10^{-5}$ Si/m. The sharp maximum between $f = 10^6$ and 10^7 Hz continues but only at decreasing radial distances. Finally, in Fig. 10(a) where $\sigma_{e2} = 4 \times 10^{-4}$ Si/m, and 4×10^{-3} Si/m in Fig. 10(b), the exponential attenuation is so great at the high frequencies that the maximum in the radial range near $f = 10^7$ Hz occurs only at very short distances. Furthermore, since α_2 increases with frequency, the largest values of $|E_{1\rho}|$ occur at the lowest frequency.

In Figs. 11 and 12 are shown graphs of $|E_{1\rho}|$ like those in Figs. 6 and 7 but now with the dipole and point of observation further from the boundary in the sea water. Specifically, $z = d = 1.5$ m. Contour diagrams like those in Figs. 8-10 are shown in Figs. 13-15. It is seen that when $\sigma_{e2} < 4 \times 10^{-5}$ Si/m, the relative maxima in the radial range have moved from near $f = 10^7$ Hz when $z = d = 0.15$ m, to near $f = 10^5$ Hz when $z = d = 1.5$ m, and that they are substantially smaller. For example, with $\sigma_{e2} = 4 \times 10^{-8}$ Si/m the maximum range for $|E_{1\rho}| = -225$ dB is $\rho = 10$ km with $z = d = 1.5$ m, instead of $\rho \sim 500$ km with $z = d = 0.15$ m. There is no corresponding decrease in the range at low frequencies since there the exponential attenuation is small. Unless both the transmitting and receiving antennas are very close to the ocean-lithosphere boundary and $\sigma_{e2} < 4 \times 10^{-6}$ Si/m, the greatest radial range for any given value of $|E_{1\rho}|$ occurs at very low frequencies.

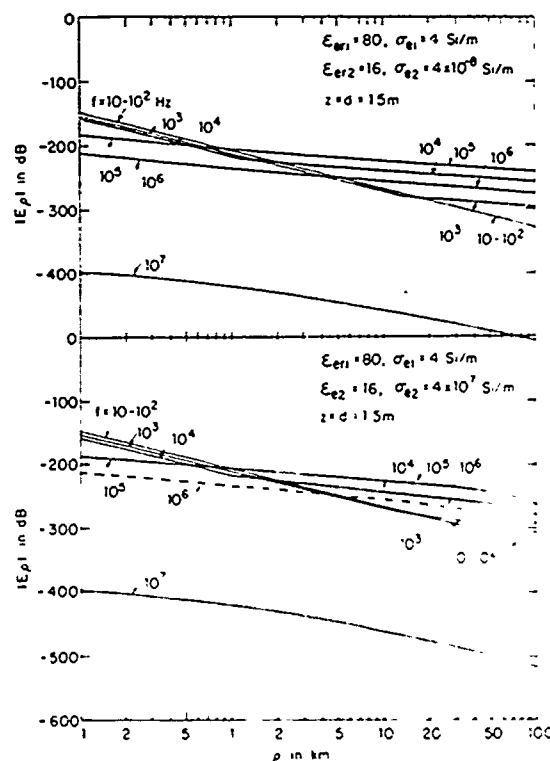


Fig. 11. Magnitude of E_ρ in sea water bounded by lithosphere, $z = d = 1.5$ m.

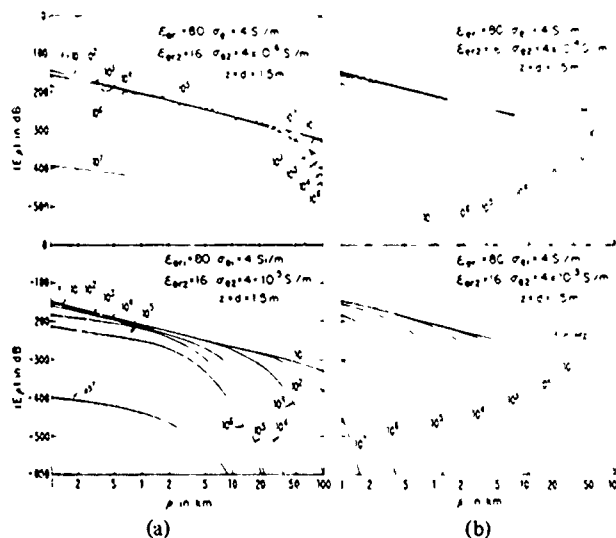


Fig. 12. Magnitude of E_ρ in sea water bounded by lithosphere, $z = d = 1.5$ m.

When z and d are sufficiently small and $\sigma_{e2} \leq 4 \times 10^{-6}$ Si/m, the greatest radial range occurs at an optimum frequency. This occurs with $f = 10^5$ to 10^7 Hz when $z = d$ is in the range from 1.5 m to 0.15 m.

IV. GENERALIZATION TO ARBITRARY LOCATIONS OF THE SOURCE AND RECEIVER

The graphs of $|E_{1\rho}|$ shown in the several figures apply to the special case $z = d$ when the dipole and the point of observation are at the same distance in the sea from the lithosphere boundary. Approximate values of $|E_{1\rho}|$ at dif-

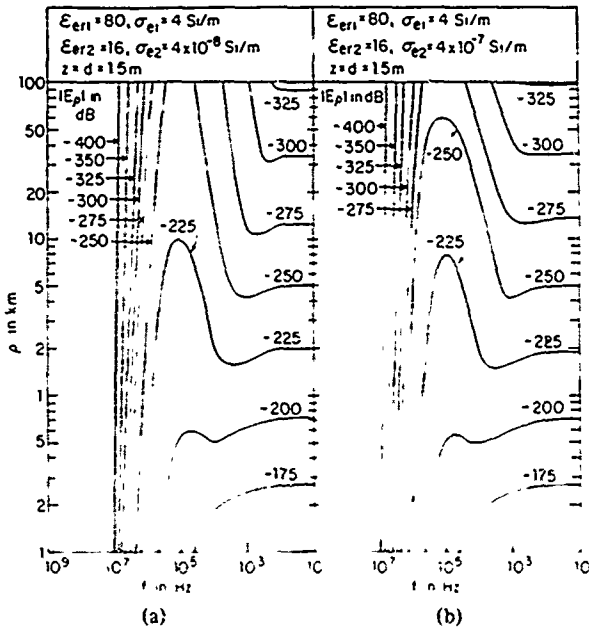


Fig. 13. Contours of constant $|E_\rho|$ in sea water bounded by lithosphere; $z = d = 1.5$ m.

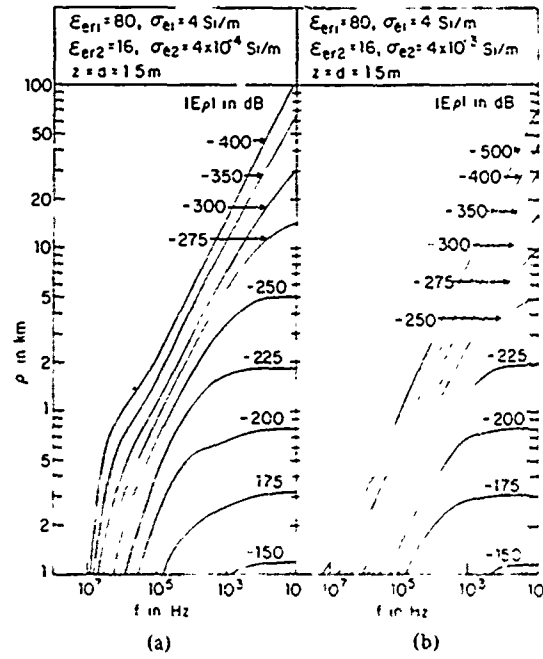


Fig. 15. Contours of constant $|E_\rho|$ in sea water bounded by lithosphere; $z = d = 1.5$ m.

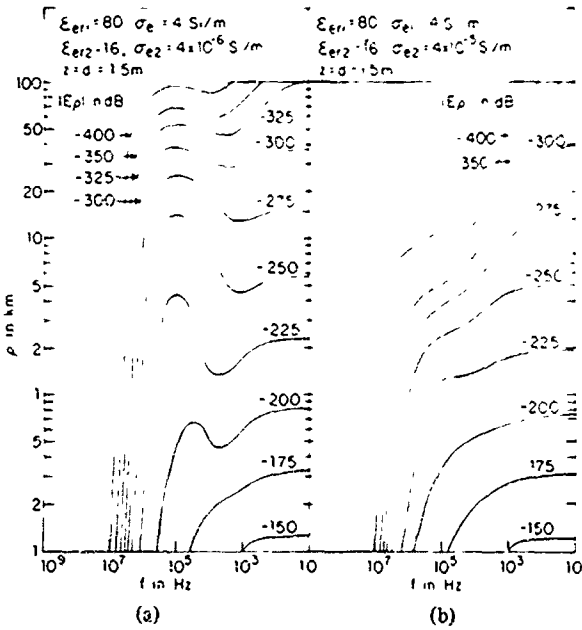


Fig. 14. Contours of constant $|E_\rho|$ in sea water bounded by lithosphere; $z = d = 1.5$ m.

ferent values of z and d are readily obtained from the known values at $z = d = 0.15$ m or $z = d = 1.5$ m if use is made of the simple formula (4) in which z and d occur only in the exponential $e^{ik_1(z+d)}$. Let $(E_{1\rho})_1$ be the known value at $z_1 = d_1 = 0.15$ m, and $(E_{1\rho})_2$ the unknown value at z_2 when the dipole is at d_2 . It is not assumed that $z_2 = d_2$. Clearly, from (4)

$$(E_{1\rho})_2 = (E_{1\rho})_1 \exp[ik_1(z_2 - z_1 + d_2 - d_1)] \quad (5)$$

and

$$|E_{1\rho}|_2 = |E_{1\rho}|_1 \exp[-\alpha_1(z_2 - z_1 + d_2 - d_1)]. \quad (6)$$

Also,

$$\begin{aligned} 20 \log_{10} |E_{1\rho}|_2 &= 20 \log_{10} |E_{1\rho}|_1 \\ &\quad - 20\alpha_1(z_2 - z_1 + d_2 - d_1) \\ &\quad \times 0.4343 \text{ dB referred to } 1 \text{ V/m} \end{aligned} \quad (7)$$

where $\log_{10} e = 0.4343$.

V. CONCLUSIONS CONCERNING LATERAL-WAVE PROPAGATION ALONG THE OCEAN-LITHOSPHERE BOUNDARY

The several graphs in Figs. 6-15 lead to the following general conclusions regarding lateral-wave transmission, along a plane boundary between sea water and the lithospheric rock, when the source is a horizontal electric dipole in the sea water at the distance d from the boundary and the point of observation is also in the sea water at the distance z from the boundary and the radial distance ρ from the source. 1) If the conductivity of the lithosphere is greater than $\sigma_{e2} = 4 \times 10^{-6}$ Si/m, transmission over distances greater than $\rho = 50$ km experiences the smallest decrease with distance when the frequency is as low as possible. This is true for all values of $z = d \geq 15$ cm. 2) If the conductivity of the lithosphere is significantly smaller than $\sigma_{e2} = 4 \times 10^{-6}$ Si/m, there is an optimum frequency between 1 and 10 MHz at which the radial range has a large relative maximum that may be substantially greater than the radial distance for $|E_{1\rho}|$ at other frequencies including the very low. Furthermore, an effective directional array with significant gain can be constructed for both the transmitter and the receiver for use at frequencies in the 1-10 MHz range. 3) Unless both the transmitting and receiving antennas are in the sea very close to the boundary surface with the lithosphere, the exponential term $e^{-\alpha_1(z+d)}$ greatly reduces the level of the transmitted field at all radial distances

and at all frequencies. This decrease is largest at high frequencies and smallest at low frequencies since α_1 increases with frequency.

REFERENCES

- [1] H. A. Wheeler, "Radio-wave propagation in the earth's crust," *J. Res. Nat. Bur. Stand.*, vol. 65D, pp. 189-191, 1961.
- [2] H. Mott and A. W. Biggs, "Very-low-frequency propagation below the bottom of the sea," *IEEE Trans. Antennas Propagat.*, vol. AP-11, pp. 232-239, May 1963.
- [3] S. B. Levin, "Lithospheric propagation—A review," Conference Proc. no. 20, pp. 147-178, in *Subsurface Communications*, NATO 12th Symposium of Avionics Panel of AGARD, Paris, France, 1966.
- [4] D. Staiman and T. Tamir, "Nature and optimisation of the ground (lateral) wave excited by submerged antennas," *Proc. Inst. Elec. Eng. (London)*, vol. 113, pp. 1299-1310, Aug 1966.
- [5] J. R. Wait, "Electromagnetic propagation in idealized earth crust waveguide," *Radio Sci.*, vol. 1, pp. 913-924, Aug 1966.
- [6] R. Gabillard, P. Degauque, and J. R. Wait, "Subsurface electromagnetic telecommunications—A review," *IEEE Trans. Comm. Tech.*, vol. COM-19, pp. 1217-1228, Dec. 1971.
- [7] G. L. Brown and A. F. Gangi, "Electromagnetic modelling studies of lithospheric propagation," *IEEE Trans. Geosci. Electron.*, vol. GE-1, pp. 17-23, Jan. 1961.
- [8] E. A. Frieman and N. M. Kroll, "Lithospheric propagation for undersea communication," Tech. Rep. (JASON) JSR-73-5, Stanford Res. Inst., Menlo Park, CA, Nov. 1973.
- [9] A. Baños, Jr., *Dipole Radiation in the Presence of a Conducting Half-Space*. New York: Pergamon, 1966.
- [10] R. W. P. King and B. Sandler, "Subsurface communication between dipoles in general media," *IEEE Trans. Antennas Propagat.*, vol. AP-25, pp. 770-775, Nov. 1977.
- [11] D. M. Bubenik and A. C. Fraser Smith, "ULF/ELF electromagnetic fields generated in a sea of finite depth by a submerged vertically directed harmonic magnetic dipole," *Radio Sci.*, vol. 13, pp. 1011-1020, 1978.
- [12] R. W. P. King, B. H. Sandler, and L. C. Shen, "A comprehensive study of subsurface propagation from horizontal electric dipoles," to be published.
- [13] R. W. P. King and G. S. Smith, *Antennas in Matter Fundamentals, Theory, and Applications*. Cambridge, MA: The M.I.T. Press, (in press)

Lateral waves: a new formula and interference patterns

T. T. Wu and R. W. P. King

Gordon McKay Laboratory, Harvard University, Cambridge, Massachusetts 02138

(Received June 23, 1981; revised September 28, 1981; accepted October 6, 1981.)

A new simple formula is derived as an approximation for the general exact integrals for the radial component of the electric field generated by a horizontal electric dipole in a half-space of water or earth near its boundary with air. The field in the water or earth is investigated as a function of radial distance from the source for $\epsilon_r = 80, 20$, and 4, over wide ranges of conductivities and frequencies. Special attention is paid to the ranges in which the direct wave from the dipole produces an interference pattern of standing waves when it interacts with the lateral wave. For selected values of the parameters the radial electric field computed from the new simple formula is compared with the field evaluated numerically from the exact integrals. The agreement is excellent when the ratio of wave numbers characteristic of the denser half-space and air is large, quite good even when this ratio is as small as 2.

1 INTRODUCTION

The study and understanding of lateral-electromagnetic-wave propagation from horizontal electric dipoles located near the surface of the earth (in salt or fresh water, dry or moist soil or sand, frozen earth or ice) have been handicapped by the complexity of the exact general integrals that characterize all six components of the electromagnetic field in both the earth and in the air above it. Between the pioneer work of Sommerfeld [1909, 1926] and the appearance of the comprehensive treatise by Baños [1966], many attempts were made to obtain useful approximate formulas. These were successful only in a limited sense in severely restricted ranges of the parameters and variables. Many investigators have been preoccupied with propagation in and over sea water and at very low frequencies for which all parts of the earth's surface behave like conductors [Bannister and Dube, 1978]. More recently, attention has been directed to the numerical evaluation of the complex Sommerfeld integrals that occur in the general formulas for the lateral-wave field [Siegel and King, 1970, 1971, 1973; Bubenik, 1977; King and Sandler, 1977; Rahmat-Samii et al., 1981]. A comprehensive tabulation of the numerically calculated radial component of the electric field of a horizontal electric dipole in a half-space with a wide range of values of permittivity and

conductivity at frequencies from 10 Hz to 1 GHz and a radial range from 0.5 m to 100 km has been completed [King and Smith, 1981]. Extensive graphical representations of the magnitude of this field have been published [King et al., 1980; King and de Bettencourt, 1979].

Significantly, none of the available approximate formulas—including those of Baños [1966]—is adequate to provide insight into the complicated nature of the field generated by a horizontal electric dipole in a homogeneous half-space near its boundary with air. So-called 'physical explanations' [Lytle et al., 1976] also fail to do so. The complete picture is, of course, contained in the general integral formulas, but these are too complicated to provide physical insight by inspection and their evaluation by numerical methods has not been sufficiently fine-grained to reveal some of their most interesting and important characteristics. A full understanding of the properties of lateral waves can best be obtained from simple and accurate formulas for the components of the electromagnetic field. Since the radial electric field is the most important component, attention is directed to it. The other components will be treated in another paper.

In the analysis to follow the complex wave number of region 1 with $z > 0$ (water, earth, etc.) is $k_1 = \beta_1 + i\alpha_1 = \omega(\mu_1\bar{\epsilon}_1)^{1/2}$, where $\bar{\epsilon}_1 = \epsilon_1 + i\sigma_1/\omega$ and $\epsilon_1 = \epsilon_0\epsilon_{r1}$. The wave number of region 2 with $z < 0$ (air) is $k_2 = \beta_2 - i\alpha_2 = \omega(\mu_2\bar{\epsilon}_2)^{1/2}$. It is assumed that $\mu_1 = \mu_2 = \mu_0$; for air $\bar{\epsilon}_2 = \epsilon_0$, $\alpha_2 = 0$.

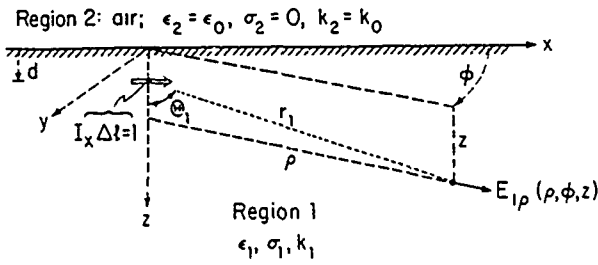


Fig. 1. Radial component of electric field at (ρ, ϕ, z) due to x -directed dipole at $(0, 0, d)$

2 AN APPROXIMATE THEORETICAL FORMULA FOR THE RADIAL ELECTRIC FIELD

The general integral for the radial component $E_{1\rho}$ of the electric field at the point (ρ, ϕ, z) in region 1 due to an x directed, horizontal electric dipole in the same region at the point $(0, 0, d)$ is (King and Smith [1981], p. 617, eq. (5.9)):

$$E_{1\rho} = -\frac{\omega\mu_0}{4\pi k_1^2} \cos \phi \left(\int_0^\infty \{k_1^2 J_0(\lambda\rho) - (\lambda^2/2)[J_0(\lambda\rho) - J_2(\lambda\rho)]\} \gamma_1^{-1} e^{-\gamma_1(z-d)} \lambda d\lambda \right. \\ \left. + \int_0^\infty \{(\gamma_1 Q/2)[J_0(\lambda\rho) - J_2(\lambda\rho)] - (k_1^2 P/2\gamma_1)[J_0(\lambda\rho) + J_2(\lambda\rho)]\} e^{-\gamma_1(z+d)} \lambda d\lambda \right) \quad (1)$$

where, with $\mu_1 = \mu_2 = \mu_0$,

$$P = (\gamma_2 - \gamma_1)/(\gamma_2 + \gamma_1) \\ Q = (\bar{\epsilon}_1 \gamma_2 - \bar{\epsilon}_2 \gamma_1)/(\bar{\epsilon}_1 \gamma_2 + \bar{\epsilon}_2 \gamma_1) \\ \gamma_i^2 = k_i^2 - \lambda^2 \quad (2)$$

The location of the dipole at $(0, 0, d)$ and the point (ρ, ϕ, z) where $E_{1\rho}$ is calculated are shown in Figure 1.

The second integral in (1) can be expressed as the sum of two integrals as follows.

$$F'_0(\rho, z+d) + F_1(\rho, z+d) = \int_0^\infty \{(\gamma_1/2)[J_0(\lambda\rho) - J_2(\lambda\rho)] \\ + (k_1^2/2\gamma_1)[J_0(\lambda\rho) + J_2(\lambda\rho)]\} e^{-\gamma_1(z+d)} \lambda d\lambda \\ + \int_0^\infty \{(\gamma_1/2)[Q-1][J_0(\lambda\rho) - J_2(\lambda\rho)] - (k_1^2/2\gamma_1) \\ \cdot [P+1][J_0(\lambda\rho) + J_2(\lambda\rho)]\} e^{-\gamma_1(z+d)} \lambda d\lambda \quad (3)$$

The first integral in (1) can be rearranged with the relation $\gamma_1^2 = k_1^2 - \lambda^2$ to have the same form, except for the exponential, as the first integral in (3). It is

$$F_0(\rho, z-d) = \int_0^\infty \{(\gamma_1/2)[J_0(\lambda\rho) - J_2(\lambda\rho)] \\ + (k_1^2/2\gamma_1)[J_0(\lambda\rho) + J_2(\lambda\rho)]\} e^{-\gamma_1(z-d)} \lambda d\lambda \quad (4)$$

It follows that (1) can be expressed in the following form:

$$E_{1\rho} = -\frac{\omega\mu_0}{4\pi k_1^2} \cos \phi [F_0(\rho, z-d) \\ - F'_0(\rho, z+d) - F_1(\rho, z+d)] \quad (5)$$

where $F_0(\rho, z-d)$ is defined in (4) and where $F'_0(\rho, z+d)$ and $F_1(\rho, z+d)$ are, respectively, the first and second integrals in (3). Note that

$$Q-1 = -2\bar{\epsilon}_2 \gamma_1/(\bar{\epsilon}_1 \gamma_2 - \bar{\epsilon}_2 \gamma_1) \quad (6)$$

$$P+1 = 2\gamma_2/(\gamma_2 - \gamma_1) \quad (7)$$

The integral $F_1(\rho, z+d)$ given in (3) can be expressed as the sum of two integrals. Thus, with

$$F_1(\rho, z+d) = F_2(\rho, z+d) - F_3(\rho, z+d) \quad (8)$$

$$F_2(\rho, z+d) = -\bar{\epsilon}_2 \int_0^\infty [\gamma_1^2/(\bar{\epsilon}_1 \gamma_2 - \bar{\epsilon}_2 \gamma_1)] \\ \cdot [J_0(\lambda\rho) - J_2(\lambda\rho)] e^{-\gamma_1(z+d)} \lambda d\lambda \quad (9)$$

$$F_3(\rho, z+d) = -k_1^2 \int_0^\infty \{(\gamma_2/\gamma_1)/(\gamma_2 - \gamma_1)\} \\ \cdot [J_0(\lambda\rho) + J_2(\lambda\rho)] e^{-\gamma_1(z+d)} \lambda d\lambda \quad (10)$$

The first problem is to evaluate F_0 , F'_0 , F_2 , and F_3 . This is carried out subject to two conditions. The first requirement is that the wave number k_1 of region 1 (in which the antenna is immersed and the field calculated) be much greater in magnitude than k_2 for region 2. Specifically,

$$k_1^2 \gg k_2^2 \quad (11)$$

The second requirement is an approximation needed to simplify the integrations in (3), the integral (4) is considered separately after (3) has been evaluated. The well-known exponential decay of a plane wave entering a dissipative medium combined with the reciprocal theorem, the available approximate formulas of Baños in their ranges of validity, extensive numerical computations from (1), and a series of mea-

surements all indicate that the dependence on the depth d of the source and the depth z of the point of observation of the part of E_{10} with the exponential $\exp[i\gamma_1(z+d)]$ should be well approximated (at least when $\rho^2 \gg z^2$ and $\rho^2 \gg d^2$) by setting $\gamma_1 \sim k_1$ in the exponential factor $\exp[i\gamma_1(z+d)]$ in (1). The consequences of this assumption must be verified by direct comparison of calculations from the approximate formula to be derived with the numerical evaluation of (1). With this substitution, the functions $F(\rho, z+d)$ can be expressed as follows:

$$\begin{aligned} F'_0(\rho, z+d) &\sim F'_0(\rho, 0)e^{ik_1(z+d)} \\ F_1(\rho, z+d) &\sim F_1(\rho, 0)e^{ik_1(z+d)} \end{aligned} \quad (12)$$

In (12) and with (4),

$$\begin{aligned} F_0(\rho, 0) = F'_0(\rho, 0) &= \int_0^\infty \{(\gamma_1/2)[J_0(\lambda\rho) - J_2(\lambda\rho)] \\ &\quad - (k_1^2/2\gamma_1)[J_0(\lambda\rho) + J_2(\lambda\rho)]\} \lambda d\lambda \end{aligned} \quad (13)$$

and, with $F_1(\rho, 0) = F_2(\rho, 0) + F_3(\rho, 0)$

$$\begin{aligned} F_2(\rho, 0) = -\bar{\epsilon}_2 \int_0^\infty [\gamma_1^2/(\bar{\epsilon}_1\gamma_2 - \bar{\epsilon}_2\gamma_1)] \\ \cdot [J_0(\lambda\rho) - J_2(\lambda\rho)] \lambda d\lambda \end{aligned} \quad (14)$$

$$\begin{aligned} F_3(\rho, 0) = -k_1^2 \int_0^\infty [(\gamma_2'\gamma_1)/(\gamma_2 + \gamma_1)] \\ \cdot [J_0(\lambda\rho) + J_2(\lambda\rho)] \lambda d\lambda \end{aligned} \quad (15)$$

The function $F'_0(\rho, 0)$ as given by (13) can be expressed in terms of two integrals that can be integrated. Specifically,

$$F'_0(\rho, 0) = (1/2)[I_1(k_1) + k_1^2 I_4(k_1)] \quad (16)$$

where,

$$\begin{aligned} I_1(k) &= \int_0^\infty (k^2 - \lambda^2)^{-1/2} [J_0(\lambda\rho) - J_2(\lambda\rho)] \lambda d\lambda \\ &= -2I_2(k) + k^2 I_4(k) \end{aligned} \quad (17)$$

$$\begin{aligned} I_2(k) &= \int_0^\infty (k^2 - \lambda^2)^{-1/2} [J_0(\lambda\rho) + J_2(\lambda\rho)] \lambda d\lambda \\ &= \frac{2k}{\rho^2} + \frac{2i}{\rho} e^{ik\rho} \end{aligned} \quad (18)$$

$$I_4(k) = \int_0^\infty (k^2 - \lambda^2)^{-1/2} [J_0(\lambda\rho) + J_2(\lambda\rho)] \lambda d\lambda$$

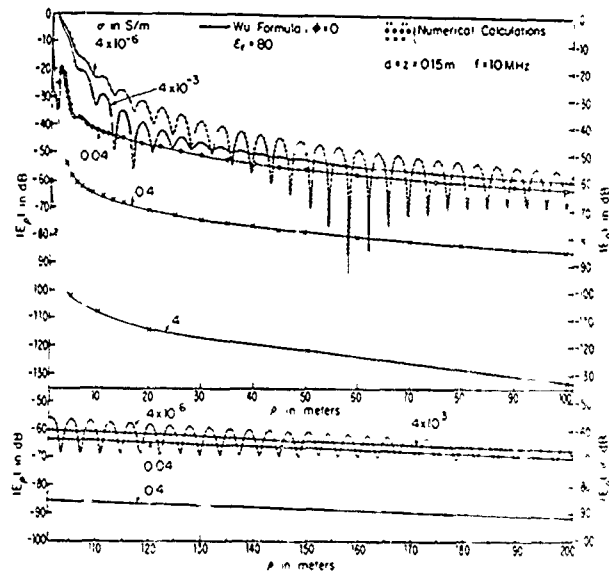


Fig. 2: $|E_p|$ at depth z of horizontal electric dipole at depth d in water below air

$$= \frac{2}{k\rho^2} (1 - e^{ik\rho}) \quad (19)$$

The indicated evaluation of these integrals is outlined in appendix A. With these values, (16) gives

$$\begin{aligned} F_0(\rho, 0) = F'_0(\rho, 0) &= -I_2(k_1) + k_1^2 I_4(k_1) \\ &= -2e^{ik_1\rho} \left[\frac{k_1}{\rho^2} + \frac{i}{\rho^3} \right] \end{aligned} \quad (20)$$

The function $F_2(\rho, 0)$ defined in (14) can be rearranged as follows. Note that with $\mu_1 = \mu_2 = \mu_0$, $\bar{\epsilon}_2/\bar{\epsilon}_1 = k_2^2/k_1^2$.

$$F_2(\rho, 0) = -(k_2^2/k_1^2)[I_1(k_2) - (k_1^2 - k_2^2)I_3(k_2)] + G(\rho) \quad (21)$$

where

$$\begin{aligned} G(\rho) &= -\bar{\epsilon}_2 \int_0^\infty \gamma_1^2 \left[\frac{1}{\bar{\epsilon}_1\gamma_2 + \bar{\epsilon}_2\gamma_1} - \frac{1}{\bar{\epsilon}_1\gamma_2} \right] \\ &\quad \cdot [J_0(\lambda\rho) - J_2(\lambda\rho)] \lambda d\lambda \end{aligned} \quad (22)$$

$$\begin{aligned} I_3(k) &= \int_0^\infty (k^2 - \lambda^2)^{-1/2} [J_0(\lambda\rho) - J_2(\lambda\rho)] \lambda d\lambda \\ &= -\frac{2i}{\rho} e^{ik\rho} - I_4(k) \end{aligned} \quad (23)$$

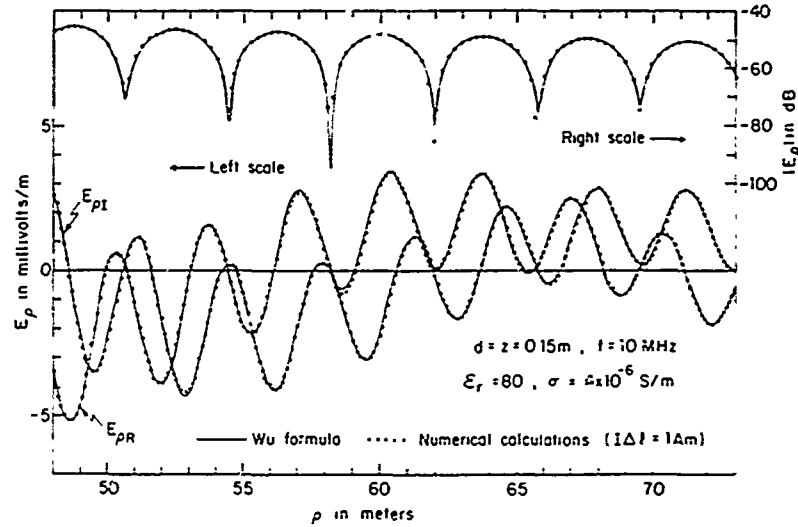


Fig 2b. Real and imaginary parts and magnitude of E_p in critical range, Wu's formula (35) and numerical calculations from exact integrals (1)

The function $I_3(k)$ is evaluated in appendix A, the function $G(\rho)$ in appendix B. With (17) and (23) and from (11), $k_1^2 - k_2^2 \sim k_1^2$, (21) becomes

$$\begin{aligned} F_2(\rho, 0) &\sim -(k_2^2/k_1^2)[-2I_2(k_2) - k_2^2 I_4(k_2) + k_1^2 I_3(k_2)] - G(\rho) \\ &\sim -(k_2^2/k_1^2)[-2I_2(k_2) - k_1^2 I_4(k_2) - (2ik_1^2/\rho)e^{ik_1\rho}] - G(\rho) \end{aligned} \quad (24)$$

The function $F_3(\rho, 0)$ defined in (15) can be expressed as follows:

$$\begin{aligned} F_3(\rho, 0) &= -k_1^2 \left[I_4(k_1) - \frac{1}{k_1^2 - k_2^2} I_2(k_1) + \frac{1}{k_1^2 - k_2^2} I_2(k_2) \right] \\ &\sim -k_1^2 I_4(k_1) + I_2(k_1) - I_2(k_2) \end{aligned} \quad (25)$$

When (25) is combined with (24), it follows that

$$\begin{aligned} F_1(\rho, 0) &= F_2(\rho, 0) + F_3(\rho, 0) \sim 2(k_2^2/k_1^2)I_2(k_2) \\ &\quad + (2k_2^2/\rho)e^{ik_2\rho} + k_2^2 I_4(k_2) - k_1^2 I_4(k_1) \\ &\quad + I_2(k_1) - I_2(k_2) + G(\rho) \end{aligned} \quad (26)$$

With (18) and (19), this becomes:

$$F_1(\rho, 0) = 2e^{ik_2\rho} \left[\frac{ik_2^2}{\rho} - \frac{k_2}{\rho^2} - \frac{i}{\rho^3} \right] + 2e^{ik_1\rho} \left[\frac{k_1}{\rho^2} + \frac{i}{\rho^3} \right] + G(\rho) \quad (27)$$

When (20) and (27) are combined in (5) with (12),

the resulting formula is:

$$\begin{aligned} E_{1\rho} &= -\frac{\omega\mu_0}{2\pi k_1^2} \cos \phi \left\{ e^{ik_2 z - d_1} \left(e^{ik_2\rho} \left[\frac{ik_2^2}{\rho} - \frac{k_2}{\rho^2} - \frac{i}{\rho^3} \right] - \frac{G(\rho)}{2} \right) \right. \\ &\quad \left. + (1/2)F_0(\rho, z - d) \right\} \end{aligned} \quad (28)$$

With (B16) of appendix B, the complete formula is

$$\begin{aligned} E_{1\rho} &= -\frac{\omega\mu_0}{2\pi k_1^2} \cos \phi \left\{ e^{ik_2 z - d_1} e^{ik_2\rho} \right. \\ &\quad \cdot \left[\frac{ik_2^2}{\rho} - \frac{k_2}{\rho^2} - \frac{i}{\rho^3} - \frac{k_2^4}{k_1} \left(\frac{\pi}{k_2\rho} \right)^{1/2} \right. \\ &\quad \left. \left. \times e^{-ik_2\rho k_1^2/2k_1^2} \mathcal{F} \right] - (1/2)F_0(\rho, z - d) \right\} \end{aligned} \quad (29)$$

where

$$\mathcal{F} = \frac{1}{2} - C[k_2\rho(k_2^2/2k_1^2)] - i \left\{ \frac{1}{2} - S[k_2\rho(k_2^2/2k_1^2)] \right\} \quad (30)$$

and C and S are the Fresnel integrals as defined in the Jahnke-Emde Tables of Functions.

The integral $F_0(\rho, z - d)$ as given by (4) is simply the field of a horizontal dipole at $(0, 0, d)$ in an infinite homogeneous region characterized by ϵ_1 and k_1 . In this case, $Q = P = 0$ in (1) and the entire field is given by the first integral, which is necessarily equivalent to the well-known formula for the field of an

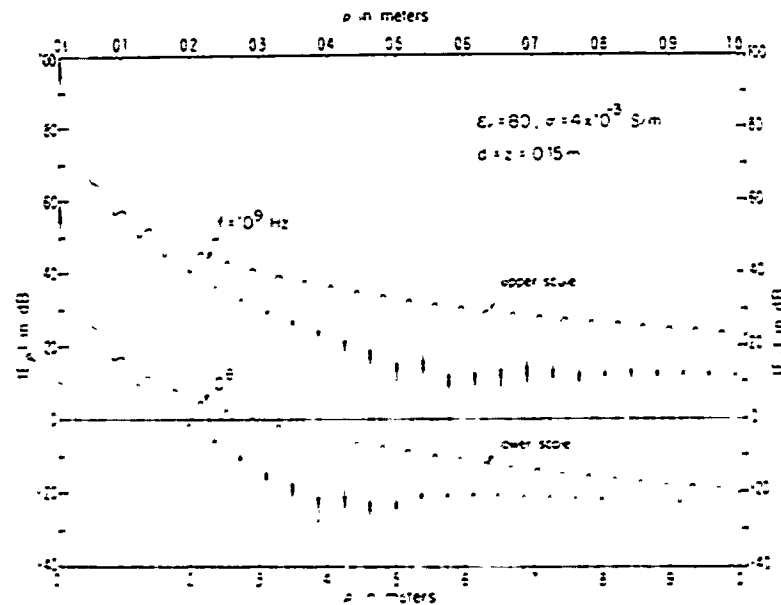


Fig. 3a. E_p of dipole in lake water parallel to its interface with air

infinitesimal dipole. For an x directed dipole with moment $I\Delta l = 1$ at $(0, 0, d)$ on the z axis, the radial component of the electric field is given by

$$(E_p)_r = \frac{\omega\mu_0}{4\pi k^2} \cos\phi e^{-kz} \left\{ \frac{ik^2}{r_1} - \frac{k}{r_1^2} - \frac{1}{r_1^3} \right\}$$

$$- \left[\frac{ik^2}{r} - \frac{3k}{r^2} - \frac{3}{r^3} \right] \sin^2\Theta_1 \quad (31)$$

where Θ_1 is the angle subtended by the radial line $r_1 = [p^2 + (z - d)^2]^{1/2}$ and the positive z axis (Figure 1). With

$$p^2 \gg z^2 \quad p^2 \gg d^2 \quad (32)$$

$r_1 \sim p$, $\Theta_1 \sim \pi/2$ in amplitude factors, so that

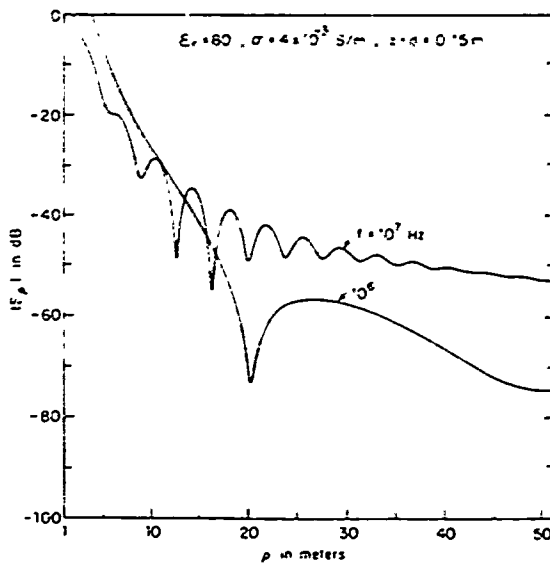


Fig. 3b. E_p of dipole in lake water parallel to its interface with air

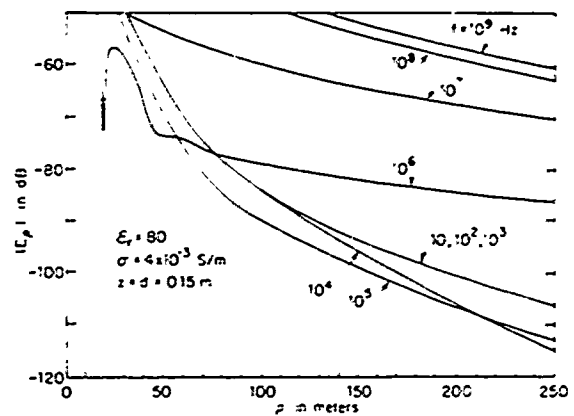


Fig. 3c. E_p of dipole in lake water parallel to its interface with air

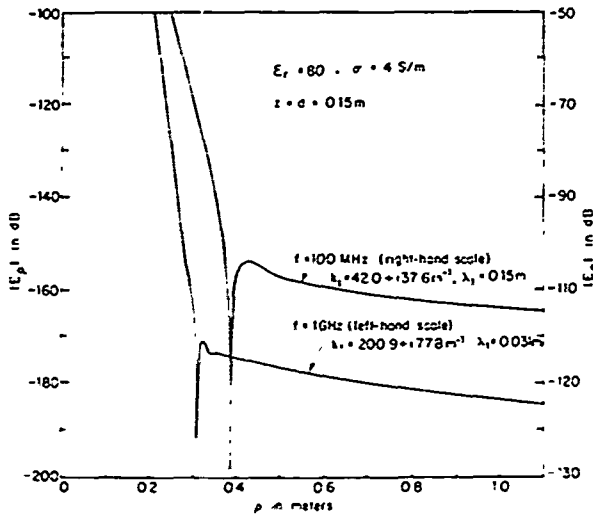


Fig 4 E_p of dipole in sea water parallel to its interface with air

$$\begin{aligned} |E_{p,r}| &\sim \frac{\omega \mu_0}{2\pi k_1^2} \cos \phi e^{ik_1 z} \left[\frac{k_1}{p^2} - \frac{1}{p} \right] \\ &= -\frac{\omega \mu_0}{4\pi k_1^2} \cos \phi F_0(p, z-d) \end{aligned} \quad (32)$$

It follows that

$$F_0(p, z-d) \sim -2e^{ik_1 z} \left[\frac{k_1}{p^2} - \frac{1}{p} \right] \quad (34)$$

(Note that $F_0(p, 0)$ in (20) agrees exactly with $F_0(p, 0)$ as obtained from (34) when $z = d$.) With (34), the expression (29) becomes:

$$\begin{aligned} E_{ip} &= -\frac{\omega \mu_0}{2\pi k_1^2} \cos \phi \left\{ e^{ik_1 z-d} e^{ik_2 p} \right. \\ &\quad \cdot \left[\frac{ik_1^2}{p} - \frac{k_1}{p^2} - \frac{1}{p^3} - \frac{k_2^2}{k_1} \left(\frac{\pi}{k_2 p} \right)^{1/2} \right. \\ &\quad \times \left. \left. e^{-k_2 \sqrt{p^2 + (z-d)^2}} \right] - e^{ik_1 p^2 + (z-d)^2} \left[\frac{k_1}{p^2} - \frac{1}{p} \right] \right\} \end{aligned} \quad (35)$$

\mathcal{F} is given by (30). This is the final approximate formula for E_{ip} . Note its simplicity as compared with the exact formula (1). It is completely general except for the conditions (11) and (32), i.e., $|k_1^2| \gg |k_2^2|$, $p^2 \gg z^2$, $p^2 \gg d^2$. It agrees exceedingly well with the numerical evaluation of the exact integrals when $|k_1^2| \gg |k_2^2|$ and quite well even when $|k_1^2/k_2^2|$ is as small as 4. This is shown on selected graphs in the extensive set computed from (35).

3. THE RADIAL ELECTRIC FIELD INTERFERENCE PATTERNS

The general expression (35) for the radial component of the electric field at a depth z in a half-space of earth or water and at a radial distance p from a unit horizontal electric dipole at a depth d consists of two principal parts. These are characterized respectively by the functions $f_L(p, z, d) = f_L(p) \exp [ik_2 p + ik_1(z-d)]$ and $f_D(p, z, d) = f_D(p) \exp \{ik_1[p^2 - (z-d)^2]^{1/2}\}$, where $f_L(p)$ and $f_D(p)$ are the quantities in square brackets in (35). Clearly, $f_L(p, z, d)$ is a lateral wave that travels upward from the dipole to the surface a distance d in region 1 (earth or water), then continues radially outward along the surface in region 2 (air), and finally proceeds downward in region 1 a distance z to the point of observation at (p, z) . On the other hand, $f_D(p, z, d)$ is a direct wave that travels from the source to the point of observation entirely in region 1. The amplitudes of these waves decrease with radial distance according to quite different functions. When $z = d$, these are $f_L(p) \exp (ik_2 p)$ and $f_D(p) \exp (ik_1 p)$. Since the wavelength in air is $\lambda_2 = 2\pi/\beta_2$ and that in the earth or water is $\lambda_1 = 2\pi/\beta_1$ ($k_2 = \beta_2 + i\alpha_2 \sim \beta_2$; $k_1 = \beta_1 + i\alpha_1$) with $\beta_1 \gg \beta_2$, it follows that $\lambda_2 \gg \lambda_1$. The superposition of the two waves produces a standing wave pattern with a complicated structure dominated by the wavelength λ .

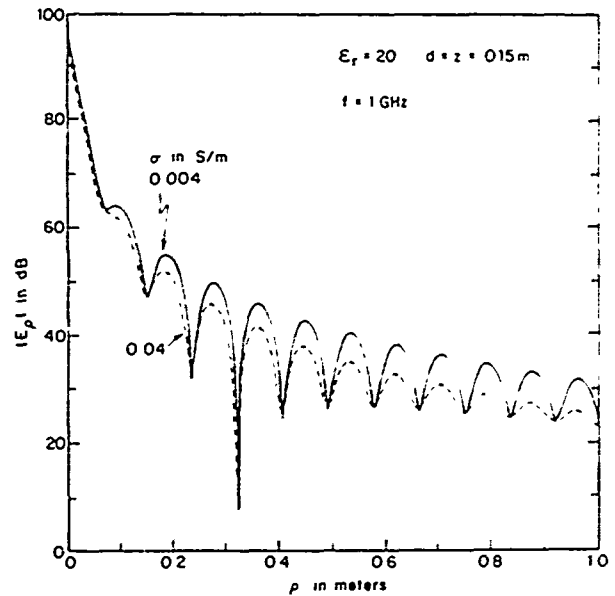


Fig 5 $|E_p|$ at depth z due to horizontal dipole ($I\Delta l = 1$) at depth d in region 1 below air; $f = 1$ GHz. Wu's formula

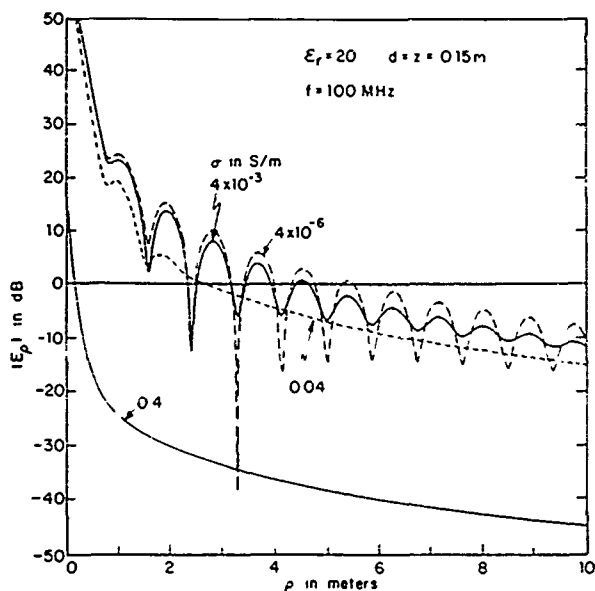


Fig 6 E_p at depth z due to horizontal dipole ($I\Delta l = 1$) at depth d in region 1 below air, $f = 100$ MHz, Wu's formula

In Figure 2a is shown E_{1p} in water as a function of the radial distance ρ when $z = d = 0.15$ m and $f = 10$ MHz. Graphs are provided for $\epsilon_r = 80$ and five values of σ_1 ranging from 4×10^{-6} S/m to 4 S/m. The top and bottom graphs in Figure 2a for distilled water with $\sigma_1 = 4 \times 10^{-6}$ S/m are primarily of theoretical interest. α_1 is so small that the direct wave is attenuated only slowly. As a consequence, the

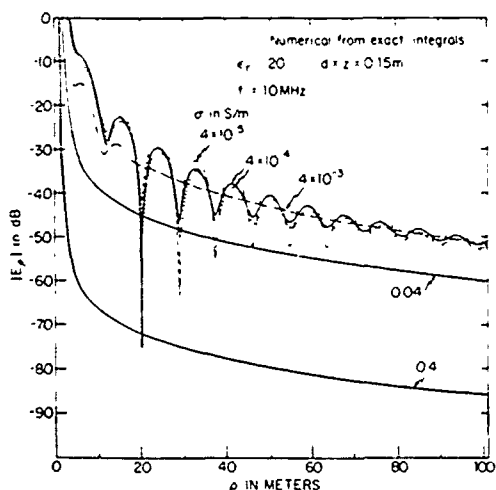


Fig 7 $|E_p|$ at depth z due to horizontal dipole ($I\Delta l = 1$) at depth d in region 1 below air, $f = 10$ MHz, Wu's formula

standing wave persists for a large radial distance. The curves in solid line are calculated from (35), the dotted curve is evaluated numerically from the general formula (1), both with $\phi = 0^\circ$. The central section of the graph for $|E_{1p}|$ and the associated real and imaginary parts, $E_p = E_{pR} + iE_{pI} = |E_p| \exp i\theta_p$, are shown in Figure 2b on a larger scale. The agreement with the numerical calculations from (1) is seen to be excellent.

The graph in Figure 2a for $\sigma_1 = 4 \times 10^{-3}$ S/m characterizes $|E_{1p}|$ in lake water. Owing to the much greater value of the attenuation constant α_1 in $k_1 = \beta_1 + i\alpha_1$, the amplitude of the direct wave decreases quite rapidly so that the standing-wave pattern that characterizes the interference between it and the lateral wave diminishes to a negligible amplitude in about 50 m. In less-pure lake water with $\sigma_1 = 0.04$ S/m, the standing wave persists only out to about $\rho = 8$ m. With $\sigma_1 = 0.4$ S/m and in sea water with $\sigma_1 = 4$ S/m, the direct wave has a negligible amplitude even at $\rho = 1$ m. Note that the graphs calculated from the approximate formula (35) are all in excellent agreement with the corresponding numerical values calculated from (1).

The standing-wave patterns at $f = 1$ GHz and 100 MHz in lake water with $\sigma_1 = 4 \times 10^{-3}$ S/m are shown in Figure 3a. Since the wavelength in the water is much shorter than with $f = 10$ MHz, the deepest minima occur near $\rho = 0.57$ m with $f = 1$ GHz and $\rho = 4$ m with $f = 100$ MHz instead of near $\rho \sim 58$ m with $f = 10$ MHz. However, since α_1 is substantially smaller at the higher frequencies, the standing-wave amplitude decreases only slowly with radial distance. Graphs of $|E_{1p}|$ for lake water over a wide range of frequencies are shown in Figures 3b and 3c to different scales. A significant standing wave

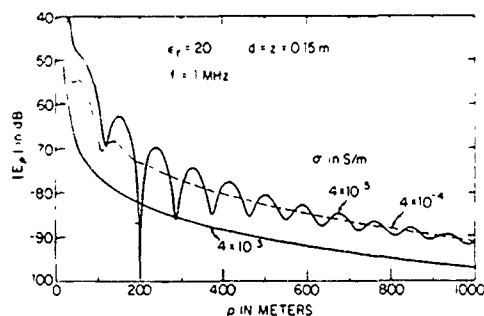


Fig 8 $|E_p|$ at depth z due to horizontal dipole ($I\Delta l = 1$) at depth d in region 1 below air, $f = 1$ MHz, Wu's formula

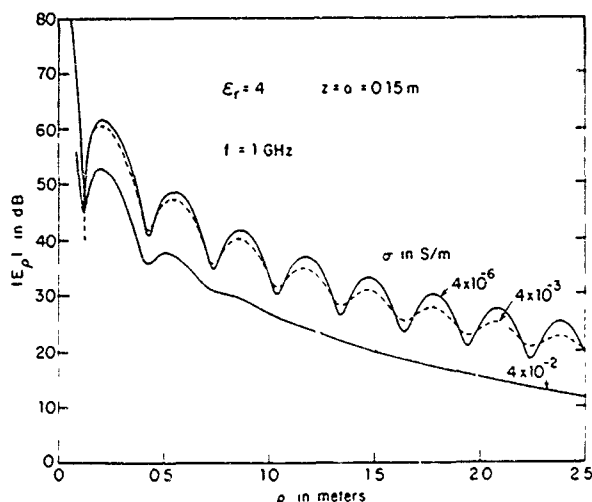


Fig 9 $|E_\rho|$ at depth z due to horizontal dipole ($I\Delta l = 1$) at depth d in region 1 below air, $f = 1$ GHz, Wu's formula

occurs when $f = 1$ MHz. Graphs of $|E_\rho|$ in sea water ($\sigma_1 = 4$ S/m) at the high frequencies $f = 100$ MHz and $f = 1$ GHz are shown in Figure 4 at very close range. It is seen that standing waves exist out 30–40 cm from the source.

Graphs like those in Figures 3 and 4 for water with $\epsilon_{1r} = 80$ are shown in Figures 5 through 8, respectively, at $f = 1$ GHz, 100 MHz, 10 MHz, and 1 MHz for a material medium with $\epsilon_{1r} = 20$ and a range of values of σ_1 . The interference patterns generated by the superposition of the direct and lateral waves are similar to those in water with the standing wave dominated by the wavelength characteristic of the material

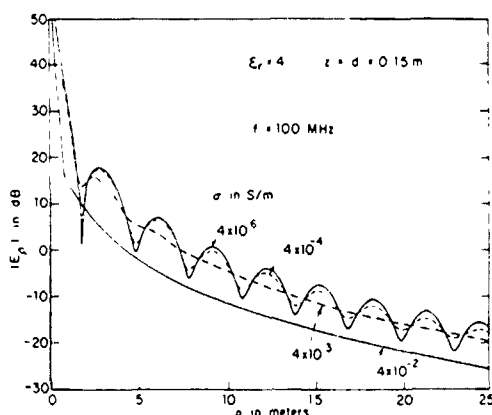


Fig 10 $|E_\rho|$ at depth z due to horizontal dipole ($I\Delta l = 1$) at depth d in region 1 below air, $f = 100$ MHz, Wu's formula

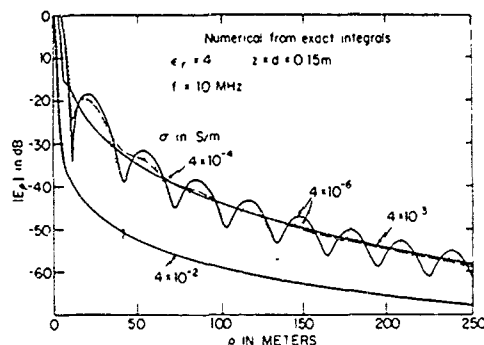


Fig 11 $|E_\rho|$ at depth z due to horizontal dipole ($I\Delta l = 1$) at depth d in region 1 below air, $f = 10$ MHz, Wu's formula

medium at each frequency. A comparison of the calculations from (35) with those from the exact integrals (1) is shown in Figure 7. The agreement is very good.

Graphs for dry earth with $\epsilon_{1r} = 4$ and several values of σ_1 are in Figures 9 through 11, respectively, at $f = 1$ GHz, 100 MHz, and 10 MHz. Typical standing-wave patterns are obtained. As seen from Figure 11, the agreement between $|E_\rho|$ as calculated from the newly derived approximate formula (35) and by numerical integration from the exact integrals (1) is not as good with $\epsilon_{1r} = 4$ as with $\epsilon_{1r} = 80$ or 20. This is to be expected since the condition (11) is not well satisfied. However, whereas the amplitude of the standing-wave pattern is not quite accurate, the agreement in the actual location of the standing waves is excellent.

4 CONCLUSION

A new simple and accurate formula has been derived for the radial electric field of a horizontal electric dipole in a dissipative or dielectric half-space near its boundary with air. The interference patterns generated by the direct and lateral waves that originate at the dipole are examined in detail for three values of ϵ_{1r} , numerous values of σ_1 , and a wide range of frequencies. The accuracy of the new formula is confirmed by comparison with numerically evaluated results. In terms of computer time the new formula (35) can be evaluated in fractions of a minute as compared with hours for the complete numerical integration of (1). When similar expressions are made available for the other five components of the electromagnetic field, it will be possible to study the more compli-

cated properties of lateral waves including especially reflection at and transmission across boundaries.

APPENDIX A THE INTEGRALS $I(k)$

Let the four integrals $I_1(k) \dots I_4(k)$ defined in (17)–(19) and (23) be considered in turn. Clearly,

$$I_1(k) = 2 \int_0^x (k^2 - \lambda^2)^{1/2} J_0(\lambda \rho) \lambda d\lambda - I_2(k) \quad (\text{A1})$$

With the substitution $(d/d\lambda)[\lambda J_1(\lambda \rho)] = \lambda \rho J_0(\lambda \rho)$ and integration by parts,

$$\begin{aligned} 2 \int_0^x (k^2 - \lambda^2)^{1/2} J_0(\lambda \rho) \lambda d\lambda &= (2/\rho) \int_0^x \lambda^2 (k^2 - \lambda^2)^{-1/2} \\ &\cdot J_1(\lambda \rho) d\lambda = (-2/\rho) \int_0^x [(k^2 - \lambda^2)^{1/2} \\ &- k^2 (k^2 - \lambda^2)^{-1/2}] J_1(\lambda \rho) d\lambda \end{aligned} \quad (\text{A2})$$

With

$$2J_1(\lambda \rho)/\lambda \rho = J_0(\lambda \rho) - J_2(\lambda \rho) \quad (\text{A3})$$

it follows directly from the definitions (17) and (18) that

$$2 \int_0^x (k^2 - \lambda^2)^{1/2} J_0(\lambda \rho) \lambda d\lambda = -I_2(k) + k^2 I_4(k) \quad (\text{A4})$$

Hence,

$$I_1(k) = -2I_2(k) - k^2 I_4(k) \quad (\text{A5})$$

With (A3) and $J_1(\lambda \rho) = -(1/\rho)(\partial/\partial \lambda)J_0(\lambda \rho)$, $I_2(k)$ as defined in (18) becomes

$$I_2(k) = -\frac{2}{\rho^2} \int_0^x (k^2 - \lambda^2)^{1/2} \frac{\partial}{\partial \lambda} J_0(\lambda \rho) d\lambda \quad (\text{A6})$$

Integration by parts gives

$$I_2(k) = \frac{2k}{\rho^2} - \frac{2}{\rho^2} \int_0^x (k^2 - \lambda^2)^{1/2} J_0(\lambda \rho) \lambda d\lambda \quad (\text{A7})$$

With Bateman, Higher Transcendental Functions II, p. 95 (52), the integral in (A7) integrates into $-(i/\rho)e^{ik\rho}$ so that

$$I_2(k) = \frac{2k}{\rho^2} + \frac{2i}{\rho^3} e^{ik\rho} \quad (\text{A8})$$

It follows directly from (18) that

$$I_3(k) = 2 \int_0^x (k^2 - \lambda^2)^{-1/2} J_0(\lambda \rho) \lambda d\lambda - I_4(k) \quad (\text{A9})$$

Here the integral is the same as that in (A7) so that

$$I_3(k) = -\frac{2i}{\rho} e^{ik\rho} - I_4(k) \quad (\text{A10})$$

With (A3) used in (19) and the temporary substitution $k = i\beta$,

$$\begin{aligned} I_4(k) &= -\frac{2i}{\rho} \int_0^x (\lambda^2 + \beta^2)^{-1/2} J_1(\lambda \rho) d\lambda \\ &= -\frac{2i}{\rho} [I_{1/2}(\beta \rho/2) K_{1/2}(\beta \rho/2)] \end{aligned} \quad (\text{A11})$$

where $I_{1/2}$ and $K_{1/2}$ are the modified Bessel functions of order $1/2$. However, $I_{1/2}(z) = (2/\pi z)^{1/2} \sinh z$, $K_{1/2}(z) = (\pi/2z)^{1/2} e^{-z}$ so that $I_{1/2}(z)K_{1/2}(z) = (1/2z)(1 - e^{-2z})$. It follows that (A11) becomes

$$I_4(k) = -\frac{2i}{\rho} \cdot \frac{1}{\beta \rho} (1 - e^{-\beta \rho}) = \frac{2}{k \rho^2} (1 - e^{ik\rho}) \quad (\text{A12})$$

With (A5), (A8), (A10), and (A12), the formulas in (17)–(19) and (23) are obtained.

APPENDIX B THE FUNCTION $G(\rho)$

The function $G(\rho)$ is defined by

$$\begin{aligned} G(\rho) &= -\bar{\epsilon}_2 \int_0^x (k_1^2 - \lambda^2) \left[\frac{1}{\bar{\epsilon}_1 (k_2^2 - \lambda^2)^{1/2} + \bar{\epsilon}_2 (k_1^2 - \lambda^2)^{1/2}} \right. \\ &\quad \left. - \frac{1}{\bar{\epsilon}_1 (k_2^2 - \lambda^2)^{1/2}} \right] [J_0(\lambda \rho) - J_2(\lambda \rho)] \lambda d\lambda \end{aligned} \quad (\text{B1})$$

It is clear that the integrand is very large only when λ is near k_2 so that in the range of significance, $k_1^2 \gg \lambda^2$. For all but small arguments,

$$J_p(\lambda \rho) \approx \frac{1}{2} H_p^{(1)}(\lambda \rho) \approx \frac{1}{(2\pi\lambda\rho)^{1/2}} e^{i(\lambda\rho - \pi/4 - 1/2)} \quad (\text{B2})$$

so that

$$\begin{aligned} J_0(\lambda \rho) - J_2(\lambda \rho) &\sim \frac{1}{(2\pi\lambda\rho)^{1/2}} e^{i\lambda\rho} [e^{-i\pi/4} - e^{-i\pi/4 - 1/2}] \\ &= \left(\frac{2}{\pi\lambda\rho} \right)^{1/2} e^{i(\lambda\rho - \pi/4)} \end{aligned} \quad (\text{B3})$$

The integral is

$$\begin{aligned} G(\rho) &\sim -\bar{\epsilon}_2 k_1^2 \int_0^x \left[\frac{1}{\bar{\epsilon}_1 (k_2^2 - \lambda^2)^{1/2} + \bar{\epsilon}_2 k_1} - \frac{1}{\bar{\epsilon}_1 (k_2^2 - \lambda^2)^{1/2}} \right] \\ &\cdot \left(\frac{2}{\pi\lambda\rho} \right)^{1/2} e^{i(\lambda\rho - \pi/4)} \lambda d\lambda \end{aligned} \quad (\text{B4})$$

530 WU AND KING

Now let the variable of integration be changed with

$$\lambda = k_2(1 + m\tau) \quad d\lambda = k_2 m d\tau \quad (\text{B5})$$

where the parameter

$$m = k_2^2/2k_1^2 \quad (\text{B6})$$

is very small since $|k_2^2| \ll |k_1^2|$ and τ is the dimensionless variable of integration. It follows that

$$\lambda^2 = k_2^2(1 + 2m\tau + m^2\tau^2) \sim k_2^2(1 + 2m\tau)$$

or

$$\lambda \sim k_2(1 + 2m\tau)^{1/2} = k_2(1 + m\tau) \quad (\text{B7})$$

and

$$(k_2^2 - \lambda^2)^{1/2} = (-2m\tau)^{1/2} k_2 \quad (\text{B8})$$

It follows that with

$$\alpha = mk_2\rho = k_2^2\rho/2k_1^2 \quad (\text{B9})$$

(B4) becomes

$$G(\rho) = -\tilde{\epsilon}_2 k_1^2 \int_{-\infty}^{\infty} \left[\frac{1}{\tilde{\epsilon}_1 k_2(-2m\tau)^{1/2} - \tilde{\epsilon}_2 k_1} - \frac{1}{\tilde{\epsilon}_1 k_2(-2m\tau)^{1/2}} \right] \cdot \left(\frac{2}{\pi k_2 \rho} \right)^{1/2} e^{i(k_2\rho - \tau/4)} e^{i\alpha\tau} m k_2^2 d\tau \quad (\text{B10})$$

Since $m = k_2^2/2k_1^2 \ll 1$, it is adequate to write $\lambda \sim k_2$ in amplitudes but not in the exponents. Also, since $\lambda = 0$ corresponds to $\tau = -1/m$, a very large negative quantity, the lower limit can be made $-\infty$. Thus, with $\tilde{\epsilon}_1 k_2(2m)^{1/2}/\tilde{\epsilon}_2 k_1 = 1$, (B10) can be written:

$$G(\rho) \sim -k_1 k_2^2 m \left(\frac{2}{\pi k_2 \rho} \right)^{1/2} e^{i(k_2\rho - \tau/4)} H(\alpha) \quad (\text{B11})$$

where

$$H(\alpha) = \int_{-\infty}^{\infty} \left[\frac{1}{\sqrt{-\tau} - 1} - \frac{1}{\sqrt{-\tau}} \right] e^{i\alpha\tau} d\tau \quad (\text{B12})$$

With considerable manipulation this integral can be reduced to

$$H(\alpha) = 2\sqrt{\pi} e^{i\pi/4} e^{-i\alpha} \int_0^{\infty} \frac{e^{-t}}{\sqrt{t}} dt \quad (\text{B13})$$

In the notation of Jahnke-Emde, Tables of Functions, p. 36, Dover Publ., 1945, the Fresnel integrals are defined as follows:

$$C(z) + iS(z) = \int_0^z \frac{e^{it}}{\sqrt{2\pi t}} dt \quad (\text{B14})$$

It follows that, since $C(\infty) = S(\infty) = 1/2$, (B13) has the following form:

$$H(\alpha) = 2\pi\sqrt{2} e^{i\pi/4} e^{-i\alpha} \left\{ \left[\frac{1}{2} - C(\alpha) \right] - i \left[\frac{1}{2} - S(\alpha) \right] \right\} \quad (\text{B15})$$

Accordingly, (B11) can be expressed in terms of the Fresnel integrals. Thus,

$$G(\rho) = -2(k_2^2/k_1) \left(\frac{\pi}{k_2\rho} \right)^{1/2} e^{i(k_2\rho - \tau/4)} \cdot \left\{ \left[\frac{1}{2} - C(\alpha) \right] - i \left[\frac{1}{2} - S(\alpha) \right] \right\} \quad (\text{B16})$$

where $\alpha = k_2\rho(k_2^2/2k_1^2)$.

Acknowledgments Computations from the approximate and the exact formulas were carried out by B. H. Sandler. This research was supported in part by the Office of Naval Research under contract N00014-79-C-0419 and in part by the Joint Services Electronics program under contract N00014-75-C-0648, both with Harvard University.

REFERENCES

- Bannister, P. R., and R. L. Dube (1978). Simple expressions for horizontal electric dipole quasi-static range subsurface-to-subsurface and subsurface-to-air propagation. *Radio Sci.* 13, 501-507.
- Baños, Jr., A. (1966). *Dipole Radiation in the Presence of a Conducting Half-Space*. Pergamon, New York.
- Bubenik, D. M. (1977). A practical method for the numerical evaluation of Sommerfeld integrals. *IEEE Trans. Antennas Propagat.* AP-25, 904-906.
- King, R. W. P., and J. T. deBettencourt (1979). Lateral-wave propagation of electromagnetic waves in the lithosphere. *IEEE Trans. Geosci. Electron.* GE-17, 86-92.
- King, R. W. P., and B. H. Sandler (1977). Subsurface communication between dipoles in general media. *IEEE Trans. Antennas Propagat.* AP-25, 770-775.
- King, R. W. P., and G. S. Smith (1981). *Antennas in Matter*. MIT Press, Cambridge, Mass.
- King, R. W. P., B. H. Sandler, and L. C. Shen (1980). A comprehensive study of subsurface propagation from horizontal electric dipoles. *IEEE Trans. Geosci. Remote Sensing*, GE-18, 225-233.
- Lytie, R. J., E. K. Miller, and D. L. Lager (1976). A physical explanation of electromagnetic surface wave for muds. *Radio Sci.* 11, 235-243.
- Rahmat-Samii, Y., R. Mittra, and P. Parhami (1981). Evaluation of Sommerfeld integrals for lossy half-space problems. *Electromagnetics*, 1, 1-28.

- Siegel, M., and R. W. P. King (1970), Electromagnetic fields in a dissipative half-space: A numerical approach, *J. Appl. Phys.*, 41, 2415-2423.
- Siegel, M., and R. W. P. King (1971), Radiation from linear antennas in a dissipative half-space, *IEEE Trans. Antennas Propagat*, AP-19, 477-485.
- Siegel, M., and R. W. P. King (1973), Electromagnetic propagation between antennas submerged in the ocean, *IEEE Trans Antennas Propagat*, AP-21, 507-513.
- Sommerfeld, A. (1909), Über die Ausbreitung der Wellen in der drahtlosen Telegraphie, *Ann Physik*, 28, 665-736.
- Sommerfeld, A. (1926), Über die Ausbreitung der Wellen in der drahtlosen Telegraphie, *Ann. Physik*, 81, 1135-1153.

Lateral waves: new formulas for $E_{1\phi}$ and E_{1z}

T. T. Wu and R. W. P. King

Gordon McKay Laboratory, Harvard University, Cambridge, Massachusetts 02138

(Received August 12, 1981; revised October 19, 1981; accepted October 20, 1981)

New simple formulas are derived as an approximation for the exact general integrals for the transverse and vertical components of the electric field generated by a horizontal electric dipole in a half-space of water or earth near its boundary with air. These formulas supplement the earlier derivation of the more important radial component.

1 FORMULATION FOR $E_{1\phi}$

The transverse component of the electric field $E_{1\phi}$ at the point (ρ, ϕ, z) in region 1 due to an x directed horizontal electric dipole in the same region at the point $(0, 0, d)$ is [King and Smith, 1981, p. 617, equation (5.10)]

$$E_{1\phi} = \frac{\omega\mu_1}{4\pi k_1^2} \sin \phi \left(\int_0^\infty \{k_1^2 J_0(\lambda\rho) - (\lambda^2/2)[J_0(\lambda\rho) - J_2(\lambda\rho)]\} \cdot \gamma_1^{-1} e^{\gamma_1(z-d)} \lambda d\lambda - \int_0^\infty \{(\gamma_1 Q/2)[J_0(\lambda\rho) - J_2(\lambda\rho)] - (k_1^2 P/2\gamma_1)[J_0(\lambda\rho) - J_2(\lambda\rho)]\} e^{\gamma_1(z-d)} \lambda d\lambda \right) \quad (1)$$

where, with $\mu_1 = \mu_2 = \mu_0$,

$$P = \frac{\gamma_2 - \gamma_1}{\gamma_2 + \gamma_1} \quad Q = \frac{\tilde{\epsilon}_1 \gamma_2 - \tilde{\epsilon}_2 \gamma_1}{\tilde{\epsilon}_1 \gamma_2 + \tilde{\epsilon}_2 \gamma_1} \quad \gamma_i^2 = k_i^2 - \lambda^2 \quad i = 1, 2 \quad (2)$$

This expression is like that previously analyzed in Wu and King [this issue] for $E_{1\rho}$ with two differences. These are $-\sin \phi$ replaces $\cos \phi$ and the sign of $J_2(\lambda\rho)$ is reversed throughout. It follows that $E_{1\phi}$ can be expressed as follows, paralleling equation (5) in Wu and King [this issue]:

$$E_{1\phi} = \frac{\omega\mu_0}{4\pi k_1^2} \sin \phi \cdot [G_0(\rho, z-d) + G'_0(\rho, z+d) + G_1(\rho, z+d)] \quad (3)$$

where

$$G_0(\rho, z-d) = \int_0^\infty \{(\gamma_1/2)[J_0(\lambda\rho) + J_2(\lambda\rho)]$$

$$- (k_1^2/2\gamma_1)[J_0(\lambda\rho) - J_2(\lambda\rho)]\} e^{\gamma_1(z-d)} \lambda d\lambda \quad (4)$$

$$G'_0(\rho, z-d) = \int_0^\infty \{(\gamma_1/2)[J_0(\lambda\rho) - J_2(\lambda\rho)] - (k_1^2/2\gamma_1)[J_0(\lambda\rho) - J_2(\lambda\rho)]\} e^{\gamma_1(z-d)} \lambda d\lambda \quad (5)$$

$$G_1(\rho, z-d) = G_2(\rho, z-d) - G_3(\rho, z-d) \quad (6)$$

$$G_2(\rho, z-d) = -\tilde{\epsilon}_2 \int_0^\infty \left[\frac{\gamma_1^2}{\tilde{\epsilon}_1 \gamma_2 - \tilde{\epsilon}_2 \gamma_1} \right] \cdot [J_0(\lambda\rho) + J_2(\lambda\rho)] e^{\gamma_1(z-d)} \lambda d\lambda \quad (7)$$

$$G_3(\rho, z-d) = -k_1^2 \int_0^\infty \left[\frac{\gamma_2}{\gamma_1(\gamma_2 + \gamma_1)} \right] \cdot [J_0(\lambda\rho) - J_2(\lambda\rho)] e^{\gamma_1(z-d)} \lambda d\lambda \quad (8)$$

2 EVALUATION OF $G_1(\rho, z-d)$

The evaluation of $G_1(\rho, z-d)$ as defined in (6) with (7) and (8) will be carried out subject to the restriction

$$|k_1|^2 \gg |k_2|^2 \quad (9)$$

and with the approximation

$$G_1(\rho, z-d) \sim G_1(\rho, 0) e^{i k_1(z-d)} \quad (10)$$

which is discussed in Wu and King [this issue]. Since $G_1(\rho, 0) = G_2(\rho, 0) + G_3(\rho, 0)$, it remains to evaluate

$$G_2(\rho, 0) = -\tilde{\epsilon}_2 \int_0^\infty \left[\frac{\gamma_1^2}{\tilde{\epsilon}_1 \gamma_2 - \tilde{\epsilon}_2 \gamma_1} \right] [J_0(\lambda\rho) + J_2(\lambda\rho)] \lambda d\lambda \quad (11)$$

$$G_3(\rho, 0) = -k_1^2 \int_0^\infty \left[\frac{\gamma_2}{\gamma_1(\gamma_2 + \gamma_1)} \right] [J_0(\lambda\rho) - J_2(\lambda\rho)] \lambda d\lambda \quad (12)$$

The integrals can be expressed in terms of the previously evaluated four integrals, viz.,

$$I_1(k) = \int_0^\infty (k^2 - \lambda^2)^{1/2} [J_0(\lambda\rho) - J_2(\lambda\rho)] \lambda d\lambda$$

$$= -2I_2(k) - k^2 I_3(k) = -\frac{2k}{\rho^2} - e^{ik\rho} \left(\frac{2k}{\rho^2} - \frac{4i}{\rho^3} \right) \quad (13)$$

$$I_2(k) = \int_0^\infty (k^2 - \lambda^2)^{-1/2} [J_0(\lambda\rho) - J_2(\lambda\rho)] \lambda d\lambda = \frac{2k}{\rho^2} + \frac{2i}{\rho^3} e^{ik\rho} \quad (14)$$

$$I_3(k) = \int_0^\infty (k^2 - \lambda^2)^{-1} [J_0(\lambda\rho) - J_2(\lambda\rho)] \lambda d\lambda$$

$$= -\frac{2i}{\rho} e^{ik\rho} - I_4(k) = -\frac{2}{k\rho^2} - e^{ik\rho} \left(\frac{2}{k\rho^2} - \frac{2i}{\rho} \right) \quad (15)$$

$$I_4(k) = \int_0^\infty (k^2 - \lambda^2)^{-1} [J_0(\lambda\rho) - J_2(\lambda\rho)] \lambda d\lambda$$

$$= \frac{2}{k\rho^2} (1 - e^{ik\rho}) \quad (16)$$

The reversal of sign of $J_2(\lambda\rho)$ is equivalent to an interchange of $I_1(k)$ with $I_2(k)$ and of $I_3(k)$ with $I_4(k)$. It follows from (21) in *Wu and King* [this issue] that

$$G_2(\rho, 0) = -(k_2^2/k_1^2)[I_2(k_2) - (k_1^2 - k_2^2)I_3(k_2)] - H(\rho) \quad (17)$$

where

$$H(\rho) = -\bar{\epsilon}_2 \int_0^\infty \gamma_1^2 \left[\frac{1}{\bar{\epsilon}_1 \gamma_2 + i\gamma_1} - \frac{1}{\bar{\epsilon}_1 \gamma_2} \right] \cdot [J_0(\lambda\rho) + J_2(\lambda\rho)] \lambda d\lambda \quad (18)$$

With (24) in *Wu and King* [this issue], (17) becomes

$$G_2(\rho, 0) = -(k_2^2/k_1^2)[-2I_1(k_2) + k_2^2 I_3(k_2) + k_1^2 I_4(k_2)] + H(\rho) \quad (19)$$

Similarly, with (25) in *Wu and King* [this issue],

$$G_3(\rho, 0) = -k_1^2 I_3(k_1) + I_1(k_1) - I_1(k_2) \quad (20)$$

These can be added and terms of the order k_2^2/k_1^2 neglected. With (13)–(16), the result is:

$$G_1(\rho, 0) \sim 4e^{ik_1\rho} \left(\frac{ik_1^2}{2\rho} - \frac{k_1}{\rho^2} - \frac{i}{\rho^3} \right) + 4e^{ik_2\rho} \left(\frac{k_2}{\rho^2} + \frac{i}{\rho^3} \right) + H(\rho) \quad (21)$$

The function $H(\rho)$ is evaluated in appendix A. The result is

$$H(\rho) = \frac{2ik_2^4}{k_1} \frac{\pi^{1/2}}{(k_2\rho)^{3/2}} e^{ik_2\rho} e^{-ik_2\rho k_1^2/2k_1^2} \mathcal{F} \quad (22)$$

where

$$\mathcal{F} = \frac{1}{2} - C[k_2\rho(k_2^2/2k_1^2)] + i \left\{ \frac{1}{2} - S[k_2\rho(k_2^2/2k_1^2)] \right\} \quad (23)$$

In (23), C and S are the Fresnel integrals as defined in Jahnke-Emde, *Tables of Functions*.

3 EVALUATION OF $G_0(\rho, z-d)$ AND $G_1(\rho, z-d)$

In the evaluation of $F'_0(\rho, z+d)$ in *Wu and King* [this issue] the same approximation was made as in the evaluation of $F_1(\rho, z+d)$. That is, it was assumed that $F'_0(\rho, z+d) \sim F'_0(\rho, 0)e^{ik_1(z-d)}$. This was done because the terms involving $e^{ik_1(z-d)}$ as a factor in $F'_0(\rho, z+d)$ exactly cancelled those in $F_1(\rho, z+d)$ and therefore a parallel treatment of the integrals involving $e^{i\gamma_1(z-d)}$ was indicated. The corresponding terms in $G'_0(\rho, z+d)$ add to those in $G_1(\rho, z+d)$. In this case it would appear that somewhat greater accuracy could be achieved by using the exact expressions for both $G'_0(\rho, z+d)$ and $G_0(\rho, z-d)$. Specifically, since $G_0(\rho, z-d)$ is the direct contribution to $E_{1\phi}$ by the horizontal dipole as if in an infinite medium and $G'_0(\rho, z+d)$ is the contribution of its image, the relevant formulas can be written down directly.

For an x directed dipole with the moment $I\Delta l = 1$ A m at $(0, 0, d)$ on the z axis, the ϕ component of the electric field is given by

$$(E_{1\phi})_e = -\frac{\omega\mu_0}{4\pi k_1^2} e^{ik_1 r_1} \sin \phi \left[\frac{ik_1^2}{r_1} - \frac{k_1}{r_1^2} - \frac{i}{r_1^3} \right]$$

$$= \frac{\omega\mu_0}{4\pi k_1^2} \sin \phi G_0(\rho, z-d) \quad (24)$$

Similarly, the ϕ component of the electric field of an image dipole at $(0, 0, -d)$ is

$$(E_{1\phi})_i = -\frac{\omega\mu_0}{4\pi k_1^2} e^{ik_1 r_2} \sin \phi \left[\frac{ik_1^2}{r_2} - \frac{k_1}{r_2^2} - \frac{i}{r_2^3} \right]$$

$$= \frac{\omega\mu_0}{4\pi k_1^2} \sin \phi G'_0(\rho, z+d) \quad (25)$$

where

$$r_1 = [\rho^2 + (z-d)^2]^{1/2} \quad r_2 = [\rho^2 + (z+d)^2]^{1/2} \quad (26)$$

Clearly,

$$G_0(\rho, z-d) = -e^{ik_1 r_1} \left[\frac{ik_1^2}{r_1} - \frac{k_1}{r_1^2} - \frac{i}{r_1^3} \right] \quad (27)$$

$$G'_0(\rho, z-d) = -e^{ik_1 r_2} \left[\frac{ik_1^2}{r_2} - \frac{k_1}{r_2^2} - \frac{i}{r_2^3} \right] \quad (28)$$

Subject to the conditions $\rho^2 \gg z^2$, $\rho^2 \gg d^2$, it is a good approximation to set $r_1 \sim r_2 \sim \rho$ in amplitudes, but not in exponents. With this approximation,

$$G_0(\rho, z-d) - G'_0(\rho, z-d) \sim -[e^{ik_1 r_1} - e^{ik_1 r_2}] \cdot \left[\frac{ik_1^2}{\rho} - \frac{k_1}{\rho^2} - \frac{i}{\rho^3} \right] \quad (29)$$

4 THE COMPLETE FORMULA FOR $E_{1\phi}$

The final approximate formula for $E_{1\phi}$ is given by (3) with (29) and (10) with (21) and (22). It is

$$E_{1\phi} = \frac{\omega\mu_0}{\pi k_1^2} \sin \phi \cdot \left\{ e^{ik_1(z+d)} e^{ik_2 \rho} \left[\frac{k_2}{\rho^2} + \frac{i}{\rho^3} - \frac{ik_2^4}{2k_1(k_2\rho)^{3/2}} e^{-ik_2\rho} \frac{\pi^{1/2}}{2} \mathcal{F} \right] - e^{ik_1(z-d+\rho)} \left[\frac{ik_1^2}{2\rho} - \frac{k_1}{\rho^2} - \frac{i}{\rho^3} \right] - \frac{1}{4} [e^{ik_1 r_1} + e^{ik_1 r_2}] \left[\frac{ik_1^2}{\rho} - \frac{k_1}{\rho^2} - \frac{i}{\rho^3} \right] \right\} \quad (30)$$

where r_1 and r_2 are defined in (26) and \mathcal{F} is in (23).

The formula with $z = d = 0$ is of interest. This has the following much simpler form:

$$E_{1\phi} \sim \frac{\omega\mu_0}{\pi k_1^2} \sin \phi \left\{ e^{ik_2 \rho} \left[\frac{k_2}{\rho^2} + \frac{i}{\rho^3} - \frac{ik_2^4}{2k_1(k_2\rho)^{3/2}} e^{-ik_2\rho} \frac{\pi^{1/2}}{2} \mathcal{F} \right] - \frac{1}{2} e^{ik_1 \rho} \left[\frac{k_1}{\rho^2} + \frac{i}{\rho^3} \right] \right\} \quad (31)$$

The $1/\rho$ terms are seen to cancel. This suggests that the corresponding terms in (30), viz., $(ik_1^2/2\rho) [e^{ik_1(z+d+\rho)} - (1/2)(e^{ik_1 r_1} + e^{ik_1 r_2})]$, should perhaps also cancel, but do not owing to the approximation in the factor $e^{ik_1(z+d+\rho)}$ which is not physically meaningful.

All terms that involve $e^{ik_1 \rho}$ relate to the direct field from the dipole and its reflection from the boundary and not to the lateral-wave term which has the coefficient $e^{ik_1(z+d)} e^{ik_2 \rho}$. They can contribute significantly to the field near the source and to the interference pattern. They are not important in determining the field at distant points.

5. FORMULATION FOR E_{1z}

The vertical component of the electric field, E_{1z} , at the point (ρ, ϕ, z) in region 1 due to an x directed, horizontal electric dipole in the same region at the point $(0, 0, d)$ is [King and Smith, 1981, p. 618, equation (5.11)]:

$$E_{1z} = \frac{i\omega\mu_1}{4\pi k_1^2} \cos \phi \int_0^\infty [-e^{i\gamma_1 z-d} - Qe^{i\gamma_1 z-d}] J_1(\lambda\rho) \lambda^2 d\lambda \quad (32)$$

where Q is in (2) and the upper sign is for $z > d$, the lower sign for $0 \leq z \leq d$. With $\mu_1 = \mu_2 = \mu_0$, let (32) be written as the sum of three integrals as follows:

$$E_{1z} = \frac{i\omega\mu_0}{4\pi k_1^2} \cos \phi [H_0(\rho, z-d) - H'_0(\rho, z-d) + H_1(\rho, z-d)] \quad (33)$$

where

$$H_0(\rho, z-d) = \int_0^\infty e^{i\gamma_1 z-d} J_1(\lambda\rho) \lambda^2 d\lambda \quad (34)$$

$$H'_0(\rho, z+d) = \int_0^\infty e^{i\gamma_1 z+d} J_1(\lambda\rho) \lambda^2 d\lambda \quad (35)$$

$$H_1(\rho, z-d) = \int_0^\infty e^{i\gamma_1 z-d} (Q-1) J_1(\lambda\rho) \lambda^2 d\lambda = -2\tilde{\epsilon}_2 \int_0^\infty e^{i\gamma_1 z-d} \left[\frac{\gamma_1}{\tilde{\epsilon}_1 \gamma_2 + \tilde{\epsilon}_2 \gamma_1} \right] J_1(\lambda\rho) \lambda^2 d\lambda \quad (36)$$

6 EVALUATION OF $H_1(\rho, z+d)$

The evaluation of $H_1(\rho, z+d)$ as defined in (36) is carried out subject to (9) and with an approximation that corresponds to (10), viz.,

$$H_1(\rho, z+d) \sim H_1(\rho, 0) e^{i\gamma_1(z+d)} \quad (37)$$

The function $H_1(\rho, 0)$ can be expanded in the manner carried out in (11). Thus,

$$H_1(\rho, 0) = -2\bar{\epsilon}_2 \int_0^\infty \gamma_1 \left[\frac{1}{\bar{\epsilon}_1 \gamma_2} + \frac{1}{\bar{\epsilon}_1 \gamma_2 + \bar{\epsilon}_2 \gamma_1} - \frac{1}{\bar{\epsilon}_1 \gamma_2} \right] J_1(\lambda \rho) \lambda^2 d\lambda \quad (38)$$

$$= -2 \frac{\bar{\epsilon}_2}{\bar{\epsilon}_1} \int_0^\infty \frac{\gamma_1}{\gamma_2} J_1(\lambda \rho) \lambda^2 d\lambda + K(\rho) \quad (39)$$

where

$$K(\rho) = -2\bar{\epsilon}_2 \int_0^\infty \gamma_1 \left[\frac{1}{\bar{\epsilon}_1 \gamma_2 + \bar{\epsilon}_2 \gamma_1} - \frac{1}{\bar{\epsilon}_1 \gamma_2} \right] J_1(\lambda \rho) \lambda^2 d\lambda \quad (40)$$

is evaluated in appendix B. The evaluation of the integral in (39) is carried out with the help of the following approximate procedure:

$$J_1(k_1, k_2, \lambda) = \frac{\gamma_1}{\gamma_2} = \frac{(k_1^2 - \lambda^2)^{1/2}}{(k_2^2 - \lambda^2)^{1/2}} \sim f_1 + f_2 - f_3 \quad (41)$$

where, with $|k_1^2| \gg |k_2^2|$, and $\beta = -ik_1$ or $k_1 = i\beta$,

$$f_1 \sim f[k_1, k_2, \lambda \sim O(k_1)] = \frac{(k_1^2 - \lambda^2)^{1/2}}{(-\lambda^2)^{1/2}} = \frac{(\lambda^2 - k_1^2)^{1/2}}{\lambda} = \frac{(\lambda^2 + \beta^2)^{1/2}}{\lambda} \quad (42)$$

$$f_2 \sim f[k_1, k_2, \lambda \sim O(k_2)] = \frac{k_1}{(k_2^2 - \lambda^2)^{1/2}} \quad (43)$$

$$f_3 \sim f[\lambda \sim O(k_2)] = f_2[\lambda \sim O(k_1)] = \frac{k_1}{i\lambda} \quad (44)$$

Thus, with (42)–(44),

$$\frac{\gamma_1}{\gamma_2} \sim \frac{(\lambda^2 + \beta^2)^{1/2}}{\lambda} + \frac{k_1}{(k_2^2 - \lambda^2)^{1/2}} + \frac{ik_1}{\lambda} \quad (45)$$

and with (45) in (39)

$$H_1(\rho, 0) = -2 \frac{k_2^2}{k_1^2} \left\{ \int_0^\infty (\lambda^2 + \beta^2)^{1/2} J_1(\lambda \rho) \lambda d\lambda - k_1 \int_0^\infty \frac{J_1(\lambda \rho) \lambda^2}{(k_2^2 - \lambda^2)^{1/2}} d\lambda + ik_1 \int_0^\infty J_1(\lambda \rho) \lambda d\lambda \right\} + K(\rho) \\ = -2 \frac{k_2^2}{k_1^2} \{ I_5(k_1) + k_1 I_6(k_2) + ik_1 I_7 \} + K(\rho) \quad (46)$$

where the three integrals I_5 , I_6 , and I_7 are evaluated in appendix C. They are

$$I_5(k_1) = -\frac{ik_1}{\rho^2} [1 + ie^{ik_1 \rho}] \quad (47)$$

$$I_6(k_2) = -\left[\frac{k_2}{\rho} + \frac{i}{\rho^2} \right] e^{ik_2 \rho} \quad (48)$$

$$I_7 = \frac{1}{\rho^2} \quad (49)$$

The function $K(\rho)$ is in appendix B. The result is

$$K(\rho) = \frac{2ik_2^5}{k_1^2} \left(\frac{\rho}{k_2 \rho} \right)^{1/2} e^{ik_2 \rho} e^{-ik_2 \rho (k_1^2/2k_2^2)} \mathcal{F} \quad (50)$$

where \mathcal{F} is defined in (23).

With (47)–(50), (37) becomes

$$H_1(\rho, z+d) \sim 2 \frac{k_2^2}{k_1} e^{ik_1(z-d)} \left\{ e^{ik_2 \rho} \left[\frac{k_2}{\rho} + \frac{i}{\rho^2} + \frac{ik_2^3}{k_1} \right. \right. \\ \left. \left. + \left(\frac{\pi}{k_2 \rho} \right)^{1/2} e^{-ik_2 \rho (k_1^2/2k_2^2)} \mathcal{F} \right] - \frac{e^{ik_1 \rho}}{\rho^2} \right\} \quad (51)$$

7. EVALUATION OF $H_0(\rho, z-d)$ AND $H'_0(\rho, z-d)$

As in the evaluation of the corresponding terms in $E_{1\phi}$, the exact formulas will be used for both $H_0(\rho, z-d)$ and $H'_0(\rho, z+d)$. As before, these are the contributions by the dipole source at $(0, 0, d)$ and the identical image at $(0, 0, -d)$. The formula for the z component of the electric field in an infinite homogeneous medium due to a horizontal x directed dipole at $(0, 0, d)$ is

$$(E_{1z})_e = \frac{i\omega\mu_0}{4\pi k_1^2} e^{ik_1 r_1} \frac{x(z-d)}{r_1^2} \left(\frac{k_1^2}{r_1} - \frac{3ik_1}{r_1^2} - \frac{3}{r_1^3} \right) \\ = \frac{i\omega\mu_0}{4\pi k_1^2} \cos \phi H_0(\rho, z-d) \quad (52)$$

with

$$r_1 = [\rho^2 + (z-d)^2]^{1/2} \quad (53)$$

The corresponding expression for the image of the source at $(0, 0, -d)$ is

$$(E_{1z})_i = \frac{i\omega\mu_0}{4\pi k_1^2} e^{ik_1 r_2} \frac{x(z+d)}{r_2^2} \left(\frac{k_1^2}{r_2} + \frac{3ik_1}{r_2^2} - \frac{3}{r_2^3} \right) \\ = \frac{i\omega\mu_0}{4\pi k_1^2} \cos \phi H'_0(\rho, z+d) \quad (54)$$

with

$$r_2 = [\rho^2 + (z+d)^2]^{1/2} \quad (55)$$

With the conditions $\rho^2 \gg z^2$, $\rho^2 \gg d^2$ in amplitudes, these formulas become

$$(E_{1z})_e \sim \frac{i\omega\mu_0}{4\pi k_1^2} e^{ik_1 r_1} \frac{x(z-d)}{\rho^2} \left(\frac{k_1^2}{\rho} + \frac{3ik_1}{\rho^2} - \frac{3}{\rho^3} \right) \quad (56)$$

$$(E_{1z})_i \sim \frac{i\omega\mu_0}{4\pi k_1^2} e^{ik_1 r_2} \frac{x(z+d)}{\rho^2} \left(\frac{k_1^2}{\rho} + \frac{3ik_1}{\rho^2} - \frac{3}{\rho^3} \right) \quad (57)$$

With $x/\rho = \cos \phi$, the sum of the functions $H_0(\rho, z-d)$ and $H'_0(\rho, z+d)$ becomes

$$H_0(\rho, z-d) + H'_0(\rho, z+d) = \left[\frac{z-d}{\rho} e^{ik_1 r_1} + \frac{z+d}{\rho} e^{ik_1 r_2} \right] \left[\frac{k_1^2}{\rho} + \frac{3ik_1}{\rho^2} - \frac{3}{\rho^3} \right] \quad (58)$$

8 THE COMPLETE FORMULA FOR E_{1z}

The final approximate formula for E_{1z} is given by (33) with (51) and (58). It is

$$E_{1z} = \frac{i\omega\mu_0}{2\pi k_1^2} \cos \phi \left(\frac{k_1^2}{k_1} e^{ik_1(z-d)} + \left\{ e^{ik_1 z} \left[\frac{k_2}{\rho} + \frac{1}{\rho^2} + \frac{ik_2^2}{k_1} \left(\frac{\pi}{k_2 \rho} \right)^{1/2} e^{-ik_2 \rho (k_1^2 + 2k_2^2)^{-1/2}} \right] - \frac{e^{ik_1 \rho}}{\rho^2} \right\} + \frac{1}{2} \left[\frac{z-d}{\rho} e^{ik_1 r_1} + \frac{z+d}{\rho} e^{ik_1 r_2} \right] \left[\frac{k_1^2}{\rho} + \frac{3ik_1}{\rho^2} - \frac{3}{\rho^3} \right] \right) \quad (59)$$

with r_1 and r_2 defined in (26) and $\bar{\mathcal{F}}$ in (23).

9 CONCLUSION AND COMPARISON WITH NUMERICAL VALUES

In order to check the accuracy of the newly derived simple formulas for $E_{1\phi}$ and E_{1z} , the general integrals (1) and (32) were evaluated numerically (this evaluation is due to L. C. Shen) for a critical range of the radial distance ρ with the depths d of the dipole and z of the point where the field is calculated chosen to be different. The denser region 1 is salt water with $\epsilon_{1r} = 45$ and $\sigma_1 = 3.5$ S/m at $f = 600$ MHz; the second region is air. Since agreement at very large distances is no problem, special attention is directed to the range within 20 air wavelengths of the dipole. This is of importance since the new approximate formulas are good approximations only when $\rho^2 \gg d^2$, $\rho^2 \gg z^2$, which may be interpreted as $\rho \geq 5d$ and $\rho \geq 5z$.

Graphs showing $|E_{1\phi}|$ and $|E_{1z}|$ and also $|E_{1\rho}|$ in the range $0.001 \leq \rho \leq 10$ m for the numerical calculations and $0.01 \leq \rho \leq 10$ m for the approximate formulas are shown in Figure 1. The agreement is seen

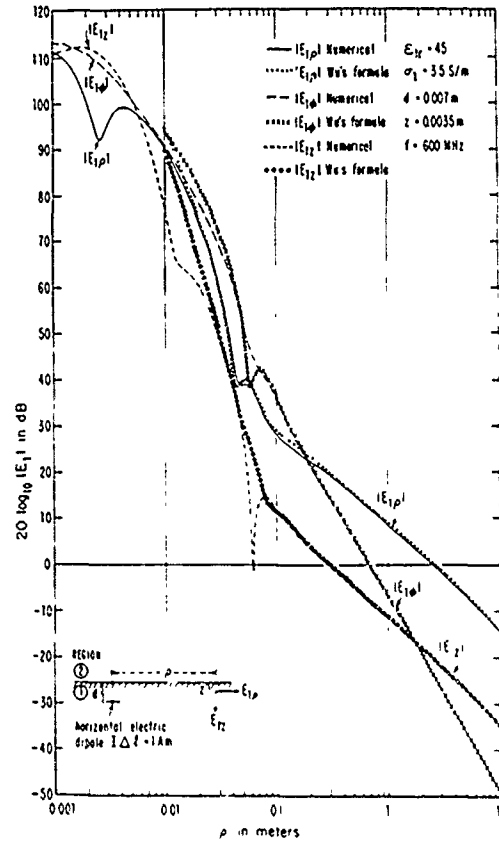


Fig. 1 The three components of the electric field at depth z due to a horizontal electric dipole at depth d in salt water. Restriction on Wu's formula $\rho \geq 5d = 0.035$ m.

to be excellent when $\rho \geq 5d = 0.035$ m except in a narrow range near $\rho = 0.07$ m where the direct and lateral waves interfere, as discussed in *Wu and King* [this issue]. Very small changes in frequency significantly alter the interference pattern so that close agreement in a small range near such a region cannot be expected. At lower frequencies the direct field is attenuated much more rapidly, so that interference phenomena do not occur in the practical ranges. Even in the case at hand, the range where the interference is significant is only 7 or 8 cm from the source. At greater distances, all three approximate formulas are highly accurate.

APPENDIX A EVALUATION OF THE FUNCTION $H(\rho)$

The function $H(\rho)$ is defined in (18). It differs from $G(\rho)$ in *Wu and King* [this issue] only in the sign of $J_2(\lambda\rho)$. Thus, whereas in (B3) of *Wu and King* [this

issue] the following function and its approximation occur:

$$J_0(\lambda\rho) - J_2(\lambda\rho) \sim \left(\frac{2}{\pi\lambda\rho}\right)^{1/2} e^{i(\lambda\rho - \pi/4)} \quad (A1)$$

the function $H(\rho)$ involves instead

$$\begin{aligned} J_0(\lambda\rho) - J_2(\lambda\rho) &= \frac{2}{\lambda\rho} J_1(\lambda\rho) \sim \frac{2}{\lambda\rho} \cdot \frac{1}{(2\pi\lambda\rho)^{1/2}} e^{i(\lambda\rho - 3\pi/4)} \\ &= \frac{-i}{\lambda\rho} \left(\frac{2}{\pi\lambda\rho}\right)^{1/2} e^{i(\lambda\rho - \pi/4)} \end{aligned} \quad (A2)$$

Clearly, (A1) and (A2) differ only by the factor $-i/\lambda\rho$. Since in the evaluation of $G(\rho)$, λ is replaced by k_2 in amplitudes, the final expression for $H(\rho)$ differs from that for $G(\rho)$ only in the factor $-i/k_2\rho$. Thus, with (B16) of *Wu and King* [this issue]:

$$\begin{aligned} H(\rho) &= 2i(k_2^2/k_1) \frac{\pi^{1/2}}{(k_2\rho)^{3/2}} e^{ik_2\rho} e^{-i\alpha} \\ &\cdot \left\{ \left[\frac{1}{2} - C(\alpha) \right] - i \left[\frac{1}{2} - S(\alpha) \right] \right\} \end{aligned} \quad (A3)$$

where $\alpha = k_2\rho(k_2^2/2k_1^2)$.

APPENDIX B THE FUNCTION $K(\rho)$

The function $K(\rho)$ is defined in (40). It is

$$\begin{aligned} K(\rho) &= -2\tilde{\epsilon}_2 \int_0^\infty (k_1^2 - \lambda^2)^{1/2} \\ &\cdot \left[\frac{1}{\tilde{\epsilon}_1(k_2^2 - \lambda^2)^{1/2} + \tilde{\epsilon}_2(k_1^2 - \lambda^2)^{1/2}} \right. \\ &\left. - \frac{1}{\tilde{\epsilon}_1(k_2^2 - \lambda^2)^{1/2}} \right] J_1(\lambda\rho) \lambda^2 d\lambda \end{aligned} \quad (B1)$$

As in the comparable integral in $H(\rho)$, which is evaluated in appendix A, significant contributions from the integrand occur only when λ is of the order of k_2 and therefore in this range $|k_1^2| \gg \lambda^2$, $(k_1^2 - \lambda^2)^{1/2} \sim k_1$. The same approximation of the Bessel function can be made. It is

$$\begin{aligned} J_1(\lambda\rho) &\sim \frac{1}{2} H_1^{(1)}(\lambda\rho) \sim \frac{1}{(2\pi\lambda\rho)^{1/2}} e^{i(\lambda\rho - \pi/4)} \\ &= \frac{-i}{(2\pi\lambda\rho)^{1/2}} e^{i(\lambda\rho - \pi/4)} \end{aligned} \quad (B2)$$

With these approximations, (B1) becomes

$$\begin{aligned} K(\rho) &\sim i\tilde{\epsilon}_2 k_1 \int_0^\infty \left[\frac{1}{\tilde{\epsilon}_1(k_2^2 - \lambda^2)^{1/2} + \tilde{\epsilon}_2 k_1} - \frac{1}{\tilde{\epsilon}_1(k_2^2 - \lambda^2)^{1/2}} \right] \\ &\cdot \left(\frac{2}{\pi\lambda\rho}\right)^{1/2} e^{i(\lambda\rho - \pi/4)} \lambda^2 d\lambda \end{aligned} \quad (B3)$$

This differs from $G(\rho)$ in (B4) of *Wu and King* [this issue] only in a factor $-i\lambda/k_1$. Since in the evaluation of $G(\rho)$ the approximation $\lambda \sim k_2$ was made in amplitudes, this ratio is simply $|k_2/k_1|$. That is, $K(\rho) \sim -(ik_2/k_1)G(\rho)$. With (B16) in *Wu and King* [this issue]:

$$K(\rho) \sim 2i(k_2^2/k_1^2) \left(\frac{\pi}{k_2\rho}\right)^{1/2} e^{ik_2\rho} e^{-ik_2\rho k_1^2/2k_1^2} \mathcal{F} \quad (B4)$$

APPENDIX C THE INTEGRALS I

With $\beta = -ik_1$ and $J_{-1}(z) = -J_1(z)$, the following integral must be evaluated:

$$\begin{aligned} I_3(k_1) &= \int_0^\infty (\lambda^2 - \beta^2)^{1/2} J_1(\lambda\rho) \lambda d\lambda \\ &= - \int_0^\infty (\lambda^2 + \beta^2)^{1/2} J_{-1}(\lambda\rho) \lambda d\lambda \end{aligned} \quad (C1)$$

This is accomplished with formula (4) on p. 435 of Watson's *Bessel Functions* with $\nu = -1$, $a = \rho$, $x = \lambda$, and $k = \beta$. Thus,

$$I_3(k_1) = -\frac{\beta^2}{2\rho} I_{-1}\left(\frac{1}{2}\beta\rho\right) K_{-1}\left(\frac{1}{2}\beta\rho\right) \lim_{\nu \rightarrow -1} \frac{\Gamma(\nu+1)}{\Gamma(2\nu+1)} \quad (C2)$$

With the relation $\Gamma(\nu) = \nu^{-1}\Gamma(\nu+1)$, it follows that $\Gamma(\nu+1) = (\nu+1)^{-1}\Gamma(\nu+2)$. Also $\Gamma(2\nu+1) = (2\nu+1)^{-1}\Gamma(2\nu+2) = (2\nu+1)^{-1}(2\nu+2)^{-1}\Gamma(2\nu+3)$. Hence,

$$\lim_{\nu \rightarrow -1} \frac{\Gamma(\nu+1)}{\Gamma(2\nu+1)} = \lim_{\nu \rightarrow -1} \frac{(2\nu+1)(2\nu+2)}{\nu-1} \frac{\Gamma(\nu+2)}{\Gamma(2\nu+3)} = -2 \quad (C3)$$

so that

$$I_3(k_1) = \frac{\beta^2}{\rho} I_{-1}\left(\frac{1}{2}\beta\rho\right) K_{-1}\left(\frac{1}{2}\beta\rho\right) \quad (C4)$$

For large arguments, $\beta\rho > 1$, $I_{-1}(\beta\rho/2) \sim (1/\pi\beta\rho)^{1/2} e^{\beta\rho/2} (1 + ie^{-\beta\rho})$, $K_{-1}(\beta\rho/2) \sim (\pi/\beta\rho)^{1/2} e^{-\beta\rho/2}$. Hence,

$$I_3(k_1) = \frac{\beta^2}{\rho} \cdot \frac{1}{\beta\rho} (1 + ie^{-\beta\rho}) = \frac{ik_1}{\rho^2} (1 + ie^{ik_1\rho}) \quad (C5)$$

The second integral to be evaluated is

$$I_6(k_2) = \int_0^\infty \frac{J_1(\lambda\rho)\lambda^2}{(k_2^2 - \lambda^2)^{1/2}} d\lambda = \int_0^\infty \frac{\lambda\rho}{2} [J_0(\lambda\rho) - J_2(\lambda\rho)] \cdot \frac{\lambda^2}{(k_2^2 - \lambda^2)^{1/2}} d\lambda \quad (C6)$$

$$= \frac{\rho}{2} \{-I_2(k_2) - k_2^2 I_4(k_2)\} \quad (C7)$$

where $I_2(k_2)$ and $I_4(k_2)$ are given in (14) and (16). With these,

$$I_6(k_2) = \frac{\rho}{2} \left[-\frac{2k_2}{\rho^2} - \frac{2i}{\rho^3} e^{ik_2\rho} - \frac{2k_2}{\rho^2} - \frac{2k_2}{\rho^2} e^{ik_2\rho} \right] = -\left[\frac{k_2}{\rho} + \frac{i}{\rho^2} \right] e^{ik_2\rho} \quad (C8)$$

The third integral is

$$I_7 = \int_0^\infty J_1(\lambda\rho)\lambda d\lambda = \frac{2\rho\Gamma(3/2)}{\rho^3\pi^{1/2}} = \frac{1}{\rho^2} \quad (C9)$$

This is evaluated with formula (5) on p. 386 of Watson's Bessel Functions. In that formula set $a = 0$, $v = 1$, $b = \rho$, $t = \lambda$. Also note that $\Gamma(3/2) = (1/2)!\pi^{1/2}/2$.

Acknowledgments Computations from the approximate formulas were carried out by B. H. Sandler. This research was supported in part by the Office of Naval Research under contract N00014-79-C-0419 and in part by the Joint Services Electronics Program under contract N00014-75-C-0648, both with Harvard University.

REFERENCES

- King, R. W. P., and G. S. Smith (1981). *Antennas in Motion*. The MIT Press, Cambridge, Mass.
- Wu, T. T., and R. W. P. King (this issue). Lateral waves: A new formula and interference patterns. *Radio Sci.*

Correction to "Lateral waves: New formulas for $E_{1\phi}$ and E_{1z} " by T. T. Wu and R. W. P. King

(Received May 8, 1984.)

In the paper "Lateral waves: New formulas for $E_{1\phi}$ and E_{1z} " by T. T. Wu and R. W. P. King (*Radio Science*, 17(3), 532-537, 1982), the following changes in sign should be made:

Equation (52): insert a minus sign after each equals sign.

Equation (54): insert a minus sign after each equals sign.

Equations (56) and (57): insert a minus sign after the asymptotic proportion sign.

Equation (58): insert a minus sign after the equals sign.

Equation (59): change plus to minus at beginning of the third line. The authors thank P. Bannister for discovering this error. The corrected formula (59) gives the interference dip near $\rho \approx 0.08$ m in Figure 1 in agreement with the numerically calculated curve.

If approximations of the type (10) and (37) are applied only to integrals that involve $\exp(ik_2\rho)$ and not

to those that involve $\exp(ik_1\rho)$, the latter can all be evaluated exactly with the help of formula (52) of Bateman [1953, p. 95] or formula 6.637(1) of Gradshteyn and Ryzhik [1980, p. 719]. The only resulting change is the replacement of $\exp[ik_1(z+d+\rho)]$ in (30) and (59) by $\exp(ik_1r_2)$ with $r_2 = [\rho^2 + (z+d)^2]^{1/2}$. This change leads to slightly better agreement with the numerically evaluated components in a narrow range near the lower limit of ρ in the conditions $\rho \geq 5d$, $\rho \geq 5z$. It becomes significant only when interference minima occur in this range. These are very sensitive to small changes.

REFERENCES

- Bateman, H., *Higher Transcendental Functions*, vol. II, 396 pp., McGraw-Hill, New York, 1957.
- Gradshteyn, I. S. and I. M. Ryzhik, *Tables of Integrals, Series and Products*, 1160 pp., Academic, New York, 1980.

New formulas for the electromagnetic field of a vertical electric dipole in a dielectric or conducting half-space near its horizontal interface

Ronald W. P. King

Cardon McKay Laboratory, Harvard University, Cambridge, Massachusetts 02138

(Received 23 May 1982; accepted for publication 6 August 1982)

New formulas are derived for the electromagnetic field of a vertical electric dipole in a conducting or dielectric half-space. These continuously approximate in accuracy the general complex integrals over the entire practical range, yet are quite simple. They supplement similar formulas for the horizontal electric dipole with which they are compared, and provide the means for studying the interference patterns between the direct and lateral components of the waves and the reflection and transmission of lateral waves at boundaries.

PACS numbers: 41.10.Hv

I. INTRODUCTION

The electromagnetic field generated by a vertical electric dipole has been studied extensively beginning with the classical work of Sommerfeld.^{1,2} An historical review with extensive references is in the authoritative book by Baños³ in which the horizontal and vertical electric and magnetic dipoles are investigated in detail. However, the final formulation in this book consists, on the one hand, of unevaluated complex integrals from which the electromagnetic field is to be determined by differentiation and, on the other hand, of approximate formulas for restricted, generally nonoverlapping ranges of the parameters and variables. These are designated near field, intermediate field, and asymptotic field. Similar expressions are given by Wait and Campbell.⁴ For a complete physical understanding of the direct and lateral-wave components of the electromagnetic field, their interaction, and their reflection and transmission at boundaries, the general integrals are too involved and the approximate formulas neither very accurate nor very useful since they have different forms in disconnected ranges. In order to overcome these difficulties, the general integrals have been evaluated directly, subject to conditions that are easily satisfied, and simple, accurate formulas have been obtained that are valid over the entire practical range. The newly derived formulas for the horizontal electric dipole have already been reported⁵⁻⁷; it is the purpose of this paper to derive comparable ones for the vertical electric dipole. Actually, they are required in a theoretical and experimental⁸ study of lateral-wave propagation. Although the general integrals for the field can be obtained from the formulation of Baños³ in terms of potential functions, a more direct derivation from Maxwell's equations in the manner carried out for the horizontal electric dipole⁹ is more convenient and is outlined in the following.

II. DERIVATION OF THE GENERAL INTEGRALS FOR THE FIELD

The geometry and notation underlying the analysis are shown in Fig. 1. The vertical electric dipole with unit moment ($|d| = 1$ A m) is located on the downward-directed z axis at a distance d from the origin of coordinates on the interface, the xy plane. Interest is in the electromagnetic field

at an arbitrary point (x, y, z) in rectangular or (ρ, ϕ, z) in cylindrical coordinates. The conducting or dielectric half-space is Region 1 ($z > 0$); Region 2 is air ($z < 0$). The two regions are characterized by the complex wave numbers $k_1 = \beta_1 + i\alpha_1 = \omega(\mu_1\epsilon_1)^{1/2}$, where $\epsilon_1 = \epsilon_1 + i\sigma_1/\omega$ and $\epsilon_1 = \epsilon_0\epsilon_{r1}$; $k_2 = \beta_2 + i\alpha_2 = \omega(\mu_2\epsilon_2)^{1/2}$. It is assumed that $\mu_1 = \mu_2 = \mu_0$; for air, $\epsilon_2 = \epsilon_0$, $\alpha_2 = 0$.

Maxwell's equations for the two regions with the time dependence $e^{-i\omega t}$ are

$$\nabla \times \mathbf{E}_j = i\omega \mathbf{B}_j = i\omega(\hat{x}B_{jx} + \hat{y}B_{jy}); \quad B_{jz} = 0, \quad (1)$$

$$\begin{aligned} \nabla \times \mathbf{B}_j &= -\frac{ik_j^2}{\omega} \mathbf{E}_j + \mu_0 \hat{z} J_z; \\ J_z &= \delta(x)\delta(y)\delta(z-d), \quad j=1, 2. \end{aligned} \quad (2)$$

As discussed in conjunction with the horizontal electric dipole,⁹ it is convenient to use the transform

$$\begin{aligned} \mathbf{E}(x, y, z) &= (2\pi)^{-2} \int_{-\infty}^{\infty} d\xi \int_{-\infty}^{\infty} d\eta e^{i\xi x + i\eta y} \bar{\mathbf{E}}(\xi, \eta, z); \\ \bar{J}_z(\xi, \eta, z) &= \delta(z-d). \end{aligned} \quad (3)$$

With it, the transformed Maxwell equations are

$$\begin{aligned} i\eta \bar{E}_{jx} - \partial \bar{E}_{jy} / \partial z &= i\omega \bar{B}_{jx}, \quad \partial \bar{E}_{jx} / \partial z - i\xi \bar{E}_{jz} = i\omega \bar{B}_{jy}, \\ i\xi \bar{E}_{jy} - i\eta \bar{E}_{jx} &= 0; \\ -\partial \bar{B}_{jy} / \partial z &= -i(k_j^2/\omega) \bar{E}_{jx}, \\ \partial \bar{B}_{jx} / \partial z &= -i(k_j^2/\omega) \bar{E}_{jy}, \\ i\xi \bar{B}_{jy} - i\eta \bar{B}_{jx} &= -i(k_j^2/\omega) \bar{E}_{jz} + \mu_0 \delta(z-d). \end{aligned} \quad (4)$$

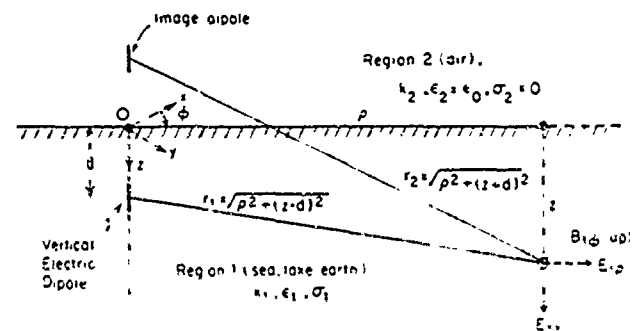


FIG. 1. Vertical dipole at depth d in Region 1, electromagnetic field calculated at (ρ, z) .

It follows that $\bar{E}_x = (\eta/\xi)\bar{E}_y$, $\bar{B}_x = -(\xi/\eta)\bar{B}_y$. Suitable combinations of the above equations yield ordinary differential equations for \bar{B}_x and \bar{B}_y . They are

$$\begin{aligned} [(d^2/dz^2) + \gamma_j^2]\bar{B}_x &= -i\eta\mu_0\delta(z-d); \\ \bar{B}_y &= -(\xi/\eta)\bar{B}_x, \end{aligned} \quad (6)$$

with

$$\gamma_j = (k_j^2 - \xi^2 - \eta^2)^{1/2}, \quad j = 1, 2. \quad (7)$$

Also,

$$\bar{E}_x = -i\omega/k_j^2 \partial \bar{B}_y / \partial z = i\omega/k_j^2 \xi / \eta \partial \bar{B}_x / \partial z, \quad (8)$$

$$\bar{E}_y = i\omega/k_j^2 \partial \bar{B}_x / \partial z, \quad (9)$$

$$\bar{E}_z = \omega/\eta k_j^2 [(d^2/dz^2) + k_j^2] \bar{B}_x. \quad (10)$$

The solutions of Eq. (6) which do not become infinite at $z = \pm \infty$ are

$$\begin{aligned} \bar{B}_{1x}(z) &= C_1 e^{\gamma_1 z} - \eta\mu_0/2\gamma_1 e^{\gamma_1(z-d)}, \quad z > 0 \\ \bar{B}_{2x}(z) &= C_2 e^{-\gamma_2 z}, \quad z < 0. \end{aligned} \quad (11)$$

The boundary condition, $\bar{B}_x(0) = \bar{B}_y(0)$, leads to

$$C_1 = C_2 = \eta\mu_0/2\gamma_1 e^{\gamma_1 d}, \quad (12)$$

so that

$$\begin{aligned} \bar{B}_x(z) &= C_2 e^{\gamma_1 z} - \eta\mu_0/2\gamma_1 [e^{\gamma_1(z-d)} - e^{\gamma_1(z+d)}], \\ \bar{B}_y(z) &= C_2 e^{\gamma_1 z} - \eta\mu_0/2\gamma_1 [e^{\gamma_1(z-d)} - e^{\gamma_1(z+d)}]. \end{aligned} \quad (13)$$

With Eqs. 8, (11), and (13),

$$\begin{aligned} \bar{E}_x(z) &= -i\omega/k_1^2 \xi / \eta C_2 e^{\gamma_1 z} \\ &\quad - (\xi\mu_0/2) [e^{\gamma_1(z-d)} - e^{\gamma_1(z+d)}], \quad \begin{cases} z > d \\ 0 < z < d \end{cases} \\ \bar{E}_y(z) &= i\omega/k_1^2 \xi / \eta C_2 e^{\gamma_1 z}, \quad z < 0. \end{aligned} \quad (14a, 14b)$$

The boundary condition, $\bar{E}_x(0) = \bar{E}_y(0)$, leads to

$$C_2 = -\mu_0\eta k_1^2 e^{\gamma_1 d} / (k_1^2 \gamma_2 - k_2^2 \gamma_1). \quad (15)$$

When C_2 , given by Eq. (15), is substituted in Eqs. (11), (13), (14a), and (14b), the final solutions for $\bar{B}_x(z)$, $\bar{B}_y(z)$, $\bar{E}_x(z)$, and $\bar{E}_y(z)$ are obtained. The corresponding solutions for $\bar{B}_1(z)$, $\bar{B}_2(z)$, $\bar{E}_1(z)$, and $\bar{E}_2(z)$ follow from $\bar{E}_x = (\eta/\xi)\bar{E}_y$, $\bar{B}_x = -(\xi/\eta)\bar{B}_y$. Finally, $\bar{E}_z(z)$ and $\bar{B}_z(z)$ are obtained with Eq. (10). The results successively for Regions 1 and 2 are

Region 1, $z \geq 0$:

$$\begin{aligned} \bar{B}_{1x}(\xi, \eta, z) &= -\mu_0\eta \left[\frac{e^{\gamma_1(z-d)}}{2\gamma_1} - \frac{e^{\gamma_1(z+d)}}{2\gamma_1} \right. \\ &\quad \left. + \frac{k_2^2 e^{\gamma_1(z-d)}}{k_1^2 \gamma_2 + k_2^2 \gamma_1} \right], \end{aligned} \quad (16)$$

$$\bar{B}_{1y}(\xi, \eta, z) = -(\xi/\eta)\bar{B}_{1x}(\xi, \eta, z), \quad (17)$$

$$\begin{aligned} \bar{E}_{1x}(\xi, \eta, z) &= -\frac{\omega\mu_0\xi}{k_1^2} \left[\mp \frac{e^{\gamma_1(z-d)}}{2} + \frac{e^{\gamma_1(z+d)}}{2} \right. \\ &\quad \left. - \frac{k_2^2 \gamma_1 e^{\gamma_1(z-d)}}{k_1^2 \gamma_2 + k_2^2 \gamma_1} \right], \quad \begin{cases} z > d \\ 0 < z < d \end{cases} \end{aligned} \quad (18)$$

$$\bar{E}_{1y}(\xi, \eta, z) = (\eta/\xi)\bar{E}_{1x}(\xi, \eta, z), \quad (19)$$

$$\begin{aligned} \bar{E}_{1z}(\xi, \eta, z) &= -\frac{\omega\mu_0\xi^2 + \eta^2}{k_1^2} \left[\frac{e^{\gamma_1(z-d)}}{2\gamma_1} - \frac{e^{\gamma_1(z+d)}}{2\gamma_1} \right. \\ &\quad \left. + \frac{k_2^2 e^{\gamma_1(z-d)}}{k_1^2 \gamma_2 + k_2^2 \gamma_1} \right]. \end{aligned} \quad (20)$$

Region 2, $z < 0$:

$$\bar{B}_{2x}(\xi, \eta, z) = -\mu_0\eta \left[\frac{k_2^2 e^{\gamma_2 z} e^{-\gamma_1 d}}{k_1^2 \gamma_2 + k_2^2 \gamma_1} \right], \quad (21)$$

$$\bar{B}_{2y}(\xi, \eta, z) = -(\xi/\eta)\bar{B}_{2x}(\xi, \eta, z), \quad (22)$$

$$\bar{E}_{2x}(\xi, \eta, z) = -\omega\mu_0\xi \left[\frac{\gamma_2 e^{\gamma_2 z} e^{-\gamma_1 d}}{k_1^2 \gamma_2 + k_2^2 \gamma_1} \right], \quad (23)$$

$$\bar{E}_{2y}(\xi, \eta, z) = (\eta/\xi)\bar{E}_{2x}(\xi, \eta, z), \quad (24)$$

$$\bar{E}_{2z}(\xi, \eta, z) = -\omega\mu_0\xi^2 - \eta^2 \left[\frac{e^{\gamma_2 z} e^{-\gamma_1 d}}{k_1^2 \gamma_2 + k_2^2 \gamma_1} \right]. \quad (25)$$

Note that in agreement with the boundary condition, $k_1^2 \bar{E}_z(\xi, \eta, 0) = k_2^2 \bar{E}_z(\xi, \eta, 0)$. The substitution of Eqs. 16-25 into Eq. (3), yields the general integrals for the components of the electric and magnetic fields in Cartesian coordinates. These are readily converted to cylindrical coordinates with the relations $x = \rho \cos \phi$, $y = \rho \sin \phi$, $\xi = \lambda \cos \phi$, $\eta = \lambda \sin \phi$, $\rho = (x^2 + y^2)^{1/2}$, $\lambda = (\xi^2 + \eta^2)^{1/2}$, $d\xi d\eta = \lambda d\phi d\lambda$, $\xi x - \eta y = \lambda \rho \cos(\phi - \phi')$, $E_x = E_\rho \cos \phi - E_\phi \sin \phi$, $B_\phi = -B_x \sin \phi - B_y \cos \phi$. If use is made of the integral representations of the Bessel functions, specifically,

$$\begin{aligned} J_0(\lambda\rho) &= (2\pi)^{-1} \int_0^{2\pi} e^{i\lambda\rho \cos(\phi - \phi')} d\phi', \\ J_1(\lambda\rho) &= -i(2\pi)^{-1} \int_0^{2\pi} e^{i\lambda\rho \cos(\phi - \phi')} \cos \phi - \phi' d\phi'. \end{aligned}$$

it follows that $B_z(\rho, z) = 0$, $B_\phi(\rho, z) = 0$, $E_\phi(\rho, z) = 0$, $j = 1, 2$, and

$$\begin{aligned} B_{1\phi}(\rho, z) &= \frac{i\mu_0}{2\pi} \int_0^\infty \left[\frac{e^{\gamma_1(z-d)}}{2\gamma_1} - \frac{e^{\gamma_1(z+d)}}{2\gamma_1} \right. \\ &\quad \left. + \frac{k_2^2 e^{\gamma_1(z-d)}}{k_1^2 \gamma_2 + k_2^2 \gamma_1} \right] J_1(\lambda\rho) \lambda^2 d\lambda, \end{aligned} \quad (26)$$

$$\begin{aligned} E_{1\rho}(\rho, z) &= \frac{i\omega\mu_0}{2\pi k_1^2} \int_0^\infty \left[\pm \frac{e^{\gamma_1(z-d)}}{2} - \frac{e^{\gamma_1(z+d)}}{2} \right. \\ &\quad \left. + \frac{k_2^2 \gamma_1 e^{\gamma_1(z-d)}}{k_1^2 \gamma_2 + k_2^2 \gamma_1} \right] \\ &\quad \times J_1(\lambda\rho) \lambda^2 d\lambda; \quad \begin{cases} z > d \\ 0 < z < d \end{cases} \end{aligned} \quad (27)$$

$$\begin{aligned} E_{1z}(\rho, z) &= -\frac{\omega\mu_0}{2\pi k_1^2} \int_0^\infty \left[\frac{e^{\gamma_1(z-d)}}{2\gamma_1} - \frac{e^{\gamma_1(z+d)}}{2\gamma_1} \right. \\ &\quad \left. + \frac{k_2^2 e^{\gamma_1(z-d)}}{k_1^2 \gamma_2 + k_2^2 \gamma_1} \right] J_0(\lambda\rho) \lambda^2 d\lambda, \end{aligned} \quad (28)$$

for Region 1, $z \geq 0$. Similarly, for Region 2, $z < 0$:

$$B_{2\phi}(\rho, z) = \frac{i\mu_0}{2\pi} \int_0^\infty \frac{k_2^2 e^{\gamma_2 z} e^{-\gamma_1 d}}{k_1^2 \gamma_2 + k_2^2 \gamma_1} J_1(\lambda\rho) \lambda^2 d\lambda, \quad (29)$$

$$E_{2\rho}(\rho, z) = \frac{-i\omega\mu_0}{2\pi} \int_0^\infty \frac{\gamma_2 e^{\gamma_2 z} e^{-\gamma_1 d}}{k_1^2 \gamma_2 + k_2^2 \gamma_1} J_1(\lambda\rho) \lambda^2 d\lambda, \quad (30)$$

$$E_{zz}(\rho, z) = \frac{-\omega\mu_0}{2\pi} \int_0^\infty \frac{e^{\gamma_1 z} e^{-\gamma_2 z}}{k_1^2 \gamma_2 + k_2^2 \gamma_1} J_0(\lambda \rho) \lambda^3 d\lambda. \quad (31)$$

These are the desired general integrals for the electromagnetic field of the vertical dipole at $z = d$. The same expressions can be obtained from the general formulas (2.103) and (2.104) on p. 43 of Baños' book.³ It is to be noted that the expressions (7.84) and (7.85) on p. 221 of Baños' book—from which the approximate formulas for the several ranges are derived—omit the entire direct and reflected fields.

III. EVALUATION OF THE INTEGRALS FOR THE FIELD IN REGION 1

It is possible to evaluate the integrals [Eqs. (26)–(28)] for the field in Region 1 subject only to the following conditions:

$$k_1^2 > k_2^2 \text{ and } \rho^2 > z^2, \rho^2 > d^2. \quad (32)$$

Note that the condition $k_1^2 = k_2^2 \epsilon_1 + i\sigma_1/\omega > k_2^2 = k_0^2$ does not require Region 1 to be conducting. It may be lake water or earth as well as sea water, and the range of frequencies is not restricted.

The first step in the evaluation of Eqs. (26)–(28) is to note that in each formula the first term is the appropriate component of the well-known direct field ($B_{10}^d, E_{1\rho}^d, E_{1z}^d$) of the dipole as if isolated at $z = d$ in an infinite (rather than semi-infinite) Region 1. Similarly, the second term is the field ($B_{10}^L, E_{1\rho}^L, E_{1z}^L$) of an image dipole at $z = -d$ but with electric moment reversed. The remaining third term is the lateral-wave field ($B_{10}^L, E_{1\rho}^L, E_{1z}^L$). Thus,

$$B_{10}(\rho, z) = B_{10}^d(\rho, z) + B_{10}^L(\rho, z) + B_{10}^L(\rho, z),$$

$$E_{1\rho}(\rho, z) = E_{1\rho}^d(\rho, z) + E_{1\rho}^L(\rho, z) + E_{1\rho}^L(\rho, z),$$

$$E_{1z}(\rho, z) = E_{1z}^d(\rho, z) + E_{1z}^L(\rho, z) + E_{1z}^L(\rho, z).$$

Specifically, with $r_1 = [z - d]^2 - \rho^2]^{1/2}$, $r_2 = [z + d]^2 - \rho^2]^{1/2}$,

$$\begin{aligned} B_{10}^d(\rho, z) &= \frac{i\mu_0}{4\pi} \int_0^\infty \frac{e^{\gamma_1 z} e^{-\gamma_2 z}}{\gamma_1} J_1(\lambda \rho) \lambda^2 d\lambda \\ &= -\frac{\mu_0}{4\pi} e^{ik_1 r_1} \left(\frac{ik_1}{r_1} - \frac{1}{r_1^2} \right) \left(\frac{\rho}{r_1} \right), \end{aligned} \quad (33a)$$

$$\begin{aligned} B_{10}^L(\rho, z) &= -\frac{i\mu_0}{4\pi} \int_0^\infty \frac{e^{\gamma_1 z} e^{-\gamma_2 z}}{\gamma_1} J_1(\lambda \rho) \lambda^2 d\lambda \\ &= \frac{\mu_0}{4\pi} e^{ik_1 r_2} \left(\frac{ik_1}{r_2} - \frac{1}{r_2^2} \right) \left(\frac{\rho}{r_2} \right), \end{aligned} \quad (33b)$$

$$\begin{aligned} E_{1\rho}^d(\rho, z) &= \frac{i\omega\mu_0}{4\pi k_1^2} \int_0^\infty \pm e^{\gamma_1 z} e^{-\gamma_2 z} J_1(\lambda \rho) \lambda^2 d\lambda \\ &= \frac{i\omega\mu_0}{4\pi k_1^2} e^{ik_1 r_1} \left(\frac{k_1^2}{r_1} + \frac{i3k_1}{r_1^2} - \frac{3}{r_1^3} \right) \\ &\quad \times \left(\frac{\rho}{r_1} \right) \left(\frac{z-d}{r_1} \right), \end{aligned} \quad (34a)$$

$$\begin{aligned} E_{1\rho}^L(\rho, z) &= -\frac{i\omega\mu_0}{4\pi k_1^2} \int_0^\infty e^{\gamma_1 z} e^{-\gamma_2 z} J_1(\lambda \rho) \lambda^2 d\lambda \\ &= -\frac{i\omega\mu_0}{4\pi k_1^2} e^{ik_1 r_2} \left(\frac{k_1^2}{r_2} + \frac{i3k_1}{r_2^2} - \frac{3}{r_2^3} \right) \\ &\quad \times \left(\frac{\rho}{r_2} \right) \left(\frac{z+d}{r_2} \right), \end{aligned} \quad (34b)$$

$$\begin{aligned} E_{1z}^d(\rho, z) &= -\frac{\omega\mu_0}{4\pi k_1^2} \int_0^\infty \frac{e^{\gamma_1 z} e^{-\gamma_2 z}}{\gamma_1} J_0(\lambda \rho) \lambda^2 d\lambda \\ &= -\frac{\omega\mu_0}{4\pi k_1^2} e^{ik_1 r_1} \left[\left(\frac{ik_1^2}{r_1} - \frac{k_1}{r_1^2} - \frac{i}{r_1^3} \right) \right. \\ &\quad \left. - \left(\frac{z-d}{r_1} \right)^2 \left(\frac{ik_1^2}{r_1} - \frac{3k_1}{r_1^2} - \frac{3i}{r_1^3} \right) \right], \end{aligned} \quad (35a)$$

$$\begin{aligned} E_{1z}^L(\rho, z) &= \frac{\omega\mu_0}{4\pi k_1^2} \int_0^\infty \frac{e^{\gamma_1 z} e^{-\gamma_2 z}}{\gamma_1} J_0(\lambda \rho) \lambda^2 d\lambda \\ &= \frac{\omega\mu_0}{4\pi k_1^2} e^{ik_1 r_2} \left[\left(\frac{ik_1^2}{r_2} - \frac{k_1}{r_2^2} - \frac{i}{r_2^3} \right) \right. \\ &\quad \left. - \left(\frac{z+d}{r_2} \right)^2 \left(\frac{ik_1^2}{r_2} - \frac{3k_1}{r_2^2} - \frac{3i}{r_2^3} \right) \right]. \end{aligned} \quad (35b)$$

With the conditions $\rho^2 > z^2, \rho^2 > d^2, r_1 \sim r_2 \sim \rho$ in amplitudes, $\rho/r_1 \sim \rho/r_2 \sim 1$ and terms in $(z-d)^2/r_1^2$ and $(z+d)^2/r_2^2$ are negligible. It follows that

$$\begin{aligned} B_{10}^L(\rho, z) &= B_{10}^L(\rho, z) \\ &= -\frac{\mu_0}{4\pi} (e^{ik_1 r_1} - e^{ik_1 r_2}) \left(\frac{ik_1}{\rho} - \frac{1}{\rho^2} \right). \end{aligned} \quad (36)$$

$$\begin{aligned} E_{1\rho}^L(\rho, z) &= E_{1\rho}^L(\rho, z) \sim \frac{i\omega\mu_0}{4\pi k_1^2} \left(\frac{z-d}{\rho} e^{ik_1 r_1} \right. \\ &\quad \left. - \frac{z+d}{\rho} e^{ik_1 r_2} \right) \left(\frac{k_1^2}{\rho} - \frac{i3k_1}{\rho^2} - \frac{3}{\rho^3} \right). \end{aligned} \quad (37)$$

$$\begin{aligned} E_{1z}^L(\rho, z) &= E_{1z}^L(\rho, z) \\ &\sim -\frac{\omega\mu_0}{4\pi k_1^2} (e^{ik_1 r_1} - e^{ik_1 r_2}) \left(\frac{ik_1^2}{\rho} - \frac{k_1}{\rho^2} - \frac{i}{\rho^3} \right). \end{aligned} \quad (38)$$

It remains to evaluate the lateral-wave terms given by the third integral in each formula [Eqs. (26)–(28)].

The three terms to be evaluated are the following lateral-wave parts of the fields:

$$\begin{aligned} B_{10}^L(\rho, z) &= \frac{i\mu_0}{2\pi} F_{10}(\rho, z+d); \\ F_{10}(\rho, z+d) &= k_2^2 \int_0^\infty \frac{e^{\gamma_1 z} e^{-\gamma_2 z}}{k_1^2 \gamma_2 + k_2^2 \gamma_1} J_1(\lambda \rho) \lambda^2 d\lambda, \end{aligned} \quad (39)$$

$$\begin{aligned} E_{1\rho}^L(\rho, z) &= \frac{i\omega\mu_0}{2\pi k_1^2} F_{1\rho}(\rho, z+d); \\ F_{1\rho}(\rho, z+d) &= k_2^2 \int_0^\infty \frac{\gamma_1 e^{\gamma_1 z} e^{-\gamma_2 z}}{k_1^2 \gamma_2 + k_2^2 \gamma_1} J_1(\lambda \rho) \lambda^2 d\lambda, \end{aligned} \quad (40)$$

$$\begin{aligned} E_{1z}^L(\rho, z) &= -\frac{\omega\mu_0}{2\pi k_1^2} F_{1z}(\rho, z+d); \\ F_{1z}(\rho, z+d) &= k_2^2 \int_0^\infty \frac{e^{\gamma_1 z} e^{-\gamma_2 z}}{k_1^2 \gamma_2 + k_2^2 \gamma_1} J_0(\lambda \rho) \lambda^3 d\lambda. \end{aligned} \quad (41)$$

These integrals can be evaluated subject to the following approximation:

$$F_{1m}(\rho, z+d) = F_{1m}(\rho, 0) e^{ik_1 z + d}, \quad m = \phi, \rho, z. \quad (42)$$

This approximation depends on the fact that the lateral wave originates in the air above and travels vertically down as a plane wave into the denser Region 1 where it is known to advance as $e^{ik_1 z}$. The approximation has been verified for the six components of the field of the horizontal electric dipole

by direct comparison of the results obtained with Eq. (42) and by the numerical evaluation of the general integrals. The agreement is excellent over wide ranges of the electrical parameters, frequency, and radial distance. With Eq. (42), the integrals to be evaluated are

$$F_{10}(\rho, 0) = k_2^2 \int_0^\infty [k_1^2(k_2^2 - \lambda^2)^{1/2} + k_2^2(k_1^2 - \lambda^2)^{1/2}]^{-1} J_1(\lambda\rho) \lambda^2 d\lambda, \quad (43)$$

$$F_{1\rho}(\rho, 0) = k_2^2 \int_0^\infty [k_1^2(k_2^2 - \lambda^2)^{1/2} + k_2^2(k_1^2 - \lambda^2)^{1/2}]^{-1} (k_1^2 - \lambda^2)^{1/2} \times J_1(\lambda\rho) \lambda^2 d\lambda, \quad (44)$$

$$F_{1z}(\rho, 0) = k_2^2 \int_0^\infty [k_1^2(k_2^2 - \lambda^2)^{1/2} + k_2^2(k_1^2 - \lambda^2)^{1/2}]^{-1} J_0(\lambda\rho) \lambda^3 d\lambda. \quad (45)$$

These integrals all have the same denominator. With $k_1^2 \gg k_2^2$, the leading part of the integral is obtained with the denominator approximated by $k_1^{-2}(k_2^2 - \lambda^2)^{-1/2}$. It follows that it is conveniently and exactly written in the form $k_1^{-2}(k_2^2 - \lambda^2)^{-1/2} + \{ [k_1^2(k_2^2 - \lambda^2)^{1/2} + k_2^2(k_1^2 - \lambda^2)^{1/2}]^{-1} - k_1^{-2}(k_2^2 - \lambda^2)^{-1/2} \}$.

With this representation, the integrals [Eqs. (43)–(45)] can be expressed as follows:

$$F_{10}(\rho, 0) = \frac{k_2^2}{k_1^2} \int_0^\infty \frac{J_1(\lambda\rho)}{(k_2^2 - \lambda^2)^{1/2}} \lambda^2 d\lambda - G_0, \quad (46)$$

$$F_{1\rho}(\rho, 0) = \frac{k_2^2}{k_1^2} \int_0^\infty \left(\frac{k_1^2 - \lambda^2}{k_2^2 - \lambda^2} \right)^{1/2} J_1(\lambda\rho) \lambda^2 d\lambda - G_\rho, \quad (47)$$

$$F_{1z}(\rho, 0) = \frac{k_2^2}{k_1^2} \int_0^\infty \frac{J_0(\lambda\rho)}{(k_2^2 - \lambda^2)^{1/2}} \lambda^3 d\lambda - G_z. \quad (48)$$

The three integrals in Eqs. (46)–(48) are evaluated in Appendix A. The functions $G_k, k = 0, \rho, z$, are defined and evaluated in Appendix B. The results when substituted in Eqs. (46)–(48) and then in Eqs. (39)–(41) with Eq. (42) are

$$B_{10}^L(\rho, z) = -\frac{\mu_0 k_2^2}{2\pi k_1^2} e^{ik_1 z - d} e^{ik_2 \rho} \left[\frac{ik_2}{\rho} - \frac{1}{\rho^2} - \frac{k_2^3}{k_1} \left(\frac{\pi}{k_2 \rho} \right)^{1/2} e^{-ik_2 \rho k_1^2 / 2k_1^2} \mathcal{F} \right], \quad (49)$$

$$E_{1\rho}^L(\rho, z) = -\frac{\omega \mu_0 k_2^2}{2\pi k_1^3} e^{ik_1 z - d} \left\{ e^{ik_2 \rho} \left[\frac{ik_2}{\rho} - \frac{1}{\rho^2} - \frac{k_2^3}{k_1} \left(\frac{\pi}{k_2 \rho} \right)^{1/2} e^{-ik_2 \rho k_1^2 / 2k_1^2} \mathcal{F} \right] - \frac{ie^{ik_2 \rho}}{\rho^2} \right\}, \quad (50)$$

$$E_{1z}^L(\rho, z) = \frac{\omega \mu_0 k_2^2}{2\pi k_1^4} e^{ik_1 z - d} e^{ik_2 \rho} \left[\frac{ik_2}{\rho} - \frac{k_2}{\rho^2} - \frac{i}{\rho^3} - \frac{k_2^4}{k_1} \left(\frac{\pi}{k_2 \rho} \right)^{1/2} e^{-ik_2 \rho k_1^2 / 2k_1^2} \mathcal{F} \right]. \quad (51)$$

The last term, $-ie^{ik_2 \rho}/\rho^3$, in Eq. (50) actually is part of the direct field and not a lateral-wave term.

IV. COMPLETE FORMULAS FOR THE ELECTROMAGNETIC FIELD IN REGION 1 DUE TO A VERTICAL DIPOLE IN REGION 1

When the direct, reflected, and lateral-wave parts of the field are combined, the final complete formulas for the three components in Region 1 are

$$B_{10}(\rho, z) = -\frac{\mu_0}{2\pi} \left\{ \frac{k_2^2}{k_1^2} e^{ik_1 z - d} e^{ik_2 \rho} \left[\frac{ik_2}{\rho} - \frac{1}{\rho^2} - \frac{k_2^3}{k_1} \left(\frac{\pi}{k_2 \rho} \right)^{1/2} e^{-ik_2 \rho k_1^2 / 2k_1^2} \mathcal{F} \right] + \frac{1}{2} (e^{ik_2 \rho} - e^{ik_1 \rho}) \left(\frac{ik_1}{\rho} - \frac{1}{\rho^2} \right) \right\}, \quad (52)$$

$$E_{1\rho}(\rho, z) = -\frac{\omega \mu_0}{2\pi k_1^3} \left\{ \frac{k_2^2}{k_1^2} e^{ik_1 z - d} e^{ik_2 \rho} \left[\frac{ik_2}{\rho} - \frac{1}{\rho^2} - \frac{k_2^3}{k_1} \left(\frac{\pi}{k_2 \rho} \right)^{1/2} e^{-ik_2 \rho k_1^2 / 2k_1^2} \mathcal{F} \right] - \frac{ie^{ik_2 \rho}}{\rho^2} \right\} - \frac{1}{2} \left(\frac{z-d}{\rho} e^{ik_1 \rho} - \frac{z-d}{\rho} e^{ik_2 \rho} \right) \times \left(\frac{ik_2}{\rho} - \frac{3k_1}{\rho^2} - \frac{3i}{\rho^3} \right), \quad (53)$$

$$E_{1z}(\rho, z) = \frac{\omega \mu_0}{2\pi k_1^4} \left\{ \frac{k_2^2}{k_1^2} e^{ik_1 z - d} e^{ik_2 \rho} \left[\frac{ik_2}{\rho} - \frac{k_2}{\rho^2} - \frac{i}{\rho^3} - \frac{k_2^4}{k_1} \left(\frac{\pi}{k_2 \rho} \right)^{1/2} e^{-ik_2 \rho k_1^2 / 2k_1^2} \mathcal{F} \right] - \frac{1}{2} (e^{ik_2 \rho} - e^{ik_1 \rho}) \left(\frac{ik_1}{\rho} - \frac{k_1}{\rho^2} - \frac{i}{\rho^3} \right) \right\}, \quad (54)$$

where, with $C(u)$ and $S(u)$ Fresnel integrals,

$$\mathcal{F} = \frac{1}{2} - C \left[k_2 \rho k_1^2 / 2k_1^2 \right] - i \left[\frac{1}{2} - S \left[k_2 \rho k_1^2 / 2k_1^2 \right] \right], \quad (55)$$

The restrictions on Eqs. (52)–(54) are

$$k_1^2 \gg k_2^2; \quad k_2 \rho \gg 3; \quad \rho^2 \gg z^2; \quad \rho^2 \gg d^2. \quad (56)$$

Note that the restriction $k_2 \rho \gg 3$ can be removed if certain integrals are expressed in terms of Bessel functions instead of the much simpler exponentials. Note also that multiplication by k_2/k_1 yields $k_2 \rho \gg 3 k_2/k_1$, where k_2/k_1 is small. In fresh or salt water, $k_2/k_1 \leq 0.11$ so that $k_2 \rho \gg 3$ is equivalent to $k_2 \rho \gg 0.33$ or $\rho \gg 0.05 \lambda_2$. In other words, the formulas [Eqs. (52)–(54)] are good approximations continuously over the entire range included between radial distances extending from a small fraction of the wavelength λ_0 in air to infinity. It has been shown⁴⁻⁶ that the corresponding, similarly evaluated formulas for all six components of the electromagnetic field of a horizontal electric dipole are in close agreement with the general integrals. It may be assumed that the same is true of Eqs. (52)–(54).

It is interesting to note that the lateral-wave parts of the formulas [Eqs. (52)–(54)] [i.e., the parts multiplied by $\exp[ik_1(z+d)] \exp[ik_2 \rho]$] for the three components of the elec-

tromagnetic field in Region 1 are very much alike. Except for the added term i/ρ^3 in the formula for $E_{1z}(\rho, z)$, the first square brackets are the same. This means that at distances that satisfy $k_2\rho \gg 10$ where $k_1/\rho^2 \gg 1/\rho^3$, the amplitude and phase of all three components change with distance in the same manner. Quite near the dipole ($k_2\rho < 10$) $E_{1z}(\rho, z)$ behaves differently owing to the additional term i/ρ^3 .

It is interesting and significant to compare the field of the vertical dipole with the corresponding three components of the field of the horizontal electric dipole.⁵⁻⁷ Specifically, and in general, the lateral-wave parts satisfy the following relations exactly:

$$E_{1\rho h}^L(\rho, \phi, z) = [-(k_1^2/k_2^2)\cos\phi]E_{1z}^L(\rho, z), \quad (57)$$

$$E_{1z}^L(\rho, \phi, z) = [-\cos\phi]E_{1\rho v}^L(\rho, z), \quad (58)$$

where the subscripts h and v denote the horizontal and vertical dipoles and the superscript L refers to the lateral-wave part of the field only. Note that $E_{1z}^L(\rho, z)$ and, in the direction $\phi = 0$, $E_{1\rho h}^L(\rho, 0, z)$ are the axial components, respectively, of the vertical and horizontal dipoles. Similarly, $E_{1\rho v}^L(\rho, z)$ and $E_{1z}^L(\rho, \phi, z)$ are the components transverse to the axis of the dipole. When the i/ρ^3 term in the horizontal dipole it occurs in the formulas for $E_{1\rho v}$ and $B_{1\phi}$ is negligible, i.e., when $k_2\rho \gg 10$, it is possible to compare the components more directly since they then are all alike in form. In this case,

$$E_{1\rho h}^L(\rho, \phi, z) = [(k_1/k_2)\cos\phi]E_{1\rho v}^L(\rho, z), \quad (59)$$

$$E_{1z}^L(\rho, \phi, z) = [(k_1/k_2)\cos\phi]E_{1z}^L(\rho, z), \quad (60)$$

$$B_{1\phi}^L(\rho, \phi, z) = [(k_1/k_2)\cos\phi]B_{1\phi}^L(\rho, z). \quad (61)$$

In other words, except quite close to the dipoles, the lateral-wave fields of horizontal and vertical dipoles have the same radial variation with distance except that the field of the vertical dipole is rotationally symmetric; that of the horizontal dipole varies as $\cos\phi$. Most significantly, the field of the vertical dipole in Region 1 is smaller than that of the horizontal dipole in the direction $\phi = 0$ by the factor k_2/k_1 . These conclusions agree with those of Baños³ who found Eqs. (59)–(61) to be true of his approximate and discontinuous sets of quite different formulas for the intermediate and asymptotic ranges, but not for the near field.

The general integrals for the field in Region 2 (air), as given by Eqs. (29)–(31), have not been evaluated. However, with the boundary conditions, $B_{2\phi}(\rho, 0) = B_{1\phi}(\rho, 0)$, $E_{2\rho}(\rho, 0) = E_{1\rho}(\rho, 0)$, $k_2^2 E_{2z}(\rho, 0) = k_1^2 E_{1z}(\rho, 0)$, the entire field directly over the boundary surface is known. It is

$$B_{2\phi}(\rho, 0) = -\frac{\mu_0}{2\pi} \frac{k_2^2}{k_1^2} e^{ik_1 d} e^{ik_2 \rho} \left[\frac{ik_2}{\rho} - \frac{1}{\rho^2} - \frac{k_2^2}{k_1^2} \left(\frac{\pi}{k_2 \rho} \right)^{1/2} \right] \times e^{-ik_2 \rho k_2^2 / 2k_1^2} \mathcal{F}, \quad (62)$$

$$E_{2\rho}(\rho, 0) = -\frac{\omega\mu_0}{2\pi k_1^2} \left(\frac{k_2^2}{k_1^2} e^{ik_1 d} \left\{ e^{ik_2 \rho} \left[\frac{ik_2}{\rho} - \frac{1}{\rho^2} - \frac{k_2^2}{k_1^2} \left(\frac{\pi}{k_2 \rho} \right)^{1/2} \right] - \frac{ie^{ik_2 \rho}}{\rho^2} \right\} + e^{ik_1 \rho} + d^{1/2} \frac{d}{\rho} \left[\frac{ik_1^2}{\rho} - \frac{3k_1}{\rho^2} - \frac{3i}{\rho^3} \right] \right), \quad (63)$$

$$E_{2z}(\rho, 0) = \frac{\omega\mu_0}{2\pi k_1^2} e^{ik_1 d} e^{ik_2 \rho} \left[\frac{ik_2^2}{\rho} - \frac{k_2}{\rho^2} - \frac{i}{\rho^3} - \frac{k_2^2}{k_1^2} \left(\frac{\pi}{k_2 \rho} \right)^{1/2} e^{-ik_2 \rho k_2^2 / 2k_1^2} \mathcal{F} \right]. \quad (64)$$

The lateral-wave part of the field when $k_2\rho \gg 10$ has the form

$$E_{2z}^L(\rho, 0) = E_{2z}^L(\rho, 0) [\hat{z} - (k_2/k_1)\hat{\rho}].$$

This is an elliptically polarized field with a very small angle of tilt. With $(k_2^2/k_1^2) \ll 1$, the major axis of the ellipse is almost vertical and the minor axis is very small.

V. THE FIELD OF A VERTICAL DIPOLE ON THE BOUNDARY IN REGION 2 (AIR)

When the vertical dipole is in Region 2 on the boundary ($d = 0$), the electromagnetic field in Region 1 is given by Eqs. (29)–(31) with the subscripts 1 and 2 interchanged. $-z$ replaced by z , and $d = 0$. That is,

$$B_{1\phi}(\rho, z) = \frac{i\mu_0 k_1^2}{2\pi} \int_0^\infty \frac{e^{-\gamma z}}{k_1^2 \gamma_2 - k_2^2 \gamma_1} J_1(\lambda \rho) \gamma_1^2 d\lambda; \quad z \geq 0, \quad (65)$$

$$E_{1\rho}(\rho, z) = -\frac{i\omega\mu_0}{2\pi} \int_0^\infty \frac{\gamma_1 e^{-\gamma z}}{k_1^2 \gamma_2 - k_2^2 \gamma_1} J_1(\lambda \rho) \gamma_1^2 d\lambda; \quad z \geq 0, \quad (66)$$

$$E_{1z}(\rho, z) = -\frac{\omega\mu_0}{2\pi} \int_0^\infty \frac{e^{-\gamma z}}{k_1^2 \gamma_2 - k_2^2 \gamma_1} J_0(\lambda \rho) \gamma_1^2 d\lambda; \quad z \geq 0. \quad (67)$$

The integrals in these expressions are the same as those in Eqs. (39)–(41), when $d = 0$. It follows with Eqs. (49)–(51) that

$$B_{1\phi}(\rho, z) = -\frac{\mu_0}{2\pi} e^{ik_1 d} e^{ik_2 \rho} \left[\frac{ik_2}{\rho} - \frac{1}{\rho^2} - \frac{k_2^2}{k_1^2} \left(\frac{\pi}{k_2 \rho} \right)^{1/2} \right] \times e^{-ik_2 \rho k_2^2 / 2k_1^2} \mathcal{F}, \quad (68)$$

$$E_{1\rho}(\rho, z) = -\frac{\omega\mu_0}{2\pi k_1^2} \left\{ e^{ik_1 d} e^{ik_2 \rho} \left[\frac{ik_2}{\rho} - \frac{1}{\rho^2} - \frac{k_2^2}{k_1^2} \left(\frac{\pi}{k_2 \rho} \right)^{1/2} \right] \times e^{-ik_2 \rho k_2^2 / 2k_1^2} \mathcal{F} - \frac{ie^{ik_2 \rho}}{\rho^2} \right\}, \quad (69)$$

$$E_{1z}(\rho, z) = \frac{\omega\mu_0}{2\pi k_1^2} e^{ik_1 d} e^{ik_2 \rho} \left[\frac{ik_2^2}{\rho} - \frac{k_2}{\rho^2} - \frac{i}{\rho^3} - \frac{k_2^2}{k_1^2} \left(\frac{\pi}{k_2 \rho} \right)^{1/2} \right] \times e^{-ik_2 \rho k_2^2 / 2k_1^2} \mathcal{F}. \quad (70)$$

This is the field in Region 1 when a vertical dipole is located in Region 2 on the boundary surface, $d = 0$. It is seen to be greater than the corresponding lateral-wave field [Eqs. (49)–(51)] when the same dipole is in the denser Region 1 at $d = 0$ by the large factor $(k_1/k_2)^2$.

VI. CONCLUSION

Simple formulas for the electromagnetic field in a half-space Region 1 (earth, sea, lake) have been derived when the

source is a vertical electric dipole in the same region near its boundary with Region 2 (air) or on the boundary in Region 2. These complement corresponding formulas already available for the horizontal electric dipole.⁵⁻⁷ They continuously and accurately represent the general exact integrals over the full range of radial distance from a fraction of a wavelength from the source to infinity for all frequencies and electrical parameters that satisfy the conditions (56).

ACKNOWLEDGMENT

This research was supported in part by the Office of Naval Research under Contract N00014-79-C-0419 and in part by the Joint Services Electronics Program under Contract N00014-75-C-0648, both with Harvard University.

APPENDIX A: EVALUATION OF INTEGRALS

The first integral to be evaluated is

$$\int_0^\infty \frac{J_1(\lambda\rho)}{(k_2^2 - \lambda^2)^{1/2}} \lambda^2 d\lambda = -I_a(k_2) + k_2^2 I_b(k_2), \quad (\text{A1})$$

where

$$I_a(k_2) = \int_0^\infty (k_2^2 - \lambda^2)^{-1/2} J_1(\lambda\rho) d\lambda; \\ I_b(k_2) = \int_0^\infty (k_2^2 - \lambda^2)^{-1/2} J_1(\lambda\rho) d\lambda, \quad (\text{A2})$$

$$I_a(k_2) = -\frac{1}{\rho} \int_0^\infty (k_2^2 - \lambda^2)^{-1/2} \frac{\partial}{\partial \lambda} J_0(\lambda\rho) d\lambda \\ = \frac{k_2}{\rho} - \frac{1}{\rho} \int_0^\infty (k_2^2 - \lambda^2)^{-1/2} J_0(\lambda\rho) \lambda d\lambda. \quad (\text{A3})$$

With Bateman, Higher Transcendental Functions II, p. 95(52), the last integral integrates into $-(i/\rho)\exp(ik_2\rho)$ so that

$$I_a(k_2) = \frac{k_2}{\rho} + \frac{i}{\rho^2} e^{ik_2\rho}. \quad (\text{A4})$$

With $k_2 = i\beta$,

$$I_b(k_2) = -i \int_0^\infty (\lambda^2 + \beta^2)^{-1/2} J_1(\lambda\rho) d\lambda \\ = -i I_{1/2}(\beta\rho/2) K_{1/2}(\beta\rho/2), \quad (\text{A5})$$

where I and K are the modified Bessel functions. However, $I_{1/2}(z) = (2/\pi z)^{1/2} \sinh z$, $K_{1/2}(z) = (\pi/2z)^{1/2} e^{-z}$, so that $I_{1/2}(z)K_{1/2}(z) = (1/2z)(1 - e^{-2z})$ and

$$I_b(k_2) = (1/k_2\rho)(1 - e^{ik_2\rho}). \quad (\text{A6})$$

With Eqs. (A6) and (A4), Eq. (A1) becomes

$$\int_0^\infty \frac{J_1(\lambda\rho)}{(k_2^2 - \lambda^2)^{1/2}} \lambda^2 d\lambda \\ = -\frac{k_2}{\rho} - \frac{i}{\rho^2} e^{ik_2\rho} + \frac{k_2}{\rho} - \frac{k_2}{\rho} e^{ik_2\rho} \\ = -e^{ik_2\rho} \left(\frac{k_2}{\rho} + \frac{i}{\rho^2} \right). \quad (\text{A7})$$

The second integral occurs in the formulas for the field of a horizontal electric dipole. It is evaluated in Appendix C of Ref. 6. Subject to the restriction $k_1\rho \gg 3$, it has the follow-

ing simple form:

$$\int_0^\infty \left(\frac{k_1^2 - \lambda^2}{k_2^2 - \lambda^2} \right)^{1/2} J_1(\lambda\rho) \lambda^2 d\lambda \\ \sim k_1 \left[\frac{e^{ik_1\rho}}{\rho^2} - \left(\frac{k_2}{\rho} + \frac{i}{\rho^2} \right) e^{ik_2\rho} \right]. \quad (\text{A8})$$

The third integral is evaluated as follows:

$$\int_0^\infty \frac{J_0(\lambda\rho)}{(k_2^2 - \lambda^2)^{1/2}} \lambda^3 d\lambda \\ = \frac{1}{\rho} \int_0^\infty \frac{d}{d\lambda} [\lambda J_1(\lambda\rho)] \frac{\lambda^2 d\lambda}{(k_2^2 - \lambda^2)^{1/2}} \\ = -\frac{1}{\rho} \left\{ \int_0^\infty \frac{\lambda^2 J_1(\lambda\rho)}{(k_2^2 - \lambda^2)^{1/2}} d\lambda \right. \\ \left. + k_2^2 \int_0^\infty \frac{\lambda^2 J_1(\lambda\rho)}{(k_2^2 - \lambda^2)^{3/2}} d\lambda \right\}. \quad (\text{A9})$$

Here, the first integral is the same as that in (A1). The second integral is evaluated with $k_2 = i\beta$ and Eq. (2) on p. 434 of Watson's Bessel Functions with $\nu = 1, \mu = 1/2$. Specifically,

$$\int_0^\infty \frac{\lambda^2 J_1(\lambda\rho)}{(k_2^2 - \lambda^2)^{3/2}} d\lambda = i(2\beta\rho/\pi)^{1/2} K_{1/2}(\beta\rho) = ie^{ik_2\rho}. \quad (\text{A10})$$

With Eqs. (A7) and (A10) in Eq. (A9), the result is

$$\int_0^\infty \frac{J_0(\lambda\rho)}{(k_2^2 - \lambda^2)^{1/2}} \lambda^3 d\lambda = -\left(\frac{ik_2^2}{\rho} - \frac{k_2}{\rho^2} - \frac{i}{\rho^3} \right) e^{ik_2\rho}. \quad (\text{A11})$$

APPENDIX B: G FUNCTIONS

The three functions G_k , $k = \phi, \rho, z$, are defined as follows:

$$G_\phi(\rho) = k_2^2 \int_0^\infty \left[\frac{1}{k_1^2(k_2^2 - \lambda^2)^{1/2} + k_2^2(k_1^2 - \lambda^2)^{1/2}} \right. \\ \left. - \frac{1}{k_1^2(k_2^2 - \lambda^2)^{1/2}} \right] J_1(\lambda\rho) \lambda^2 d\lambda, \quad (\text{B1})$$

$$G_\rho(\rho) = k_2^2 \int_0^\infty \left[\frac{1}{k_1^2(k_2^2 - \lambda^2)^{1/2} + k_2^2(k_1^2 - \lambda^2)^{1/2}} \right. \\ \left. - \frac{1}{k_1^2(k_2^2 - \lambda^2)^{1/2}} \right] (k_1^2 - \lambda^2)^{1/2} J_1(\lambda\rho) \lambda^2 d\lambda, \quad (\text{B2})$$

$$G_z(\rho) = k_2^2 \int_0^\infty \left[\frac{1}{k_1^2(k_2^2 - \lambda^2)^{1/2} + k_2^2(k_1^2 - \lambda^2)^{1/2}} \right. \\ \left. - \frac{1}{k_1^2(k_2^2 - \lambda^2)^{1/2}} \right] J_0(\lambda\rho) \lambda^3 d\lambda. \quad (\text{B3})$$

They are closely related to the corresponding function $G(\rho)$ which occurs in the expression for the field of a horizontal electric dipole and is evaluated in Appendix B of Ref. 5. They will be evaluated in the same manner and with the same approximations.

It is evident that the significant contributions to the several integrals must come only when λ is near k_2 . This means that λ^2 can be neglected compared with k_1^2 since $|k_1^2| \gg |k_2^2|$. Let the variable of integration be changed from

λ to τ as follows:

$$\lambda = k_2(1 + m\tau), d\lambda = k_2 m d\tau, \quad (\text{B4})$$

where

$$m = k_2^2/2k_1^2 \ll 1, \quad (\text{B5})$$

and τ is a dimensionless variable of integration. It follows that

$$\lambda^2 \sim k_2^2(1 + 2m\tau); \quad \gamma_2 = (k_2^2 - \lambda^2)^{1/2} = (-2m\tau)^{1/2}k_2. \quad (\text{B6})$$

In phases, the representation of Eq. (B4) is used; in amplitudes, $\lambda \sim k_2$. For all but small arguments,

$$J_n(\lambda\rho) \sim \frac{1}{2} H_n^{(1)}(\lambda\rho) \sim (2\pi\lambda\rho)^{-1/2} e^{i[\lambda\rho - \frac{\pi}{2}(n+1)]}. \quad (\text{B7})$$

With Eqs. (B4)–(B7), the three quantities [Eqs. (B1)–(B3)] become

$$G_\delta(\rho) \sim k_2^2 \int_{-\infty}^{\infty} \left[\frac{1}{k_1^2 k_2(1 - 2m\tau)^{1/2} + k_2^2 k_1} - \frac{1}{k_1^2 k_2(1 - 2m\tau)^{1/2}} \right] \left(\frac{1}{2\pi k_2 \rho} \right)^{1/2} \times e^{i\lambda\rho - \frac{3\pi}{4} + i k_2 \rho m \tau} k_2^2 m d\tau. \quad (\text{B8})$$

Since $\lambda = 0$ corresponds to $\tau = -1/m$, a very large negative quantity, the lower limit can be made $-\infty$. Since $k_1^2 k_2(2m)^{1/2}/k_2^2 k_1 = 1$, Eq. (B8) can be written as

$$G_\delta(\rho) \sim -\frac{ik_2^5}{4k_1^3} \left(\frac{2}{\pi k_2 \rho} \right)^{1/2} e^{i\lambda\rho - \pi/4} H(k_2 \rho m), \quad (\text{B9})$$

where

$$H(k_2 \rho m) = \int_{-\infty}^{\infty} \left[\frac{1}{\sqrt{-\tau+1}} - \frac{1}{\sqrt{-\tau}} \right] e^{i\lambda\rho m \tau} d\tau. \quad (\text{B10})$$

From Eqs. (B2) and (B3), it follows that

$$G_\rho(\rho) \sim -\frac{ik_2^5}{4k_1^3} \left(\frac{2}{\pi k_2 \rho} \right)^{1/2} e^{i\lambda\rho - \pi/4} H(k_2 \rho m), \quad (\text{B11})$$

$$G_z(\rho) \sim \frac{k_2^6}{4k_1^3} \left(\frac{2}{\pi k_2 \rho} \right)^{1/2} e^{i\lambda\rho - \pi/4} H(k_2 \rho m), \quad (\text{B12})$$

with $H(k_2 \rho m)$ as defined in Eq. (B10). With considerable ma-

nipulation it can be shown that

$$H(k_2 \rho m) = 2\sqrt{\pi} e^{i\pi/4} e^{-ik_2 \rho(k_2^2/2k_1^2)} \int_{k_2 \rho m}^{\infty} t^{-1/2} e^{it} dt. \quad (\text{B13})$$

In the notation of Jahnke-Emde,¹⁰ the Fresnel integrals are defined as follows:

$$C(z) + iS(z) = \int_0^z \frac{e^{it}}{(2\pi t)^{1/2}} dt. \quad (\text{B14})$$

Hence, and with $C(\infty) = S(\infty) = 1/2$, Eq. (B13) has the following form:

$$H(k_2 \rho m) = 2\pi\sqrt{2} e^{i\pi/4} e^{-ik_2 \rho(k_2^2/2k_1^2)} \mathcal{F}, \quad (\text{B15})$$

where

$$\mathcal{F} = \frac{1}{2} - C[k_2 \rho(k_2^2/2k_1^2)] + i\left\{ \frac{1}{2} - S[k_2 \rho(k_2^2/2k_1^2)] \right\}. \quad (\text{B16})$$

With Eq. (B15) in Eqs. (B9), (B11), and (B12), the three G functions become

$$G_\delta(\rho) \sim -\frac{ik_2^5}{k_1^3} \left(\frac{\pi}{k_2 \rho} \right)^{1/2} e^{i\lambda\rho} e^{-ik_2 \rho(k_2^2/2k_1^2)} \mathcal{F}, \quad (\text{B17})$$

$$G_\rho(\rho) \sim -\frac{ik_2^5}{k_1^3} \left(\frac{\pi}{k_2 \rho} \right)^{1/2} e^{i\lambda\rho} e^{-ik_2 \rho(k_2^2/2k_1^2)} \mathcal{F}, \quad (\text{B18})$$

$$G_z(\rho) \sim \frac{k_2^6}{k_1^3} \left(\frac{\pi}{k_2 \rho} \right)^{1/2} e^{i\lambda\rho} e^{-ik_2 \rho(k_2^2/2k_1^2)} \mathcal{F}. \quad (\text{B19})$$

¹A. Sommerfeld, *Ann. Phys.* 28, 665 (1909).

²A. Sommerfeld, *Ann. Phys.* 81, 1135 (1926).

³A. Baños, Jr., *Dipole Radiation in the Presence of a Conducting Half-Space* (Pergamon, Oxford, England, 1966).

⁴J. R. Wait and L. L. Campbell, *J. Geophys. Res.* 58, 21 (1953).

⁵T. T. Wu and R. W. P. King, *Radio Sci.* 17, 521 (1982).

⁶T. T. Wu and R. W. P. King, *Radio Sci.* 17, 532 (1982).

⁷R. W. P. King and T. T. Wu (to be published).

⁸M. Brown, R. W. P. King, and T. T. Wu, *J. Appl. Phys.* 53, 3387 (1982).

⁹R. W. P. King and G. S. Smith, *Antennas in Matter* (MIT, Cambridge, Mass., 1981), Chap. 11.

¹⁰E. Jahnke and F. Emde, *Tables of Functions* (Dover, New York, 1945), p. 36.

Erratum: New formulas for the electromagnetic field of a vertical electric dipole in a dielectric or conducting half-space near its horizontal interface **[J. Appl. Phys. 53, 8476 (1982)]**

R. W. F. King

Gordon McKay Laboratory, Harvard University, Cambridge, Massachusetts 02138

A more accurate evaluation of the integrals involved in the terms with $\exp(ik_1\rho)$ in equations (50), (53), (63), and (69) shows that this exponential factor should be $\exp(ik_1r_2)$, where $r_2 = [(z+d)^2 + \rho^2]^{1/2}$. The corrected formulas are as follows:

$$E_{1\rho}^L(\rho, z) = \frac{-\omega\mu_0 k_2^2}{2\pi k_1^3} \left\{ e^{ik_1(z+d)} e^{ik_2\rho} \left[\frac{ik_2}{\rho} - \frac{1}{\rho^2} - \frac{k_2^3}{k_1} \left(\frac{\pi}{k_2\rho} \right)^{1/2} e^{-ik_2\rho(k_2^2/2k_1^2)} \mathcal{F} \right] - \frac{ie^{ik_1r_2}}{\rho^2} \right\}, \quad (50)$$

$$E_{1\rho}(\rho, z) = \frac{-\omega\mu_0}{2\pi k_1^2} \left(\frac{k_2^2}{k_1} \left\{ e^{ik_1(z+d)} e^{ik_2\rho} \left[\frac{ik_2}{\rho} - \frac{1}{\rho^2} - \frac{k_2^3}{k_1} \left(\frac{\pi}{k_2\rho} \right)^{1/2} e^{-ik_2\rho(k_2^2/2k_1^2)} \mathcal{F} \right] - \frac{ie^{ik_1r_2}}{\rho^2} \right\} - \frac{1}{2} \left(\frac{z-d}{\rho} e^{ik_1r_1} - \frac{z+d}{\rho} e^{ik_1r_2} \right) \left(\frac{ik_1^2}{\rho} - \frac{3k_1}{\rho^2} - \frac{3i}{\rho^3} \right) \right), \quad (53)$$

$$E_{2\rho}(\rho, 0) = \frac{-\omega\mu_0}{2\pi k_1^2} \left(\frac{k_2^2}{k_1} \left\{ e^{ik_1d} e^{ik_2\rho} \left[\frac{ik_2}{\rho} - \frac{1}{\rho^2} - \frac{k_2^3}{k_1} \left(\frac{\pi}{k_2\rho} \right)^{1/2} e^{-ik_2\rho(k_2^2/2k_1^2)} \mathcal{F} \right] - \frac{ie^{ik_1(\rho^2+d^2)^{1/2}}}{\rho^2} \right\} + e^{ik_1(\rho^2+d^2)^{1/2}} \frac{d}{\rho} \left(\frac{ik_1^2}{\rho} - \frac{3k_1}{\rho^2} - \frac{3i}{\rho^3} \right) \right), \quad (63)$$

and

$$E_{1\rho}(\rho, z) = \frac{-\omega\mu_0}{2\pi k_1} \left\{ e^{ik_1z} e^{ik_2\rho} \left[\frac{ik_2}{\rho} - \frac{1}{\rho^2} - \frac{k_2^3}{k_1} \left(\frac{\pi}{k_2\rho} \right)^{1/2} e^{-ik_2\rho(k_2^2/2k_1^2)} \mathcal{F} \right] - \frac{ie^{ik_1(\rho^2+z^2)^{1/2}}}{\rho^2} \right\}. \quad (69)$$

Also, the first sentence of Sec. V on p. 8480 should be amended to read "When the vertical dipole is in Region 2 on the boundary ($d = 0$), the electromagnetic field in Region 1 is given by Eqs. (29)–(31) with the subscripts 1 and 2 interchanged, $-z$ replaced by z , $I\Delta l = 1$ replaced by $I\Delta l = -1$, and $d = 0$."

Lateral-wave studies in a model lithosphere

M. F. Brown, R. W. P. King, and T. T. Wu

Gr don McKay Laboratory, Harvard University, Cambridge, Massachusetts 02138

(Received 29 October 1981; accepted for publication 1 February 1982)

An experimental basis is provided for the theoretical expressions associated with the E_p lateral-wave field due to a horizontal dipole in a conducting half-space of sea water. Both perturbed and unperturbed fields are studied in detail in a laboratory model of the lithosphere. It is found that rectilinear and wedge-shaped discontinuities at the air-water interface comprise effective perturbations of E_p , while submerged metallic cylinders do not. The effective perturbations, localized in their effect on the overall propagation of the lateral wave over several wavelengths, have geometries chosen to characterize the broad plateaus and mountains of a real lithosphere.

PACS numbers: 41.10.Hv

I. INTRODUCTION

The mathematical physics of the propagation of electromagnetic waves at the lithosphere-ocean interface is of particular relevance to geophysical exploration and subsurface communication. Modal analyses have shown that the fields involved are those associated with a general class of dipole excitation problems, in which the source dipole is located in or near an idealized planar boundary between two regions whose conductivities σ_1, σ_2 and permittivities ϵ_1, ϵ_2 may differ over a wide range.^{1,2}

The methods of the Sommerfeld solution^{3,4} for a dipole in air above the earth have been applied with some modification to infinitesimal electric or magnetic dipoles embedded horizontally in dissipative media. Since the definitive monograph of Baños⁵ appeared on this subject, three important refinements involving the electric field components may be noted. The radial electric field component in the dissipative medium ($E_{1\rho}$ component), which is the most useful for lateral-wave or "up-over-and-down" propagation (Fig. 1), has been numerically evaluated over wide ranges of distance,

frequency, and constitutive parameters.^{6,7} An insulated traveling-wave antenna suitable for subsurface communication has been designed⁸, an approximate formula for the general, exact integrals of $E_{1\rho}$ over a continuous range of the parameters has been reported.⁹

The refinements indicate that a proper choice of frequency, constitutive parameters, and antenna characteristics may be made in order to study lateral-wave propagation effectively by means of a lithosphere-ocean model in the laboratory. The purpose of the present paper is to provide an experimental basis for the theoretical $E_{1\rho}$ field associated with such a choice of values.

II. THE MODEL LITHOSPHERE

The model lithosphere of the present investigation is a logical extension of that used in earlier studies by Brown and Gangi¹⁰ and Iizuka,^{11,12} generalized to include a boundary of sea water. The boundary may be extended above the lithosphere layer by proper placement of a metal image plane. With such an extension, a planar slab of low conductivity

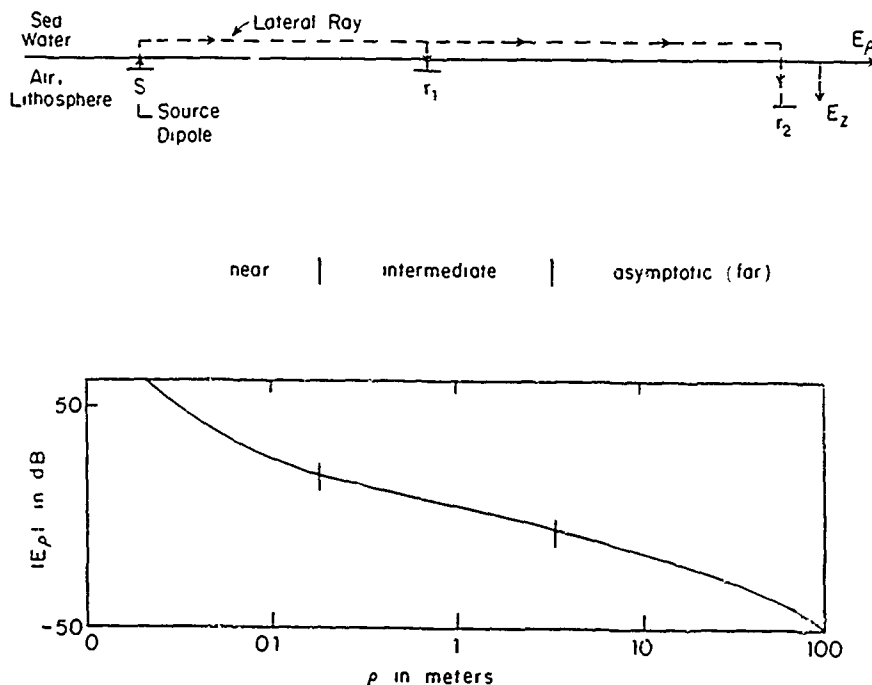
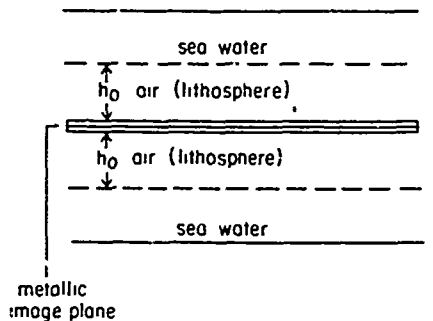
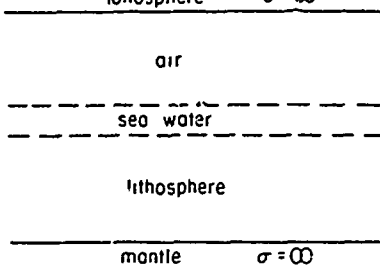


FIG 1. Lateral-wave transmission from source dipole S to receiving dipoles r_1 and r_2 (top), theoretical $|E_\rho|$ decay to 100 m (Wu's formula) in three field ranges (bottom). $f = 600$ MHz, $\epsilon_r = 60$, $\sigma = 4.15/\text{m}$, $z = d = 7$ mm

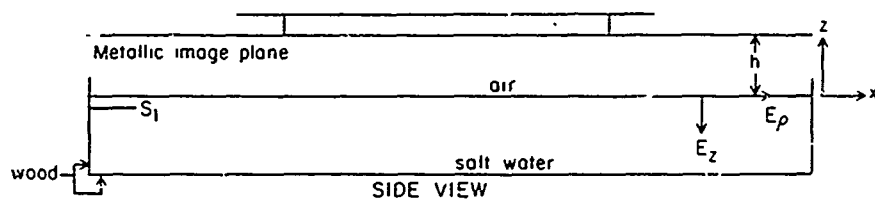


Experimental bounded model lithosphere

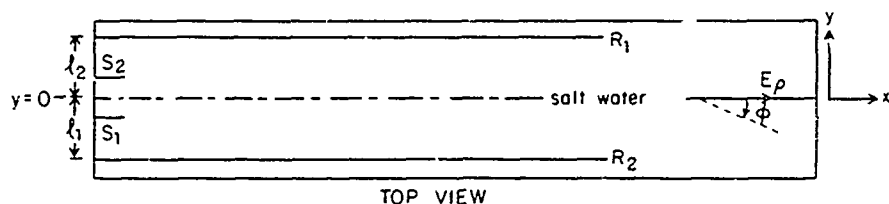


Frieman/Kroli model of the earth's crust [Ref 1]

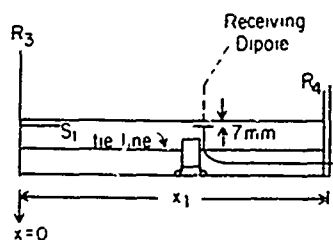
FIG 2. Model lithosphere (left) and idealized earth crust model (right). Interfaces of interest in present study shown in dashed line.



(a)



(b)



(c)

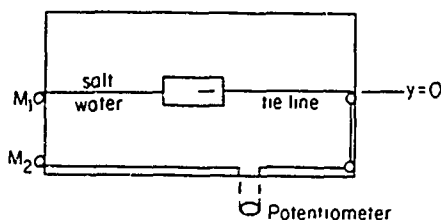
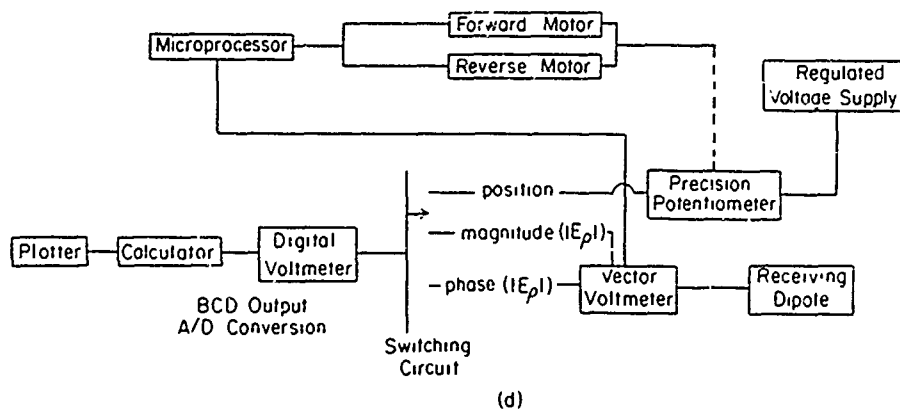


FIG 3. Experimental specifications for model lithosphere (a) Side view, with reflectors R_1 , R_2 of (b) removed. (b) Top view, with metallic image plane of (a) removed (c) Side and top views showing probe system. (d) Block diagram of electronics.



(d)

(air lithosphere, $\sigma \approx 10^{-6}$ S/m) separates two regions of high conductivity (salt water, $\sigma \approx 4$ S/m). The regions so formed may be compared with the idealized model of the earth's crust of Frieman and Kroll (Fig. 2).

The following experimental specifications are detailed in Fig. 3. The vertical, lithosphere embedded dipole of the earlier studies is replaced with a pair of horizontal traveling wave antennas located in salt water at 7 mm below the air-water interface. The specific properties and design of the antenna are discussed in Sec. III; designation is as S_1 and S_2 in Fig. 3. The bounds on the model lithosphere are indicated in Figs. 3(a) and 3(b). A metal image plane extends, at a vertical distance h in air, over a half-space of salt water formed by a rectangular enclosure ($3.66\text{m} \times 2.43\text{m} \times 30.5\text{cm}$). Dissolution of laboratory-grade NaCl (≈ 125 lb) in water brings the conductivity of the dissipative half-space to approximately 4 S/m. The precise values of the constitutive parameters of the half-space have been measured periodically using the method of Smith¹³ and an insulated microwave loop antenna specially designed at Harvard. The rectangular enclosure shown in the top view of Fig. 3(b) is fashioned of plywood with an insulating plastic liner; the 30.5-cm depth is effectively one of infinity at the frequency ($f = 600$ MHz) at which measurements are made. The planar metal boundaries R_1 - R_4 which lie along the x and y directions of the figure serve to image S_1 and S_2 transversely and longitudinally. In this way the size of the tank is effectively expanded. More importantly, R_1 and R_2 may be adjusted to favor the pure lateral-wave mode and suppress extraneous modes. Such modes originate from reflections involving the sides of the rectangular enclosure, in particular those due to the ϕ component of the field set up by S_1 and S_2 . Reflections from R_4 are less important due to the distance of R_4 from the antennas; adjustment of R_4 serves merely to shift the phase of the longitudinal standing wave.

Phase and amplitude measurements of E_p are made using the receiving dipole of Fig. 3(c) with a vector voltmeter.

The dipole, adjustable from 0 to 1 cm below the air-water interface, sits atop a plastic wheeled carriage. The submerged carriage is guided along a track at the floor of the dissipative half-space; the track follows symmetrically the axis $y = 0$. The carriage is mobilized by two synchronous motors lying behind R_3 . A nylon tie line rotates a plastic circular wheel fitted to a 10-turn, precision potentiometer to measure units of regulated voltage-distance⁻¹; the distance is incremented through control of motor revolutions by a microprocessor, which may also be programmed to switch sensitivity scales on the vector voltmeter. The electronics used in data acquisition, including an analog-to-digital conversion stage, is shown in the block diagram in Fig. 3(d).

Coaxial lines from S_1 and S_2 , precisely equal in length, are joined in a T-adaptor to a single signal line which is continuous with the output of a rf power source (Applied Microwave C201). A single-stub tuner may be used between the T-adaptor and S_1 or S_2 to correct phase differences between the two sources. A directional coupler/attenuator arrangement reduces to less than 1.4 the voltage standing-wave ratio of power reflected from S_1 and S_2 back to the rf source for protection of its output circuitry.

The operating frequency is $f = 600$ MHz which provides approximately six air wavelengths along $y = 0$, a power level of 20 W results in a -10 to -70 dB mW spread in the magnitude of the signal at the receiving dipole. With the existing choice of constitutive parameter $\sigma \approx 3.5$ S/m, the air wavelength $\lambda_a = 50.0$ cm, the water wavelength $\lambda_w \approx 6.9$ cm.

III. INSULATED TRAVELING-WAVE ANTENNA IN A SALT WATER MEDIUM

The general design criteria for the traveling-wave sub-surface-communication antenna have been formerly outlined.^{8,14} Such antennas are necessarily insulated from the surrounding conductive medium; the current characteristic

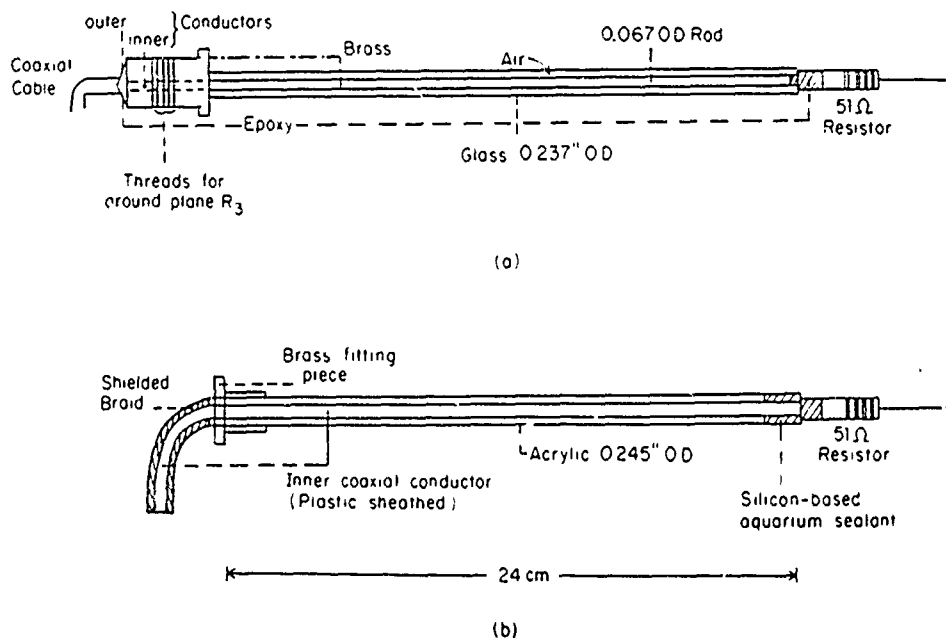


FIG. 4 (a) Glass prototype traveling-wave antenna for salt water (b) Continuously enclosed plastic version.

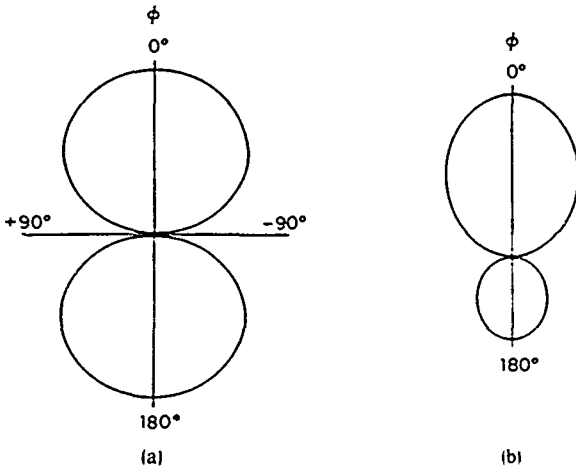


FIG. 5. Field patterns of traveling-wave antennas in dissipative medium. (a) Single element. (b) Two-element array

of a bare metal dipole attenuates rapidly when embedded in a highly conducting earth or salt water. The equivalence of the two-layered eccentrically insulated antenna with a lossy transmission line has been demonstrated¹⁵; the traveling wave is generated through placement of a resistor at a distance of approximately $\lambda_G/4$ from each end, where $\lambda_G = 2\pi k_L^{-1}$ for current of complex wave number k_L . (In the presence of the conducting image plane at $x = 0$ of Fig. 3, the antenna is fed coaxially from the end, and only one resistive termination is required.)

A glass prototype antenna designed for lateral-wave studies [Fig. 4(a)] was of limited usefulness due to thermal disruption of the epoxy-glass bond; more resilient materials were chosen to prevent infiltration of salt water. The design proven most effective utilizes a plastic enclosure which extends above the surface of the air-water interface. The seals are minimized and, where necessary, a silicon-based material of the type used for salt water aquaria has replaced the epoxy of the original design [Fig. 4(b)].

Placement of two traveling-wave antennas [designed as in Fig. 4(b)] is symmetric with respect to the central axis of the tank $y = 0$ of Fig. 3, along which measurements of E_ρ are made. Directivity of the field pattern associated with the linear broadside array so formed increases with the number of radiating broadside elements, although the two-element array is sufficiently directive for lateral-wave measurements of E_ρ . The field pattern associated with the array is shown in Fig. 5.

IV. LATERAL-WAVE FIELD IN THE ABSENCE OF OBSTACLES

The field components due to an infinitesimal horizontal dipole of unit moment ($I_x \Delta x = 1$) near a planar interface may be written in terms of the coordinates and constitutive parameters associated with the half-spaces of Fig. 6. The half-spaces are of infinite extent in each of the three coordinate directions; the air-water interface comprises the only boundary. The existing theoretical expressions for the components are of two types (hereafter designated I and II). Both types are motivated by the need for a simple, accurate formula for $E_{1\rho}$, the most important component. The general integral expression for $E_{1\rho}$ (discussed in detail in Ref. 14, p. 617) implicitly contains the interesting and complicated aspects of the field, but little physical insight is provided by inspection:

$$E_{1\rho} = \frac{-\omega\mu_0}{4\pi k_1^2} \cos \phi \left(\int_0^\infty \lambda d\lambda \{ k_1^2 J_0(\lambda\rho) - \left(\frac{\lambda^2}{2} \right) [J_0(\lambda\rho) - J_2(\lambda\rho)] \} \gamma_1^{-1} \exp(i\gamma_1|z-d|) \right. \\ \left. + \int_0^\infty \lambda d\lambda \{ (\gamma_1 Q/2) [J_0(\lambda\rho) - J_2(\lambda\rho)] - (k_1^2 P/2\gamma_1) [J_0(\lambda\rho) + J_2(\lambda\rho)] \} \exp(i\gamma_1(z+d)) \right), \quad (1)$$

where

$$P = (\gamma_2 - \gamma_1)(\gamma_2 + \gamma_1)^{-1}; \\ Q = (\bar{\epsilon}_1\gamma_2 - \bar{\epsilon}_2\gamma_1)(\bar{\epsilon}_1\gamma_2 + \bar{\epsilon}_2\gamma_1)^{-1},$$

and

$$\mu_1 = \mu_2 = \mu_0; \quad \gamma_i = (k_i^2 - \lambda^2)^{1/2}, \quad i = 1, 2.$$

The formulas of Type I, the Baños relations, are approximations of the Sommerfeld integrals over limited ranges of the parameters,⁵ and comprise a set of approximate formulas partitioned into three nonoverlapping distance domains:

Near Field:

$$E_{1\rho} = \frac{i\omega\mu_0}{2\pi k_1^2} \frac{\cos \phi}{\rho^3} \exp\{i[k_2\rho + k_1(d+z)]\}, \quad (2a)$$

Intermediate Field:

$$E_{1\rho} = - \frac{i\omega\mu_0 k_2^2}{2\pi k_1^2} \frac{\cos \phi}{\rho} \\ \times \left[1 + i \left(\frac{k_2}{k_1} \right) (i\pi k_2\rho/2)^{1/2} \right] \\ \times \exp\{i[k_2\rho + k_1(d+z)]\}, \quad (2b)$$

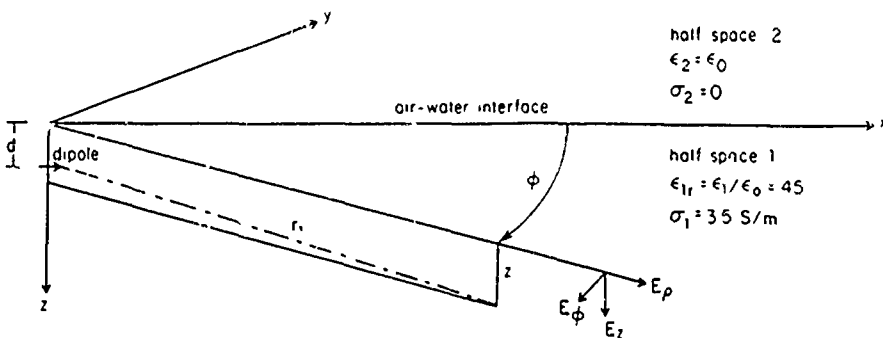


FIG. 6. Field components due to Hertzian dipole of unit moment $I_x \Delta x = 1$ near a planar interface.

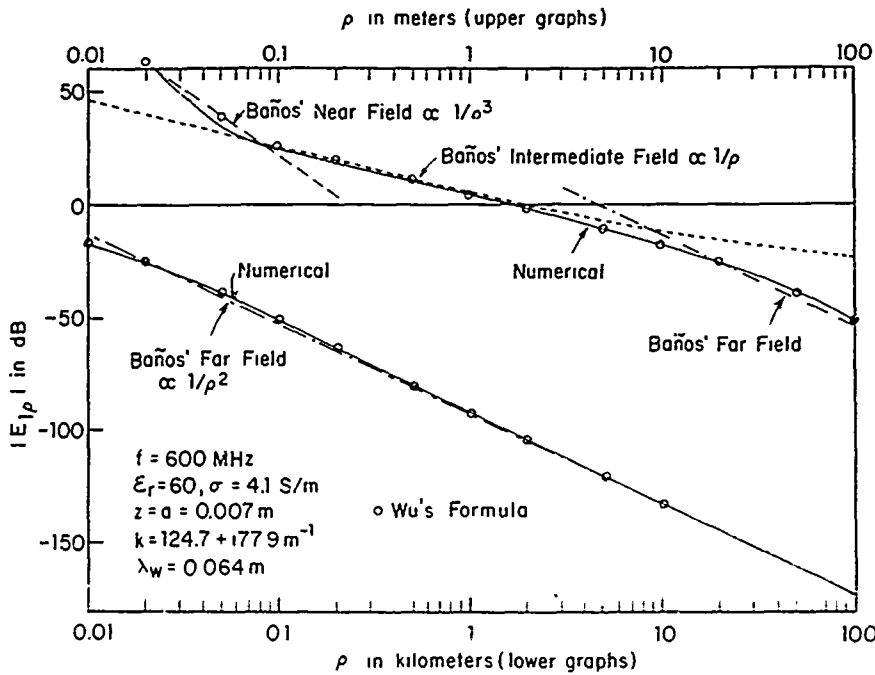


FIG. 7. Theoretical $E_{1\rho}$ for lateral wave along sea water-air boundary.

Asymptotic Field:

$$E_{1\rho} \doteq \frac{\omega\mu_0}{2\pi k_2} \frac{\cos\phi}{\rho^2} \exp\{i[k_2\rho + k_1(d+z)]\}. \quad (2c)$$

The usefulness of the Baños relations for $E_{1\rho}$ lies in the general physical meaning abstracted from the expression:

$$E_{1\rho} \sim a_0 \cos\phi F(\rho) \exp\{i[k_2\rho + k_1(d+z)]\},$$

where $a_0 = a_0(k_1, k_2)$ is an amplitude function of wave numbers, and $F(\rho) \sim \rho^{-3}$ for the near field, $F(\rho) \sim \rho^{-1}$ for the intermediate field, and $F(\rho) \sim \rho^{-2}$ for the far field, the chief limitation arises from the disconnected picture provided for $E_{1\rho}$ over its entire range. This limitation, readily apparent in

the theoretical calculations which counterpart the experimental results of the present investigation, is a pervasive one. The near-intermediate zone juncture is not explicitly expressed in the Type I formulas; the complicated nature of the field crucial to scattering and effects of finiteness in the model lithosphere are not presented in a continuous field relation.

The formula of Type II, the Wu relation, is unpartitioned into separate distance regions.⁹ The derivation of the Wu formula from the general exact integrals for $E_{1\rho}$ in Eq. (1) above is subject to two approximations: $|k_1^2| \gg |k_2^2|$ and $\rho^2 \gg z^2$, $\rho^2 \gg d^2$. Their significance is discussed elsewhere.⁹ Wu's expression for $E_{1\rho}$ is

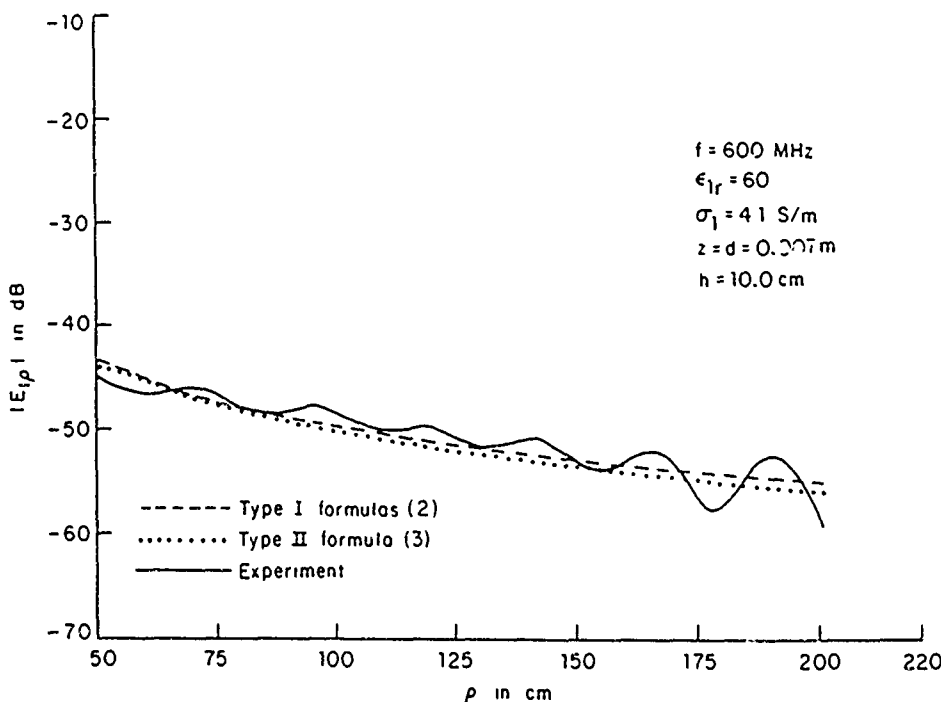


FIG. 8 Comparison of theoretical and experimental values of $E_{1\rho}$ in obstacle placement region $\rho > \lambda_a = 50.0$ cm.

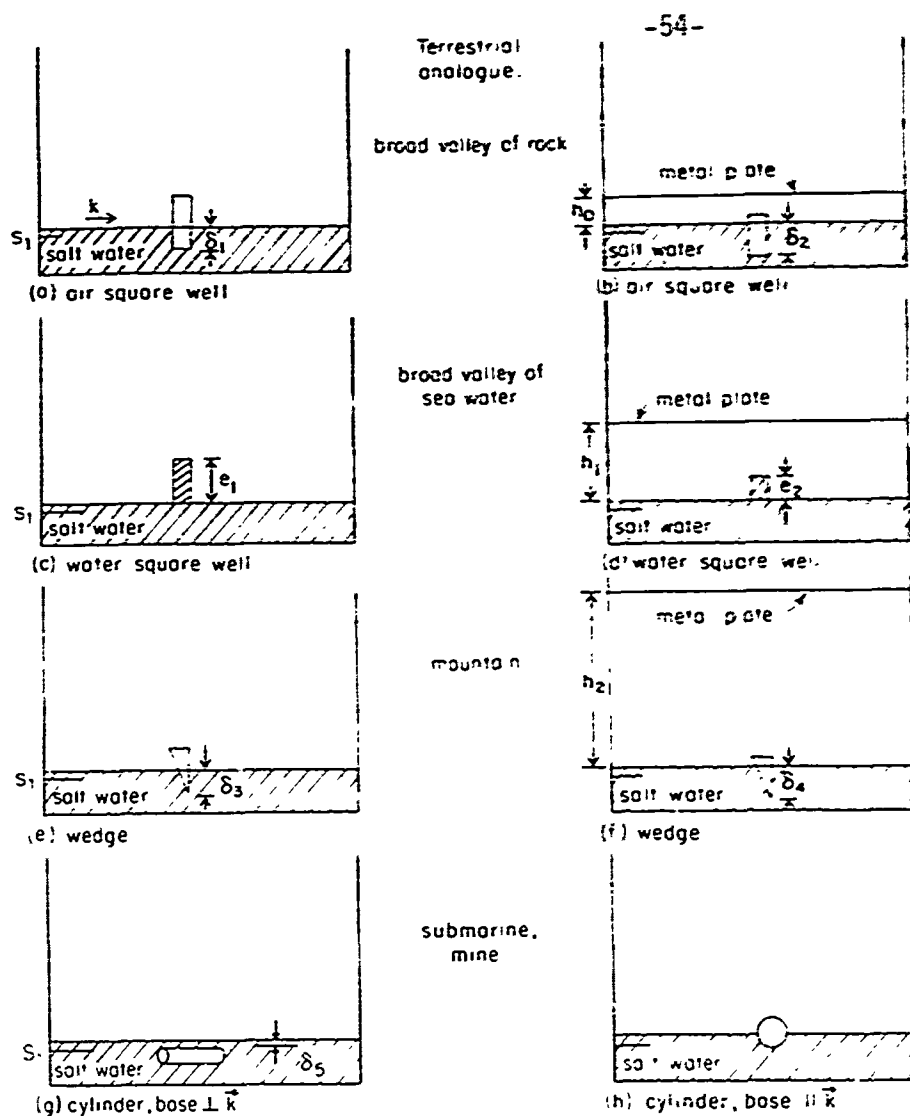


FIG. 9. Obstacle types and placement at depths δ or elevations e , for three image plate heights h .

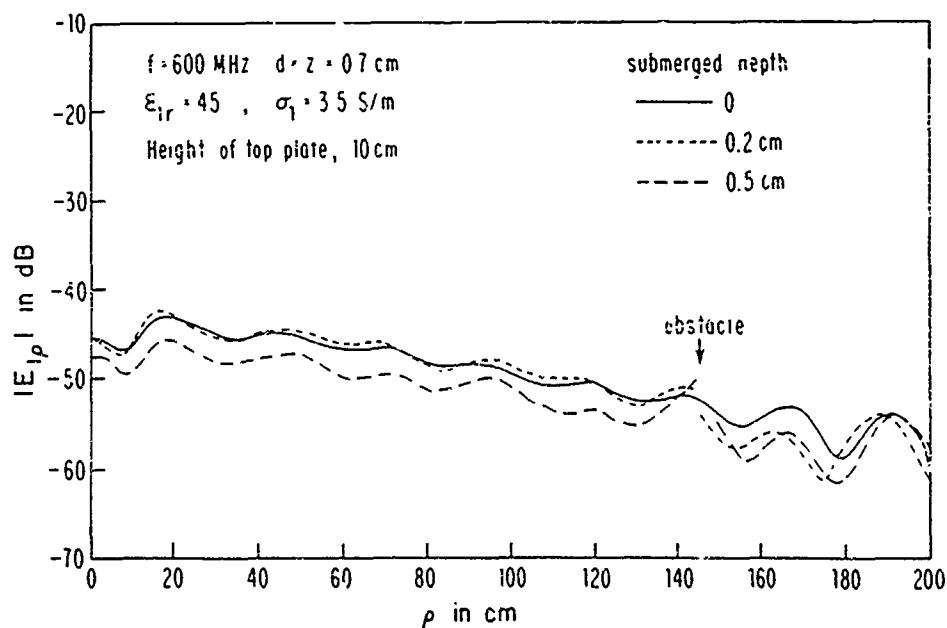


FIG. 10. Effect of rectangular depression in surface of water on $|E_{\rho}|$. Size of obstacle is $30.5 \text{ cm} \times 2 \text{ cm} \times$ submerged depth.

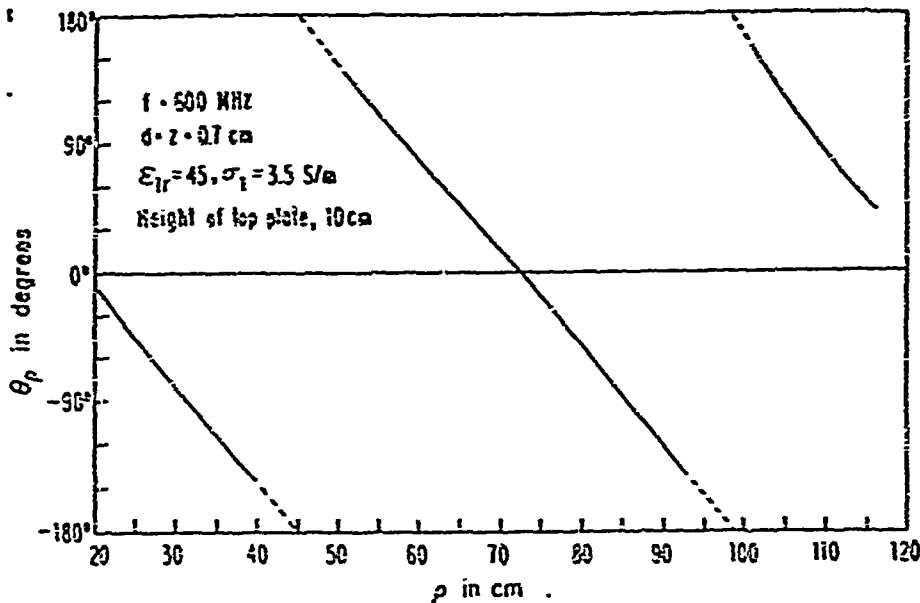


FIG. 11. Phase of E_p with smooth surface.

$$E_{ip} = -\frac{\omega\mu_0}{2\pi k_1^2} \cos \phi \left\{ \exp[ik_1(z+d)] \exp[ik_2\rho] \times \left[\frac{ik_2^2}{\rho} - \frac{k_2}{\rho^2} - \frac{i}{\rho^3} - \frac{k_2^4}{k_1} \left(\frac{\pi}{k_2\rho} \right)^{1/2} \right] \times \exp[-ik_2\rho(k_2^2/2k_1^2)] \right\} \mathcal{F} - \exp[ik_1(\rho^2 + (z-d)^2)^{1/2}] \left(\frac{k_1}{\rho^2} + \frac{i}{\rho^3} \right) \right\}, \quad (3)$$

where \mathcal{F} is given in terms of Fresnel integrals C and S as

$$\mathcal{F} = \frac{1}{2} - C[k_2\rho(k_2^2/2k_1^2)] + i\left\{ \frac{1}{2} - S[k_2\rho(k_2^2/2k_1^2)] \right\}$$

The Type I expressions (2), numerical evaluations of the general integral formula (1), and the above relation (3), designated Wu's formula, are compared in Fig. 7.

The model lithosphere of Sec. II forms a pair of half-spaces bounded in each of three coordinate directions. Thus, interest is in the field E'_{ip} of the model lithosphere of finite extent, in its relation to the E_{ip} given by (2) and (3). In particular, of primary importance are those conditions for which $|E_{ip} - E'_{ip}|$ is small. E'_{ip} is influenced by the parameters h, l_1, l_2, x_1 of Sec. II (Fig. 3) and the relation they bear to λ_a , the air wavelength. The $1/\rho$ decay predicted by (2) and (3) for the intermediate zone of the field is approximated very closely by laboratory measurements for $h \ll \lambda_a$. For h small, the other three parameters do not figure significantly in the decay rate as measured along the central axis $y = 0$ of Fig. 3, although some changes in the phase of the field are elicited. Comparison of measured and theoretically predicted fields is in Fig. 8.

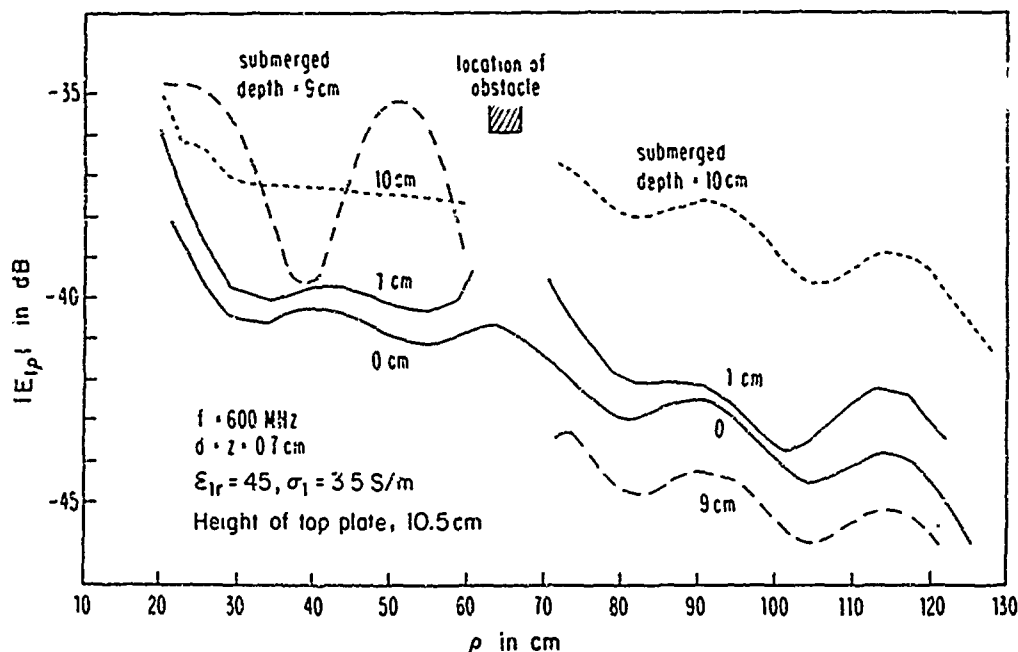


FIG. 12. Effect of rectangular depression in surface of water on $|E_p|$. Size of obstacle is 60 cm \times 4 cm \times submerged depth.

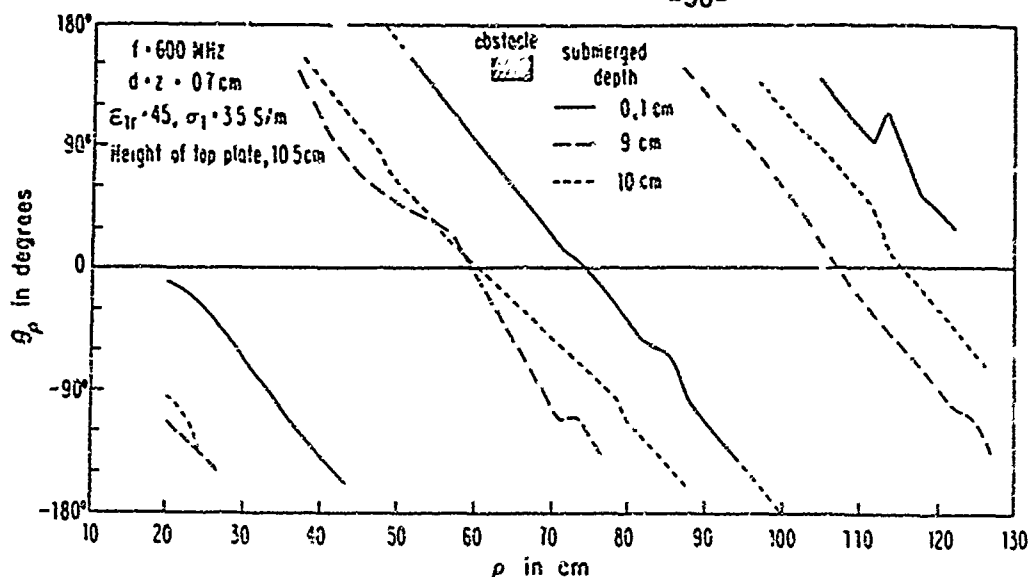


FIG. 13. Effect of rectangular depression in surface of water on phase of $E_{1\rho}$. Size of obstacle is 60 cm \times 4 cm \times submerged depth.

V. LATERAL-WAVE FIELD IN THE PRESENCE OF OBSTACLES

The types of obstacles studied and the discontinuities in conductivity which they model are shown in Fig. 9. Placement of the obstacles is symmetric about the central axis $y = 0$ of the rectangular enclosure of Fig. 3. The use of styrofoam ($\epsilon \approx 1.05$) is instrumental in the modeling of air-water discontinuities, the air square wells of Fig. 9 are formed from machined styrofoam sheets, while the water wells are styrofoam-enclosed casings of salt water. Metal cylinders, both

vertical and horizontal, are of brass.

The first set of scattering data was obtained with only a small perturbation in the path of the lateral wave. The unperturbed $E_{1\rho}$ reference field is given as a function of axial distance in the solid curve in Fig. 10. The corresponding phase curve is shown in Fig. 11. The phase is nearly linear, indicative of an almost pure traveling wave. A sheet of thickness 2.0 cm, comprising a rectangular air well, was placed with its length transverse to the radial propagation vector k . The ability of the lateral wave to propagate across the well is apparent from Fig. 10, where the dotted and dashed curves

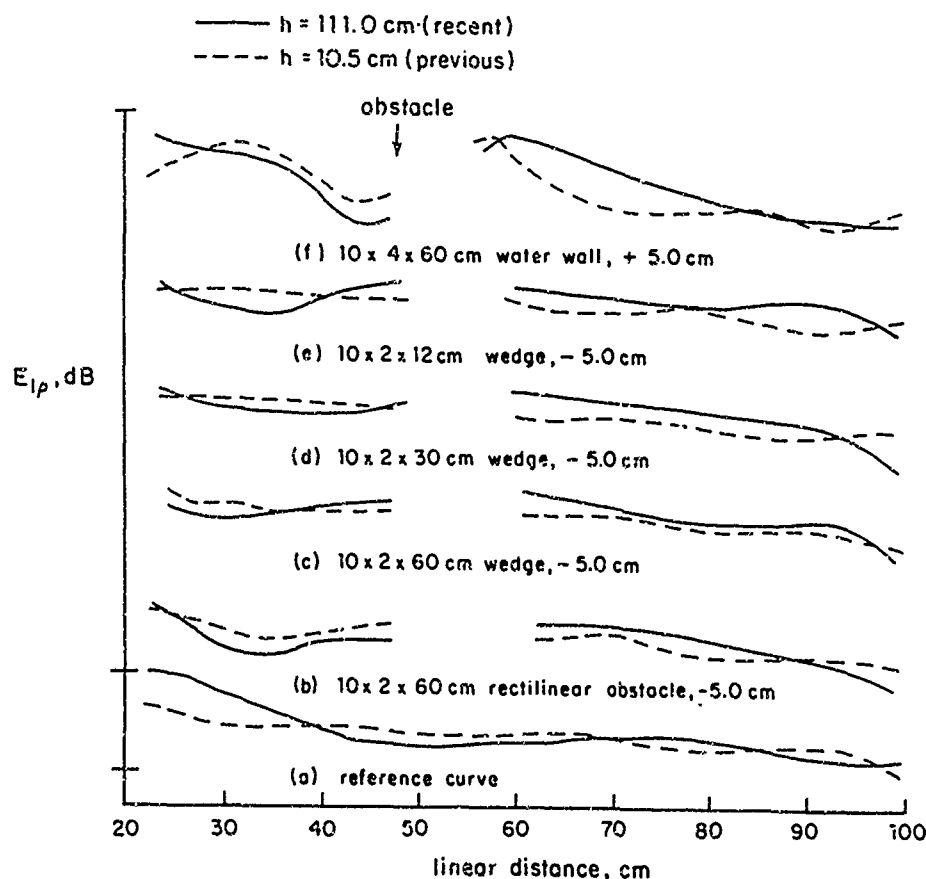


FIG. 14. Measured $|E_{1\rho}|$ reference curves and obstacle perturbations. Vertical $E_{1\rho}$ scale of -10 dB per unit length indicated applies to each curve.

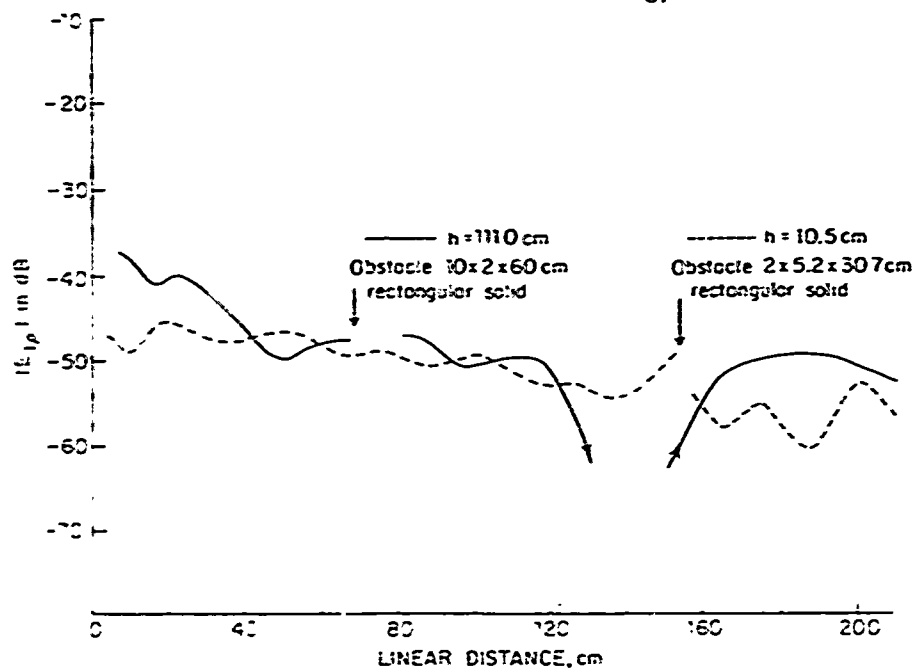


FIG. 15. Fields far from the scatterer.

signify submerged depths of 0.2 and 0.5 cm, respectively.

Measurements on deeper, thicker rectangular wells were made, data were developed from the scattering due to $40 \times 4 \times \delta$ -cm and $60 \times 4 \times \delta$ -cm wells, where δ , the submer-
sion depth of Fig. 9, ranged to 10 cm. The effects of the larger
discontinuities 40- and 60-cm transverse widths $\geq \lambda_z$, are

shown in Figs. 12 and 13 for submerged depths of 0 (unper-
turbed surface), 1, 9, and 10 cm. Several qualitative aspects
of the results are to be noted. Significant reflection occurs in
front of the obstacles, as evidenced by the strong standing
wave apparent in the 9-cm submersion, E_{1p} curve. The fully
submerged well, $\delta = 10$ cm, shows a dramatic change in

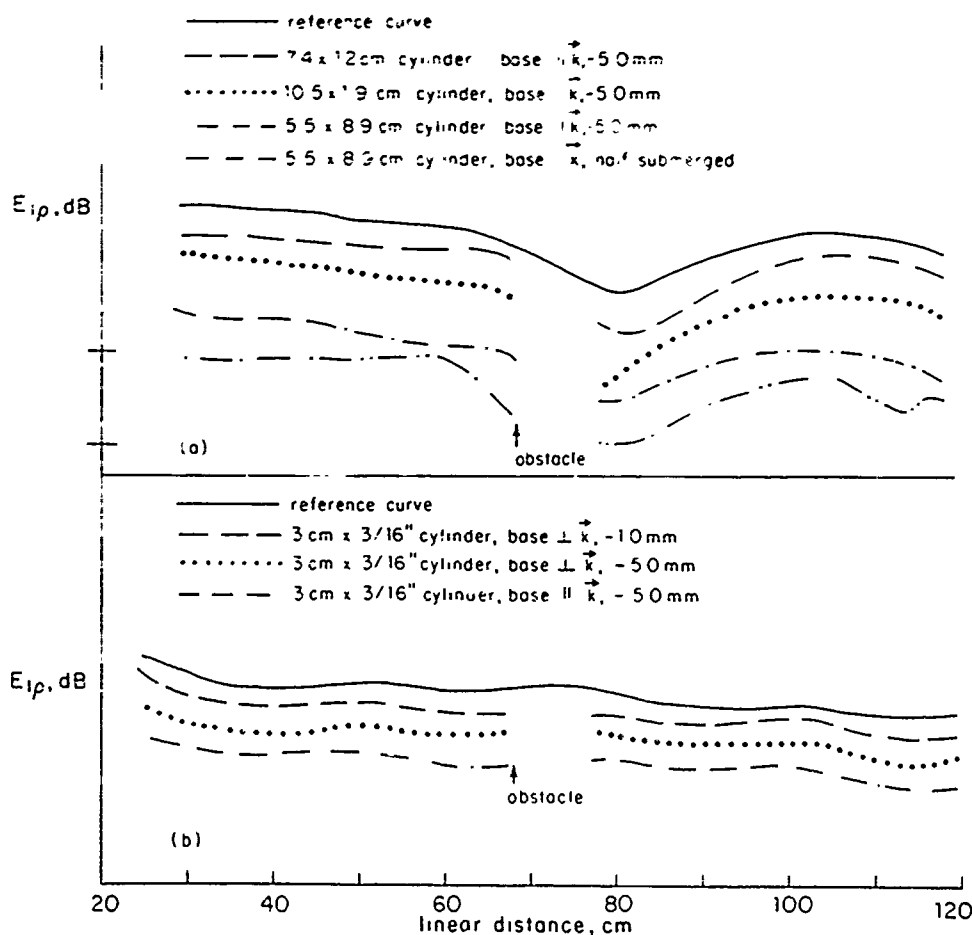


FIG. 16 Scattering from metallic cylinders. (a) $h = 252.0$ cm. (b) $h = 10.5$ cm. Vertical E_{1p} scale of -10 dB per unit length indicated applies to each curve.

field pattern from the 9-cm depth, insofar as no standing wave appears in front of it, while the propagating amplitude is, if anything, increased above the expected value. Of significance to propagation in a real lithosphere is the fact that, in all cases, the qualitative features of the incident wave are preserved downfield from the obstacle. The structure of the wave is affected only locally, within $x \approx \pm \lambda_o/2$.

Scattering by water wells and by obstacles whose shape is more characteristic of mountains, given respectively by the geometries shown in Figs. 9(c), 9(d), and in Figs. 9(e), 9(f), has been studied. In the discussion of these results a comparison is first made of data recorded at two plate separations, $h = 10.5$ cm and $h = 111.0$ cm; although close approximation of the unperturbed E_{1p} field as defined by (2) and (3) is strictly maintained for $h \ll \lambda_o$, similarly smooth curves ($h > \lambda_o$) suitable for scattering may be used. In Fig. 14 the perturbation of E_{1p} is illustrated only in the "near region" of the scatterer, i.e., at distances $x \approx \pm \lambda_o$. An important question to be addressed is whether or not the lateral wave is strongly attenuated in intensity further from the scatterer. Figure 15, in which x is scaled to 2.0 m or four wavelengths, suggests that such a reduction does not occur. The earlier data with $h = 10.5$ cm show that the incident field is not influenced strongly at distances to the left of the obstacle, which in this case was a $2 \times 5.2 \times 30.7$ -cm styro-foam rectangular solid. For the recent measurements with $h = 111.0$ cm, the obstacle was $10 \times 2 \times 60$ cm, its position shifted to the left. Downfield from the obstacle the curve goes through a minimum below -70 dB but returns at $x \approx 170$ cm to a dB level analogous to that predicted theoretically for an unbounded, unperturbed propagating lateral wave at 170 cm from its source. The minimum is due to configurational aspects of the experiment, in particular those of the upper plate, and is inherent in the reference curve for $h = 111.0$ cm. The mapping of such effects, which are most pronounced for $h \approx \lambda_o$, is too detailed and complex to warrant inclusion in this paper.

Metallic cylinders hung from nylon thread have been used as scattering objects when placed both perpendicular and parallel to the propagation vector. The overall dimensions of the objects ranged from less than λ_w to several multiples of λ_w . The results with $h = 252.0$ cm and $h = 10.5$ cm are compared in Fig. 16. In every instance, the scattering by completely submerged cylinders was too weak to provide an observable scattering pattern; partial submersion of the largest pieces resulted in a reflected and transmitted wave pattern characteristic of the inverted shallow water well [water "wall" of Figs. 9(d) and 14(f).]

VI. CONCLUSION

The decay rate predicted by existing theoretical expressions for the E_{1p} lateral-wave field due to a horizontal dipole is given an experimental basis in a model lithosphere. The measured field, under suitable configurational conditions on the lithosphere's bounding surfaces, follows the calculated field closely. Even so, curves which decay less smoothly owing to the effects of finiteness in the model lithosphere may be used for inferences regarding the fields incident upon and scattered from the various obstacles outlined in Sec. V. The incident lateral wave is only locally altered in magnitude and phase by even quite large irregularities at the air-water boundary. This localization of effects to the vicinity of the scatterer is of fundamental importance to propagation studies of the wave in a real lithosphere.

ACKNOWLEDGMENT

The advice and cooperation of Dr. L. C. Shen and Dr. J. T. deBettencourt are gratefully acknowledged. This research was supported in part by the Office of Naval Research under Contract N00014-79-C-0419 and in part by the Joint Services Electronics Program under Contract N00014-75-C-0648, both with Harvard University.

- ¹E. A. Frieman and N. M. Kroll, Tech. Rep. JASON, JSR-73-5 (Stanford Res. Inst., Menlo Park, California, 1973).
- ²J. R. Wait, *Radio Sci.* 1, 913 (1966).
- ³A. Sommerfeld, *Ann. Phys. (Leipzig)* 28, 665 (1909).
- ⁴A. Sommerfeld, *Ann. Phys. (Leipzig)* 81, 1135 (1926).
- ⁵A. Baños, Jr., *Dipole Radiation in the Presence of a Conducting Half-Space* (Pergamon, Oxford, England, 1966).
- ⁶R. W. P. King, J. T. deBettencourt, and B. H. Sandler, *IEEE Trans. Geosci. Electron.* GE-17, 86 (1979).
- ⁷R. W. P. King, B. H. Sandler, and L. C. Shen, *IEEE Trans. Geosci. Remote Sensing* GE-18, 225 (1980).
- ⁸L. C. Shen and R. W. P. King, *Proc. Inst. Electr. Eng.* 126, 793 (1979).
- ⁹T. T. Wu and R. W. P. King, *Radio Sci.* 17, (1982).
- ¹⁰G. H. Brown and A. F. Gangi, *IEEE Trans. Geosci. Electron.* GE-1, 17 (1963).
- ¹¹K. Iizuka, *IEEE Trans. Antennas Propag.* AP-19, 365 (1971).
- ¹²K. Iizuka, *IEEE Trans. Antennas Propag.* AP-20, 602 (1972).
- ¹³G. S. Smith, Tech. Rep. No. 637, Harvard University, Div. of Eng. and Appl. Phys., Cambridge, Massachusetts, 1973.
- ¹⁴R. W. P. King and G. S. Smith, *Antennas in Matter* (MIT, Cambridge, Massachusetts, 1981).
- ¹⁵L. C. Shen, *IEEE Trans. Antennas Propag.* AP-24, 894 (1976).

Lateral waves: Formulas for the magnetic field

R. W. P. King and T. T. Wu

Gordon McKay Laboratory, Harvard University, Cambridge, Massachusetts 02138

(Received 10 August 1982; accepted for publication 21 September 1982)

New simple formulas are obtained as an approximation of the exact general integrals for the components of the magnetic field generated by a horizontal electric dipole in a half-space of water or earth near its boundary with air. These formulas supplement the earlier derivation of the three components of the electric field which are repeated here for completeness. The formulas for the transverse and vertical components are needed in treating the reflection of lateral waves from plane or cylindrical boundaries.

PACS numbers: 41.10.Fiv

1. INTRODUCTION

In two recent papers,^{1,2} the following simple approximate formulas were derived from the general integrals for the three cylindrical components of the electric field generated at a point ρ, ϕ, z in a half-space of water, earth, etc., (Region 1, below air, Region 2), by a horizontal electric dipole at $\rho = 0$ and at a depth d , also in Region 1 (see Fig. 1). The wave numbers in the two regions are $k_1 = \beta_1 + i\alpha_1 = \omega(\mu_1\epsilon_1)^{1/2}$, where $\epsilon_1 = \epsilon_1 - i\sigma_1/\omega$ and $\epsilon_1 = \epsilon_0\epsilon_{1r}$; $k_2 = \beta_2 - i\alpha_2 = \omega(\mu_2\epsilon_2)^{1/2}$. It is assumed that $\mu_1 = \mu_2 = \mu_0$ and for air, $\epsilon_2 = \epsilon_0, \alpha_2 = 0$.

$$E_{1\rho} = -\frac{\omega\mu_0}{2\pi k_1^2} \cos \phi \left\{ e^{ik_1 z - d} e^{ik_2 \rho} \left[\frac{ik_1^2}{\rho} - \frac{k_2^2}{\rho^2} - \frac{i}{\rho^3} - \frac{k_2^4}{k_1 (k_2 \rho)^3} \right] \right. \\ \left. \times e^{-ik_2 \rho k_1^2 / 2k_1^2} \mathcal{F} \right\} - e^{ik_1 \rho^2 + iz - d} \left[\frac{k_1^2}{\rho^2} + \frac{i}{\rho^3} \right] \quad (1a)$$

$$E_{1\phi} = \frac{\omega\mu_0}{\pi k_1^2} \sin \phi \left\{ e^{ik_1 z - d} e^{ik_2 \rho} \left[\frac{k_2^2}{\rho^2} + \frac{i}{\rho^3} + \frac{ik_2^4}{2k_1 (k_2 \rho)^3} \right] e^{-ik_2 \rho k_1^2 / 2k_1^2} \mathcal{F} \right\} \\ + e^{ik_1 z - d - \rho} \left[\frac{ik_1^2}{2\rho} - \frac{k_1}{\rho^2} - \frac{i}{\rho^3} \right] - \frac{1}{4} [e^{ik_1 r_1} + e^{ik_1 r_2}] \left[\frac{ik_1^2}{\rho} - \frac{k_1}{\rho^2} - \frac{i}{\rho^3} \right] \quad (1b)$$

$$E_{1z} = \frac{i\omega\mu_0}{2\pi k_1^2} \cos \phi \left(\frac{k_2^2}{k_1} e^{ik_1 z + d} \left\{ e^{ik_2 \rho} \left[\frac{k_2^2}{\rho} + \frac{i}{\rho^2} + \frac{ik_2^3}{k_1} \left(\frac{\pi}{k_2 \rho} \right)^{1/2} e^{-ik_2 \rho k_1^2 / 2k_1^2} \mathcal{F} \right] - \frac{e^{ik_1 \rho}}{\rho^2} \right\} \right. \right. \\ \left. \left. + \frac{1}{2} \left[\frac{z-d}{\rho} e^{ik_1 r_1} + \frac{z+d}{\rho} e^{ik_1 r_2} \right] \left[\frac{k_1^2}{\rho} + \frac{3ik_1}{\rho^2} - \frac{3}{\rho^3} \right] \right) \right) \quad (1c)$$

In these formulas, \mathcal{F} involves the Fresnel integrals. It is defined explicitly in Eq. (21) later in this paper. These formulas were compared [see Figs. 2(a), 7, and 11 of Ref. 1, and Fig. 1 of Ref. 2] with the numerically evaluated general integrals for a wide range of values of ϵ_{1r}, σ_1 , and the radial distance ρ with very good agreement.

It is the purpose of this paper to derive corresponding approximate formulas for the components $B_{1\rho}, B_{1\phi}$, and B_{1z} of the magnetic field at ρ, ϕ, z . The last two are useful in satisfying the boundary conditions on the tangential components of the electromagnetic field that determine the reflection and transmission of cylindrical waves at cylindrical boundaries. Also useful for this purpose are the corresponding formulas for the electromagnetic field of a vertical electric dipole.³

Consider first the components $B_{1\phi}$ and B_{1z} . These are, of course, directly related to the known electric field through Maxwell's equations. The general integrals for these components in Region 1 when the source is a unit dipole ($I\Delta l = 1$ Am) are [Eqs. (5.13) and (5.14) on pg. 618 of Ref. 4]:

$$B_{1\phi} = -\frac{\mu_0}{4\pi} \cos \phi \left(\pm \int_0^\infty J_0(\lambda \rho) e^{i\gamma_1 z - d} \lambda d\lambda \right. \\ \left. + \int_0^\infty \{ (\mathcal{Q}/2) [J_0(\lambda \rho) - J_2(\lambda \rho)] \right. \right. \\ \left. \left. - (P/2) [J_0(\lambda \rho) + J_2(\lambda \rho)] \} e^{i\gamma_1 z + d} \lambda d\lambda \right) \quad (2)$$

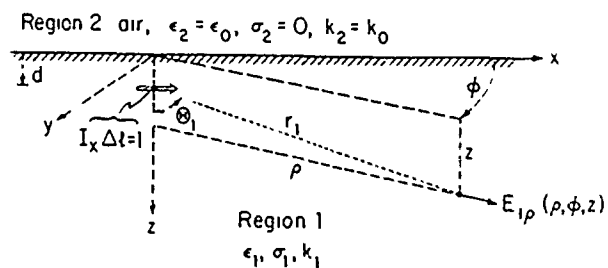


FIG. 1. Radial component of electric field at (ρ, ϕ, z) due to an x -directed dipole at $(0, 0, d)$.

$$B_{1z} = \frac{i\mu_0}{4\pi} \sin \phi \int_0^\infty [e^{\gamma_1 z - d} - P e^{\gamma_1 z + d}] \gamma_1^{-1} J_1(\lambda \rho) \lambda^2 d\lambda, \quad (3)$$

where, with $\mu_1 = \mu_2 = \mu_0$,

$$P = (\gamma_2 - \gamma_1)/(\gamma_2 + \gamma_1);$$

$$Q = (\bar{\epsilon}_1 \gamma_2 - \bar{\epsilon}_2 \gamma_1)/(\bar{\epsilon}_1 \gamma_2 + \bar{\epsilon}_2 \gamma_1); \quad (4)$$

$$\gamma_1 = (k_1^2 - \lambda^2)^{1/2}; \quad \gamma_2 = (k_2^2 - \lambda^2)^{1/2}. \quad (5)$$

The upper sign in (2) applies when $z > d$, the lower sign when $0 < z < d$.

The derivation of simple approximate formulas for $B_{1\phi}$ and B_{1z} will be carried out directly from these general integrals.

II. AN APPROXIMATE FORMULA FOR $B_{1\phi}$

As in the derivation of simple formulas for the components of the electric field from the general integrals,^{1,2} it is convenient to rearrange the second integral in (2) with the introduction of

$$P + 1 = 2\gamma_2/(\gamma_2 + \gamma_1);$$

$$Q - 1 = -2\bar{\epsilon}_2 \gamma_1/(\bar{\epsilon}_2 \gamma_1 + \bar{\epsilon}_1 \gamma_2). \quad (6)$$

Specifically, with these expressions, the second integral in Eq. (2) is given exactly by:

$$\begin{aligned} & \int_0^\infty J_0(\lambda \rho) e^{\gamma_1(z+d)} \lambda d\lambda - \int_0^\infty \left\{ \left(\frac{\bar{\epsilon}_2 \gamma_1}{\bar{\epsilon}_2 \gamma_1 + \bar{\epsilon}_1 \gamma_2} \right) \right. \\ & \times [J_0(\lambda \rho) - J_2(\lambda \rho)] + \left(\frac{\gamma_2}{\gamma_2 + \gamma_1} \right) \\ & \left. \times [J_0(\lambda \rho) + J_2(\lambda \rho)] \right\} e^{\gamma_1(z-d)} \lambda d\lambda. \end{aligned} \quad (7)$$

It is now readily seen that when $k_1 = k_2$ so that the two media are the same, the second integral in Eq. (2) vanishes. This shows that the first integral is the direct field at (ρ, ϕ, z) due to the dipole at the point $(0, 0, d)$. Since the first integral in (7) is like the first integral in (2), except for the exponential factor, it is readily identified as the field at (z, ϕ, ρ) of an image dipole at $(0, 0, -d)$. Note that the fields of the source and image dipoles are in the same direction when the point of observation satisfies the condition $z > d$. This makes the current elements in the dipole and its image in phase, so that their field components B_ϕ cancel along the plane $z = d = 0$. Since the magnetic field of an x -directed dipole is well known,⁵ the exact expressions for the two integrals can be written down. With the previously imposed condition,

$$\rho^2 \gg (z+d)^2 \gg (z-d)^2 \quad (8)$$

so that

$$r_1 = [\rho^2 + (z-d)^2]^{1/2} \sim \rho,$$

$$r_2 = [\rho^2 + (z+d)^2]^{1/2} \sim \rho \text{ in amplitudes,}$$

$$\begin{aligned} F_0(\rho, z-d) &= \pm \int_0^\infty J_0(\lambda \rho) e^{\gamma_1(z-d)} \lambda d\lambda \\ &\sim e^{ik_1 r_1} \left[\frac{ik_1}{\rho^2} - \frac{1}{\rho^3} \right] (z-d), \end{aligned} \quad (9)$$

$$\begin{aligned} F'_0(\rho, z+d) &= \int_0^\infty J_0(\lambda \rho) e^{\gamma_1(z+d)} \lambda d\lambda \\ &\sim e^{ik_1 r_2} \left[\frac{ik_1}{\rho^2} - \frac{1}{\rho^3} \right] (z+d), \end{aligned} \quad (10)$$

where the upper sign is for $z > d$, the lower sign for $0 < z < d$. Let

$$F_1(\rho, z+d) = F_2(\rho, z+d) + F_3(\rho, z+d), \quad (11)$$

where

$$\begin{aligned} F_2(\rho, z+d) &= - \int_0^\infty \left(\frac{\bar{\epsilon}_2 \gamma_1}{\bar{\epsilon}_2 \gamma_1 + \bar{\epsilon}_1 \gamma_2} \right) \\ &\times [J_0(\lambda \rho) - J_2(\lambda \rho)] e^{\gamma_1(z-d)} \lambda d\lambda, \end{aligned} \quad (12)$$

$$\begin{aligned} F_3(\rho, z+d) &= - \int_0^\infty \left(\frac{\gamma_2}{\gamma_2 + \gamma_1} \right) \\ &\times [J_0(\lambda \rho) + J_2(\lambda \rho)] e^{\gamma_1(z-d)} \lambda d\lambda. \end{aligned} \quad (13)$$

Then Eq. (2) is given by

$$\begin{aligned} B_{1\phi} &= - \frac{\mu_0}{4\pi} \cos \phi [F_0(\rho, z-d) \\ &+ F'_0(\rho, z+d) + F_1(\rho, z+d)]. \end{aligned} \quad (14)$$

Since $F_0(\rho, z-d)$ and $F'_0(\rho, z+d)$ are known, it remains to evaluate $F_1(\rho, z+d)$ as the sum of $F_2(\rho, z+d)$ and $F_3(\rho, z+d)$.

The evaluation of $F_1(\rho, z+d)$ as defined in Eq. (11) with (12) and (13), will be carried out subject to the restrictions of Eq. (8), and

$$|k_1|^2 \gg k_2^2. \quad (15)$$

The following approximation is made

$$F_1(\rho, z+d) \sim F_1(\rho, 0) e^{ik_1 z - d}. \quad (16)$$

This is discussed in Ref. 1. With (11), (12), and (13), it remains to evaluate

$$F_2(\rho, 0) = - \int_0^\infty \left(\frac{\bar{\epsilon}_2 \gamma_1}{\bar{\epsilon}_2 \gamma_1 + \bar{\epsilon}_1 \gamma_2} \right) [J_0(\lambda \rho) - J_2(\lambda \rho)] \lambda d\lambda, \quad (17)$$

$$F_3(\rho, 0) = - \int_0^\infty \left(\frac{\gamma_2}{\gamma_2 + \gamma_1} \right) [J_0(\lambda \rho) + J_2(\lambda \rho)] \lambda d\lambda. \quad (18)$$

III. EVALUATION OF $F_2(\rho, 0)$

The integrand in Eq. (17) can be expanded as follows.

$$\begin{aligned} F_2(\rho, 0) &= - \frac{\bar{\epsilon}_2}{\bar{\epsilon}_1} \int_0^\infty \frac{\gamma_1}{\gamma_2} [J_0(\lambda \rho) - J_2(\lambda \rho)] \lambda d\lambda \\ &= - \bar{\epsilon}_2 \int_0^\infty \gamma_1 \left[\frac{1}{\bar{\epsilon}_2 \gamma_1 + \bar{\epsilon}_1 \gamma_2} - \frac{1}{\bar{\epsilon}_1 \gamma_2} \right] \\ &\times [J_0(\lambda \rho) - J_2(\lambda \rho)] \lambda d\lambda. \end{aligned} \quad (19)$$

Here the second integral is closely related to the function $G(\rho)$ evaluated in Appendix B of Ref. 1. When note is taken of the fact that the integrand becomes large only when λ is near k_2 , so that $k_1^2 \gg \lambda^2$ in the range of significance, the second integral in Eq. (19) is the same as $G(\rho)/k_1$, where

$$G(\rho) = -2(k_2^4/k_1) \left(\frac{\pi}{k_2 \rho} \right)^{1/2} e^{ik_2 \rho} e^{-ik_2 \rho k_2^2/2k_1^2} \mathcal{F}. \quad (20)$$

Here

$$\mathcal{F} = \left[\frac{1}{2} - C \left(\frac{k_2^3 \rho}{2k_1^2} \right) \right] + i \left[\frac{1}{2} - S \left(\frac{k_2^3 \rho}{2k_1^2} \right) \right], \quad (21)$$

and $C(z) + iS(z) = \int_0^z (2\pi t)^{-1/2} e^{it^2} dt$ is the Fresnel integral as defined in Jahnke-Emde, *Tables of Functions* (Dover, New York, 1945), p. 36. Thus, with $\bar{\epsilon}_2/\bar{\epsilon}_1 = k_2^2/k_1^2$ and $k_1 = i\beta$,

$$F_2(\rho, 0) = \frac{k_2^2}{\beta^2} \int_0^\infty \frac{(\lambda^2 + \beta^2)^{1/2}}{(\lambda^2 - k_2^2)^{1/2}} \times [J_0(\lambda\rho) - J_2(\lambda\rho)] \lambda d\lambda + G(\rho)/k_1. \quad (22)$$

Let the following notation be introduced with reference to a function $f(\lambda, \beta, k_2)$:

$$\begin{aligned} f_1(\lambda, \beta, k_2) &= f(\lambda \sim \beta, \beta, k_2), \\ f_2(\lambda, \beta, k_2) &= f(\lambda \sim k_2, \beta, k_2), \\ f_3(\lambda, \beta, k_2) &= f_1(\lambda \sim k_2, \beta, k_2) = f_2(\lambda \sim \beta, \beta, k_2). \end{aligned}$$

With Eq. (15), the following approximate relation holds:

$$f(\lambda, \beta, k_2) \sim f_1(\lambda, \beta, k_2) + f_2(\lambda, \beta, k_2) - f_3(\lambda, \beta, k_2). \quad (23)$$

In Eq. (22), let $f(\lambda, \beta, k_2) = (\lambda^2 + \beta^2)^{1/2}/(\lambda^2 - k_2^2)^{1/2}$. Then $f_1(\lambda, \beta, k_2) = (\lambda^2 + \beta^2)^{1/2}/\lambda$; $f_2(\lambda, \beta, k_2) = \beta/(\lambda^2 - k_2^2)^{1/2}$; $f_3(\lambda, \beta, k_2) = \beta/\lambda$. With Eq. (23),

$$\begin{aligned} &(\lambda^2 + \beta^2)^{1/2}/(\lambda^2 - k_2^2)^{1/2} \\ &\sim (\lambda^2 + \beta^2)^{1/2}/\lambda + \beta/(\lambda^2 - k_2^2)^{1/2} - \beta/\lambda. \end{aligned} \quad (24)$$

With Eq. (24) in Eq. (22), this becomes

$$F_2(\rho, 0) \sim \frac{k_2^2}{\beta^2} \{I_A + 3I_B - \beta I_C\} + G(\rho)/k_1, \quad (25)$$

where

$$I_A = \int_0^\infty (\lambda^2 + \beta^2)^{1/2} [J_0(\lambda\rho) - J_2(\lambda\rho)] \lambda d\lambda, \quad (26)$$

$$I_B = \int_0^\infty (\lambda^2 - k_2^2)^{-1/2} [J_0(\lambda\rho) - J_2(\lambda\rho)] \lambda d\lambda, \quad (27)$$

and

$$I_C = \int_0^\infty [J_0(\lambda\rho) - J_2(\lambda\rho)] \lambda d\lambda. \quad (28)$$

It is shown in Appendix A that

$$\begin{aligned} I_A &= -\frac{2}{\rho} \left[\beta I_0(\beta\rho/2) K_1(\beta\rho/2) - \frac{1}{\rho} \right] \\ &\sim -\frac{2}{\rho^2} \left[\frac{1}{\beta\rho} - ie^{-\beta\rho} \left(1 + \frac{1}{2\beta\rho} \right) \right] \\ &\sim -2 \left[\frac{i}{k_1\rho^3} - ie^{ik_1\rho} \left(\frac{1}{\rho^2} + \frac{i}{2k_1\rho^3} \right) \right], \end{aligned} \quad (29)$$

where the approximate value on the right is a good approximation when $|\beta\rho| \gg 3$.

$$I_B = 2 \left[\frac{-i}{k_2\rho^2} + e^{ik_2\rho} \left(\frac{1}{\rho} + \frac{i}{k_2\rho^2} \right) \right], \quad (30)$$

$$\begin{aligned} \beta I_B &= \frac{-2k_1}{k_2\rho^2} - 2ik_1 e^{ik_2\rho} \left(\frac{1}{\rho} + \frac{i}{k_2\rho^2} \right), \\ I_C &= 0. \end{aligned} \quad (31)$$

It follows that with $\beta = -ik_1$, Eq. (25) becomes

$$\begin{aligned} F_2(\rho, 0) &\sim \frac{2}{k_1} \left[\frac{ik_2^2}{k_1^2\rho^3} - ie^{ik_2\rho} \left(\frac{k_2^2}{k_1\rho^2} + \frac{ik_2^2}{2k_1^2\rho^3} \right) \right. \\ &\quad \left. + \frac{k_2}{\rho^2} + ie^{ik_2\rho} \left(\frac{k_2^2}{\rho} + \frac{ik_2}{\rho^2} \right) \right] \\ &\quad + \frac{G(\rho)}{k_1}. \end{aligned} \quad (32)$$

IV. THE EVALUATION OF $F_3(\rho, 0)$

The integral in Eq. (18) can be rearranged as follows

$$F_3(\rho, 0) = - \int_0^\infty \frac{\gamma_2(\gamma_2 - \gamma_1)}{\gamma_2^2 - \gamma_1^2} [J_0(\lambda\rho) + J_2(\lambda\rho)] \lambda d\lambda. \quad (33)$$

In the integrand,

$$\begin{aligned} &\frac{\gamma_2(\gamma_2 - \gamma_1)}{\gamma_2^2 - \gamma_1^2} \\ &= \frac{k_2^2 - \lambda^2 - (k_2^2 - \lambda^2)^{1/2} (k_1^2 - \lambda^2)^{1/2}}{k_2^2 - k_1^2}. \end{aligned} \quad (34)$$

With $k_1 = i\beta$, this becomes

$$\begin{aligned} &\frac{\gamma_2(\gamma_2 - \gamma_1)}{\gamma_2^2 - \gamma_1^2} \\ &= \frac{(\lambda^2 - k_2^2)^{1/2} (\lambda^2 + \beta^2)^{1/2} + k_2^2 - \lambda^2}{k_2^2 + \beta^2}. \end{aligned} \quad (35)$$

The approximation (23) is now applied to $f(\lambda, \beta, k_2) = (\lambda^2 - k_2^2)^{1/2} (\lambda^2 + \beta^2)^{1/2}$ to give: $f_1(\lambda, \beta, k_2) = \lambda (\lambda^2 + \beta^2)^{1/2}$; $f_2(\lambda, \beta, k_2) = \beta (\lambda^2 - k_2^2)^{1/2}$; $f_3(\lambda, \beta, k_2) = \beta\lambda$. Therefore, with (23),

$$\begin{aligned} &\frac{\gamma_2(\gamma_2 - \gamma_1)}{\gamma_2^2 - \gamma_1^2} \sim \frac{1}{k_2^2 + \beta^2} \left[\lambda (\lambda^2 + \beta^2)^{1/2} \right. \\ &\quad \left. + \beta (\lambda^2 - k_2^2)^{1/2} - \beta\lambda + k_2^2 - \lambda^2 \right]. \end{aligned} \quad (36)$$

When Eq. (36) is substituted in Eq. (33), this can be expressed as follows

$$\begin{aligned} F_3(\rho, 0) &= - \frac{1}{k_2^2 + \beta^2} [I_D + \beta I_E \\ &\quad - \beta I_F + k_2^2 I_G - I_H], \end{aligned} \quad (37)$$

where

$$I_D = \int_0^\infty (\lambda^2 + \beta^2)^{1/2} [J_0(\lambda\rho) + J_2(\lambda\rho)] \lambda^2 d\lambda, \quad (38)$$

$$I_E = \int_0^\infty (\lambda^2 - k_2^2)^{1/2} [J_0(\lambda\rho) + J_2(\lambda\rho)] \lambda d\lambda, \quad (39)$$

$$I_F = \int_0^\infty [J_0(\lambda\rho) + J_2(\lambda\rho)] \lambda^2 d\lambda, \quad (40)$$

$$I_G = \int_0^\infty [J_0(\lambda\rho) + J_2(\lambda\rho)] \lambda d\lambda, \quad (41)$$

$$I_H = \int_0^\infty [J_0(\lambda\rho) + J_2(\lambda\rho)] \lambda^3 d\lambda. \quad (42)$$

These integrals are evaluated in Appendix A. Their values are

$$I_D = \frac{2\beta^2}{\rho^2} I_1(\beta\rho/2) K_1(\beta\rho/2) - \frac{2\beta}{\rho^3} \left[1 + ie^{-\beta\rho} \left(1 + \frac{3}{2\beta\rho} \right) \right], \quad (43)$$

where the expression on the right is a good approximation when $|\beta\rho| \gg 3$.

$$I_E = -2i \left[\frac{k_2}{\rho^2} + \frac{i}{\rho^3} e^{ik_2\rho} \right], \quad (44)$$

$$I_F = \frac{2}{\rho^3}, \quad (45)$$

$$I_G = \frac{2}{\rho^2}, \quad (46)$$

$$I_H = 0. \quad (47)$$

It follows that with $\beta = -ik_1$,

$$F_3(\rho, 0) = \frac{1}{k_1^2 - k_2^2} \left\{ -\frac{2ik_1}{\rho^3} \left[1 + ie^{ik_1\rho} \left(1 + \frac{3i}{2k_1\rho} \right) \right] - 2k_1 \left[\frac{k_2}{\rho^2} + \frac{i}{\rho^3} e^{ik_2\rho} \right] + \frac{2ik_1}{\rho^3} + \frac{2k_2^2}{\rho^2} \right\}. \quad (48)$$

When small terms of magnitude k_2^2/k_1^2 compared to one are neglected, this becomes

$$F_3(\rho, 0) \sim \frac{1}{k_1} \left\{ e^{ik_1\rho} \left[\frac{2}{\rho^3} + \frac{3i}{k_1\rho^4} \right] + \frac{2k_2^2}{k_1\rho^2} - \frac{2k_2}{\rho^2} - \frac{2i}{\rho^3} e^{ik_2\rho} \right\}. \quad (49)$$

V. FORMULA FOR B_{1z}

When Eqs. (32) and (49) are combined, and terms of order k_2^2/k_1^2 are neglected as compared with 1 and with $k_1\rho$, the result with Eq. (16) is:

$$F_1(\rho, z + d) \sim \frac{1}{k_1} \left\{ 2ie^{ik_1\rho} \left[\frac{k_2^2}{\rho} + \frac{ik_2}{\rho^2} - \frac{1}{\rho^3} \right] + e^{ik_1\rho} \left[\frac{2}{\rho^3} + \frac{3i}{k_1\rho^4} \right] + G(\rho) \right\} e^{ik_1(z+d)}. \quad (50)$$

When Eqs. (50), (9), and (10) are substituted in Eq. (14), the expression for the ϕ -component of the magnetic field assumes the following explicit but approximate form:

$$B_{1\phi} \sim -\frac{\mu_0}{2\pi k_1} \cos \left\{ e^{ik_1(z+d)} e^{ik_2\rho} \times \left[\frac{ik_2^2}{\rho} - \frac{k_2}{\rho^2} - \frac{i}{\rho^3} - \frac{k_2^4}{k_1} \left(\frac{\pi}{k_2\rho} \right)^{1/2} e^{-ik_2\rho k_2^2/2k_1} \mathcal{F} \right] + \frac{1}{2} e^{ik_1(z+d+\rho)} \left[\frac{2}{\rho^3} + \frac{3i}{k_1\rho^4} \right] + \frac{1}{2} \left[\frac{z-d}{\rho} e^{ik_1r_1} + \frac{z+d}{\rho} e^{ik_1r_2} \right] \left[\frac{ik_1^2}{\rho} - \frac{k_1}{\rho^2} \right] \right\}, \quad (51)$$

where \mathcal{F} is defined in Eq. (21). This formula makes use of the approximate values of I_A in Eq. (29) and I_D in Eq. (43). These are valid when $|k_1\rho| \gg 3$. For smaller values of $k_1\rho$, the more accurate formulas for I_A and I_D in Eqs. (29) and (43) can be used. However, the condition (8) must be satisfied.

VI. FORMULA FOR B_{1z}

The desired formula for B_{1z} can be obtained quite simply from Eq. (3) when rearranged as follows:

$$B_{1z} = \frac{i\mu_0}{4\pi} \sin \phi \int_0^\infty [e^{i\gamma_1(z-d)} - e^{i\gamma_1(z+d)} - (P-1)e^{i\gamma_1(z+d)}] \gamma_1^{-1} J_1(\lambda\rho) \lambda^2 d\lambda, \quad (52)$$

where $P-1 = (\gamma_2 - \gamma_1)/(\gamma_2 + \gamma_1) - 1 = -2\gamma_1/(\gamma_2 + \gamma_1)$. Let

$$B_{1z} = \frac{i\mu_0}{4\pi} \sin \phi [G_0(\rho, z-d) - G_0'(\rho, z+d) + G_1(\rho, z+d)]. \quad (53)$$

In this expression, the first two terms are the direct and image fields which are known. Thus, with Eq. 16(b) on p. 700 of Ref. 5 (with coordinates permuted), the direct field due to the source at $(0, 0, d)$ is given by

$$G_0(\rho, z-d) = \int_0^\infty e^{i\gamma_1(z-d)} \gamma_1^{-1} J_1(\lambda\rho) \lambda^2 d\lambda = -e^{ik_1r_1} \left(\frac{k_1}{\rho} + \frac{i}{\rho^2} \right). \quad (54)$$

Similarly, the field due to a codirectional image at $(0, 0, -d)$ is given by

$$G_0'(\rho, z+d) = \int_0^\infty e^{i\gamma_1(z+d)} \gamma_1^{-1} J_1(\lambda\rho) \lambda^2 d\lambda = -e^{ik_1r_2} \left(\frac{k_1}{\rho} + \frac{i}{\rho^2} \right). \quad (55)$$

In these expressions $r_1 = [\rho^2 + (z-d)^2]^{1/2}$, $r_2 = [\rho^2 + (z+d)^2]^{1/2}$; the approximation $r_1 \sim \rho \sim r_2$ has been used in amplitudes, since it is assumed that $\rho^2 \gg z^2$, $\rho^2 \gg d^2$.

The integral to be evaluated is

$$G_1(\rho, z+d) = 2 \int_0^\infty e^{i\gamma_1(z+d)} (\gamma_2 + \gamma_1)^{-1} J_1(\lambda\rho) \lambda^2 d\lambda. \quad (56)$$

As in previously derived formulas, this is evaluated with the approximation

$$G_1(\rho, z+d) \sim G_1(\rho, 0) e^{ik_1(z+d)}. \quad (57)$$

The justification for Eq. (57) is given in Ref. 1. Thus, the required integral is:

$$G_1(\rho, 0) = 2 \int_0^\infty (\gamma_2 + \gamma_1)^{-1} J_1(\lambda\rho) \lambda^2 d\lambda = \frac{2}{k_1^2 - k_2^2} \int_0^\infty [(k_1^2 - \lambda^2)^{1/2} - (k_2^2 - \lambda^2)^{1/2}] J_1(\lambda\rho) \lambda^2 d\lambda. \quad (58)$$

In Eq. (58), use is made of the relation $(\gamma_2 + \gamma_1)^{-1} = (\gamma_1 - \gamma_2)/(\gamma_1^2 - \gamma_2^2)$. As shown in Appendix B,

$$I_J = \int_0^\infty (k^2 - \lambda^2)^{1/2} J_1(\lambda\rho) \lambda^2 d\lambda = e^{ik\rho} \left(\frac{ik^2}{\rho^2} - \frac{3k}{\rho^3} - \frac{3i}{\rho^4} \right), \quad (59)$$

so that with $|k_1^2| \gg |k_2^2|$,

$$G_1(\rho, 0) \sim \frac{2}{k_1^2} \left[e^{ik_1 \rho} \left(\frac{ik_1^2}{\rho^2} - \frac{3k_1}{\rho^3} - \frac{3i}{\rho^4} \right) - e^{ik_2 \rho} \left(\frac{ik_2^2}{\rho^2} - \frac{3k_2}{\rho^3} - \frac{3i}{\rho^4} \right) \right]. \quad (60)$$

-63-

When Eq. (60) is substituted in Eq. (57), and this is used with Eqs. (54) and (55) in Eq. (53), the resulting expression for B_{1z} is

$$B_{1z} = -\frac{i\mu_0}{2\pi k_1^2} \sin \phi \left\{ e^{ik_1(z+d)} \left[e^{ik_1 \rho} \left(\frac{ik_1^2}{\rho^2} - \frac{3k_1}{\rho^3} - \frac{3i}{\rho^4} \right) - e^{ik_2 \rho} \left(\frac{ik_2^2}{\rho^2} - \frac{3k_2}{\rho^3} - \frac{3i}{\rho^4} \right) \right] + \frac{1}{2} [e^{ik_1 r_1} - e^{ik_1 r_2}] \left[\frac{k_1^3}{\rho} + \frac{ik_1^2}{\rho^2} \right] \right\}. \quad (61)$$

This is the final formula for B_{1z} .

VII. APPROXIMATE FORMULA FOR $B_{1\rho}$

The evaluation of the component $B_{1\rho}$ from the general integral formula [Eq. (5.12) on p. 618 of Ref. 4]:

$$B_{1\rho} = -\frac{\mu_0}{4\pi} \sin \phi \left(\pm \int_0^\infty J_0(\lambda \rho) e^{i\gamma_1 z - d} \lambda d\lambda + \int_0^\infty \{ (Q/2) [J_0(\lambda \rho) + J_2(\lambda \rho)] - (P/2) [J_0(\lambda \rho) - J_2(\lambda \rho)] \} e^{i\gamma_2 z - d} \lambda d\lambda \right), \quad (62)$$

where P and Q are defined in Eq. (4), γ_1 and γ_2 in Eq. (5), and

the sign convention is the same as for Eq. (2), leads to certain integrals which do not appear to be expressible in simple form. Its evaluation from Maxwell's equation

$$B_{1\rho} = -\frac{i}{\omega} \left[\frac{1}{\rho} \frac{\partial E_{1z}}{\partial \rho} - \frac{\partial E_{1\phi}}{\partial z} \right] \quad (63)$$

involves the potentially not highly accurate differentiation with respect to z . In the absence of a better formula, $B_{1\rho}$ will be determined from Eq. (63). Its accuracy will be checked by direct comparison with Eq. (62).

From Eq. (30) for $E_{1\phi}$ and Eq. (59) for E_{1z} in Ref. 2, it follows directly that:

$$\begin{aligned} \frac{1}{\rho} \frac{\partial E_{1z}}{\partial \rho} = & -\frac{i\omega\mu_0}{2\pi k_1} \sin \phi \left\{ \frac{k_2^2}{k_1^2} e^{ik_1(z+d)} e^{ik_2 \rho} \left[\frac{k_2}{\rho^2} + \frac{i}{\rho^3} + \frac{ik_2^3}{k_1 \rho} \left(\frac{\pi}{k_2 \rho} \right)^{1/2} \right. \right. \\ & \times e^{-ik_2 \rho (k_2^2/2k_1^2)} \left. \left. - \frac{k_2^2}{k_1^2} e^{ik_1(z+d+\rho)} \frac{1}{\rho^3} \right. \right. \\ & \left. \left. + \frac{1}{2} \left[\frac{z-d}{\rho} e^{ik_1 r_1} + \frac{z+d}{\rho} e^{ik_1 r_2} \right] \left[\frac{k_1}{\rho^2} + \frac{3i}{\rho^3} - \frac{3}{k_1 \rho^4} \right] \right\}, \quad (64) \end{aligned}$$

$$\begin{aligned} \frac{\partial E_{1\phi}}{\partial z} = & \frac{i\omega\mu_0}{2\pi k_1} \sin \phi \left\{ e^{ik_1(z+d)} e^{ik_2 \rho} \left[\frac{2k_2}{\rho^2} + \frac{2i}{\rho^3} + \frac{ik_2^3}{k_1 \rho} \left(\frac{\pi}{k_2 \rho} \right)^{1/2} e^{-ik_2 \rho (k_2^2/2k_1^2)} \right] \right. \\ & \left. + e^{ik_1(z+d+\rho)} \left[\frac{ik_1^2}{\rho} - \frac{2k_1}{\rho^2} - \frac{2i}{\rho^3} \right] \right. \\ & \left. - \frac{1}{2} \left[\frac{z-d}{\rho} e^{ik_1 r_1} + \frac{z+d}{\rho} e^{ik_1 r_2} \right] \left[\frac{ik_1^2}{\rho} - \frac{k_1}{\rho^2} - \frac{i}{\rho^3} \right] \right\}. \quad (65) \end{aligned}$$

When these are combined in Eq. (63) and terms of order k_2^2/k_1^2 are neglected, the following formula is obtained

$$\begin{aligned} B_{1\rho} \sim & -\frac{\mu_0}{2\pi k_1} \sin \phi \left\{ e^{ik_1(z+d)} e^{ik_2 \rho} \left[\frac{2k_2}{\rho^2} + \frac{2i}{\rho^3} + \frac{ik_2^3}{k_1 \rho} \left(\frac{\pi}{k_2 \rho} \right)^{1/2} e^{-ik_2 \rho (k_2^2/2k_1^2)} \right] \right. \\ & \left. + e^{ik_1(z+d+\rho)} \left[\frac{ik_1^2}{\rho} - \frac{2k_1}{\rho^2} - \frac{2i}{\rho^3} \right] \right. \\ & \left. - \frac{1}{2} \left[\frac{z-d}{\rho} e^{ik_1 r_1} + \frac{z+d}{\rho} e^{ik_1 r_2} \right] \left[\frac{ik_1^2}{\rho} - \frac{2k_1}{\rho^2} - \frac{4i}{\rho^3} + \frac{3}{k_1 \rho^4} \right] \right\}. \quad (66) \end{aligned}$$

\mathcal{F} is defined in Eq. (21). The lateral-wave term in this expression is associated entirely with $E_{1\phi}$, since the term relating it to E_{1z} is negligible.

VIII. COMPARISON WITH NUMERICAL VALUES AND CONCLUSION

In order to verify the accuracy of the three formulas for the magnetic field, the general integrals (2), (3), and (62) have been evaluated numerically for a critical range of the radial distance ρ with the depths d of the dipole and z of the point where the field is calculated chosen to be different. The denser Region 1 is characterized by $\epsilon_{1r} = 45$, $\sigma_1 = 3.5$ S/m; the frequency used is $f = 600$ MHz; the second region is air. Since the approximate formulas are quite accurate at large distances, a much more critical range within 20 air wavelengths of the dipole was examined. This is important since the new approximate formulas are assured to be good approximations only when $\rho^2 \gg d^2$, $\rho^2 \gg z^2$, which may be interpreted to mean $\rho \gg 5d$, $\rho \gg 5z$.

Graphs showing $|H_{1\rho}| = \mu_0^{-1}|B_{1\rho}|$ and $|H_{1z}| = \mu_0^{-1}|B_{1z}|$ are shown in Fig. 2, $|H_{1\phi}| = \mu_0^{-1}|B_{1\phi}|$ in Fig. 3 in the range $0.001 < \rho < 10$ m. The agreement between the numerical computations from the exact integrals and the approximate formulas is seen to be excellent in the specified range $\rho \gg 5d = 0.035$ m, except in a very narrow range between $\rho = 0.07$ and $\rho = 0.09$ m for H_{1z} , where the direct

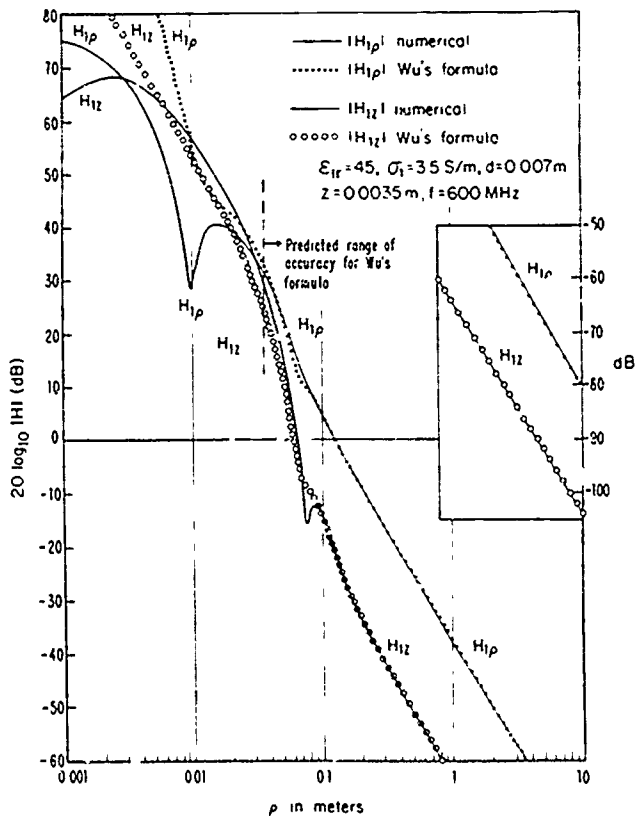


FIG. 2. The components $H_{1\rho}$ and H_{1z} of the magnetic field at depth z due to a horizontal electric dipole with unit moment ($|A| = 1$ A m) at depth d in salt water. Restriction on Wu's formulas. $\rho \gg 5d = 0.035$ m.

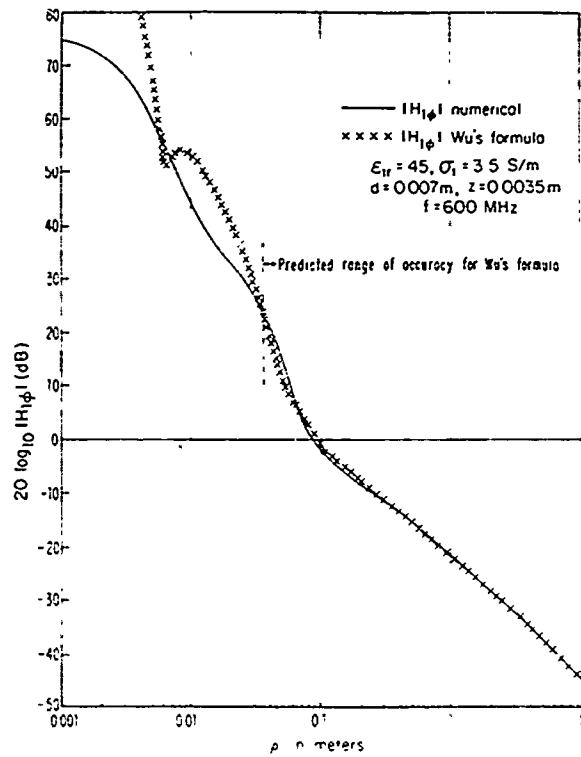


FIG. 3. The component $H_{1\phi}$ of the magnetic field at depth z due to a horizontal electric dipole with unit moment ($|A| = 1$ A m) at depth d in salt water. Restriction on Wu's formula. $\rho \gg 5d = 0.035$ m.

and lateral waves interfere.¹ Very small changes in frequency significantly alter the interference pattern so that close agreement in such a region cannot be expected. At lower frequencies, the direct wave is attenuated more rapidly, and the interference phenomena are restricted to even shorter distances from the source. As in the case of the electric field,² the range of significant interference with the parameters used is only 8 or 9 cm from the source. At all greater distances, the three approximate formulas are highly accurate and are sufficiently simple to permit very rapid calculation. Note that despite its possibly less accurate derivation, $H_{1\rho}$ is also in excellent agreement with the numerical evaluation of the exact integrals.

With the new approximate formulas for the three components of the magnetic field now added to those of the electric field already available, the complete electromagnetic field of the horizontal electric dipole in the earth or water near its interface with air has been provided in simple, continuous, and accurate form.

ACKNOWLEDGMENTS

The numerical evaluation of the general integrals was carried out by L. C. Shen, and the computations from the new approximate formulas were calculated by B. H. Sandler. This research was supported in part by the Office of Naval Research under Contract N00014-79-C-0419, and in part by the Joint Services Electronics Program under Contract N00014-75-C-0648, both with Harvard University.

In the evaluation of the several integrals, the following relations are useful:

$$J_0(z) + J_2(z) = \frac{2}{z} J_1(z) \quad (A1)$$

$$J_0(z) - J_2(z) = 2J'_1(z). \quad (A2)$$

When Eq. (A2) is used in I_A as defined in Eq. (26), this becomes:

$$I_A = \frac{2}{\rho} \int_0^\infty (\lambda^2 + \beta^2)^{1/2} \frac{\partial}{\partial \lambda} J_1(\lambda \rho) d\lambda. \quad (A3)$$

Integration by parts gives:

$$I_A = \frac{2}{\rho} [(\lambda^2 + \beta^2)^{1/2} J_1(\lambda \rho)] \Big|_0^\infty - \frac{2}{\rho} \int_0^\infty (\lambda^2 + \beta^2)^{-1/2} J_1(\lambda \rho) \lambda d\lambda. \quad (A4)$$

Here the integrated term vanishes at both limits and the remaining integral can be evaluated with Eq. (38) on p. 26 of Bateman's *Table of Integral Transforms*, Vol. II. With $\mu = 1$ in this formula, it reduces to

$$\int_0^\infty \left[1 \pm \frac{\lambda}{(\lambda^2 + \beta^2)^{1/2}} \right] J_1(\lambda \rho) d\lambda = BI_{1, \pm 1/2}(\beta \rho/2) K_{1, \pm 1/2}(\beta \rho/2). \quad (A5)$$

The addition and subtraction of the two formulas obtained with upper and lower signs gives:

$$\int_0^\infty J_1(\lambda \rho) d\lambda = \frac{1}{\rho} \int_0^\infty (\lambda^2 + \beta^2)^{-1/2} J_1(\lambda \rho) \lambda d\lambda \quad (A6)$$

$$= BI_{1, -1/2}(\beta \rho/2) K_{1, -1/2}(\beta \rho/2) - \frac{1}{\rho}. \quad (A7)$$

With $\nu = 1$, (A7) is the same as the integral in Eq. (A4). Thus,

$$I_A = -\frac{2}{\rho} [BI_0(\beta \rho/2) K_1(\beta \rho/2) - 1/\rho] \sim -\frac{2}{\rho^2} \left[\frac{1}{\beta \rho} - ie^{-\beta \rho} \left(1 + \frac{1}{2\beta \rho} \right) \right]. \quad (A8)$$

The approximate formula on the right makes use of the large argument approximations $I_0(z) \sim [e^z/(2\pi z)^{1/2}][1 + 1/8z + 9/128z^2] - [ie^{-z}/(2\pi z)^{1/2}][1 - 1/8z + 9/128z^2]$; $K_1(z) \sim (\pi/2z)^{1/2} e^{-z} [1 + 3/8z - 15/128z^2]$. It is a good approximation when $z \geq 2.5$.

The integral I_B as defined in Eq. (27) can be expanded as follows:

$$I_B = 2 \int_0^\infty (\lambda^2 - k^2)^{-1/2} J_0(\lambda \rho) \lambda d\lambda - \int_0^\infty (\lambda^2 - k^2)^{-1/2} [J_0(\lambda \rho) + J_2(\lambda \rho)] \lambda d\lambda. \quad (A9)$$

The use of Eq. (52) on p. 95 of Bateman's *Higher Transcendental Functions*, Vol. II, for the evaluation of the first integral gives:

$$\int_0^\infty (\lambda^2 - k^2)^{-1/2} J_0(\lambda \rho) \lambda d\lambda = e^{ik\rho}/\rho. \quad (A10)$$

The second integral in Eq. (A9) can be evaluated with the use of Eq. (A1) and formula (3) on p. 435 of Watson's *Bessel Functions*. With them it becomes

$$\begin{aligned} \frac{2}{\rho} \int_0^\infty (\lambda^2 - k^2)^{-1/2} J_1(\lambda \rho) d\lambda &= \frac{2}{\rho} I_{1/2}(-ik_2 \rho/2) K_{1/2}(-ik_2 \rho/2) \\ &= \frac{2i}{k_2 \rho^2} (1 - e^{ik_2 \rho}). \end{aligned} \quad (A11)$$

The final step in (A11) makes use of the formulas $I_{1/2}(z) = (2/\pi z)^{1/2} \sinh z$, $K_{1/2}(z) = (\pi/2z)^{1/2} e^{-z}$. With (A10) and (A11), it follows that:

$$I_B = 2 \left[\frac{e^{ik_2 \rho}}{\rho} - \frac{i}{k_2 \rho^2} (1 - e^{ik_2 \rho}) \right]. \quad (A12)$$

The integral I_C defined in Eq. (28) can be transformed with Eq. (A2) to give:

$$\begin{aligned} I_C &= 2 \int_0^\infty J'_1(\lambda \rho) d\lambda = \frac{2}{\rho} \int_0^\infty J'_1(z) dz \\ &= \frac{2}{\rho} J_1(z) \Big|_0^\infty = 0. \end{aligned} \quad (A13)$$

The integral I_D defined by Eq. (38) can be transformed with Eq. (A1) to give:

$$\begin{aligned} I_D &= \frac{2}{\rho} \int_0^\infty (\lambda^2 + \beta^2)^{1/2} J_1(\lambda \rho) \lambda d\lambda \\ &= -\frac{2}{\rho} \int_0^\infty (\lambda^2 + \beta^2)^{1/2} J_{-1}(\lambda \rho) \lambda d\lambda. \end{aligned} \quad (A14)$$

The application of formula (4) on p. 435 of Watson's *Bessel Functions* gives:

$$\begin{aligned} I_D &= \frac{2\beta^2}{\rho^2} I_1(\beta \rho/2) K_1(\beta \rho/2) \\ &\sim \frac{2\beta}{\rho^3} \left[1 + ie^{-\beta \rho} \left(1 + \frac{3}{2\beta \rho} \right) \right], \end{aligned} \quad (A15)$$

where the approximate formula on the right is obtained with the large argument approximations $I_1(z) \sim [e^z/(2\pi z)^{1/2}][1 - 3/8z - 15/128z^2] + [ie^{-z}/(2\pi z)^{1/2}][1 + 3/8z - 15/128z^2]$, $K_1(z) \sim (\pi/2z)^{1/2} e^{-z} [1 + 3/8z - 15/128z^2]$.

The integral I_E defined in Eq. (39) can be transformed with Eq. (A1) as follows:

$$\begin{aligned} I_E &= \frac{2}{\rho} \int_0^\infty (\lambda^2 - k^2)^{1/2} J_1(\lambda \rho) d\lambda \\ &= -\frac{2}{\rho^2} \int_0^\infty (\lambda^2 - k^2)^{1/2} \frac{\partial}{\partial \lambda} J_0(\lambda \rho) d\lambda. \end{aligned} \quad (A16)$$

This can be integrated by parts to give:

$$I_E = -\frac{2}{\rho^2} \left\{ (\lambda^2 - k_2^2)^{1/2} J_0(\lambda \rho) \right\}_0^\infty - \int_0^\infty (\lambda^2 - k_2^2)^{-1/2} J_0(\lambda \rho) \lambda d\lambda \Bigg\} \\ = -\frac{2}{\rho^2} \left(ik_2 - \frac{e^{ik_2 \rho}}{\rho} \right) = -2i \left[\frac{k_2}{\rho^2} + \frac{i}{\rho^3} e^{ik_2 \rho} \right]. \quad (A17)$$

The value Eq. (45) of the integral I_F as defined in Eq. (40) is obtained from I_E with $k_2 = 0$. I_G in Eq. (41) is integrated directly in the form:

$$I_G = \frac{2}{\rho} \int_0^\infty J_1(\lambda \rho) d\lambda = \frac{2}{\rho^2} \int_0^\infty J_1(x) dx = \frac{2}{\rho^2}. \quad (A18)$$

Similarly, I_H in Eq. (42) can be expressed as follows:

$$I_H = \frac{2}{\rho} \int_0^\infty J_1(\lambda \rho) \lambda^2 d\lambda = \frac{2}{\rho^4} \int_0^\infty J_1(x) x^2 dx \\ = \frac{2}{\rho^4} [x^2 J_2(x)]_0^\infty = 0. \quad (A19)$$

The integral is evaluated with formula (1) on p. 132 of Watson's *Bessel Functions*.

APPENDIX B: THE INTEGRAL FOR B_{12}

The integral I_J defined in Eq. (59) can be evaluated with formula (2) in Watson's *Bessel Functions*, p. 434. The substitutions $\nu = 1$ and $\mu = -3/2$ in that formula give:

$$\int_0^\infty (x^2 + k^2)^{1/2} J_1(xa) x^2 dx \\ = \frac{a^{-3/2} k^{5/2}}{2^{-3/2} \Gamma(-1/2)} K_{-5/2}(ak). \quad (B1)$$

Since $K_{-\nu}(z) = K_\nu(z)$, and $\Gamma(-1/2) = -2\Gamma(1/2) = -2\pi^{1/2}$, it follows that with $k_1 = i\beta$:

$$\int_0^\infty (k_1^2 - \lambda^2)^{1/2} J_1(\lambda \rho) \lambda^2 d\lambda \\ = i \int_0^\infty (\lambda^2 + \beta^2)^{1/2} J_1(\lambda \rho) \lambda^2 d\lambda \\ = -\frac{i\beta^2}{\rho} \left(\frac{2\beta}{\pi\rho} \right)^{1/2} K_{5/2}(\beta\rho). \quad (B2)$$

With formula (10.2.17) on p. 444 of Abramowitz and Stegun, *Handbook of Mathematical Functions*, viz.,

$$K_{5/2}(\beta\rho) = \left(\frac{\pi}{2\beta\rho} \right)^{1/2} e^{-\rho\beta} \left(1 + \frac{3}{\beta\rho} + \frac{3}{\beta^2\rho^2} \right), \quad (B3)$$

and the substitution $\beta = -ik$, the expression on the right in Eq. (60) is obtained.

¹T. T. Wu and R. W. P. King, *Radio Sci.* **17**, 521 (1982).

²T. T. Wu and R. W. P. King, *Radio Sci.* **17**, 532 (1982).

³R. W. P. King, *J. Appl. Phys.* **53**, 8476 (1982).

⁴R. W. P. King and G. S. Smith, *Antennas in Matter* (MIT, Cambridge, Massachusetts, 1981), p. 618.

⁵R. W. P. King, *Theory of Linear Antennas* (Harvard Univ., Cambridge, Massachusetts, 1956), Ch. VII.

Erratum: Lateral waves: Formulas for the magnetic field [J. Appl. Phys. 54, 507 (1983)]

R. W. P. King and T. T. Wu

Gordon McKay Laboratory, Harvard University, Cambridge, Massachusetts 02138

In Eq. (1c) the + sign at the beginning of the second line should be -. As a consequence, in Eq. (64), the + sign at the beginning of the third line should be -, and in Eq. (66) the last square bracket should be

$$\left[\frac{ik_1^2}{\rho} + \frac{2i}{\rho^3} - \frac{3}{k_1\rho^4} \right].$$

The authors thank Dr. P. Bannister for discovering this error.

In Eq. (51), a large left brace should be inserted after $\cos \phi$. Equations (A6) and (A7) have been run together. They should read

$$\int_0^\infty J_\nu(\lambda\rho)d\lambda = 1/\rho, \quad (\text{A6})$$

$$\int_0^\infty (\lambda^2 + \beta^2)^{-1/2} J_\nu(\lambda\rho) \lambda d\lambda$$

$$= \beta I_{\nu-1/2}(\beta\rho/2) K_{\nu+1/2}(\beta\rho/2) - 1/\rho. \quad (\text{A7})$$

If approximations of the type (16) and (57) viz., $F(\rho, z+d) \sim F(\rho, 0) \exp[ik_1(z+d)]$, which underlie the evaluation of the integrals for all components of the field, are used only in those integrals that involve $\exp(ik_2\rho)$ and not in those that involve $\exp(ik_1\rho)$, the latter can be evaluated exactly with the help of Bateman's¹ formula (52) or formula 6.637(1) of Gradshteyn and Ryshik.² The only resulting change in the formulas for E_{1z} , $E_{1\phi}$, $B_{1\rho}$, $B_{1\phi}$, and B_{1z} is the replacement of $\exp[ik_1(z+d)]$ wherever it occurs by $\exp(ik_1r_2)$ with $r_2 = [\rho^2 + (z+d)^2]^{1/2}$. This change leads to slightly better agreement with the numerically evaluated components in a narrow range near the lower limit of ρ in the conditions $\rho \gg 5d$, $\rho \gg 5z$. It becomes significant only when interference minima occur in this range. These are very sensitive to small changes. The complete corrected formulas are as follows:

$$E_{1\phi} = \frac{\omega\mu_0}{\pi k_1^2} \sin \phi \left[e^{ik_1(z+d)} e^{ik_2\rho} \left(\frac{k_2}{\rho^2} + \frac{i}{\rho^3} + \frac{ik_2^3}{2k_1(k_2\rho)^{3/2}} e^{-ik_2\rho k_2^{1/2}/2k_1} \mathcal{F} \right) + e^{ik_1r_2} \left(\frac{ik_1^2}{2\rho} - \frac{k_1}{\rho^2} - \frac{i}{\rho^3} \right) - \frac{1}{4} (e^{ik_1r_1} + e^{ik_1r_2}) \left(\frac{ik_1^2}{\rho} - \frac{k_1}{\rho^2} - \frac{i}{\rho^3} \right) \right], \quad (1b)$$

$$E_{1z} = \frac{i\omega\mu_0}{2\pi k_1^2} \cos \phi \left[\frac{k_2^2}{k_1} \left\{ e^{ik_1(z+d)} e^{ik_2\rho} \left[\frac{k_2}{\rho} + \frac{i}{\rho^2} + \frac{ik_2^3}{k_1(k_2\rho)^{3/2}} e^{-ik_2\rho k_2^{1/2}/2k_1} \mathcal{F} \right] - \frac{e^{ik_1r_2}}{\rho^2} \right\} - \frac{1}{2} \left(\frac{z-d}{\rho} e^{ik_1r_1} + \frac{z+d}{\rho} e^{ik_1r_2} \right) \left(\frac{k_1^2}{\rho} + \frac{3ik_1}{\rho^2} - \frac{3}{\rho^3} \right) \right], \quad (1c)$$

$$B_{1\phi} \sim \frac{-\mu_0}{2\pi k_1} \cos \phi \left\{ e^{ik_1(z+d)} e^{ik_2\rho} \left[\frac{ik_2^2}{\rho} - \frac{k_2}{\rho^2} - \frac{i}{\rho^3} - \frac{k_2^4}{k_1} \left(\frac{\pi}{k_2\rho} \right)^{1/2} e^{-ik_2\rho k_2^{1/2}/2k_1} \mathcal{F} \right] + \frac{1}{2} e^{ik_1r_2} \left(\frac{2}{\rho^3} + \frac{3i}{k_1\rho^4} \right) + \frac{1}{2} \left(\frac{z-d}{\rho} e^{ik_1r_1} + \frac{z+d}{\rho} e^{ik_1r_2} \right) \left(\frac{ik_1^2}{\rho} - \frac{k_1}{\rho^2} \right) \right\}, \quad (51)$$

$$B_{1z} \sim \frac{-i\mu_0}{2\pi k_1^2} \sin \phi \left[e^{ik_1(z+d)} e^{ik_2\rho} \left(\frac{ik_2^2}{\rho^2} - \frac{3k_2}{\rho^3} - \frac{3i}{\rho^4} \right) - e^{ik_1r_2} \left(\frac{ik_1^2}{\rho^2} - \frac{3k_1}{\rho^3} - \frac{3i}{\rho^4} \right) + \frac{1}{2} (e^{ik_1r_1} - e^{ik_1r_2}) \left(\frac{k_1^3}{\rho} + \frac{ik_1^2}{\rho^2} \right) \right], \quad (61)$$

$$\frac{1}{\rho} \frac{\partial E_{1z}}{\partial \phi} = \frac{-i\omega\mu_0}{2\pi k_1} \sin \phi \left\{ \frac{k_2^2}{k_1} \left[e^{ik_1(z+d)} e^{ik_2\rho} \left[\frac{k_2}{\rho^2} + \frac{i}{\rho^3} + \frac{ik_2^3}{k_1\rho} \left(\frac{\pi}{k_2\rho} \right)^{1/2} e^{-ik_2\rho k_2^{1/2}/2k_1} \mathcal{F} \right] - \frac{k_2^2}{k_1\rho^3} e^{ik_1r_2} \right] - \frac{1}{2} \left(\frac{z-d}{\rho} e^{ik_1r_1} + \frac{z+d}{\rho} e^{ik_1r_2} \right) \left(\frac{k_1}{\rho^2} + \frac{3i}{\rho^3} - \frac{3}{k_1\rho^4} \right) \right\}, \quad (64)$$

$$\frac{\partial E_{1\phi}}{\partial z} = \frac{i\omega\mu_0}{2\pi k_1} \sin \phi \left\{ e^{ik_1(z+d)} e^{ik_2\rho} \left[\frac{2k_2}{\rho^2} + \frac{2i}{\rho^3} + \frac{ik_2^3}{k_1\rho} \left(\frac{\pi}{k_2\rho} \right)^{1/2} e^{-ik_2\rho(k_2^2/2k_1^2)} \mathcal{F} \right] \right. \\ \left. + e^{ik_1r_2} \left(\frac{ik_1^2}{\rho} - \frac{2k_1}{\rho^2} - \frac{2i}{\rho^3} \right) - \frac{1}{2} \left(\frac{z-d}{\rho} e^{ik_1r_1} + \frac{z+d}{\rho} e^{ik_1r_2} \right) \left(\frac{ik_1^2}{\rho} - \frac{k_1}{\rho^2} - \frac{i}{\rho^3} \right) \right\} \cdot \left(\frac{z+d}{\rho} \right) \quad (65)$$

$$B_{1\rho} \sim \frac{-\mu_0}{2\pi k_1} \sin \phi \left\{ e^{ik_1(z+d)} e^{ik_2\rho} \left[\frac{2k_2}{\rho^2} + \frac{2i}{\rho^3} + \frac{ik_2^3}{k_1\rho} \left(\frac{\pi}{k_2\rho} \right)^{1/2} e^{-ik_2\rho(k_2^2/2k_1^2)} \mathcal{F} \right] \right. \\ \left. + e^{ik_1r_2} \left(\frac{ik_1^2}{\rho} - \frac{2k_1}{\rho^2} - \frac{2i}{\rho^3} \right) - \frac{1}{2} \left(\frac{z-d}{\rho} e^{ik_1r_1} + \frac{z+d}{\rho} e^{ik_1r_2} \right) \left(\frac{ik_1^2}{\rho} + \frac{2i}{\rho^3} - \frac{3}{k_1\rho^4} \right) \right\} \cdot \left(\frac{z+d}{\rho} \right) \quad (66)$$

¹H. Bateman, *Higher Transcendental Functions*, Vol II (McGraw-Hill, New York, 1953), p. 95.

²I. S. Gradshteyn and I. M. Ryshik, *Tables of Integrals, Series and Products* (Academic, New York, 1980), p. 719.

On the reflection of lateral electromagnetic waves from perpendicular boundaries

Ronald W. P. King

Gordon McKay Laboratory, Harvard University, Cambridge, Massachusetts 02138

(Received 31 October 1983; accepted for publication 3 January 1984)

Lateral electromagnetic waves propagate along the boundary between an electrically dense half space ($z \geq 0$) with the wave number k_1 (earth, water) and a less dense half space ($z < 0$) with the wave number k_2 ($|k_2|^2 < |k_1|^2$). The scattering of such waves by vertical discontinuities in the denser half space (k_1 changes to k_3) is analyzed. It is shown that the reflected field is very small even when $k_3 \rightarrow \infty$. Also analyzed are the reflections from thin vertical walls of height L of the denser medium projecting vertically into the less dense medium. These are studied specifically when the walls are made of metal. It is shown that reflections are small when $k_2 L \ll 1$, but very significant when $k_2 L > 1$. The standing-wave patterns due to incident and reflected lateral waves are determined and shown graphically.

PACS numbers: 41.10.Hv

I. INTRODUCTION

The propagation of electromagnetic waves along boundaries has been of interest to physicists since the early work of Sommerfeld. It is involved in geophysical exploration, over-the-horizon radar and remote sensing. Some of the most interesting applications are related to regions of the earth that are near the boundaries between quite different materials. Examples include the surface of the earth (soil, ice, salt, and fresh water) adjacent to air; the sea bottom (rock, sediment) next to salt water. In some instances the regions along the bounding surfaces are relatively smooth, in others they are interrupted by discontinuities, projections, and depressions. The propagation of electromagnetic waves along boundaries between quite different media is predominantly by lateral waves. This is well understood along smooth boundaries,^{1,2} but the scattering of lateral waves at boundaries and discontinuities is not well understood. It is the purpose of this paper to analyze the reflection and scattering of lateral waves at vertical discontinuities on both sides of the boundary between air and earth (water).

When a horizontal dipole antenna is located in the earth or water (Region 1) parallel to its plane boundary with air (Region 2), a complicated electromagnetic field is generated in both regions. This is described accurately and in general by complex integrals for each of the six components of the electromagnetic field.^{3,4} It has been interpreted in terms of simple approximate formulas due to Baños⁵ that are valid in limited ranges of the parameters and variables and, more recently, in terms of quite accurate general formulas.⁶⁻⁸ These last are restricted only by the conditions

$$|k_1|^2 > |k_2|^2; \rho_2 \gg z^2, \rho^2 \gg d^2; |k_1 \rho| > 3, \quad (1)$$

where $k_1 = \beta_1 + i\alpha$ is the wave number of the earth or water, $k_2 = k_0$ is the real wave number of air, d is the depth below the surface of the source dipole, and the point of observation is specified by the cylindrical coordinates ρ, ϕ, z , with Region 1 defined by $z \geq 0$, Region 2 by $z < 0$. The positive x axis lies along the axis of the dipole and is the origin for the cylindrical coordinate ϕ . This is shown in Fig. 1.

The first part of this investigation is concerned with the behavior of the field generated by the dipole when the properties of the denser Region 1 change discontinuously as at the edge of a lake or ocean. Specifically, for convenient measurements in the laboratory, attention is directed to the nature of the electromagnetic field when the denser region consists of a semi-infinite cylinder, Region 1, defined by $0 < \rho \leq \rho_b, 0 \leq z < \infty$, and the rest of the half space, Region 3, defined by $\rho_b \leq \rho < \infty, 0 \leq z < \infty$. The half space $-\infty < z \leq 0$ is Region 2, air; it extends over both Regions 1 and 3. The horizontal dipole with unit moment $p_x = I_x \Delta l = 1$ A m is located on the z axis in Region 1 at $z = d$. The arrangement is shown in Fig. 2(a).

The second part of the investigation deals with the effect on the field generated by the horizontal dipole in Region 1 due to a projection of Region 3 into Region 2 (air) as when an island rises out of the sea or a mountain projects up from a plain. Again for convenience in the laboratory, only the extreme case is considered when Region 3 at $\rho_b \leq \rho < \infty, 0 \leq z < \infty$ consists of aluminum and the projection into Region 2 ($-\infty < z \leq 0$) is an aluminum cylinder of height L and radius ρ_b . Region 1 at $0 \leq \rho \leq \rho_b, 0 \leq z < \infty$ continues as salt water. This choice of Region 3 and its extension into Region 2 provides a measure of the maximum possible effect due to a vertical projection. The arrangement is shown schematically in Fig. 2(b).

II. THE LATERAL-WAVE FIELD

Before considering the field in the three regions of Fig. 2(a), it is expedient to review the field for the simpler configuration of Fig. 1, where the entire lower half space is the homogeneous Region 1. The cylindrical components of the field in Region 1 are given by $E_1 = E_L + E_D, B_1 = B_L + B_D$, where the subscript L refers to the lateral-wave part of the field and the subscript D to the direct field.⁶⁻⁸ The nature of the two parts is illustrated for the radial component of the electric field for which the lateral-wave part is [see Eq. (35) of Ref. 6]

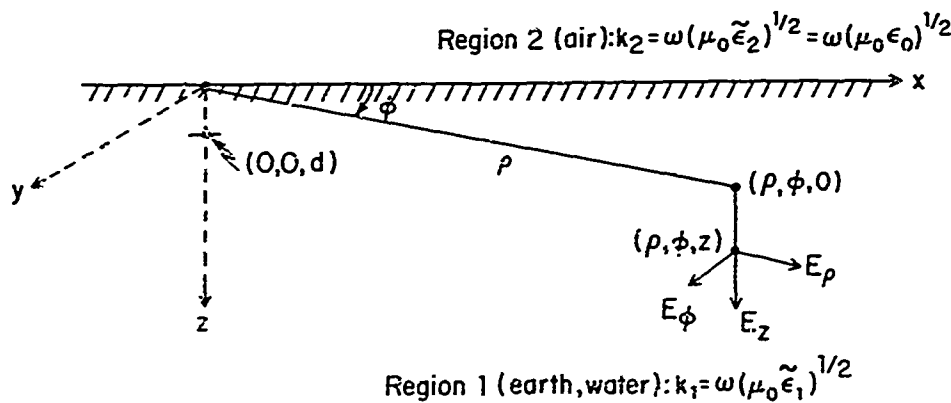


FIG. 1 Field of horizontal electric dipole at depth d in water or earth.

$$E_{1\rho L}(\rho, \phi, z) = E_{1\rho L}(\rho, 0, 0) \cos \phi e^{ik_1 z}, \quad (2)$$

$$E_{1\rho L}(\rho, 0, 0) = -\frac{\omega \mu_0}{2\pi k_1^2} e^{ik_1 d} e^{ik_1 \rho} \left[\frac{ik_1^2}{\rho} - \frac{k_2^2}{\rho^2} - \frac{i}{\rho^3} - \frac{k_1^4}{k_1} \left(\frac{\pi}{k_2 \rho} \right)^{1/2} \right. \\ \left. \times e^{-ik_2 \rho (k_2^2/2k_1^2)} \mathcal{F}(k_2 \rho, k_1) \right], \quad (3)$$

where

$$\mathcal{F}(k_2 \rho, k_1) = \frac{1}{2} - C_2[k_2 \rho (k_2^2/2k_1^2)] \\ + i \left\{ \frac{1}{2} - S_2[k_2 \rho (k_2^2/2k_1^2)] \right\}, \quad (4)$$

and C_2 and S_2 are the Fresnel integrals as defined in the Jahne-Emde Tables of Functions. The first three terms in the square bracket in Eq. (3) are simple powers of the inverse

radial distance; taken together they will be called the *radial or ρ term*. The remaining fourth term involves the Fresnel integrals; it is called the *Fresnel term*. The *direct term* is

$$E_{1\rho D}(\rho, \phi, z) = \frac{\omega \mu_0}{2\pi k_1^2} \cos \phi e^{ik_1 r} \left[\frac{k_1}{\rho^2} + \frac{i}{\rho^3} \right], \quad (5)$$

where $r = [\rho^2 + (z-d)^2]^{1/2}$ and $\rho^2 \gg z^2$. In Fig. 3 are shown the magnitudes of the radial and Fresnel terms of $E_{1\rho L}(\rho, 0, z)$ together with $|E_{1\rho D}(\rho, 0, z)|$ as functions of the radial distance ρ from the source when Region 1 is salt water. It is seen that the direct wave decays very rapidly and is negligible only a small fraction of the wavelength in air from the source. Beyond this short distance, the radial term of the lateral wave is greatest for a little more than two air wavelengths when the Fresnel term becomes comparable and even slightly larger.

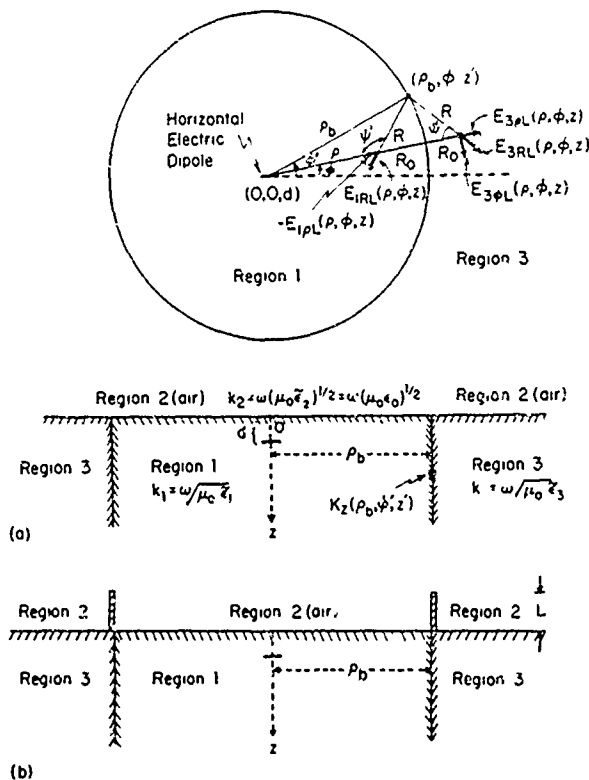


FIG. 2. (a) Horizontal electric dipole in cylindrical Region 1 surrounded by Region 3, all below Region 2 (air). (b) The same with cylindrical projection of Region 3 into Region 2 to height L at $\rho = \rho_b$.

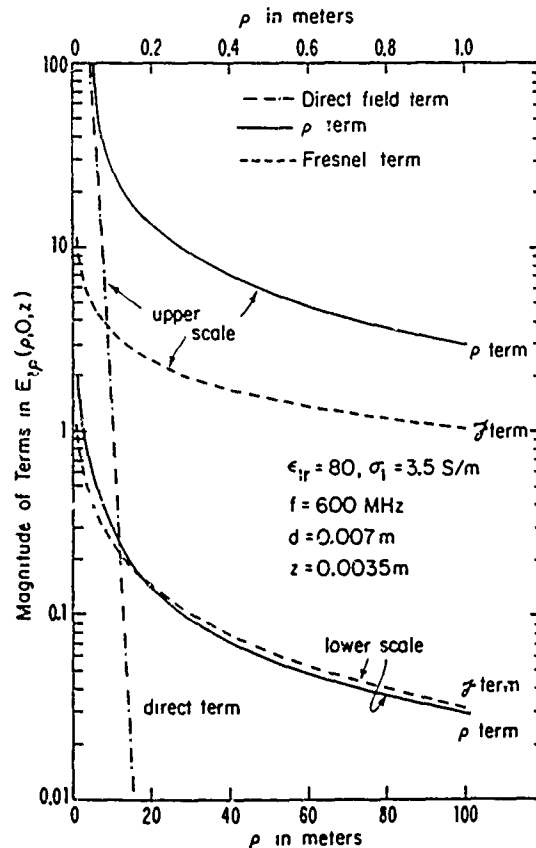


FIG. 3. Magnitudes of direct and lateral-wave terms of $E_{1\rho}(\rho, 0, z)$ in dB referred to 1 V/m. [See Eqs. (2)-(5).]

In this paper attention is directed to the reflection and transmission of the field generated by a horizontal electric dipole at boundaries that are sufficiently far from the source to make the direct wave negligible. Accordingly, only the lateral-wave parts of the other components of the field in Region 1 need be listed. They are [see Eqs. (30) and (59) of Ref. 7]

$$E_{1\phi L}(\rho, \phi, z) = E_{1\phi L}(\rho, 0, 0) \sin \phi e^{ik_1 z}, \quad (6)$$

$$E_{1\phi L}(\rho, 0, 0) = \frac{\omega \mu_0}{\pi k_1^2} e^{ik_1 d} e^{ik_2 \rho} \left[\frac{k_2}{\rho^2} + \frac{i}{\rho^3} + \frac{ik_2^3}{2k_1 \rho} \left(\frac{\pi}{k_2 \rho} \right)^{1/2} \right] \times e^{-ik_2 \rho (k_2^2/2k_1^2)} \mathcal{F}(k_2 \rho, k_1), \quad (7)$$

$$E_{1zL}(\rho, \phi, z) = E_{1zL}(\rho, 0, 0) \cos \phi e^{ik_1 z}, \quad (8)$$

$$E_{1zL}(\rho, 0, 0) = \frac{\omega \mu_0 k_2^2}{2\pi k_1^3} e^{ik_1 d} e^{ik_2 \rho} \left[\frac{ik_2}{\rho} - \frac{1}{\rho^2} - \frac{k_2^3}{k_1} \left(\frac{\pi}{k_2 \rho} \right)^{1/2} \right] \times e^{-ik_2 \rho (k_2^2/2k_1^2)} \mathcal{F}(k_2 \rho, k_1). \quad (9)$$

The associated components of the magnetic field are⁸

$$B_{1\rho L}(\rho, \phi, z) = -(k_1/\omega) E_{1\phi L}(\rho, \phi, z), \quad (10)$$

$$B_{1\phi L}(\rho, \phi, z) = (k_1/\omega) E_{1\rho L}(\rho, \phi, z), \quad (11)$$

$$B_{1zL}(\rho, \phi, z) = B_{1zL}(\rho, 0, 0) \sin \phi e^{ik_1 z}, \quad (12)$$

$$B_{1zL}(\rho, 0, 0) = -\frac{i\mu_0}{2\pi k_1^2} e^{ik_1 d} e^{ik_2 \rho} \left(\frac{ik_2^2}{\rho^2} - \frac{3k_2}{\rho^3} - \frac{3i}{\rho^4} \right). \quad (13)$$

These six components are associated in two groups of three, viz., an electric-type field consisting of the transverse component $B_{1\phi L}(\rho, \phi, z)$ and the two components $E_{1\rho L}(\rho, \phi, z)$ and $E_{1zL}(\rho, \phi, z)$, respectively, longitudinal in the two directions of propagation, and a magnetic-type field consisting of the transverse component $E_{1\phi L}(\rho, \phi, z)$ and the two components $B_{1\rho L}(\rho, \phi, z)$ and $B_{1zL}(\rho, \phi, z)$, respectively, in the two directions of propagation. Of these two groups, the first dominates at all but very short distances since it contains terms of the order $1/\rho$, whereas the leading term in

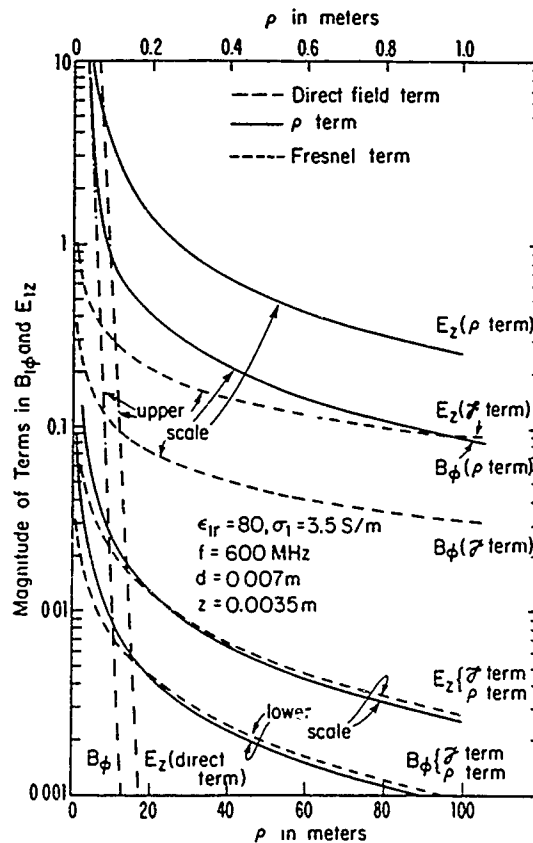


FIG. 4. Magnitudes of direct and lateral-wave terms of $E_{1\rho}(\rho, 0, z)$ and $B_{1\phi}(\rho, 0, z)$ in dB referred to 1 V/m [See Eqs. (2)-(5)]

the second group is of order $1/\rho^2$. In the following analysis, attention is directed primarily to the properties of the field as governed by the leading components $E_{1\rho L}(\rho, \phi, z)$, $E_{1zL}(\rho, \phi, z)$, and $B_{1\phi L}(\rho, \phi, z)$. Figure 4 shows the relative magnitudes of the lateral-wave terms and the direct wave for $E_{1z}(\rho, 0, z)$ and $B_{1\phi}(\rho, 0, z)$.

The associated field in the air is given by

$$E_{2\rho L}(\rho, \phi, z) = -\frac{\omega \mu_0}{2\pi k_1} \cos \phi e^{ik_1 d} e^{ik_2 \rho} \left(\frac{ik_2}{r_0} - \frac{1}{r_0^2} - \frac{i}{k_2 r_0^3} \right) \left\{ \frac{z}{r_0} + \frac{k_2}{k_1} [1 + G(k_2 \rho, k_1)] \right\}, \quad (14)$$

$$E_{2zL}(\rho, \phi, z) = \frac{\omega \mu_0}{2\pi k_1} \cos \phi e^{ik_1 d} e^{ik_2 \rho} \left[\frac{ik_2}{r_0} - \frac{1}{r_0^2} \right] \left[\frac{\rho}{r_0} \right] [1 + G(k_2 \rho, k_1)], \quad (15)$$

$$B_{2\phi L}(\rho, \phi, z) = -\frac{i\mu_0}{2\pi k_1} \cos \phi e^{ik_1 d} e^{ik_2 \rho} \left[\frac{k_2^2}{r_0} + \frac{ik_2}{r_0^2} - \frac{1}{r_0^3} \right] [1 + G(k_2 \rho, k_1)], \quad (16)$$

where

$$G(k_2 \rho, k_1) = i(2\pi R)^{1/2} e^{-i\pi(R+Z)/R} \left(\frac{1}{2} - C_2 \left[\frac{(R+Z)^2}{R} \right] + i \left[\frac{1}{2} - S_2 \left[\frac{(R+Z)^2}{R} \right] \right] \right), \quad (17)$$

and

$$R = k_2 \rho (k_2^2/2k_1^2), \quad Z = k_2 z (k_2^2/2k_1^2), \quad r_0 = (\rho^2 + z^2)^{1/2}. \quad (18)$$

The field in Region 2 at the surface $z = 0$ is

$$E_{2\rho L}(\rho, \phi, 0) = -\frac{\omega \mu_0}{2\pi k_1^2} \cos \phi e^{ik_1 d} e^{ik_2 \rho} \left[\frac{ik_2^2}{\rho} - \frac{k_2}{\rho^2} - \frac{i}{\rho^3} - \frac{k_2^4}{k_1} \left(\frac{\pi}{k_2 \rho} \right)^{1/2} e^{-ik_2 \rho (k_2^2/2k_1^2)} \mathcal{F}(k_2 \rho, k_1) \right], \quad (19)$$

$$E_{2zL}(\rho, \phi, 0) = \frac{\omega \mu_0}{2\pi k_1} \cos \phi e^{ik_1 d} e^{ik_2 \rho} \left[\frac{ik_2}{\rho} - \frac{1}{\rho^2} - \frac{k_2^3}{k_1} \left(\frac{\pi}{k_2 \rho} \right)^{1/2} e^{-ik_2 \rho (k_2^2/2k_1^2)} \mathcal{F}(k_2 \rho, k_1) \right], \quad (20)$$

$$B_{2\phi L}(\rho, \phi, 0) = (k_1/\omega) E_{2\rho L}(\rho, \phi, 0). \quad (21)$$

In Eqs. (19)–(21) only the leading term in $G(k_2 \rho, k_1)$ is retained when z is set equal to zero. $\mathcal{F}(k_2 \rho, k_1)$ is given in Eq. (4). The formulas (3), (9), and (11) with Eqs. (19)–(21) satisfy the correct boundary conditions at $z = 0$, viz.,

$$E_{1\rho L}(\rho, \phi, 0) = E_{2\rho L}(\rho, \phi, 0), \quad (22a)$$

$$E_{1zL}(\rho, \phi, 0) = (k_2^2/k_1^2) E_{2zL}(\rho, \phi, 0), \quad (22b)$$

$$B_{1\phi L}(\rho, \phi, 0) = B_{2\phi L}(\rho, \phi, 0). \quad (22c)$$

The electric field in the two regions is composed of the two components $E_{zL}(\rho, \phi, z)$ and $E_{\rho L}(\rho, \phi, z)$. They have the approximate forms shown below when $(k_2 \rho)^2 \gg 1$ so that the $1/\rho^3$ term is negligible:

$$E_{1L}(\rho, \phi, z) = E_{1\rho L}(\rho, \phi, z) [\hat{\rho} - \hat{z} k_2/k_1], \quad (23)$$

$$E_{2L}(\rho, \phi, z) = E_{2\rho L}(\rho, \phi, z) [\hat{\rho} - \hat{z} k_1/k_2]. \quad (24)$$

Since $|k_1|^2 \gg k_2^2$, it is clear that E_ρ dominates in Region 1 and E_z in Region 2. Note that $E_{1\rho L}(\rho, \phi, 0) = E_{2\rho L}(\rho, \phi, 0)$. The electric field in both regions is elliptically polarized with the major axis of the ellipse tilted from the vertical z axis by the angles

$$\theta_{2z} = \frac{1}{2} \tan^{-1} \left[\frac{2\beta_1 k_2 / |k_1|^2}{1 - |k_2/k_1|^2} \right] \sim k_2 \beta_1 / |k_1|^2, \quad (25)$$

$$\theta_{1z} = \frac{\pi}{2} - \frac{1}{2} \tan^{-1} \left[\frac{2\beta_1 k_2 / |k_1|^2}{1 - |k_2/k_1|^2} \right] \sim \frac{\pi}{2} - k_2 \beta_1 / |k_1|^2. \quad (26)$$

III. CONDITIONS AT A DISCONTINUITY IN THE LOWER HALF SPACE: THE FIELD BEYOND THE BOUNDARY

When the lower half space ($z > 0$) consists of a cylindrical Region 1 ($0 < \rho < \rho_b$, $z > 0$) characterized by the wave number $k_1 = \beta_1 + i\alpha_1 = \omega(\mu_0 \epsilon_1)^{1/2}$ and of the rest of the half space, Region 3 ($\rho_b < \rho < \infty$, $z > 0$), characterized by the wave number $k_3 = \beta_3 + i\alpha_3 = \omega(\mu_0 \epsilon_3)^{1/2}$, as shown in Fig. 2, a lateral electromagnetic wave is incident on the boundary $\rho = \rho_b$, $z > 0$. Here the wave is partly reflected, partly transmitted. Let the three components of the lateral-wave field be considered in turn. In writing the several components, let the following notation be used for the amplitude function:

$$f(k_2 \rho, k_n) = \left[\frac{ik_2^3}{\rho} - \frac{k_2}{\rho^2} - \frac{i}{\rho^3} - \frac{k_2^4}{k_n} \left(\frac{\pi}{k_2 \rho} \right)^{1/2} \times e^{-ik_2 \rho (k_2^2/2k_n^2)} \mathcal{F}(k_2 \rho, k_n) \right]; \quad n = 1, 3, \quad (27)$$

$$\mathcal{F}(k_2 \rho, k_n) = \frac{1}{2} - C_2 [k_2 \rho (k_2^2/2k_n^2)] + i \left\{ \frac{1}{2} - S_2 [k_2 \rho (k_2^2/2k_n^2)] \right\}; \quad n = 1, 3. \quad (28)$$

A. Magnetic field

The lateral-wave part of the incident magnetic field in Region 2 ($z < 0$, air) along its boundary with Region 1 ($0 < \rho < \rho_b$, $z > 0$) is given by Eq. (21), viz.,

$$[B_{2\phi L}(\rho, \phi, 0)]_1 = -\frac{\mu_0}{2\pi k_1} \cos \phi e^{ik_1 d} e^{ik_2 \rho} f(k_2 \rho, k_1); \quad \rho < \rho_b. \quad (29a)$$

The corresponding formula for the field along the boundary with Region 3 ($\rho_b < \rho < \infty$, $z > 0$) is given by Eq. (29a) with k_1 replaced by k_3 [except in $\exp(ik_1 d)$] and the amplitude adjusted to be continuous with $[B_{2\phi L}(\rho, \phi, 0)]_1$ at $\rho = \rho_b$. Specifically,

$$[B_{2\phi L}(\rho, \phi, 0)]_3 = -\frac{\mu_0 R_{13}}{2\pi k_3} \cos \phi e^{ik_1 d} \times e^{ik_2 \rho} f(k_2 \rho, k_3); \quad \rho > \rho_b, \quad (29b)$$

where

$$R_{13} = \frac{k_3 f(k_2 \rho_b, k_1)}{k_1 f(k_2 \rho_b, k_3)}. \quad (30)$$

It follows that in general:

$$B_{1\phi L}(\rho, \phi, z) = -\frac{\mu_0}{2\pi k_1} \cos \phi e^{ik_1(d-z)} e^{ik_2 \rho} \times f(k_2 \rho, k_1); \quad \rho < \rho_b, \quad (31a)$$

$$B_{3\phi L}(\rho, \phi, z) = -\frac{\mu_0 R_{13}}{2\pi k_3} \cos \phi e^{ik_1 d} e^{ik_2 \rho} \times f(k_2 \rho, k_3); \quad \rho > \rho_b. \quad (31b)$$

The general boundary condition for the magnetic field is

$$B_{1\phi L}(\rho_b, \phi, z) - B_{3\phi L}(\rho_b, \phi, z) = -\mu_0 K_z(\rho_b, \phi, z), \quad (32)$$

where $K_z(\rho_b, \phi, z)$ is the surface density of current along the boundary surface. With Eqs. (31a) and (31b) it is

$$\begin{aligned} \mu_0 K_z(\rho_b, \phi, z) &= -[B_{2\phi L}(\rho_b, \phi, 0)]_1 e^{ik_1 z} \\ &\quad + [B_{2\phi L}(\rho_b, \phi, 0)]_3 e^{ik_3 z} \\ &= -[B_{2\phi L}(\rho_b, \phi, 0)]_1 (e^{ik_1 z} - e^{ik_3 z}). \end{aligned} \quad (33)$$

The second equation follows since, with Eqs. (29a) and (29b) and (30), $[B_{2\phi L}(\rho_b, \phi, 0)]_3 = [B_{2\phi L}(\rho_b, \phi, 0)]_1$. Note that at $z = 0$, $K_z(\rho_b, \phi, z) = 0$.

B. Component of the electric field normal to the boundary

The equation of continuity provides the surface density of charge on the boundary. It is

$$\begin{aligned} \eta(\rho_b, \phi, z) &= -\frac{i}{\omega} \frac{\partial K_z(\rho_b, \phi, z)}{\partial z} = -\frac{[B_{2\phi L}(\rho_b, \phi, 0)]_1}{\omega \mu_0} \\ &\quad \times (k_1 e^{ik_1 z} - k_3 e^{ik_3 z}). \end{aligned} \quad (34)$$

This charge is related to the normal component of the electric field at the boundary by the condition:

$$\bar{\epsilon}_1 E_{1\rho L}(\rho_b, \phi, z) - \bar{\epsilon}_3 E_{3\rho L}(\rho_b, \phi, z) = -\eta(\rho_b, \phi, z). \quad (35)$$

Since $\bar{\epsilon} = k^2/\omega^2\mu_0$ and

$$E_{1\rho L}(\rho, \phi, z) = (\omega/k_1) B_{1\phi L}(\rho, \phi, z) \\ = (\omega/k_1) [B_{2\phi L}(\rho, \phi, 0)]_1 e^{ik_1 z}, \quad (36a)$$

$$E_{3\rho L}(\rho, \phi, z) = (\omega/k_3) B_{3\phi L}(\rho, \phi, z) \\ = (\omega/k_3) [B_{2\phi L}(\rho, \phi, 0)]_3 e^{ik_3 z}, \quad (36b)$$

it follows that at the boundary $\rho = \rho_b$, Eq. (35) gives

$$(\omega \bar{\epsilon}_1/k_1) [B_{2\phi L}(\rho_b, \phi, 0)]_1 e^{ik_1 z} \\ - (\omega \bar{\epsilon}_3/k_3) [B_{2\phi L}(\rho_b, \phi, 0)]_3 e^{ik_3 z} = -\eta(\rho_b, \phi, z), \quad (37)$$

or

$$\eta(\rho_b, \phi, z) = -\frac{[B_{2\phi L}(\rho_b, \phi, 0)]_1}{\omega\mu_0} (k_1 e^{ik_1 z} - k_3 e^{ik_3 z}). \quad (38)$$

The last equation follows since $[B_{2\phi L}(\rho_b, \phi, 0)]_3 = [B_{2\phi L}(\rho_b, \phi, 0)]_1$. It is in agreement with Eq. (34). The electric fields $E_{1\rho L}(\rho, \phi, z)$ and $E_{3\rho L}(\rho, \phi, z)$ are given by

$$E_{1\rho L}(\rho, \phi, z) = -\frac{\omega\mu_0}{2\pi k_1^2} \cos \phi e^{ik_1(d+z)} \\ \times e^{ik_1 \rho f(k_2 \rho, k_1)}; \quad \rho < \rho_b, \quad (39a)$$

$$E_{3\rho L}(\rho, \phi, z) = -\frac{\omega\mu_0 R_{13}}{2\pi k_3^2} \cos \phi e^{ik_3 d} \\ \times e^{ik_3 \rho f(k_2 \rho, k_3)}; \quad \rho > \rho_b. \quad (39b)$$

C. Vertical electric field

The z -directed currents $K_z(\rho_b, \phi, z)$ given in Eq. (33) generate a scattered field that travels in both directions from the boundary. It consists of a reflected field that travels radially inward from the boundary in Region 1, radially outward in Region 3. On both sides of the boundary $\rho = \rho_b$, the z component of the scattered field, $E_z^s(\rho, \phi, z)$, can be determined from the boundary condition for E_z at $\rho = \rho_b$. Since the component of the electric field tangent to a boundary is continuous across that boundary, it follows that the total z component of the electric field at the boundary must be continuous. This means

$$E_{1zL}(\rho_b, \phi, z) - E_z^s(\rho_b, \phi, z) = E_{3zL}(\rho_b, \phi, z) \\ + E_z^s(\rho_b, \phi, z), \quad (40a)$$

or

$$E_z^s(\rho_b, \phi, z) = \frac{1}{2} [E_{1zL}(\rho_b, \phi, z) - E_{3zL}(\rho_b, \phi, z)]. \quad (40b)$$

Here,

$$E_{1zL}(\rho, \phi, z) = \frac{\omega\mu_0}{2\pi k_1} \frac{k_2^2}{k_1^2} \cos \phi e^{ik_1(d+z)} \\ \times e^{ik_1 \rho f(k_2 \rho, k_1)} \quad (41a)$$

and

$$E_{3zL}(\rho, \phi, z) = \frac{\omega\mu_0 R_{13}}{2\pi k_3} \frac{k_2^2}{k_3^2} \cos \phi e^{ik_3 d} \\ \times e^{ik_3 \rho f(k_2 \rho, k_3)}, \quad (41b)$$

where

$$f_V(k_2 \rho, k_n) = \left[\frac{ik_2}{\rho} - \frac{1}{\rho^2} - \frac{k_2^2}{k_n} \left(\frac{\pi}{k_2 \rho} \right)^{1/2} e^{-ik_2 \rho(k_2^2/2k_n^2)} \right. \\ \left. \times \mathcal{F}(k_2 \rho, k_n) \right]; \quad n = 1, 3, \quad (42)$$

and $\mathcal{F}(k_2 \rho, k_n)$ is given in Eq. (28). It follows that

$$E_z^s(\rho_b, \phi, z) = \frac{\omega\mu_0}{4\pi} \cos \phi e^{ik_1 d} \\ \times e^{ik_1 z} \left\{ \frac{k_2^2}{k_1^3} e^{ik_1 z} f_V(k_2 \rho_b, k_1) \right. \\ \left. - R_{13} \frac{k_2^2}{k_3^3} e^{ik_3 z} f_V(k_2 \rho_b, k_3) \right\}. \quad (43)$$

This is the z component of the field on each side of the boundary surface generated by the surface density of current $K_z(\rho_b, \phi, z)$ and surface density of charge $\eta(\rho_b, \phi, z)$. It remains to determine $E_z^s(\rho, \phi, z)$ and $E_\rho^s(\rho, \phi, z)$ for both $\rho < \rho_b$ and $\rho > \rho_b$. The former is the field reflected back into Region 1, the latter the field transmitted forward into Region 3.

IV. THE SCATTERED FIELD DUE TO A DISCONTINUITY IN THE LOWER HALF SPACE

The field scattered at the boundary, $\rho = \rho_b, z \geq 0$, in the form of a reflected field in Region 1 ($\rho < \rho_b, z \geq 0$) and a transmitted field in Region 3 ($\rho > \rho_b, z \geq 0$) is generated by the currents $K_z(\rho_b, \phi, z)$ on the boundary surface. Since these currents are all perpendicular to the boundary $z = 0$ between Region 2 and Regions 1 and 3, they can be represented by a suitable distribution of *vertical* (i.e., z -directed) electric dipoles. The complete field of a single vertical electric dipole with unit moment ($Idz = 1$ A m) is given by the following three components, each with a direct and lateral-wave part⁹.

$$B_{1\phi}^V(\rho, z) = B_{1\phi L}^V(\rho, z) + B_{1\phi D}^V(\rho, z), \quad (44)$$

$$B_{1\phi L}^V(\rho, z) = -\frac{\mu_0 k_2^2}{2\pi k_1^2} e^{ik_1(z+d)} e^{ik_1 \rho f(k_2 \rho, k_1)}, \quad (45)$$

$$B_{1\phi D}^V(\rho, z) = -\frac{\mu_0}{4\pi} (e^{ik_1 r_1} - e^{ik_1 r_2}) \left(\frac{ik_1}{\rho} - \frac{1}{\rho^2} \right), \quad (46)$$

$$E_{1\rho}^V(\rho, z) = E_{1\rho L}^V(\rho, z) + E_{1\rho D}^V(\rho, z), \quad (47)$$

$$E_{1\rho L}^V(\rho, z) = -\frac{\omega\mu_0 k_2^2}{2\pi k_1^3} e^{ik_1(z+d)} e^{ik_1 \rho f(k_2 \rho, k_1)}, \quad (48)$$

$$E_{1\rho D}^V(\rho, z) = \frac{\omega\mu_0}{2\pi k_1^2} \left\{ e^{ik_1(z+d)} e^{ik_1 \rho} \frac{ik_2^2}{k_1 \rho^2} + \frac{1}{2} \left[\frac{z-d}{\rho} e^{ik_1 r_1} \right. \right. \\ \left. \left. - \frac{z+d}{\rho} e^{ik_1 r_2} \right] \left(\frac{ik_1^2}{\rho} - \frac{3k_1}{\rho^2} - \frac{3i}{\rho^3} \right) \right\}, \quad (49)$$

$$E_{1z}^V(\rho, z) = E_{1zL}^V(\rho, z) + E_{1zD}^V(\rho, z), \quad (50)$$

$$E_{1zL}^V(\rho, z) = \frac{\omega\mu_0}{2\pi k_1^2} \frac{k_2^2}{k_1^2} e^{ik_1(z+d)} e^{ik_1 \rho f(k_2 \rho, k_1)}, \quad (51)$$

$$E_{1zD}^V(\rho, z) = -\frac{\omega\mu_0}{4\pi k_1^2} (e^{ik_1 r_1} - e^{ik_1 r_2}) \left(\frac{ik_1^2}{\rho} - \frac{k_1}{\rho^2} - \frac{i}{\rho^3} \right), \quad (52)$$

where $r_1 = [(z-d)^2 + \rho^2]^{1/2}$, $r_2 = [(z+d)^2 + \rho^2]^{1/2}$ in the exponents, $r_1 \approx r_2 \approx \rho$ in the amplitudes, and $f(k_2, \rho, k_1)$ and $f_V(k_2, \rho, k_1)$ are given in Eqs. (27) and (42), respectively. These formulas are good approximations when $|k_1^2| \gg |k_2^2|$, $|k_1 \rho| \gg 3$, $\rho^2 \gg z^2$, $\rho^2 \gg d^2$. It is to be noted that

$$E_{1\rho L}(\rho, \phi, z) = [(-k_1^2/k_2^2)\cos\phi] E_{1zL}^V(\rho, z), \quad (53)$$

$$E_{1zL}(\rho, \phi, z) = [-\cos\phi] E_{1\rho L}^V(\rho, z), \quad (54)$$

where the components with the superscript V apply to the vertical electric dipole, and those without the superscript to the horizontal electric dipole at the same depth. Note also that the radial electric field of a horizontal dipole is an order of magnitude greater than that of a vertical dipole since

$$E_{1\rho L}(\rho, 0, z) \sim (k_1/k_2) E_{1\rho L}^V(\rho, z). \quad (55)$$

The radial component of the lateral-wave electric field at ρ, ϕ, z due to a single vertical electric dipole with unit electric moment $Idz = 1$ A m at ρ_b, ϕ', z' is

$$E_{1RL}^V(R, z) = -\frac{\omega\mu_0 k_2^2}{2\pi k_1^3} e^{ik_1(z+z')} e^{ik_2 R} f_V(k_2 R, k_1), \quad \rho < \rho_b, \quad (56)$$

$$E_{3RL}^V(R, z) = -\frac{\omega\mu_0 k_2^2}{2\pi k_3^3} e^{ik_1(z+z')} e^{ik_2 R} f_V(k_2 R, k_3), \quad \rho > \rho_b, \quad (57)$$

where

$$f_V(k_2 R, k_n) = \left[\frac{ik_2}{R} - \frac{1}{R^2} - \frac{k_2^3}{k_n} \left(\frac{\pi}{k_2 R} \right)^{1/2} \right] \times e^{-ik_2 R (k_2^2/2k_n^2)} \mathcal{F}(k_2 R, k_n), \quad n = 1, 3, \quad (58a)$$

and

$$R = [\rho_b^2 + \rho^2 - 2\rho\rho_b \cos(\phi - \phi')]^{1/2} \quad (58b)$$

is the radial distance from the dipole, $[R^2 + (z-z')^2]^{1/2}$ is the distance between the dipole at ρ_b, ϕ', z' and the point of observation at ρ, ϕ, z .

The element of surface current at ρ_b, ϕ', z' is readily obtained from Eq. (33). It is

$$Idz' = dK_z(\rho_b, \phi', z') = -\mu_0^{-1} [B_{2\phi L}(\rho_b, 0, 0)]_1 (e^{ik_1 z} - e^{ik_1 z'}) \cos\phi' \rho_b d\phi' dz'. \quad (59)$$

Hence, the scattered radial lateral-wave electric fields due to a vertical line source extending from $z' = 0$ to $z' = \infty$ and of width $\rho_b d\phi'$ are

$$dE_{1RL}^V(R, z) = -\mu_0^{-1} [B_{2\phi L}(\rho_b, 0, 0)]_1 \int_0^\infty dz' E_{1RL}^V(R, z) (e^{ik_1 z} - e^{ik_1 z'}) \rho_b \cos\phi' d\phi', \quad \rho < \rho_b, \quad (60a)$$

$$dE_{3RL}^V(R, z) = -\mu_0^{-1} [B_{2\phi L}(\rho_b, 0, 0)]_1 \int_0^\infty dz' E_{3RL}^V(R, z) (e^{ik_1 z} - e^{ik_1 z'}) \rho_b \cos\phi' d\phi', \quad \rho > \rho_b. \quad (60b)$$

With Eqs. (56) and (57) it follows that the integrals with respect to z' are simple and readily carried out. They are

$$\int_0^\infty (e^{ik_1 z'} - e^{ik_1 z}) e^{ik_1 z'} dz' = \frac{i(k_3 - k_1)}{2k_1(k_3 + k_1)}, \quad (61a)$$

$$\int_0^\infty (e^{ik_1 z'} - e^{ik_1 z}) e^{ik_1 z'} dz' = \frac{i(k_3 - k_1)}{2k_3(k_3 + k_1)}. \quad (61b)$$

With these integrals, Eqs. (60a) and (60b) become:

$$dE_{1RL}^V(R, z) = \frac{i\omega k_2^2 (k_3 - k_1)}{4\pi k_1^4 (k_3 + k_1)} [B_{2\phi L}(\rho_b, 0, 0)]_1 e^{ik_1 z} e^{ik_2 R} f_V(k_2 R, k_1) \rho_b \cos\phi' d\phi', \quad (62)$$

$$dE_{3RL}^V(R, z) = \frac{i\omega k_2^2 (k_3 - k_1)}{4\pi k_3^4 (k_3 + k_1)} [B_{2\phi L}(\rho_b, 0, 0)]_1 e^{ik_1 z} e^{ik_2 R} f_V(k_2 R, k_3) \rho_b \cos\phi' d\phi', \quad (63)$$

where $f_V(k_2 R, k_n)$ is given in Eq. (58a). These are cylindrical waves centered at the vertical line source at ρ_b, ϕ' , they are rotationally symmetric within each region.

In order to simplify the determination of the complete field due to all of the line sources distributed around the cylindrical boundary at $\rho = \rho_b$, let the field be examined specifically along the radial line $\phi = 0$ along which $E_{1\rho L}(\rho, \phi, z)$ due to the dipole at $(0, 0, d)$ has its maximum. Along this line the resultant radial electric field due to vertical line elements $K_z(\rho_b, \phi')$ and $K_z(\rho_b, -\phi')$ is directed radially inward toward the origin in Region 1, radially outward in Re-

gion 3, as shown in Fig. 5. In order to represent the outward traveling waves from these sources at the observation point $(\rho, 0, z)$, the distance R in the exponents has the following form:

$$R = A \pm B, \quad (64a)$$

where

$$A = (\rho - \rho_b \cos\phi') \cos\psi'; \quad B = \rho_b \sin\phi' \sin\psi'. \quad (64b)$$

The angle ψ' in Region 1 ($\rho < \rho_b$) and Region 3 ($\rho > \rho_b$) is shown in Fig. 5. It is given by $\cos\psi' = (\rho - \rho_b \cos\phi')/R$ or by $\sin\psi' = (\rho_b \sin\phi')/R$. The upper sign in Eq. (64a) ap-

plies to distances R from (ρ_b, ϕ') , the lower sign to distances R from $(\rho_b, -\phi')$. Note that in Region 1, $\rho < \rho_b$ and $\pi/2 < \psi' < \pi$ when $\rho < \rho_b \cos \phi'$; $(\pi - \phi')/2 < \psi' < \pi/2$ when $\rho_b \cos \phi' < \rho < \rho_b$. In Region 3, $\rho > \rho_b$ and $0 < \psi' < (\pi - \phi')/2$. In amplitudes the magnitude of R is

$$R = [\rho^2 + \rho_b^2 - 2\rho\rho_b \cos \phi']^{1/2}. \quad (65)$$

With Eqs. (62), (63), and (64a) and (64b), the scattered fields at $(\rho, 0, z)$ due to the continuous distribution of surface current $K_z(\rho_b, \phi', z')$ on the boundary at $\rho = \rho_b$ are

$$E_{1\rho L}^s(\rho, 0, z) = \frac{i\omega k_2^2(k_3 - k_1)}{2\pi k_1^4(k_3 + k_1)} [B_{2\phi L}(\rho_b, 0, 0)]_1 e^{ik_2 z} \int_0^\pi e^{ik_2 A} \left\{ \left(\frac{ik_2}{R} - \frac{1}{R^2} \right) \cos k_2 B - \frac{k_2^3}{k_1} \left(\frac{\pi}{k_2 R} \right)^{1/2} e^{-ik_2 A (k_2^2/2k_1^2)} \right. \\ \left. \times \cos [k_2 B (1 - k_2^2/2k_1^2)] \mathcal{F}(k_2 R, k_1) \right\} \rho_b \cos \psi' \cos \phi' d\phi', \quad \rho < \rho_b, \quad (66)$$

$$E_{3\rho L}^s(\rho, 0, z) = \frac{i\omega k_2^2(k_3 - k_1)}{2\pi k_3^4(k_3 + k_1)} [B_{2\phi L}(\rho_b, 0, 0)]_1 e^{ik_2 z} \int_0^\pi e^{ik_2 A} \left\{ \left(\frac{ik_2}{R} - \frac{1}{R^2} \right) \cos k_2 B - \frac{k_2^3}{k_3} \left(\frac{\pi}{k_2 R} \right)^{1/2} e^{-ik_2 A (k_2^2/2k_3^2)} \right. \\ \left. \times \cos [k_2 B (1 - k_2^2/2k_3^2)] \mathcal{F}(k_2 R, k_3) \right\} \rho_b \cos \psi' \cos \phi' d\phi', \quad \rho > \rho_b \quad (67)$$

In these formulas, $R = [\rho^2 + \rho_b^2 - 2\rho\rho_b \cos \phi']^{1/2}$, $A = (\rho - \rho_b \cos \phi')^2/R$, $B = (\rho_b \sin \phi')^2/R$, and

$$[B_{2\phi L}(\rho_b, 0, 0)]_1 = -\frac{\mu_0}{2\pi k_1} e^{ik_2 d} e^{ik_2 \rho_b} f(k_2 \rho_b, k_1) = (k_1/\omega) E_{1\rho L}(\rho_b, 0, 0). \quad (68)$$

In Region 1 where $\rho < \rho_b \cos \phi'$, $\cos \psi'$ is negative so that $\exp(ik_2 A) = \exp(ik_2 \rho_b |\cos \psi'| \cos \phi') \exp(-ik_2 \rho |\cos \psi'|)$. This is a radially inward traveling wave. In Region 1 where $\rho_b > \rho > \rho_b \cos \phi'$ and in Region 3, $\cos \psi'$ is positive so that $\exp(ik_2 A) = \exp(-ik_2 \rho_b |\cos \psi'| \cos \phi') \exp(ik_2 \rho |\cos \psi'|)$ which represents a radially outward traveling wave.

Since $[B_{2\phi L}(\rho_b, 0, 0)]_1 = B_{1\phi L}(\rho_b, 0, 0) = (k_1/\omega) E_{1\rho L}(\rho_b, 0, 0)$, the scattered radial electric field in Region 1 can be expressed in terms of the radial electric field incident on the boundary in Region 1. That is

$$e_{1\rho L}(\rho, 0, z) \equiv \frac{E_{1\rho L}^s(\rho, 0, z)}{E_{1\rho L}(\rho_b, 0, 0)} = \frac{ik_2^2(k_3 - k_1)}{2\pi k_1^4(k_3 + k_1)} \int_0^\pi e^{ik_2 A} \left\{ \left(\frac{ik_2}{R} - \frac{1}{R^2} \right) \cos k_2 B - \frac{k_2^3}{k_1} \left(\frac{\pi}{k_2 R} \right)^{1/2} e^{-ik_2 A (k_2^2/2k_1^2)} \right. \\ \left. \times \cos [k_2 B (1 - k_2^2/2k_1^2)] \mathcal{F}(k_2 R, k_1) \right\} \rho_b \cos \psi' \cos \phi' d\phi'. \quad (69)$$

Similarly, with $[B_{2\phi L}(\rho_b, 0, 0)]_1 = [B_{2\phi L}(\rho_b, 0, 0)]_3 = B_{3\phi L}(\rho_b, 0, 0) = (k_3/\omega) E_{3\rho L}(\rho_b, 0, 0)$, the scattered radial electric field in Region 3 can be expressed in terms of the radial electric field incident on the boundary in Region 3. That is,

$$e_{3\rho L}(\rho, 0, z) \equiv \frac{E_{3\rho L}^s(\rho, 0, z)}{E_{3\rho L}(\rho_b, 0, 0)} = \frac{ik_2^2(k_3 - k_1)}{2\pi k_3^4(k_3 + k_1)} \int_0^\pi e^{ik_2 A} \left\{ \left(\frac{ik_2}{R} - \frac{1}{R^2} \right) \cos k_2 B - \frac{k_2^3}{k_3} \left(\frac{\pi}{k_2 R} \right)^{1/2} e^{-ik_2 A (k_2^2/2k_3^2)} \right. \\ \left. \times \cos [k_2 B (1 - k_2^2/2k_3^2)] \mathcal{F}(k_2 R, k_3) \right\} \rho_b \cos \psi' \cos \phi' d\phi', \quad (70)$$

where \mathcal{F} is given in Eq. (28).

The evaluation of the integrals in Eqs. (66)–(70) has not been accomplished in closed form. Presumably they must be evaluated numerically.

V. THE TOTAL LATERAL-WAVE ELECTRIC FIELD IN THE PRESENCE OF A DISCONTINUITY IN THE LOWER HALF SPACE

The total radial lateral-wave electric field along the central radius $\phi = 0$ in each region is the sum of the incident and scattered fields. Thus,

$$E_{1\rho L}^t(\rho, 0, z) = E_{1\rho L}(\rho, 0, z) + E_{1\rho L}^s(\rho, 0, z), \quad (71)$$

where $E_{1\rho L}(\rho, 0, z)$ is given by Eq. (39a) with $\phi = 0$ and Eq. (27), and $E_{1\rho L}^s(\rho, 0, z)$ is given by Eq. (66). Similarly,

$$E_{3\rho L}^t(\rho, 0, z) = E_{3\rho L}(\rho, 0, z) + E_{3\rho L}^s(\rho, 0, z), \quad (72)$$

where $E_{3\rho L}(\rho, 0, z)$ is given by Eq. (39b) with $\phi = 0$ and Eq. (27), and $E_{3\rho L}^s(\rho, 0, z)$ is obtained from Eq. (67). These expressions can also be written as follows.

$$E_{1\rho L}^t(\rho, 0, z) = -\frac{\omega\mu_0}{2\pi k_1^2} e^{ik_2 d + z} [e^{ik_2 \rho} f(k_2 \rho, k_1) + e^{ik_2 \rho_b} f(k_2 \rho_b, k_1) e_{1\rho L}(\rho, 0, z)]; \\ (\rho_b - \rho)^2 > z^2, \quad |k_1(\rho_b - \rho)| > 3, \quad (73)$$

$$E_{3\rho L}^t(\rho, 0, z) = -\frac{\omega\mu_0 R_{13}}{2\pi k_3^2} e^{ik_2 d} e^{ik_2 z} [e^{ik_2 \rho} f(k_2 \rho, k_3) + e^{ik_2 \rho_b} f(k_2 \rho_b, k_3) e_{3\rho L}(\rho, 0, z)]; \\ (\rho - \rho_b)^2 > z^2, \quad |k_3(\rho - \rho_b)| > 3, \quad (74)$$

where $f(k_2 \rho, k_n)$ is defined in Eq. (27), R_{13} in Eq. (30), and $e_{1\rho L}(\rho, 0, z)$ and $e_{3\rho L}(\rho, 0, z)$ are given, respectively, in Eqs. (69) and (70). These formulas give only the lateral-wave field in media in which the direct field decays rapidly. Even in these they are not complete near the source dipole or the boundary at $\rho = \rho_b$ where the direct field is also significant.

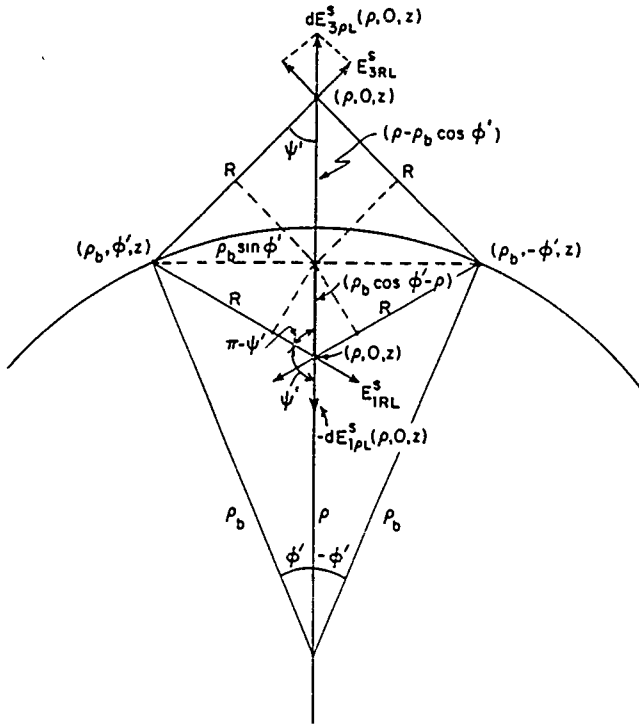


FIG. 5. Notation with respect to two points of observation at $(\rho, 0, z)$ with $\rho < \rho_b$ and $\rho > \rho_b$.

VI. NUMERICAL EVALUATION OF THE SCATTERED ELECTRIC FIELD DUE TO A VERTICAL DISCONTINUITY IN THE DENSER REGION

The radial component of the incident electric field in Region 1 $[E'_{1\rho}(\rho, 0, z)]$ due to a horizontal electric dipole with unit electric moment at depth $d = 0.15$ m has been evaluated at depth $z = 0.15$ m from Eqs. (2) and (3) with $\phi = 0$ and $k_1 = 129.4 + i64.1 \text{ m}^{-1}$, $k_2 = 4\pi \text{ m}^{-1}$ ($\sigma_1 = 3.5 \text{ S/m}$, $\epsilon_{1r} = 80$, $f = 600 \text{ MHz}$) over the range $0.5 < \rho < \rho_b = 1.86$ m. The magnitude $|E'_{1\rho}(\rho, 0, z)|$ is shown at the top of Fig. 6. For comparison, the quantity $|E'_{1\rho}(1, 0, z)|/\rho$ is also shown. Evidently, the range of ρ is in the $1/\rho$ section of the lateral-wave field.

The lateral-wave field scattered from the boundary at $\rho = \rho_b$ between Regions 1 and 3 and observed at depth $z = 0.15$ m is shown at the bottom of Fig. 6 when Region 1, $\rho < \rho_b$, is salt water ($\sigma_1 = 3.5 \text{ S/m}$, $\epsilon_{1r} = 80$) for three different media in Region 3 ($\rho > \rho_b$). These are characterized by $\sigma_3 = 0.0035 \text{ S/m}$, $\epsilon_{3r} = 80$ for lake water; $\sigma_3 = 0.35 \text{ S/m}$, $\epsilon_{3r} = 80$ for somewhat salty water; and $\sigma_3 = \infty$ for a perfect conductor (well approximated by metal). In each case, $f = 600 \text{ MHz}$. The quantity actually shown is the ratio $|E'_{1\rho L}(\rho, 0, 0.15)| = |E'_{1\rho L}(\rho, 0, 0.15)/E'_{1\rho L}(1.86, 0, 0.15)|$ given in Eq. (69). This is the normalized amplitude of the inward traveling cylindrical wave that is generated by the surface currents $K_z(\rho_b, \phi', z')$ all around the cylindrical boundary $\rho = \rho_b, 0 < z'$, and is observed along the radial line $\phi = 0$. The small oscillations are a consequence of the rotationally unsymmetric distribution of the source currents, $K_z(\rho_b, \phi', z') = K_z(\rho_b, 0, z')\cos\phi'$, and the cylindrical shape of the boundary. They would be absent if $K_z(\rho_b, \phi', z')$ were rotationally symmetric, i.e., independent of ϕ' .

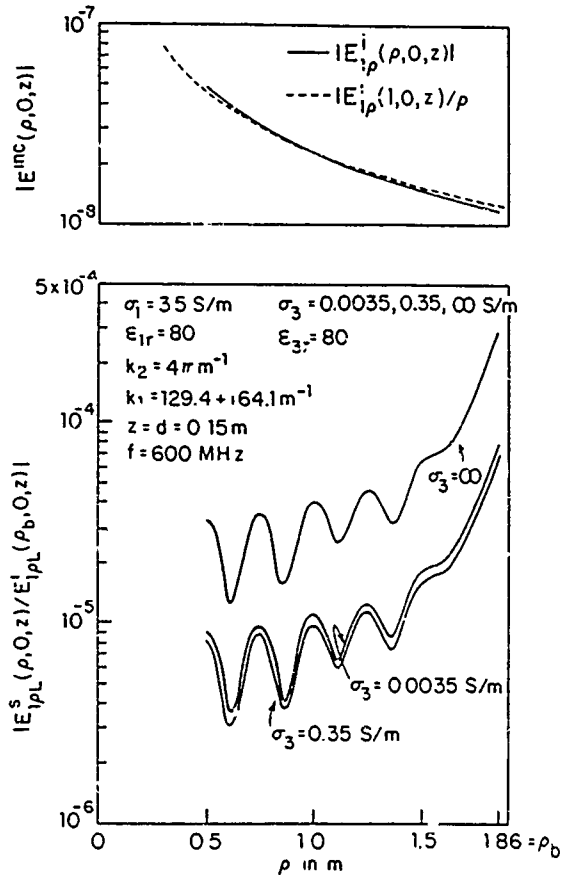


FIG. 6. Incident and scattered fields in Region 1 ($\rho < \rho_b$, $z > 0$)

What is primarily significant about the scattered field is its very small amplitude. Even when Region 3 is perfectly conducting (metal), the relative average amplitude of the scattered field when compared with the incident field is between 3×10^{-4} near $\rho = \rho_b$ and 2×10^{-5} near $\rho = 0.5$ m. This is so small that the resultant total radial electric field given by Eq. (73) differs negligibly from the incident field. The conclusion follows that the reflection of lateral waves from discontinuities or changes in the properties of the half space $z > 0$ are insignificant so long as the ratio $|k^2(z < 0)/k^2(z > 0)|$ remains small and the scattering discontinuity includes only vertical boundaries within the relatively short distances from the surface for which $|e^{kz}| = e^{-\alpha z}$ is significant. Since the scattered field transmitted into Region 3 ($\rho > \rho_b$) has a magnitude that is comparable to that of the field reflected into Region 1, the lateral wave that continues beyond the boundary, i.e., $\rho > \rho_b$, is given essentially by the first term in Eq. (74) with only an insignificant contribution from the second term—the field generated by the current $K_z(\rho_b, \phi', z')$ on the bounding surface, $\rho = \rho_b, z > 0$.

In practice, these results indicate that when a lateral wave traveling along the surface of the ocean encounters the shoreline of a low island or continent, significant reflections do not come from vertical components of induced current on the boundary. This is readily understood if it is recalled that the energy carried by lateral waves actually enters the denser half space from above and travels down into it. Thus, vertical boundaries are perpendicular to the dominant $E_{1\rho}$ component, parallel to the very much smaller E_{1z} component.

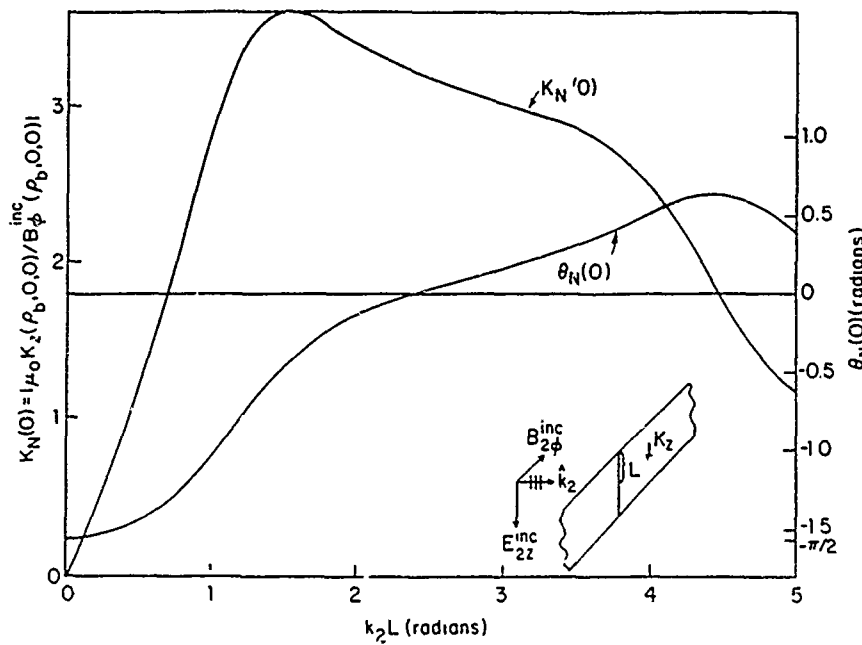


FIG. 7. Current density on infinite strip of height $2L$ in H -polarized field. (Data of Myers)

VII. THE FIELD SCATTERED BY A METAL WALL AT $\rho = \rho_b$ IN REGION 2

Although the components $E_{1z}(\rho, \phi, z)$ and $E_{3z}(\rho, \phi, z)$ in the denser half space are relatively very small, the component $E_{2z}(\rho, \phi, z)$ in the air is relatively large. This is a consequence of the boundary condition: $k_1^2 E_{1z}(\rho, \phi, 0) = k_2^2 E_{2z}(\rho, \phi, 0)$, $i = 1$ or 3 , and the assumed inequalities, $k_1^2 \gg k_2^2$. It follows that a vertical scattering obstacle in Region 2 (air, $z < 0$) is a much more effective scatterer than a comparable obstacle in the denser half space ($z > 0$). The scattered field generated by such an obstacle is readily determined when the height L of the obstacle is not electrically great, i.e., $k_2 L \ll 1$. When this is true, the incident field in Region 2 due to a horizontal electric dipole in Region 1 is obtained directly from the field in Region 1 with the help of the boundary conditions. Over Region 1, it is given by Eq. (15). Sufficiently near the surface, this reduces to Eq. (20). The associated magnetic field is given by Eq. (21).

The magnetic field incident on a metal cylinder of height L and radius ρ_b is $B_{2\phi}(\rho, \phi, 0)$ as given by Eq. (21), provided $k_2 L \ll 1$. It will be assumed that a reasonably good approximation is obtained when $k_2 L < 1.5$. In order to determine the current induced in the metal cylinder, use is made of the analysis of Myers¹⁰ who determined the current in and the scattered field of an infinitely wide strip of height $2L$ in a normally incident plane electromagnetic wave with either E or H polarization. Since salt water is a good reflector of electromagnetic waves, the current density induced on the metal cylinder of height L over salt water with $\rho_b \gg L$, $\rho_b \gg \lambda_2$, is well approximated by the current induced on the upper half of an isolated infinitely wide strip of height $2L$ in an H -polarized field. Myers reduced the determination of the current density to a differential equation which he solved numerically. The surface density of current on the strip determined by Myers can be expressed in a notation appropriate for the metal cylinder of large radius ρ_b and small height L in the form:

$$K_z(\rho_b, 0, z) = K_z(\rho_b, 0, 0)g(z) = -\mu_0^{-1}B_\phi^{\text{inc}}(\rho_b, 0, 0) \times K_N(z)e^{i\theta_N(z)}, \quad (75)$$

where $K_z(\rho_b, 0, 0)$ is the current density at the center of the strip or at the base of the cylinder, $z = 0$. It is tabulated by Myers in the normalized form

$$K_N(0)e^{i\theta_N(0)} = -\mu_0 K_z(\rho_b, 0, 0) / B_\phi^{\text{inc}}(\rho_b, 0, 0) = K_z(\rho_b, 0, 0) / H_\phi^{\text{inc}}(\rho_b, 0, 0). \quad (76)$$

The numerical values of the amplitude $K_N(0)$ and the argument $\theta_N(0)$ of the normalized current density are shown graphically in Fig. 7 as a function of L . It is seen that a maximum current is obtained near $k_2 L = 1.5$ or $L \sim \lambda_2/4$. The transverse distribution of current on the strip is $g(z)$. When $k_2 L$ is sufficiently small,

$$g(z) \sim (1 - z^2/L^2)^{1/2}. \quad (77)$$

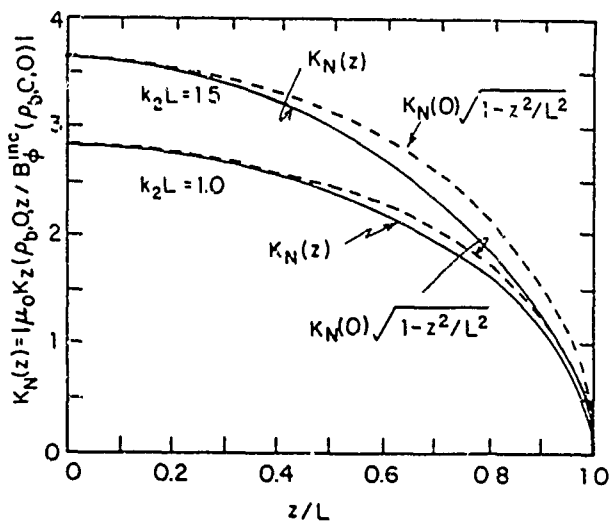


FIG. 8. Actual and approximate normalized distributions of current on strip in H -polarized, normally incident field. (Data of Myers.)

Actual distributions $K_N(z)$ as determined by Myers for $k_2L = 1.0$ and 1.5 are shown in Fig. 8 together with the quantity $K_N(0)(1 - z^2/L^2)^{1/2}$. It is seen that even when k_2L is as large as 1.5 , the approximation is acceptable. The argument $\theta_N(z)$ is not shown, but Myer's results show that $\theta_N(z) \sim \theta_N(0)$ within a few percent when $k_2L < 1.5$. It follows that for $k_2L < 1.5$, the current density on the cylindrical metal wall is well approximated by

$$K_{2z}(\rho_b, \phi', z') \sim -\mu_0^{-1} B_{2\phi L}(\rho_b, 0, 0) K_N(0) e^{i\theta_N(0)} \times [1 - (z'/L)^2]^{1/2} \cos \phi', \quad (78)$$

where $K_N(0)$ and $\theta_N(0)$ are given in Fig. 7.

Corresponding to Eq. (59) for the element of surface current on the boundary at ρ_b, ϕ', z' between Regions 1 and 3 with $z' > 0$, the element of surface current on the metal cylinder at ρ_b, ϕ', z' in Region 2 with $-L < z' < 0$ is

$$Idz' = dK_z(\rho_b, \phi', z') = -\mu_0^{-1} B_{2\phi L}(\rho_b, 0, 0) K_N(0) e^{i\theta_N(0)} \times [1 - (z'/L)^2]^{1/2} \cos \phi' \rho_b d\phi' dz'. \quad (79)$$

And corresponding to Eq. (60a), the scattered radial lateral-wave electric field at the depth z in Region 1 due to a vertical line source in Region 2 extending from $z' = -L$ to $z' = 0$ and of width $\rho_b d\phi'$ is

$$[dE_{iRL}^s(R, z)]_2 = -\mu_0^{-1} B_{2\phi L}(\rho_b, 0, 0) \times \int_{-L}^0 dz' [E_{iRL}^s(R, z)]_2 K_N(0) e^{i\theta_N(0)} \times [1 - (z'/L)^2]^{1/2} \rho_b \cos \phi' d\phi'; \quad (80)$$

$\rho < \rho_b,$

where $[E_{iRL}^s(R, z)]_2$ is the radial electric field in Region 1 due to a unit vertical electric dipole at $\rho_b, \phi', 0$ in Region 2 (air). It is given by Eq. (56) with $z' = 0$ and multiplied by the factor k_2^2/k_1^2 . With it and

$$\int_{-L}^0 [1 - (z'/L)^2]^{1/2} dz' = -\pi L/4,$$

Eq. (80) becomes

$$[dE_{iRL}^s(R, z)]_2 = -\frac{\omega L}{8k_1} K_N(0) e^{i\theta_N(0)} B_{2\phi L}(\rho_b, 0, 0) e^{ik_1 z} \times e^{ik_2 R} f_V(k_2 R, k_1) \rho_b \cos \phi' d\phi'. \quad (81)$$

This field can be compared with Eq. (62) when Region 2 is a metal so that $k_3 \rightarrow \infty$, viz.,

$$dE_{iRL}^s(R, z) = \frac{i\omega k_2^2}{4\pi k_1^4} B_{2\phi L}(\rho_b, 0, 0) e^{ik_1 z} \times e^{ik_2 R} f_V(k_2 R, k_1) \rho_b \cos \phi' d\phi'. \quad (82)$$

The ratio of Eq. (81) to Eq. (82) is

$$R = \frac{-\omega L K_N(0) e^{i\theta_N(0)} / 8k_1}{i\omega k_2^2 / 4\pi k_1^4} = \frac{\pi k_2 L}{2} \frac{k_1^3}{k_2^2} K_N(0) e^{i(\theta_N(0) + \pi/2)}. \quad (83)$$

Since this expression is independent of ϕ' , the integrated scattered field in Region 1 due to the sheet of current induced in the metal cylinder in Region 2 is given by Eq. (66)

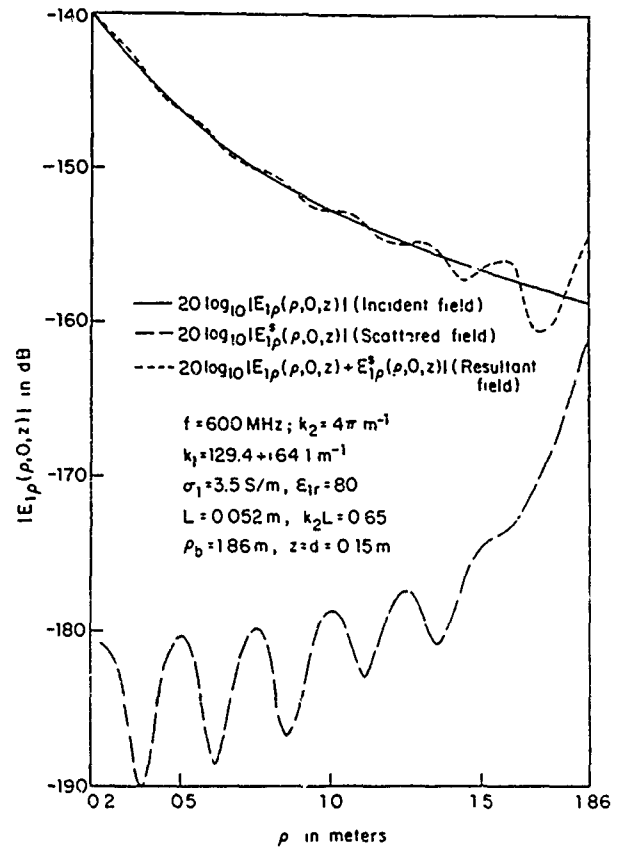


FIG. 9. Standing waves due to reflection from metal wall of height $L = 5.2$ cm $= 0.10\lambda_2$ at $\rho = \rho_b = 1.86$ m.

with $k_3 \rightarrow \infty$ and multiplied by R as given in Eq. (83). The total radial lateral-wave electric field along the central radius $\phi = 0$ at (ρ, z) in Region 1 is the sum of the incident and scattered fields as given in Eq. (71). It is

$$E_{i\rho L}^s(\rho, 0, z) = E_{i\rho L}(\rho, 0, z) + [E_{i\rho L}^s(\rho, 0, z)]_2 = E_{i\rho L}(\rho, 0, z) + RE_{i\rho L}^s(\rho, 0, z), \quad (84)$$

where $E_{i\rho L}^s(\rho, 0, z)$ is the scattered field calculated from Eq. (66) with $k_3 \rightarrow \infty$. It is represented by the curve marked $\sigma_3 = \infty$ in the lower part of Fig. 6. Calculations of the total field given by Eq. (84) have been made with $k_2L = 0.65$ for which $K_N(0) = 1.63$, $\theta_N(0) = -1.370$ and $R = 2.5 \times 10^3 e^{i1.581}$, and for $k_2L = 1.5$ for which $K_N(0) = 3.40$, $\theta_N(0) = -0.4685$, and $R = 12.9 \times 10^3 e^{i2.482}$. Graphs of the magnitude of the incident, scattered, and total fields for these two heights of the metal wall are shown respectively in Figs. 9 and 10 with $f = 600$ MHz and $\rho_b = 1.86$ m. At this frequency, the height of the metal wall is $L = 5.2$ cm in Fig. 9, $L = 11.9$ cm in Fig. 10. It is seen that at the lower height the reflected field and the amplitude of the standing waves are quite small. At the greater height (Fig. 10), the reflected field is much greater and significant standing waves are produced, especially near the reflecting wall at $\rho_b = 1.86$ m. Note that the small oscillations in the reflected waves do not significantly affect the standing-wave pattern of the total field. This is determined largely by the interaction of the incident field and the traveling-wave part of the reflected field.

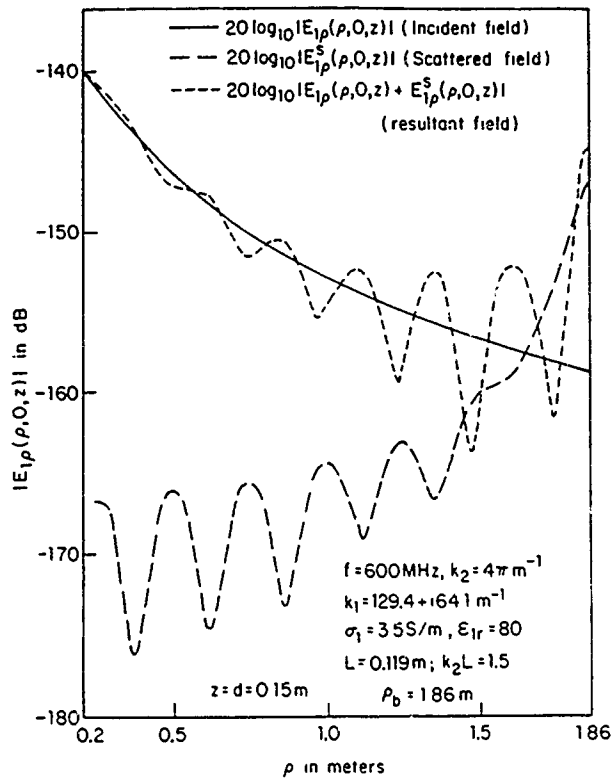


FIG 10 Standing waves due to reflection from metal walls of height $L = 11.9 \text{ cm} = 0.24\lambda_2$ at $\rho = \rho_b = 1.86 \text{ m}$.

VIII. CONCLUSION

An analysis has been made of the reflection of lateral electromagnetic waves traveling along the boundary between two half spaces, characterized by the wave numbers k_1 and k_2 that differ significantly so that $|k_1|^2 \gg |k_2|^2$. The reflecting boundaries consist of two types: (a) Vertical discontinuities in the denser medium (earth, water) in the form of changes in the wave number from k_1 to k_3 with $|k_3|^2 \gg |k_2|^2$; (b) vertical projections into the less dense medium in the form of thin walls of the denser medium. The analysis shows that reflections from the discontinuities in the denser half space are extremely small even when k_1

changes from a value characteristic of salt water to a value $k_3 \rightarrow \infty$ characteristic of a perfect conductor (metal). Reflections from metal walls in air when $k_3 \sim \infty$ are much larger but still quite small when the height of the wall is a tenth of a wavelength or less. They are very significant when the wall is a quarter-wavelength high. These results are readily understood if it is recalled that the vertical unit dipole in air is very superior to the vertical unit dipole in salt water as a generator of lateral waves. It follows that the vertical current induced on the metal surface in air generates a relatively strong reflected lateral-wave field in the salt water, the vertical current induced on the vertical metal (or other) surface in the salt water generates a relatively very small reflected lateral-wave field even with equal currents. Actually, the current along the metal surface in the salt water is rapidly attenuated with depth z owing to the factor $e^{ik_3 z} = e^{-\alpha_3 z} e^{i\beta_3 z}$.

ACKNOWLEDGMENTS

The author wishes to thank Barbara H. Sandler for carrying out the numerical calculations and Margaret Owens for correcting the manuscript. This work was supported in part by the Joint Services Electronics Program under Contract N00014-75-C-0648 and in part by the Office of Naval Research under Contract N00014-79-C-0419, both with Harvard University.

- ¹R. W. P. King, B. H. Sandler, and L. C. Shen, *IEEE Trans. Geosci. Remote Sensing* GE-18, 225 (1980).
- ²R. W. P. King, J. T. dePettencourt, and B. H. Sandler, *IEEE Trans. Geosci. Electron.* GE-17, 36 (1979).
- ³R. W. P. King and G. S. Smith, *Antennas in Matter* (MIT, Cambridge, Massachusetts, 1981).
- ⁴A. Baños, Jr., *Dipole Radiation in the Presence of a Conducting Half-Space* (Pergamon, Oxford, England, 1966), pp. 197–198, Eqs. (7.1)–(7.7).
- ⁵A. Baños, Jr., *Dipole Radiation in the Presence of a Conducting Half-Space* (Pergamon, Oxford, England, 1966), Chap. 7.
- ⁶T. T. Wu and R. W. P. King, *Radio Sci.* 17, 521 (1982).
- ⁷T. T. Wu and R. W. P. King, *Radio Sci.* 17, 532 (1982).
- ⁸R. W. P. King and T. T. Wu, *J. Appl. Phys.* 54, 507 (1983).
- ⁹R. W. P. King, *J. Appl. Phys.* 53, 8476 (1982).
- ¹⁰J. M. Myers, Ph.D. thesis (Harvard University, 1962) (unpublished).

Experiments on the reflection of lateral electromagnetic waves

M. F. Brown, R. W. P. King, and T. T. Wu

Grordon McKay Laboratory, Harvard University, Cambridge, Massachusetts 02138

(Received 28 October 1983; accepted for publication 3 January 1984)

The measured reflections of lateral waves at discontinuities and boundaries are shown for two frequencies. A cylindrical model lithosphere bounded at its perimeter in seven distinct ways is utilized. The resulting fields are compared with the theory of normally incident lateral waves.

PACS numbers: 41.10.Hv

I. INTRODUCTION

The electromagnetic field components associated with lateral-wave propagation and reflection can be measured in a model lithosphere.¹ The reflection process which occurs at discontinuities in such a model is quite complicated, when the source is a horizontal electric dipole, all six components of the electromagnetic field are involved. A choice of measured fields and boundary geometries characterized by simplicity is therefore the most meaningful in an initial experimental basis for theory. In the present study, plots of the cylindrical radial component $E_{1\rho}$ in the denser medium (Region 1) are presented. The directional strength attributed to the component² renders it useful as a source of reflected and scattered fields when incident upon isolated obstacles. For example, the scattering due to rectilinear extensions of air into salt water has been analyzed by charting the magnitude and phase of $E_{1\rho}$.¹ The vertical field in air which accompanies surface-wave propagation at the planar abutment of two regions (one or both of which may be described by complex wave numbers) is likewise important and interesting and has been investigated using open-ended waveguides.³⁻⁵

The dependence of both air and dense-medium field components upon the cylindrical variables ρ , ϕ , and z has been expressed in various ways since the original formulation of vertical dipole fields above the earth by Sommerfeld,⁶ although for indoor measurements the recently derived formula for the $E_{1\rho}$ component of the companion paper⁷ is particularly useful. It is important to note that reflections ascribed to plane waves at boundaries between material media with their attendant Fresnel coefficients do not form an adequate basis for the description of the reflected surface waves of the present paper. Quite close to the interface between air and a conducting half space, some qualitative aspects of plane waves have been measured, however, and in the limit of high frequencies spherical waves incident upon planar surfaces may be regarded as bundles of homogeneous plane waves,⁸ each element of which is reflected, transmitted, and refracted as prescribed by geometrical optics.

The reflection of electromagnetic surface waves at non-planar and perturbed planar bounding surfaces has been discussed to some extent in terms of the effects of rough material surfaces⁹ and high-frequency waves backscattered from salt water.¹⁰ The discussions indicate the need for studies in which scatterers project into both conducting and less dense half spaces. In the present study, simple combinations of horizontal and vertical metal planes so oriented are chosen as discontinuities.

II. REFLECTIONS FROM OBJECTS OUTSIDE THE IDEAL MODEL

The apparatus for the excitation of lateral waves in a shallow tank of salt water by a horizontal electric dipole (monopole with image) is the same as that described in Ref. 1. In order to avoid troublesome reflections from the side walls, the rectilinear tank used in the earlier investigations has been adapted to a circular symmetry. In this way, only radially directed waves are involved at normal incidence at circular boundaries. The adaptation is shown schematically in Fig. 1. With it, the measured data for $E_{1\rho}$ show an even closer correspondence to theoretical predictions than previously reported.

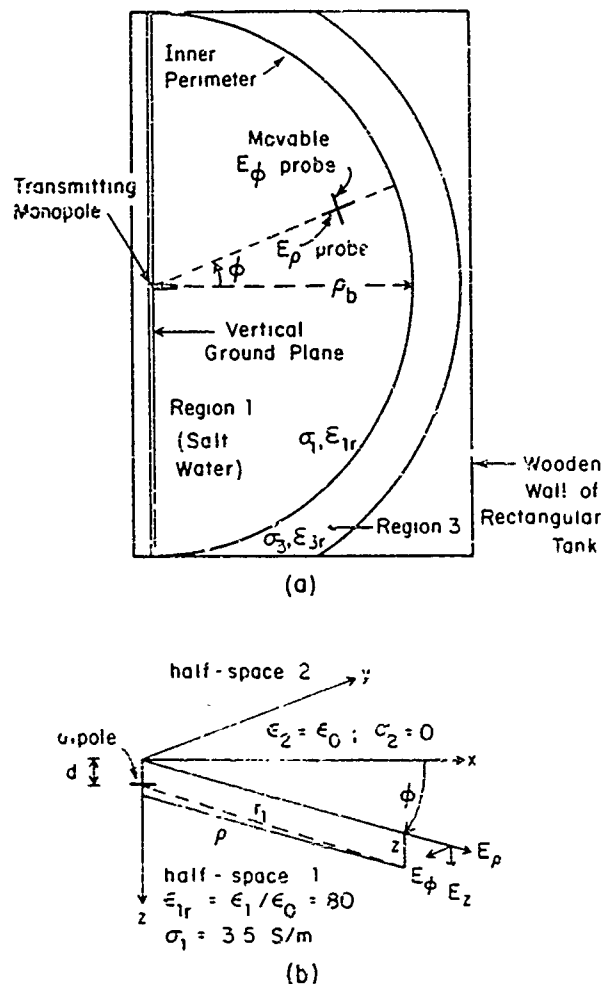


FIG. 1. (a) Schematic diagram of semi-circular tank, (b) Field components of Hertzian dipole near planar interface; $I_0 \Delta x = 1 \text{ A m}$.

ed, and movable metallic sheets to reduce reflections from the side walls have been eliminated.

Initially, measurements were made with a metal top plate quite close to the air-salt water boundary. However, theory predicts that the surface waves in the presence of the top plate are exponentially attenuated with distance instead of according to the combination of powers of inverse distances and error functions that characterize true lateral waves under an unbounded air space. Although the actual magnitudes of the decaying fields are very similar over the distances involved in the tank, it seemed desirable to remove the top plate. This necessarily introduces some reflection from the ceiling of the laboratory and the metal pipes that are close to it. These are between 2.5 and 3 m above the surface of the water. At $f = 644$ MHz, this height is of the order of 6 wavelengths, at $f = 1.5$ GHz of the order of 15 wavelengths. The observed effect of the reflections is quite small at the lower frequency, much smaller at the higher frequency. However, since interesting reflections at the cylindrical boundary can also be very small, it is desirable to obtain an accurate picture of the detailed nature of the effect of reflections from the ceiling so that they may be identified and separated from radial reflections at the cylindrical boundary when these are very small. When the ceiling is sufficiently far away—five or more wavelengths—the direct reflection is so small that multiple reflections can be disregarded at least in order to obtain a qualitative or semi-quantitative measure of the nature and significance of observable interference patterns. An approximate analysis is given in the Appendix together with graphs of the theoretical interference patterns obtained when the ceiling is represented first by a metal plate and then by an approximation of a line source that generates an approximate plane wave normally incident on the water surface of the tank along the radial line where the measurements of $E_{1\rho}$ are made. These can be compared with observed patterns which, in general, involve three waves: (1) The direct lateral waves with both vertical and radial components traveling radially outward from the source, (2) reflections from the cylindrical boundary in the form of lateral waves traveling radially inward toward the source and producing a regular standing-wave pattern, and (3) transverse plane waves coming from the ceiling at normal or near normal incidence and polarized with the electric field in the radial direction. These produce interference patterns with traveling and standing lateral waves that are quite different from ordinary standing waves produced by similar waves traveling in opposite directions.

III. MEASUREMENTS AT $f = 1.5$ GHz

The excitation of lateral surface waves by a radio-frequency source and the mechanisms of data acquisition in the cylindrical tank are identical to those described in Ref. 1. Changes other than those relating to side walls and top plate are restricted to radial discontinuities and adjustable parameters in the complex wave number of Region 1 defined by

$$k_1 = \omega \mu_1 \epsilon_{e1}^{1/2} (1 + i\sigma_{e1}/\omega\epsilon_{e1})^{1/2}. \quad (1)$$

Here, ϵ_{e1} is the real effective permittivity, σ_{e1} the real effective conductivity, $\mu_1 = \mu_0$, and $\omega = 2\pi f$.

The first physical configuration used in the measurements is shown in Fig. 2(a). The associated $E_{1\rho}$ field has been plotted over four air wavelengths ($\lambda_2 = 20.0$ cm). $E_{1\rho}$ as a function of ρ is shown in Fig. 3(a) where the field intensity is, as indicated, 10 dB per given vertical increment. For the combination of the two homogeneous Regions 1 (salt water, and 3 (metal) in contact in the z direction along the cylinder $\rho = \rho_0$ and having a continuous uniform (unstepped) interface with air (Region 2), little reflection is evident. There is a very small undulation with maxima separated by distances only slightly greater than λ_2 . This must be due to very small reflections from the ceiling like those in the middle of Fig. A2 in the Appendix, but with smaller amplitudes.

Simple variations on the above placement of metal planes can now be made. They correspond roughly to inversions about $z = 0$ [Fig. 2(b)] and serve to conjoin theory and experiment (see Sec. V). Since energy is absorbed rapidly with depth in the denser medium, the vertical metal plane need be only several skin depths deep. Measured results for an extension of the vertical metallic boundary to $L = 15$ cm above the water surface are shown in Fig. 3(b). The undulatory pattern suggests reflections from both the radial boundary and the ceiling of the general type shown at the bottom of Fig. A2.

The complete theoretical formula for the unperturbed $E_{1\rho}$ field in Region 1 is⁷

$$E_{1\rho} = -\frac{\omega\mu_0}{2\pi k_1^2} \cos \phi \left\{ e^{ik_1(z+d)} e^{ik_1\rho} \left[\frac{ik_1^2}{\rho} - \frac{k_1^2}{\rho^2} - \frac{i}{\rho^3} - \frac{k_1^4}{k_1} \left(\frac{\pi}{k_2\rho} \right)^{1/2} e^{-ik_2\rho(k_1^2/2k_2^2)} \mathcal{F}(k_2\rho, k_1) \right] - e^{ik_1(\rho^2 - (z+d)^2)^{1/2}} \left(\frac{k_1}{\rho^2} + \frac{i}{\rho^3} \right) \right\}, \quad (2)$$

where $\mathcal{F}(k_2\rho, k_1)$ is defined in terms of the Fresnel integrals¹¹ C_2 and S_2 as

$$\mathcal{F}(k_2\rho, k_1) = (1/2) - C_2[k_2\rho(k_1^2/2k_2^2)] + i\{(1/2) - S_2[k_2\rho(k_1^2/2k_2^2)]\}. \quad (3)$$

A graph of the magnitude of the field calculated from Eq. (2) for $d = 0$ is given in Fig. 3(c). The decay rate with radial distance follows very closely that of the curve for minimally perturbed $E_{1\rho}$ in Fig. 3(a). The relative decay rate is a criterion conveniently employed to test the adherence of minimally perturbed fields measured in the model lithosphere to precise theory for freely propagating $E_{1\rho}$.

IV. MEASUREMENTS AT $f = 644$ MHz

Reflections from configurations of perimetrical metal sheets including the vertical one directly treated by theory⁷ are of interest. Thus, in addition to the simple combination of vertical and horizontal metal sheets described in Sec. III, measurements involving single vertical sheets of various heights L above the surface combined with a dense-medium corner [Figs. 2(c)–2(g)] have been made. The reflecting corner, or 90° wedge which is formed with air is labeled $c_{2,3}$ in Fig. 2(c). The data at 644 MHz are concerned primarily with the effects of vertical sheets, particularly the high ones. With

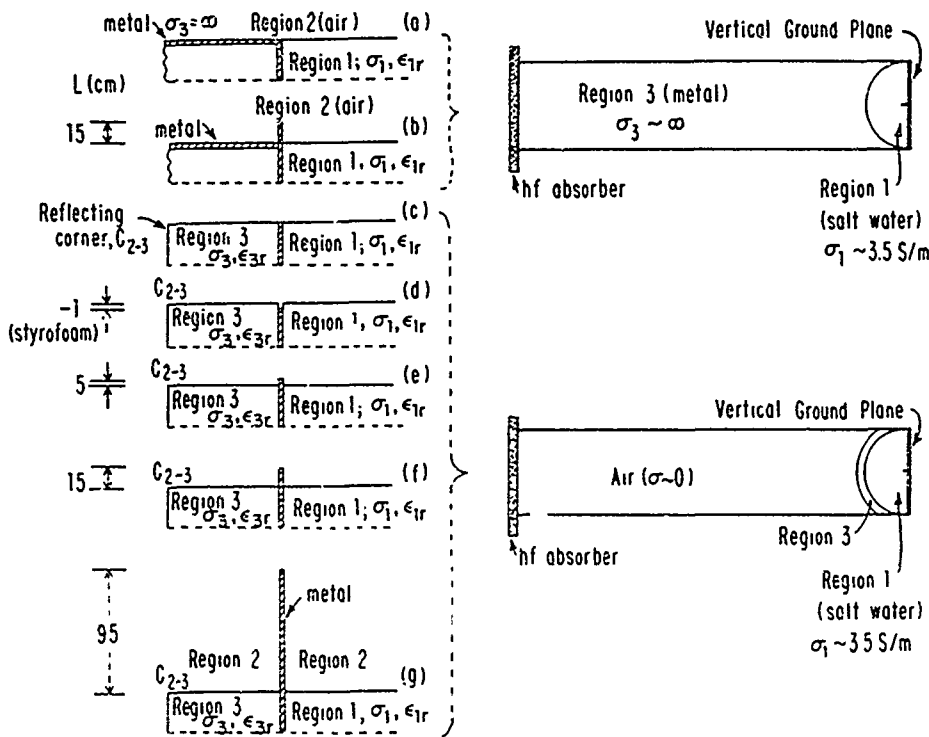


FIG. 2. Configurations of discontinuities at perimeter of model lithosphere. Side views (left); top views (right).

$L \geq 5 \text{ cm}$, reflections from the corner $c_{2,3}$ are expected to become relatively insignificant with increasing L since the corner is in the geometrical optics shadow of the higher sheets. At 644 MHz, an integral number (precisely four) air wavelengths are contained radially within the circularly bounded model lithosphere. Since the wavelength is much longer than that used to obtain the results of Sec. III, measurements have been taken over a longer radial distance. In presenting the data in Figs. 4 and 5, a larger dB scale has been used to magnify the standing-wave character of multiply-reflected lateral waves.

At sheet heights $L = 0, -1$, and 5 cm [configurations of Fig. 2(c)–2(e)], traveling waves with a superimposed small interference pattern are observed (Fig. 4). A comparison with Fig. A1 in the Appendix shows that they closely resemble the dashed curve 3 in their intermodal spacing ($\lambda_2 = 46.6 \text{ cm}$) and decay rate, which is in close agreement with Eq. (2).

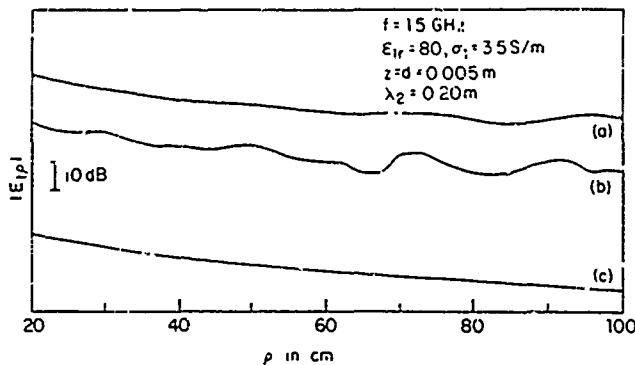


FIG. 3. $E_1 \rho$ vs distance in Region 1. (a) Measured, configuration of Fig. 2(a); (b) Measured, configuration of Fig. 2(b); (c) Theoretical (unperturbed) Arbitrary relative amplitudes.

The patterns of the curves for $L = -1$ and 0 cm are clearly interference patterns of the type shown in Fig. A1, curve 3, due to reflections from the ceiling. They are not standing-wave patterns due to reflections of the radially directed cylindrical wave. The same is also true of the solid line curve in Fig. 4 which was observed with a cylindrical wall of height $L = 5 \text{ cm}$ above the surface at $\rho = \rho_b = 1.86 \text{ m}$. A comparison with the broken-line curve in Fig. A3—which gives the theoretical equivalent as a superposition of the direct lateral wave, a lateral wave reflected from the cylindrical boundary, and a plane wave reflected from the ceiling—is in good agreement. The lateral-wave reflections at the 5-cm-high metal wall are so small compared with the reflections from the ceiling that they produce only a minor perturbation of the typical interference pattern due to reflections from the

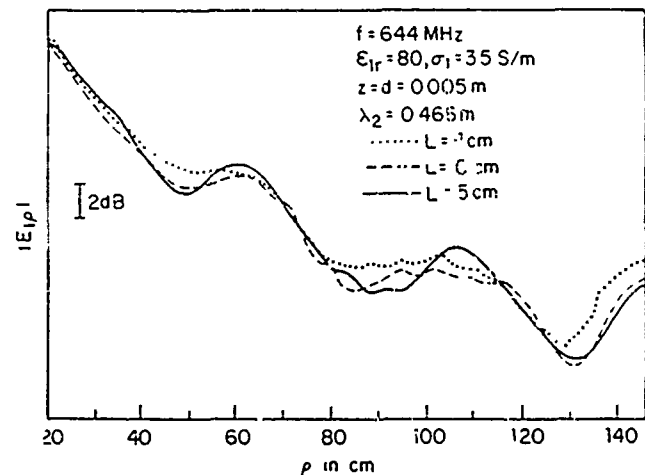


FIG. 4. $E_1 \rho$ vs distance in Region 1. Measured, configurations of Fig. 2(c)–2(e). Arbitrary relative amplitudes.

ceiling. This is true in both theoretical and measured curves.

The small undulations particularly evident at $\rho \sim 75$ –125 cm in Fig. 4 are not present when $|E_{1\rho}|$ vs ρ is plotted on a 2 dB per vertical increment scale for metal sheets higher than $L = 5.0$ cm. The effect of the boundary at $c_{2,3}$ is to generate a cylindrical wave (much like that of a scattered plane wave incident upon a Sommerfeld right-angle wedge). This cylindrical wave occurs as an implicit contribution to the net interference pattern at $\rho \sim 75$ –125 cm. The net pattern is expected to be complicated for L small.

In Fig. 5(c) the counterpart of the $L = 15$ -cm vertical extension of Sec. III is plotted. The configuration is that of Fig. 2(f). Compared to the curve for $L = 5$ cm in Fig. 4, pronounced radial standing waves are now apparent. The effects of reflections from the ceiling with their spacing near $\lambda_2 \simeq 47$ cm between maxima are overwhelmed by the much larger reflections from the cylindrical boundary to form normal standing waves with $\lambda_2/2$ spacing between adjacent minima. In Fig. 5(a) is the quite similar curve for $L = 95$ cm, but with a much higher standing-wave ratio. As the sheet attains such increased heights, its effects provide a closer and closer approximation to an image plane. The specular-reflection result from an infinite vertical metal plane at $\rho = 1.86$ m is shown in Fig. 5(b); it is obtained from Eq. (2) without the last term (which contributes only at distances very close to the source dipole). It is

$$E_{1\rho} = -\frac{\omega\mu_0}{2\pi k_1^2} e^{ik_1(z+d)} \left\{ e^{ik_1\rho} \left[\frac{ik_2^2}{\rho} - \frac{k_2}{\rho^2} - \frac{i}{\rho^3} - \frac{k_2^4}{k_1} \left(\frac{\pi}{k_2\rho} \right)^{1/2} \right] \times e^{-ik_2\rho(k_2^2/2k_1^2)} \mathcal{F}(k_2\rho, k_1) \right\} - e^{ik_1\rho} \left[\frac{ik_2^2}{\rho_1} - \frac{k_2}{\rho_1^2} - \frac{i}{\rho_1^3} - \frac{k_2^4}{k_1} \left(\frac{\pi}{k_2\rho_1} \right)^{1/2} \right] \times e^{-ik_2\rho_1(k_2^2/2k_1^2)} \mathcal{F}(k_2\rho_1, k_1) \right\}, \quad (4)$$

where $\rho_1 = 2\rho_b - \rho$ for the tank of radius ρ_b , and $\mathcal{F}(k_2\rho, k_1)$ is given by Eq. (3). Of course, in the limit of precise adherence to image theory, the boundary sheet needs to be infinite and planar, not finite and slightly curved. Some effects due to small reflections from the ceiling are evident in the relative magnitudes of successive maxima and minima in the experimental curves [Figs. 5(a) and 5(c)] as compared with the theoretical curve [Fig. 5(b)].

V. THEORY AND EXPERIMENT

The configurations of Figs. 2(a) and 2(b) with $k_2 L < 1$ are accurate models of the half spaces depicted in Figs. 2(a) and 2(b) in Ref. 7. The configurations of Fig. 2(b) with $k_2 L > 1$ and 2(c)–2(g) have related, albeit more complicated, theoretical formulations.

The magnitude of the perturbation due to the discontinuity between Regions 1 and 3 where $z > 0$ [Fig. 2(a)] is, according to the theory, very small. The importance of this calculation is in its prediction of the relative scattering ability of discontinuities above and below the $z = 0$ plane of Fig. 2(a). For, if the radial reflection is of very small order, the

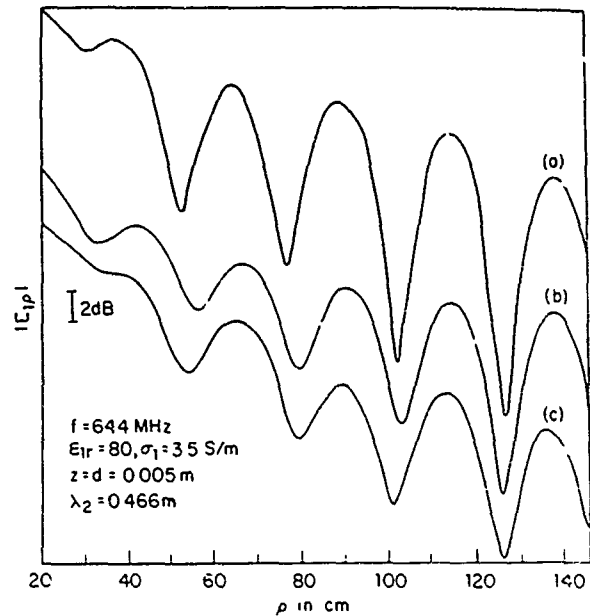


FIG. 5 $E_{1\rho}$ vs distance in Region 1 (a) Measured, configuration of Fig. 2(g); (b) Theoretical (specular reflection); (c) Measured, configuration of Fig. 2(f). Arbitrary relative amplitudes.

oscillations measured in the $E_{1\rho}$ pattern [Fig. 3(a)] must be due to other sources, notably the reflections from the ceiling. In view of the fact that the skin depth at 1.5 GHz is very small at the surface of the vertical metallic layer of Region 3, and the fact that energy is dissipated rapidly with distance from boundaries in Region 1, the effects of the finiteness of the model lithosphere in Region 1 for $z > 0$ are unlikely to influence the $E_{1\rho}$ component significantly. In the absence of low-conductivity discontinuities in the denser medium (the presence of which is addressed in Ref. 1), the source of scattering must lie in the upper ($z < 0$) half space. A test of the relative scattering abilities may thus be made through a comparison of the effects of high-conductivity perturbations for both $z > 0$ and $z < 0$.

It is shown in Ref. 7 that the reflection from Region 3 ($\rho \geq \rho_b$, $z \geq 0$) is very small even when this is a metal. It follows that the reflection from a vertical metal sheet at $\rho = \rho_b$, $z \geq 0$ should likewise be small. No significant change in the measured field in Fig. 3(a) was produced by such a sheet. No perturbative effects on the curve of Fig. 3(a) were observed upon submersion of an extensive array of conducting objects in Region 1 (including plates, rods, and metal cylinders). Thus, it would appear that the very small reflection predicted theoretically from vertical discontinuities in the denser half space is a general result for high-conductivity objects in a half space (Region 1) for which $|k_1|^2 \gg |k_2|^2$.

The results of scattering from boundaries at $\rho = \rho_1$, $z < 0$, as shown in Fig. 2(b), make it clear that sufficiently tall metal objects in air have large reflection coefficients and are therefore, strong generators of standing-wave patterns in $E_{1\rho}$. Measured standing-wave patterns due to such reflectors in the configurations of Figs. 2(e)–2(g) show them to produce significant standing waves comparable to those of more complicated structures in the half space $z < 0$; those due to

the configurations of Figs. 2(c) and 2(d) suggest that dense-medium corners such as $c_{2,3}$ may be comparable to short conducting objects in the region $z < 0$ in their ability to reflect incident lateral waves.

VI. THE MEDIUM-SCATTERER COMPLEMENTARITY

In the first experimental basis¹ for formula (2) of the present paper, low-conductivity (Styrofoam) discontinuities in the dissipative medium of a pair of half spaces were shown to cause significant reflections. In that study the reflections were localized to the vicinity of the rectilinear Styrofoam depressions. In the present study, high-conductivity (metallic) extensions in air are shown to cause reflections. Here the extensions are really total enclosures; the reflections are more systemic (multiply reflected lateral waves). In the earlier experiments, isolated Styrofoam and plastic extensions in air produced a negligible scattering pattern; indeed, much of the experimental technique depended on this fact. In the present study, highly conducting bodies of extensive size with vertical boundaries in the dissipative half space are shown to produce very small scattering. For either localized or extensive scattering, the observations suggest that a symmetric role is played by the medium and the scatterer. Scattering is maximized when a high (low)-conductivity discontinuity penetrates a low (high)-conductivity half space.

VII. CONCLUSION

In confirmation of theoretical predictions,⁷ measured scattering by objects of high conductivity in Region 2 ($z < 0$) is significant. On the other hand, the scattered field from such objects in Region 1 ($z > 0$) is so small that it must be inferred indirectly. Measurements show that, relative to reflections from obstacles in Region 2, the effects in Region 1 are very small, in agreement with theoretical calculations.

ACKNOWLEDGMENTS

This work was supported in part by the Office of Naval Research under Contract N00014-79-C-0419 and in part by the Joint Services Electronics Program under Contract N00014-75-C-0648, both with Harvard University.

APPENDIX: REFLECTIONS FROM THE CEILING

Measurements of the properties of lateral electromagnetic waves in an indoor tank require an understanding of the nature and magnitude of reflections not only from the radial boundary $\rho = \rho_b = 1.86$ m of the semicircular volume of salt water, but also from the concrete ceiling at a height $D \sim 2.5$ – 2.75 m and from four copper pipes just below it. Of primary interest is the effect of such reflections on a simple traveling lateral wave characterized in the water by

$$E_{1\rho}(\rho, 0, z) = -\frac{\omega\mu_0}{2\pi k_1} e^{ik_1(z+d)} e^{ik_2\rho} f(k_2\rho, k_1) \equiv Be^{i\theta_B} \quad (\text{A1})$$

$$|E_{1\rho}(\rho, 0, z) + E_{1\rho}^c(\rho, 0, z)| = \left| Be^{i\theta_B} + A(\Theta_1) e^{i\Theta_1} \frac{e^{ik_2 r}}{r_0} \right|$$

$$= \left[B^2 + \frac{2A(\Theta_1)B}{r_0} \cos(k_2 r_0 + \theta_A - \theta_B) + \frac{A^2(\Theta_1)}{r_0^2} \right]^{1/2}. \quad (\text{A7})$$

where B is the magnitude, θ_B the angle of $E_{1\rho}(\rho, 0, z)$. In Eq. (A1),

$$f(k_2\rho, k_1) = \frac{ik_2^2}{\rho} - \frac{k_2}{\rho^2} - \frac{i}{\rho^3} - \frac{k_2^4}{k_1} \left(\frac{\pi}{k_2\rho} \right)^{1/2} \times e^{-ik_2\rho(k_2^2/2k_1^2)} \mathcal{F}(k_2\rho, k_1), \quad (\text{A2})$$

$$\mathcal{F}(k_2\rho, k_1) = (1/2) - C_2[k_2\rho(k_2^2/2k_1^2)] + i\{(1/2) - S_2[k_2\rho(k_2^2/2k_1^2)]\}. \quad (\text{A3})$$

Here C_2 and S_2 are Fresnel integrals. The direct-field terms that involve $e^{ik_1 r}$, $r = [\rho^2 + (z-d)^2]^{1/2}$, have been omitted in Eq. (A1) since they are negligible beyond a very short distance from the source. Graphs of $20 \log_{10}|E_{1\rho}(\rho, 0, z)|$ as defined in Eq. (A1) are shown in solid lines in Fig. A1 at $f = 600$ MHz and in Fig. A2 at $f = 1.5$ GHz. For the calculations, $\sigma_1 = 3.5$ S/m and $\epsilon_{1r} = 80$.

Also of interest in a tank of finite radial extension is the effect of reflections from the ceiling on a standing lateral wave due to the interaction of reflections from the circular boundary at $\rho = \rho_b = 1.86$ m with the outward traveling lateral wave from the source. Since these latter can be quite small, they could have an amplitude comparable with or even smaller than the amplitude of reflected waves incident on the tank from the ceiling.

Let the ceiling be approximated initially by an infinite highly conducting plane at the height D from the surface of the water. The reflected field corresponds to that of an image source with reversed electric moment at the depth d in an image tank of salt water at a distance $2D$ from the actual water. The radial electric field on the surface of the water at $z = 0$, above the point $(\rho, 0, z)$ where $E_{1\rho}(\rho, 0, z)$ is to be calculated, is

$$E_{1\rho}^c(\rho, 0, 0) \sim -\frac{\omega\mu_0}{2\pi k_1} e^{ik_1 d} e^{ik_2 r_0} \frac{2ik_2 D}{r_0^2} = -\frac{i\omega\mu_0 k_2}{2\pi k_1} e^{ik_1 d} \frac{e^{ik_2 r_0}}{r_0} \cos \Theta_1, \quad (\text{A4})$$

where $r_0 = (\rho^2 + 4D^2)^{1/2}$ and Θ_1 is the angle of incidence, $\cos \Theta_1 = 2D/r_0$. The field transmitted into the water is

$$E_{1\rho}^c(\rho, 0, z) \sim E_{1\rho}^c(\rho, 0, 0) \frac{e^{ik_1 z} 2k_2 \cos \Theta_1}{k_2 \cos \Theta_1 + (k_1^2 - k_2^2 \sin^2 \Theta_1)^{1/2}} \quad (\text{A5})$$

$$\sim -\frac{i\omega\mu_0 k_2^2}{\pi k_1} \frac{\cos^2 \Theta_1}{k_2 \cos \Theta_1 + k_1} e^{ik_1 d} \frac{e^{ik_2 r_0}}{r_0} = A(\Theta_1) e^{i\Theta_1} \frac{e^{ik_2 r_0}}{r_0}. \quad (\text{A6})$$

In Eq. (A6) use has been made of the inequality $k_2^2 \ll |k_1|^2$ to simplify the reflection factor; $A(\Theta_1)$ is a real magnitude.

When the field in Eq. (A6) is combined with that in Eq. (A1), the result is

When $2D$ and, hence, r_0 are sufficiently large, $B^2 \gg A^2(\theta_i)/r_0^2$ so that

$$|E_{1\rho}(\rho, 0, z) + E_{1\rho}^c(\rho, 0, z)| \sim B + \frac{A(\theta_i)}{r_0} \cos(k_2 r_0 + \theta_A - \theta_B). \quad (\text{A8})$$

This field has been evaluated at $f = 600$ MHz with $2D = 5.25$ m and $d = z = 0.15$ m. It is shown in dotted line as curve 2 in Fig. A1. It represents the interference pattern between a lateral wave traveling along the air-water boundary and a singly reflected wave from a metal ceiling at the distance $D = 2.625$ m. Actually, the field incident from the image source is largely reflected at the surface of the water so that multiple reflections occur that involve the distances $2r_0$, $4r_0$, etc. Since the first reflected field is quite small compared with the lateral-wave field, the much smaller higher-order reflections can be neglected in this qualitative and semi-quantitative study.

An interesting modification of the field reflected from the ceiling is to assume it to be a normally incident plane wave obtained from Eq. (A8) by setting $\theta_i = \pi/2$ and $r_0 = 2D$. When this is done, Eq. (A8) becomes

$$|E_{1\rho}(\rho, 0, z) + E_{1\rho}^c(\rho, 0, z)| \sim B + (A/2D) \cos(2k_2 D + \theta_A - \theta_B). \quad (\text{A9})$$

This field is also shown graphically in Fig. A1 by curve 3 in dashed line. It resembles the curve obtained with the dipole image but the distance between successive maxima is λ_2 , the wavelength in air, and not a distance greater than λ_2 that increases with angle.

In order to investigate the effect of reflections from the ceiling on a standing-wave pattern of lateral waves, it is ne-

cessary to include a reflecting boundary that provides a radially inward traveling wave. This is most simply and accurately done with a metal image plane at $\rho = \rho_b$. This provides an inward traveling wave along the radial line $\phi = 0$ apparently originating at an image dipole at $(2\rho_b, 0, z)$. The unit dipole moment in the image is the negative of that in the source. The field is given by

$$E_{1\rho}^r(\rho_i, 0, z) = \frac{\omega\mu_0}{2\pi k^2} e^{ik_1(z+d)} e^{ik_2\rho_i} f(k_2\rho_i, k_1) = -C e^{i\theta_c}, \quad (\text{A10})$$

where $\rho_i = 2\rho_b - \rho$. When Eq. (A10) is combined with Eq. (A1), the magnitude of the resulting field is

$$|E_{1\rho}(\rho, 0, z) + E_{1\rho}^r(\rho_i, 0, z)| = [B^2 - 2BC \cos(\theta_B - \theta_c) + C^2]^{1/2}. \quad (\text{A11})$$

When $\rho_i = 2\rho_b - \rho$ is sufficiently large compared with ρ so that $B^2 \gg C^2$, Eq. (A11) is approximated by

$$|E_{1\rho}(\rho, 0, z) + E_{1\rho}^r(\rho_i, 0, z)| \sim B - C \cos(\theta_B - \theta_c). \quad (\text{A12})$$

Calculations have been made from Eq. (A12) at $f = 1.5$ GHz for salt water with $\sigma_1 = 3.5$ S/m and $\epsilon_{1r} = 80$ so that $k_1 = 289.8 + i71.2 \text{ m}^{-1}$ and $k_2 = 10\pi \text{ m}^{-1}$. With $\rho_b = 1.86$ m, the condition $B^2 \gg C^2$ is quite well satisfied in the range $\rho \leq 1.0$ m. Specifically at $\rho = 0.1$ m, $C^2/B^2 = 1.7 \times 10^{-4}$, at $\rho = 1$ m, $C^2/B^2 = 0.081$. The graph of Eq. (A12) is shown in broken line at the top of Fig. A2 together with the solid-line curve of B alone. The interaction of the two traveling waves moving in opposite directions produces a typical standing-wave pattern with successive maxima or minima separated by the distance $\lambda_2/2$. The standing-wave ratio (SWR) at

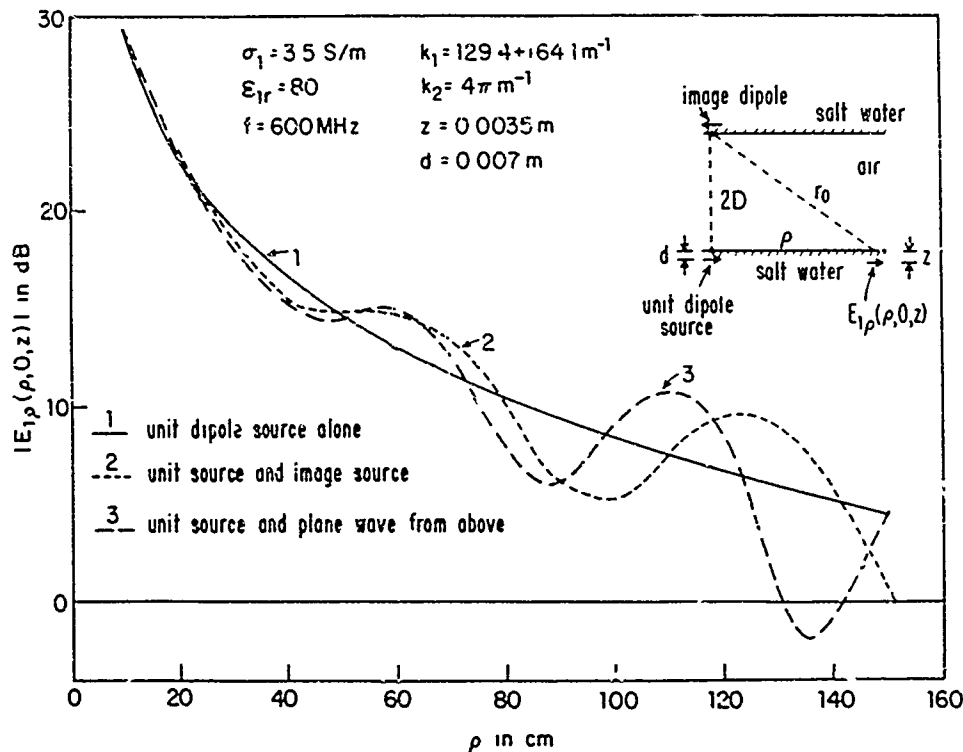


FIG A1 Interference patterns due to reflections from the ceiling and a traveling lateral wave, $f = 600$ MHz

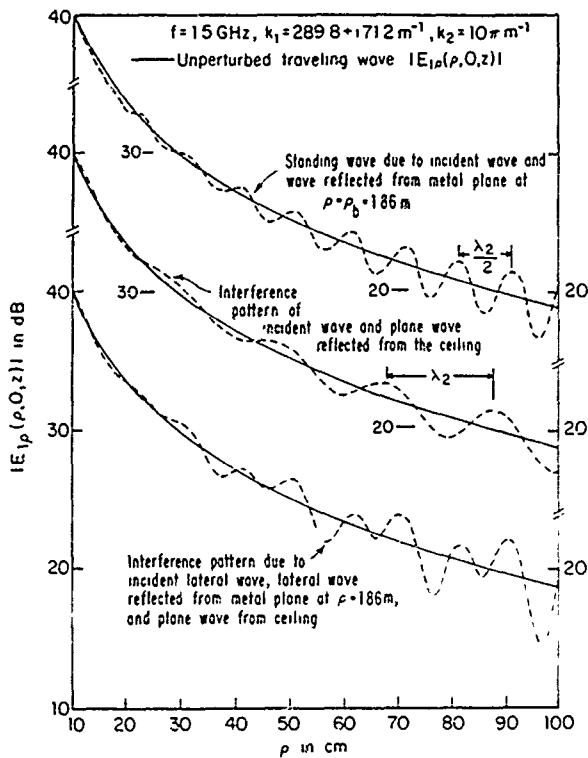


FIG A2 Standing wave and interference patterns due to reflections from a metal plate at $\rho = 1.86$ m and from the ceiling; $f = 1.5$ GHz

$\rho \sim 0.5$ m is $\text{SWR} \sim 1.25$, at $\rho \sim 0.9$, $\text{SWR} \sim 1.66$.

The interaction of plane-wave reflections from the ceiling with the incident lateral-wave field has been calculated at 1.5 GHz. The resulting interference pattern is shown by the broken-line graph at the center of Fig. A2. This is quite similar to the corresponding graph in Fig. A1, but the amplitude of the reflected field has been made relatively smaller by a factor 1/2. That is, in Eq. (A9) the amplitude of the incident plane wave is taken to be $A/4D$ instead of $A/2D$ in order to make it comparable to the amplitude of the radially reflected waves considered below. As before, the successive maxima of the interference pattern are separated by a distance close to λ_2 .

When these reflections from the ceiling are combined with the reflections from the metal wall at $\rho = \rho_b$, the resulting field is

$$|E_{1p}(\rho, 0, z) + E_{1p}^r(\rho, 0, z) + E_{1p}^c(\rho, 0, z)| \\ \sim B - C \cos(\theta_B - \theta_C) + (A/2D) \cos(2k_2 D + \theta_A - \theta_B). \quad (\text{A13})$$

This formula assumes that $B^2 \gg C^2$, $B^2 \gg (A/2D)^2$, and $B^2 \gg CA/2D$. Calculations from Eq. (A13) (again with $A/2D$ replaced by $A/4D$) at $f = 1.5$ GHz are shown by the broken-line curve at the bottom of Fig. A2. The combined standing-wave interference pattern is seen to have successive maxima that are separated by about $\lambda_2/2$ as in the standing-wave pattern at the top, but these maxima are alternately increased and decreased by the reflected field from the ceiling with its interval between maxima near λ_2 . The detailed nature of this type of pattern necessarily depends on the relative magnitudes and phases of the lateral waves traveling in

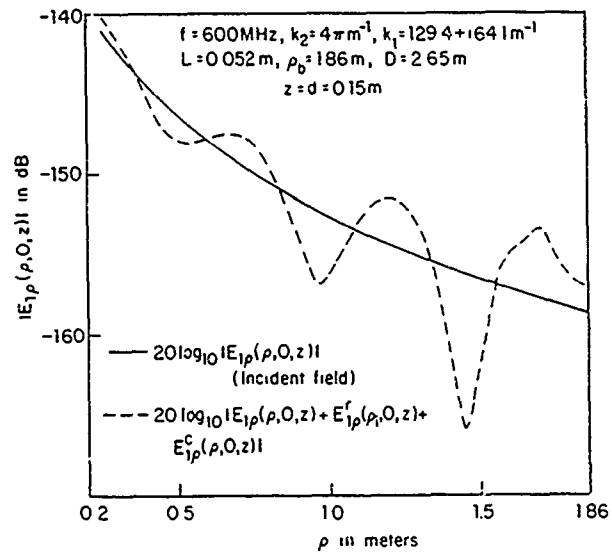


FIG A3 Superposition of incident lateral wave, lateral wave reflected from vertical metal wall of height L , and plane wave reflected from ceiling, $f = 600$ MHz

the horizontal direction and the waves reflected from the ceiling and traveling in the vertical direction. Either of these can dominate if its amplitude is significantly greater than the amplitude of the other with corresponding potentially very large differences in the shape of the standing wave and interference pattern.

An interesting second application of Eq. (A13) is to the reflections from a cylindrical metal wall of height L above the surface for which measurements are reported in Fig. 4 at $f = 644$ MHz and analytically determined graphs are in Fig. 9 of Ref. 7 for $f = 600$ MHz. Both graphs apply to a cylindrical Region 1 of radius $\rho_b = 1.86$ m containing salt water with $\sigma_1 = 3.5$ S/m and $\epsilon_{r1} = 80$. When Eq. (A13) is applied to the standing-wave data shown in Fig. 9 of Ref. 7 at $f = 600$ MHz and with $2D = 5.25$ m, the broken-line graph in Fig. A3 is obtained. The plane wave from the ceiling clearly dominates with only small variations due to the reflections from the cylindrical metal wall of height $L = 5.2$ cm at $\rho_b = 1.86$ m.

¹M. F. Brown, R. W. P. King, and T. T. Wu, *J. Appl. Phys.* 53, 5387 (1982).

²R. W. P. King, J. T. deBettencourt, and B. H. Sandler, *IEEE Trans. Geosci. Electron.* GE-17, 86 (1979).

³R. J. King and S. W. Maley, *Radio Sci.* 69 D, 1375 (1965).

⁴R. J. King and S. W. Maley, *Radio Sci.* 1, 111 (1966).

⁵R. J. King, S. H. Cho, D. L. Jaggard, G. E. Bruckner, and C. H. Hustig, *IEEE Trans. Antennas Propag.* AP-22, 550 (1974).

⁶R. W. P. King and G. S. Smith, *Antennas in Matter* (MIT, Cambridge, Mass., 1981), Ch. 11.

⁷R. W. P. King, *J. Appl. Phys.* 55, 3916 (1984).

⁸L. M. Brekhovskikh, *Waves in Layered Media* (Academic, New York, 1960).

⁹P. Beckman, "Rough Surface Effects," Chap. 3 in *Electromagnetic Probing in Geophysics*, edited by J. R. Wait (Golem, Boulder, Colo., 1971).

¹⁰D. D. Crombie, "Backscatter of HF Radio Waves from the Sea," Chap. 4 in *Electromagnetic Probing in Geophysics*, edited by J. R. Wait (Golem, Boulder, Colo., 1971).

¹¹E. Jahnke and F. Emde, *Tables of Functions* (Dover, New York, 1945), p. 36.

Lateral Waves Near the Air-Sea Boundary and Atmospheric Noise

J. T. DeBETTENCOURT

Considering attenuated atmospheric radio noise, useful signal-to-noise ratios are obtained with lateral waves between submerged horizontal dipoles for an air-sea model

I INTRODUCTION

Lateral electromagnetic waves traveling along the air-sea surface have been examined in [1] for use as a means of communication with submarines using a variety of antennas. Here we consider the case for antennas that are horizontally polarized, immersed in the sea, and radially disposed, see Fig. 1(a). This is the case, beyond the near field and in the direction $\phi = 0$ along the antenna axis, the radial component E_{1r} in a cylindrical coordinate system (ρ, ϕ, z) is the strongest. The subscript 1 pertains to the sea (Region 1) and subscript 2 to the air (Region 2). Dipole depths are d and z for the transmitting and receiving dipoles, respectively. A simple but accurate formula for E_{1r} has been described in [2] along with its derivation and significance. Numerous computations have been carried out and the relevant curves plotted. Rather long ranges are indicated from the standpoint of useful field strengths in the MF-HF region. However, since in the spectrum of frequencies below 10 MHz or so, atmospheric noise may be a limitation, it is expedient to examine some aspects of this question.

II ATMOSPHERIC NOISE

Of the various components of noise external to a receiver, the most important source is that due to thunderstorm activity in the MF-HF part of the spectrum. (Man-made noise for other wise quiet

receiving sites is neglected.) Such atmospheric noise is statistically quite variable, depending upon the location on the earth, time of day, season of the year, and frequency.¹ These dependencies have been studied for years and charts have been prepared to show variations. The charts are found in publications such as CCIR Report No. 322 [3].

What is plotted in the charts is the value of the median external atmospheric noise factor F_{am} versus frequency for given 4-h time blocks for the different seasons. This factor is determined from noise voltages induced in loops (usually) or vertical whip antennas. The noise field behavior is assumed in the theory to be that of a surface wave near the receiver. The theory has been treated, for example, in [4]. Here, the overburden will be replaced by the sea, the geometry is shown in Fig. 1(b).

The atmospheric noise fields are essentially vertically polarized in Fig. 1(b) with the vertical electric field strength $E_v = |E_v^n|$ at the surface related to the external noise factor F_{am} as follows:

$$E_v^n = 160 \beta_0^2 F_{am} k T B \quad (1)$$

where $\beta_0 = 2\pi/\lambda_0$, λ_0 is the wavelength in air, k is Boltzmann's constant, T is the absolute temperature, and B is the receiver noise bandwidth. In the MKS system, E_v is in volts/meter or in decibels

$$E_v(\text{dB} \geq 1 \mu\text{V/m}) = -125.56 + F_{am}(\text{dB}) + 20 \log_{10} f_{\text{kHz}} + 10 \log_{10} B_{\text{kHz}} \quad (2)$$

where the rms value of E_v is used and the subscript on f and B means frequencies in kilohertz. Night-time summer noise fields are largest in the northern hemisphere in general.

III THEORY OF NOISE ATTENUATION

Referring to Fig. 1(b), there is in the air a small horizontal noise component of the electric field, E_{2h}^n , in addition to the vertical one E_{2v}^n . The wave tilt for noise fields is defined at the surface in air at P_2 as follows:

$$W_2 = \left| \frac{E_{2h}^n}{E_{2v}^n} \right|^n = \left| \frac{1}{N_{12}} \right|^n = \left| \frac{1}{(\tilde{\epsilon}_v)^{1/2}} \right|^n \quad (3)$$

where N_{12} is the refractive index of water relative to air and $\tilde{\epsilon}_v$ is the complex relative dielectric constant $\tilde{\epsilon}_v = \epsilon_v(1 - jp_v)$ with $p_v = \sigma_v/\omega\epsilon_v$, the loss tangent and σ_v , the conductivity in siemens/meter.

There is a similar wave tilt at the point P_1 at the depth z in the water:

$$W_1 = \left| \frac{E_{1h}}{E_{1v}} \right|^n = N_{12}^n = (\tilde{\epsilon}_v)^{n/2} \quad (4)$$

These relations assume that N_{12} is large compared with unity, which is true for sea water with real relative dielectric constant $\epsilon_v = 80$ and loss tangent $p_v = 60\sigma_v/\omega\epsilon_v$. It is also assumed that atmospheric noise in a given time block is omnidirectional in azimuth. It follows that

$$\left| \frac{E_{1h}}{E_{2h}} \right|^n = \frac{1}{|N_{12}|^2} = \frac{1}{\tilde{\epsilon}_v} \quad (5)$$

At $z = 0$, $E_{1h} = E_{2h}$ by continuity. Thus the horizontal component in air, E_{2h}^n , is smaller than the vertical component E_{2v}^n , but in water the horizontal component E_{1h}^n far exceeds the vertical component E_{1v}^n .

¹As a first approximation, such noise is azimuthally nondirectional.

Manuscript received August 4, 1983; revised March 17, 1984. This research was supported in part by the Office of Naval Research under Contract N00014-79-C-0419 with Harvard University.

The author is with the Gordon McKay Laboratory, Harvard University, Cambridge, MA 02138, USA.

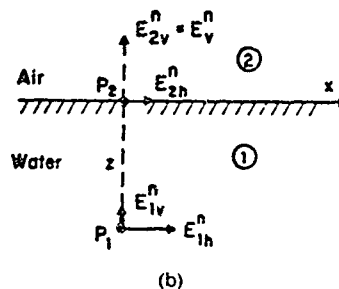
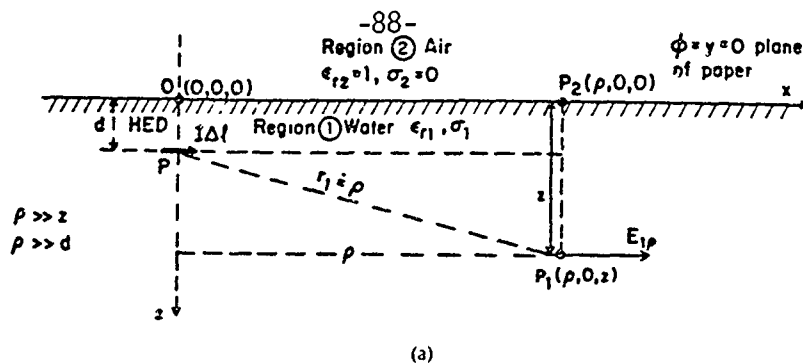


Fig. 1. Signal and atmospheric noise at subsurface point P_1 (a) Signal electrical field $E_{1\rho}$ at $P_1(\rho, \phi, z)$ due to HED at $P(0, 0, d)$ in sea water (b) Atmospheric radio noise E_2^n at P_2 on surface attenuated to E_1^n at P_1 in sea at depth z

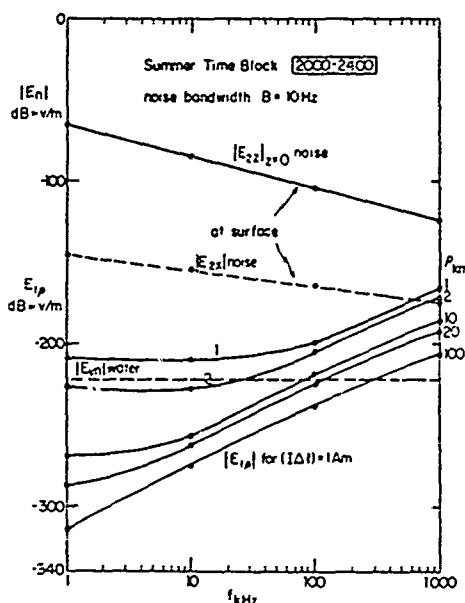


Fig. 2. Lateral waves and atmospheric noise

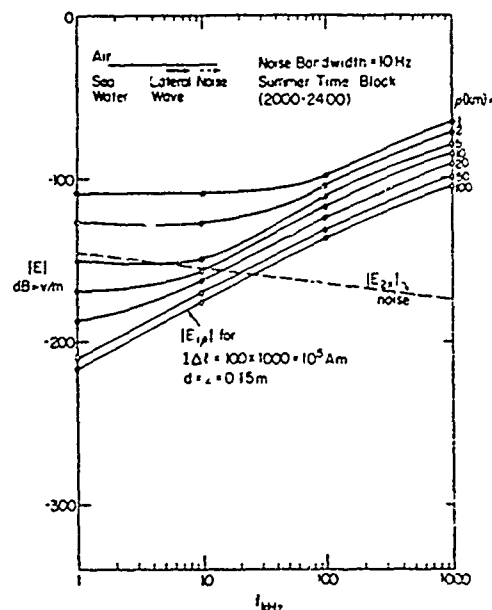


Fig. 3. Lateral waves and atmospheric noise

Because of the interest in the radial component $|E_{1\rho}|$ of the lateral wave, it is appropriate to concentrate on the horizontal component of noise in the water in the antenna direction. Since both the lateral wave $|E_{1\rho}|$ and the horizontal noise $|E_{1h}^n|$ decay exponentially with depth, the signal-to-noise ratio (S/N) at the receiver is determined at the surface, down to depths where the external atmospheric noise has been attenuated to the level of the internal noise of the receiver.

The horizontal noise level, from (3), has a field strength

$$|E_{2h}^n| = |E_{2v}^n / N_{12}| = |E_{2v}^n| / |\tilde{\epsilon}_{1r}|^{1/2} \quad (6)$$

But for sea water at MF-HF, the loss tangent ρ_1 is large so that

$$\tilde{\epsilon}_{1r} = \epsilon_{1r}(1 - j\rho_1) \approx -j60\sigma_1\lambda_0 \quad (7)$$

IV. CALCULATIONS

Calculations have been made for sea water ($\epsilon_{1r} = 80$, $\sigma_1 = 4 \text{ S/m}$). The vertical noise is for the worst time conditions of summer-time, time block (2000–2400) for Eastern U.S.A. at 40° N latitude, to typify results. The values of f_{sm} have been converted into $E_1 = |E_{1\rho}|_{z=0}$ according to (1) and (2), they are plotted in Fig. 2 as the uppermost curve. The horizontal component at the surface in air or in the water is the next lower dashed curve, $|E_{2h}^n| \approx |E_{2v}^n|_{\text{noise}}$. The lowest dashed curve is the vertical component $|E_{1v}^n| = |E_{2v}^n|$ in the water only. The noise bandwidth is assumed to be 10 Hz, and $z = 0$.

The solid curves for $E_{1\rho}$ are the field strengths of the $|E_{1\rho}|$ component of the lateral-wave field generated by an infinitesimal horizontal electric dipole with unit moment in the sea as calculated from a recently derived simple formula by Wu and King [2]. If it is

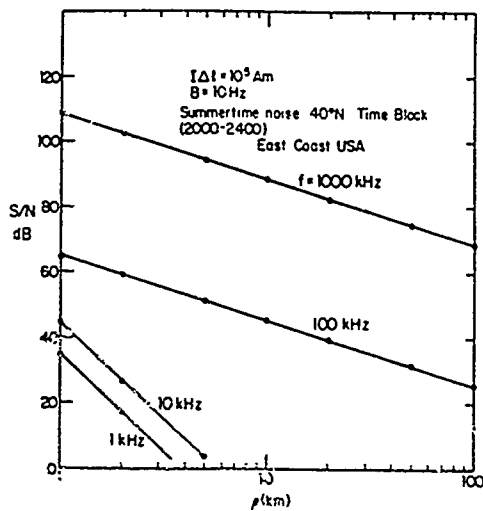


Fig. 4. Signal-to-noise ratio, lateral waves near air-sea boundary

possible to enhance the unit dipole moment ($I\Delta l = 1 \text{ A} \cdot \text{m}$) to a more practical value, then useful values of S/N will result. A typical lateral-wave system could consist of $I\Delta l \approx 100 \times 1000 = 10^5 \text{ A} \cdot \text{m}$. The curves for E_{lo} in Fig. 2 would, in this case, be raised 100 dB. This result is shown in Fig. 3. Thus at a frequency as high as 1 MHz, useful S/N ratios would result.

The resulting signal-to-noise ratios have been plotted as functions of the radial range ρ in Fig. 4. Even more optimistic values would obtain at $f = 10^6 \text{ Hz}$ (not shown) since there is an optimum at that frequency for the lateral wave.

V. CONCLUSION

Useful signal-to-noise ratios are obtainable with lateral waves between submerged horizontal dipoles for an air-sea model. These results infer useful communication to submarines using lateral waves limited by attenuated atmospheric noise for shallow depths. For greater depths, lower frequencies should give more optimum signal-to-noise ratios; this will be reported on in a future paper.

REFERENCES

- [1] R. W. P. King and M. F. Brown, "Lateral electromagnetic waves along plane boundaries: A summarizing approach," *Proc. IEEE*, vol. 72, no. 5, pp. 595-611, May 1984.
- [2] T. T. Wu and R. W. P. King, "Lateral waves: A new formula and interference patterns," *Radio Sci.*, vol. 17, pp. 521-531, May-June 1982.
- [3] CCIR Report No. 322, "World distribution and characteristics of atmospheric radio noise," Documents of the Xth Plenary Assembly, Geneva 1963, Geneva, Switzerland, ITU 1964, Figs. 19a, b.
- [4] J. T. deBettencourt, "Theory of attenuation of atmospheric noise and interference by the overburden," in J. T. deBettencourt and R. A. Butcliffe, "Studies in deep strata communications," Final Report AFCRD Contract AF19(604)-8359, Raytheon Co., Oct. 1962, appendix G.

Lateral Electromagnetic Waves Along Plane Boundaries: A Summarizing Approach

RONOLD W. P. KING, LIFE FELLOW, IEEE, AND MICHAEL FRANKLIN BROWN

Lateral electromagnetic waves along a plane boundary between homogeneous half-spaces are reviewed. The electromagnetic fields generated by vertical and horizontal electric dipoles near the boundary between air and the earth (salt or fresh water, soil, ice, etc.) are summarized in terms of a new unified theory of lateral-wave propagation. Complete theoretically determined fields are displayed and compared with measured fields at $f = 600$ kHz relative to the boundary between air and salt water ($\sigma = 3.5$ S/m, $\epsilon_r = 80$). Near, intermediate, and asymptotic fields are related graphically to the new general theory and to the approximate and restricted formulas of Norton and Baños as well as to the Zenneck wave. Application is made to the specific problem of communication with submerged submarines by means of transmitters consisting of electrically short monopoles in air and horizontal traveling-wave antennas and directional arrays in sea water. The properties of the antennas are evaluated in the frequency range $10 \leq f \leq 30$ kHz which is optimum for receiver depths near 10 m and at $f = 1$ kHz which is optimum for depths up to 50 m. The effects of reflections from the ionosphere and of the earth's curvature are not included.

I. INTRODUCTION

The propagation of electromagnetic waves in the presence of a boundary between two quite different materials like air and earth (salt and fresh water, soil, sand, ice, etc.) has been of long-standing interest in classical electromagnetism. It has application in all radio communication between points near the surface of the earth and this is true whether the transmitting and receiving antennas are both in the air (broadcast radio), both in the earth (communication between tunnels, mine shafts, submarines), or one is in each medium (communication with submarines). It underlies geophysical exploration by means of electromagnetic waves generated and received by antennas on the surface of the earth, or on the floor of the ocean.

A. Surface Waves, Zenneck Waves

Surface waves along cylindrical conductors of infinite length in air were analyzed by Sommerfeld in 1899 [1]. Inside the cylinder the field is distributed in the well-known

manner commonly referred to as skin effect. Outside the conductor the electric field is elliptically polarized with a large radial and small axial component in the direction of propagation. The two components are not in phase. The analogous phenomenon for a plane surface was discussed by Zenneck in 1907 [2] and related to the propagation of radio waves over the surface of the earth. With the existence and significance of the ionosphere still unknown, Zenneck sought to explain the long-distance propagation of radio waves in terms of a surface wave that decays less rapidly than the familiar $1/r$ decrease for space waves. The properties of radial cylindrical surface waves (Zenneck waves) as possible solutions of Maxwell's equations are well described by Barlow and Cullen [3]. They give formulas for the field along the boundary between a conducting or dielectric half-space (Region 1, $z \geq 0$, σ , ϵ_r) with complex wavenumber $k_1 = \beta_1 + i\alpha_1 = k_2(\epsilon_r + i\sigma/\omega\epsilon_0)^{1/2}$ and air (Region 2, $z \leq 0$) with wavenumber $k_2 = \omega(\mu_0\epsilon_0)^{1/2}$. The time dependence is $e^{-i\omega t} = e^{i\omega t}$. If the condition

$$|k_1|^2 \gg k_2^2 \quad \text{or} \quad |k_1| \gg 9k_2 \quad (1)$$

is imposed, the following considerably simplified formulas (which serve present purposes) are obtained in the cylindrical coordinates ρ, ϕ, z .

In Region 1

$$\begin{aligned} B_{1\phi} &= \mu_0 A e^{ik_1 z} H_1^{(1)}(k_2 \rho) \\ E_{1\rho} &= -(\omega/k_1) B_{1\phi} \\ E_{1z} &= \frac{i\omega\mu_0 k_2}{k_1^2} A e^{ik_1 z} H_0^{(1)}(k_2 \rho) \end{aligned} \quad (2)$$

In Region 2

$$\begin{aligned} B_{2\phi} &= \mu_0 A e^{-i(k_2^2/k_1^2)z} H_1^{(1)}(k_2 \rho) \\ E_{2\rho} &= -(\omega/k_1) B_{2\phi} \\ E_{2z} &= \frac{i\omega\mu_0}{k_1^2} A e^{-i(k_2^2/k_1^2)z} H_0^{(1)}(k_2 \rho) \end{aligned} \quad (3)$$

where the H 's are Hankel functions and A is an amplitude that depends on the nature of an unspecified source at the origin. Note that the field decays exponentially as $\exp(-\alpha_1 z)$ in the conducting or dielectric half-space, more slowly as $\exp[-\alpha_1(k_2^2/k_1^2)z]$ in the air. Clearly, it is bound quite closely to a region on each side of the surface $z = 0$. When $k_2 \rho \gg 10$, the asymptotic forms of the Hankel functions are

Manuscript received July 6, 1983; revised February 13, 1984. This research was supported in part by the Joint Services Electronics Program under Contract N00014-75-C-0648 with Harvard University. The experimental work was supported in part by the Office of Naval Research under Contract N00014-79-C-0419 with Harvard University.

The authors are with the Gordon McKay Laboratory, Division of Applied Sciences, Harvard University, Cambridge, MA 02138, USA.

good approximations, i.e.,

$$H_0^{(1)}(k_2 \rho) \sim (2/\pi k_2 \rho)^{1/2} \exp[i(k_2 \rho - \pi/4)]$$

$$H_1^{(1)}(k_2 \rho) \sim (2/\pi k_2 \rho)^{1/2} \exp[i(k_2 \rho - 3\pi/4)].$$

It follows that when $k_2 \rho \geq 10$, the entire surface-wave field decreases as $\rho^{-1/2}$ with increasing radial distance ρ . This is the essential characteristic of the Zenneck wave.

In 1909, Sommerfeld [4] determined the complete electromagnetic field of a vertical dipole on the surface of the earth and verified that his complicated general solution actually contained the surface-wave term with its $\rho^{-1/2}$ rate of decrease. This seemed to confirm the possibility of attributing long-distance radio transmission to the Zenneck surface wave. However, no later than 1935 Sommerfeld [5] in a re-examination of his theory concluded that the surface-wave term could not be separated from the other terms in the complete solution for the field of the vertical dipole. He also stated that there were no possible circumstances under which the Zenneck surface wave could exist alone or even form the principal part of the complete representation of the outward traveling waves from the dipole. Nevertheless, the existence or nonexistence of the Zenneck surface wave continued as the controversial subject of a long series of papers. Since the details are ably summarized by Baños [6], they are not repeated here. Useful discussions are in Hill and Wait [7] and Wait and Hill [8].

B Surface Waves in the Field of a Vertical Dipole on the Earth, The Formula of Norton

Even though the surface-wave term in the formula for the field of a vertical electric dipole over the earth has no application to phenomena now attributed to reflections from the ionosphere, it is nevertheless a significant term in the radiation field. This arises from the fact that the field in the absence of the surface-wave term vanishes along the surface of the earth, i.e., when $\Theta = \pi/2$ [9]. This is readily understood from the formula for the field of an electrically short vertical dipole with unit electric moment ($I\Delta l = 1$ A·m) at a height d over the earth [Fig. 1(a)]. It is

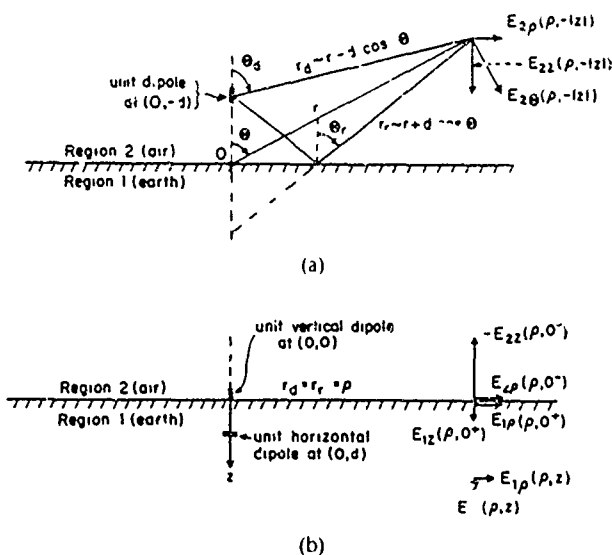


Fig. 1. (a) Vertical dipole with unit electric moment ($I\Delta l = 1$ A·m) at height d over earth (b) Unit vertical dipole at surface, unit horizontal dipole at depth d

-91-

$$E_{2\theta} = -\frac{i\omega\mu_0}{4\pi} \frac{e^{ik_2 r}}{r} A_e(\Theta) \sin \Theta \quad (4)$$

where Θ is measured from the vertical axis and

$$A_e(\Theta) = e^{-ik_2 d \cos \Theta} + f_{er} e^{ik_2 d \cos \Theta} \quad (5)$$

is the field factor. The plane-wave reflection coefficient $f_{er} = |f_{er}| \exp(i\psi_{er})$ is defined as follows in terms of the square of the complex index of refraction, $N^2 = (k_1/k_2)^2 = \epsilon_1/\epsilon_2 = \epsilon_{1r} + i\sigma_1/\omega\epsilon_0$

$$f_{er} = \frac{\cos \Theta - \Delta(\Theta)}{\cos \Theta + \Delta(\Theta)} \quad (6a)$$

where $\Delta(\Theta)$ is the normalized surface impedance defined by

$$\Delta(\Theta) = Z_s(\Theta)/\zeta_0 = (N^2 - \sin^2 \Theta)^{1/2}/N^2, \quad \zeta_0 = (\mu_0/\epsilon_0)^{1/2} \quad (6b)$$

At normal incidence $\Theta = 0$ and $Z_s(0) \equiv Z_s = \omega\mu_0/k_1 = (\mu_0/\epsilon_1)^{1/2}$. The magnitude of f_{er} has values near 1 when $\Theta = 0$ and $\pi/2$ and has a deep minimum between 0 and $\pi/2$ at the Brewster angle. Graphs of $|f_{er}|$ and ψ_{er} are shown in Fig. 2(a) and (b) for a range of values of N^2 appropriate to earth and water. The field factor $A_e(\Theta) \sin \Theta$ is shown in Fig. 3 for a dipole on the earth ($d = 0$). It is seen that the field has a maximum between $\Theta = 60^\circ$ and 90° , depending on the value of N , but vanishes at $\Theta = \pi/2$ for all N except $N = \infty$, the value for a perfect conductor for which the maximum occurs at $\Theta = \pi/2$. It is virtually $\pi/2$ for a metal surface. The corresponding field patterns for a quarter-wave monopole on the earth are shown in Fig. 4. They are seen to vanish at $\Theta = \pi/2$ except when the earth is replaced by a perfect conductor. Note that the larger N^2 the closer to $\Theta = \pi/2$ is the maximum in the field pattern and the steeper is the drop to zero at $\Theta = \pi/2$. This means that a receiving antenna located at a sufficient height can experience a near-maximum field. Actually, the field at $\Theta = \pi/2$ is not zero as indicated by the space-wave terms but is determined by a surface-wave term which must be added to (4). It is significant only when Θ is near or at $\pi/2$.

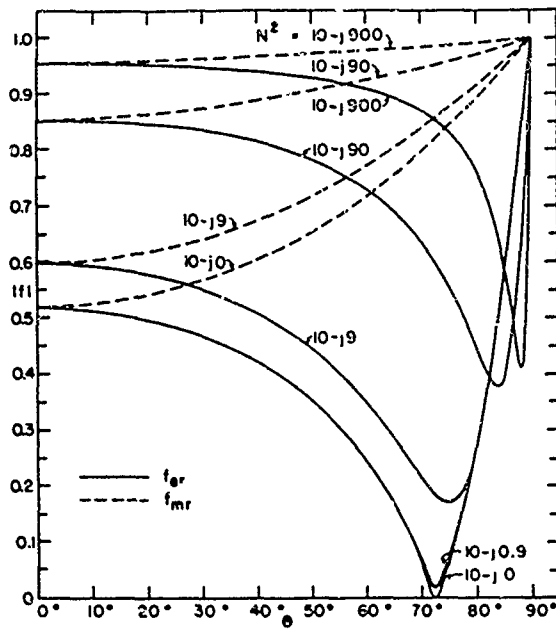
In order to make Sommerfeld's complicated solution with its complex integrals convenient for engineering use, Norton [10] in 1936, and with the help of expressions for the ground-wave potential due to van der Pol and Niessen [11] and the electric field due to Wise [12], reduced the surface-wave term to simple formulas and graphs. These involved approximations that restricted their ranges of validity. He then compared the fields obtained from them with available experimental results in order to determine these ranges. He was careful to point out that "when the theory is used to predict the field intensity in other frequency and distance ranges than those for which it has been checked, there is the possibility of error due to leaving out some factor which becomes important in these new situations." A useful discussion and correction of Norton's work is in a paper by R. J. King [13].

Norton's surface-wave term in the field of a unit ($I\Delta l = 1$ A·m) electric dipole in Region 2 (air) on the boundary ($d = 0$) with Region 1 (earth) is [Fig. 1(b)]

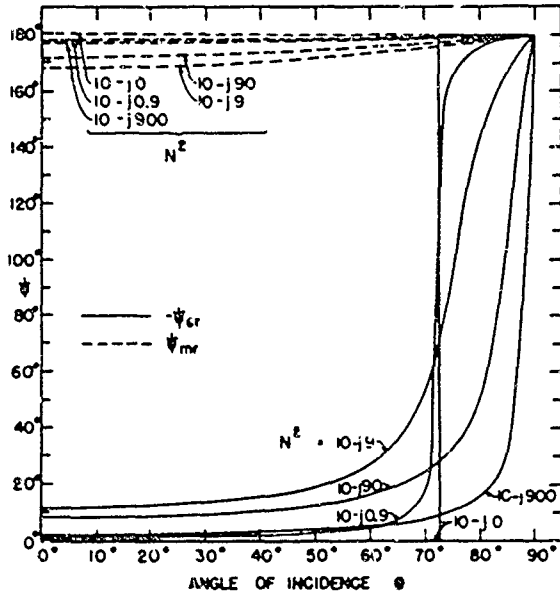
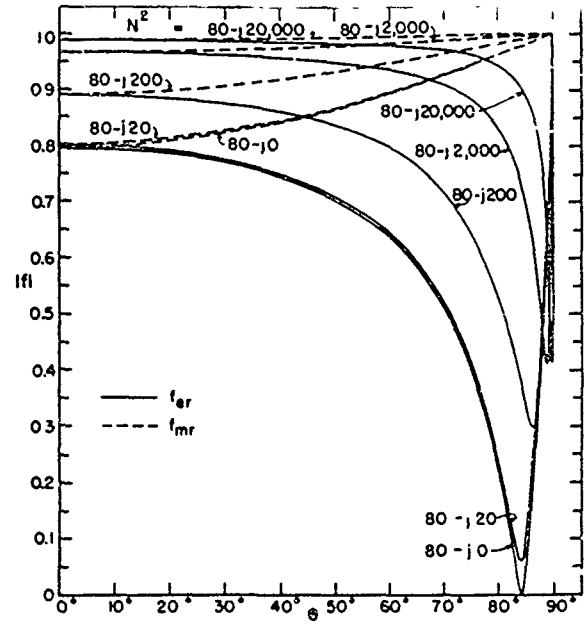
$$E_{2z}(\rho, 0) = \frac{i\omega\mu_0}{2\pi} \frac{e^{ik_2 \rho}}{\rho} F_e \quad (7)$$

where

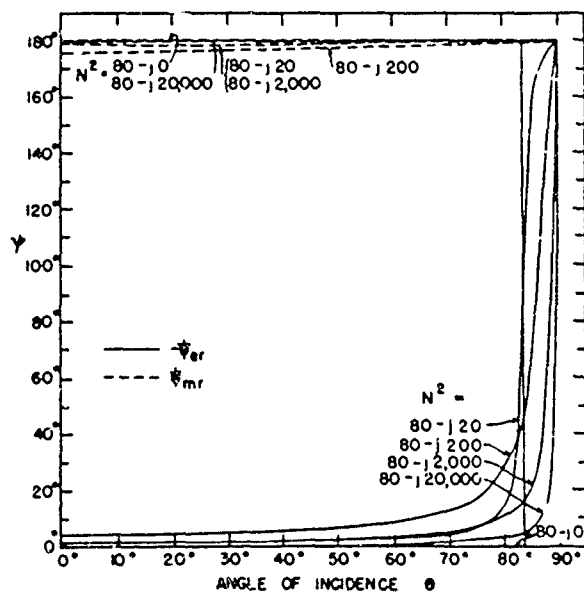
$$F_e = 1 + i(\pi\rho)^{1/2} e^{-\rho} [1 - \text{erf}(-i\rho^{1/2})] \quad (8)$$



-92-



(a)



(b)

Fig. 2. Reflection coefficients f_{er} and f_{mr} . (a) $\epsilon_r = 10$ (b) $\epsilon_r = 80$ Note that $j = -i$

and the numerical distance is defined by

$$p = |p|e^{i\phi} = ik_2\rho(k_1^2/2k_2^2) \quad (9)$$

The error function is

$$\text{erf}(z) = \frac{2}{\pi^{1/2}} \int_0^z e^{-t^2} dt \quad (10)$$

Norton provided graphs and tables of F_e as a function of the magnitude and argumen of the so-called numerical distance p . Their quantitative significance is considered later. A useful alternative form of (7) is in terms of the Fresnel integral

$$C_2(z) + iS_2(z) = \int_0^z \frac{e^{-t^2}}{(2\pi t)^{1/2}} dt \quad (11)$$

With it, (7) becomes

$$E_{2z}(\rho, 0) = \frac{\omega\mu_0}{2\pi} e^{ik_2\rho} \left[\frac{1}{\rho} - \frac{k_1^2}{k_2} \left(\frac{\pi}{k_2\rho} \right)^{1/2} e^{-ik_2\rho(k_1^2/2k_2^2)} \mathcal{F}(k_2\rho, k_1) \right] \quad (12)$$

with

$$\mathcal{F}(k_2\rho, k_1) = \frac{1}{2}(1+i) - C_2[k_2\rho(k_1^2/2k_2^2)] - iS_2[k_2\rho(k_1^2/2k_2^2)] \quad (13)$$

The leading term for very large values of $k_2\rho$, i.e., when $k_2\rho \gg \pi|k_1^2/k_2^2|$, is

$$E_{2z}(\rho, 0) \sim -\frac{\omega\mu_0}{2\pi} \frac{k_1^2}{k_2^3} \frac{e^{ik_2\rho}}{\rho^2} \quad (14)$$

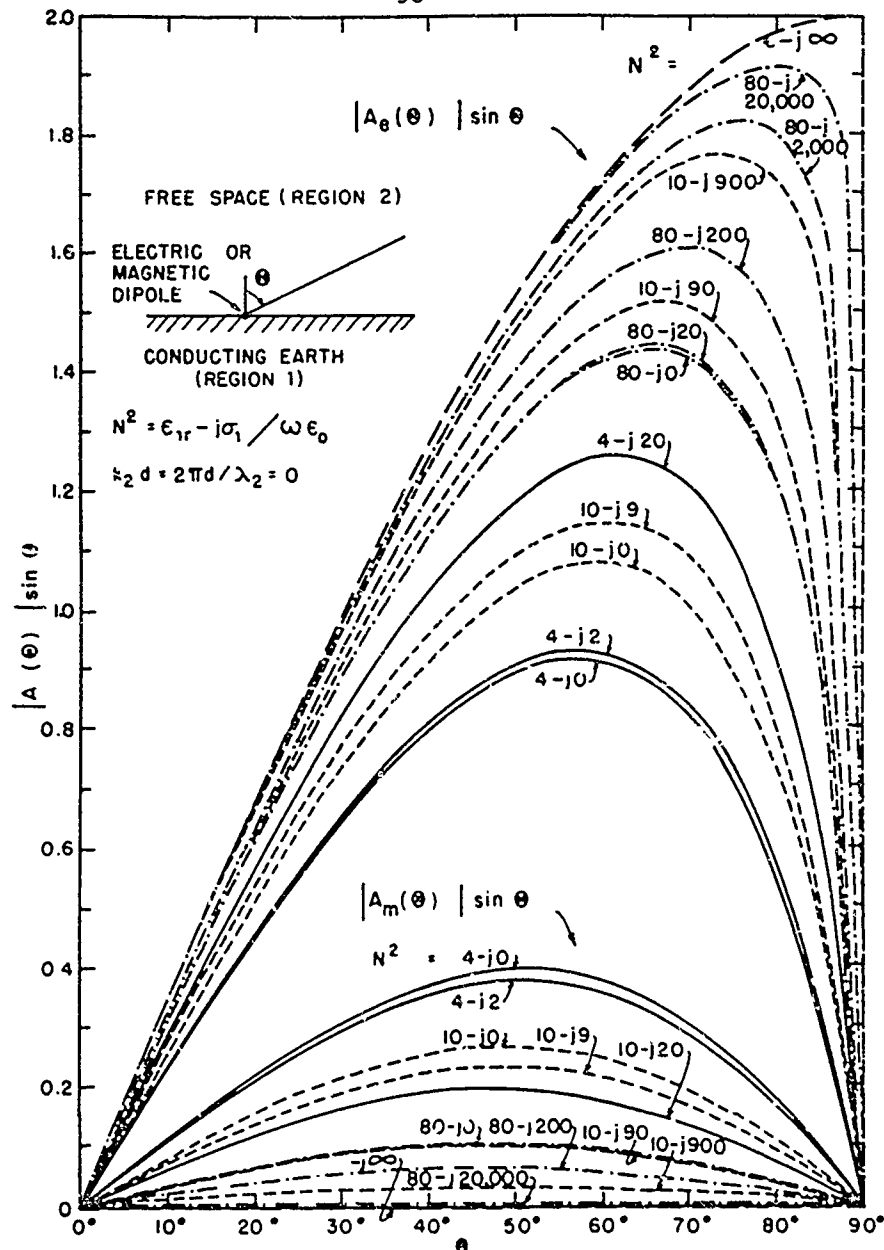


Fig. 3. Field factors of vertical electric and magnetic dipoles on conducting earth, $d = 0$. Note that $j = -i$.

For small and intermediate values of $k_2 \rho$, i.e., $k_2 \rho \ll \pi^{1/2} k_1^2 / k_2^2$,

$$E_{2z}(\rho, 0) \sim \frac{\omega \mu_0}{2\pi} e^{i k_2 \rho} \left[\frac{1}{\rho} - \frac{1}{2} (1+i) \frac{k_1^2}{k_2} \left(\frac{\pi}{k_2 \rho} \right)^{1/2} \right] \sim \frac{i \omega \mu_0}{2\pi} \frac{e^{i k_2 \rho}}{\rho} \quad (15)$$

The Zenneck surface wave is explicitly contained in (15) where it is the second term which varies with distance as $\rho^{-1/2}$. However, as predicted by Sommerfeld, it is not the dominant term since it is multiplied by the small factor k_2/k_1 . As ρ increases, the valid range of (15) is passed and (12) must be used. Finally, for sufficiently large ρ where it might be expected that the $\rho^{-1/2}$ term would dominate over the ρ^{-1} term, the Fresnel integral contributes major factors such that the ρ^{-1} term is canceled exactly and the

$\rho^{-1/2}$ term becomes a ρ^{-2} term as in (14). Thus the Zenneck surface wave, while present formally, is only a relatively small part of the complete surface wave.

The problem treated by Sommerfeld and evaluated by Norton concerned propagation over a plane earth. An extension of this work to the spherical earth is contained in a treatise by Bremner [14] and in a recent paper by Hill and Wait [15].

C Approximate Formulas, Numerical Results

Following the work of Norton, which addressed primarily the problem of surface-wave communication between vertical antennas in the air on the surface of the earth, interest turned to the problem of communicating with submarines. Extensive studies were carried out relating especially to the electromagnetic fields generated by hori-

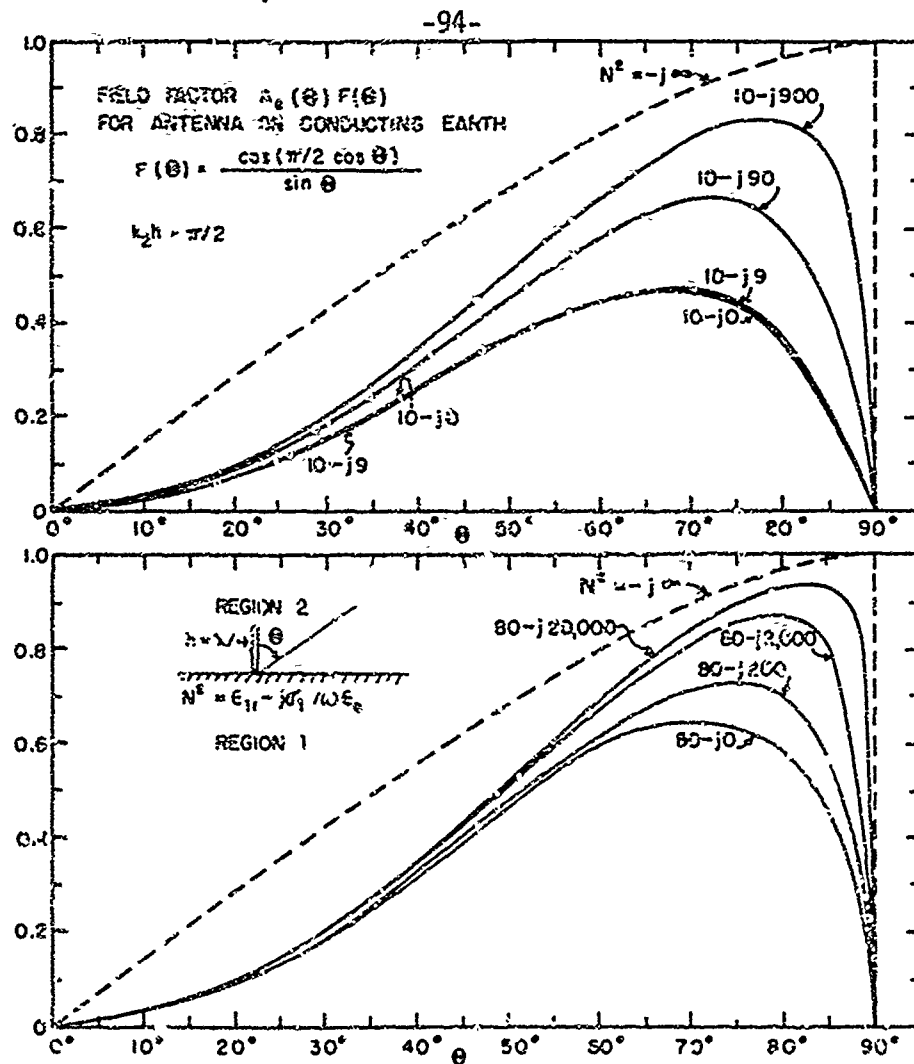


Fig. 4. Vertical field pattern of $\lambda/4$ monopole on a conducting earth or water. Note that $j = -1$.

zontal and vertical electric and magnetic dipoles in the sea. This work included an extensive series of papers by Wait [16] and reports by Baños and Wesley which culminated in the exhaustive book by Baños [6] in 1966. In this, the entire problem is reformulated, general integrals are obtained for the potential functions and expressions for the components of the electromagnetic field in both regions. These are then simplified to obtain sets of illuminating approximate formulas valid in restricted nonoverlapping ranges of the variables and parameters referred to as the asymptotic, intermediate, and near-field ranges. They are defined as follows.

near field	$k_2 \rho < 1 < k_1 \rho $	
intermediate field	$ k_2 \rho (k_2^2 / 2k_1^2) < 1 < k_2 \rho$	
asymptotic field	$1 \ll k_2 \rho (k_2^2 / 2k_1^2) $	(16)

Extensive graphs of the components of the electric field of a horizontal electric dipole as calculated from Baños' approximate formulas are in King and Smith [17] for wide ranges of the material parameters, the frequency, and radial distance. Their quantitative significance is considered later.

Electromagnetic waves are highly attenuated in sea water except at very low frequencies, for which practical distances are in the near field. Accordingly, the problem of com-

municating with submarines was studied primarily in terms of near-field or quasi-static formulas [18].

When high-speed computers became available, attention was directed to the numerical evaluation of the Sommerfeld integrals [19]–[22] and extensive systematic calculations were made of the fields of horizontal electric dipoles in air-bounded media ranging from sea water to dry earth over a wide range of frequencies [23]–[25], [17, ch. 11], and in rock-bounded sea water [26]. These have been compared with calculations from Baños' approximate formulas [17, ch. 11]. Extensive measurements of electromagnetic fields due to antennas in sea water [27] and lake water [28] have been made and compared with the appropriate numerical results and with Baños' approximate formulas.

II. A NZW REPRESENTATION OF AN OLD THEORY

Although the electromagnetic fields generated by vertical and horizontal dipoles above and below the boundary between two quite different material media have been formally available in terms of general integrals for many years, a clear understanding of their characteristics, similarities, and differences has been difficult to obtain because of the complexity of the formulas. Following Sommerfeld, these have, in general, been expressed in terms of deriva-

tives of the Hertz potentials. A somewhat different insight is obtained from the explicit integrals for the components of the electric and magnetic fields. For the horizontal electric dipole these are given in [17, pp. 617, 618]; for the vertical electric dipole in [29, eqs. (26)–(31)]. An example of the type of integral involved is the radial component of the electric field at a depth z in Region 1 (earth) of a horizontal unit electric dipole ($I\Delta l = 1 \text{ A} \cdot \text{m}$) located at the depth d also in Region 1 [Fig. 1(b)]

$$E_{\rho}(\rho, \phi, z) = -\frac{\omega\mu_0}{4\pi k_1^2} \cos\phi \left(\int_0^{\infty} \{k_1^2 b(\lambda\rho) - (\lambda^2/2)[b_0(\lambda\rho) - b_2(\lambda\rho)]\} \gamma_1^{-1} e^{\gamma_1(z-d)} \lambda d\lambda \right. \\ \left. + \int_0^{\infty} \{(\gamma_1 Q/2)[b_0(\lambda\rho) - b_2(\lambda\rho)] - (k_1^2 P/2\gamma_1)[b_0(\lambda\rho) + b_2(\lambda\rho)]\} e^{\gamma_1(z-d)} \lambda d\lambda \right) \quad (17)$$

where, with $\mu_1 = \mu_2 = \mu_0$, $P = (\gamma_2 - \gamma_1)/(\gamma_2 + \gamma_1)$, $Q = (k_1^2 \gamma_2 - k_2^2 \gamma_1)/(k_1^2 \gamma_2 + k_2^2 \gamma_1)$, $\gamma_1^2 = k_1^2 - \lambda^2$. The location of the dipole at $(0, 0, d)$ and the point (ρ, ϕ, z) , where E_{ρ} is evaluated, are shown in Fig. 5. The formulas for the other

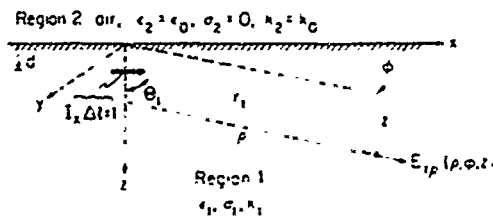


Fig. 5. Radial component of electric field at (ρ, ϕ, z) due to x -directed dipole at $(0, 0, d)$.

five components of the electromagnetic field are similar, as are the formulas for the three components of the rotationally symmetric field of a vertical dipole at $(0, 0, d)$.

A. New Simple Formulas

A careful study of all of the general integrals in the light of the known properties of the field from numerical calculations, approximate formulas, and measurements has shown that they can be evaluated in closed form subject to quite simple and readily satisfied conditions. They are

$$|k_1| \geq 3k_2 \quad \rho \geq 5d \quad \rho \geq 5z \quad |k_1\rho| \geq 3. \quad (18)$$

With (18), the surface-wave parts of the three components of the electromagnetic field of the vertical electric dipole [29] and of all six components of the field of the horizontal electric dipole [30]–[32] can be expressed in terms of the following radial functions:

$$f(k_2\rho, k_1) = \frac{ik_2}{\rho} - \frac{1}{\rho^2} - \frac{k_2^3}{k_1} \left(\frac{\pi}{k_2\rho} \right)^{1/2} e^{-ik_2\rho(k_1^2/2k_2^2)} \\ \cdot \mathcal{F}(k_2\rho, k_1) \quad (19)$$

$$g(k_2\rho, k_1) = f(k_2\rho, k_1) - \frac{i}{k_2\rho^3} \quad (20)$$

$$h(k_2\rho, k_1) = \frac{2}{\rho^2} + \frac{2i}{k_2\rho^3} + \frac{ik_2^3}{k_1\rho} \left(\frac{\pi}{k_2\rho} \right)^{1/2} e^{-ik_2\rho(k_1^2/2k_2^2)} \\ \cdot \mathcal{F}(k_2\rho, k_1) \quad (21)$$

where

$$\mathcal{F}(k_2\rho, k_1) = \frac{1}{2}(1+i) - C_2[k_2\rho(k_1^2/2k_2^2)] \\ - iS_2[k_2\rho(k_1^2/2k_2^2)] \quad (22)$$

$$C_2(u) + iS_2(u) = \int_0^u (2\pi t)^{-1/2} e^{-t} dt \quad (23)$$

$$k_1^2 = \omega^2\mu_0(\epsilon_1 + i\sigma_1/\omega) \quad k_2^2 = \omega^2\mu_0\epsilon_0. \quad (24)$$

Note that when $k_2\rho \geq 3$, $g(k_2\rho, k_1) \sim f(k_2\rho, k_1)$ since $|i/k_2\rho^3|$ is then negligible compared to

$$\left| \frac{ik_2}{\rho} - \frac{1}{\rho^2} \right|$$

Note also that when $k_2\rho \gg |k_1^2/k_2^2|$

$$f(k_2\rho, k_1) \sim g(k_2\rho, k_1) \rightarrow -k_1^2/k_2^2\rho^2 \quad (25)$$

since

$$(k_1^2/k_1)(\pi/k_2\rho)^{1/2} \exp[-ik_2\rho(k_1^2/2k_2^2)] \mathcal{F}(k_2\rho, k_1) \\ \rightarrow (ik_1/\rho) + (k_1/k_2\rho)$$

Similarly

$$h(k_2\rho, k_1) \rightarrow 1/\rho^2. \quad (26)$$

When the source dipole is located at depth d in Region 1 (earth, water, etc.), each component of the electromagnetic field consists of two distinct parts. The distinguishing feature of the terms in the two parts are the factors $\exp(ik_1r)$ and $\exp(ik_2\rho)$. Each term associated with the direct field includes an exponential factor with the wavenumber $k = \beta_1 + i\alpha_1$ and, therefore, the attenuation factor $\exp(-\alpha_1 r)$. Each term associated with the lateral-wave field includes the factor $\exp(ik_2\rho)$. For all practically available materials that form the surface of the earth, the attenuation constant α_1 is significant and the direct field decays rapidly with distance. Only quite close to the source is the magnitude of the direct field comparable with that of the lateral-wave field. Here it can produce an interference pattern. This is observable for low-conductivity lake water and for salt water at very high frequencies. Formulas that include the direct field of each component are given in [29]–[32]. They will be indicated only by a letter D and not written explicitly since they are of no significance in even short-distance propagation over the earth. When the source is on the surface in Region 2 (air), there is no direct field; the lateral field is the entire field.

The three components of the rotationally symmetric electromagnetic field of a vertical electric dipole in Region 2 on the surface and in Region 1 at any depth $d \geq 0$ are given in Table 1. The six components of the field of a horizontal electric dipole at depth $d \geq 0$ in Region 1 are listed in Table 2. These latter are conveniently separated into a field of electric type consisting of E_ρ , E_z , and B_ϕ with an angular dependence $\cos\phi$ and a field of magnetic type that includes B_ρ , B_z , and E_ϕ with an angular dependence $\sin\phi$.

Table 1 Electromagnetic Field of a Vertical Electric Dipole with Unit Moment ($I\Delta l = 1 \text{ A} \cdot \text{m}$) On or Below the Surface Between Region 1 ($z \geq 0$, Earth, Water, etc.) and Region 2 ($z \leq 0$, Air): $A = \omega\mu_0/2\pi$

Component of the Field	Dipole in Region 2 at $(0, 0, 0)$, i.e., on Surface	Dipole in Region 1 at $(0, 0, d)$, i.e., at depth d
$E_{1\rho}(\rho, z)$	$-Ak_1^{-1}f(k_2\rho, k_1)e^{k_2z}e^{k_1x}$	$-Ak_2^2k_1^{-3}f(k_2\rho, k_1)e^{k_2z}e^{k_1(x+d)} + D_{\rho f}^v$
$E_{1z}(\rho, z)$	$Ak_2k_1^{-2}g(k_2\rho, k_1)e^{k_2z}e^{k_1x}$	$Ak_2^3k_1^{-4}g(k_2\rho, k_1)e^{k_2z}e^{k_1(x+d)} + D_{zf}^v$
$B_{1\phi}(\rho, z)$	$k_1\omega^{-1}E_{1\phi}(\rho, z)$	$-A\omega^{-1}k_2^2k_1^{-2}f(k_2\rho, k_1)e^{k_2z}e^{k_1(x+d)} + D_{\phi f}^v$
$E_{2\rho}(\rho, 0)$	$E_{1\rho}(\rho, 0)$	$E_{1\rho}(\rho, 0)$
$E_{2z}(\rho, 0)$	$k_1^2k_2^{-2}E_{1z}(\rho, 0)$	$k_1^2k_2^{-2}E_{1z}(\rho, 0)$
$B_{2\phi}(\rho, 0)$	$B_{1\phi}(\rho, 0)$	$B_{1\phi}(\rho, 0)$

Table 2 Electromagnetic Field of a Horizontal Electric Dipole with Unit Moment ($I\Delta l = 1 \text{ A} \cdot \text{m}$) On or Below the Surface Between Region 1 ($z \geq 0$, Earth, Water, etc.) and Region 2 ($z \leq 0$, Air): $A = \omega\mu_0/2\pi$

Component of the Field	Dipole in Region 1 at $(0, 0, d)$, i.e., at depth d
$E_{1\rho}(\rho, \phi, z)$	$-Ak_2k_1^{-1}g(k_2\rho, k_1)e^{k_2z}e^{k_1(x+d)}\cos\phi + D_{\rho f}^h$
$E_{1z}(\rho, \phi, z)$	$Ak_2^2k_1^{-3}f(k_2\rho, k_1)e^{k_2z}e^{k_1(x+d)}\cos\phi + D_{zf}^h$
$B_{1\phi}(\rho, \phi, z)$	$-A\omega^{-1}k_2^2k_1^{-2}g(k_2\rho, k_1)e^{k_2z}e^{k_1(x+d)}\cos\phi + D_{\phi f}^h$
$B_{1\rho}(\rho, \phi, z)$	$-A\omega^{-1}k_2k_1^{-1}h(k_2\rho, k_1)e^{k_2z}e^{k_1(x+d)}\sin\phi + D_{\rho f}^h$
$B_{1z}(\rho, \phi, z)$	$-A\omega^{-1}k_2k_1^{-1}\left[\frac{1}{\rho^2} - \frac{3}{\rho^4} - \frac{3}{k_2\rho^4}\right]e^{k_2z}e^{k_1(x+d)}\sin\phi + D_{zf}^h$
$E_{1\phi}(\rho, \phi, z)$	$Ak_2k_1^{-1}h(k_2\rho, k_1)e^{k_2z}e^{k_1(x+d)}\sin\phi + D_{\phi f}^h$
$E_{2\rho}(\rho, \phi, 0)$	$E_{1\rho}(\rho, \phi, 0)$
$E_{2z}(\rho, \phi, 0)$	$k_1^2k_2^{-2}E_{1z}(\rho, \phi, 0)$
$B_{2\phi}(\rho, \phi, 0)$	$B_{1\phi}(\rho, \phi, 0)$
$B_{2\rho}(\rho, \phi, 0)$	$B_{1\rho}(\rho, \phi, 0)$
$B_{2z}(\rho, \phi, 0)$	$B_{1z}(\rho, \phi, 0)$
$E_{2\phi}(\rho, \phi, 0)$	$E_{1\phi}(\rho, \phi, 0)$

All six components of the field of a horizontal electric dipole as computed from the new formulas (that are expressed only in terms of simple functions and Fresnel integrals) have been compared with corresponding numerical evaluations of the general integrals [30]–[32] with excellent

agreement over the entire range permitted by the conditions (18). The formula for each component is continuous and agrees with the asymptotic, intermediate, and near-field formulas of Baños [6] in the ranges where the latter are good approximations. Since the complete new formulas

include the direct field, interference patterns between the surface-wave field and the direct field are observed. These occur only very near the source unless the conductivity of Region 1 is quite low. Extensive graphs of such patterns are in [30].

B. The Fields of Vertical and Horizontal Unit Dipoles for the Air-Sea Water Boundary at $f = 600$ MHz

In order to present a complete picture of the properties of the components of the electromagnetic field of vertical and horizontal dipoles and compare them with fields measured in a model tank, the frequency $f = 600$ MHz was chosen with Region 1 salt water ($\sigma_1 = 3.5$ S/m, $\epsilon_r = 80$, $k_1 = \beta_1 + i\alpha_1 = 129.4 + i64.1 = 144.4e^{0.46} \text{ m}^{-1}$) and Region 2 air ($k_2 = 4\pi \text{ m}^{-1}$). Graphs of the magnitudes of the components of the electric field computed from the formulas in the first column of Table 1 for the vertical dipole in air and from Table 2 for the horizontal dipole in salt water are shown in Fig. 6. For the horizontal dipole, the

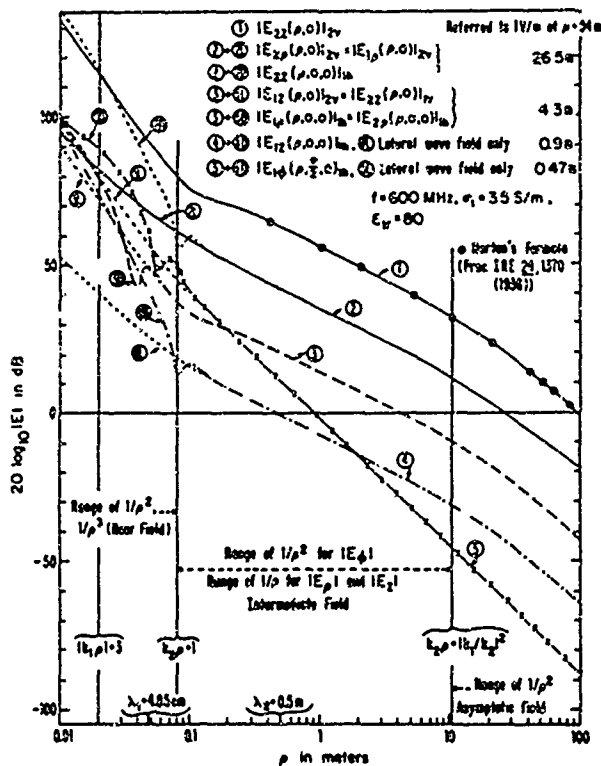


Fig. 6. Components of electric field $E(\rho, z)$ of unit vertical electric dipole ($IAI = 1 \text{ A} \cdot \text{m}$) in air (Region 2, $z \leq 0$), and $E(\rho, \phi, z)$ of unit horizontal electric dipole in sea water (Region 1, $z \geq 0$) near the surface ($z \sim 0$). [Subscript notation: first, field in Region 1 or 2; second, component of field; third, source dipole in Region 1 or 2, fourth, vertical or horizontal dipole.]

complete field including contributions from the direct-field terms are shown; also shown are the parts due to only the lateral-wave terms. Small interference patterns occur where the magnitudes of the direct and surface waves are comparable. No graphs are shown for the vertical dipole when it is in salt water since (as is readily verified from Table 1) the fields in this case are insignificant compared to the fields of the same dipole in air because of the very small

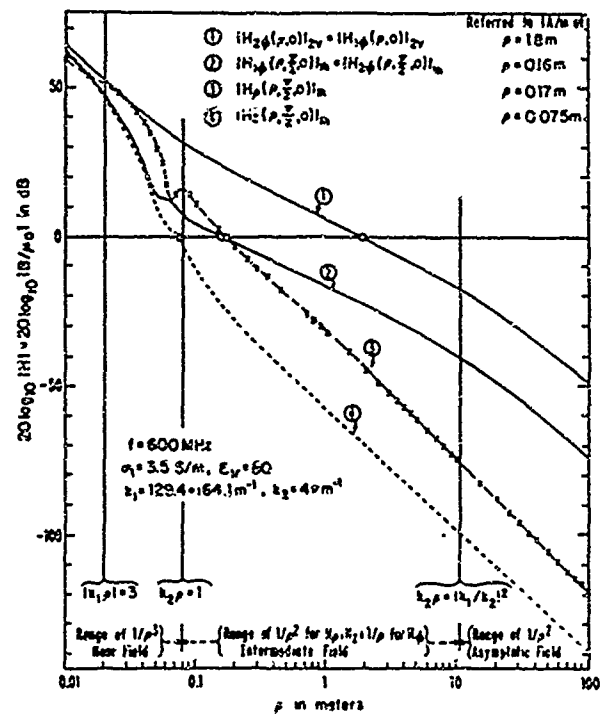


Fig. 7. Components of magnetic field $H(\rho, z)$ of unit vertical electric dipole in air and $H(\rho, \phi, z)$ of unit horizontal electric dipole in sea water

factor (k_2^2/k_1^2). For the case at hand, $|k_2^2/k_1^2| = 0.0076$ or $20 \log_{10} |k_2^2/k_1^2| = -42.4$ dB. Graphs of the components of the magnetic field are shown in Fig. 7. On the graphs, the electrical distances $|k_1 \rho| = 3$, $k_2 \rho = 1$, and $k_2 \rho = |k_2^2/k_1^2|$ are indicated. Note that $|k_1 \rho| \geq 3$ ($\rho \geq 2 \text{ cm}$) is the range of accuracy of the formulas for the fields, $k_2 \rho = 1$ ($\rho = 8 \text{ cm}$) is the boundary between the near and intermediate ranges, and $k_2 \rho = |k_2^2/k_1^2|$ ($\rho = 10.5 \text{ m}$) is the boundary between the intermediate and asymptotic fields. It is seen that the direct field is generally significant only in the near field, i.e., when $k_2 \rho < 1$, or $\rho < 8 \text{ cm}$ at $f = 600$ MHz.

Curve ① in Fig. 6 is the vertical electric field in air on the surface at $(\rho, 0)$ due to a vertical electric dipole in air and on the surface at $(0, 0)$. It is denoted by $|E_{22}(\rho, 0)|_{2v}$, where the first subscripts indicate the z -component in Region 2 and the second pair of subscripts indicates a vertical dipole in Region 2 also on the surface. The crosses along the curve were obtained from Norton's "ground-wave term" (7) using his tabulation of the function F_p defined in (8). The associated radial component is represented by curve ② + ②L. It is smaller than the z -component by the factor k_2/k_1 . Curve ② + ②L is reproduced in Fig. 8 together with the magnitudes of the separate parts of the formula. These include the term $B \exp(ik_2 \rho) [(ik_2/\rho) - 1/\rho^2]$ which is dominated by $1/\rho^2$ when ρ is small, by $1/\rho$ when ρ is large. Also included is the Fresnel integral term $|BF|$ which conforms precisely to the Zenneck wave when $\rho \leq 1 \text{ m}$. When $\rho \geq 30 \text{ m}$, the Fresnel integral term has the asymptotic form given following (25). This includes a $1/\rho$ term that cancels the $1/\rho$ term in $|BF|$ and a term $k_2^2/k_1^2 \rho^2$ which determines the asymptotic field. The two vertical lines $k_2 \rho = 1$ and $k_2 \rho = |k_2^2/k_1^2|$ are also shown. These are the approximate demarcation lines of the near field [$k_2 \rho <$

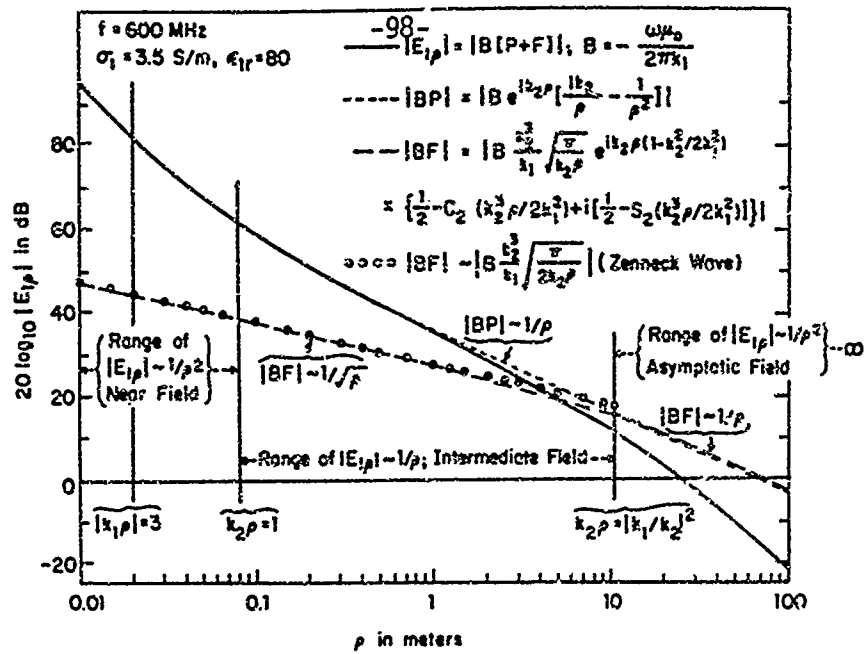


Fig. 8. Radial electric field $E_p(\rho, z)$ at surface ($z = 0$) of sea water due to vertical electric dipole ($I\Delta l = 1 \text{ A} \cdot \text{m}$) in air on surface ($d = 0$) of water (Referred to 1 V/m at $\rho = 25 \text{ m}$)

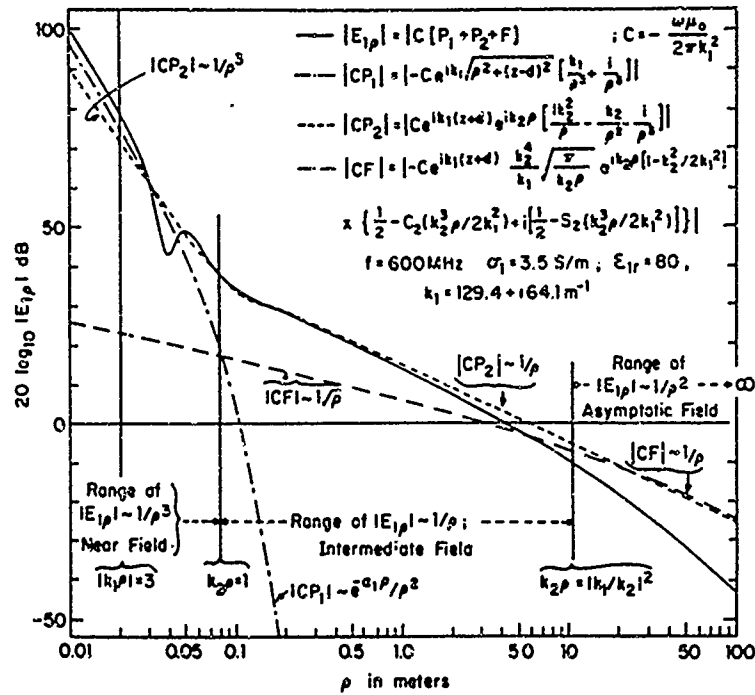


Fig. 9. Radial electric field $E_p(\rho, \phi, z)$ near surface ($z = 0, \phi = 0$) of unit ($I\Delta l = 1 \text{ A} \cdot \text{m}$) horizontal electric dipole at depth $d = 0$ in sea water (Referred to 1 V/m at $\rho = 4.7 \text{ m}$)

1, $E_p(\rho, 0) \sim 1/\rho^2$, the intermediate field [$1 < k_2\rho < |k_1/k_2|^2$, $E_p(\rho, 0) \sim 1/\rho$], and the asymptotic field [$|k_1/k_2|^2 < k_2\rho < \infty$; $E_p(\rho, 0) \sim 1/\rho^2$] which characterize the field of the vertical electric dipole when the dipole and the point of observation are on the surface in air (Region 2). Note that in this case there is no direct field and the formulas in Table 1 give the complete field.

Curve (3) + (3L) in Fig. 6 represents $|E_{1z}(\rho, 0)|_{2v}$. That is, the z -component of the electric field in Region 1 due to a

vertical dipole in Region 2 on the boundary $z = 0$. Curve (3) + (3D) represents $|E_{1p}(\rho, 0, 0)|_{1n} = |E_{2p}(\rho, 0, 0)|_{1n}$, i.e., the radial electric field at the boundary due to a horizontal electric dipole in Region 1 at (0, 0). It includes the contribution of the direct-field terms. It is reproduced in Fig 9 together with its constituent parts. These include the direct field CP_1 which decreases exponentially with distance; the terms CP_2 which decrease as $1/\rho^3$ for small values of ρ , as $1/\rho$ for large values, and the Fresnel integral term which

decreases as $1/\rho^{1/2}$ when ρ is not too large and then, for large values of ρ , as $(ik_2/\rho) + (k_1^2/k_2^2\rho^2)$. When $k_2\rho < 1$, the direct-field term is significant and combines with the surface-wave term in an interference pattern. In general, $|E_p(\rho, 0, 0)|_{1h}$ decreases as $1/\rho^3$ in the near field, as $1/\rho$ in the intermediate range, and as $1/\rho^2$ in the asymptotic range. Curve (4) + (4D) is the magnitude of the complete component $|E_{1z}(\rho, 0, 0)|_{1h}$ (including the direct field) of the horizontal dipole source; curve (4) + (4L) is the lateral-wave part.

Curve (5) + (5D) in Fig. 6 is for $|E_{1\phi}(\rho, \pi/2, 0)|_{1h}$, i.e., for the transverse component of the electric field in Region 1 due to a horizontal electric dipole also in Region 1 near the surface. It decreases as $1/\rho^3$ for small values of ρ and as $1/\rho^2$ in both the intermediate and asymptotic ranges so that, while initially larger than $|E_{1z}(\rho, 0, 0)|_{1h}$ by a factor 2, it rapidly decreases to much smaller values as ρ increases. Curve (5) + (5L) is the lateral-wave part of $|E_{1\phi}(\rho, \pi/2, 0)|_{1h}$, i.e., the field without the contributions by the direct-field terms.

In Fig. 7 for the magnetic field, curve (1) is for the complete magnetic field $H_\phi = B_\phi/\mu_0$ of the vertical dipole (there is no direct field), curve (2) is for the same component for the horizontal dipole including the direct-field terms. B_ϕ is associated with E_z and E_ρ , curves (3) and (4) are for $H_\rho = B_\rho/\mu_0$ and $H_z = B_z/\mu_0$ associated with E_ϕ . Note that E_ϕ , B_ρ , and B_z have the directional factor $\sin\phi$, E_ρ , E_z , and B_ϕ the factor $\cos\phi$.

It is evident from these figures and Tables 1 and 2 that the largest field (both E_z and E_ρ) along the surface in air is generated by a unit vertical dipole in air. This also generates the largest $E_{1\phi}$ in Region 1. The corresponding field of the unit horizontal dipole in the water is smaller by the factor k_1/k_2 . The field of the unit vertical dipole in the water is smaller by the factor $(k_2/k_1)^2$.

C. Elliptical Polarization

The lateral-wave electric field in both regions is elliptically polarized with a component of the electric field in the direction of propagation. Specifically from Table 1 for the vertical dipole on the surface in Region 2

$$\vec{E}_2(\rho, 0) = -\frac{\omega\mu_0}{2\pi k_1} f(k_2\rho, k_1) e^{ik_2\rho} \cdot \left[\hat{\rho} - z \frac{k_1 g(k_2\rho, k_1)}{k_2 f(k_2\rho, k_1)} \right] \quad (27)$$

$$\vec{E}_1(\rho, z) = -\frac{\omega\mu_0}{2\pi k_1} f(k_2\rho, k_1) e^{ik_2\rho} e^{ik_1 z} \cdot \left[\hat{\rho} - z \frac{k_2 g(k_2\rho, k_1)}{k_1 f(k_2\rho, k_1)} \right] \quad (28)$$

At distances $k_2\rho \geq 10$, $g(k_2\rho, k_1) \sim f(k_2\rho, k_1)$ so that the instantaneous values of the electric vectors are

$$\vec{E}_2(\rho, 0; t) = \text{Re} \left\{ K(\rho) e^{-i\theta_K(\rho, 0)} \cdot [\hat{\rho} e^{-i\omega t} - z |k_1/k_2| e^{-i(\omega t + \theta_1)}] \right\} \quad (29)$$

$$\vec{E}_1(\rho, z; t) = \text{Re} \left\{ K(\rho) e^{-i\theta_K(\rho, z)} \cdot [\hat{\rho} e^{-i\omega t} - z |k_2/k_1| e^{-i(\omega t + \theta_1)}] \right\} \quad (30)$$

where $\theta_1 = \tan^{-1}(\alpha_1/\beta_1)$ and $K(\rho) \exp[-i\theta_K(\rho, z)] = -(\omega\mu_0/2\pi k_1) f(k_2\rho, k_1) \exp(ik_2\rho) \exp(ik_1 z)$. These

equations reduce, respectively, to

$$|k_2/k_1|^2 E_{2z}^2(\rho, 0, t) - 2|k_2/k_1| E_{2z}(\rho, 0, t) E_{2\rho}(\rho, 0, t) \cos\theta_1 + E_{2\rho}^2(\rho, 0, t) - \sin^2\theta_1 = 0 \quad (31)$$

$$|k_1/k_2|^2 E_{1z}^2(\rho, z, t) - 2|k_1/k_2| E_{1z}(\rho, z, t) E_{1\rho}(\rho, z, t) \cos\theta_1 + E_{1\rho}^2(\rho, z, t) - \sin^2\theta_1 = 0. \quad (32)$$

These are equations of ellipses with their major axes rotated with respect to the z -axis by the wave-tilt angles

$$\theta = \frac{1}{2} \tan^{-1} \left[\frac{2|k_2/k_1| \cos\theta_1}{1 - |k_1^2/k_2^2|} \right] = \frac{1}{2} \tan^{-1} \frac{2k_2\beta_1}{|k_1|^2} - \frac{k_2\beta_1}{|k_1|^2} - \frac{k_2}{|k_1|\sqrt{2}} \quad (33)$$

$$\theta = \frac{\pi}{2} - \frac{1}{2} \tan^{-1} \frac{2k_2\beta_1}{|k_1|^2} - \frac{\pi}{2} - \frac{k_2\beta_1}{|k_1|^2} - \frac{\pi}{2} - \frac{k_2}{|k_1|\sqrt{2}} \quad (34)$$

The last steps in (33) and (34) apply to salt water for which $\beta_1 = \alpha_1 = |k_1|/\sqrt{2}$. These equations indicate that the lateral wave that travels radially outward along the surface $z = 0$ in Region 2 consists of a linearly polarized transverse magnetic field $B_{2\phi}(\rho, 0)$ and an elliptically polarized electric field with the major axis inclined slightly from the plane perpendicular to the direction of propagation $\hat{\rho}$, since $|E_{2z}/E_{2\rho}| \sim |k_1/k_2|$. Similarly, the wave that travels vertically downward into Region 1 consists of a linearly polarized transverse magnetic field $B_{1\phi}(\rho, z)$ and an elliptically polarized electric field with its major axis inclined slightly from the plane perpendicular to the direction of propagation \hat{z} , since $|E_{1\rho}/E_{1z}| \sim |k_2/k_1|$.

D. Comparison with Measurements

Since the general integrals for the fields of unit dipoles near a plane boundary between different media are exact solutions of Maxwell's equations, they require no experimental verification. The approximations involved in the representation of these integrals by simple formulas are quantitatively clear and, in the range specified for them, corroborating measurements are not essential. However, both the general integrals and their approximate representations are idealizations in the sense that they apply to two homogeneous and different semi-infinite half-spaces with a smooth plane boundary. In order to have them as useful tools in the practical experimental study of the propagation of electromagnetic waves along the boundaries of finite regions that may have irregularities, obstacles, and discontinuities, it is desirable to investigate experimentally the degree in which conditions can be provided in the laboratory that approximate the ideal. Accordingly, a series of experiments has been carried out to observe the radial electric field due to a horizontal electric monopole (with image in a vertical ground plane) just below the surface of salt water in a small indoor tank. These are described in [33]. Results relevant to the present work are the measurement in amplitude and phase of the radial component $E_{1\rho}(\rho, \phi, z)$ due to a horizontal electric dipole at depth d in salt water. The aspects of interest are the field distribution along the radial line $\phi = 0$ (which should have the form $\exp(ik_2\rho)/\rho$ in the intermediate zone), the field pattern as a function of ϕ (which should have the form $\cos\phi$ for a

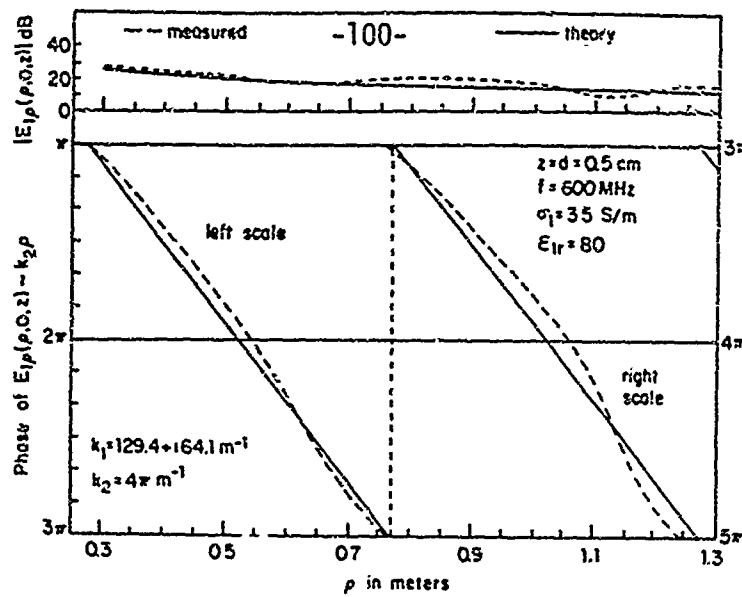


Fig. 10. Measured magnitude and phase of $E_p(p, 0, z) \sim \exp(ik_1 p)/p$ (intermediate range)

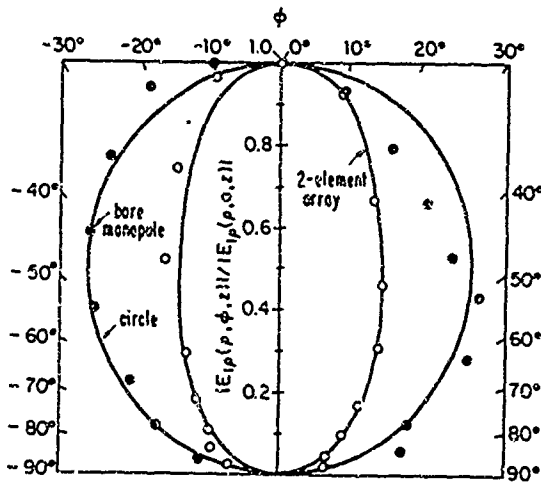


Fig. 11 Measured lateral-wave field pattern of a short bare monopole and a two-element array of insulated traveling-wave antennas; $p = 0.8$ m, $z = d = 0.5$ cm, $f = 600$ MHz

short bare dipole), and the amplitude as a function of the combined depths of the source and receiving dipoles (which should behave like $\exp[-\alpha_1(z+d)] \exp[i\beta_1(z+d)] \times \exp(ik_2 p)$). Measured graphs of the amplitude and phase along the radial line $\phi = 0$ are shown in Fig. 10, the measured field pattern is in Fig. 11, and the decrease in amplitude and change in phase with depth are shown in Fig. 12. All of the measured graphs are in good agreement with the theory. A small standing wave due to both the finite size of the semi-circular tank and small reflections from the ceiling is the principal difference between measurement and theory. Also of interest and shown in Fig. 11 is the measured directional field pattern of a two-element array of horizontal traveling-wave insulated monopoles. The antennas are described in [33].

E. Summary

Surface waves along the plane boundary between two half-spaces characterized by the wavenumbers k_1 and k_2

with $|k_1/k_2|^2 \gg 1$ can be excited by suitable sources in either region near the boundary. With the direct field, they constitute the entire field along the surface in Region 2 and at all points in Region 1. Their essential characteristics are contained in the formula $A(k_2/k_1)F(p)\exp(ik_2 p)\exp[ik_1(z+d)]$. This indicates that a source at a depth d in Region 1 at $p = 0$ generates a lateral wave that propagates vertically upward to the surface [$\exp(ik_1 d) = \exp(-\alpha_1 d)\exp(i\beta_1 d)$], then proceeds radially outward along the surface [$\exp(ik_2 p)$], and finally propagates vertically downward to the point of observation at the point (p, ϕ, z) [$\exp(ik_1 z) = \exp(-\alpha_1 z)\exp(i\beta_1 z)$]. If the source is at the surface, $d = 0$, the wave proceeds directly along the surface. The radially

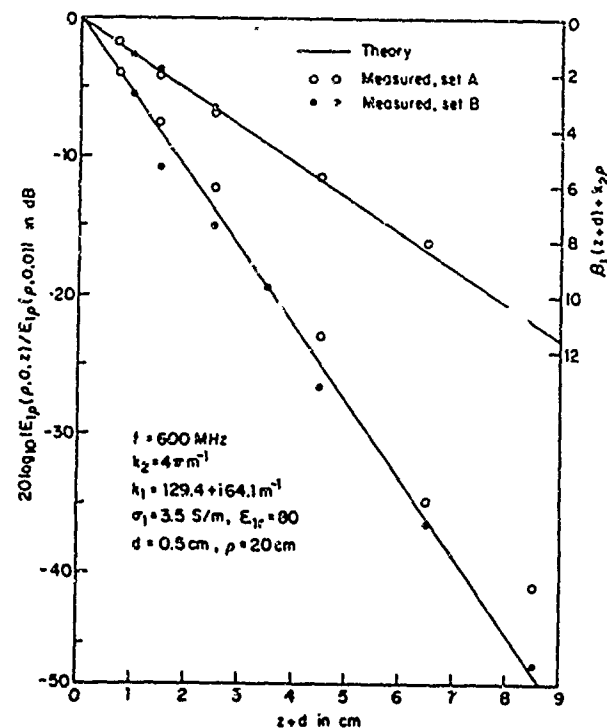


Fig. 12. Experimental test of $|E_p(p, 0, z)| \sim \exp[-\alpha_1(z+d)] \exp[i\beta_1(z+d) + k_2 p]$.

outward traveling wave decreases in amplitude according to $F(\rho)$. This includes three regions: a) the near field, $k_2\rho < 1$, $F(\rho) \sim 1/\rho^2$ for a vertical dipole in Region 2, $F(\rho) \sim 1/\rho^3$ for a horizontal dipole in Region 1, b) the intermediate field, $1 < k_2\rho < |k_1/k_2|^2$, $F(\rho) \sim 1/\rho$ for electric-type field (E_ρ, E_z, B_ϕ), $F(\rho) \sim 1/\rho^2$ for magnetic-type field (B_ρ, B_z, E_ϕ); c) the asymptotic field, $|k_1/k_2|^2 < k_2\rho$, $F(\rho) \sim 1/\rho^2$. The amplitude factor $A(k_2/k_1)$ is greatest for the field of a vertical dipole on the surface in Region 2, smaller by a factor (k_2/k_1) for a horizontal dipole in Region 1, and smallest by a factor $(k_2/k_1)^2$ for a vertical dipole in Region 1.

The complete fields due to dipoles in Region 1 include a set of direct-field terms with the factors $\exp(ik_1r_1)$ or $\exp(ik_1r_2)$, where $r_1 = [(z-d)^2 + \rho^2]^{1/2}$ and $r_2 = [(z+d)^2 + \rho^2]^{1/2}$. These are generally significant only in the near field when Region 1 is at least moderately dissipative. For very pure lake water at high frequencies, the direct-field terms are significant much further out. They combine with the lateral-wave field to produce an interference pattern. For long-distance transmission over the earth's surface, the direct-field terms can usually be ignored.

The theory has been presented for a perfectly nonconducting Region 2. If Region 2 is somewhat conducting (rock instead of air), all formulas remain valid with $k_2 = \beta_2 + i\alpha_2$, complex. The first inequality in (18) becomes $|k_1| \geq 3|k_2|$; the other are unchanged.

F. Limitations

The simplified theory which has been summarized in the preceding sections is a complete and quantitatively accurate representation of electromagnetic surface waves along the boundary between two half-spaces that satisfy the specified conditions. When applied to practical situations such as propagation over the earth, the geometry of two half-spaces with a plane boundary may not be an adequate approximation. In particular, for large distances, the curvature of the earth must be considered. There are no comparably simple formulas for the propagation of surface waves over a spherical earth. However, methods for correcting the fields over a plane earth so they apply to a spherical earth are available [34], [35].

A further complicating factor in problems relating to the propagation over the earth is the presence of the ionosphere [36]. In effect, this changes the two-medium problem into one involving three media with the air bounded both above and below so that multiple reflections can occur. Since the surface wave is significant only within a few wavelengths of the air-earth interface, it may be presumed that its general form remains valid with a superimposed reflected field from the ionosphere except when the height of the ionosphere is less than one or two wavelengths. An analysis of the three-layer problem specifically to determine its relation to the surface wave in the two-layer problem is in progress.

In the following example of the application of the new simple formulas for the surface wave, no account is taken of the curvature of the earth or of the presence of the ionosphere.

III. THE LATERAL-WAVE FIELD OF PRACTICAL ANTENNAS; APPLICATION TO COMMUNICATION WITH SUBMARINES

The electromagnetic fields represented by the formulas in Tables 1 and 2 and the graphs in Figs. 6-9 are generated by

idealized extensionless dipoles with unit electric moments, $|\Delta\mathcal{L}| = 1 \text{ A} \cdot \text{m}$. Here I is a uniform current in amperes in an infinitesimal length $\Delta\mathcal{L}$. Practical antennas in Region 2 may be bare vertical monopoles and arrays of such monopoles on the surface or horizontal traveling-wave antennas (Beverage antennas) or arrays of such antennas close to the surface. Useful antennas for Region 1 are insulated traveling-wave elements either used singly or in arrays designed to provide a radially progressive field with a maximum vertically upward. In order to describe and compare the properties of such antennas, they will be treated specifically as applied to communication with submarines.

A. Communication with Submarines

Radio communication with submerged submarines by means of electromagnetic waves is made difficult by high attenuation in sea water. Since the amplitude of a transmitted signal decreases exponentially with the distance of travel through the water [$\exp(-\alpha_1 r)$, $\alpha_1 = \{\omega\mu_0\sigma/2\}^{1/2}$], it is essential that the path in the water be short and the frequency low so that $\alpha_1 r$ is not too large. The shortest distance is in transmission vertically downward into the ocean. Hence, obvious locations for the source are on an aircraft, the space shuttle, or a satellite. Less obviously but no less effectively, vertically downward transmission can be achieved with lateral waves. All components of the lateral-wave field propagate along the surface of the ocean without exponential attenuation until directly over the submarine and then travel vertically downward so that the entire exponential attenuation is in the factor $\exp(-\alpha_2 z)$ for a vertical or horizontal transmitting antenna on the surface or in $\exp[-\alpha_2(z+d)]$ for a horizontal transmitting antenna at the depth d . The attenuation constant α_2 as a function of frequency and the magnitude of $\exp(-\alpha_2 s)$ as a function of the total depth $s = z + d$ with the frequency as the parameter are shown in Fig. 13 for salt water. The advantages of the lower frequencies are obvious.

In order to determine the optimum frequency for long-distance communication with submarines, it is not sufficient to examine only the decrease in amplitude with depth. It is also necessary to consider the decrease in amplitude with radial distance. This differs considerably for the several components of the lateral-wave field. Except quite near the source, the largest component is $E_{1\rho}$; it is the most useful for long-distance communication. $E_{1\rho}(\rho, 0)$ due to a unit vertical dipole on the surface in air is greater than $E_{1\rho}(\rho, 0, 0)$ due to a unit horizontal dipole in the sea at the surface by the factor (k_1/k_2) . $E_{1\rho}(\rho, 0)$ due to the vertical dipole also has the advantage that in the near field it decreases only as $1/\rho^2$ and not as $1/\rho^3$ as does $E_{1\rho}(\rho, 0, 0)$ due to a horizontal dipole. For both dipoles the intermediate field is characterized by $1/\rho$, the asymptotic field by $1/\rho^2$. Graphs of $|E_{1\rho}(\rho, 0)|_{2v}$ as a function of radial distance from $\rho = 0.1 \text{ m}$ to 10000 km with the frequency as the parameter are shown in Fig. 14 for a unit vertical dipole in air. The corresponding graphs of $|E_{1\rho}(\rho, 0, 0)|_{1h}$ for a unit horizontal dipole in sea water are in Fig. 15. The boundaries $k_2\rho = 1$ and $k_2\rho = |k_1^2/k_2^2|$, respectively, between the near and intermediate, and intermediate and asymptotic regions are indicated. These are important since the desirable range is always the intermediate one where the field decreases slowly as $1/\rho$ with distance. The limits of this range together with the amplitudes of the radial electric field in sea water just below the surface are listed in Table 3 against the

Table 3 Intermediate Ranges in Distance and Amplitude

f	Intermediate Range	Vertical Dipole in Air	Horizontal Dipole in Sea Water
		$20 \log_{10} E_v(\rho, 0) $	$20 \log_{10} E_h(\rho, 0, 0) $
10^1	5000 to beyond 10 000 km	-327 to -335 dB	-428 to -434 dB
10^2	500 to beyond 10 000 km	-277 to -306	-358 to -394
10^3	50 to beyond 10 000 km	-227 to -276	-306 to -354
10^4	5 to beyond 10 000 km	-177 to -246	-248 to -314
10^5	500 m to beyond 10 000 km	-127 to -216	-188 to -274
10^6	50 m to 3000 km	-77 to -176	-128 to -225
10^7	5 m to 30 km	-27 to -107	-68 to -144
10^8	0.5 to 300 m	23 to -38	-8 to -66

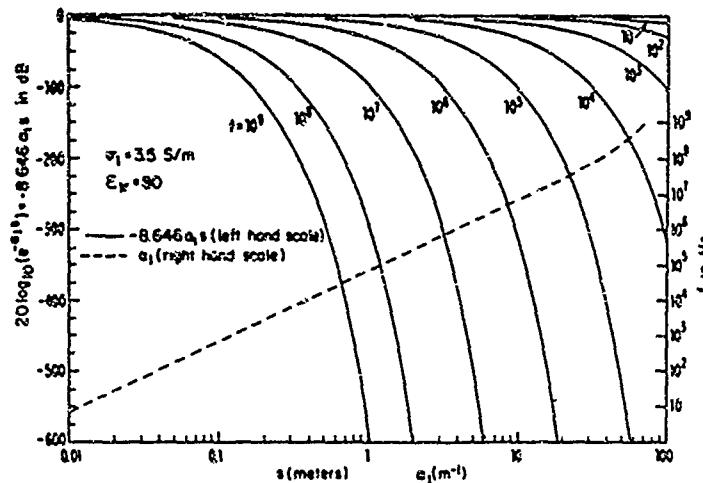


Fig. 13. Decrease in amplitude with depth $s = z - d$ in sea water, attenuation constant α_1 as a function of frequency

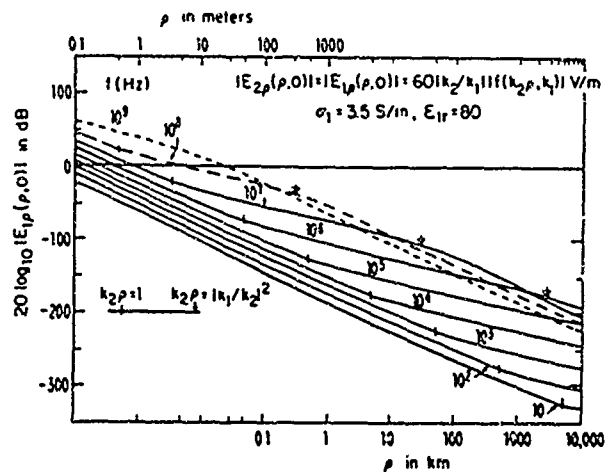


Fig. 14. Magnitude of $E_v(\rho, 0)$ due to vertical unit electric dipole in air above the surface of sea water.

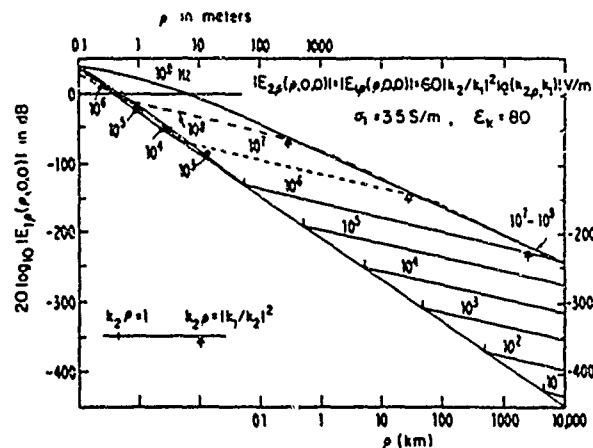


Fig. 15. Magnitude of $E_h(\rho, 0, 0)$ due to horizontal unit electric dipole in salt water just below the surface with air

frequency. In order to extend outward to 10 000 km and inward to 50 km, the best frequency lies between 1 and 100 kHz. This frequency range encompasses amplitude ranges from -276 to -127 dB for the unit vertical dipole in air and from -354 to -188 dB for the unit horizontal dipole in salt water, all referred to 1 V/m.

The decrease in amplitude with radial distance is one of the important quantities in long-distance communication. The other is the decrease in amplitude with depth in the sea water. This involves only the distance z from the surface to the antenna of the submarine for the vertical unit dipole in air, the combined distance $z + d$ (including the

depth z of the submarine's antenna and the depth d of the transmitting unit dipole) for the horizontal dipole in sea water. What is the optimum frequency for a preassigned depth? This is readily determined when the radial range is restricted to the intermediate zone where the frequency is low enough so that $k_1 = (i\omega\mu_0\sigma_1)^{1/2}$. With $(\omega\mu_0/2\pi k_2) = 60 \Omega$

$$|E_v(\rho, z)|_{2v} = \frac{60k_2^2}{\rho|k_1|} e^{-\alpha_1 z}$$

$$|E_h(\rho, 0, z)|_{1h} = \frac{60k_2^2}{\rho|k_1|} e^{-\alpha_1(z-d)}$$

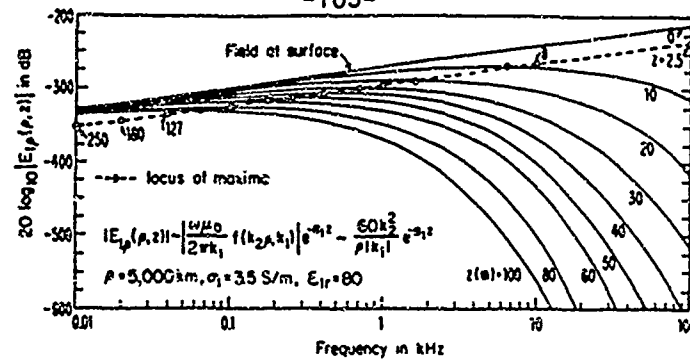


Fig. 16. Magnitude of $E_p(p, z)$ at depth z and $\rho = 5000$ km due to vertical electric dipole in air on the surface of sea water as a function of the frequency with z as parameter

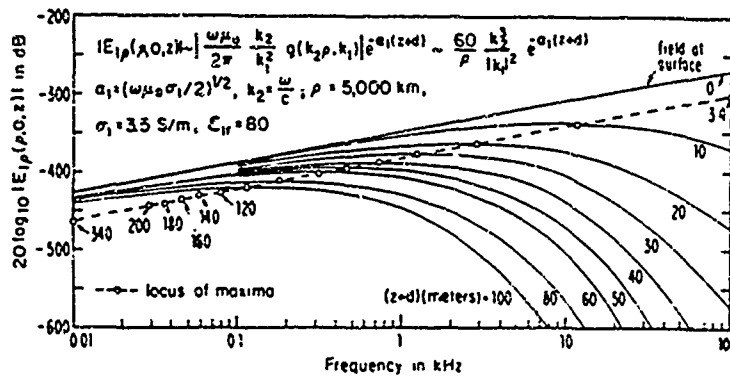


Fig. 17. Magnitude of $E_p(p, 0, z)$ at depth z and $\rho = 5000$ km due to horizontal electric dipole at depth d in sea water as a function of frequency with $z + d$ as parameter

If $\partial|E_p(p, z)|/\partial z$ is equated to zero, it turns out that the depth for maximum field is given by $\alpha_1 z = 3$ for the vertical dipole, $\alpha_1 z = 4$ for the horizontal dipole. It follows that the maximizing condition is $1z^2 = 9/\pi\mu_0\sigma_1$ for the vertical, $1z^2 = 16/\pi\mu_0\sigma_1$ for the horizontal dipole. Graphs of $|E_p(p, z)|$, and $|E_p(p, 0, z)|$, are shown in Figs. 16 and 17 for $\rho = 5000$ km as a function of frequency from 0.01 to 100 kHz with z or $z + d$ as the parameter. The field at the surface ($z = 0$, $z + d = 0$) is also shown, together with the locus of maximum field for each value of z or $z + d$. It is seen that the greater z or $z + d$, the lower must be the frequency if the maximum field for the particular value of z or $z + d$ is to be available. On the other hand, the magnitude of the available maximum decreases significantly as the frequency is lowered. In general, for depths in the ocean of less than 50 m, frequencies in the range from 1 to 30 kHz are most useful.

B. The Field of Vertical Antennas in Region 2 (Air) on the Surface of Region 1 (the Sea)

The electromagnetic fields represented by the formulas in Tables 1 and 2 and the graphs in Figs. 6-9 are generated by idealized dipoles with unit electric moments, $I\Delta\ell = 1$ A m, where I is the uniform current in amperes and $\Delta\ell$ is the length in meters. Practical vertical antennas on the earth are usually bare monopoles of length h and radius a . For antennas with the electrical lengths $k_2 h \leq \pi/2$, the distribution of current for calculating the radiated field is adequately approximated by

tion of current for calculating the radiated field is adequately approximated by

$$I_z(z) = V_0 \sin k_2(h - z)/Z_0 \sin k_2 h \quad (35)$$

where Z_0 is the driving-point impedance. In calculating the field in the equatorial plane, the antenna can be represented by an equivalent monopole with the uniform current $I_z(0)$ and an effective length h_e defined by

$$I_z(0)h_e = \int_0^h I_z(z) dz. \quad (36)$$

The electrical effective length is

$$k_2 h_e = \int_0^h [\sin k_2(h - z)/\sin k_2 h] k_2 dz = \tan(k_2 h/2) \quad (37)$$

For an electrically short antenna with $(k_2 h)^2 \ll 1$, $h_e \sim h/2$. If the antenna is sufficiently top-loaded

$$h_e \sim h. \quad (38)$$

The field in the equatorial plane of the vertical monopole is well approximated by the field of the unit dipole multiplied by $I_z(0)h_e$. Directivity in the equatorial plane can be achieved with arrays of monopoles in the usual manner.

A practical vertical antenna designed to excite surface waves along the surface of the sea is the VLF antenna at Cutler, ME, USA [36]. It operates in the frequency range

from 10 to 30 kHz and consists of two base-driven vertical monopoles erected on a peninsula with an extensive radial ground system that ends in the ocean. The distance between the two antennas is of the order of $b = 1.9$ km, but since this is only 0.064 to 0.192 wavelength, the field pattern is a broad oval that does not differ greatly from a circle when the two antennas are driven in phase. Each element is 298 m high, but the six huge diamond-shaped panels of conductors that serve as the top load are arranged in an umbrella fashion with an outer height of 243 m. The effective length of the array with dual operation is only $h_e = 147$ m at $f = 14$ kHz and $h_e = 151$ m at $f = 28.5$ kHz. These correspond, respectively, to electrical lengths of $k_2 h_e = 0.043$ and $k_2 h_e = 0.090$. The associated radiation resistances are $R_r = 40k_2^2 h_e^2 \sim 0.074$ and 0.32Ω . With a total current of 2000 A equally divided between the two elements, the effective electric moments are $I(0)h_e = 2.94 \times 10^5 \text{ A} \cdot \text{m}$ at $f = 14$ kHz and $I(0)h_e = 3.02 \times 10^5 \text{ A} \cdot \text{m}$ at $f = 28.5$ kHz. The radiated powers are $P_r = I^2(0)R_r = 0.30$ and 1.28 MW.

It is evident from Fig. 1b that the frequencies from 14 to 28.5 kHz are near optimum for depths of the order of $z = 10$ m when $\rho = 5000$ km. The field decreases very rapidly at greater depths unless lower frequencies are used. This means that a submarine or its antenna must rise to within 10–20 m of the surface. Let it be assumed that submarines make use of a trailing-wire antenna with an effective length for reception of the order of 1 km and that the sensitivity of the receiver is sufficient to detect voltages across its terminals as small as $0.01 \mu\text{V}$. This means that the exciting fields along the antenna must be no smaller than $10^{-5} \mu\text{V/m}$ or -220 dB referred to 1 V/m . From Fig. 1b it is seen that the field at $\rho = 5000$ km, $z = 10$ m, is -270 dB at $f = 14$ kHz and -279 dB at $f = 28.5$ kHz for electric moments of $1 \text{ A} \cdot \text{m}$. For the moments $2.94 \times 10^5 \text{ A} \cdot \text{m}$ and $3.02 \times 10^5 \text{ A} \cdot \text{m}$, the fields are increased, respectively, by 109 and 110 dB to the values -161 and -169 dB which are large enough to be detected. At depths greater than $z = 10$ m, the field strength decreases rapidly. Specifically at $\rho = 5000$ km and $z = 20$ and 30 m, Fig. 1b shows that the fields are reduced, respectively, to -201 and -241 dB at $f = 14$ kHz and to -209 and -280 dB at $f = 28.5$ kHz. Those for $z = 30$ m are below the limit of detectability.

It may be concluded that for distances up to 5000 km and receiver depths of the order of 10 m, top-loaded, electrically short, vertical monopoles like those at Cutler, ME, operate effectively at frequencies between 10 and 30 kHz with currents up to 2000 A. If useful signals are to be received at greater depths, e.g., up to $z = 40$ m, much greater currents and much higher and more directive antennas are required. In view of the already large physical size of the Cutler system, no significant increase seems practical. Due to corona, a significant increase in voltage and current is also ruled out. Actually, Fig. 1b shows that in order to reach depths of 40 to 50 m, a frequency no higher than 1 kHz should be used. A decrease in frequency from 10 to 1 kHz would involve an increase in the dimensions of an antenna like that at Cutler by a factor of 10. This is not realistic. Hence, for communicating with submarines, vertical dipoles are generally practical at radial distances ρ up to 5000 km only if the depth of the receiving antenna is not deeper than $z \sim 10$ m. This conclusion does not include possible reflections from the ionosphere—which might

substantially increase the signal—nor the effect of the curvature of the earth which reduces the signal.

C. The Field of Horizontal Antennas Near the Air-Sea Surface

1) *The Wave Antenna or Eccentrically Insulated Antenna on the Surface in Air:* An alternative to a high (but electrically short) vertical monopole with an extensive, nondirectional top load for exciting surface waves is the directional Beverage or wave antenna. This is made up of a short vertical monopole of height d with a top load that consists of a very long horizontal wire of length h parallel to the sea or earth. This is connected to the sea or earth by a vertical wire and a series resistor so selected that the current on the horizontal wire is a traveling wave. In effect this antenna is an eccentrically insulated wire lying on the surface of the sea or earth. The effective thickness of the air insulation is the height d . A complete analysis of this antenna for both transmission and reception in terms of the accurate theory of the horizontal-wire antenna [37], [38], is in [39]. The formulas for the wavenumber $k_t = \beta_t + i\alpha_t$ of the current $I_t(x) \sim I_t(0) \exp(ik_t x)$ on the horizontal wire and the characteristic impedance Z_c in $I_t(0) = V_0^2/Z_c$ are given in [37]. Significant gain can be achieved when the antenna is near the optimum length $h_m = \pi/(\beta_t - k_2)$. This is very large except when d is small and the horizontal wire is quite close to the surface of the sea or earth. The directivity can be increased further if a number of wires with the same length are arranged parallel to one another at the same height and spaced by $\lambda_t/2$ in an upward-downward directed broadside array of traveling-wave elements. Spacings less than $\lambda_t/2$ can be used, but the directivity is reduced. The disadvantage of such an array is the very large area required (hundreds of square kilometers in the 10–30-kHz range) for wires in air close to the surface of the sea or earth.

2) *Insulated Antennas in the Sea.* Instead of locating a horizontal traveling-wave antenna at a small height d above the surface of the sea, it is possible to place it at a small depth d in the sea. For this purpose, it should consist of a conductor (radius a , length h) enclosed in an insulating sheath (outer radius b) and driven at $x = 0$ against a bare monopole of length $l = \lambda_1/4$ (where λ_1 is the wavelength in sea water) and impedance Z_0 . Because of the rapid exponential decrease of the current along bare conductors in salt water, longer antennas offer no advantages and have essentially the same impedance. The conductor is terminated at $z = h$ in a similar monopole in series with an impedance Z . This impedance is adjusted so that $Z + Z_c = Z_0$ and the current on the horizontal wire is a pure traveling wave, $I_t(x) = I_t(0) \exp(ik_t x)$, $0 \leq x \leq h$, with $I_t(0) = V_0^2/(Z_c + Z_0)$. Here the wavenumber $k_t = \beta_t + i\alpha_t$ and the characteristic impedance Z_c are given by [17, p. 15]

$$k_t = k_2 \left[1 + \frac{H_0^{(1)}(k_2 b)}{k_1 b \ln(b/a) H_1^{(1)}(k_1 b)} \right]^{1/2} \quad (39)$$

$$Z_c = 60(k_1/k_2) \ln(b/a) \Omega. \quad (40)$$

At radial distances ρ_0 that are large compared to the length h , i.e., $\rho_0^2 \gg h^2$, a typical component of the field of the antenna is well approximated by

$$[E_{1p}(\rho_0, \phi_0, z)]_{ant} = E_{1p}(\rho_0, \phi_0, z) \times \int_{-l}^{l+h} I_x(x') e^{-\alpha_1 x' \cos \phi_0} dx' \quad (41)$$

where $E_{1p}(\rho_0, \phi_0, z)$ is the field of a unit horizontal dipole at the origin. Since the bare terminating sections in sea water are very short compared to the length h , a simple and satisfactory approximation is to carry the integration in (41) only from 0 to h . That is,

$$[E_{1p}(\rho_0, \phi_0, z)]_{ant} = E_{1p}(\rho_0, \phi_0, z) I_x(0) h_e(\phi_0) \quad (42)$$

where the effective length is

$$h_e(\phi_0) = \int_0^h e^{i\alpha_1(k_1 - k_2 \cos \phi_0)x} dx = \frac{i[1 - e^{i\alpha_1(k_1 - k_2 \cos \phi_0)h}]}{k_1 - k_2 \cos \phi_0} \quad (43)$$

Of primary interest is the magnitude of the field in the direction of maximum, $\phi_0 = 0$. With $k_1 = \beta_1 + i\alpha_1$, the magnitude of the effective length is

$$|h_e(0)| = [1 - 2e^{-\alpha_1 h} \cos(\beta_1 - k_2)h + e^{-2\alpha_1 h}]^{1/2} \times [\alpha_1^2 + (\beta_1 - k_2)^2]^{-1/2} \quad (44)$$

This has a maximum near $(\beta_1 - k_2)h = \pi$ or $h = \pi/(\beta_1 - k_2)$, where

$$|h_e(0)|_{max} = [1 + e^{-\alpha_1 h}] [\alpha_1^2 + (\beta_1 - k_2)^2]^{-1/2} \quad (45)$$

Let the antenna consist of a conductor with length h and radius $a = 0.735$ cm in a thin-walled air-filled plastic tube with radius $b = 4.41$ cm so that $b/a = 6$ and $\ln(b/a) = 1.792$. When operated in sea water ($\sigma_1 = 4$ S/m) at $f = 14$ kHz, $k_1 = 2.92 \times 10^{-4} \text{ m}^{-1}$, $k_2 = \beta_1 + i\alpha_1 = (i\omega\mu\sigma_1)^{1/2} = 0.66e^{i\pi/4} = 0.47(1 + i) \text{ m}^{-1}$, so that $k_1 b = 0.66 \times 4.41 \times 10^{-4} e^{i\pi/4} = 2.91 \times 10^{-4} e^{i\pi/4}$. The small argument forms of the Hankel functions give $H_0^{(1)}(k_1 b) \sim 1 + (2i/\pi) [0.5772 + \ln(k_1 b/2)] = 0.5 - i2.325 = 2.38e^{-i1.10}$, $k_1 b H_1^{(1)}(k_1 b) \sim -2i/\pi = -i0.636$. It follows from (39) and (40) that

$$k_1 = \beta_1 + i\alpha_1 = 5.11 \times 10^{-4} e^{i0.12} = (5.10 + i0.36) \times 10^{-4} \text{ m}^{-1} \quad (46)$$

$$Z_c = 188.2 + i13.4 \Omega \quad (47)$$

With $\alpha_1 = 0.36 \times 10^{-4} \text{ m}^{-1}$ and $\beta_1 = 5.1 \times 10^{-4} \text{ m}^{-1}$, it follows that

$$h_m = \frac{\pi}{(\beta_1 - k_2)} = \frac{\pi \times 10^4}{(5.1 - 2.92)} = 14.4 \text{ km} \quad (48)$$

Also

$$h_e(0) = \frac{1 + e^{-\alpha_1 h}}{[\alpha_1^2 + (\beta_1 - k_2)^2]^{1/2}} = \frac{1 + e^{-0.518}}{[(0.36)^2 + (2.18)^2]^{1/2}} \times 10^4 = 7.2 \text{ km} \quad (49)$$

The radial electric field of the traveling-wave antenna in the direction $\phi_0 = 0$ is

$$[E_{1p}(\rho_0, 0, z)]_{ant} = I_x(0) h_e(0) E_{1p}(\rho_0, 0, z)_{d=0} e^{i\alpha_1 z} \quad (50)$$

With Fig. 17 at $z = 10$ m, $f = 14$ kHz,

$$20 \log_{10} |E_{1p}(\rho_0, 0, z)|_{ant} = 20 \log_{10} [I_x(0) h_e(0) e^{-\alpha_1 z}] - 340 \text{ dB} \quad (51)$$

Let the current in the element be $I_x(0) = 100$ A, and the depth d of the antenna be 1 m, so that $\exp(-\alpha_1 d) = 0.625$. Then, with $\rho_0 = 5000$ km, $z = 10$ m,

$$20 \log_{10} |E_{1p}(\rho_0, 0, z)|_{ant} = 113 - 340 = -227 \text{ dB}$$

for a single traveling-wave element. For 100 such elements spaced at 25 m, there is an additional gain of 40 dB so that $20 \log_{10} |E_{1p}(\rho_0, 0, z)|_{ant}$ is -187 dB referred to 1 V/m at $f = 14$ kHz. At $f = 28.5$ kHz, $\exp(-\alpha_1 d) = 0.51$ and the corresponding values are $105 - 345 = -240$ dB for one element and -200 dB for 100 elements with $z = 10$ m. In spite of the very extensive broadside array (consisting of 100 parallel traveling-wave antennas each of length 14.4 km [or 7.48 km for 28.5 kHz] at the depth $d = 1$ m separated by distances of 25 m so that an area of 2.5×14.4 [or 7.48] km is required) carrying a total of 10^4 A, the electric field at $\rho_0 = 5000$ km, $z = 10$ m, is substantially smaller than that generated by the electrically short vertical monopoles.

Unlike the vertical monopole, the horizontal subsurface array can be enlarged to operate at 1 kHz, the frequency preferred for communicating with receivers at depths in the 30-50-m range. With $a = 0.735$ cm, $b = 4.41$ cm, the relevant quantities at $f = 1$ kHz are: $k_1 = 2.09 \times 10^{-5} \text{ m}^{-1}$, $k_2 = 0.178e^{i\pi/4} = 0.126(1 + i) \text{ m}^{-1}$, $k_1 b = 0.0078e^{i\pi/4}$, $H_0^{(1)}(k_1 b) = 0.5 - i3.16 = 3.20e^{-i1.41}$, $k_1 b H_1^{(1)}(k_1 b) = -i0.636$ so that

$$k_1 = \beta_1 + i\alpha_1 = (4.07 + i0.24) \times 10^{-5} \text{ m}^{-1} \quad (52)$$

$$Z_c = 209.7 + i12.5 \Omega \quad (53)$$

$$h_m = 159 \text{ km} \quad h_e(0) = 84.4 \text{ km} \quad (54)$$

With these values, the field at $\rho_0 = 5000$ km and the depth $z = 20$ m due to a unit horizontal dipole at the surface is obtained from Fig. 17 to be -368 dB referred to 1 V/m. For an array of 100 traveling-wave antennas each at depth $d = 1$ m, of length $h = 15.3$ km, and carrying 100 A, the field is

$$20 \log_{10} |E_{1p}(\rho_0, 0, z)|_{ant} = 20 \log_{10} [10^4 \times 84.4 \times 10^3 \times e^{-0.126}] - 368 = 177 - 368 = -191 \text{ dB} \quad (55)$$

At $z = 30$ m, the field is -201 dB, and at $z = 40$ m, -211 dB. These are all greater than the minimum detectable -220 dB. The corresponding values at $f = 14$ kHz with the vertical dipoles in air are: -201 , -241 , and -279 dB, of which only the field at depth $z = 20$ m is detectable. Thus an array of 100 horizontal traveling-wave antennas at depth $d = 1$ m can be constructed in an area of 159×2.5 km to generate a much greater field than that available from the largest practical, vertical top-loaded monopole. A large amount of power is required since the input power to each element is $P_i = |I_x(0)|^2 R_c = 2.10$ MW or a total of $P_{100} = 210$ MW. However, if communication with submarines at depths up to 50 m and at distances up to 5000 km is required, an array can be constructed in an area of 150 square miles of the ocean to achieve the purpose.

For long-distance communication with submarines, the

best frequencies for receiving-antenna depths of the order of 10 m are in the 10–30-kHz range and the preferred transmitters make use of well-designed vertical top-loaded monopoles in air like those at Cutler, ME. For depths up to 50 m, the best frequencies are near 1 kHz and a possible transmitter makes use of an extensive upward-directed broadside array of optimized insulated traveling-wave antennas in the ocean near its surface.

ACKNOWLEDGMENT

The authors are grateful to J. G. Heacock of the Office of Naval Research for his continued interest in this project. The authors also wish to thank the staff of the Harvard Scientific Instrumentation Shop for their assistance in the design and construction of the technical devices associated with the experimental setup, Barbara H. Sandler for carrying out the numerical calculations, and Margzret Owens for correcting the manuscript.

REFERENCES

- [1] A. Sommerfeld, "Electromagnetic waves near wires," *Wied Annalen*, vol. 67, pp. 233–290, 1899.
- [2] J. Zenneck, "Propagation of plane electromagnetic waves along a plane conducting surface and its bearing on the theory of transmission in wireless telegraphy," *Ann d Phys*, vol. 23, pp. 846–866, Sept. 1907.
- [3] H. M. Barlow and A. L. Cullen, "Surface waves," *Proc Inst Elec Eng (London)*, pt. III, vol. 100, pp. 329–341, Nov. 1953.
- [4] A. Sommerfeld, "Propagation of waves in wireless telegraphy," *Ann d Phys*, vol. 28, pp. 665–736, Mar. 1909; *Ann d Phys*, vol. 81, pp. 1135–1153, Dec. 1926.
- [5] ———, in *Differential u. Integralgleichungen der Mechanik u. Physik*, vol. II, P. Frank and R. v. Mises, Eds., Braunschweig, Germany: Vieweg and Son, 1935, pp. 932–933.
- [6] A. Baños, Jr., *Dipole Radiation in the Presence of a Conducting Half-Space*, Oxford, England: Pergamon, 1968, pp. 151–158.
- [7] D. A. Hill and J. R. Wait, "Excitation of the Zenneck surface wave by vertical apertures," *Radio Sci.*, vol. 13, pp. 969–977, 1978.
- [8] J. R. Wait and D. A. Hill, "Excitation of the HF surface wave by vertical and horizontal antennas," *Radio Sci.*, vol. 14, pp. 767–780, 1979.
- [9] R. W. P. King, *Theory of Linear Antennas*, Cambridge, MA: Harvard Univ. Press, 1956, ch. VII, sec. 7–18.
- [10] K. A. Norton, "The propagation of radio waves over the surface of the earth and in the upper atmosphere," *Proc IRE*, vol. 24, pp. 1367–1387, Oct. 1936.
- [11] B. van der Pol and K. F. Niessen, "Propagation of electromagnetic waves over a plane earth," *Ann d. Phys.*, vol. 6, pp. 273–295, Aug. 1930.
- [12] W. H. Wise, "Earthed condenser aerial radiation formulae," *Proc. IRE*, vol. 19, pp. 1684–1689, Sept. 1931.
- [13] R. J. King, "Electromagnetic wave propagation over a constant impedance plane," *Radio Sci.*, vol. 4, pp. 255–258, Mar. 1969.
- [14] H. Bremmer, *Terrestrial Radio Waves*, New York: Elsevier, 1949.
- [15] D. A. Hill and J. R. Wait, "Ground wave attenuation for a spherical earth with arbitrary surface impedance," *Radio Sci.*, vol. 15, pp. 637–643, 1980.
- [16] J. R. Wait, "Theory of ground wave propagation," in *Electromagnetic Probing in Geophysics*, J. R. Wait, Ed., Boulder, CO: Golem Press, 1971, ch. 5, see also, [6, pp. 240–241], for a list of relevant papers by J. R. Wait.
- [17] R. W. P. King and G. S. Smith, *Antennas in Matter*, Cambridge, MA: M.I.T. Press, 1981, pp. 640–646, figs. 11.7.1a–11.7.3c.
- [18] P. R. Bannister and R. L. Dube, "Simple expressions for horizontal electric dipole quasi-static range subsurface-to-subsurface and subsurface-to-air propagation," *Radio. Sci.*,

- vol. 13, pp. 501–507, May–June 1978.
- [19] M. Siegel and R. W. P. King, "Electromagnetic fields in a dissipative half-space: A numerical approach," *J. Appl Phys.*, vol. 41, pp. 2415–2423, May 1970.
- [20] M. Siegel and R. W. P. King, "Radiation from linear antennas in a dissipative half-space," *IEEE Trans. Antennas Propagat.*, vol. AP-19, pp. 477–485, July 1971.
- [21] R. J. Lytle, E. K. Miller, and D. L. Lager, "A physical explanation of electromagnetic surface wave formulas," *Radio Sci.*, vol. 11, pp. 235–243, Apr. 1976.
- [22] D. M. Bubenik, "A practical method for the evaluation of Sommerfeld integrals," *IEEE Trans. Antennas Propagat.*, vol. AP-25, pp. 904–906, Nov. 1977.
- [23] Y. Rahmat-Samii, R. Mittra, and P. Parhami, "Evaluation of Sommerfeld integrals for lossy half-space problems," *Electromagnetics*, vol. 1, pp. 1–28, Apr. 1981.
- [24] R. W. P. King and B. H. Sandler, "Subsurface communication between dipoles in general media," *IEEE Trans. Antennas Propagat.*, vol. AP-25, pp. 770–775, Nov. 1977.
- [25] R. W. P. King, B. H. Sandler, and L. C. Shen, "A comprehensive study of subsurface propagation from horizontal electric dipoles," *IEEE Trans. Geosci. Remote Sensing*, vol. GE-18, pp. 225–233, July 1980.
- [26] R. W. P. King, J. T. deBettencourt, and B. H. Sandler, "Lateral-wave propagation in the lithosphere," *IEEE Trans. Geosci. Electron.*, vol. GE-17, pp. 86–92, July 1979.
- [27] M. Siegel and R. W. P. King, "Electromagnetic propagation between antennas submerged in the ocean," *IEEE Trans. Antennas Propagat.*, vol. AP-21, pp. 507–513, July 1973.
- [28] L. C. Shen, R. W. P. King, and R. M. Sorbello, "Measured field of a directional antenna submerged in a lake," *IEEE Trans. Antennas Propagat.*, vol. AP-24, pp. 891–894, Nov. 1976; Correction, vol. AP-26, pp. 872–873, Nov. 1978.
- [29] R. W. P. King, "New formulas for the electromagnetic field of a vertical electric dipole in a dielectric or conducting half-space near its horizontal interface," *J. Appl Phys.*, vol. 53, pp. 8476–8482, Dec. 1982.
- [30] T. T. Wu and R. W. P. King, "Lateral waves: A new formula and interference patterns," *Radio Sci.*, vol. 17, pp. 521–531, May–June 1982.
- [31] T. T. Wu and R. W. P. King, "Lateral waves: New formulas for E_y and E_z ," *Radio Sci.*, vol. 17, pp. 532–538, May–June 1982.
- [32] R. W. P. King and T. T. Wu, "Lateral waves: New formulas for the magnetic field," *J. Appl Phys.*, vol. 54, pp. 537–544, Feb. 1983.
- [33] M. F. Brown, R. W. P. King, and T. T. Wu, "Lateral-wave studies in a model lithosphere," *J. Appl Phys.*, vol. 53, pp. 3387–3396, May 1982.
- [34] K. A. Norton, "The calculations of ground-wave field intensity over a finitely conducting spherical earth," *Proc. IRE*, vol. 29, pp. 623–639, Dec. 1941.
- [35] *Recommendations and Reports of the CCIR, 1975, Vol. 1, Propagation in Non-ionized Media*, Geneva, Switzerland: International Telecommunication Union, 1978, pp. 36, 37.
- [36] A. D. Watt, *VLF Radio Engineering*, Oxford, England: Pergamon, 1967.
- [37] R. W. P. King, T. T. Wu, and L. C. Shen, "The horizontal-wire antenna over a conducting or dielectric half-space: Current and admittance," *Radio Sci.*, vol. 9, pp. 701–709, July 1974.
- [38] R. M. Sorbello, R. W. P. King, K.-M. Lee, L. C. Shen, and T. T. Wu, "The horizontal-wire antenna over a dissipative half-space: Generalized formula and measurements," *IEEE Trans. Antennas Propagat.*, vol. AP-25, pp. 850–854, Nov. 1977.
- [39] R. W. P. King, "The wave antenna for transmission and reception," *IEEE Trans. Antennas Propagat.*, vol. AP-31, pp. 956–965, Nov. 1983.

Supplementary General References

- M. L. Burrows, *ELF Communication Antennas*, Stevenage, England: Peter Peregrinus, 1978.
- L. B. Felsen and N. Marcuvitz, *Radiation and Scattering of Waves*, Englewood Cliffs, NJ: Prentice-Hall, 1973.
- H. Jasik, Ed., *Antenna Engineering Handbook*, New York: McGraw-Hill, 1961.
- Special issue on ELF Communications, *IEEE Trans. Commun.*, vol. COM-22, Apr. 1978.

Scattering of lateral waves by buried or submerged objects. I. The incident lateral-wave field

Ronald W. P. King

Gordon McKay Laboratory, Harvard University, Cambridge, Massachusetts 02138

(Received 5 September 1984; accepted for publication 18 October 1984)

The components of the lateral-wave field generated by vertical and horizontal antennas near the plane interface between air and earth (soil, water, etc.) are determined at points near the surface in air and at all points in the earth. This is the field incident on and scattered from inhomogeneities and objects in the earth.

I. INTRODUCTION

The detection and localization of buried or submerged objects or inhomogeneities in a dissipative half-space from measurements of a scattered electromagnetic field are of current interest. Investigations on this subject have been devoted primarily to plane waves incident on the surface of the earth from the air above at an arbitrary angle.^{1,2} This study is concerned with the incident fields generated by horizontal and vertical antennas on the surface of the earth. The complete fields of such antennas can now be expressed in simple and accurate form thanks to the availability of new formulas³⁻⁶ that are excellent approximations of the rigorous general integrals.

II. THE ELECTROMAGNETIC FIELD OF INFINITESIMAL HORIZONTAL AND VERTICAL ELECTRIC DIPOLES WITH UNIT ELECTRIC MOMENT

The components of the electromagnetic field at (ρ, ϕ, z) in cylindrical coordinates of an infinitesimal horizontal electric dipole with unit moment $Idl = 1$ A m at the surface of the earth in air (Region 2, $z < 0$) over a dissipative half-space (Region 1, $z > 0$) are (see Fig. 1)

$$E_{1\rho}(\rho, \phi, z) = \frac{-\omega\mu_0 k_2}{2\pi k_1^2} \cos \phi e^{ik_1 z} g(k_2 \rho, k_1) \\ = (\omega/k_1) B_{1\phi}(\rho, \phi, z), \quad (1a)$$

$$E_{1\phi}(\rho, \phi, z) = \frac{\omega\mu_0 k_2}{\pi k_1^2} \sin \phi e^{ik_1 z} h(k_2 \rho, k_1) \\ = -(\omega/k_1) B_{1\rho}(\rho, \phi, z), \quad (1b)$$

$$E_{1z}(\rho, \phi, z) = \frac{\omega\mu_0 k_2^2}{2\pi k_1^3} \cos \phi e^{ik_1 z} f(k_2 \rho, k_1), \quad (1c)$$

$$B_{1z}(\rho, \phi, z) = \frac{\mu_0 k_2^2}{2\pi k_1^2} \sin \phi e^{ik_1 z} e^{ik_1 z} \\ \times \left(\frac{1}{\rho^2} + \frac{3i}{k_2 \rho^3} - \frac{3}{k_2^2 \rho^4} \right), \quad (1d)$$

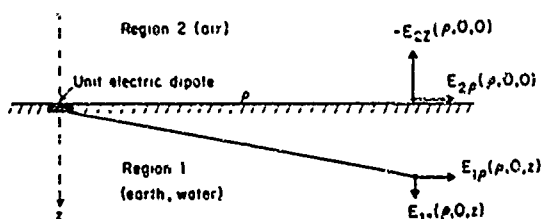


FIG. 1. Components of electric field due to unit electric dipole in earth or water very near the surface ($z \sim 0$).

where

$$f(k_2 \rho, k_1) = e^{ik_1 \rho} \left[\frac{ik_2}{\rho} - \frac{1}{\rho^2} - \frac{k_2^3}{k_1} \left(\frac{\pi}{k_2 \rho} \right)^{1/2} \right. \\ \left. \times e^{-ik_2^2 \rho / 2k_1^2} \mathcal{F}(k_2 \rho, k_1) \right], \quad (2)$$

$$g(k_2 \rho, k_1) = e^{ik_1 \rho} \left[\frac{ik_2}{\rho} - \frac{1}{\rho^2} - \frac{i}{k_2 \rho^3} - \frac{k_2^2}{k_1} \left(\frac{\pi}{k_2 \rho} \right)^{1/2} \right. \\ \left. \times e^{-ik_2^2 \rho / 2k_1^2} \mathcal{F}(k_2 \rho, k_1) \right], \quad (3)$$

$$h(k_2 \rho, k_1) = e^{ik_1 \rho} \left[\frac{1}{\rho^2} + \frac{i}{k_2 \rho^3} + \frac{ik_2^2}{2k_1} \frac{\pi^{1/2}}{(k_2 \rho)^{3/2}} \right. \\ \left. \times e^{-ik_2^2 \rho / 2k_1^2} \mathcal{F}(k_2 \rho, k_1) \right], \quad (4)$$

and

$$\mathcal{F}(k_2 \rho, k_1) = \frac{1}{2}(1+i) - C_2(k_2^2 \rho / 2k_1^2) - iS_2(k_2^2 \rho / 2k_1^2). \quad (5)$$

Here $C_2(u)$ and $S_2(u)$ are Fresnel integrals defined by

$$C_2(u) + iS_2(u) = \int_0^u (2\pi t)^{-1/2} e^{it} dt. \quad (6)$$

The field at the surface $z \sim 0$ in air is

$$E_{2\rho}(\rho, \phi, 0) = E_{1\rho}(\rho, \phi, 0) = (\omega/k_1) B_{2\phi}(\rho, \phi, 0), \quad (7a)$$

$$E_{2\phi}(\rho, \phi, 0) = E_{1\phi}(\rho, \phi, 0) = -(\omega/k_1) B_{2\rho}(\rho, \phi, 0), \quad (7b)$$

$$E_{2z}(\rho, \phi, 0) = (k_1^2/k_2^2) E_{1z}(\rho, \phi, 0), \quad (7c)$$

$$B_{2z}(\rho, \phi, 0) = B_{1z}(\rho, \phi, 0). \quad (7d)$$

All of these formulas are excellent approximations subject only to the following conditions:

$$|k_1| > 3k_2, \quad |k_1 \rho| > 3, \quad \rho^2 \gg z^2. \quad (8)$$

The corresponding expressions for the rotationally symmetric field of an infinitesimal vertical electric dipole with unit moment in air on the surface of the dissipative half-space are given by

$$E_{1\rho}(\rho, z) = \frac{-\omega\mu_0}{2\pi k_1} e^{ik_1 z} f(k_2 \rho, k_1) = (\omega/k_1) B_{1\phi}(\rho, z), \quad (9)$$

$$E_{1z}(\rho, z) = \frac{\omega\mu_0 k_2}{2\pi k_1^2} e^{ik_1 z} g(k_2 \rho, k_1). \quad (10)$$

$$E_{2\rho}(\rho, 0) = E_{1\rho}(\rho, 0) = (\omega/k_1) B_{2\phi}(\rho, 0) \quad (11)$$

$$E_{2z}(\rho, 0) = (k_1^2/k_2^2) E_{1z}(\rho, 0). \quad (12)$$

Note that the field of the vertical dipole is a function of ρ and z only, that of the horizontal dipole of ρ , ϕ and z . The fields of a unit horizontal dipole just above or just below the surface are related to those of a unit vertical dipole in air just above the surface as follows:

$$E_{1\rho\phi}(\rho, \phi, z) = [-\cos \phi] E_{1z}(\rho, z), \quad (13)$$

$$E_{1z\phi}(\rho, \phi, z) = [(k_2/k_1)^2 \cos \phi] E_{1\rho}(\rho, z), \quad (14)$$

$$B_{1\phi\phi}(\rho, \phi, z) = \left\{ (k_2/k_1) \frac{g(k_2 \rho, k_1)}{f(k_2 \rho, k_1)} \cos \phi \right\} B_{1z}(\rho, z), \quad (15)$$

$$E_{2\rho\phi}(\rho, \phi, 0) = [-\cos \phi] E_{2z}(\rho, 0), \quad (16)$$

$$E_{2z\phi}(\rho, \phi, 0) = [-\cos \phi] E_{2\rho}(\rho, 0), \quad (17)$$

$$B_{2\phi\phi}(\rho, \phi, 0) = \left\{ (k_2/k_1) \frac{g(k_2 \rho, k_1)}{f(k_2 \rho, k_1)} \cos \phi \right\} B_{2z}(\rho, 0). \quad (18)$$

III. THE FIELD OF HORIZONTAL ANTENNAS OF FINITE LENGTH WITH OPEN ENDS

A practical antenna is a center-driven horizontal dipole of half-length h and radius a , located in air at an electrically small height d over the dissipative half-space (Fig. 2). Actually, such an antenna is equivalent to an eccentrically insulated antenna lying on the surface of the half-space.⁷⁻⁹ The effective thickness of the insulation is d . The current in such an antenna is given by⁷

$$I_x(x') = \frac{I_x(0) \sin k_L(h - |x'|)}{\sin k_L h};$$

$$\times I_x(0) = V_0 Y_a. \quad (19)$$

The complex wave number is

$$k_L = \beta_L + i\alpha_L$$

$$= k_2 \left\{ 1 + \frac{2}{\ln(2d/a)} \left[\frac{1}{(2k_1 d)^2} - \frac{K_1(2k_1 d)}{2k_1 d} \right] \right\}$$

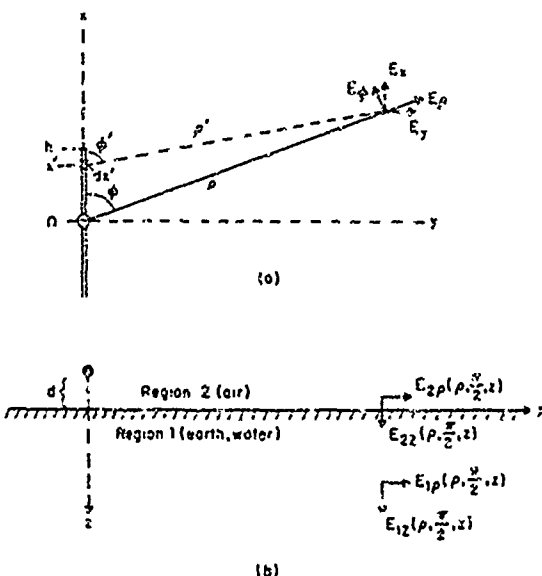


FIG. 2. Horizontal electric dipole at height d over the earth. (a) Top view. (b) Side view.

$$+ \frac{\ln(2k_1 d)}{4k_1 d}$$

$$- \left\{ \frac{2k_1 d}{3} + \frac{(2k_1 d)^3}{45} + \frac{(2k_1 d)^5}{1875} + \dots \right\}^{1/2}. \quad (20)$$

The input impedance is

$$Z_{in} = Y_{in}^{-1} = Z_c \tan k_L h, \quad (21)$$

where

$$Z_c = \frac{\xi_2 k_1}{2\pi \xi_2} \ln(2d/a);$$

$$\xi_2 = 120\pi \Omega. \quad (22)$$

At moderate distances from the dipole, the approximations $\rho' = [\rho^2 + x'^2 - 2\rho x' \cos \phi]^{1/2} \sim \rho - x' \cos \phi$ in phases and $\rho' \sim \rho$ in amplitudes can be used. With these approximations, the field of the entire dipole is given by

$$[E_{1\rho}(\rho, \phi, z)]_{HA} = \bar{E}_{1\rho}(\rho, \phi, z) \int_{-h}^h I_x(x') \times e^{-ik_2 \rho \cos \phi dx'}. \quad (23)$$

With Eq. (19) the integral is

$$I_x(0) M_0(\phi) = \frac{I_x(0)}{\sin k_L h} \int_{-h}^h \sin k_L(h - |x'|) \times e^{-ik_2 \rho \cos \phi dx'}$$

$$= \frac{2I_x(0)k_L}{\sin k_L h} \left(\frac{\cos[k_L h \cos \phi] - \cos k_L h}{k_L^2 - k_2^2 \cos^2 \phi} \right). \quad (24)$$

Note that when the antenna is electrically short so that $k_L^2 h^2 \ll 1$, $|k_L^2| h^2 \ll 1$,

$$I_x(0) M_0(\phi) \sim \frac{2I_x(0)k_L}{k_L h} \frac{k_L^2 h^2 - k_2^2 h^2 \cos^2 \phi}{2(k_L^2 - k_2^2 \cos^2 \phi)} = I_x(0)h. \quad (25)$$

The complete field in Region 1 and the field along the surface in Region 2 of the horizontal-wire antenna are given by Eqs. (1a)-(1d) and Eqs. (7a)-(7d) multiplied by $I_x(0) M_0(\phi)$ as given in Eq. (24).

IV. THE FIELD OF A HORIZONTAL ANTENNA OF FINITE LENGTH TERMINATED IN GROUNDED VERTICAL MONOPOLES

An alternative arrangement of the horizontal electric dipole over earth or salt water is with the ends grounded by vertical conductors, each of length d in air and of sufficient length in the earth or salt water to be effective ground connections with negligible impedance. When this is the case, the current on the terminated horizontal-wire antenna is

$$I_x(x') = \frac{I_x(0) \cos k_L(h - |x'|)}{\cos k_L h} = I_x(h) \cos k_L(h - |x'|). \quad (26)$$

When this expression is substituted in Eq. (23) to obtain the field of the horizontal part of the antenna, the integral is readily evaluated to give

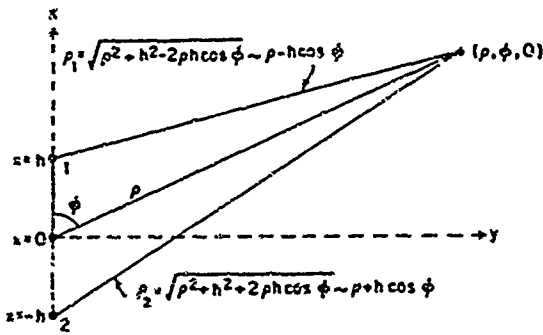


FIG. 3. Radial distances from vertical elements 1 and 2 to field point (ρ, φ, 0).

$$I_x(h)M_h(\phi) = 2I_x(h) \times \left(\frac{k_L \sin k_L h - k_2 \cos \phi \sin(k_2 h \cos \phi)}{k_L^2 - k_2^2 \cos^2 \phi} \right). \quad (27)$$

Note that when the antenna is electrically short with $k_L^2 h^2 \ll 1$, $|k_L^2| h^2 \ll 1$,

$$I_x(h)M_h(\phi) \sim 2I_x(h) \left(\frac{k_L^2 h - k_2^2 h \cos^2 \phi}{k_L^2 - k_2^2 \cos^2 \phi} \right) = 2I_x(h)h \sim 2I_x(0)h. \quad (28)$$

The complete field of the horizontal element is given by Eqs. (1a)–(1d) and Eqs. (7a)–(7d) multiplied by $I_x(h)M_h(\phi)$ as given in Eq. (27).

Each of the vertical elements at $x = \pm h$, $y = 0$, consists of a part of length h in air and a part of length l in the earth or salt water. Let each be electrically short in the respective medium; that is, let

$$(k_2 l)^2 \ll 1, \quad (k_1 l)^2 \ll 1. \quad (29)$$

The current in the vertical elements in air is essentially constant in amplitude over the length so that the electric moments are $I_x(h)d = I_x(h)d$ at $x = h$, $y = 0$, and $I_x(-h)d = I_x(-h)d = -I_x(h)d$ at $x = -h$, $y = 0$.

The radial electric field of a vertical electric dipole with unit moment is given in Eq. (9). The radial electric field of the two vertical monopoles with equal and opposite electric moments is

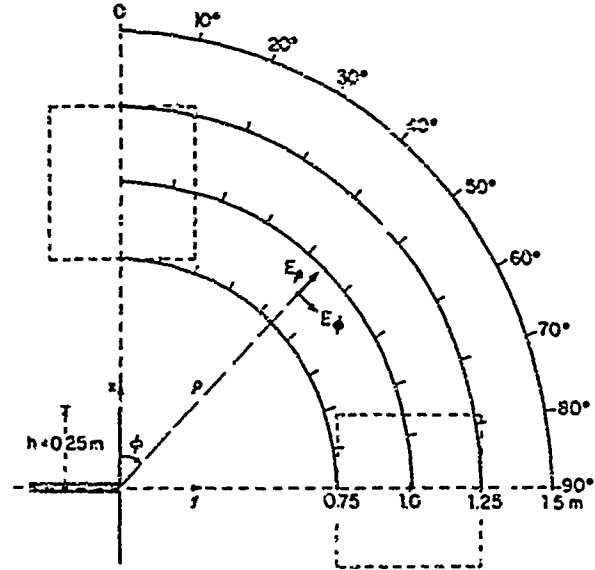


FIG. 4. Range of calculation of field of horizontal half-wave dipole: $0.75 < \rho < 1.5$ m, $0^\circ < \phi < 90^\circ$. Areas of primary interest: $-0.25 < x < 0.25$ m, $0.75 < y < 1.25$ m; and $0.75 < x < 1.25$ m, $-0.25 < y < 0.25$ m.

$$[E_{1\rho}(\rho, z)]_{\text{VA}} = E_{1\rho}(\rho, z) \times (e^{ik_2 h \cos \phi} - e^{-ik_2 h \cos \phi}) 2I_x(h) d = iE_{1\rho}(\rho, z) I_x(h) d \sin(k_2 h \cos \phi). \quad (30)$$

It has been assumed—as indicated in Fig. 3—that ρ is sufficiently large so that the radial distances ρ_1 and ρ_2 to the point (ρ, φ) are well approximated by $\rho_1 \sim \rho_2 \sim \rho$ in amplitudes and by $\rho_1 = \rho - h \cos \phi$, $\rho_2 = \rho + h \cos \phi$ in phases. The other components are obtained in the same manner. It is readily shown that the contributions to the field by the short vertical sections in the earth or salt water are negligibly small.⁶

Thus, the complete field due to the two vertical dipoles is given by Eqs. (9)–(12) with each component multiplied by $iI_x(h)d \sin(k_2 h \cos \phi)$. The complete field due to the horizontal and vertical elements can be expressed as follows, first for the field at any depth z in Region 1, then for the field on the surface $z = 0$ in Region 2. In the formulas $I_x(h)$ has been set equal to 1 A. The subscript CA indicates the field of the complete antenna.

$$[E_{1\rho}(\rho, \phi, z)]_{\text{CA}} = \frac{-\omega\mu_0}{2\pi k_1} e^{ik_1 z} \left(\frac{k_2}{k_1} g(k_2 \rho, k_1) M_h(\phi) \cos \phi + idf(k_2 \rho, k_1) \sin(k_2 h \cos \phi) \right), \quad (31)$$

$$[E_{1\phi}(\rho, \phi, z)]_{\text{CA}} = \frac{\omega\mu_0 k_2}{\pi k_1^2} e^{ik_1 z} h (k_2 \rho, k_1) M_h(\phi) \sin \phi, \quad (32)$$

$$[E_{1z}(\rho, \phi, z)]_{\text{CA}} = \frac{\omega\mu_0 k_2}{2\pi k_1^2} e^{ik_1 z} \left(\frac{k_2}{k_1} f(k_2 \rho, k_1) M_h(\phi) \cos \phi + idg(k_2 \rho, k_1) \sin(k_2 h \cos \phi) \right), \quad (33)$$

$$[B_{1\rho}(\rho, \phi, z)]_{\text{CA}} = \frac{-k_1}{\omega} [E_{1\phi}(\rho, \phi, z)]_{\text{CA}}, \quad (34)$$

$$[B_{1\phi}(\rho, \phi, z)]_{\text{CA}} = \frac{k_1}{\omega} [E_{1\rho}(\rho, \phi, z)]_{\text{CA}}, \quad (35)$$

$$[B_{1z}(\rho, \phi, z)]_{\text{CA}} = \frac{\mu_0 k_2^2}{2\pi k_1^2} e^{ik_1 z} e^{ik_2 \rho} \left(\frac{1}{\rho^2} + \frac{3i}{k_2 \rho^3} - \frac{3}{k_2^2 \rho^4} \right) \sin \phi, \quad (36)$$

$$[E_{2\rho}(\rho, \phi, 0)]_{CA} = [E_{1\rho}(\rho, \phi, 0)]_{CA}; \quad [B_{2\rho}(\rho, \phi, 0)]_{CA} = [B_{1\rho}(\rho, \phi, 0)]_{CA}, \quad (37)$$

$$[E_{2\phi}(\rho, \phi, 0)]_{CA} = [E_{1\phi}(\rho, \phi, 0)]_{CA}; \quad [B_{2\phi}(\rho, \phi, 0)]_{CA} = [B_{1\phi}(\rho, \phi, 0)]_{CA}, \quad (38)$$

$$[E_{2z}(\rho, \phi, 0)]_{CA} = (k_1^2/k_2^2)[E_{1z}(\rho, \phi, 0)]_{CA}; \quad [B_{2z}(\rho, \phi, 0)]_{CA} = [B_{1z}(\rho, \phi, 0)]_{CA}. \quad (39)$$

Note that the vertical elements contribute only to E_ρ , E_z , and B_z so that E_ϕ , B_ρ , and B_ϕ are determined entirely by the horizontal part of the antenna. Except for the relatively small differences between $M_0(\phi)$ as given by Eq. (24) and $M_A(\phi)$ as given by Eq. (27), these components are like those of the open-ended horizontal dipole. Depending on the height d , the contributions to E_ρ , E_z , and B_z by the vertical elements may be relatively small or very significant.

V. THE CALCULATED FIELD OF THE HORIZONTAL HALF-WAVE DIPOLE

The components $[E_\rho(\rho, \phi, 0)]_{HA}$ and $[E_\phi(\rho, \phi, 0)]_{HA}$ have been calculated [from Eqs. (1a) and (1b) with Eqs. (23), (24), and $I_x(0) = 1$ A] over the range $0.75 < \rho < 1.5$ m, $0^\circ < \phi < 90^\circ$, as indicated schematically in Fig. 4. Here the area of primary interest for the components $E_\phi(\rho, \phi, 0)$ and

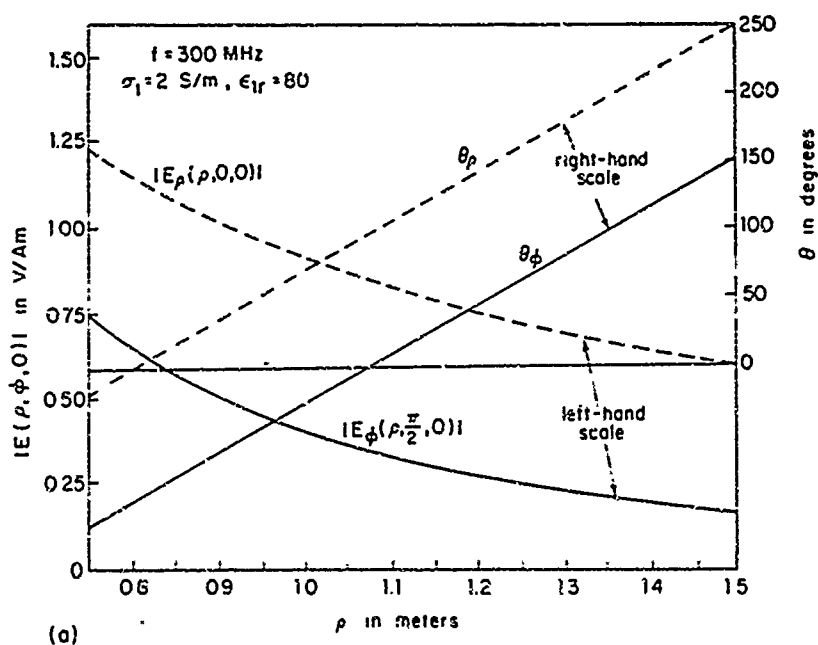
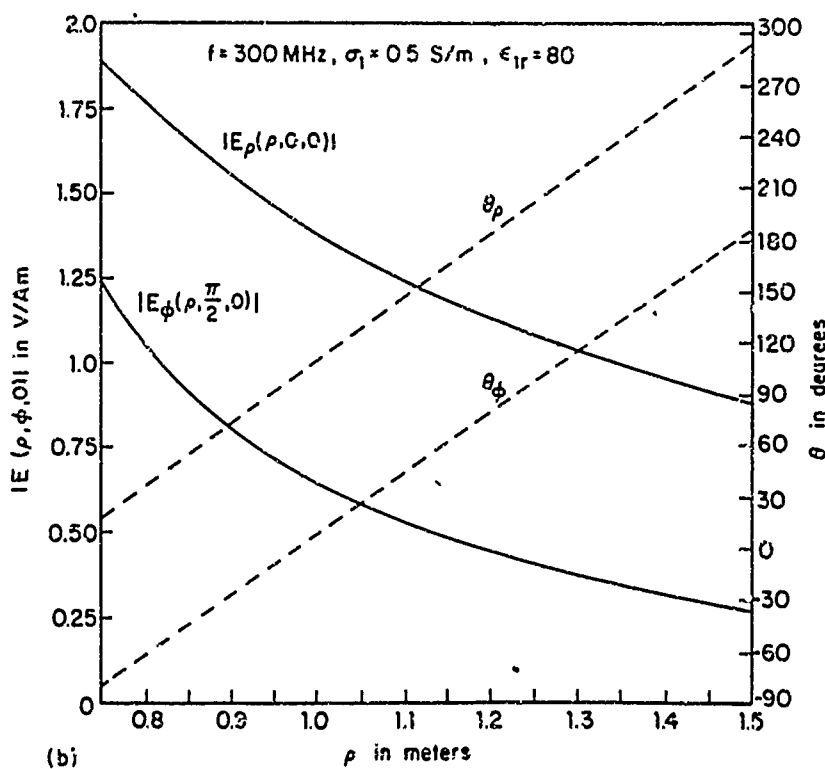


FIG. 5. E_ρ along x axis, E_ϕ along y axis; field of horizontal half-wave dipole. (a) $\sigma_1 = 2$ S/m, $\epsilon_{1r} = 80$. (b) $\sigma_1 = 0.5$ S/m, $\epsilon_{1r} = 80$.

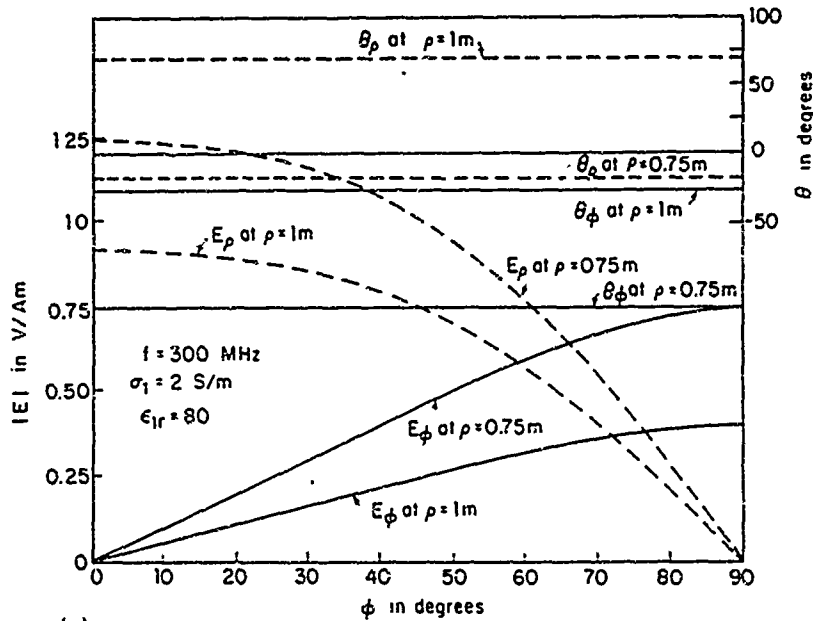


$B_\rho(\rho, \phi, 0) = -(k_1/\omega)E_\phi(\rho, \phi, 0)$ is
 $0.75 < y < 1.25$ m, $-0.25 < x < 0.25$ m. The corresponding
 area for the components $E_\rho(\rho, \phi, 0)$ and $B_\phi(\rho, \phi, 0)$
 $= (k_1/\omega)E_\rho(\rho, \phi, 0)$ is $0.75 < x < 1.25$ m, $-0.25 < y < 0.25$ m.

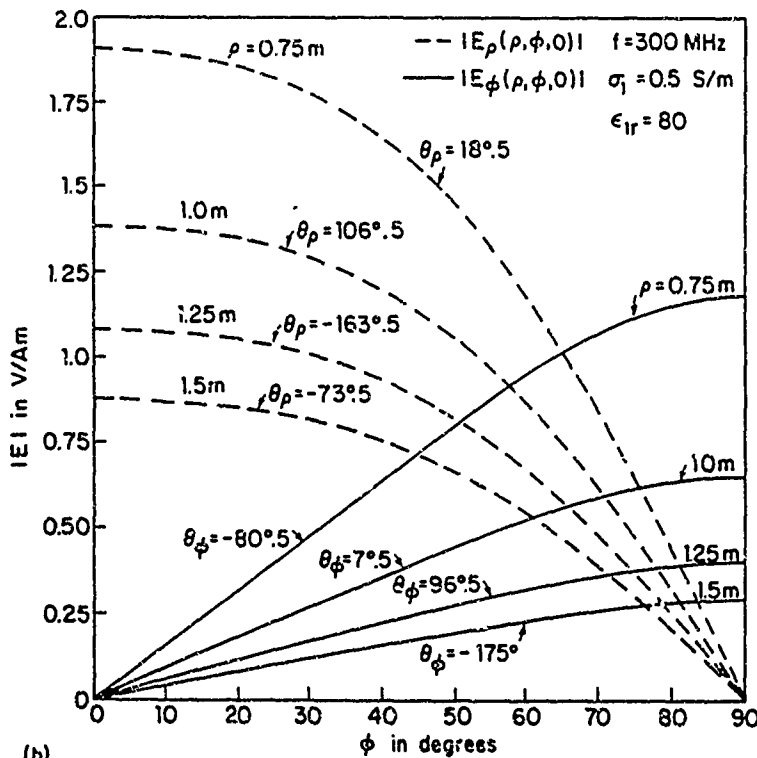
Graphs of $E_\rho(\rho, 0, 0)$ and $E_\phi(\rho, \pi/2, 0)$ in both amplitude
 and phase are plotted as functions of ρ in Fig. 5(a) for $\sigma_1 = 2$
 S/m, $\epsilon_{1r} = 80$ and in Fig. 5(b) for $\sigma_1 = 0.5$ S/m, $\epsilon_{1r} = 80$.
 Note that $E_\rho(\rho, \pi/2, 0)$ and $E_\phi(\rho, 0, 0)$ are both zero. The
 magnitude of $E_\rho(\rho, 0, 0)$ is substantially greater than
 $E_\phi(\rho, \pi/2, 0)$. Both components have amplitudes that de-
 crease with increasing radial distance and phases that are
 linearly increasing as required for an outward traveling
 wave.

Corresponding graphs of $E_\rho(1, \phi, 0)$ and $E_\phi(1, \phi, 0)$ are

shown in Fig. 6. Since the radius $\rho = 1$ m is a surface of
 constant phase for the outward traveling waves, the phases
 θ_ρ and θ_ϕ are both constant as ϕ is varied. The amplitudes of
 the two components are very different in their dependence
 on ϕ . $E_\rho(1, \phi, 0)$ has its maximum at $\phi = 0$ and decreases to
 zero at $\phi = 90^\circ$; $E_\phi(1, \phi, 0)$ is zero at $\phi = 0$ and increases to its
 maximum at $\phi = 90^\circ$. It is seen that in the range from 70° to
 90° , $|E_\phi(1, \phi, 0)|$ is almost constant, whereas $|E_\rho(1, \phi, 0)|$ de-
 creases almost linearly to a sharp null at $\phi = 90^\circ$. The fields
 in the range from $\phi = 90^\circ$ to $\phi = 110^\circ$ are readily obtained by
 symmetry. Also shown in Fig. 6 are the fields at $\rho = 0.75$ m.
 They behave like those at $\rho = 1$ m, but with larger ampli-
 tude. Figure 6(b) also shows the fields at $\rho = 1.25$ m and
 $\rho = 1.5$ m.



(a)



(b)

FIG. 6. E_ρ and E_ϕ as functions of ϕ ; field of hori-
 zontal half-wave dipole. (a) $\sigma_1 = 2$ S/m, $\epsilon_{1r} = 80$.
 (b) $\sigma_1 = 0.5$ S/m, $\epsilon_{1r} = 80$.

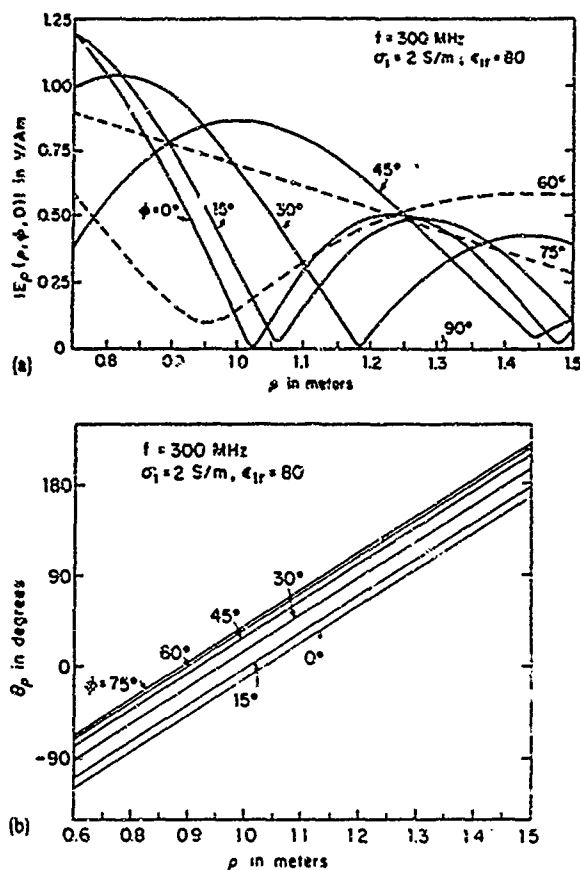


FIG. 7. E_ρ along radial lines; field of terminated half-wave dipole. (a) Magnitude. (b) Phase.

VI. THE CALCULATED FIELD OF THE TERMINATED HORIZONTAL HALF-WAVE DIPOLE

The components $[E_{2\rho}(\rho, \phi, 0)]_{CA}$ and $[E_{2\phi}(\rho, \phi, 0)]_{CA}$ as given by Eqs. (37) and (38) with Eqs. (31) and (32) have been calculated over the range $0.75 \leq \rho \leq 1.5$ m, $0^\circ \leq \phi \leq 90^\circ$ as indicated schematically in Fig. 4. Graphs of $E_\rho(\rho, \phi, 0) = |E_\rho(\rho, \phi, 0)| \exp(i\theta_\rho)$ are shown in Fig. 7 along radial lines with ϕ as the parameter and in Fig. 8 as a function of ϕ for four radial distances. Since the amplitude of $E_\rho(\rho, \phi, 0)$ is due to contributions from the long horizontal part and the two short vertical terminations which are a half-wavelength apart and driven 180° out of phase, a complicated pattern is to be expected. In the specific case under study, $2h = \lambda_2/2$ and $d = 0.025\lambda_2$. Since the field of a unit vertical element is greater than that of a unit horizontal element by a factor k_1/k_2 and since $2k_2h \sim \pi$, $|k_1d| \sim 0.6\pi$, the contributions from the two vertical terminations are larger in magnitude than the contribution from the horizontal element. It follows that large fluctuations in amplitude are to be expected over the range of ϕ , and also over that part of the range of ρ where $f(k_2\rho, k_1)$ differs significantly from $g(k_2\rho, k_1)$. At large distances, these functions are essentially equal. Such changes in amplitude are evident in both Figs. 7(a) and 8(a). On the other hand, with the approximation involved in the use of Eq. (23), all waves travel outward from the origin so that the phase varies linearly with radial distance along each radial line as shown in Fig. 7(b). However, the contours of constant phase

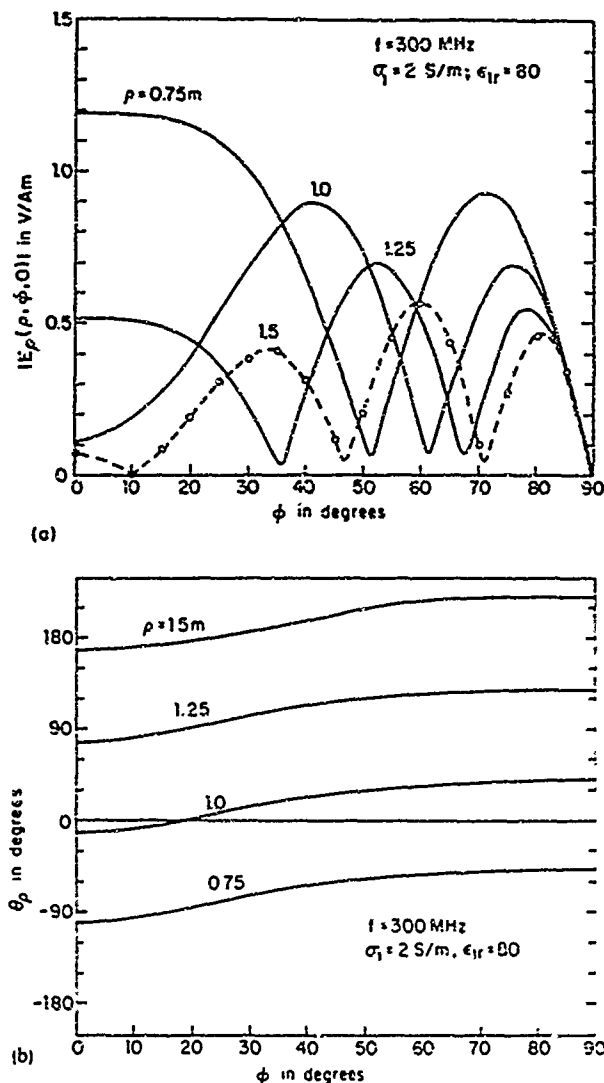


FIG. 8. E_ρ as a function of ϕ , field of terminated half-wave dipole. (a) Magnitude. (b) Phase.

are not exactly circles since the phase varies with ϕ as shown in Fig. 8(b). The contributions by the currents in the vertical terminations can be reduced greatly by making them much shorter.

Since the component $E_\phi(\rho, \phi, 0) = |E_\phi(\rho, \phi, 0)| \exp(i\theta_\phi)$

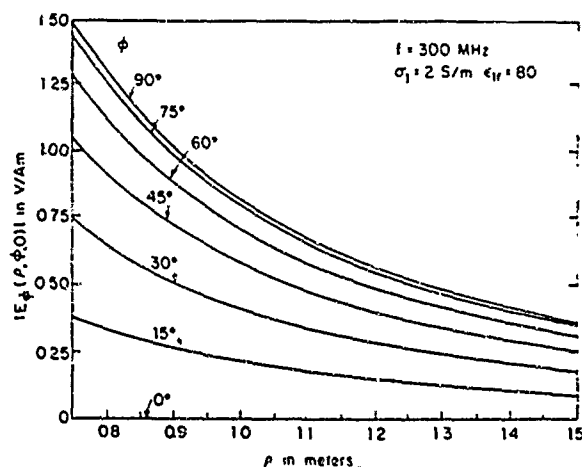


FIG. 9. E_ϕ along radial lines, field of terminated half wave dipole

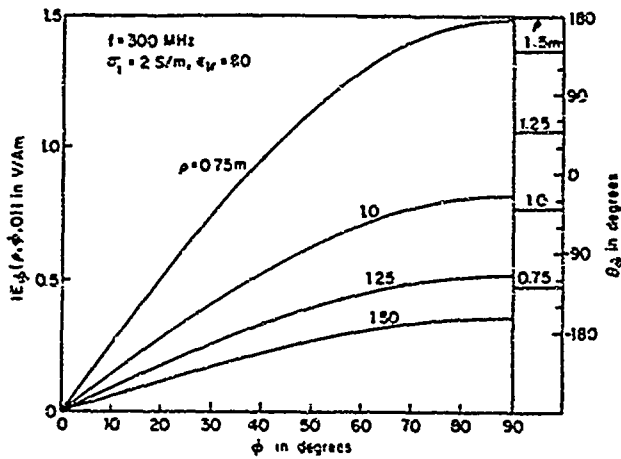


FIG. 10. E_ϕ as a function of ϕ ; field of terminated half-wave dipole

depends only on the current in the horizontal part of the antenna, its properties are much simpler than those of $E_\rho(\rho, \phi, 0)$. The magnitude is shown in Fig. 9 along radial lines with ϕ as parameter. The phase is not shown since it varies linearly with radial distance. $E_\phi(\rho, \phi, 0)$ as a function of ϕ with ρ as the parameter is shown in Fig. 10 in both amplitude and phase. The phase θ_ϕ is independent of ϕ since circles are contours of constant phase. These curves are very similar to those in Figs. 5 and 6 for the open-ended horizontal dipole. Since the current amplitude in the terminated antenna is greatest at $x = \pm h$, the effective electric moment is substantially greater and E_ϕ is almost double that for the open-ended antenna with the same length and maximum current.

VII. CONCLUSION

The complete electromagnetic field parallel to the surface of salt water has been determined when the source is a horizontal electric dipole either with open ends or grounded at its ends. The dipole is in the air at a small height d above the water. The components actually evaluated are the tan-

gential components $E_\rho(\rho, \phi, 0)$ and $E_\phi(\rho, \phi, 0)$ of the electric field. The associated tangential components of the magnetic field are given by $B_\phi(\rho, \phi, 0) = (k_1/\omega)E_\rho(\rho, \phi, 0)$ and $B_\rho(\rho, \phi, 0) = -(k_1/\omega)E_\phi(\rho, \phi, 0)$. The vertical components $E_{zz}(\rho, \phi, 0)$ and $B_{zz}(\rho, \phi, 0)$ are not required.

The field of the open-ended dipole is simpler than that of the terminated dipole since the currents in the vertical terminations of the latter generate a significant field consisting of the three components E_ρ , E_z , and B_ϕ . The combined field of the horizontal and vertical members of the complete antenna can be quite complicated if the height d , and with it the length d of the vertical elements, is sufficient to make the contributions from them comparable to that from the horizontal element.

At close range E_ρ and E_ϕ are comparable in magnitude. At distances for which $k_2\rho > 1$, E_ρ is significantly greater since it decreases only as $1/\rho$ whereas E_ϕ decreases as $1/\rho^2$.

The cylindrical components E_ρ and E_ϕ are individually simpler than the related Cartesian components E_x and E_y .

ACKNOWLEDGMENTS

The author wishes to thank Ms. B. H. Sandler for carrying out the numerical calculations and Ms. M. Owens for correcting the manuscript. This research was supported in part by the Joint Services Electronics Program under Contract N00014-84-K-0465 with Harvard University

- ¹H. S. Tuan and R. W. P. King, Radio Sci. 1, 1309 (1966).
- ²H. S. Tuan and R. W. P. King, Radio Sci. 3, 577 (1968).
- ³T. T. Wu and R. W. P. King, Radio Sci. 17, 521 (1982).
- ⁴T. T. Wu and R. W. P. King, Radio Sci. 17, 532 (1982); 19, 1422 (1984).
- ⁵R. W. P. King and T. T. Wu, J. Appl. Phys. 54, 307 (1983); 6, 3365 (1984).
- ⁶R. W. P. King, J. Appl. Phys. 53, 8476 (1982); 6, 3366 (1984).
- ⁷R. W. P. King, T. T. Wu and L. C. Shen, Radio Sci. 9, 701 (1974).
- ⁸R. M. Sorbello, R. W. P. King, K.-M. Lee, L. C. Shen, and T. T. Wu, IEEE Trans. Antennas Propagat. AP-25, 850 (1977).
- ⁹R. W. P. King, IEEE Trans. Antennas Propagat. AP-31, 956 (1983).

Scattering of lateral waves by buried or submerged objects. II. The electric field on the surface above a buried insulated wire

Ronald W. P. King

Gordon McKay Laboratory, Harvard University, Cambridge, Massachusetts 02138

(Received 5 September 1984; accepted for publication 18 October 1984)

The electric field on the surface of the earth in an area above a buried insulated conductor is determined when the active source is a horizontal dipole also on the surface of the earth at some distance away. This is accomplished by first evaluating the current induced in the wire by the lateral-wave field incident from the transmitter and then calculating the reradiated field just above the surface. Two orientations are considered. The field at the center of the buried conductor is (1) parallel to $E_{1\rho}(\rho, 0, z)$ and (2) parallel to $E_{1\phi}(\rho, \pi/2, z)$. In an area above the conductor, the incident, scattered and total fields are evaluated for the conditions of a laboratory model. It is concluded that the method is potentially useful for locating buried or submerged regions with significantly different wave numbers from that of the surrounding earth.

I. INTRODUCTION

The problem of interest is to determine the nature of the interference pattern generated by the superposition of an incident lateral wave with the field scattered by a buried object or region with different electrical parameters. The incident lateral-wave field is maintained by a horizontal dipole in the air (Region 2, $z < 0$, wave number k_2) just above the surface of the earth (Region 1, $z > 0$, wave number k_1); the total field, i.e., the incident plus scattered fields, is to be observed in the air also just above the surface of the earth.

Note that this problem is related to that treated by Tuan and King,^{1,2} but the incident field is now a lateral wave generated by a horizontal electric dipole on the surface of the earth and not a plane wave incident at an arbitrary angle. It is also related to the problem analyzed by King and Shen,³ but in that the scattering antenna is in the air above the surface of the earth and the incident field is a plane wave arriving at an arbitrary angle.

The scattering object to be studied in this paper is a horizontal insulated conductor. This provides a scattered field that is readily calculated and combined with the incident field to obtain a total field that exhibits interference phenomena. These are potentially useful in locating a buried object from measurements made on the surface of the earth.

II. THE INCIDENT FIELD

The incident field is that described in Part I.⁴ It is generated by a horizontal electric dipole parallel to the x axis with its center at the origin of the x_0, y_0 coordinates in air just above the surface of the earth or—in the laboratory experiment—just above the surface of salt water. Of particular interest are the two areas shown in Fig. 1(a) of which Area I is symmetrically located along the x_0 axis, Area II is symmetrically located along the y_0 axis. Since the axis of the driven dipole is parallel to the x axis, it follows that $E_{1\rho}(\rho, \phi, z)$ and $B_{1\phi}(\rho, \phi, z)$ are the principal components of the incident field in Area I with ϕ near zero, $E_{1\phi}(\rho, \phi, z)$ and $B_{1\rho}(\rho, \phi, z)$ in Area II with ϕ near $\pi/2$. Note that along the respective axes $E_{1\rho}(\rho, 0, z) \sim E_{1x}(x_0, 0, z)$; $E_{1\phi}(\rho, \pi/2, z) \sim -E_{1z}(0, y_0, z)$. The expressions for these fields at radial distances ρ from the

source and at depth z below the surface are

$$E_{1\rho}^{inc}(\rho, \phi, z) = -Gg(k_2\rho, k_1)\cos\phi e^{ik_2z} \\ = (\omega/k_1)B_{1\phi}^{inc}(\rho, \phi, z), \quad (1)$$

$$E_{1\phi}^{inc}(\rho, \phi, z) = 2Gh(k_2\rho, k_1)\sin\phi e^{ik_2z} \\ = -(\omega/k_1)B_{1\rho}^{inc}(\rho, \phi, z), \quad (2)$$

with

$$G = \frac{\omega\mu_0 k_2}{2\pi k_1^2} I_1(0)M_0(\phi), \quad (3)$$

$$g(k_2\rho, k_1) = g_0(k_2\rho, k_1)e^{ik_2\rho} \\ = \left[\frac{ik_2}{\rho} - \frac{1}{\rho^2} - \frac{i}{k_2\rho^3} - \frac{k_2^3}{k_1} \left(\frac{\pi}{k_2\rho} \right)^{1/2} \right] \\ \times e^{-ik_2\rho/2k_1^2} \mathcal{F}(k_2\rho, k_1) e^{ik_2\rho}, \quad (4)$$

$$h(k_2\rho, k_1) = h_0(k_2\rho, k_1)e^{ik_2\rho} \\ = \left(\frac{1}{\rho^2} + \frac{i}{k_2\rho^3} + \frac{ik_2^3}{2k_1} \frac{\pi^{1/2}}{(k_2\rho)^{3/2}} \right) \\ \times e^{-ik_2\rho/2k_1^2} \mathcal{F}(k_2\rho, k_1) e^{ik_2\rho}, \quad (5)$$

where

$$\mathcal{F}(k_2\rho, k_1) = \frac{1}{2}(1+i) - C_2(k_2^3\rho/2k_1^2) - iS_2(k_2^3\rho/2k_1^2), \quad (6a)$$

$$C_2(u) + iS_2(u) = \int_0^u (2\pi t)^{-1/2} e^{it} dt. \quad (6b)$$

In Eq. (3), $I_1(0)$ is the x -directed current at the center of the transmitting antenna and

$$M_0(\phi) = \frac{2k_L}{\sin k_L h} \left(\frac{\cos(k_2 h \cos\phi) - \cos k_L h}{k_L^2 - k_2^2 \cos^2\phi} \right). \quad (7)$$

The last formula applies to an insulated dipole of half-length h and with open ends. This will be used as the source

III. THE CURRENT INDUCED IN A BURIED INSULATED CONDUCTOR BY THE RADIAL ELECTRIC FIELD

When an insulated conductor with length $2l$ is located at depth d in the earth within the area close to the x_0 axis, as

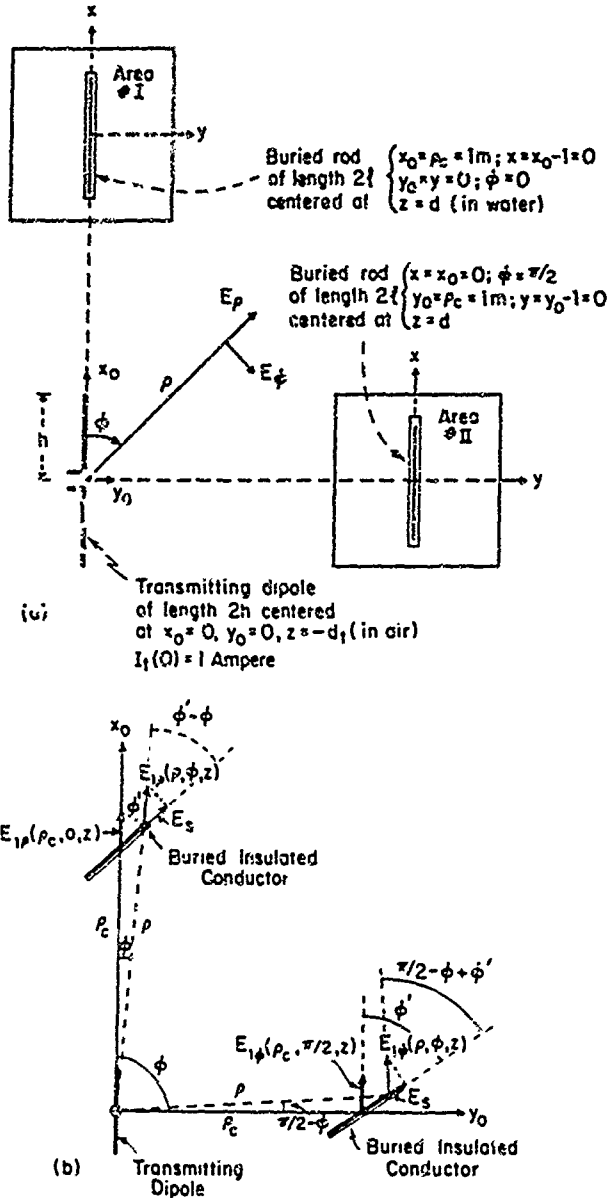


FIG. 1. Two locations of a buried insulated conductor relative to a transmitting dipole on the surface of the earth. (a) Orientations of scattering antenna in areas of interest. (b) General orientations of scattering antenna.

shown in Fig. 1(b) on the upper left, the subtended angle $\pm \phi$ and with it $\sin \phi$ are small so that the component $E_{1\phi}^{inc}(\rho, \phi, d) = E_{1\phi}^{inc}(\rho, 0, d) \sin \phi$ is small compared to $E_{1\rho}^{inc}(\rho, \phi, d) = E_{1\rho}^{inc}(\rho, 0, d) \cos \phi$. It follows that the current induced in the conductor is due primarily to $E_{1\rho}^{inc}(\rho, \phi, d)$. For simplicity let the center of the conductor be located on the plane $y_0 = 0$ at the distance $x_0 = \rho = \rho_c$ from the center of the driven dipole. The distance along the conductor from its center is s' which extends from $s' = -l$ to $s' = l$. The conductor subtends the angle ϕ' with the plane $y_0 = 0$. It is par-

allel to the boundary surface $z = 0$ and lies in the plane $z = d$.

The radial incident electric field at the center of the conductor is

$$E_{1\rho}^{inc}(\rho_c, 0, d) = -G_{00}(k, \rho_c, k_1) e^{ik\rho_c} e^{ik_1 d}. \quad (8)$$

The radial field at a distance s' along the conductor is

$$E_{1\rho}^{inc}(\rho, \phi, d) = -G_{00}(k, \rho, k_1) \cos \phi e^{ik\rho} e^{ik_1 d}. \quad (9)$$

The distance ρ can be expressed in terms of ρ_c and s' . Thus,

$$\rho = (\rho_c^2 + s'^2 + 2\rho_c s' \cos \phi')^{1/2} \sim \rho_c + s' \cos \phi'. \quad (10)$$

The component of the radial electric field along the buried conductor is

$$E_s = E_{1\rho}^{inc}(\rho, \phi, d) \cos(\phi' - \phi) \sim E_{1\rho}^{inc}(\rho_c, 0, d) \cos \phi' e^{ik\rho_c} e^{ik_1 d}. \quad (11)$$

It is this field that induces the current in the conductor.

An insulated wire in a Region 1 with $|k_1| > 3k$, (where k , is the wave number of the insulating sheath) behaves like a transmission line with the complex wave number k_L and characteristic impedance Z_c . Owing to the proximity of the air-earth boundary at the distance d from the insulated wire, there is a significant downward reflected wave that interacts with the current in the conductor. The reflection coefficient for the electric field—which is perpendicular to the plane of incidence—is

$$f_{mr} = \frac{k_1 - k_2}{k_1 + k_2} \sim 1,$$

when k_1 is large compared to k_2 . The reflected field is thus equivalent to that of an image conductor at $z = -d$ with currents in the same direction as in the buried conductor. Hence, k_L' and Z_c' must be approximated by the values for two coupled insulated antennas excited in phase. These are⁵

$$k_L' = k_1 \left(1 + \frac{H_0^{(1)}(k, b) + H_0^{(1)}(2k_1 d)}{k_1 b \ln(b/a) H_1^{(1)}(k, b)} \right)^{1/2}, \quad (12)$$

$$Z_c' = \frac{\omega \mu_0 k_L'}{2\pi k_1^2} \ln(b/a). \quad (13)$$

In these formulas a is the radius of the conductor and b the outer radius of the insulating sheath.

The increment of current at s in the insulated conductor with open ends due to an incremental voltage $E_s ds'$ at s' is

$$dI_s = \frac{-iE_s ds'}{Z_c'} \left(\frac{\sin k_L'(l+s') \sin k_L'(l-s)}{\sin 2k_L' l} \right) \quad (14)$$

$$dI_s = \frac{-iE_s ds'}{Z_c'} \left(\frac{\sin k_L'(l-s') \sin k_L'(l+s)}{\sin 2k_L' l} \right) \quad (15)$$

The current due to the field along the entire length is

$$I_s = \frac{-i}{Z_c' \sin 2k_L' l} \left(\sin k_L'(l-s) \int_{-l}^s E_s \sin k_L'(l+s') ds' + \sin k_L'(l+s) \int_s^l E_s \sin k_L'(l-s') ds' \right). \quad (16)$$

With Eq. (11),

$$I_s \sim \frac{-iE_{1\rho}^{\text{inc}}(\rho_c, 0, d)\cos\phi'}{Z_c'\sin 2k_L' l} \left(\sin k_L'(l-s) \int_{-l}^s e^{ik_L's'\cos\phi'} \sin k_L'(l+s')ds' \right. \\ \left. + \sin k_L'(l+s) \int_s^l e^{ik_L's'\cos\phi'} \sin k_L'(l-s')ds' \right). \quad (17)$$

With $u = l + s'$ in the first integral and $u = l - s'$ in the second integral, Eq. (17) can be expressed as follows:

$$I_s = \frac{-iE_{1\rho}^{\text{inc}}(\rho_c, 0, d)\cos\phi'}{Z_c'\sin 2k_L' l} \left(\sin k_L'(l-s) e^{-ik_L'l\cos\phi'} \int_0^{l+s} e^{ik_L'u\cos\phi'} \sin k_L'u du \right. \\ \left. - \sin k_L'(l+s) e^{ik_L'l\cos\phi'} \int_{l-s}^0 e^{-ik_L'u\cos\phi'} \sin k_L'u du \right). \quad (18)$$

These integrals are in the form

$$\int e^{ax} \sin bx dx = \frac{e^{ax}(a \sin bx - b \cos bx)}{a^2 + b^2}. \quad (19)$$

With Eq. (19) and considerable rearrangement, the following final formula is obtained for the current induced by the radial electric field:

$$I_s = \frac{ik_L'E_{1\rho}^{\text{inc}}(\rho_c, 0, d)\cos\phi'}{Z_c'(k_L'^2 - k_2^2 \cos^2\phi')} \\ \times \left[e^{ik_L's\cos\phi'} - \left(\frac{\sin(k_L' + k_2 \cos\phi')l}{\sin 2k_L'l} \right) e^{ik_L's} \right. \\ \left. - \left(\frac{\sin(k_L' - k_2 \cos\phi')l}{\sin 2k_L'l} \right) e^{-ik_L's} \right]. \quad (20)$$

The induced current is seen to consist of three traveling waves. Two advance in the positive s direction, the one with the phase velocity $(\omega/k_2 \cos\phi')$, the other with the phase velocity (ω/β_L') . The third wave travels in the negative s direction also with the phase velocity (ω/β_L') . The amplitudes are so disposed that $I_s(\pm l) = 0$. Of particular interest is the direction $\phi' = 0$ of maximum $E_{1\rho}^{\text{inc}}(\rho_c, \phi, d)$. For this orientation, $s = x$ and

$$I_s = \frac{ik_L'E_{1\rho}^{\text{inc}}(\rho_c, 0, d)}{Z_c'(k_L'^2 - k_2^2)} \left[e^{ik_L'x} - \left(\frac{\sin(k_L' + k_2)l}{\sin 2k_L'l} \right) e^{ik_L'x} \right. \\ \left. - \left(\frac{\sin(k_L' - k_2)l}{\sin 2k_L'l} \right) e^{-ik_L'x} \right]. \quad (21)$$

IV. THE CURRENT INDUCED BY THE TRANSVERSE ELECTRIC FIELD

When the buried conductor is located at a depth d in the earth with its center in the plane $x_0 = 0$ in the area along the y_0 axis as shown in Fig. 1(b) on the lower right, the transverse incident electric field at the center of the conductor is

$$E_{1\phi}^{\text{inc}}(\rho_c, \pi/2, d) = 2Gh_0(k_2\rho_c, k_1)e^{ik_2\rho_c}e^{ik_1d}. \quad (22)$$

The transverse incident field at a distance s' along the conductor is

$$E_{1\phi}^{\text{inc}}(\rho, \phi, d) = 2Gh_0(k_2\rho, k_1)\sin\phi e^{ik_2\rho}e^{ik_1d}. \quad (23)$$

The distance ρ can be expressed in terms of ρ_c and s' as follows:

$$\rho = [\rho_c^2 + s'^2 - 2\rho_c s' \cos(\pi/2 + \phi')]^{1/2} \\ = (\rho_c^2 + s'^2 + 2\rho_c s' \sin\phi')^{1/2} \\ \sim \rho_c + s' \sin\phi'. \quad (24)$$

The component of $E_{1\phi}^{\text{inc}}(\rho, \phi, d)$ along the axis of the buried conductor is

$$E_s = E_{1\phi}^{\text{inc}}(\rho, \phi, d)\cos(\pi/2 - \phi + \phi') \\ \sim E_{1\phi}^{\text{inc}}(\rho_c, \pi/2, d)\cos\phi' e^{ik_2\rho}e^{ik_1d}. \quad (25)$$

It is this field that induces the current in the buried conductor.

The current due to the field along the entire length is given by Eq. (16) with Eq. (25). It is

$$I_s \sim \frac{-iE_{1\phi}^{\text{inc}}(\rho_c, \pi/2, d)\cos\phi'}{Z_c'\sin 2k_L' l} \left(\sin k_L'(l-s) \int_{-l}^s e^{ik_L's'\sin\phi'} \sin k_L'(l+s')ds' \right. \\ \left. + \sin k_L'(l+s) \int_s^l e^{ik_L's'\sin\phi'} \sin k_L'(l-s')ds' \right). \quad (26)$$

The integrals in Eq. (26) are like those in Eq. (17) with $\sin\phi'$ appearing in place of $\cos\phi'$ in the exponents. It follows with Eq. (20) that

$$I_s = \frac{ik_L'E_{1\phi}^{\text{inc}}(\rho_c, \pi/2, d)\cos\phi'}{Z_c'(k_L'^2 - k_2^2 \sin^2\phi')} \left[e^{ik_L's\sin\phi'} - \left(\frac{\sin(k_L' + k_2 \sin\phi')l}{\sin 2k_L'l} \right) e^{ik_L's} \right. \\ \left. - \left(\frac{\sin(k_L' - k_2 \sin\phi')l}{\sin 2k_L'l} \right) e^{-ik_L's} \right]. \quad (27)$$

This is the induced current when the conductor is located with its center at depth d below the y_0 axis. Of primary interest is the field in the direction $\phi = \pi/2$ with $\phi' = 0$. Here $E_{1\phi}^{inc}(\rho_c, \phi, d)$ has its maximum and the buried conductor is oriented to have its axis along that maximum. Here $s = x$ and

$$I_x = \frac{iE_{1\phi}^{inc}(\rho_c, \pi/2, d)}{Z_c' k_L'} \left(1 - \frac{e^{ik_L'x} + e^{-ik_L'x}}{2 \cos k_L' l} \right) \\ = \frac{-iE_{1\phi}^{inc}(\rho_c, \pi/2, d)}{Z_c' k_L'} \frac{\cos k_L' x - \cos k_L' l}{\cos k_L' l} \quad (28)$$

This expression has been derived in an earlier paper.⁶ It represents a pure standing wave. Note that the incident field has the same amplitude and phase at all points along the conductor.

V. THE DIRECT SCATTERED FIELD JUST BELOW THE SURFACE OF THE EARTH

The currents Eqs. (20) or (21) and Eqs. (27) or (28) generate the scattered or reradiated field. Of interest is the field on the surface ($z = -0$) in air in an area above the buried conductor, but it is first necessary to calculate the field on the surface ($z = +0$) in the earth. This can be evaluated from the known distribution of current. For simplicity let this be done when the buried conductor is oriented for maximum induced current, i.e., parallel to the x axis so that the current Eq. (21) applies to the region along the x_0 axis (Area I), the current Eq. (28) to the region along the y_0 axis (Area II). The scattered field at $z = +0$ due to an x -directed dipole with current $I_x dx'$ at the point $(x', 0, d)$ has the following components:

$$dE_{1x}^{scat}(x, y, 0) = \frac{i\omega\mu_0 I_x dx'}{4\pi} \left(\frac{e^{ik_1 r}}{r} + \frac{1}{k_1^2} \frac{\partial^2}{\partial x^2} \frac{e^{ik_1 r}}{r} \right) \\ = \frac{i\omega\mu_0 I_x dx'}{4\pi} e^{ik_1 r} \left[\frac{1}{r} \left(1 - \frac{(x-x')^2}{r^2} \right) + \frac{i}{k_1 r^2} \left(1 - \frac{3(x-x')^2}{r^2} \right) - \frac{1}{k_1^2 r^3} \left(1 - \frac{3(x-x')^2}{r^2} \right) \right], \quad (29)$$

$$dE_{1y}^{scat}(x, y, 0) = -\frac{i\omega\mu_0 I_x dx'}{4\pi} \frac{1}{k_1^2} \frac{\partial^2}{\partial x \partial y} \frac{e^{ik_1 r}}{r} \\ = -\frac{i\omega\mu_0 I_x dx'}{4\pi} e^{ik_1 r} \frac{y(x-x')}{r^2} \left(\frac{k_1^2}{r} + \frac{3ik_1}{r^2} - \frac{3}{r^3} \right), \quad (30)$$

where

$$r = [(x-x')^2 + y^2 + d^2]^{1/2}, \quad (31)$$

and x, y are coordinates referred to the point $\varphi_c, \phi_c, 0$ on the surface directly above the center of the scattering element. In terms of $x_0, y_0, x = x_0 - \rho_c \cos \phi_c$ and $y = y_0 - \rho_c \sin \phi_c$. In Area I, when $\phi_c = 0, x = x_0 - \rho_c$ and $y = y_0$; in Area II, when $\phi_c = \pi/2, x = x_0$ and $y = y_0 - \rho_c$.

The field reradiated by the entire antenna is

$$E_{1x}^{scat}(x, y, 0) = \frac{i\omega\mu_0}{4\pi} \int_{-l}^l I_x(x') \left(\frac{e^{ik_1 r}}{r} + \frac{1}{k_1^2} \frac{\partial^2}{\partial x^2} \frac{e^{ik_1 r}}{r} \right) dx', \quad (32)$$

$$E_{1y}^{scat}(x, y, 0) = -\frac{i\omega\mu_0}{4\pi k_1^2} \int_{-l}^l I_x(x') \frac{\partial^2}{\partial x \partial y} \frac{e^{ik_1 r}}{r} dx', \quad (33)$$

where

$$I_x(x') = \frac{ik_L' E_{1\phi}^{inc}(\rho_c, 0, d)}{Z_c'(k_L'^2 - k_1^2)} (e^{ik_L'x'} - B e^{-ik_L'x'} - C e^{-ik_L'x'}), \quad (34a)$$

with

$$B = \frac{\sin(k_L' l + k_2 l)}{\sin 2k_L' l}, \quad C = \frac{\sin(k_L' l - k_2 l)}{\sin 2k_L' l} \quad (34b)$$

for the conductor along the x_0 axis, and

$$I_x(x') = \frac{-iE_{1\phi}^{inc}(\rho_c, \pi/2, d)}{Z_c' k_L'} \frac{\cos k_L' x' - \cos k_L' l}{\cos k_L' l} \quad (35)$$

for the conductor along the y_0 axis.

If use is made of the fact that $\partial^2/\partial x'^2 = \partial^2/\partial x^2$ in the second term in Eq. (32), and it is integrated twice by parts, noting that $I_x(\pm l) = 0$, the result is

$$E_{1x}^{scat}(x, y, 0) = \frac{i\omega\mu_0}{4\pi} \int_{-l}^l \left(I_x(x') + \frac{1}{k_1^2} \frac{\partial^2 I_x(x')}{\partial x'^2} \right) \\ \times \frac{e^{ik_1 r}}{r} dx' + c_x(l), \quad (36)$$

where

$$c_x(l) = \frac{-i\omega\mu_0}{4\pi k_1^2} \frac{\partial I_x(x')}{\partial x'} \frac{e^{ik_1 r}}{r} \Big|_{-l}^l \\ = \frac{\omega^2 \mu_0}{4\pi k_1^2} \left(q(l) \frac{\exp(ik_1 r_{1l})}{r_{1l}} - q(-l) \frac{\exp(ik_1 r_{2l})}{r_{2l}} \right), \quad (37)$$

with $r_{1l} = [(l-x)^2 + y^2 + d^2]^{1/2}$, and $r_{2l} = [(l+x)^2 + y^2 + d^2]^{1/2}$. The last form follows with the equation of continuity, viz., $\partial I_x(x')/\partial x' - i\omega q(x') = 0$, where $q(x')$ is the charge per unit length on the conductor at x' .

The second derivative of the current in Eq. (36) is readily evaluated using either Eq. (34a) or (35). In both cases the second term in the integrand in Eq. (36) consists of terms of the form $(k_2/k_1)^2 I_x(x'), (k_L'/k_1)^2 I_x(x')$. Since $|k_2/k_1|^2 \ll 1$ and $|k_L'/k_1|^2 \ll 1$, these terms are negligible and Eq. (36) reduces to

$$E_{1x}^{\text{scat}}(x, y, 0) = \frac{i\omega\mu_0}{4\pi} \int_{-l}^l I_x(x') \frac{e^{ik_1 r}}{r} dx' + c_x(l). \quad (38)$$

With $\partial/\partial x = -\partial/\partial x'$ in Eq. (33), an integration by parts results in

$$\begin{aligned} E_{1x}^{\text{scat}}(x, y, 0) &= \frac{i\omega\mu_0}{4\pi k_1^2} \int_{-l}^l \frac{\partial I_x(x')}{\partial x'} \frac{\partial}{\partial y} \left(\frac{e^{ik_1 r}}{r} \right) dx' \\ &= \frac{i\omega\mu_0}{4\pi k_1^2} \int_{-l}^l \frac{\partial I_x(x')}{\partial x'} \frac{y}{r} \frac{\partial}{\partial r} \left(\frac{e^{ik_1 r}}{r} \right) dx'. \end{aligned} \quad (39)$$

With Eq. (34a) or (35), $\partial I_x(x')/\partial x'$ includes only terms with the factor k_2 or k_L . Thus, when compared with Eq. (38), Eq. (39) has the factors k_2/k_1 or k_L/k_1 and y/r . Both of these are small and their product makes $E_{1y}^{\text{scat}}(x, y, 0)$ small compared with $E_{1x}^{\text{scat}}(x, y, 0)$. It follows that $E_{1x}^{\text{scat}}(x, y, 0)$ is the component of the scattered field that is of interest in locating the scattering object. This is true for either location of the buried insulated wire.

It remains to evaluate the first term in Eq. (38) with $I_x(x')$ given by Eqs. (34a) and (35). These are

$$\mathcal{I}_1 = E_{1\rho}^{\text{inc}}(\rho_c, 0, d) D_1 \int_{-l}^l \left(\frac{e^{ik_1 r + k_2 x'}}{r} - B \frac{e^{ik_1 r + k_L x'}}{r} - C \frac{e^{ik_1 r - k_L x'}}{r} \right) dx', \quad (40)$$

where B and C are given in Eqs. (34b) and where

$$D_1 = \frac{-\omega\mu_0 k_L}{4\pi Z_c'(k_L'^2 - k_2'^2)}, \quad (41)$$

and

$$\mathcal{I}_2 = E_{1\rho}^{\text{inc}}(\rho_c, \pi/2, d) D_2 \int_{-l}^l \left(\frac{e^{ik_1 r}}{r} - \frac{e^{ik_1 r + k_L x'} + e^{ik_1 r - k_L x'}}{2 \cos k_L' l} \right) dx', \quad (42)$$

where

$$D_2 = \frac{-\omega\mu_0}{4\pi Z_c' k_L'}. \quad (43)$$

The associated values of $c_x(l)$ in Eq. (37), for $I_x(x')$ in Eq. (34a), are

$$c_{1x}(l) = E_{1\rho}^{\text{inc}}(\rho_c, 0, d) D_1 C_{1x}(l), \quad (44a)$$

$$C_{1x}(l) = \frac{-i}{k_1^2} \left\{ \left[k_2 e^{ik_1 l} - k_L' (B e^{ik_1 l} - C e^{-ik_1 l}) \right] \frac{\exp(ik_1 r_{1l})}{r_{1l}} - \left[k_2 e^{-ik_1 l} - k_L' (B e^{-ik_1 l} - C e^{ik_1 l}) \right] \frac{\exp(ik_1 r_{2l})}{r_{2l}} \right\}. \quad (44b)$$

For $I_x(x')$ in Eq. (35), the corresponding formulas are

$$c_{2x}(l) = E_{1\rho}^{\text{inc}}(\rho_c, \pi/2, d) D_2 C_{2x}(l), \quad (45a)$$

$$C_{2x}(l) = \frac{-k_L'}{k_1^2} \left(\frac{\exp(ik_1 r_{1l})}{r_{1l}} + \frac{\exp(ik_1 r_{2l})}{r_{2l}} \right) \tan k_L' l. \quad (45b)$$

It is seen from Eqs. (40) and (42) that there are two types of integrals to be evaluated. These are

$$J_1(k_1) = \int_{-l}^l \frac{e^{ik_1 r}}{r} dx' \quad (46)$$

and

$$J_2(k_2) = \int_{-l}^l \frac{e^{ik_1 r + k_2 x'}}{r} dx', \quad (47)$$

and similar integrals J_L with k_2 replaced by $\pm k_L'$. The second integral can be reduced to the form of the first subject to the following inequalities:

$$d^2 \ll l^2; \quad y^2 \ll l^2; \quad k_1 l \gg 1; \quad k_1^2 \gg k_2^2; \quad k_1^2 \gg k_L'^2. \quad (48)$$

These require the buried wire to be long compared to its depth.

It is shown in Appendix A that Eq. (47) can be approximated by

$$J_2(k_2) = \int_{-l}^l \frac{e^{ik_1 r + k_2 x'}}{r} dx' \sim \begin{cases} e^{ik_2 x} \int_{-l}^l \frac{e^{ik_1 r}}{r} dx', & x \leq l, \\ e^{ik_1 l} \int_{-l}^l \frac{e^{ik_1 r}}{r} dx', & x \geq l \end{cases}, \quad (49)$$

where

$$k_{12} = \beta_{12} + i\alpha_{12} = \sqrt{k_1^2 - k_2^2}. \quad (50)$$

In effect, the transformation is equivalent to $x' \rightarrow x$, $x' \leq l$, and $x' \rightarrow l$, $x' \geq l$ in the exponential (but not in $r = [(x - x')^2 + y^2 + d^2]^{1/2}$) with a simultaneous change in wave number, $k_1 \rightarrow k_{12} = (k_1^2 - k_2^2)^{1/2}$. Since $k_2^2 \ll k_1^2$, this is a small change that would be negligible in the amplitude but is significant in the phase. Physically this approximation

is related to the fact that the principal contribution to the field at x is due to the nearest part of the current in the buried conductor, namely, that at $x' = x$. Since this does not involve only a vertical distance, there must be a simultaneous correction in the effective wave number.

The integrals [Eqs. (46) and (49)] are generalized exponential integrals as shown in Appendix B. Specifically,

$$J_1(k_1) = \bar{E}(\delta_{11}, A_{11}, U_1) + \bar{E}(\delta_{11}, A_{11}, U_2), \quad (51)$$

$$J_2(k_2) = e^{ik_2 x} [\bar{E}(\delta_{12}, A_{12}, U_{12}) + \bar{E}(\delta_{12}, A_{12}, U_{22})]. \quad (52)$$

Similar integrals occur with k_2 replaced by $\pm k_L$. They are

$$J_L(\pm k_L) = e^{\pm ik_L x} [\bar{E}(\delta_{1L}, A_{1L}, U_{1L}) + \bar{E}(\delta_{1L}, A_{1L}, U_{2L})]. \quad (53)$$

In these formulas,

$$\delta_1 = \alpha_1/\beta_1; \quad \delta_{12} = \alpha_{12}/\beta_{12}; \quad \delta_{1L} = \alpha_{1L}/\beta_{1L}; \quad (54)$$

$$A_1 = \beta_1 \sqrt{y^2 + d^2}; \quad A_{12} = \beta_{12} \sqrt{y^2 + d^2}; \quad A_{1L} = \beta_{1L} \sqrt{y^2 + d^2}; \quad (55)$$

$$U_1 = \beta_1(l - x); \quad U_{12} = \beta_{12}(l - x); \quad U_{1L} = \beta_{1L}(l - x); \quad (56)$$

$$U_2 = \beta_1(l + x); \quad U_{22} = \beta_{12}(l + x); \quad U_{2L} = \beta_{1L}(l + x); \quad (57)$$

and

$$k_1 = \beta_1 + i\alpha_1; \quad k_{12} = \sqrt{k_1^2 - k_2^2} = \beta_{12} + i\alpha_{12}; \quad k_{1L} = \sqrt{k_1^2 - k_L^2} = \beta_{1L} + i\alpha_{1L}. \quad (58)$$

The complete expressions for Eq. (38) are

$$E_{1x}^{\text{scat}}(x, y, 0) = E_{1p}^{\text{inc}}(\rho_c, 0, d) D_1 \{ e^{ik_2 x} [\bar{E}(\delta_{12}, A_{12}, U_{12}) + \bar{E}(\delta_{12}, A_{12}, U_{22})] - [Be^{ik_L x} + Ce^{-ik_L x}] [\bar{E}(\delta_{1L}, A_{1L}, U_{1L}) + \bar{E}(\delta_{1L}, A_{1L}, U_{2L})] + C_{1x}(l) \}, \quad x < l, \quad (59)$$

for $I_x(x')$ given in Eq. (34a) and

$$E_{1x}^{\text{scat}}(x, y, 0) = E_{1p}^{\text{inc}}(\rho_c, \pi/2, d) D_2 \left\{ [\bar{E}(\delta_{11}, A_{11}, U_1) + \bar{E}(\delta_{11}, A_{11}, U_2)] - \frac{\cos k_L x}{\cos k_L l} [\bar{E}(\delta_{1L}, A_{1L}, U_{1L}) + \bar{E}(\delta_{1L}, A_{1L}, U_{2L})] + C_{2x}(l) \right\}, \quad x < l, \quad (60)$$

for $I_x(x')$ given in Eq. (35). Formulas for the range $|x| > l$ are like Eqs. (59) and (60) with x where it appears explicitly in the three exponentials in Eq. (59) and in the cosine in Eq. (60) replaced by l .

VI. THE SCATTERED FIELD IN AIR JUST ABOVE THE SURFACE OF THE EARTH

The direct reradiated field from the buried insulated wire is partly transmitted into the air, partly reflected back into the earth. Direct comparison with the numerical evaluation of the exact integrals⁷ has shown that the electric field in the air directly above a buried unit dipole is accurately given by the direct field multiplied by the plane-wave transmission coefficient. It is to be expected that this can be generalized to small angles from the vertical. The plane-wave transmission coefficient when the electric field is perpendicular to the plane of incidence is

$$f = \frac{2 \cos \theta}{\cos \theta + [(k_2/k_1)^2 - \sin^2 \theta]^{1/2}}, \quad (61a)$$

or

$$f = \frac{2d}{d + [(k_2/k_1)^2 - (x' - x)^2 - y^2]^{1/2}}, \quad (61b)$$

since $\cos \theta = d/r$ and $\sin \theta = [(x' - x)^2 + y^2]^{1/2}/r$. Since

$(k_2/k_1)^2$ is small and $r^2 \sim (x' - x)^2 + y^2$, it follows that

$$f \sim \frac{2d}{d + i[(x' - x)^2 + y^2]^{1/2}}. \quad (62)$$

Because $l^2 \gg d^2$, the direct field at any point $(x, y = 0)$ is due primarily to the part of the buried wire directly below $(x, y = 0)$ —that is, the part near $x' = x$ so long as $x' < l$. When $x > l$, $x' \sim l$. Thus, extending the approximation in Eq. (49),

$$f \sim \frac{2d}{d + iy}, \quad x < l, \quad (63a)$$

$$f \sim \frac{2d}{d + i[(l - x)^2 + y^2]^{1/2}}, \quad x > l. \quad (63b)$$

These are constants in the integration with respect to x' . Hence, the transmitted fields are given by Eqs. (59) and (60) multiplied by $2d/(d + iy)$ when $x < l$ and by Eqs. (59) and (60) with $x = l$ in the exponentials and cosine and multiplied by $2d/[d + i[(l - x)^2 + y^2]^{1/2}]$ when $x > l$. The complete final formulas for the direct scattered field just above the surface of the earth are

$$E_{2x}^{\text{scat}}(x, y, 0) = \left(\frac{2d D_1 E_{1p}^{\text{inc}}(\rho_c, 0, d)}{d + iy} \right) \left\{ e^{ik_2 x} [\bar{E}(\delta_{12}, A_{12}, U_{12}) + \bar{E}(\delta_{12}, A_{12}, U_{22})] - [Be^{ik_L x} + Ce^{-ik_L x}] [\bar{E}(\delta_{1L}, A_{1L}, U_{1L}) + \bar{E}(\delta_{1L}, A_{1L}, U_{2L})] + C_{1x}(l) \right\}, \quad x < l, \quad (64a)$$

$$E_{2x}^{scat}(x,y,0) = \left(\frac{2dD_1 E_{1\rho}^{inc}(\rho_c, 0, d)}{d + i[(l-x)^2 + y^2]^{1/2}} \right) \left\{ e^{ik_z l} [\bar{E}(\delta_{12} A_{12}, U_{12}) + \bar{E}(\delta_{12} A_{12}, U_{22})] \right. \\ \left. - (B e^{ik_z l} + C e^{-ik_z l}) [\bar{E}(\delta_{1L} A_{1L}, U_{1L}) + \bar{E}(\delta_{1L} A_{1L}, U_{2L})] + C_{1x}(l) \right\}, \quad x > l, \quad (65)$$

when the current is given by Eq. (34a). The corresponding expressions for the current in Eq. (35) are

$$E_{2x}^{scat}(x,y,0) = \left(\frac{2dD_2 E_{1\rho}^{inc}(\rho_c, \pi/2, d)}{d + iy} \right) \left\{ [\bar{E}(\delta_{11} A_{11}, U_{11}) + \bar{E}(\delta_{11} A_{11}, U_{21})] \right. \\ \left. - \frac{\cos k_z l x}{\cos k_z l} [\bar{E}(\delta_{1L} A_{1L}, U_{1L}) + \bar{E}(\delta_{1L} A_{1L}, U_{2L})] + C_{2x}(l) \right\}, \quad x < l, \quad (66)$$

$$E_{2x}^{scat}(x,y,0) = \left(\frac{2dD_2 E_{1\rho}^{inc}(\rho_c, \pi/2, d)}{d + i[(l-x)^2 + y^2]^{1/2}} \right) \left\{ [\bar{E}(\delta_{11} A_{11}, U_{11}) + \bar{E}(\delta_{11} A_{11}, U_{21})] \right. \\ \left. - \bar{E}(\delta_{1L} A_{1L}, U_{1L}) - \bar{E}(\delta_{1L} A_{1L}, U_{2L}) + C_{2x}(l) \right\}, \quad x > l. \quad (67)$$

VII. THE TOTAL ELECTRIC FIELD IN THE AIR JUST ABOVE THE SURFACE OF THE EARTH

The electric field incident from the transmitting antenna in Region 2 (air) is obtained directly from the boundary conditions $E_{1\rho}(\rho, \phi, 0) = E_{2\rho}(\rho, \phi, 0)$ and $E_{1\phi}(\rho, \phi, 0) = E_{2\phi}(\rho, \phi, 0)$ with Eqs. (1) and (2) at $z = 0$. The x component is

$$E_{2x}^{inc}(\rho, \phi, 0) = E_{2\rho}^{inc}(\rho, \phi, 0) \cos \phi + E_{2\phi}^{inc}(\rho, \phi, 0) \sin \phi \\ = -Gg(k_{2\rho}, k_1) \cos^2 \phi + 2Gh(k_{2\rho}, k_1) \sin^2 \phi. \quad (68)$$

In Cartesian coordinates, $\rho = \sqrt{x_0^2 + y_0^2}$, $\cos \phi = x_0/\sqrt{x_0^2 + y_0^2}$, and $\sin \phi = y_0/\sqrt{x_0^2 + y_0^2}$. Hence,

$$E_{2x}^{inc}(x_0, y_0, 0) = \frac{-G}{(x_0^2 + y_0^2)} \left[x_0^2 g(k_2 \sqrt{x_0^2 + y_0^2}, k_1) \right. \\ \left. - 2y_0^2 h(k_2 \sqrt{x_0^2 + y_0^2}, k_1) \right], \quad (69)$$

where the amplitude G is defined in Eq. (3). Since interest is in the distribution of the field relative to the scattering object, the x, y coordinate system with origin at the point $(\rho_c, \phi_c, 0)$ directly above the center of each scattering antenna is used. As shown in Fig. 1(a), when the antenna is located in Area I with $\phi_c = 0$, $x_0 = x + \rho_c$ and $y_0 = y$; when located in Area II with $\phi_c = \pi/2$, $x_0 = x$ and $y_0 = y + \rho_c$. In all of the calculations, ρ_c has been set equal to 1 m.

The scattered fields on the surface in Region 2 (air) are given by Eqs. (64)–(67). The total fields in the two locations with the associated induced currents Eqs. (34a) and (35) are

$$E_{2x}^t(x, y, 0) = E_{2x}^{inc}(x, y, 0) + E_{2x}^{scat}(x, y, 0), \quad (70)$$

where $E_{2x}^{inc}(x, y, 0)$ is given by Eq. (69) and $E_{2x}^{scat}(x, y, 0)$ is obtained from Eqs. (64) and (65) with Eq. (8) for the current Eq. (34a) in the buried antenna with center at $x_0 = \rho_c = 1$ m, $y_0 = 0$, and from Eqs. (66) and (67) with Eq. (22) for the current Eq. (35) in the buried antenna with center at $x_0 = 0$, $y_0 = \rho_c = 1$ m.

The properties of the total field at any point $(x, y, 0)$ as a function of the depth d of the buried antenna are readily determined. Thus,

$$|E_{2x}^t(x, y, 0)| = |E_{2x}^{inc}(x, y, 0) [1 + K e^{-\alpha_1 d} e^{i(\psi + \beta_1 d)}]|,$$

where $K e^{i\psi} = E_{2x}^{scat}(x, y, 0)/E_{2x}^{inc}(x, y, 0)$. Or

$$|E_{2x}^t(x, y, 0)| = |E_{2x}^{inc}(x, y, 0)| \\ \times \{ [1 + K e^{-\alpha_1 d} \cos(\psi + \beta_1 d)]^2 \\ + K^2 e^{-2\alpha_1 d} \sin^2(\psi + \beta_1 d) \}^{1/2} \\ = |E_{2x}^{inc}(x, y, 0)| \{ 1 + 2K e^{-\alpha_1 d} \cos(\psi + \beta_1 d) \\ + K^2 e^{-2\alpha_1 d} \}^{1/2}. \quad (71)$$

Evidently, the total field varies periodically with $\beta_1 d$. Thus, there are maxima near $(\psi + \beta_1 d) = n\pi$ with n even, viz.,

$$|E_{2x}^t(x, y, 0)|_{\max} \sim |E_{2x}^{inc}(x, y, 0)| (1 + K e^{-\alpha_1 d}), \quad (72)$$

and minima near $(\psi + \beta_1 d) = n\pi$ with n odd, viz.,

$$|E_{2x}^t(x, y, 0)|_{\min} \sim |E_{2x}^{inc}(x, y, 0)| (1 - K e^{-\alpha_1 d}). \quad (73)$$

It is seen that the amplitude of the oscillation decreases exponentially with depth as $\exp(-\alpha_1 d) = \exp(-d/d_s)$ where d_s is the skin depth.

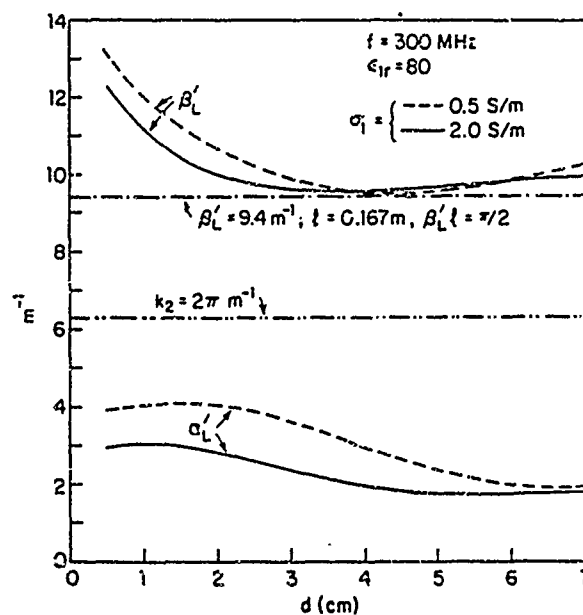


FIG. 2. Wave number $k_L' = \beta_L' + i\alpha_L'$ for induced current on insulated scattering rod: Area I.

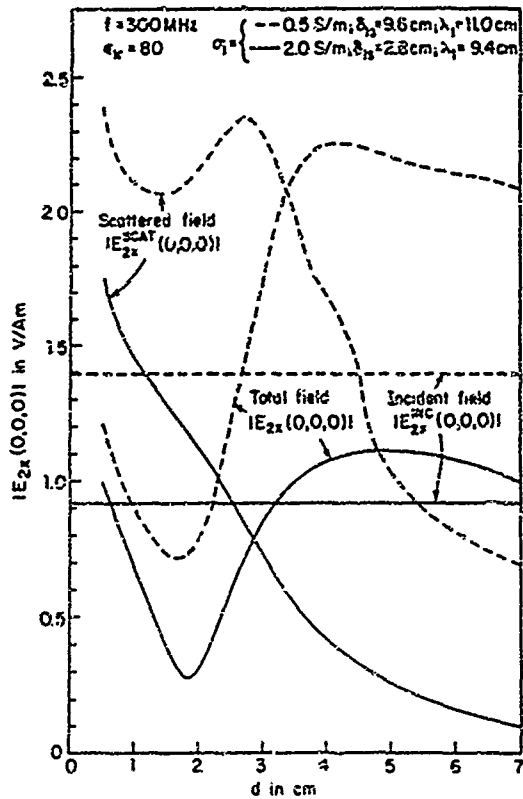


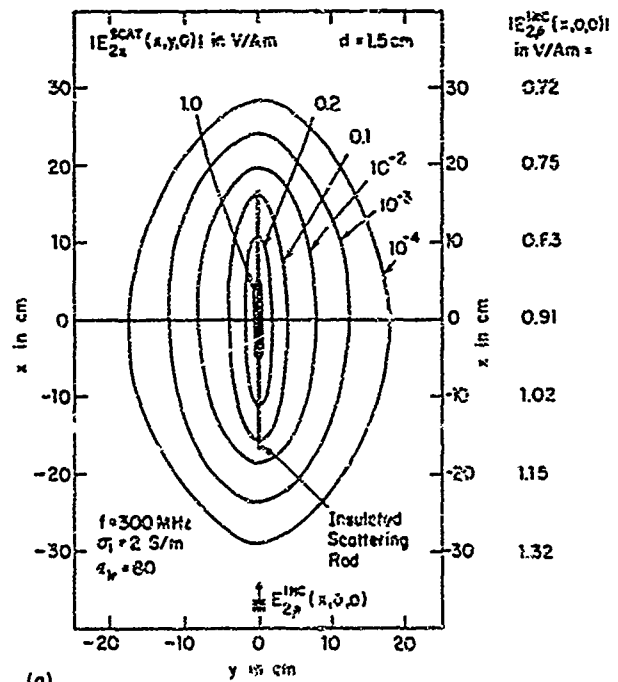
FIG. 3. Electric field in air over insulated scattering rod at depth d in salt water: Area I.

VIII. CALCULATED FIELDS FOR THE LABORATORY MODEL: AREA I

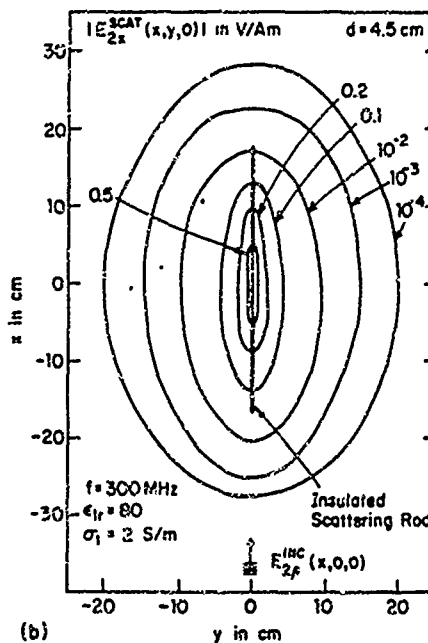
Of interest in the air above a buried scattering object are the incident lateral-wave field, the scattered field, and the total field—which is the only one actually measured and

used in locating buried objects. Calculations have been made of these fields in Area I at $f = 300$ MHz for the horizontal half-wave transmitting dipole described in Sec. V of Part I⁴ and a metal scattering rod of length $2l = 33.4$ cm, radius $a = 0.159$ cm, encased in a styrofoam insulating sheath with outer radius $b = 0.413$ cm. The specified length was chosen in order to have a scattering rod of constant length near resonance, viz., $\beta_1 l \sim \pi/2$ for all values of the depth d in the range $0 < d < 8$ cm.

Graphs of $\beta_1 l$ and $\alpha_1 l$ in the wave number k_1 of the current in the scattering rod as a function of the depth d are shown in Fig. 2. Since k_1 varies with d , the length $2l = 33.4$



(a)



(b)

FIG. 5. Contour diagram of scattered electric field on surface above insulated scatterer of length $2l = 33.4$ cm at depth d in salt water ($\epsilon_1 = 66.5 + i35.6 \text{ m}^{-1}$): Area I. (a) $d = 1.5$ cm. (b) $d = 4.5$ cm

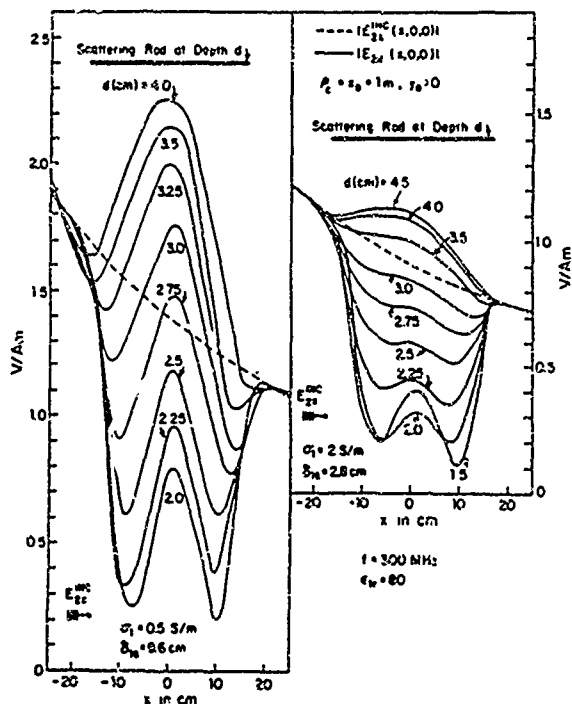


FIG. 4. Electric field directly over insulated scattering rod ($y = 0$): Area I.

cm is chosen so that β_z is near its minimum and $\beta_z/\lambda \approx \pi/2$. The ambient medium is salt water with relative permittivity $\epsilon_r = 80$ and conductivity $\sigma_1 = 2$ S/m for one set of data, $\sigma_1 = 0.5$ S/m for a second set of data.

Consider first the field at the point $x = y = 0$ directly above the center of the scattering rod as a function of its depth d when the medium is salt water with the conductivities $\sigma_1 = 2$ and 0.5 S/m. This is shown in Fig. 3. The incident lateral-wave field is independent of d but is greater when the conductivity is smaller due to the factor k_z^2 in the denominator of the amplitude G_z given by Eq. (3). The magnitude of the scattered field decreases with depth, but is also modified by the coupling of the insulated rod to the image, especially with the lower conductivity. The magnitude of the total field oscillates about the incident field. The distance between the maximum and minimum values depends on the interaction of the scattering antenna with its image and

differs substantially from $\lambda_1/2$, the value it would have for a large planar scattering object.

In Fig. 4 the total electric field along the x axis directly over the scattering rod is shown for $\sigma_1 = 2$ S/m with a skin depth $\delta_{1s} = 2.3$ cm on the right, $\sigma_1 = 0.5$ S/m with a skin depth $\delta_{1s} = 9.6$ cm on the left. The variable is the distance x from the point directly over the center of the scatterer; the parameter is the depth d . Also shown (in broken line) is the incident field. The effect of the scattered field in distorting the incident field is, of course, much greater when the scatterer is in the medium of lower conductivity where all depths are smaller than the skin depth. In the medium with higher conductivity, the effect of the scattered field decreases rapidly at depths greater than the skin depth, but is still significant at twice the skin depth. Actually more important than the skin depth is the phase of the scattered field relative to that of the incident field as determined by the depth of the scatterer.

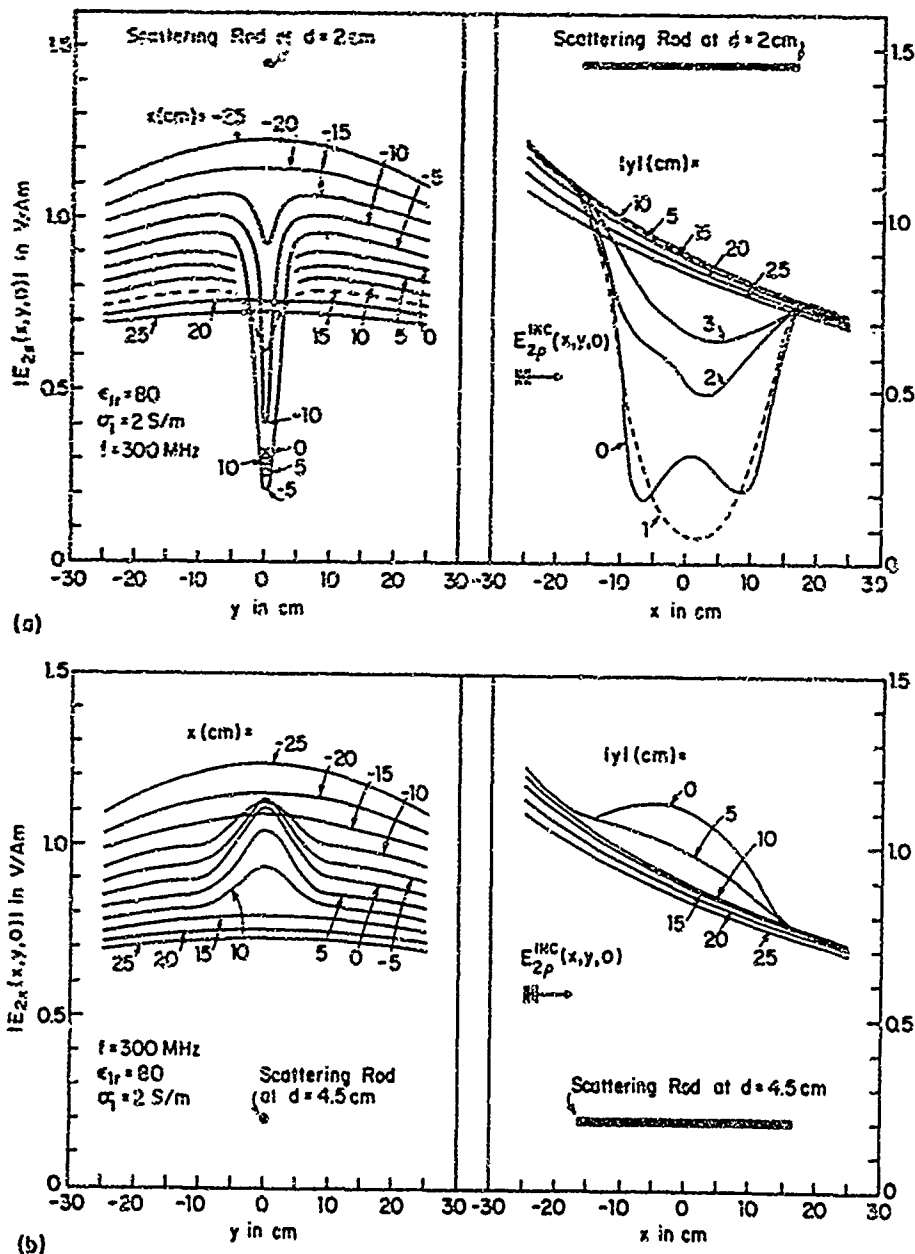


FIG. 6. Electric field in air above insulated scattering rod of length $2l = 33.4$ cm at depth d in salt water ($\sigma_1 = 2$ S/m): Area I. (a) $d = 2$ cm. (b) $d = 4.5$ cm.

When the two fields are in phase, the magnitude of the total field is greater than that of the incident field; when they are 180° out of phase, the magnitude of the total field is reduced below that of the incident field. Since the incident field is a progressive wave traveling lengthwise over the rod, whereas the current in the scattering rod is a superposition of a traveling wave with the wave number k_L and a standing wave with the wave number k_L , the differences between the phases of the incident and scattered field over the length of the rod vary. This accounts for the asymmetric patterns and the fact that the transition from a "mountain" to a "valley" in the total field is not uniform over the length of the wire so that there is always an observable effect although this can be quite small (as with $d \sim 3.25$

cm) compared to the high "mountains" at greater depths and the deep "valleys" at smaller depths.

A more detailed study of the total field over Area I has been carried out specifically with $d = 2$ cm with a deep "valley" over the scatterer and with $d = 4.5$ cm for $\sigma_1 = 2$ S/m and $d = 4.0$ cm for $\sigma_1 = 0.5$ S/m, both with a high "mountain" over the scatterer.

Contour diagrams of the magnitude of the scattered field in Area I with $d = 1.5$ cm and $d = 4.5$ cm for $\sigma_1 = 2$ S/m are shown in Fig. 5. For both depths the scattered field increases steeply directly over the scattering rod. The largest field is directly over the center of the rod. Similar diagrams can be obtained when $\sigma_1 = 0.5$ S/m.

The total field with $\sigma_1 = 2$ S/m is shown in Fig. 6(a) for

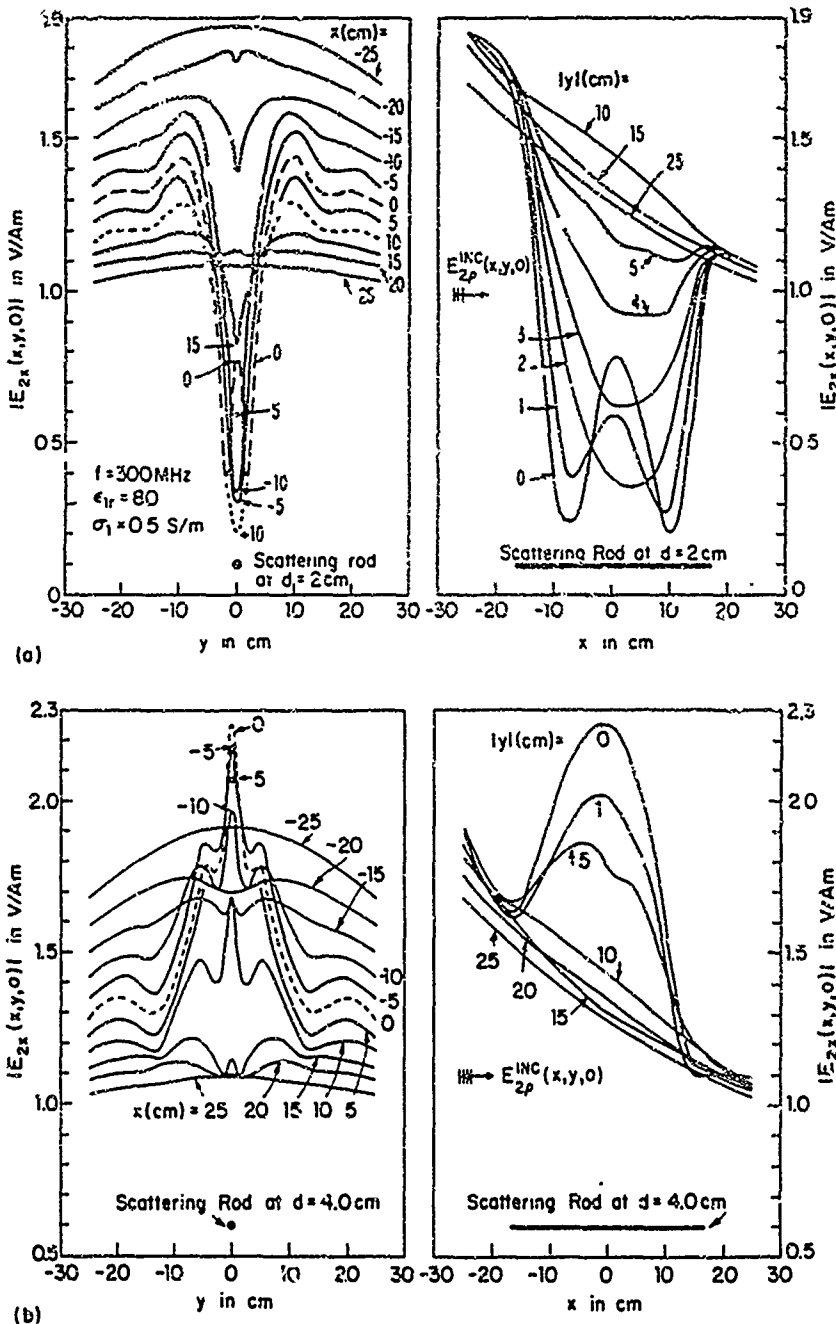


FIG. 7. Electric field in air above insulated scattering rod of length $2l = 33.4$ cm at depth d in salt water ($\sigma_1 = 0.5$ S/m): Area I. (a) $d = 2$ cm. (b) $d = 4.0$ cm.

$d = 2$ cm and in Fig. 6(b) for $d = 4.5$ cm. In these curves, y is the variable and x the parameter on the left, and vice versa on the right. In Fig. 6(a) the magnitude of the field is characterized by a deep and very narrow "valley" over the insulated conductor since the incident and scattered fields are nearly out of phase. In Fig. 6(b) the "valley" is replaced by a high narrow "mountain" since the incident and scattered fields are almost in phase. The valley and mountain are symmetric in y but asymmetric in x because the phase and magnitude of the incident field vary along the length of the scattering rod. Similar curves for $\sigma_1 = 0.5$ S/m are in Fig. 7. It is evident from these diagrams that measurements made of $|E_{2x}(x,y,0)|$ with a receiving dipole moved along the surface. If the water should clearly indicate the presence and location of the buried object. Alternatively, a receiving loop can be used to measure $|B_z(x,y,0)|$ with substantially the same results. This follows from Eqs. (1) and (2).

IX. CALCULATED FIELDS FOR THE LABORATORY MODEL: AREA II

The field over the insulated conductor when located in Area II differs from that in Area I in the following ways. The component of the electric field parallel to the x -directed scatterer is primarily E_x instead of E_y . Since E_x decreases with radial distance much more rapidly than E_y , the incident field is smaller even at one wavelength from the transmitting antenna. The current induced in the scattering rod is due primarily to E_x and this is practically constant in amplitude and phase over the entire scatterer. Consequently, the induced current consists almost entirely of a simple standing wave with a nearly constant phase along the entire length of the rod. As a result, the scattered field and its interference pattern with the incident field are simpler. Figure 8 for Area

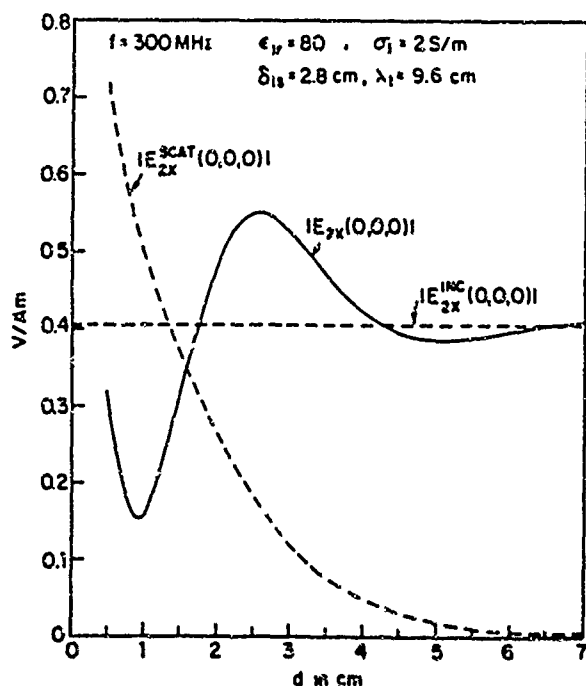
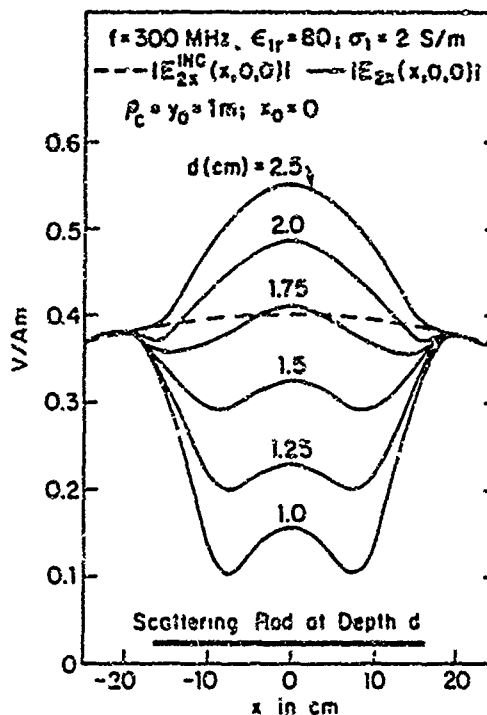
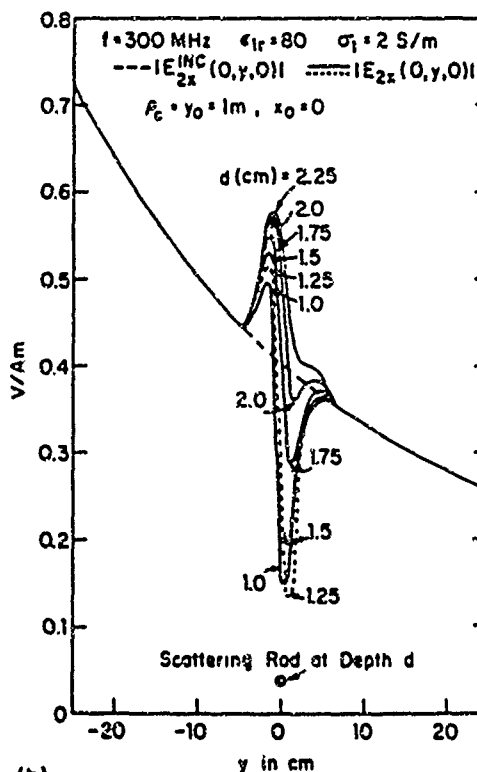


FIG. 8. Electric field in air over insulated scattering rod at depth d in salt water: Area II.

II corresponds to Fig. 3 for Area I with $\sigma_1 = 2$ S/m. The amplitudes of all of the fields are seen to be substantially smaller. Figure 9 illustrates the interference patterns generated by the scattered field on the surface above the scattering rod with the depth d as the parameter. In Fig. 9(a), as in Fig. 4, the field is represented lengthwise directly above the scattering rod. It is symmetric in x . In Fig. 9(b), the field is shown



(a)



(b)

FIG. 9. Electric field over insulated scattering rod: Area II (a) $y = 0$. (b) $x = 0$.

along a line perpendicular to and crossing above the center of the scattering rod. It corresponds to Fig. 6 at $x = 0$ for a wider range of values of d . Depending on the depth d , the scattered field augments or decreases the incident field to form sharp "mountains" or deep "valleys." Note that these are asymmetric in y .

It is seen that the general nature of the field in Area II resembles that in Area I. Except quite close to the transmitter, the amplitude of the incident field is smaller because E_0 decreases as $1/\rho^2$, E_p as $1/\rho$ after the initial ranges with $1/\rho^3$ decreases. In general, E_p is to be preferred.

X. CONCLUSION

The application of lateral electromagnetic waves generated by a dipole lying on the surface of the earth or sea to locate a buried or submerged object has been analyzed in detail when the scattering obstacle is an insulated metal rod near resonance at the operating frequency. It is clearly demonstrated that a significant change in the electric field over the volume occupied by the scattering object is observed and that this is sufficiently localized to permit an accurate bounding of the area above the object. It is anticipated that a somewhat smaller response will occur when the buried rod is bare metal. The scattering from objects like a metal disk or any region with a wave number that is significantly different from that of the ambient medium will be investigated quantitatively since the method has definite promise for discovering and locating underground oil fields. Note that the approach in this paper is quite different from that of Mahmoud *et al.*⁸ for the infinitely long cylinder.

ACKNOWLEDGMENTS

The author wishes to thank Professor T. T. Wu for his evaluation of the integrals in the Appendices, Ms. B. H. Sandler for carrying out the numerical calculations, and Ms. M. Owens for correcting the manuscript. This research was supported in part by the Joint Services Electronics Program under Contract N00014-84-K-0465 with Harvard University.

APPENDIX A: EVALUATION OF AN INTEGRAL

In order to evaluate Eq. (40) consider first the integral

$$\mathcal{J} = \int_{-\infty}^{\infty} \frac{e^{ik_1 r + kx}}{r} dx', \quad (A1)$$

where

$$k = k_2 \text{ or } k = \pm k_L \text{ and } r = [(x' - x)^2 + y^2 + d^2]^{1/2}. \text{ Let } x' = x + \sqrt{y^2 + d^2} \sinh \phi, \quad dx' = \sqrt{y^2 + d^2} \cosh \phi d\phi, \\ r = \sqrt{y^2 + d^2} (\sinh^2 \phi + 1) = \sqrt{y^2 + d^2} \cosh \phi.$$

It follows that

$$\mathcal{J} = e^{ikx} \int_{-\infty}^{\infty} \exp[i\sqrt{y^2 + d^2}(k_1 \cosh \phi + k \sinh \phi)] d\phi. \quad (A2)$$

Now let $k_1 = A \cosh \alpha$, $k = A \sinh \alpha$, $A = \sqrt{k_1^2 - k^2}$; $\phi + \alpha = \theta$. Then, $k_1 \cosh \phi + k \sinh \phi = A(\cosh \alpha \cosh \phi + \sinh \alpha \sinh \phi) = A \cosh \theta$, and

$$\mathcal{J} = \int_{-\infty}^{\infty} \frac{e^{ik_1 r + kx}}{r} dx' \\ = e^{ikx} \int_{-\infty}^{\infty} \exp(i\sqrt{k_1^2 - k^2} \cosh \theta) d\theta \\ = \pi i e^{ikx} H_0^{(1)}(\sqrt{k_1^2 - k^2} \sqrt{y^2 + d^2}). \quad (A3)$$

It follows formally that with $k = 0$,

$$\int_{-\infty}^{\infty} \frac{e^{ik_1 r}}{r} dx' = \pi i H_0^{(1)}(k_1 \sqrt{y^2 + d^2}). \quad (A4)$$

Therefore, with $\sqrt{k_1^2 - k^2}$ substituted for k_1 ,

$$\int_{-\infty}^{\infty} \frac{\exp(i\sqrt{k_1^2 - k^2} r)}{r} dx' \\ = \pi i H_0^{(1)}(\sqrt{k_1^2 - k^2} \sqrt{y^2 + d^2}). \quad (A5)$$

With Eq. (A3), it also follows that

$$\int_{-\infty}^{\infty} \frac{e^{ik_1 r + kx}}{r} dx' = e^{ikx} \int_{-\infty}^{\infty} \frac{\exp(i\sqrt{k_1^2 - k^2} r)}{r} dx'. \quad (A6)$$

This transformation applies when $k = k_2$ or $k = \pm k_L$.

Subject to the conditions (48) which require l to be large compared with y and d (which occur in $r = [(x' - x)^2 + y^2 + d^2]^{1/2}$), it can be assumed that Eq. (A6) is a good approximation when the infinite limits are replaced by the large but finite ones, viz., $\pm l$. That is,

$$\int_{-l}^l \frac{e^{ik_1 r + kx}}{r} dx' \sim e^{ikx} \int_{-l}^l \frac{\exp(i\sqrt{k_1^2 - k^2} r)}{r} dx', \quad x < l. \quad (A7)$$

This approximation is best when $|x'| < l$, but should be acceptable when $|x'| < l$. Since $|x'|$ can never exceed l , the appropriate form of Eq. (A7) for $x > l$ is

$$\int_{-l}^l \frac{e^{ik_1 r + kx}}{r} dx' \sim e^{ikl} \int_{-l}^l \frac{\exp(i\sqrt{k_1^2 - k^2} r)}{r} dx'. \quad (A8)$$

This maintains continuity between $x < l$ and $x > l$.

APPENDIX B: EVALUATION OF EXPONENTIAL INTEGRALS

The integrals in Eqs. (46) and (49) can be expanded as follows:

$$\mathcal{J} = \int_0^l \left(\frac{e^{ikr_1}}{r_1} + \frac{e^{ikr_2}}{r_2} \right) dx', \quad (B1)$$

where

$$k = \beta + i\alpha \text{ stands for } k_1 \text{ in Eq. (46) or } k_{12} \text{ in Eq. (49),} \quad (B2)$$

and

$$r_1 = \sqrt{(x' - x)^2 + y^2 + d^2}, \\ r_2 = \sqrt{(x' + x)^2 + y^2 + d^2}. \quad (B3)$$

Now let the following short-hand notation be introduced:

$$U = \beta(x' - x) \text{ in the first term in Eq. (B1),} \\ U = \beta(x' + x) \text{ in the second term in Eq. (B1),} \\ A = \beta\sqrt{y^2 + d^2}, \quad W = \sqrt{U^2 + A^2}, \quad \delta = \alpha/\beta, \quad (B4)$$

Also let

$$U_0 = \beta x, \quad U_1 = \beta(l - x), \quad U_2 = \beta(l + x). \quad (\text{B5})$$

With this notation Eq. (B1) becomes

$$J = \int_{-U_0}^{U_1} \frac{e^{-\delta W} e^{iW}}{W} dU + \int_{U_0}^{U_2} \frac{e^{-\delta W} e^{iW}}{W} dU. \quad (\text{B6})$$

The generalized exponential integral can now be defined as follows:

$$\bar{E}(\delta, A, U) \equiv \int_0^U \frac{e^{-\delta W} e^{iW}}{W} dU. \quad (\text{B7})$$

With Eq. (B7), Eq. (B6) becomes:

$$J = \bar{E}(\delta, A, U_1) + \bar{E}(\delta, A, U_2), \quad (\text{B8})$$

since $\bar{E}(\delta, A, -U_0) = -\bar{E}(\delta, A, U_0)$. This is usually more convenient in the alternative form:

$$\bar{E}(\delta, A, U) = \sinh^{-1}(U/A) - E(\delta, A, U), \quad (\text{B9})$$

where

$$\bar{E}(\delta, A, U) = \int_0^U \frac{1 - e^{-\delta W} e^{-iW}}{W} dU. \quad (\text{B10})$$

The function $E(\delta, A, U)$ has been tabulated when $\alpha/\beta = 0$,⁹ and when $\delta = (\alpha/\beta) = 1$.¹⁰

¹H. S. Tuan and R. W. P. King, *Radio Sci.* 3, 1309 (1966).

²H. S. Tuan and R. W. P. King, *Radio Sci.* 3, 577 (1966).

³R. W. P. King and L. C. Shen, *IEEE Trans. Antennas Propagat.* AP-30, 1165 (1982).

⁴R. W. P. King, *J. Appl. Phys.* 57, 1433 (1985).

⁵R. W. P. King and L. C. Shen, *J. Appl. Phys.* 47, 5226 (1976).

⁶R. W. P. King, *IEEE Trans. Antennas Propagat.* AP-24, 327 (1976).

⁷R. W. P. King and L. C. Shen, *Radio Sci.* 14, 1049 (1979).

⁸S. F. Mahmoud, S. M. Ali, and J. R. Wait, *Radio Sci.* 16, 1285 (1981).

⁹Staff of the Computation Laboratory, *Tables of Generalized Sine and Cosine Integral Functions* (Harvard University, Cambridge, MA, 1949).

¹⁰Staff of the Computation Laboratory, *Tables of Generalized Exponential Integral Functions* (Harvard University, Cambridge, MA, 1949).

Electromagnetic surface waves: New formulas and their application to determine the electrical properties of the sea bottom

Ronald W. P. King

Gordon McKay Laboratory, Harvard University, Cambridge, Massachusetts 02138

(Received 24 January 1985; accepted for publication 22 July 1985)

Electromagnetic surface waves can propagate along boundaries between electrically different media like air and earth or sea water and rock. They have unusual properties that make them valuable tools in geophysical prospecting and diagnostics. They are not suited to deep sounding. Much of the current theory for their geophysical application has been limited to ranges of the parameters and variables that permit the use of Norton's graphs which were developed for radio communication over the earth. A recently derived set of accurate, very general, and simple formulas for the surface-wave fields of antennas near a boundary surface has provided an expanded horizon for understanding and using surface waves as distinct from plane waves that travel down into the earth. The new formulas are given and used to assist in the interpretation of available measurements and then applied to the determination of the average conductivity and permittivity of the part of the lithosphere very close to the sea bottom where the lateral waves travel.

I. INTRODUCTION

An important application of classical physics is to geophysical prospecting and diagnostics. Among the electrical methods used for these purposes, electromagnetic surface waves have found only limited application. This may be due in part to the complexity of the underlying Sommerfeld integrals in which the numerous parameters and variables occur in physically obscure combinations, and in part to preoccupation with ranges of parameters and variables of interest in radio communication over the surface of the earth. Simple functional relationships, which form the basis of effective methods of measurement, are not evident in the rigorous integrals and no general perspective is provided by numerous approximate formulas for limited, nonoverlapping ranges of the variables and parameters. This is illustrated in the use of surface waves to measure the electrical properties of the earth.¹⁻³ On the other hand, geophysical studies that use natural electromagnetic fields originating in the Earth's magnetosphere and ionosphere⁴ do not involve lateral waves.

When both the transmitting and receiving antennas are vertical monopoles on the surface of the earth, the entire field along that surface consists of the ground or surface wave (with possible contributions from ionospheric reflections). In the absence of a simple formula for the vertical component $E_z(\rho, 0)$ of the electric field at the radial distance ρ from the source, use is made of the well-known curves of Norton⁵ (see Fig. 1) which represent the magnitude of the electric field as a function of the radial distance contained in the "numerical distance" $p = |\rho| \exp(ib) = ik_2 \rho / 2k_1^2$, where k_1 is the complex wave number of the earth and k_2 the real wave number of the air. A logarithmic curve-matching procedure is used to determine the electrical properties of the earth from the measured decay rate with radial distance of $|E_z(\rho, 0)|$. However, and this is obvious from Fig. 1, there is very little spread between Norton's curves over the full range of possible values of k_1 , as contained in the angle b of the complex numerical

distance, so that highly accurate measured data on the decay rate of the electric field are required.

References to electromagnetic surface waves^{1,3} are often limited to those generated by vertical antennas in the air above the surface of the earth. This is also true of many experimental investigations,⁶⁻⁹ in which the field in the air over the earth is evaluated or measured directly or in models. The theoretically determined field is usually separated into a direct wave, a reflected wave, and a surface wave. Since the direct and reflected waves cancel along the boundary, the entire field there is that maintained by the surface wave which includes the error-function or Fresnel-integral term represented by Norton's curves.

A systematic study of the properties of the complete field generated by vertical and horizontal electric dipoles at and near the boundary between two electrically different half-spaces can lead to the discovery and development of more general and sensitive applications of surface waves than are contained in Norton's curves. This possibility appears not to have been recognized heretofore, perhaps because of the complicated nature of the Sommerfeld-integral

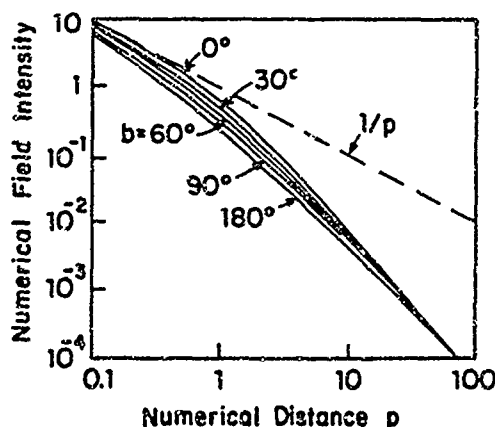


FIG. 1. Decay of ground wave intensity with propagation distance (Norton's graphs).

representation¹⁰ and the lack of continuity in various approximate formulas.^{3,10-14} Some of the interesting properties of lateral waves have become evident from numerical evaluations of the general integrals for the boundary between air and the earth (sea, lake, etc.)¹⁵⁻²⁰ and for the sea water-lithosphere boundary.^{20,21} Significantly, even these detailed and comprehensive evaluations failed to discover and display the

startling interference patterns resulting from the interaction of the direct fields from the source and its image with the lateral-wave field. This became evident from the new analytical formulas²² to be discussed below in another application. It is hoped that these formulas can add physical insight to the numerical evaluation of the Sommerfeld integrals in recent studies of the oceanic crust.^{23,24}

II. THE FIELDS OF THE HORIZONTAL AND VERTICAL ELECTRIC DIPOLES: TWO-LAYER PROBLEM

The complete electromagnetic field at any point due to a unit x -directed horizontal electric dipole at a height d in Region 1 ($z > 0$, wave number $k_1 = \omega[\mu_0(\epsilon_1 + i\sigma_1/\omega)]^{1/2}$, sea water) above Region 2 ($z < 0$, wave number $k_2 = \omega[\mu_0(\epsilon_2 + i\sigma_2/\omega)]^{1/2}$, rock or deep sediment) is determined by King and Smith [Ref. 20, pp. 607-620] directly from Maxwell's equations. At the point (ρ, ϕ, z) in cylindrical coordinates in Region 1, a typical component in integral form is

$$E_{1\rho}(\rho, \phi, z) = -\frac{\omega\mu_0}{4\pi k_1^2} \cos \phi \left(\int_0^\infty \{(\gamma_1 Q/2)[J_0(\lambda\rho) - J_2(\lambda\rho)] - (k_1^2 P/2\gamma_1)[J_0(\lambda\rho) + J_2(\lambda\rho)]\} e^{\gamma_1(z+d)} \lambda d\lambda \right. \\ \left. + \int_0^\infty \{k_1^2 J_0(\lambda\rho) - (\lambda^2/2)[J_0(\lambda\rho) - J_2(\lambda\rho)]\} \gamma_1^{-1} e^{\gamma_1(z-d)} \lambda d\lambda \right). \quad (1)$$

Similar integrals for the other five components in Region 1 and the six components of the field in Region 2 are in Ref. 20 [Chap. 11, Eqs. (5.10)-(5.20)]. When $\mu_1 = \mu_2 = \mu_0$,

$$P = (\gamma_2 - \gamma_1)/(\gamma_1 + \gamma_2), \quad Q = (k_1^2 \gamma_2 - k_2^2 \gamma_1)/(k_1^2 \gamma_2 + k_2^2 \gamma_1); \quad (2)$$

$$\gamma_1 = (k_1^2 - \lambda^2)^{1/2}, \quad \gamma_2 = (k_2^2 - \lambda^2)^{1/2}. \quad (3)$$

The time dependence is $e^{-i\omega t}$ and ϕ is measured from the positive x axis.

In recent applications to the lithosphere all six formulas were rederived²⁵ in a form specialized to low frequencies so that the condition $\omega\epsilon \ll \sigma$ with $k^2 \sim i\omega\mu_0\sigma$ is applicable to both Regions 1 and 2. When applied to homogeneous half-spaces, the "response functions" of the sea-lithosphere boundary are $R_{TE} = -P$, $R_{TM} = -Q$, where P and Q are given in Eq. (2). In the discussion of the integral formulas for the six components, the following statement was made²⁵: "The mathematical complexity...masks their conceptual simplicity. In each case the first terms, involving the coefficients R_{TE} and R_{TM} , represent the electromagnetic field due to an image current induced in the conducting earth, while the second terms represent the primary field in the ocean." This statement is not quite complete. The first terms also include the very important surface wave that propagates radially outward and actually dominates the field along the boundary. The field associated with the surface wave is quite complicated. It is perhaps well to add that while the coefficients R_{TE} and R_{TM} are indeed analogs of the reflection coefficients of electromagnetic theory, this is only in a formal sense that applies to the elementary generalized plane waves in the integrands and involves complex angles. The integrat-

ed field^{22,25-27}—which cannot be represented by plane waves—includes not only the reflected wave but also the outward-traveling surface wave. Subject only to the following conditions:

$$|z_1| > 3|z_2|; \quad |k_1\rho| > 3; \quad \rho > 5|z|, \quad \rho > 5d, \quad (4)$$

and with the notation

$$f(k_2\rho, k_1) = \frac{i}{k_2\rho^3} \\ = g(k_2\rho, k_1) \\ = \frac{ik_2}{\rho} - \frac{1}{\rho^2} - \frac{i}{k_2\rho^3} \\ - \frac{k_2^3}{k_1} \left(\frac{\pi}{k_2\rho} \right)^{1/2} e^{-ik_2^3\rho/2k_1^2} \mathcal{F}(k_2\rho, k_1), \quad (5)$$

and

$$\mathcal{F}(k_2\rho, k_1) = \frac{1}{2}(1+i) - C_2(k_2^3\rho/2k_1^2) - iS_2(k_2^3\rho/2k_1^2), \quad (6)$$

where

$$C_2(u) + iS_2(u) = \int_0^u (2\pi t)^{-1/2} e^{it} dt, \quad (7)$$

the six components of the integrated field in Region 1 ($z > 0$ sea water) are

$$E_{1\rho}(\rho, \phi, z) = -\frac{\omega\mu_0}{2\pi k_1^2} \cos \phi \left[k_2 g(k_2\rho, k_1) e^{ik_2\rho} e^{ik_1(z+d)} - \left(\frac{k_1}{\rho^2} + \frac{i}{\rho^3} \right) e^{ik_1 r_1} \right], \quad (8)$$

$$E_{1\phi}(\rho, \phi, z) = \frac{\omega\mu_0}{\pi k_1^2} \sin \phi \left[e^{ik_1(z+d)} e^{ik_1\rho} \left(\frac{k_2}{\rho^2} + \frac{i}{\rho^3} + \frac{ik_2^4}{2k_1} \frac{\pi^{1/2}}{(k_2\rho)^{3/2}} e^{-ik_2^3\rho/2k_1^2} \mathcal{F}(k_2\rho, k_1) \right) \right. \\ \left. + e^{ik_1 r_1} \left(\frac{ik_1^2}{2\rho} - \frac{k_1}{\rho^2} - \frac{i}{\rho^3} \right) - \frac{1}{4} (e^{ik_1 r_1} + e^{ik_1 r_2}) \left(\frac{ik_1^2}{\rho} - \frac{k_1}{\rho^2} - \frac{i}{\rho^3} \right) \right], \quad (9)$$

$$E_{1z}(\rho, \phi, z) = \frac{\omega \mu_0}{2\pi k_1^2} \cos \phi \left[\frac{k_2^2}{k_1} \left(f(k_2 \rho, k_1) e^{ik_2 \rho} e^{ik_1(z+d)} - \frac{ie^{ik_1 r_1}}{\rho^2} \right) - \frac{1}{2} \left(\frac{z-d}{\rho} e^{ik_1 r_1} + \frac{z+d}{\rho} e^{ik_1 r_2} \right) \left(\frac{ik_1^2}{\rho} - \frac{3k_1}{\rho^2} - \frac{3i}{\rho^3} \right) \right], \quad (10)$$

$$B_{1\rho}(\rho, \phi, z) = -\frac{\mu_0}{2\pi k_1} \sin \phi \left\{ e^{ik_1(z+d)} e^{ik_2 \rho} \left[\frac{2k_2}{\rho^2} + \frac{2i}{\rho^3} + \frac{ik_2^2}{k_1 \rho} \left(\frac{\pi}{k_2 \rho} \right)^{1/2} e^{-ik_2^2 \rho / 2k_1} \mathcal{F}(k_2 \rho, k_1) \right] \right. \\ \left. + e^{ik_1 r_1} \left(\frac{ik_1^2}{\rho} - \frac{2k_1}{\rho^2} - \frac{2i}{\rho^3} \right) - \frac{1}{2} \left(\frac{z-d}{\rho} e^{ik_1 r_1} + \frac{z+d}{\rho} e^{ik_1 r_2} \right) \left(\frac{ik_1^2}{\rho} + \frac{2i}{\rho^3} - \frac{3}{k_1 \rho^4} \right) \right\}, \quad (11)$$

$$B_{1\phi}(\rho, \phi, z) = -\frac{\mu_0}{2\pi k_1} \cos \phi \left[k_2 g(k_2 \rho, k_1) e^{ik_2 \rho} e^{ik_1(z+d)} + \frac{1}{2} \left(\frac{2}{\rho^3} + \frac{3i}{k_1 \rho^4} \right) e^{ik_1 r_1} + \frac{1}{2} \left(\frac{z-d}{\rho} e^{ik_1 r_1} + \frac{z+d}{\rho} e^{ik_1 r_2} \right) \left(\frac{ik_1^2}{\rho} - \frac{k_1}{\rho^2} \right) \right], \quad (12)$$

$$B_{1z}(\rho, \phi, z) = \frac{\mu_0}{2\pi k_1^2} \sin \phi \left[e^{ik_1(z+d)} e^{ik_2 \rho} \left(\frac{k_2^2}{\rho^2} + \frac{3ik_2}{\rho^3} - \frac{3}{\rho^4} \right) - e^{ik_1 r_1} \left(\frac{k_1^2}{\rho^2} + \frac{3ik_1}{\rho^3} - \frac{3}{\rho^4} \right) - \frac{1}{2} (e^{ik_1 r_1} - e^{ik_1 r_2}) \left(\frac{ik_1^2}{\rho} - \frac{k_1^2}{\rho^2} \right) \right]. \quad (13)$$

The distances r_1 and r_2 from the source dipole and its image to the point of observation, respectively, are

$$r_1 = [\rho^2 + (z-d)^2]^{1/2}; \quad r_2 = [\rho^2 + (z+d)^2]^{1/2}. \quad (14)$$

The formulas (8)–(13) are accurate equivalents of the general integrals throughout the indicated range which excludes only a small region close to the source. They have been extensively checked numerically and experimentally over wide ranges of the parameters and variables. Even in the very sensitive ranges where the interaction of the primary and image fields with the lateral-wave field produces sharp interference maxima and minima, the representation is quantitatively accurate.

The formulas (8)–(13), unlike the integrals they represent, explicitly show that the field consists of three parts. These are (1) the direct field from the source dipole at $(0,0,d)$ given by all terms with the exponential factor $e^{ik_1 r_1}$; (2) the reflected field or field from an image dipole at $(0,0,-d)$ given by the sum of terms with the exponential factor $e^{ik_1 r_2}$; and (3) the lateral-wave field with the exponential factors $e^{ik_1(z+d)} e^{ik_2 \rho}$ which represents a wave that travels down from the source a distance d in sea water (Region 1) to the ocean floor, then proceeds radially outward a distance ρ parallel to that floor in the lithosphere (Region 2), and finally propagates upward from the sea floor a distance z into the ocean to the point of observation at (ρ, ϕ, z) . The amplitude of the lateral wave is determined by the exponential attenuation $e^{-\alpha_1(z+d)}$ for the vertical up-and-down paths in the sea water, and by $e^{-\alpha_2 \rho}$ for the horizontal path in the lithosphere. In addition, it decreases by functions of the type $g(k_2 \rho, k_1)$, given in Eq. (5), which involve inverse powers of the radial distance ρ and a Fresnel-integral term. When Region 1 is sea water, the direct and reflected fields are much more rapidly attenuated with radial distance than the lateral wave since they experience the exponential attenuations $e^{-\alpha_1 r_1}$ and $e^{-\alpha_1 r_2}$ with $\alpha_1 \gg \alpha_2$. It follows that at all distances for which $e^{-\alpha_1 \rho} \ll e^{-\alpha_2 \rho}$, the field is dominated by the radially outward-traveling surface wave.

Of particular interest is the depth of penetration into Region 2 of the lateral wave. This has been determined²⁷

from the locus of the Poynting vector in Region 2 beginning near the dipole and proceeding to the radial distance ρ_0 where it crosses the surface from Region 2 into Region 1. At the relatively low frequencies useful in measurements near the sea floor, for which $k_1 \sim (i\omega\mu_0\sigma_1)^{1/2}$, $k_2 \sim (i\omega\mu_0\sigma_2)^{1/2}$, the locus is defined in terms of $z' = -z, z < 0$, by

$$z' = -(\sigma_2/\sigma_1)^{1/2} \rho \ln(\rho/\rho_0), \quad (15)$$

with a maximum penetration $z'_m = (\sigma_2/\sigma_1)^{1/2} \rho_0/e$, where $e = 2.718$. Also determined is the fraction of the total power P_T in Region 2 that continues on in Region 2 beyond a radius ρ_0 as a spherical wave and the fraction that is diverted as a lateral wave that reaches the boundary surface between the radii $\rho = \rho_0$ and $\rho = 2.718\rho_0$. With P_L the power in the lateral wave and P_S the power in the spherical wave, the ratios are

$$P_L/P_T = (\sigma_2/\sigma_1)^{1/2}; \quad P_S/P_T = 1 - (\sigma_2/\sigma_1)^{1/2}. \quad (16)$$

General integrals for $E_\rho(\rho, z)$, $E_z(\rho, z)$, and $B_\phi(\rho, z)$ in both regions due to a vertical electric dipole at $z = d$ in Region 1 are in Ref. 28 together with integrated formulas. The lateral-wave parts of the field in Region 1 are given by

$$E_{1\rho}^L(\rho, z) = -E_{1z}^L(\rho, 0, z), \quad (17)$$

$$E_{1z}^L(\rho, z) = -(k_2^2/k_1^2) E_{1\rho}^L(\rho, 0, z), \quad (18)$$

where the subscripts v and h refer to vertical and horizontal dipoles.

III. LATERAL WAVES AND VERTICALLY LAYERED MEDIA

Studies of the oceanic crust^{23,24,29} are not limited to a lithosphere modeled as a homogeneous half-space. They also treat the more general problem of a lithosphere (Region 2, $z < 0$) with a conductivity that is a function of the vertical coordinate, $\sigma_2 = \sigma_2(z)$, that varies discontinuously from layer to layer. The sea boundary of the horizontally layered region is characterized by generalized reflection coefficients or response functions R_{TE} and R_{TM} obtained with a one-dimensional recurrence formula similar to that derived and used for downward-traveling plane waves.⁴ Note that in transmission from the air (wave number k_2) into the earth

(wave number k_1) the ratio $|k_1/k_2|$ is large so that the electromagnetic field is a locally plane wave propagating normally to the surface. Also the plane-wave impedance is determined only by the conductivity and frequency and does not depend on the incident wave structure. The situation is very different when the primary field is generated by a horizontal dipole in the sea water above the surface of the lithosphere. Transmission is now from a region with large wave number into one with a much smaller wave number so that the field transmitted into the lithosphere, even when represented by elementary plane waves, bends away from and not towards the normal. Furthermore, the field in the sea water now includes a surface wave in addition to any partially reflected wave.

A study of the Poynting vector in both regions³⁰ shows that the field from the horizontal dipole in the sea at $z = d$ enters the adjacent lithosphere only in a narrow cone directly below the dipole. This suggests that the field in the lithosphere can be determined at points that are not too close by evaluating the primary tangential electric field on the boundary surface and using this, in the form of an equivalent magnetic surface current $\mathbf{K}_m = \hat{n} \times \mathbf{E}$, as the new source for the electromagnetic field in the lithosphere. The components $K_{my} \approx E_x$ and $K_{mx} \approx -E_y$ at $z = 0$ due to the x -directed unit dipole at $z = d$ are readily evaluated from well-known formulas. The contribution by an image at $z = -d$ with an equal unit electric moment in phase must, of course, be included since the large value of $|k_1/k_2|$ yields a reflection coefficient corresponding approximately to that when $B_{\text{mag}} \sim 0$ at $z = 0$. For calculating the field at sufficiently large distances, the magnetic moment of the entire magnetic surface current \mathbf{K}_m can be evaluated and lumped at the origin as the moment of a magnetic dipole. Thus with

$$\int_{-\infty}^{\infty} \int_{-\infty}^{\infty} E_x dx dy = (-2\omega\mu_0/k_1)e^{ik_1d};$$

$$\int_{-\infty}^{\infty} \int_{-\infty}^{\infty} E_y dx dy = 0,$$

it follows that the equivalent magnetic dipole at $z = 0$ is y directed with a magnetic moment $(-2\omega\mu_0/k_1)e^{ik_1d}$. It is the approximate effective source of the sufficiently distant field in the lithosphere. The well-known field of such a magnetic dipole for the specified orientation and magnetic moment and with $r_0 = (\rho^2 + z^2)^{1/2}$ is

$$E_{2\rho}(\rho, \phi, z) = -\frac{\omega\mu_0}{2\pi k_1} e^{ik_1d} \cos \phi \left(\frac{z}{r_0} \right) \left(\frac{ik_2}{r_0} - \frac{1}{r_0^2} \right) e^{ik_2r_0}, \quad (19)$$

$$E_{2\phi}(\rho, \phi, z) = \frac{\omega\mu_0}{2\pi k_1} e^{ik_1d} \sin \phi \left(\frac{z}{r_0} \right) \left(\frac{ik_2}{r_0} - \frac{1}{r_0^2} \right) e^{ik_2r_0}, \quad (20)$$

$$E_{2z}(\rho, \phi, z) = \frac{\omega\mu_0}{2\pi k_1} e^{ik_1d} \cos \phi \left(\frac{\rho}{r_0} \right) \left(\frac{ik_2}{r_0} - \frac{1}{r_0^2} \right) e^{ik_2r_0}, \quad (21)$$

$$B_{2\rho}(\rho, \phi, z) = -\frac{\mu_0 k_2}{2\pi k_1} e^{ik_1d} \sin \phi$$

$$\times \left[\frac{ik_2 z^3}{r_0^3} + \frac{(2\rho^2 - z^2)}{r_0^2} \left(\frac{1}{r_0} + \frac{i}{k_2 r_0^2} \right) \right] e^{ik_2r_0}, \quad (22)$$

$$B_{2\phi}(\rho, \phi, z) = -\frac{\mu_0 k_2}{2\pi k_1} e^{ik_1d} \cos \phi$$

$$\times \left(\frac{ik_2}{r_0} - \frac{1}{r_0^2} - \frac{i}{k_2 r_0^2} \right) e^{ik_2r_0}, \quad (23)$$

$$B_{2z}(\rho, \phi, z) = \frac{\mu_0 k_2}{2\pi k_1} e^{ik_1d} \sin \phi$$

$$\times \left(\frac{\rho z}{r_0^2} \right) \left(\frac{ik_2}{r_0} - \frac{3}{r_0^2} - \frac{3i}{k_2 r_0^2} \right) e^{ik_2r_0}. \quad (24)$$

Formulas (19)–(24) are good approximations of the field in the lithosphere ($z < 0$) when $|k_1 r_0| \gg 1$ and $|z|$ is not too small. However, the field along the boundary ($z = 0$) in the lithosphere is accurately known from the boundary conditions and Eqs. (5)–(13). Thus,

$$E_{2\rho}(\rho, \phi, 0) = E_{1\rho}(\rho, \phi, 0),$$

$$E_{2\phi}(\rho, \phi, 0) = E_{1\phi}(\rho, \phi, 0); \quad (25)$$

$$E_{2z}(\rho, \phi, 0) = (k_1^2/k_2^2) E_{1z}(\rho, \phi, 0),$$

$$B_{2\rho}(\rho, \phi, 0) = B_{1\rho}(\rho, \phi, 0). \quad (26)$$

It is the field given by Eqs. (19)–(24) that is incident on the first horizontal layer in the lithosphere provided this is not too close to the sea floor. If it is quite close, the field is given by Eqs. (19)–(24) with added terms that contain the surface wave.²⁷ The partial reflection and transmission of the spherical wave represented by Eqs. (19)–(24) at successive horizontal surfaces of discontinuity for $\sigma_2(z)$ are, of course, different from those of a downward-traveling plane wave. Calculation of the upward reflected field can be made using Eqs. (19)–(24) and a perfectly reflecting surface at the optimum depth.²⁷ These show that the reflected spherical wave contributes less than 40% to the total field in the sea with at least 60% contributed by the lateral wave. For other than optimum depth the lateral wave contributes as much as 90% or more to the total field.

The simple solution (8)–(10) for the electric field in sea water above a lithosphere modeled as a homogeneous isotropic half-space has no direct application to a horizontally layered lithosphere. However, it does permit useful insights into important aspects of the numerically evaluated layered models in their relation to both the half-space model and measured results. In order to illustrate this, consider the measured data of Young and Cox²⁴ that were obtained with the arrangement shown in the upper part of Fig. 2 (which corresponds to a part of their Fig. 2). The insulated transmitting dipole T is at a distance $\rho = 18.9$ km along the sea floor from the crossed-dipole receiving antenna R . The angle between the transmitting antenna and the radial line ρ is ϕ in the notation of Eqs. (8)–(13). Vectors to represent the components $E_{1\rho}(\rho, \phi, 0)$ and $E_{1\phi}(\rho, \phi, 0)$ at R are shown in the figure. The two arms of the crossed-dipole receiving antenna used by Young and Cox were not aligned to measure $E_{1\rho}$ and $E_{1\phi}$, respectively, but rather the components E_x and E_y along the arbitrary X and Y directions shown in the diagram. The angle between Y and ρ is ψ . The angles ϕ and ψ are not specified by Young and Cox²⁴ except as indicated in the dia-

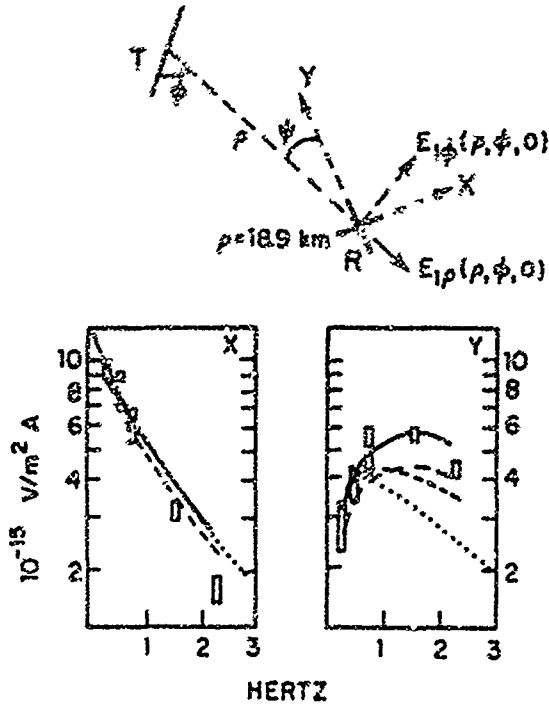


FIG. 2. Traced from Figs. 2 and 3 of Young and Cox (Ref. 24).

gram in Fig 2 E_x and E_y can be expressed in terms of the basic horizontal components $E_{1\rho}(\rho, \phi, 0) = E_{1\rho}(\rho, 0, 0)\cos\phi$ and $E_{1\phi}(\rho, \phi, 0) = E_{1\phi}(\rho, \pi/2, 0)\sin\phi$ as follows:

$$E_x = E_{1\rho}(\rho, \phi, 0)\sin\psi + E_{1\phi}(\rho, \phi, 0)\cos\psi, \quad (27)$$

$$E_y = -E_{1\rho}(\rho, \phi, 0)\cos\psi + E_{1\phi}(\rho, \phi, 0)\sin\psi. \quad (28)$$

When ψ is small, E_x is dominated by $E_{1\phi}(\rho, \phi, 0)$. E_y by $E_{1\rho}(\rho, \phi, 0)$. The measured data of Young and Cox²⁴ are shown by the boxes in their Fig. 3 which is reproduced here as part of Fig 2. $|E_x|$ is seen to decrease rapidly and smoothly as the frequency is increased from 0.25 to 2.25 Hz. On the other hand, $|E_y|$ increases to a maximum near $f = 1$ Hz and then decreases. Together with their measured data, Young and Cox²⁴ also showed numerically calculated graphs of $|E_x|$ and $|E_y|$ for a lithosphere represented successively by (a) a homogeneous isotropic half-space with $\sigma_2 = 0.004$ S/m (dotted lines), and (b) a stack of eight horizontal layers in a total depth of 33 km (dashed and solid-line curves), as depicted in their Fig. 4. All four graphs of $|E_x|$ are reproduced in Fig. 2. Although they are calculated for four very different models, they differ negligibly from one another and all agree well with the measured values. The corresponding graphs of $|E_y|$ differ significantly from one another and only the one "best-fit" curve (in solid lines) agrees reasonably well with the measured data. All have maxima but these occur at different frequencies: that for the half-space model with

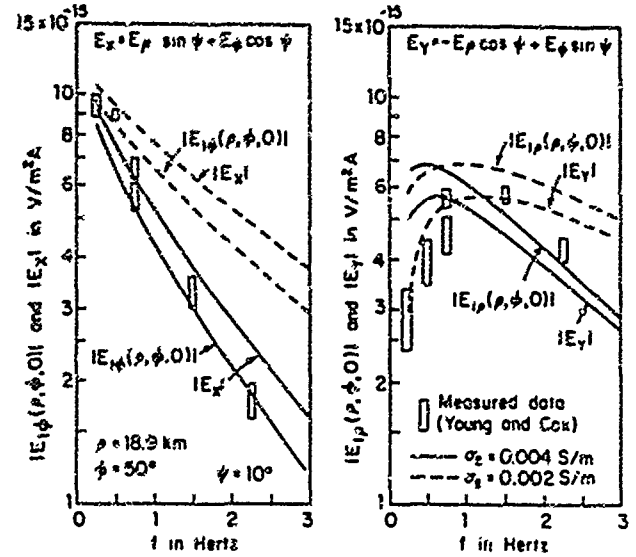


FIG. 3. $|E_{1\rho}(\rho, \phi, 0)|$ and $|E_{1\phi}(\rho, \phi, 0)|$ calculated from Eqs. (8) and (9); $|E_x|$ and $|E_y|$ with measured data of Young and Cox (Ref. 24).

$\sigma_2 = 0.004$ S/m is near $f = 0.5$ Hz; that for the "best fit" is near $f = 1$ Hz.

The comparison of the numerically calculated fields for the four models with the measured data and the selection of a "best-fit model" raise interesting questions. First, why is the frequency dependence of E_x different from that of E_y ? Second, how can E_y be sensitive to all eight layers whereas E_x is not? $|E_x|$ as calculated for the half-space model is in good agreement with the measurements and the presence of the hypothetical eight layers with any one of three different combinations of conductivity has virtually no effect on the field. If only $|E_x|$ had been measured, the obvious conclusion would have been that the lithosphere is a homogeneous isotropic half-space with $\sigma_2 = 0.004$ S/m. For $|E_y|$ the situation is very different. The field of the half-space model with $\sigma_2 = 0.004$ S/m is in poor agreement with measurements, its maximum is clearly at the wrong frequency, and the three different layered models all lead to different fields—all in better agreement with the measurements than the half-space model. It is from E_y that the "best-fit" layered model was selected. But how can E_x be almost totally transmitted through, while E_y is significantly reflected from some or all of the laterally homogeneous layers?

The entire problem is illuminated with the help of the integrated formulas (8) and (9). For the range $0.25 < f < 3$ Hz, $\sigma_1 = 3.2$ S/m, the specified distance $\rho = 18.9$ km between transmitting and receiving antennas, and $z = d = 1$ m, all contributions from direct and reflected fields are negligible, the same is true of the Fresnel-integral term of the lateral-wave field. Also, $e^{ik_1 d} \sim 1$. It follows that the complete accurate expressions for the components (8) and (9) are

$$E_{1\rho}(\rho, \phi, 0) = \frac{\cos\phi}{2\pi\sigma_1} e^{ik_1\rho} \left(\frac{1}{\rho^3} - \frac{ik_2}{\rho^2} - \frac{k_2^2}{\rho} \right) = -\frac{i\cos\phi}{2\pi\sigma_1} \frac{e^{-\alpha_1\rho} e^{i\alpha_2\rho}}{\rho^3} [\alpha_2\rho + 2\alpha_2^2\rho^2 + i(1 + \alpha_2\rho)], \quad (29a)$$

$$E_{1\phi}(\rho, \phi, 0) = \frac{\sin\phi}{\pi\sigma_1} e^{ik_1\rho} \left(\frac{1}{\rho^3} - \frac{ik_2}{\rho^2} \right) = -\frac{i\sin\phi}{\pi\sigma_1} \frac{e^{-\alpha_1\rho} e^{i\alpha_2\rho}}{\rho^3} [\alpha_2\rho + i(1 + \alpha_2\rho)], \quad (29b)$$

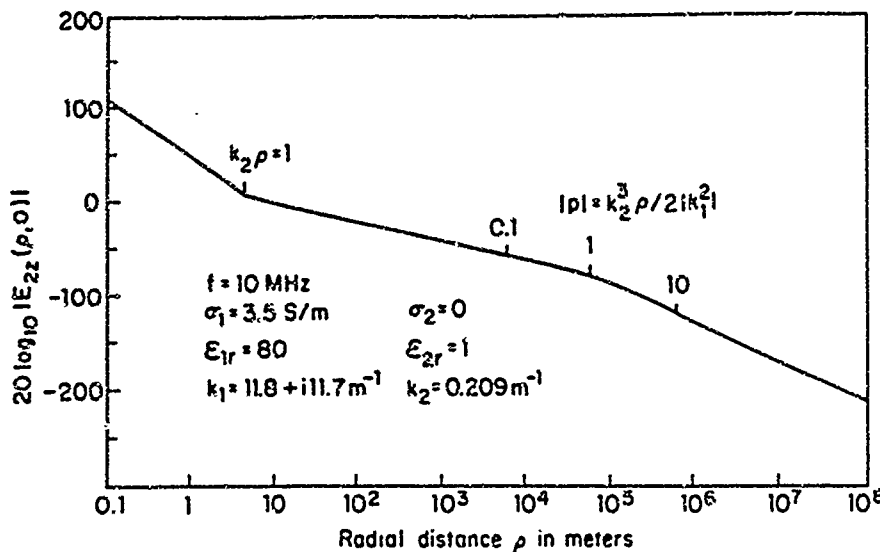


FIG. 4. $E_z(\rho, 0)$ of vertical unit dipole in air (Region 2) on the surface of sea water (Region 1); $f = 10$ MHz.

where $k_2 = (1 + i\alpha_2)$; $k_2^2 = 2i\alpha_2^2$; $\alpha_2 = (\omega\mu_0\sigma_2/2)^{1/2}$. $|E_{1\rho}(\rho, \phi, 0)|$ has a maximum at $\alpha_2\rho = (1 + \sqrt{5})/2 = 1.618$. With $\rho = 18.9$ km, this gives $f_m\sigma_2 = 1.84 \times 10^{-3}$, so that with $\sigma_2 = 0.004$ S/m, $f_m = 0.46$ Hz in precise agreement with the calculated graph of Young and Cox shown in Fig. 2 in dotted line. The maximizing frequency for $\sigma_2 = 0.002$ S/m is $f_m = 0.92$ Hz.

The angles ϕ and ψ are not given by Young and Cox. With the choice $\phi = 50^\circ$ and $\psi = 10^\circ$, graphs calculated from Eqs. (29a) and (29b) with Eqs. (27) and (28) of $|E_{1\rho}(\rho, 50^\circ, 0)|$ and $|E_Y|$, and of $|E_{1\phi}(\rho, 50^\circ, 0)|$ and $|E_X|$, are shown in Fig. 3 for both $\sigma_2 = 0.004$ S/m and $\sigma_2 = 0.002$ S/m. It is evident from these graphs that in order to have a maximum of $|E_Y|$ near $f = 1$ Hz to agree with the measured data of Young and Cox, it is necessary to choose $\sigma_2 = 0.002$ S/m. On the other hand, in order to have $|E_X|$ agree with the measured data, it is necessary that $\sigma_2 = 0.004$ S/m. If measurements had been restricted to E_Y [or better to $E_{1\rho}(\rho, 0, 0)$ as in the work of Chave and Cox²³], the good agreement with the measured data would suggest that the *half-space model* with $\sigma_2 = 0.002$ S/m is correct. On the other hand, if only E_X [or better $E_{1\phi}(\rho, \pi/2, 0)$] had been measured, the equally good agreement with the measured data would indicate a *half-space model* with $\sigma_2 = 0.004$ S/m. No reflecting layers are indicated in either case. If both E_X and E_Y are measured as by Young and Cox,²⁴ the two conclusions are inconsistent and the choice $\sigma_2 = 0.004$ S/m is made to agree with the half-space model for E_X and a particular eight-layered region in a depth of 33 km is designed to agree with E_Y . This leaves unresolved the fact that none of the three eight-layered models has any significant effect on $|E_X|$. Since $E_X \sim E_\phi$ and $E_Y \sim -E_\rho$ with ψ small, the essential difference between E_X and E_Y is that the former (of magnetic type with B_ρ, B_z) is perpendicular, the latter (of electric type with E_ρ, E_ϕ) is parallel to the plane of incidence with respect to partial reflection from any horizontal surface. Since the reflection coefficients for the two polarizations have opposite signs but almost equal magnitudes for small angles of incidence, it is necessary that the electric-type reflections reaching the point of observation from the several layers effectively cancel or that there be no reflections of electric type from

any of the eight boundaries. This is difficult to visualize for all three models at all frequencies.

A possible alternative model is suggested by the observation that E_{1Y} is in good agreement with measurements when $\sigma_2 = 0.002$ S/m and simultaneously E_{1X} is in good agreement with measurements when $\sigma_2 = 0.004$ S/m. (Region 1 is sea water, Region 2 is rock.) Note that with the angle ψ small, $E_X \sim E_\phi$ and $E_Y \sim -E_\rho$; also, E_ρ, E_z , and B_ϕ are a field of electric type; E_ϕ, B_ρ , and B_z a field of magnetic type. Furthermore, the two parts of the field, while not independent, are not closely coupled, so that the components $E_{1\rho} \sim -E_{1Y}$ and E_{1z} could be determined by the large component $E_{2z} = J_{2z}/\sigma_{2z}$ while $E_{1\phi} \sim E_{1X}$ is determined by $E_{2\phi} \sim E_{2X} = J_{2X}/\sigma_{2X}$. These considerations and the measurements of Young and Cox²⁴ suggest that σ_z might actually have somewhat different values for the z -directed currents in the lithosphere $J_{2z} = \sigma_z E_{2z}$ which determine E_{1z} and $E_{1\rho} \sim -E_{1Y}$ than for the ϕ -directed currents $J_{2\phi} = \sigma_z E_{2\phi}$ which determine $E_{1\phi} \sim E_{1X}$. It seems quite possible that all measured data would be well satisfied by a half-space model of the lithosphere that is homogeneous but one-dimensionally anisotropic, with $\sigma_{2X} = \sigma_{2Y} = 0.004$ S/m and $\sigma_{2z} = 0.002$ S/m. This model actually fits into the assumption of purely horizontal layering but the layers consist of a stack of relatively thin horizontal slabs with conductivities that alternate between $\sigma_X = \sigma_Y = 0.004$ S/m and a lower value such that the effective conductivity $\sigma_z = 0.002$ S/m. Such a model requires no reflections from deeper, widely spaced horizontal layers to explain the observed data.

An analytical study of the one-dimensionally anisotropic half-space beginning with Maxwell's equations and paralleling the analysis^{22,23,26} for the isotropic half-spaces has been completed and will be published. It confirms the validity of the half-space model with $\sigma_{2X} = \sigma_{2Y} = 0.004$ S/m and $\sigma_{2z} = 0.002$ S/m. It also provides answers to previously raised questions regarding the different behavior of E_X and E_Y .

Anisotropy in conductivity is found in various stratified media including alternating layers of dense rock with low conductivity and less dense rock with higher conductivity. In such media the conductivity transverse to the bedding

surfaces is always smaller than that along the bedding surfaces.³¹ For horizontal bedding surfaces this means that σ_{2x} is smaller than $\sigma_{2y} = \sigma_{2z}$, e.g., $\sigma_{2x} = 0.002$ S/m, $\sigma_{2y} = \sigma_{2z} = 0.004$ S/m. Anisotropy in conductivity is also found in only slightly stratified hard clay (for which a conductivity ratio of 2 is appropriate) and in rocks with different conductivities along the principal crystallographic axes. It may be added that an inclined stratification must also exhibit different conductivities to the horizontal components of current parallel to the bedding surfaces and the vertical component J_z .

IV. USEFUL CHARACTERISTICS OF THE NEW FORMULAS FOR THE TWO-LAYER PROBLEM

The dominant lateral-wave parts of the electromagnetic field of a vertical or horizontal electric dipole near the sea floor have properties that are useful for studying the earth's crust near the sea bottom. Some of these are described in the following.

A. Vertical dipole

Consider first the vertical electric dipole with unit electric moment ($Ih_e = 1$ A m) located at $d = 0$ in Region 2 (air; $z < 0$) on the boundary of Region 1 (earth, sea; $z > 0$). The rotationally symmetric electromagnetic field on the boundary ($z = 0$) in air consists of the following three components in cylindrical coordinates:

$$E_{2\rho}(\rho, 0) = -\frac{\omega\mu_0}{2\pi k_1} f(k_2\rho, k_1) e^{ik_1\rho} = \frac{\omega}{k_1} B_{2\phi}(\rho, 0), \quad (30)$$

$$E_{2z}(\rho, 0) = \frac{\omega\mu_0}{2\pi k_2} g(k_2\rho, k_1) e^{ik_2\rho}, \quad (31)$$

where $f(k_2\rho, k_1)$ and $g(k_2\rho, k_1)$ are defined in Eq. (5). Since the ratio $E_{2\rho}(\rho, 0)/E_{2z}(\rho, 0) = -k_2 f(k_2\rho, k_1)/k_1 g(k_2\rho, k_1)$, it follows that—except very close to the source— $E_{2z}(\rho, 0)$ is the dominant component of the elliptically polarized electric field. Note that when Region 2 is air, $\omega\mu_0/2\pi k_2 = 60\Omega$. This includes the factor $Ih_e = 1$ A m.

When $k_2\rho > 8|k_1^2/k_2^2|$, the function $\mathcal{F}(k_2\rho, k_1)$ in $f(k_2\rho, k_1)$ and $g(k_2\rho, k_1)$ cancels both the exponential and the square root preceding it in Eq. (5) and the resulting expression includes the term $-ik_2/\rho$. The simple result is

$$f(k_2\rho, k_1) \sim g(k_2\rho, k_1) = -\frac{1}{\rho^2} \left(\frac{k_1^2}{k_2^2} + 1 \right) \sim -\frac{k_1^2}{k_2^2 \rho^2}, \quad (32)$$

so that, for $k_2\rho > 8|k_1^2/k_2^2|$,

$$E_{2z}(\rho, 0) \sim -\frac{\omega\mu_0 k_1^2}{2\pi k_2^2} \frac{e^{ik_1\rho}}{\rho^2}, \quad (33)$$

$$E_{2\rho}(\rho, 0) \sim -(k_2/k_1) E_{2z}(\rho, 0). \quad (34)$$

A graph of $20 \log_{10}|E_{2z}(\rho, 0)|$ as calculated from Eq. (31) at $f = 10$ MHz is shown in Fig. 4 for an air-sea boundary. In general, there are three distinct ranges in terms of the radial distance ρ . These are the *near field*, defined by $k_2\rho < 1$, where $E_{2z}(\rho, 0) \sim 1/\rho^3$; the *intermediate field*, defined by $1 < k_2\rho < 8|k_1^2/k_2^2|$, where $E_{2z}(\rho, 0) \sim 1/\rho$; and the *asymptotic field*, defined by $k_2\rho > 8|k_1^2/k_2^2|$, where $E_{2z}(\rho, 0) \sim 1/\rho^2$. Note that the rate of decrease in amplitude with radial dis-

tance is independent of k_1 in each of the three ranges. Only in a transition range from the intermediate to the asymptotic field, where the amplitude factor changes in a manner that involves k_1 , is the decay rate with radial distance dependent on k_1 . As shown in Fig. 4, the radial range characterized by $0.1 < |p| < 10$, where $|p|$ is the magnitude of the "numerical distance" $p = ik_1^2 \rho / 2k_2^2$, encompasses the transition region that is described by Norton's graphs (Fig. 1). In this relatively small range the decay rate is complicated in that it changes from $1/\rho$ to $1/\rho^2$ in a manner that involves k_1 . Over all parts of the entire range except in this region of transition, $E_{2z}(\rho, 0)$ behaves very simply; $E_{2z}(\rho, 0) \sim e^{ik_1\rho}/\rho^3$, $e^{ik_1\rho}/\rho$, $e^{ik_2\rho}/\rho^2$, respectively, in the near, intermediate, and asymptotic zones. As shown in Fig. 5, such ranges exist at all frequencies with differences that involve a shifting of the transition regions and an expansion or contraction of the ranges between and beyond them. It is in terms of the simple and quite accurate relations:

$$g(k_2\rho, k_1) \sim \frac{ik_2}{\rho} - \frac{1}{\rho^2} - \frac{i}{k_2\rho^3}; \quad |k_2/k_1| < \rho < 8|k_1^2/k_2^2|, \quad (35)$$

$$g(k_2\rho, k_1) \sim -\frac{k_1^2}{k_2^2 \rho^2}; \quad 8|k_1^2/k_2^2| < k_2\rho < \infty, \quad (36)$$

that new tools can be found for geophysical prospecting. Moreover, since the decay rate with radial distance of $E_{2z}(\rho, 0)$ is independent of k_1 except in the transition range near $k_2\rho = 8|k_1^2/k_2^2|$, this region is severely restricted in its usefulness for the determination of k_1 . Its use even in the transition range is hampered by the lack of spread of Norton's curves (Fig. 1).

An insulated vertical antenna that extends all the way from the floor to the surface of the ocean has been proposed³²⁻³⁴ for generating a magnetic field along the sea floor which can be measured to determine the conductivity σ_2 of the suboceanic crust. The method is designed for very low frequencies ($< 1/32$ Hz) for which the depth $D \sim 2$ km of the ocean satisfies the inequality $|k_1 D| < 2$. With $k_2 \sim 0.1k_1$, the measurements are in the range $\rho < 20$ km or $k_2\rho < 2$. The

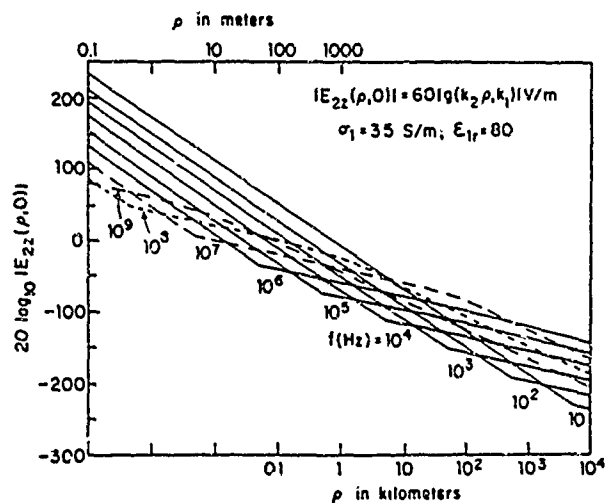


FIG. 5. Magnitude of $E_{2z}(\rho, 0)$ due to a vertical unit electric dipole in air above the surface of sea water; $f = 10^{-10^9}$ Hz.

fields along the boundaries between the sea and the air and between the sea and the sea floor are due entirely to surface waves since the direct and reflected fields cancel. In particular, the magnetic field on the sea floor generated by the vertical antenna when carrying a current I_z such that $I_z D = 1$ A m is given by

$$B_{1z}^L(\rho, 0) = -\frac{\mu_0}{2\pi k_1^2} \left[\left(\frac{ik_2^2}{\rho} - \frac{k_2^2}{\rho^2} \right) e^{ik_2 \rho} + \left(\frac{ik_0^2}{\rho} - \frac{k_0^2}{\rho^2} \right) e^{ik_0 \rho} e^{ik_1 D} \right]. \quad (37)$$

(Note that multiple reflections between the two bounding surfaces are negligible since $e^{-2\alpha_1 D} = 0.06$.) The first term in Eq. (37) is the lateral wave in the lithosphere along the sea floor with $k_2 = \beta_2 + i\alpha_2 = (1+i)(\omega\mu_0\sigma_2/2)^{1/2}$; the second term is the lateral wave in air along the surface of the sea with $k_0 = \omega/c$. This latter is negligible since $e^{-\alpha_1 D} = 0.24$ and $k_0 \ll k_2$. The conductivity σ_2 is readily determined from measured values of $|B_{1z}|$ as a function of ρ in the simple form given by the first term in Eq. (37).

B. Horizontal dipole

For applications on the sea bottom where Region 1 is salt water ($z \geq 0$) and Region 2 is rock or sediment ($z < 0$), the source and the points of observation of the field are advantageously kept in the sea water if only for practical reasons of deployment and mobility. Since the field of a unit horizontal electric dipole in sea water at the ocean bottom is an order of magnitude greater than the field of a unit vertical dipole at the same location, it is desirable to examine its properties. The electromagnetic field of an x -directed horizontal dipole located in Region 1 (sea water) at a small distance d from the boundary with Region 2 (rock, sediment) has the six components given in Eqs. (8)–(13). These can be separated into two groups of three. Except close to the source, the dominant group is that of electric type with $E_{1\rho}(\rho, \phi, z)$, $E_{1z}(\rho, \phi, z)$, and $B_{1\phi}(\rho, \phi, z)$. The lateral-wave parts of these are

$$E_{1\rho}^L(\rho, \phi, z) = -\frac{\omega\mu_0 k_2}{2\pi k_1^2} g(k_2 \rho, k_1) e^{ik_2 \rho} e^{ik_1(z+d)} \cos \phi$$

$$= \frac{\omega}{k_1} B_{1\phi}(\rho, \phi, z), \quad (38a)$$

$$E_{1z}^L(\rho, \phi, z) = \frac{\omega\mu_0 k_2^2}{2\pi k_1^3} f(k_2 \rho, k_1) e^{ik_2 \rho} e^{ik_1(z+d)} \cos \phi, \quad (38b)$$

where $f(k_2 \rho, k_1)$ and $g(k_2 \rho, k_1)$ are given in Eq. (5) and approximated in Eq. (32) for large $k_2 \rho$. Note that the ratio $E_{1\rho}^L(\rho, \phi, z)/E_{1z}^L(\rho, \phi, z) = -k_2 g(k_2 \rho, k_1)/k_2 f(k_2 \rho, k_1)$ so that $E_{1\rho}^L(\rho, \phi, z)$ dominates except very close to the source. The second group of components of magnetic type includes $E_{1\phi}(\rho, \phi, z)$, $B_{1\rho}(\rho, \phi, z)$, and $B_{1z}(\rho, \phi, z)$. In the electrical near-field and a short distance beyond, $E_{1\phi}(\rho, \phi, z)$ is comparable

to $E_{1\rho}(\rho, \phi, z)$ and equally useful for purposes of measurement. However, since none of the components in the second group has an intermediate range in which the field decreases as $e^{ik_2 \rho}/\rho$, $E_{1\phi}(\rho, \phi, z)$ decreases with distance much more rapidly than $E_{1\rho}(\rho, \phi, z)$. Therefore, the latter is to be preferred when larger electrical distances are involved.

The expression (38a) for $E_{1\rho}^L(\rho, \phi, z)$ reveals an important property of lateral waves: The radial decrease in amplitude along the surface of Region 1 (sea water) is insensitive to $k_1 = \beta_1 + i\alpha_1 = \omega[\mu_0(\epsilon_1 + i\sigma_1/\omega)]^{1/2}$ but potentially very sensitive to $k_2 = \beta_2 + i\alpha_2 = \omega[\mu_0(\epsilon_2 + i\sigma_2/\omega)]^{1/2}$. This is of no interest when Region 2 is air with $\alpha_2 = 0$. But when Region 2 is rock or sediment on the bottom of the sea, the possibilities are very interesting. With $\phi = 0$ and $z + d$ kept small and constant [$(z + d) \sim 0$],

$$E_{1\rho}^L(\rho, 0, 0) \sim -\frac{\omega\mu_0 k_2}{2\pi k_1^2} g(k_2 \rho, k_1) e^{-\alpha_2 \rho} e^{ik_2 \rho}. \quad (39)$$

When $|k_2 \rho| < 1$, $g(k_2 \rho, k_1) \sim (-i/k_2 \rho^3)$, $e^{ik_2 \rho} \sim 1$ so that the quasi-static field is

$$E_{1\rho}^L(\rho, 0, 0) \sim \frac{i\omega\mu_0}{2\pi k_1^2 \rho^3}. \quad (40)$$

Since it is independent of k_2 , it is useless for the determination of k_2 . This range is indicated in Fig. 6 which is a representation of Eq. (39) for three values of σ_2 . The location of $|k_2 \rho| = 1$ is shown for each. The quasi-static form (40) corresponds to the straight line well to the left of the points $|k_2 \rho| = 1$.

When $|k_2 \rho|$ becomes greater than 1, $g(k_2 \rho, k_1) \sim ik_2/\rho$ so that

$$E_{1\rho}^L(\rho, 0, 0) \sim -\frac{i\omega\mu_0 k_2^2}{2\pi k_1^2} \frac{e^{-\alpha_2 \rho} e^{ik_2 \rho}}{\rho};$$

$$1 < |k_2 \rho| < 8 |k_1^2/k_2^2|. \quad (41)$$

The radial decrease in amplitude is governed by $e^{-\alpha_2 \rho}/\rho$. The behavior of the quantity $20 \log_{10} |E_{1\rho}^L(\rho, 0, 0)|$ as a function of the radial distance ρ at selected fixed frequencies is shown in Figs. 6 and 7, as a function of the frequency at selected radial distances in Fig. 8. The rapid exponential decrease is seen to be critically dependent on σ_2 when this is not too small. Clearly, the observation of the range of ρ and f where the decrease occurs is a promising means for the determination of σ_2 or α_2 .

V. THE DETERMINATION OF THE CONDUCTIVITY AND PERMITTIVITY OF AN IDEALIZED TWO-LAYERED SEA BOTTOM

For initial simplicity it is advantageous to consider an idealized sea bottom that consists of a smooth plane boundary between sea water and rock or sediment, the effect of a boundary surface that is not smooth is considered in Sec. VII. The depth of the sea water and of the rock or sediment are required to be sufficient so that each is well approximated by a half-space. This excludes very shallow water and applies only to a layer of sediment that is either electrically so thin that it can be ignored or is so thick that reflections from

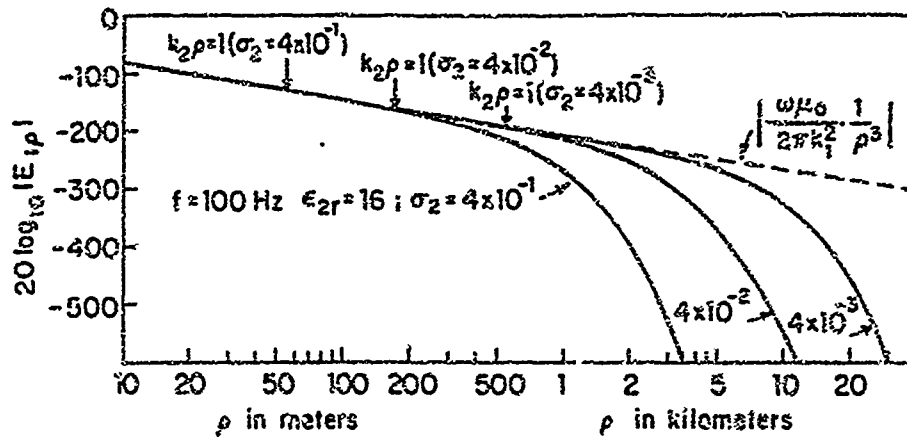


FIG. 6. Radial electric field at $z = 15$ cm in sea water ($\sigma_1 = 3.5$ S/m, $\epsilon_1 = 80$) above rock or deep sediment ($\sigma_2, \epsilon_2 = 16$) as a function of radial distance from unit horizontal electric dipole at height $d = 15$ cm above sea bottom; $f = 100$ Hz.

the rock beyond it are negligible. The intermediate three-layer problem—which applies specifically to a layer of sediment with arbitrary thickness between sea water and rock—has been analyzed by Dunn.³⁵⁻³⁷ Formulas corresponding to Eqs. (8)–(13) have been obtained and will be applied in later work to develop methods for measuring the conductivity and permittivity of rock when this is covered by a layer of sediment with electrical properties intermediate to those of rock and sea water. Methods to determine the thickness and conductivity of the sediment will also be sought. *Only the limiting cases of the three-layer problem when the intermediate layer is either very thick or very thin are treated in this paper.* They provide an essential background for understanding the significantly more complicated general case. Earlier analyses of the three-layer problem³²⁻⁴¹ are concerned primarily with a waveguide-like structure consisting of a low-conductivity layer bounded above and below by half-spaces with high conductivity.

The formula (38a) for the radial electric field of a horizontal electric dipole at a height d in sea water (Region 1, $z > 0$) above a half-space of rock or sediment (Region 2, $z < 0$) represents a lateral wave that proceeds downward from the source in the sea water ($e^{ik_1 d}$), then horizontally along the boundary in the rock or sediment [$g(k_2 \rho, k_1) e^{ik_2 \rho}$], and finally upward in the sea water to the point of observation ($e^{ik_1 z}$). The total phase change is $\beta_1(z + d) + \beta_2 \rho$. The decrease in amplitude is $e^{-\alpha_1(z+d)} e^{-\alpha_2 \rho} |g(k_2 \rho, k_1)|$. The significant observation regarding these simple relations is that they provide the means for determining α_2 and β_2 for the rock or sediment from measurements made only in the adjacent accessible sea water. From α_2 and β_2 , ϵ_2 , and σ_2 are readily calculated since $(\beta_2 + i\alpha_2)^2 = \omega^2 \mu_0 \epsilon_2 + i\omega \mu_0 \sigma_2$ so that

$$\epsilon_2 = (\beta_2^2 - \alpha_2^2) / \omega^2 \mu_0, \quad \sigma_2 = 2\alpha_2 \beta_2 / \omega \mu_0. \quad (42)$$

When $\sigma_2 \gg \omega \epsilon_2$ as at low frequencies and high conductivities, $\beta_2 \sim \alpha_2$, ϵ_2 is irrelevant, and

$$\sigma_2 = 2\alpha_2^2 / \omega \mu_0. \quad (43)$$

The graphs in Figs. 6 and 7 show $|E_{1\rho}^L(\rho, 0, z)|$ as a function of ρ at $f = 0.1, 1, 10$, and 100 kHz. They include ranges with a significant exponential decay given by $|e^{ik_2 \rho}| = e^{-\alpha_2 \rho}$. An alternative, shown in Fig. 8, is $|E_{1\rho}^L(\rho, 0, z)|$ as a function of the frequency at selected radial distances, but with $(z + d)$ sufficiently small so that $|e^{ik_1(z+d)}| \sim 1$. In both cases σ_2 is the parameter. At the lower frequencies and higher conductivities, the graphs in Fig. 8 are similar to those in Fig. 7. Since α_2 is not linear in the frequency and decreases to small values when σ_2 is reduced, $e^{-\alpha_2 \rho}$ with ρ fixed has a rapid decrease only when $\alpha_2 \sim (\omega \mu_0 \sigma_2 / 2)^{1/2}$ and approaches unity when $\sigma_2 \ll \omega \epsilon_2$. This behavior is illustrated in Fig. 9 which shows α_2 / β_2 as a function of the frequency. A rapid exponential decay occurs only in ranges where α_2 / β_2 is not much smaller than one. When $\sigma_2 \gg \omega \epsilon_2$, the factor k_2^2 / k_1^2 which occurs in the expression (41) for $E_{1\rho}^L(\rho, 0, 0)$ in the intermediate zone reduces to σ_2 / σ_1 , which is independent of the frequency, so that when $\alpha_1(z + d) \ll 1$,

$$E_{1\rho}^L(\rho, 0, 0) \sim \frac{i\omega \mu_0 \sigma_2}{2\pi \sigma_1 \rho} e^{-\alpha_1 \rho} e^{i\beta_1 \rho}. \quad (44)$$

This is essentially what is represented in Fig. 8 when σ_2 is not too small and f not too high so that a rapid exponential decay with frequency occurs. Where this is true, the graphs of Fig. 8 are as useful as those of Figs. 6 and 7 for determining α_2 .

The graphs of $E_{1\rho}$ in Fig. 8(d) are an expanded form—on a dB scale—of the numerically calculated results shown by Chave and Cox²³ in their Fig. 2. The data for $\rho = 1, 2$, and

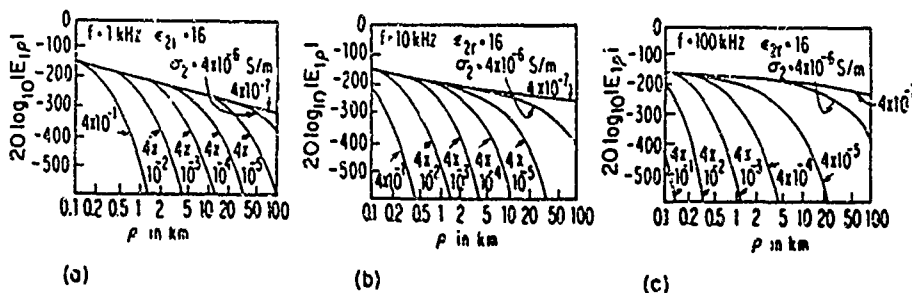


FIG. 7. Radial electric field at $z = 15$ cm in seawater ($\sigma_1 = 4$ S/m, $\epsilon_1 = 80$) above rock or deep sediment ($\sigma_2, \epsilon_2 = 16$) as a function of radial distance from unit horizontal electric dipole at height $d = 15$ cm above sea bottom. (a) $f = 1$ kHz, (b) $f = 10$ kHz, (c) $f = 100$ kHz.

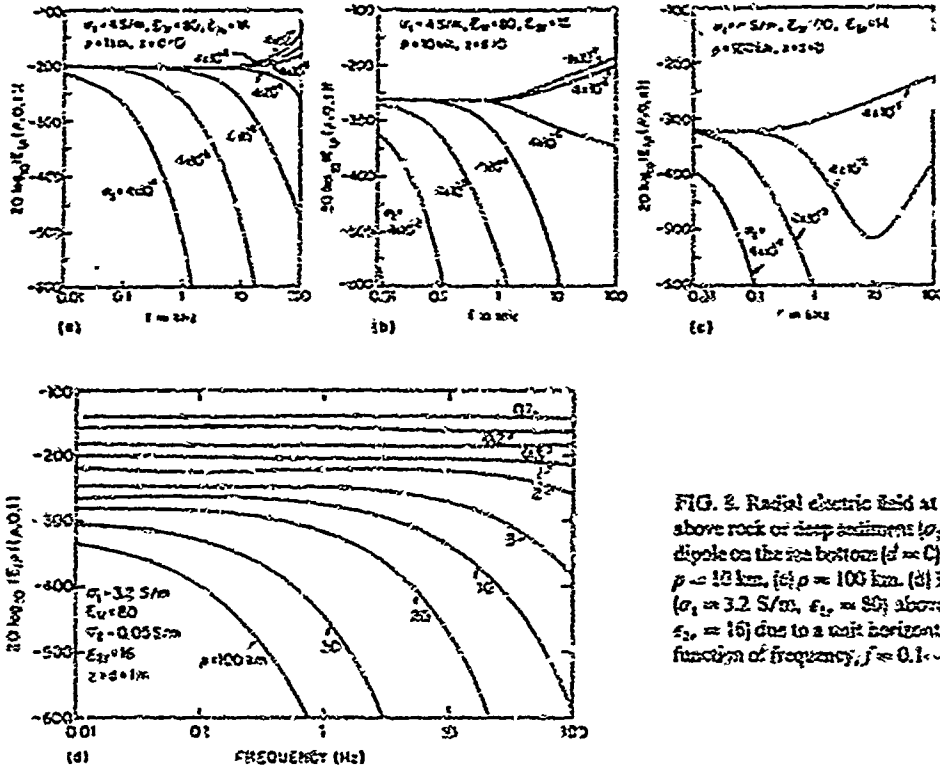


FIG. 8. Radial electric field at $x = 0$ in sea water ($\sigma_1 = 3.2$ S/m, $\epsilon_1 = 80$) above rock or deep sediment ($\sigma_2, \epsilon_2 = 16$) due to a unit horizontal electric dipole on the sea bottom ($d = 0$) as a function of frequency. (a) $\rho = 1$ km, (b) $\rho = 10$ km, (c) $\rho = 100$ km. (d) Radial electric field at $x = 1$ m in sea water ($\sigma_1 = 3.2$ S/m, $\epsilon_1 = 80$) above rock or deep sediment ($\sigma_2 = 0.05$ S/m, $\epsilon_2 = 16$) due to a unit horizontal dipole at $d = 1$ m above sea bottom as a function of frequency, $f = 0.1 - 100$ kHz.

5 km are in quantitative agreement. Corresponding sets of curves for the other five components of the field were also calculated from the simple formulas (8)–(13) but are not shown. Note that there is no need to calculate the phase since in the range of interest where the lateral-wave part of the field dominates, it is contained in the simple term $e^{i\beta_2 \rho}$ in $e^{i\beta_2 \rho} = e^{-\alpha_2 \rho} e^{i\beta_2 \rho}$.

5. The measurement of α_2

A schematic diagram of an apparatus for carrying out measurements from which α_2 of the sea bottom can be determined is included in Fig. 10. It is similar to that used by

Young and Cox²⁴ in that it consists of a transmitting antenna in the form of an insulated conductor lying on the bottom of the ocean with its axis in the direction $\phi = 0$ along which observations are to be made. Power to the antenna is supplied by a cable to the surface where a boat or float is located. The antenna generates an electromagnetic field that is complicated near the antenna, but is limited to a surface wave beyond a short distance. Its dominant components are $E_{1\rho}(\rho, \phi, z)$ as given by Eq. (38a) and $B_{1\phi}(\rho, \phi, z)$. These have their maxima in the direction $\phi = 0$ along the axis of the antenna. In order to determine α_2 in $k_2 = \beta_2 + i\alpha_2$, measurements are needed that permit the construction of graphs like those in Figs. 6 and 7 or like those in Fig. 8. This can be

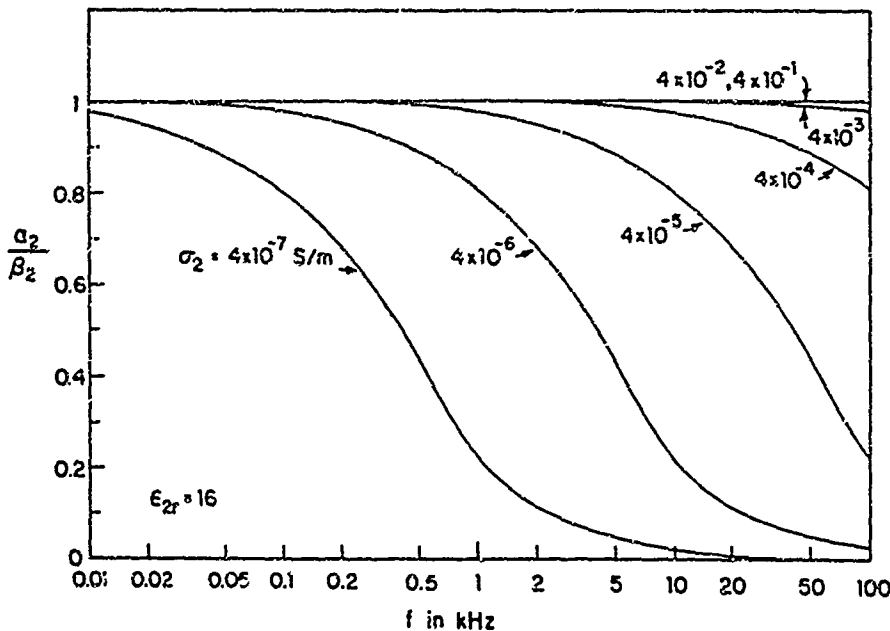


FIG. 9. Ratio of attenuation to phase constant in $k_2 = \beta_2 + i\alpha_2$ for $E_{1\rho}$ in sea water bounded by rock or sediment.

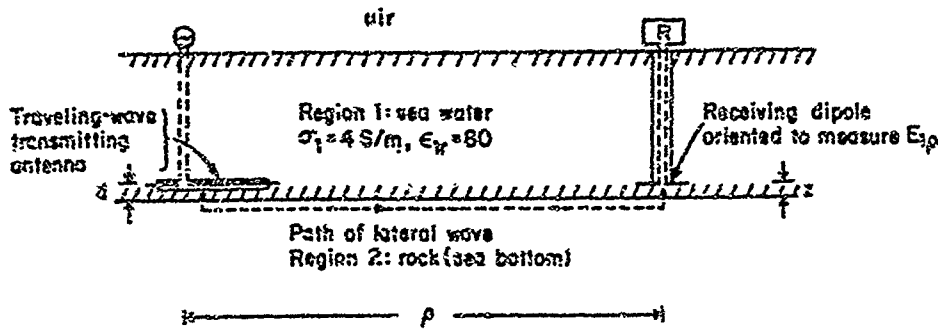
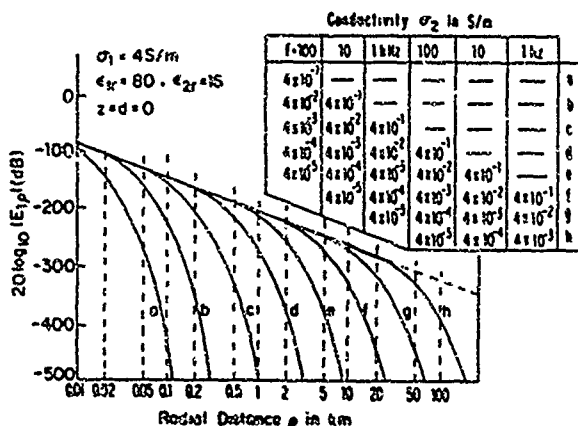


FIG. 10. Schematic diagram of directional transmitter and receiver near the bottom of the sea.

accomplished by lowering a receiving dipole to the bottom of the ocean at a succession of known radial distances (or by dragging a suitably protected antenna along the bottom) and observing $|E_{1\rho}(\rho, 0, z)|$ at each location at selected frequencies. From these data, graphs can be constructed of the measured relative values of $20 \log_{10} |E_{1\rho}(\rho, 0, z)|$ both as functions of the radial distance at each frequency and as functions of the frequency at each radial distance. The particular curve that includes a rapid exponential decrease with increasing radial distance or increasing frequency can then be used to determine α_2 . The calculation of α_2 from curves like Figs. 6 and 7 in conjunction with Eq. (39) is simpler since when ρ is the variable at a fixed frequency, k_1 is a constant. On the other hand, when f is the variable, k_1 also varies but it is known quite accurately for salt water at each frequency. Note that in Eq. (44), which is adequate in the useful range of the frequency, the frequency dependence on k_1 disappears when $(z+d)$ is sufficiently small.

Alternatively, and especially in the ranges $0.1 < f < 100$ kHz, $4 \times 10^{-5} < \sigma_2 < 0.4$ S/m, the graphs in Figs. 6 and 7 can be combined and extended into the single set shown in Fig. 11. Here each curve can represent up to six combinations of frequency and conductivity and σ_2 can be determined by interpolation between adjacent measured curves.

It is interesting to note that the numerically calculated graph of $E_{1\rho}$ in Fig. 4 of the paper by Chave and Cox²³ agrees exactly with the piece of the curve g in Fig. 11 between $\rho = 0.5$ and $\rho = 15$ km. Furthermore, their numerically calculated graph for the phase of $E_{1\rho}$ agrees with $\beta_2 \rho$ in the exponential factor $e^{ik_2 \rho} = e^{-\alpha_2 \rho} e^{i\beta_2 \rho}$.



The last step is valid when $\beta_2^2 \rho_0^2 \gg 1$.

The procedure for measuring β_2 is first to locate the point $\rho = \rho_0$ halfway between the antennas where $|E_{1\rho}(\rho_0, 0, z)| = 0$ and where the receiver at the sea bottom should record a null. This is now moved toward transmitter 2 until a minimum is located at $\beta_2 x = \pi$. From the measured distance x between the null and the first minimum, β_2 is determined from

$$\beta_2 = \pi/x. \quad (50)$$

A check on this value can be obtained from the location at $-x$ of the corresponding minimum toward transmitter 1. This gives $\beta_2 = -\pi/x$.

From the measured values of α_2 and β_2 , σ_2 and ϵ_2 are evaluated from Eq. (42).

VI. THE RANGE OF CONDUCTIVITY OF THE SEA BOTTOM

The graphs in Figs. 6, 7, and 8 represent $20 \log_{10} |E_{1\rho}|$ for values of the conductivity σ_2 that extend from 0.4 to less than 4×10^{-3} S/m. This wide range is considered in order to provide a complete picture of all possibilities to which a two-layer theory might have application. These include only simple situations in which the sea water is separated from a floor of basaltic rock by a layer of sediment that is either electrically sufficiently thin to be ignorable, or thick enough to make reflections from the rock negligible. The intermediate three-layer problem is not included here. The range of conductivities from $\sigma = 4 \times 10^{-3}$ to $\sigma = 4 \times 10^{-1}$ S/m is suggested by selected observations.^{29,32-44} Note that the condition $|k_1/k_2| \gg 3$ can be satisfied in the entire range when the boundary is with sea water where $\sigma \approx 4$ S/m.

In order to determine σ_2 of the sea bottom when this is in the range of $0.4 < \sigma_2 < 4 \times 10^{-3}$ S/m, the graph in Fig. 7(a) for $f = 1$ kHz is useful. It shows that the field at $\rho = 1$ km has the maximum value $20 \log_{10} |E_{1\rho}(\rho, 0, 0)| \sim -200$ dB due to a source with the electric moment $|J_x(0)h_x| = 1$ A m. The location of the exponential decrease—which occurs between $\rho = 1$ km and $\rho = 50$ km—can be determined if measurements can be made down to $20 \log_{10} |E_{1\rho}(\rho, 0, 0)| = -250$ dB per unit electric moment. With a transmitting antenna that is designed to provide an effective electric moment $|J_x(0)h_x| \sim 3 \times 10^5$ A m, the minimum level of -250 dB is raised to -140 dB. The corresponding minimum electric field that must be measured is $|E_{1\rho}(\rho, 0, 0)| \sim 0.1 \mu\text{V/m}$. If the receiving antenna has an effective length of 10 m, the required sensitivity of the receiver is $1 \mu\text{V}$.

If the receiving antenna is located on the sea bottom at successive radial distances between $\rho = 1$ km and $\rho = 50$ km from the source, the radial electric field can be measured at each location. A measured curve with an exponential decay like those in Fig. 7(a) suffices to determine σ_2 if it is in the specified range.

The effect of noise on lateral-wave propagation is treated by deBettencourt.⁴⁵ The design of efficient and practical antennas for use on the sea floor is an important and theoretically involved problem. It will be treated in a separate paper.

VII. PROPAGATION OF LATERAL WAVES IN THE PRESENCE OF IRREGULARITIES AND DISCONTINUITIES IN THE BOUNDING SURFACE

The formulas for the complete electromagnetic field generated by horizontal and vertical dipoles near the boundary between Regions 1 and 2 ($|k_1/k_2| \gg 3$) apply specifically to smooth plane boundary surfaces. The nature of propagation along other types of surfaces has been treated by Bahar,⁴⁶ Beckman,⁴⁷ and Crombie.⁴⁸ But these studies are concerned primarily with the use of observations of the electromagnetic field made in the air above the earth or sea to determine the nature of nonuniformities in the surface or the properties of the earth. The latter is possible for smooth surfaces only in the range of parameters and variables where the decay rate of the field with distance depends on the electrical properties of both the bounding media—a range near $|k_2\rho| \sim |k_1^2/k_2^2|$ —and even here it is not very sensitive to the properties of Region 1. In this range the electromagnetic field depends on the variables and parameters in a very complicated manner so that it is not well suited to a study of the electrical properties of the sea bottom. Specifically, if the wide range over which the electric field depends on the radial distance in the form $e^{i\alpha_2\rho}/\rho$ is selected, a study of the scattering or reflection from and the propagation across discontinuities and irregularities can be carried out in a straightforward manner. Extensive experimental investigations⁴⁹⁻⁵¹ have been carried out in this range in a model tank on the transmission across and reflection from a variety of irregularities and discontinuities along an air-salt water boundary. Theoretical studies⁵² on the reflection of lateral waves from and their transmission across vertical discontinuities and obstacles have also been made. These all indicate that vertical projections and depressions of height L do not significantly affect the propagation of surface waves provided L is electrically small in terms of the wave number k_2 , that is, $|k_2 L| \ll 1$, and their radial distance from the source satisfies $|k_2\rho| > |k_1/k_2|$. The values of L for which $|k_2 L| = 1$ are listed in Table I for a range of frequencies and conductivities. It is seen that these are relatively large so that lateral-wave measurements along a fairly rough and irregular sea bottom should be possible.

VIII. CONCLUSION

New simple formulas, that accurately represent surface wave propagation along a smooth boundary between two homogeneous and isotropic half-spaces with significantly different wave numbers in the range of useful frequencies,

TABLE I. Height L for which the electrical height is $|k_2 L| = 1$

f (kHz)	$L = k_2^{-1} $ in m				
	$\sigma_2(\text{S/m}) = 4 \times 10^{-1}$	4×10^{-2}	4×10^{-3}	4×10^{-4}	4×10^{-5}
0.01	178	560	1780
0.1	56	178	560	1780	...
1	17.8	56	178	560	1780
10	...	17.8	56	178	560
100	17.8	56	110

have been applied to the determination of the conductivity and permittivity of the sea bottom. Since the lateral waves generated by one horizontal electric dipole in the sea and received by another at a radial distance ρ do not penetrate deeply into the ocean floor, they are useful primarily in determining the average conductivity and permittivity of the material fairly close to the boundary. For this, a two-layer theory may be adequate. Since the field of a horizontal electric dipole at a given radial distance along the sea floor includes a lateral wave along the boundary surface and possible reflections of the spherical wave that travels down into the earth from horizontal layers with different conductivities, its use as a source in deep sounding requires careful study. The interesting possibility of an anisotropy in conductivity in the shallow depth sampled by the surface wave, which has now been analyzed,³³ invites serious consideration.

ACKNOWLEDGMENTS

The author is indebted to John G. Heacock for helpful discussions and for supplying important data and references. He also wishes to thank Barbara H. Sandler for carrying out the numerical calculations and Margaret Owens for correcting the manuscript. This research was supported in part by the Office of Naval Research under Contract N00014-79-C-0419 and in part by the Joint Services Electronics Program under Contract N00014-84-K-0465, both with Harvard University.

- ¹G. V. Keller and F. C. Frischknecht, *Electrical Methods in Geophysical Prospecting* (Pergamon, Oxford, England, 1966).
- ²S. W. Maley, in *Electromagnetic Probing in Geophysics*, edited by J. R. Wait (Golem, Boulder, CO 1971), Chap. 2.
- ³J. R. Wait, Ed., *Electromagnetic Probing in Geophysics* (Golem, Boulder, CO, 1971).
- ⁴I. I. Rokityanski, *Geoelectromagnetic Investigation of the Earth's Crust and Mantle* (Springer, Berlin, 1982).
- ⁵K. A. Norton, *Proc. IRE* 29, 623 (1941).
- ⁶R. J. King and S. W. Maley, *Radio Sci. J. Res. NBS* 69D, 1375 (1965).
- ⁷R. J. King and S. W. Maley, *Radio Sci.* 1, 111 (1966).
- ⁸R. J. King, S. H. Cho, D. L. Jaggard, G. E. Bruckner, and C. H. Hustig, *IEEE Trans. Antennas Propagat.* AP-22, 550 (1974).
- ⁹R. J. King, *Radio Sci.* 17, 1103 (1982).
- ¹⁰A. Baños, Jr., *Dipole Radiation in the Presence of a Conducting Half-Space* (Pergamon, Oxford, England, 1966).
- ¹¹A. Wolf, *Geophysics* 11, 518 (1946).
- ¹²J. R. Wait and L. L. Campbell, *J. Geophys. Res.* 58, 21 (1953).
- ¹³J. R. Wait and L. L. Campbell, *J. Geophys. Res.* 58, 167 (1953).
- ¹⁴J. R. Wait, *Can. J. Phys.* 39, 1017 (1961).
- ¹⁵M. Siegel and R. W. P. King, *J. Appl. Phys.* 41, 2415 (1970).
- ¹⁶M. Siegel and R. W. P. King, *IEEE Trans. Antennas Propagat.* AP-19, 477 (1971).
- ¹⁷M. Siegel and R. W. P. King, *IEEE Trans. Antennas Propagat.* AP-21, 507 (1973).
- ¹⁸R. W. P. King and B. H. Sandler, *IEEE Trans. Antennas Propagat.* AP-25, 770 (1977).
- ¹⁹R. W. P. King, B. H. Sandler, and L. C. Shen, *IEEE Trans. Geosci. Remote Sensing* GE-18, 225 (1980).
- ²⁰R. W. P. King and G. S. Smith, *Antennas in Matter* (M.I.T., Cambridge, MA, 1981), Chap. 11.
- ²¹R. W. P. King, J. T. deBettencourt, and B. H. Sandler, *IEEE Trans. Geosci. Electron.* GE-17, 86 (1979).
- ²²T. T. Wu and R. W. P. King, *Radio Sci.* 17, 521 (1982).
- ²³A. D. Chave and C. S. Cox, *J. Geophys. Res.* 87, 3327 (1982).
- ²⁴P. D. Young and C. S. Cox, *Geophys. Res. Lett.* 8, 1043 (1981).
- ²⁵T. T. Wu and R. W. P. King, *Radio Sci.* 17, 532 (1982); *Radio Sci.* 19, 1422 (1984).
- ²⁶R. W. P. King and T. T. Wu, *J. Appl. Phys.* 54, 507 (1983); *J. Appl. Phys.* 54, 3365 (1984).
- ²⁷R. W. P. King, M. Owens, and T. T. Wu, *Radio Sci.* (to be published).
- ²⁸R. W. P. King, *J. Appl. Phys.* 53, 2476 (1982); *J. Appl. Phys.* 56, 3366 (1984).
- ²⁹C. S. Cox and A. D. Chave, "Controlled source electromagnetic exploration of the continental shelves and oceanic lithosphere," presented at the 1983 International IEEE/AP-S Symposium, Houston, Texas (May 1983) (unpublished).
- ³⁰R. W. P. King, L. C. Shen, and T. T. Wu, *Electromagnetics* 1, 51 (1981).
- ³¹E. I. Parkhomenko, *Electrical Properties of Rocks* (Plenum, New York, 1967), pp. 87, 134-136.
- ³²R. N. Edwards, L. K. Law, and J. M. DeLaurier, *J. Geophys. Res.* 86, 11609 (1981).
- ³³R. N. Edwards, D. C. Nobes, and E. Gómez-Treviño, *Geophysics* 49, 566 (1984).
- ³⁴R. N. Edwards, L. K. Law, P. A. Wolfgram, D. C. Nobes, M. N. Bone, D. F. Trigg, and J. M. DeLaurier, *Geophysics* 50, 153 (1985).
- ³⁵J. M. Dunn, "Effect of perfectly conducting top plate on lateral-wave propagation," presented at the 1983 International IEEE/AP-S Symposium, Houston, Texas (May 1983) (unpublished).
- ³⁶J. M. Dunn, "Experimental study of lateral-wave propagation with a conducting top plate," presented at the 1984 International IEEE/AP-S Symposium, Boston, MA (June 1984) (unpublished).
- ³⁷J. M. Dunn, "Lateral waves in three-layered media," presented at the 1984 International IEEE/AP-S Symposium, Boston, MA (June 1984) (unpublished).
- ³⁸L. M. Brekhovskikh, *Waves in Layered Media* (Academic, New York, 1960).
- ³⁹J. R. Wait, *Radio Sci.* 1, 913 (1966).
- ⁴⁰J. R. Wait, in *Antenna Theory, Part II*, edited by R. E. Collin and F. J. Zucker (McGraw-Hill, New York, 1969), Chap. 24.
- ⁴¹J. R. Wait, *Wave Propagation Theory* (Pergamon, New York, 1981), Chap. 13.
- ⁴²G. L. Simmons, L. Caruso, and F. Miller, "Complex dielectric properties of several igneous and metamorphic rocks," Technical Report of Department of Earth and Planetary Sciences, M.I.T., under Contract N00014-76-C-0478 (1980).
- ⁴³M. Talwani, W. Hay, and W. B. F. Ryan, "Deep drilling results in the Atlantic Ocean: Continental margins and paleoenvironment," *Maurice Ewing Series*, Vol. 3 (American Geophysical Union, Washington, DC, 1979).
- ⁴⁴K. Becker, R. P. Von Herzen, T. J. G. Francis, R. N. Anderson, J. Honnorez, A. C. Adamson, J. C. Alt, R. Emmermann, P. O. Kempton, H. Kinoshita, C. Laverne, M. J. Mott, and R. L. Newmark, *Nature* 300, 594 (1982).
- ⁴⁵J. T. deBettencourt, *Proc. IEEE* 72, 1219 (1984).
- ⁴⁶E. Bahar, in *Electromagnetic Probing in Geophysics*, edited by J. R. Wait (Golem, Boulder, CO, 1971), Chap. 6.
- ⁴⁷P. Beckman, in *Electromagnetic Probing in Geophysics*, edited by J. R. Wait (Golem, Boulder, CO, 1971) (Chap. 3).
- ⁴⁸D. D. Crombie, in *Electromagnetic Probing in Geophysics*, edited by J. R. Wait (Golem, Boulder, CO, 1971) (Chap. 4).
- ⁴⁹M. F. Brown, R. W. P. King, and T. T. Wu, *J. Appl. Phys.* 53, 3387 (1982).
- ⁵⁰M. F. Brown, R. W. P. King, and T. T. Wu, "The propagation and reflection of lateral waves," presented at the 1983 International IEEE/AP-S Symposium, Houston, Texas (May 1983) (unpublished).
- ⁵¹M. F. Brown, R. W. P. King, and T. T. Wu, *J. Appl. Phys.* 55, 3927 (1984).
- ⁵²R. W. P. King, *J. Appl. Phys.* 55, 3916 (1984).
- ⁵³W. -Y. Pan, *J. Appl. Phys.* (to be published).

Surface-wave propagation along the boundary between sea water and one-dimensionally anisotropic rock

Wei-Yan Pan^{a)}

Gordon McKay Laboratory, Harvard University, Cambridge, Massachusetts 02138

(Received 10 May 1985; accepted for publication 22 August 1985)

New formulas for the components of the electromagnetic surface wave propagating along the boundary between sea water (Region 1) and a one-dimensionally anisotropic rock (Region 2) have been obtained. The conductivity of the rock is taken to be $\sigma_x = \sigma_y = \sigma_T$, $\sigma_z = \sigma_L$, where z is perpendicular to the boundary. Both σ_L and σ_T are constant. When $\sigma_L = \sigma_T$, the new formulas coincide with those of Wu and King [Radio Sci. 17, 521, 532 (1982); J. Appl. Phys. 54, 507 (1983)] for an isotropic medium. When $\sigma_L \neq \sigma_T$, the lateral-wave part of the field is separated into two terms of which the first is of electric type with the wave number $k_2 = k_L$, and the second is of magnetic type with $k_2 = k_T$. The new formulas can be used to interpret recent measurements of the oceanic crust.

1. INTRODUCTION

Electromagnetic surface waves propagate along boundaries between electrically different media like air and earth or rock and sea water. They constitute a major part of the field near the boundary when this is generated by antennas located on or close to the boundary. This means that they play an important role in geophysical prospecting and diagnostics when both the source and the receiver are located on the sea floor. Recently, numerical evaluations of the general integrals for the complete electromagnetic field (which includes the lateral wave) have been used to investigate the electrical conductivity structure of the oceanic crust under the assumption that it is horizontally layered.¹⁻³ The source used in these investigations was a horizontal electric dipole near the sea bottom. Two arbitrarily oriented horizontal components E_x and E_y of the electromagnetic field were measured with a crossed-dipole receiving antenna at a distance of 18.9 km from the source for a range of frequencies between 0.25 and 2.25 Hz. From a comparison of the measured data with the numerically calculated curves for models of the crust consisting of eight layers with different conductivities and thicknesses to a depth of over 30 km, the "best fit" model was determined. The models investigated did not include a horizontal stratification of the rock in the form of relatively thin layers that alternate with higher and lower conductivities. Such a model is well approximated by a half-space that is homogeneous but anisotropic in conductivity with the conductivity $\sigma_z = \sigma_L$ perpendicular to the bedding surfaces different from the conductivity $\sigma_x = \sigma_y = \sigma_T$ parallel to these surfaces.⁴ An anisotropic model of this type has been suggested.^{5,6} Since the maximum depth of penetration of lateral waves reaching a point 18.9 km distant in an isotropic rock with $\sigma_2 \sim 0.004$ S/m under sea water with $\sigma_1 \sim 4$ S/m is only about 220 m,⁷ such a stratification does not have to extend far into the crust.

In order to confirm the suggested anisotropic model,⁵ it is necessary to carry out a complete analysis of the field gen-

erated by a horizontal electric dipole on the sea floor above a homogeneous but one-dimensionally anisotropic half-space of rock, and to compare this with the available measurements.³ It is the purpose of this paper to carry out such a study as an interesting and useful alternative for interpreting the measured data.

II. THE INTEGRAL SOLUTION

The coordinate system is that shown in Fig. 1. The half-space $z > 0$ (Region 1) is filled with sea water characterized by the permeability $\mu_1 = \mu_0$, permittivity ϵ_1 , and conductivity σ_1 . The rest of space, $z < 0$ (Region 2), is occupied by rock with $\mu_2 = \mu_0$; $\epsilon_x = \epsilon_y = \epsilon_T$, $\epsilon_z = \epsilon_L$; and $\sigma_x = \sigma_y = \sigma_T$, $\sigma_z = \sigma_L$. The unit horizontal electric dipole is x directed at $(0,0,d)$.

Maxwell's equations, with the time dependence $e^{-i\omega t}$, are

$$\nabla \times E_j = i\omega B_j, \quad (1)$$

$$\nabla \times B_j = \mu_j(-i\omega \epsilon_j E_j + J), \quad (2)$$

$$J = \delta(x)\delta(y)\delta(z-d)\hat{x}, \quad (3)$$

where \hat{x} is the unit vector in the x direction and the subscript

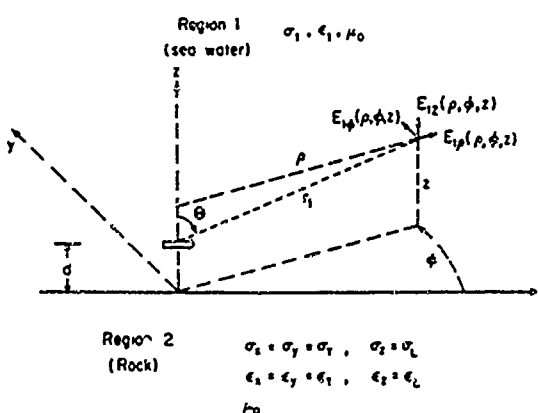


FIG. 1. Components of electric field at (ρ, ϕ, z) due to an x -directed unit dipole ($I\Delta l = 1$ A m) located at $(0,0,d)$ in sea water (Region 1) over one-dimensionally anisotropic rock (Region 2).

^{a)} Visiting scholar from the People's Republic of China.

$j = 1, 2$ distinguishes $z > 0$ and $z < 0$, respectively. In Eq. (2),

$$\bar{\epsilon}_1 = \begin{bmatrix} \epsilon_1 + i\sigma_1/\omega & 0 & 0 \\ 0 & \epsilon_1 + i\sigma_1/\omega & 0 \\ 0 & 0 & \epsilon_1 + i\sigma_1/\omega \end{bmatrix}, \quad (4)$$

$$\bar{\epsilon}_2 = \begin{bmatrix} \epsilon_T + i\sigma_T/\omega & 0 & 0 \\ 0 & \epsilon_T + i\sigma_T/\omega & 0 \\ 0 & 0 & \epsilon_L + i\sigma_L/\omega \end{bmatrix}. \quad (5)$$

The integral solutions of the field may be derived in a manner similar to that used by King and Smith.² Let

$$E(x, y, z) = \frac{1}{(2\pi)^2} \int_{-\infty}^{\infty} d\xi \int_{-\infty}^{\infty} d\eta e^{i\xi x + i\eta y} \bar{E}(\xi, \eta, z). \quad (6)$$

Similar transforms apply to B and J . Thus with Eq. (3)

$$\bar{J}(\xi, \eta, z) = \delta(z - d) \bar{J}. \quad (7)$$

From Maxwell's equations, the Fourier transforms of the field components in Region 1 satisfy the following equations:

$$i\eta \bar{E}_{1x} - \frac{\partial}{\partial z} \bar{E}_{1y} = i\omega \bar{B}_{1x}, \quad (8)$$

$$\frac{\partial}{\partial z} \bar{E}_{1x} - i\xi \bar{E}_{1y} = i\omega \bar{B}_{1y}, \quad (9)$$

$$i\xi \bar{E}_{1y} - i\eta \bar{E}_{1x} = i\omega \bar{B}_{1z}, \quad (10)$$

$$i\eta \bar{B}_{1x} - \frac{\partial}{\partial z} \bar{B}_{1y} = -i\omega \mu_0 \bar{\epsilon}_1 \bar{E}_{1x} + \mu_0 \delta(z - d), \quad (11)$$

$$\frac{\partial}{\partial z} \bar{B}_{1x} - i\xi \bar{B}_{1y} = -i\omega \mu_0 \bar{\epsilon}_1 \bar{E}_{1y}, \quad (12)$$

$$i\xi \bar{B}_{1y} - i\eta \bar{B}_{1x} = -i\omega \mu_0 \bar{\epsilon}_1 \bar{E}_{1z}. \quad (13)$$

In Region 2, the conductivity and permittivity of the rock have two different values in the horizontal and vertical directions so that the field components in the rock satisfy

$$i\eta \bar{E}_{2x} - \frac{\partial}{\partial z} \bar{E}_{2y} = i\omega \bar{B}_{2x}, \quad (14)$$

$$\frac{\partial}{\partial z} \bar{E}_{2x} - i\xi \bar{E}_{2y} = i\omega \bar{B}_{2y}, \quad (15)$$

$$i\xi \bar{E}_{2y} - i\eta \bar{E}_{2x} = i\omega \bar{B}_{2z}, \quad (16)$$

$$i\eta \bar{B}_{2x} - \frac{\partial}{\partial z} \bar{B}_{2y} = -i\omega \mu_0 \bar{\epsilon}_T \bar{E}_{2x}, \quad (17)$$

$$\frac{\partial}{\partial z} \bar{B}_{2x} - i\xi \bar{B}_{2y} = -i\omega \mu_0 \bar{\epsilon}_T \bar{E}_{2y}, \quad (18)$$

$$i\xi \bar{B}_{2y} - i\eta \bar{B}_{2x} = -i\omega \mu_0 \bar{\epsilon}_L \bar{E}_{2z}, \quad (19)$$

where

$$\bar{\epsilon}_j = \epsilon_j + i\sigma_j/\omega, \quad j = 1, L, T. \quad (20)$$

Equations (8)–(19) may be used to solve for \bar{E}_y , \bar{E}_z , \bar{B}_y , and \bar{B}_z in terms of \bar{E}_x and \bar{B}_x . The results are

$$\bar{B}_{1x} = \frac{1}{k_1^2 - \xi^2} \left(i\xi \frac{\partial}{\partial z} \bar{B}_{1x} - \omega \mu_0 \bar{\epsilon}_1 \eta \bar{E}_{1x} \right), \quad (21)$$

$$\bar{E}_{1y} = \frac{1}{k_1^2 - \xi^2} \left(i\omega \frac{\partial}{\partial z} \bar{B}_{1x} - \xi \eta \bar{E}_{1x} \right), \quad (22)$$

$$\bar{B}_{1y} = \frac{1}{k_1^2 - \xi^2} \left(-\xi \eta \bar{B}_{1x} - i\omega \mu_0 \bar{\epsilon}_1 \frac{\partial}{\partial z} \bar{E}_{1x} \right), \quad (23)$$

$$\bar{E}_{1x} = \frac{1}{k_1^2 - \xi^2} \left(\omega \eta \bar{B}_{1x} + i\xi \frac{\partial}{\partial z} \bar{E}_{1x} \right), \quad (24)$$

$$\bar{B}_{2x} = \frac{1}{k_T^2 - \xi^2} \left(i\xi \frac{\partial}{\partial z} \bar{B}_{2x} - \omega \mu_0 \bar{\epsilon}_T \eta \bar{E}_{2x} \right), \quad (25)$$

$$\bar{E}_{2y} = \frac{1}{k_T^2 - \xi^2} \left(i\omega \frac{\partial}{\partial z} \bar{B}_{2x} - \xi \eta \bar{E}_{2x} \right), \quad (26)$$

$$\bar{B}_{2y} = \frac{1}{k_L^2 - \xi^2} \left(-\xi \eta \bar{B}_{2x} - i\omega \mu_0 \bar{\epsilon}_L \frac{\partial}{\partial z} \bar{E}_{2x} \right), \quad (27)$$

$$\bar{E}_{2x} = \frac{1}{k_L^2 - \xi^2} \left(\omega \eta \bar{B}_{2x} + i\xi \frac{\partial}{\partial z} \bar{E}_{2x} \right), \quad (28)$$

where

$$k_j^2 = \omega^2 \mu_0 \bar{\epsilon}_j, \quad j = 1, L, T. \quad (29)$$

The substitution of Eqs. (21)–(24) into Eqs. (8) and (11) leads to the following ordinary differential equations for \bar{E}_{1x} and \bar{B}_{1x} :

$$\frac{\partial^2}{\partial z^2} \bar{B}_{1x} + \gamma_1^2 \bar{B}_{1x} = 0, \quad (30)$$

$$\frac{\partial^2}{\partial z^2} \bar{E}_{1x} + \gamma_1^2 \bar{E}_{1x} = \frac{k_1^2 - \xi^2}{i\omega \bar{\epsilon}_1} \delta(z - d), \quad (31)$$

where

$$\gamma_1 = (k_1^2 - \xi^2 - \eta^2)^{1/2}. \quad (32)$$

The imaginary part of the square root is positive.

Because of the radiation condition as $z \rightarrow \infty$, the solutions in Region 1 may be expressed as

$$\bar{E}_{1x} = C_2 e^{\gamma_1 z} - \frac{k_1^2 - \xi^2}{i\omega \bar{\epsilon}_1 \gamma_1} e^{\gamma_1 d} \sin \gamma_1 z, \quad 0 < z < d, \quad (33)$$

$$\bar{E}_{1x} = \left(C_2 - \frac{k_1^2 - \xi^2}{i\omega \bar{\epsilon}_1 \gamma_1} \sin \gamma_1 d \right) e^{\gamma_1 z}, \quad d < z, \quad (34)$$

$$\bar{B}_{1x} = \mu_0 C_1 e^{\gamma_1 z}, \quad 0 < z. \quad (35)$$

In Region 2, equations for \bar{B}_{2x} and \bar{E}_{2x} can be obtained with the substitution of Eqs. (25)–(28) into Eqs. (14) and (17). The results are

$$\frac{1}{k_T^2 - \xi^2} \frac{\partial^2}{\partial z^2} \bar{B}_{2x} + \left(1 - \frac{\eta^2}{k_L^2 - \xi^2} \right) \bar{B}_{2x} + \frac{i\xi \eta}{\omega} \left(\frac{1}{k_T^2 - \xi^2} - \frac{1}{k_L^2 - \xi^2} \right) \frac{\partial}{\partial z} \bar{E}_{2x} = 0, \quad (36)$$

$$\frac{k_L^2}{k_L^2 - \xi^2} \frac{\partial^2}{\partial z^2} \bar{E}_{2x} + \left(k_T^2 - \frac{k_T^2 \eta^2}{k_T^2 - \xi^2} \right) \bar{E}_{2x} - i\omega \xi \eta \left(\frac{1}{k_L^2 - \xi^2} - \frac{1}{k_T^2 - \xi^2} \right) \frac{\partial}{\partial z} \bar{B}_{2x} = 0. \quad (37)$$

If the solutions of \bar{B}_{2x} and \bar{E}_{2x} are assumed to have the forms

$$\bar{B}_{2x} = A e^{-\gamma_2 z}, \quad (38)$$

$$\bar{E}_{2x} = B e^{-\gamma_2 z}, \quad (39)$$

and these are substituted in Eqs. (36) and (37), the following algebraic equations are obtained:

$$\left(1 - \frac{\gamma^2}{k_T^2 - \xi^2} - \frac{\eta^2}{k_L^2 - \xi^2}\right) A + \frac{\xi\eta\gamma}{\omega} \left(\frac{1}{k_T^2 - \xi^2} - \frac{1}{k_L^2 - \xi^2}\right) B = 0, \quad (40)$$

$$- \omega\xi\eta\gamma \left(\frac{1}{k_L^2 - \xi^2} - \frac{1}{k_T^2 - \xi^2}\right) A + \left(k_T^2 - \frac{k_T^2\eta^2}{k_T^2 - \xi^2} - \frac{k_L^2\gamma^2}{k_L^2 - \xi^2}\right) B = 0. \quad (41)$$

The nonzero solution should satisfy the following equation:

$$\gamma^4 k_L^2 + \gamma^2 [(k_L^2 + k_T^2)(\xi^2 + \eta^2) - 2k_L^2 k_T^2] + k_T^2 (k_L^2 - \xi^2 - \eta^2)(k_T^2 - \xi^2 - \eta^2) = 0. \quad (42)$$

The solutions for γ are

$$\gamma_0 = (k_T^2 - \lambda^2)^{1/2}, \quad (43)$$

$$\gamma_e = [k_T^2 - (k_T^2/k_L^2)\lambda^2]^{1/2}, \quad (44)$$

where

$$\lambda^2 = \xi^2 + \eta^2. \quad (45)$$

The imaginary parts of γ_0 and γ_e should be positive when λ is real. The A and B coefficients in Eqs. (38) and (39) should satisfy

$$\frac{B_0}{A_0} = -\frac{\omega\eta}{\xi\gamma_0}, \quad (46)$$

$$\frac{\bar{B}_e}{A_e} = \frac{\omega\xi\gamma_e}{k_T^2\eta}. \quad (47)$$

From Eqs. (25)–(28) all of the components in Region 2 can be obtained. They are

$$\bar{B}_{2x} = \mu_0(A_0 e^{-\gamma_0 z} + A_e e^{-\gamma_e z}), \quad (48)$$

$$\bar{E}_{2x} = -\frac{\omega\mu_0\eta}{\xi\gamma_0} A_0 e^{-\gamma_0 z} + \frac{\omega\mu_0\xi\gamma_e}{k_T^2\eta} A_e e^{-\gamma_e z}, \quad (49)$$

$$\bar{B}_{2y} = \mu_0 \left(\frac{\eta}{\xi} A_0 e^{-\gamma_0 z} - \frac{\xi}{\eta} A_e e^{-\gamma_e z} \right), \quad (50)$$

$$\bar{E}_{2y} = \omega\mu_0 \left(\frac{A_0}{\gamma_0} e^{-\gamma_0 z} + \frac{A_e \gamma_e}{k_T^2} e^{-\gamma_e z} \right), \quad (51)$$

$$\bar{B}_{2x} = \frac{\lambda^2 \mu_0}{\xi\gamma_0} A_0 e^{-\gamma_0 z}, \quad (52)$$

$$\bar{E}_{2x} = \frac{\lambda^2 \omega\mu_0}{k_L^2 \eta} A_e e^{-\gamma_e z}. \quad (53)$$

On the boundary $z=0$, with the conditions $\bar{B}_{1x} = \bar{B}_{2x}|_{z=0}$ and $k_1^2 \bar{E}_{1x} = k_L^2 \bar{E}_{2x}|_{z=0}$, the coefficients A_0 and A_e may be expressed in terms of C_1 and C_2 as follows:

$$A_0 = -\frac{\xi\gamma_0}{\lambda^2(k_1^2 - \xi^2)} (\xi\gamma_1 C_1 + \omega\bar{\epsilon}_1 \eta C_2), \quad (54)$$

$$A_e = \frac{k_1^2 \eta}{\lambda^2 \omega\mu_0} \left(\frac{\omega\mu_0 \eta C_1 - \xi\gamma_1 C_2}{k_1^2 - \xi^2} - \frac{\xi}{\omega\bar{\epsilon}_1} e^{\gamma_1 d} \right). \quad (55)$$

From the conditions $\bar{E}_{2y} = \bar{E}_{1y}|_{z=0}$ and $\bar{B}_{2y} = \bar{B}_{1y}|_{z=0}$, the following equations may be obtained:

$$-\frac{\omega\mu_0\gamma_1}{k_1^2 - \xi^2} C_1 - \frac{\xi\eta}{k_1^2 - \xi^2} C_2 - \frac{\omega\mu_0}{\gamma_0} A_0 - \frac{\omega\mu_0\gamma_e}{k_T^2} A_e = 0, \quad (56)$$

$$-\frac{\xi\eta}{k_1^2 - \xi^2} C_1 + \frac{\omega\bar{\epsilon}_1\gamma_1}{k_1^2 - \xi^2} C_2 - \frac{\eta}{\xi} A_0 + \frac{\xi}{\eta} A_e = -e^{\gamma_1 d}. \quad (57)$$

The coefficients C_1 and C_2 are derived from Eqs. (54)–(57). They are

$$C_1 = \frac{\xi\eta e^{\gamma_1 d}}{\lambda^2 M_0 N_e} (k_1^2 \gamma_0 \gamma_e - k_T^2 \gamma_1^2), \quad (58)$$

$$C_2 = -\frac{\omega\mu_0 e^{\gamma_1 d}}{\lambda^2 M_0 N_e} \{ \lambda^2 N_e + \xi^2 [\gamma_1 (\gamma_0 \gamma_e - k_T^2) - \lambda^2 \gamma_e] \}, \quad (59)$$

where

$$M_0 = \gamma_1 + \gamma_0, \quad (60)$$

$$N_e = k_T^2 \gamma_1 + k_1^2 \gamma_e. \quad (61)$$

In Region 1, when $0 < z < d$, the components of the electromagnetic field are

$$E_{1x} = \frac{1}{(2\pi)^2} \int_{-\infty}^{\infty} d\xi \int_{-\infty}^{\infty} d\eta e^{i\xi x + i\eta y} \left(\frac{-\omega\mu_0 e^{i\gamma_1(z+d)}}{\lambda^2 M_0 N_e} \{ \lambda^2 N_e + \xi^2 [\gamma_1 (\gamma_0 \gamma_e - k_T^2) - \lambda^2 \gamma_e] \} - \frac{e^{i\gamma_1 d}}{i\omega\bar{\epsilon}_1 \gamma_1} (k_1^2 - \xi^2) \sin \gamma_1 z \right), \quad (62)$$

$$E_{1y} = \frac{1}{(2\pi)^2} \int_{-\infty}^{\infty} d\xi \int_{-\infty}^{\infty} d\eta e^{i\xi x + i\eta y} \xi \eta \left(\frac{\omega\mu_0 e^{i\gamma_1(z+d)}}{\lambda^2 M_0 N_e} (k_T^2 \gamma_1 + \lambda^2 \gamma_e - \gamma_1 \gamma_0 \gamma_e) + \frac{e^{i\gamma_1 d}}{i\omega\bar{\epsilon}_1 \gamma_1} \sin \gamma_1 z \right), \quad (63)$$

$$E_{1z} = \frac{1}{(2\pi)^2} \int_{-\infty}^{\infty} d\xi \int_{-\infty}^{\infty} d\eta e^{i\xi x + i\eta y} \xi \left(\frac{\omega\mu_0 \gamma_e e^{i\gamma_1(z+d)}}{N_e} - \frac{e^{i\gamma_1 d}}{\omega\bar{\epsilon}_1} \cos \gamma_1 z \right), \quad (64)$$

$$B_{1x} = \frac{\mu_0}{(2\pi)^2} \int_{-\infty}^{\infty} d\xi \int_{-\infty}^{\infty} d\eta e^{i\xi x + i\eta y} \xi \eta \frac{e^{i\gamma_1(z+d)}}{\lambda^2 M_0 N_e} (k_1^2 \gamma_0 \gamma_e - k_T^2 \gamma_1^2), \quad (65)$$

$$B_{1y} = -\frac{\mu_0}{(2\pi)^2} \int_{-\infty}^{\infty} d\xi \int_{-\infty}^{\infty} d\eta e^{i\xi x + i\eta y} \left(\frac{e^{i\gamma_1(z+d)}}{\lambda^2 M_0 N_e} [\lambda^2 \gamma_1 N_e + \xi^2 (k_1^2 \gamma_0 \gamma_e - k_T^2 \gamma_1^2)] - e^{i\gamma_1 d} \cos \gamma_1 z \right), \quad (66)$$

$$B_{1z} = \frac{\mu_0}{(2\pi)^2} \int_{-\infty}^{\infty} d\xi \int_{-\infty}^{\infty} d\eta e^{i\xi x + i\eta y} \eta \left(\frac{e^{i\gamma_1 z + d_1}}{M_0} - \frac{ie^{i\gamma_1 z}}{\gamma_1} \sin \gamma_1 z \right). \quad (67)$$

It is now convenient to introduce the cylindrical coordinates ρ, ϕ, z with

$$x = \rho \cos \phi, \quad y = \rho \sin \phi, \quad (68)$$

$$\xi = \lambda \cos \phi', \quad \eta = \lambda \sin \phi', \quad (69)$$

and the integral representation of the Bessel functions, viz.,

$$J_n(\lambda \rho) = \frac{i^{-n}}{2\pi} \int_0^{2\pi} e^{i\lambda \rho \cos \theta} e^{in\theta} d\theta. \quad (70)$$

With Eqs. (68)–(70) the components of the field in Region 1 may be rewritten as follows:

$$E_{1\rho} = -\frac{\omega\mu_0}{4\pi k_1^2} \cos \phi \left[\int_0^\infty \left(k_1^2 J_0(\lambda \rho) - \frac{\lambda^2}{2} [J_0(\lambda \rho) - J_2(\lambda \rho)] \right) \frac{e^{i\gamma_1 z - d_1}}{\gamma_1} \lambda d\lambda \right. \\ \left. + \int_0^\infty \left(\frac{\gamma_1 Q_e}{2} [J_0(\lambda \rho) - J_2(\lambda \rho)] - \frac{k_1^2 P_0}{2\gamma_1} [J_0(\lambda \rho) + J_2(\lambda \rho)] \right) e^{i\gamma_1 z + d_1} \lambda d\lambda \right], \quad (71)$$

$$E_{1\phi} = \frac{\omega\mu_0}{4\pi k_1^2} \sin \phi \left[\int_0^\infty \left(k_1^2 J_0(\lambda \rho) - \frac{\lambda^2}{2} [J_0(\lambda \rho) + J_2(\lambda \rho)] \right) \frac{e^{i\gamma_1 z - d_1}}{\gamma_1} \lambda d\lambda \right. \\ \left. + \int_0^\infty \left(\frac{\gamma_1 Q_e}{2} [J_0(\lambda \rho) + J_2(\lambda \rho)] - \frac{k_1^2 P_0}{2\gamma_1} [J_0(\lambda \rho) - J_2(\lambda \rho)] \right) e^{i\gamma_1 z + d_1} \lambda d\lambda \right], \quad (72)$$

$$E_{1z} = \frac{i\omega\mu_0}{4\pi k_1^2} \cos \phi \int_0^\infty \left[\pm e^{i\gamma_1 z - d_1} + Q_e e^{i\gamma_1 z + d_1} \right] J_1(\lambda \rho) \lambda^2 d\lambda, \quad (73)$$

$$B_{1\rho} = -\frac{\mu_0}{4\pi} \sin \phi \left[\pm \int_0^\infty J_0(\lambda \rho) e^{i\gamma_1 z - d_1} \lambda d\lambda + \int_0^\infty \left(\frac{Q_e}{2} [J_0(\lambda \rho) - J_2(\lambda \rho)] - \frac{P_0}{2} [J_0(\lambda \rho) + J_2(\lambda \rho)] \right) e^{i\gamma_1 z + d_1} \lambda d\lambda \right], \quad (74)$$

$$B_{1\phi} = -\frac{\mu_0}{4\pi} \cos \phi \left[\pm \int_0^\infty J_0(\lambda \rho) e^{i\gamma_1 z - d_1} \lambda d\lambda + \int_0^\infty \left(\frac{Q_e}{2} [J_0(\lambda \rho) - J_2(\lambda \rho)] - \frac{P_0}{2} [J_0(\lambda \rho) + J_2(\lambda \rho)] \right) e^{i\gamma_1 z + d_1} \lambda d\lambda \right], \quad (75)$$

$$B_{1z} = \frac{i\mu_0}{4\pi} \sin \phi \int_0^\infty \left[e^{i\gamma_1 z - d_1} - P_0 e^{i\gamma_1 z + d_1} \right] J_1(\lambda \rho) \frac{\lambda^2}{\gamma_1} d\lambda. \quad (76)$$

Where two signs appear, the upper one is for the range $d < z$, the lower one for $0 \leq z \leq d$. Also

$$Q_e = \frac{k_1^2 \gamma_e - k_1^2 \gamma_1}{k_1^2 \gamma_e + k_1^2 \gamma_1}, \quad (77)$$

$$P_0 = \frac{\gamma_0 - \gamma_1}{\gamma_0 + \gamma_1}. \quad (78)$$

Expressions (71)–(76) are very similar to the corresponding formulas with Region 2 isotropic.⁸ The only differences are contained in the factors P and Q which have been changed here to P_0 and Q_e .

III. SIMPLIFICATION OF THE FORMULAS

The integral expressions (71)–(76) are not convenient to evaluate or to obtain useful physical insights. For geophysical applications, accurate, general and simpler formulas for the surface-wave field are needed. With isotropic media, such a set of formulas has been obtained.^{9–11} With the same procedure, a set of similar formulas may be derived for the one-dimensionally anisotropic case.

A. Formulation for $E_{1\rho}$

Expression (71) may be rewritten in the form

$$E_{1\rho} = -\frac{\omega\mu_0}{4\pi k_1^2} \cos \phi [F_0(\rho, z - d) \\ + F_1(\rho, z + d) + F_2(\rho, z + d)], \quad (79)$$

where

$$F_0(\rho, z - d) = \int_0^\infty \left(\frac{\gamma_1}{2} [J_0(\lambda \rho) - J_2(\lambda \rho)] \right. \\ \left. + \frac{k_1^2}{2\gamma_1} [J_0(\lambda \rho) + J_2(\lambda \rho)] \right) e^{i\gamma_1 z - d_1} \lambda d\lambda, \quad (80)$$

$$F_1(\rho, z + d) = \int_0^\infty \left(\frac{\gamma_1}{2} [J_0(\lambda \rho) - J_2(\lambda \rho)] \right. \\ \left. + \frac{k_1^2}{2\gamma_1} [J_0(\lambda \rho) + J_2(\lambda \rho)] \right) e^{i\gamma_1 z + d_1} \lambda d\lambda, \quad (81)$$

and

$$F_2(\rho, z + d) = F_3(\rho, z + d) + F_4(\rho, z + d), \quad (82)$$

with

$$F_2(\rho, z+d) = -k_T^2 \int_0^\infty \frac{\gamma_1^2}{k_1^2 \gamma_e + k_T^2 \gamma_1} \times [J_0(\lambda \rho) - J_2(\lambda \rho)] e^{i\gamma_1(z+d)} \lambda d\lambda, \quad (83)$$

$$F_3(\rho, z+d) = -k_1^2 \int_0^\infty \frac{\gamma_0}{\gamma_1(\gamma_0 + \gamma_1)} \times [J_0(\lambda \rho) + J_2(\lambda \rho)] e^{i\gamma_1(z+d)} \lambda d\lambda. \quad (84)$$

The functions $F_0(\rho, z-d)$, $F'_0(\rho, z+d)$, and $F_1(\rho, z+d)$ stand for the direct wave, the reflected wave, and the lateral wave, respectively. The direct-wave and reflected-wave terms are exactly the same as with an isotropic medium.⁹ They have been simplified in Ref. 9 as follows:

$$F_0(\rho, z-d) = -2e^{ik_1 r_1} \left(\frac{k_1}{\rho^2} + \frac{i}{\rho^3} \right), \quad (85)$$

$$F'_0(\rho, z+d) \approx F'_0(\rho, 0) e^{i\gamma_1(z+d)} \\ = -2e^{i\gamma_1(z+d-\rho)} \left(\frac{k_1}{\rho^2} + \frac{i}{\rho^3} \right), \quad (86)$$

where

$$r_1 = [\rho^2 + (z-d)^2]^{1/2}. \quad (87)$$

For the lateral-wave terms F_2 and F_3 , the only differences between Eqs. (83) and (84) and the corresponding formulas for an isotropic medium⁹ are that the factor γ_2 has been replaced, respectively, by γ_e and γ_0 . With the same approximation as in the isotropic case, they may be simplified as

$$F_2(\rho, z+d) \approx F_2(\rho, 0) e^{i\gamma_e(z+d)}, \quad (88)$$

$$F_3(\rho, z+d) \approx F_3(\rho, 0) e^{i\gamma_0(z+d)}, \quad (89)$$

where

$$F_2(\rho, 0) = -k_T^2 \int_0^\infty \frac{\gamma_1^2}{k_1^2 \gamma_e + k_T^2 \gamma_1} [J_0(\lambda \rho) - J_2(\lambda \rho)] \lambda d\lambda \\ = -\frac{k_L k_T}{k_1^2} [I_1(k_L) + (k_1^2 - k_L^2) I_3(k_L)] + G(\rho), \quad (90)$$

$$F_3(\rho, 0) = -k_1^2 \int_0^\infty \frac{\gamma_0}{\gamma_1(\gamma_0 + \gamma_1)} [J_0(\lambda \rho) + J_2(\lambda \rho)] \lambda d\lambda \\ = -k_1^2 \left[I_4(k_1) - \frac{1}{k_1^2 - k_T^2} I_2(k_1) + \frac{1}{k_1^2 - k_T^2} I_2(k_T) \right]. \quad (91)$$

The four functions $I(k)$ are integrals that satisfy the following simple formulas⁹:

$$I_1(k) = \int_0^\infty (k^2 - \lambda^2)^{1/2} [J_0(\lambda \rho) - J_2(\lambda \rho)] \lambda d\lambda \\ = -2I_2(k) + k^2 I_4(k), \quad (92)$$

$$I_2(k) = \int_0^\infty (k^2 - \lambda^2)^{1/2} [J_0(\lambda \rho) + J_2(\lambda \rho)] \lambda d\lambda \\ = \frac{2k}{\rho^2} + \frac{2i}{\rho^3} e^{ik\rho}, \quad (93)$$

$$I_3(k) = \int_0^\infty (k^2 - \lambda^2)^{-1/2} [J_0(\lambda \rho) - J_2(\lambda \rho)] \lambda d\lambda \\ = -\frac{2i}{\rho} e^{ik\rho} - I_4(k), \quad (94)$$

$$I_4(k) = \int_0^\infty (k^2 - \lambda^2)^{-1/2} [J_0(\lambda \rho) + J_2(\lambda \rho)] \lambda d\lambda \\ = \frac{2}{k\rho^2} (1 - e^{ik\rho}). \quad (95)$$

The function $G(\rho)$ in Eq. (90) is the following integral:

$$G(\rho) = -k_T^2 \int_0^\infty \gamma_1^2 \left(\frac{1}{k_1^2 \gamma_e + k_T^2 \gamma_1} - \frac{1}{k_1^2 \gamma_e} \right) \\ \times [J_0(\lambda \rho) - J_2(\lambda \rho)] \lambda d\lambda \\ = -k_L k_T \int_0^\infty \gamma_1^2 \left(\frac{1}{k_1^2 \gamma_e^* + k_L k_T \gamma_1} - \frac{1}{k_1^2 \gamma_e^*} \right) \\ \times [J_0(\lambda \rho) - J_2(\lambda \rho)] \lambda d\lambda, \quad (96)$$

where

$$\gamma_e^* = (k_L^2 - \lambda^2)^{1/2}. \quad (97)$$

$G(\rho)$ is evaluated in the Appendix with the result

$$G(\rho) = -\frac{2k_L k_T^2}{k_1} \left(\frac{\pi}{k_L \rho} \right)^{1/2} e^{ik_L \rho} e^{-ik_L \rho (k_T^2/2k_1^2)} \mathcal{F}, \quad (98)$$

where

$$\mathcal{F} = \frac{1}{2}(1+i) - C_2 [k_L \rho (k_T^2/2k_1^2)] - iS_2 [k_L \rho (k_T^2/2k_1^2)]. \quad (99)$$

The Fresnel integral is defined as follows:

$$C_2(z) + iS_2(z) = \int_0^z \frac{e^{it}}{(2\pi t)^{1/2}} dt. \quad (100)$$

The substitution of Eqs. (85), (86), (90), and (91) into Eq. (79) with Eqs. (82), (88)–(95), and (98), with the omission of small terms of the order $k_L k_T/k_1^2$ compared with 1, leads to the following formula for $E_{1\rho}$:

$$E_{1\rho} = -\frac{\omega\mu_0}{2\pi k_1^2} \cos \phi \left(e^{i\gamma_1(z+d)} \left[e^{ik_L \rho} \left[\frac{ik_L k_T}{\rho} - \frac{k_T}{\rho^2} - \frac{k_L^2 k_T^2}{k_1} \left(\frac{\pi}{k_L \rho} \right)^{1/2} e^{-ik_L \rho (k_T^2/2k_1^2)} \mathcal{F} \right] - \frac{i}{\rho^3} e^{ik_L \rho} \right] - e^{ik_1 r_1} \left(\frac{k_1}{\rho^2} + \frac{i}{\rho^3} \right) \right). \quad (101)$$

B. Formulation for E_{1z}

The integral expression (72) may be rewritten in the form

$$E_{1z} = \frac{\omega\mu_0}{4\pi k_1^2} \sin \phi [G_0(\rho, z-d) \\ + G'_0(\rho, z+d) + G_1(\rho, z+d)], \quad (102)$$

where $G_0(\rho, z-d)$, $G'_0(\rho, z+d)$, and $G_1(\rho, z+d)$ are the direct wave, reflected wave, and lateral wave, respectively. The functions G_0 and G'_0 coincide with the corresponding formulas for an isotropic Region 2.¹⁰ They are

$$G_0(\rho, z-d) = \int_0^\infty \left(\frac{\gamma_1}{2} [J_0(\lambda\rho) + J_2(\lambda\rho)] + \frac{k_1^2}{2\gamma_1} [J_0(\lambda\rho) - J_2(\lambda\rho)] \right) e^{\gamma_1(z-d)} \lambda d\lambda$$

$$= -e^{ik_1 r_1} \left(\frac{ik_1^2}{r_1} - \frac{k_1}{r_1^2} - \frac{i}{r_1^3} \right), \quad (103)$$

$$G'_0(\rho, z+d) = \int_0^\infty \left(\frac{\gamma_1}{2} [J_0(\lambda\rho) + J_2(\lambda\rho)] + \frac{k_1^2}{2\gamma_1} [J_0(\lambda\rho) - J_2(\lambda\rho)] \right) e^{\gamma_1(z+d)} \lambda d\lambda$$

$$= -e^{ik_1 r_2} \left(\frac{ik_1^2}{r_2} - \frac{k_1}{r_2^2} - \frac{i}{r_2^3} \right), \quad (104)$$

where r_1 is given in Eq. (87) and

$$r_2 = [\rho^2 + (z+d)^2]^{1/2}. \quad (105)$$

The lateral-wave term is

$$G_1(\rho, z+d) = G_2(\rho, z+d) + G_3(\rho, z+d), \quad (106)$$

with

$$G_2(\rho, z+d) = -k_T^2 \int_0^\infty \frac{\gamma_1^2}{k_1^2 \gamma_1 + k_T^2 \gamma_1} [J_0(\lambda\rho) + J_2(\lambda\rho)] \times e^{\gamma_1(z+d)} \lambda d\lambda, \quad (107)$$

$$G_3(\rho, z+d) = -k_1^2 \int_0^\infty \frac{\gamma_0}{\gamma_1(\gamma_0 + \gamma_1)} [J_0(\lambda\rho) - J_2(\lambda\rho)] \times e^{\gamma_1(z+d)} \lambda d\lambda. \quad (108)$$

With the same procedure as used in Ref. 10, the following expressions can be obtained:

$$G_2(\rho, z+d) \approx G_2(\rho, 0) e^{ik_1(z+d)}, \quad (109)$$

$$G_3(\rho, z+d) \approx G_3(\rho, 0) e^{ik_1(z+d)}, \quad (110)$$

where

$$G_2(\rho, 0) = -\frac{k_L k_T}{k_1^2} [I_2(k_L) + (k_1^2 - k_L^2) I_4(k_L)] + H(\rho), \quad (111)$$

$$G_3(\rho, 0) = -k_1^2 I_3(k_1) + I_1(k_1) - I_1(k_T). \quad (112)$$

In Eq. (111) the function $H(\rho)$ is the integral

$$H(\rho) = -k_L k_T \int_0^\infty \gamma_1^2 \left(\frac{1}{k_1^2 \gamma_1^2 + k_L k_T \gamma_1} - \frac{1}{k_1^2 \gamma_1^2} \right) \times [J_0(\lambda\rho) + J_2(\lambda\rho)] \lambda d\lambda. \quad (113)$$

It is evaluated in the Appendix with the result

$$H(\rho) = \frac{2ik_L^2 k_T^2}{k_1} \frac{\pi^{1/2}}{(k_L \rho)^{3/2}} e^{ik_L \rho} e^{-ik_L \rho^2 / 2k_1^2} \mathcal{F}. \quad (114)$$

The factor \mathcal{F} is defined in Eq. (99).

The substitution of Eqs. (103), (104), (111), and (112) into Eq. (102) with Eqs. (106), (109), (110), and (114) leads to the following final approximate formula for $E_{1\phi}$:

$$E_{1\phi} = \frac{\omega\mu_0}{\pi k_1^2} \sin \phi \left\{ e^{ik_1(z+d)} \left[e^{ik_L \rho} \left(\frac{k_T}{2\rho^2} + \frac{ik_L^2 k_T^2}{2k_1} \frac{\pi^{1/2}}{(k_L \rho)^{3/2}} e^{-ik_L \rho^2 / 2k_1^2} \mathcal{F} \right) + e^{ik_T \rho} \left(\frac{k_T}{2\rho^2} + \frac{i}{\rho^3} \right) \right] \right.$$

$$\left. + e^{ik_1 r_2} \left(\frac{ik_1^2}{2\rho} - \frac{k_1}{\rho^2} - \frac{i}{\rho^3} \right) - \frac{1}{4} (e^{ik_1 r_1} + e^{ik_1 r_2}) \left(\frac{ik_1^2}{\rho} - \frac{k_1}{\rho^2} - \frac{i}{\rho^3} \right) \right\}. \quad (115)$$

C. Formulation for E_{1z}

With a similar procedure, expression (73) can be rewritten as

$$E_{1z} = \frac{i\omega\mu_0}{4\pi k_1^2} \cos \phi [E_0(\rho, z-d) + H'_0(\rho, z+d) + H_1(\rho, z+d)]. \quad (116)$$

The direct-wave term H_0 and the reflected-wave term H'_0 are identical to those in Ref. 10, viz.,

$$H_0(\rho, z-d) = \pm \int_0^\infty e^{\gamma_1(z-d)} J_1(\lambda\rho) \lambda^2 d\lambda, \quad (117)$$

$$H'_0(\rho, z+d) = \int_0^\infty e^{\gamma_1(z+d)} J_1(\lambda\rho) \lambda^2 d\lambda. \quad (118)$$

They reduce to the simple formula

$$H_0(\rho, z-d) + H'_0(\rho, z+d)$$

$$= -\left(\frac{z-d}{\rho} e^{ik_1 r_1} + \frac{z+d}{\rho} e^{ik_1 r_2} \right) \left(\frac{k_1^2}{\rho} + \frac{3ik_1}{\rho^2} - \frac{3}{\rho^3} \right). \quad (119)$$

The lateral-wave term,

$$H_1(\rho, z+d) = \int_0^\infty e^{\gamma_1(z+d)} (Q_c - 1) J_1(\lambda\rho) \lambda^2 d\lambda$$

$$= -2k_T^2 \int_0^\infty e^{\gamma_1(z+d)} \frac{\gamma_1}{k_1^2 \gamma_1 + k_T^2 \gamma_1} J_1(\lambda\rho) \lambda^2 d\lambda, \quad (120)$$

may be approximated as

$$H_1(\rho, z+d) \approx H_1(\rho, 0) e^{ik_1(z+d)}, \quad (121)$$

with

$$H_1(\rho, 0) = -2k_1^2 \int_0^\infty \gamma_1 \left(\frac{1}{k_1^2 \gamma_1} + \frac{1}{k_1^2 \gamma_1 + k_1^2 \gamma_1} - \frac{1}{k_1^2 \gamma_1} \right) \times J_1(\lambda \rho) \lambda^2 d\lambda \\ = -\frac{2k_L k_T}{k_1^2} \int_0^\infty \frac{\gamma_1}{\gamma_1^2} J_1(\lambda \rho) \lambda^2 d\lambda + K(\rho), \quad (122)$$

where

$$K(\rho) = -2k_L k_T \int_0^\infty \gamma_1 \left(\frac{1}{k_1^2 \gamma_1^2 + k_L k_T \gamma_1} - \frac{1}{k_1^2 \gamma_1^2} \right) \times J_1(\lambda \rho) \lambda^2 d\lambda. \quad (123)$$

With $|k_1^2| \gg |k_L^2|$ and $\beta = -ik_1$, the following approximation can be obtained¹⁰:

$$f(k_1, k_L, \lambda) = \frac{\gamma_1}{\gamma_1^2} \sim \frac{(\lambda^2 + \beta^2)^{1/2}}{\lambda} + \frac{k_1}{(k_L^2 - \lambda^2)^{1/2}} + \frac{ik_1}{\lambda}, \quad (124)$$

so that

$$H_1(\rho, 0) \approx -\frac{2k_L k_T}{k_1} \left[\frac{e^{ik_L \rho}}{\rho^2} - \left(\frac{k_L}{\rho} + \frac{i}{\rho^2} \right) e^{ik_L \rho} \right] + K(\rho). \quad (125)$$

The function $K(\rho)$ may be evaluated with a method similar to that used for $G(\rho)$ and $H(\rho)$. The result is

$$K(\rho) = \frac{2ik_L^2 k_1^2}{k_1^2} \left(\frac{\pi}{k_L \rho} \right)^{1/2} e^{ik_L \rho} e^{-ik_L \rho k_1^2} \mathcal{F}. \quad (126)$$

The final formula for E_{1z} is

$$E_{1z} = \frac{i\omega\mu_0}{2\pi k_1^2} \cos \phi \left(\frac{k_L k_T}{k_1} \left\{ e^{ik_1(z+d)} e^{ik_L \rho} \left[\frac{k_L}{\rho} + \frac{i}{\rho^2} \right] + \frac{ik_T k_L^2}{k_1} \left(\frac{\pi}{k_L \rho} \right)^{1/2} e^{-ik_L \rho k_1^2 / 2k_1^2} \mathcal{F} \right\} - \frac{e^{ik_1 r_2}}{\rho^2} \right) \\ - \frac{1}{2} \left(\frac{z-d}{\rho} e^{ik_1 r_1} + \frac{z+d}{\rho} e^{ik_1 r_2} \right) \times \left(\frac{k_1^2}{\rho} + \frac{3ik_1}{\rho^2} - \frac{3}{\rho^3} \right). \quad (127)$$

D. Formulation for B_{1z}

The integral expression (76) is identical to the corresponding formula for an isotropic medium¹¹ except that the factor γ_2 (in P) has been changed to γ_0 (in P_0). It follows that the final formula is

$$B_{1z} = -\frac{i\mu_0}{2\pi k_1^2} \sin \phi \left[e^{ik_1(z+d)} e^{ik_L \rho} \left(\frac{ik_L^2}{\rho^2} - \frac{3k_T}{\rho^3} - \frac{3i}{\rho^4} \right) - e^{ik_1 r_2} \left(\frac{ik_1^2}{\rho^2} - \frac{3k_1}{\rho^3} - \frac{3i}{\rho^4} \right) \right. \\ \left. + \frac{1}{2} (e^{ik_1 r_1} - e^{ik_1 r_2}) \left(\frac{k_1^3}{\rho} + \frac{ik_1^2}{\rho^2} \right) \right]. \quad (128)$$

E. Formulation for $B_{1\theta}$

The integral expression (75) may be rewritten as follows:

$$B_{1\theta} = -\frac{\mu_0}{4\pi} \cos \phi [F_0(\rho, z-d) + F_0'(\rho, z+d) + F_1(\rho, z+d)]. \quad (129)$$

The direct-wave term F_0 and the reflected-wave term F_0' are like those in the corresponding formula in Ref. 11. They are

$$F_0(\rho, z-d) = \pm \int_0^\infty e^{i\gamma_1(z-d)} J_0(\lambda \rho) \lambda d\lambda \\ \approx e^{ik_1 r_1} \left(\frac{ik_1}{\rho^2} - \frac{1}{\rho^3} \right) (z-d), \quad (130)$$

$$F_0'(\rho, z+d) = \int_0^\infty e^{i\gamma_1(z+d)} J_0(\lambda \rho) \lambda d\lambda \\ \approx e^{ik_1 r_2} \left(\frac{ik_1}{\rho^2} - \frac{1}{\rho^3} \right) (z+d). \quad (131)$$

The lateral-wave term F_1 is

$$F_1(\rho, z+d) = F_2(\rho, z+d) + F_3(\rho, z+d), \quad (132)$$

where

$$F_2(\rho, z+d) = -k_L k_T \int_0^\infty \frac{\gamma_1}{k_L k_T \gamma_1 + k_1^2 \gamma_1^2} [J_0(\lambda \rho) - J_2(\lambda \rho)] \\ \times e^{i\gamma_1(z+d)} \lambda d\lambda \\ \approx F_2(\rho, 0) e^{ik_1(z+d)}, \quad (133)$$

$$F_3(\rho, z+d) = -\int_0^\infty \frac{\gamma_0}{\gamma_0 + \gamma_1} [J_0(\lambda \rho) + J_2(\lambda \rho)] \\ \times e^{i\gamma_1(z+d)} \lambda d\lambda \\ \approx F_3(\rho, 0) e^{ik_1(z+d)}. \quad (134)$$

The integral $F_3(\rho, 0)$ is the same as in Ref. 11, viz.,

$$F_3(\rho, 0) = \frac{1}{k_1} \left[e^{ik_L \rho} \left(\frac{2}{\rho^3} + \frac{3i}{k_L \rho^4} \right) + \frac{2k_L^2}{k_1 \rho^2} - \frac{2k_T}{\rho^2} - \frac{2i}{\rho^3} e^{ik_L \rho} \right]. \quad (135)$$

The integral $F_2(\rho, 0)$ may be rewritten as follows:

$$F_2(\rho, 0) = -\frac{k_L k_T}{k_1^2} \int_0^\infty \frac{\gamma_1}{\gamma_1^2} [J_0(\lambda \rho) - J_2(\lambda \rho)] \lambda d\lambda \\ - k_L k_T \int_0^\infty \gamma_1 \left(\frac{1}{k_L k_T \gamma_1 + k_1^2 \gamma_1^2} - \frac{1}{k_1^2 \gamma_1^2} \right) \\ \times [J_0(\lambda \rho) - J_2(\lambda \rho)] \lambda d\lambda. \quad (136)$$

With the same procedure used in Ref. 11, the function $F_2(\rho, 0)$ is derived to be

$$F_2(\rho, 0) \approx \frac{2ik_L k_T}{k_1} e^{ik_L \rho} \left(\frac{1}{\rho} + \frac{i}{k_L \rho^2} \right) \\ - \frac{2ik_L k_T}{k_1^2} \left(\frac{1}{\rho^2} + \frac{i}{2k_L \rho^3} \right) e^{ik_L \rho} \\ + \frac{2k_T}{k_1 \rho^2} + \frac{2ik_L k_T}{k_1^2 \rho^3} + \frac{G(\rho)}{k_1}. \quad (137)$$

The final formula for $B_{1\theta}$ is

$$B_{1\phi} = -\frac{\mu_0}{2\pi k_1} \cos \phi \left(e^{ik_1(z+d)} \left\{ e^{ik_L \rho} \left[\frac{ik_L k_T}{\rho} - \frac{k_T}{\rho^2} - \frac{k_L^2 k_T^2}{k_1} \left(\frac{\pi}{k_L \rho} \right)^{1/2} e^{-ik_L \rho (k_T^2/2k_1)} \mathcal{F} \right] - \frac{i}{\rho^3} e^{ik_T \rho} \right\} \right. \\ \left. + \frac{1}{2} e^{ik_1 r_2} \left(\frac{2}{\rho^3} + \frac{3i}{k_1 \rho^4} \right) + \frac{1}{2} \left(\frac{z-d}{\rho} e^{ik_1 r_1} + \frac{z+d}{\rho} e^{ik_1 r_2} \right) \left(\frac{ik_1^2}{\rho} - \frac{k_1}{\rho^2} \right) \right). \quad (138)$$

F. Formulation for $B_{1\rho}$

The formula for $B_{1\rho}$ is derived as in Ref. 11 from the Maxwell equation

$$B_{1\rho} = -\frac{i}{\omega} \left(\frac{1}{\rho} \frac{\partial E_{1z}}{\partial \phi} - \frac{\partial E_{1\phi}}{\partial z} \right) \quad (139)$$

With the expressions (126) for E_{1z} and (115) for $E_{1\phi}$, the final formula for $B_{1\rho}$ is

$$B_{1\rho} = -\frac{\mu_0}{2\pi k_1} \sin \phi \left(e^{ik_1(z+d)} \left\{ e^{ik_L \rho} \left[\frac{k_T}{\rho^2} + \frac{ik_L k_T^2}{k_1 \rho} \left(\frac{\pi}{k_L \rho} \right)^{1/2} e^{-ik_L \rho (k_T^2/2k_1)} \mathcal{F} \right] + e^{ik_T \rho} \left(\frac{k_T}{\rho^2} + \frac{2i}{\rho^3} \right) \right\} \right. \\ \left. + e^{ik_1 r_2} \left(\frac{ik_1^2}{\rho} - \frac{2k_1}{\rho^2} - \frac{2i}{\rho^3} \right) - \frac{1}{2} \left(\frac{z-d}{\rho} e^{ik_1 r_1} + \frac{z+d}{\rho} e^{ik_1 r_2} \right) \left(\frac{ik_1^2}{\rho} + \frac{2i}{\rho^3} - \frac{3}{k_1 \rho^4} \right) \right). \quad (140)$$

IV. DISCUSSION AND CALCULATION

From the formulas for the components of the electromagnetic field near the surface of the one-dimensionally anisotropic rock, it is seen that the electromagnetic field in Region 1 still consists of three kinds of waves, viz., the direct wave, reflected wave, and lateral wave. The first two are exactly the same as when Region 2 is isotropic. This is not true, however, of the lateral-wave term which now appears separated into two groups. The first group includes terms from the five components E_{1z} , $E_{1\rho}$, $E_{1\phi}$, $B_{1\phi}$, and $B_{1\rho}$ with the wave number $k_2 = k_L$. The second group includes terms from the five components B_{1z} , $B_{1\rho}$, $B_{1\phi}$, $E_{1\phi}$, and $E_{1\rho}$ with the wave number $k_2 = k_T$. They correspond, respectively, to waves of the electric type (TM type) and of the magnetic type (TE type) propagating along the surface in the rock.

At large distances, when $|k_L \rho (k_T^2/2k_1)| \gg 1$, the Fresnel-integral term may be approximated by

$$e^{-ik_L \rho (k_T^2/2k_1)} \mathcal{F} \approx \frac{ik_1}{k_T} \left(\frac{1}{\pi k_L \rho} \right)^{1/2} \left(1 - \frac{ik_1^2}{k_T^2 k_L \rho} \right). \quad (141)$$

With this and $|k_1^2| \gg |k_T^2|$, it follows that the components of the lateral-wave part of the electromagnetic far field may be simplified as follows:

$$E_{1\rho}^L \approx \frac{\omega \mu_0}{2\pi k_1^2} \cos \phi e^{ik_1(z+d)} \left(\frac{k_1^2}{k_T \rho^2} e^{ik_L \rho} + \frac{i}{\rho^3} e^{ik_T \rho} \right), \quad (142)$$

$$E_{1\phi}^L \approx \frac{\omega \mu_0}{2\pi k_1^2} \sin \phi e^{ik_1(z+d)} \left(\frac{ik_1^2}{k_T k_L \rho^3} e^{ik_L \rho} + \frac{k_T}{\rho^2} e^{ik_T \rho} \right), \quad (143)$$

$$E_{1z}^L \approx -\frac{\omega \mu_0}{2\pi k_1^2} \cos \phi e^{ik_1(z+d)} \frac{k_1 k_L}{k_T \rho^2} e^{ik_L \rho}, \quad (144)$$

$$B_{1\phi}^L \approx \frac{\mu_0}{2\pi k_1} \cos \phi e^{ik_1(z+d)} \left(\frac{k_1^2}{k_T \rho^2} e^{ik_L \rho} + \frac{i}{\rho^3} e^{ik_T \rho} \right), \quad (145)$$

$$B_{1\rho}^L \approx -\frac{\mu_0}{2\pi k_1} \sin \phi e^{ik_1(z+d)} \left(\frac{ik_1^2}{k_T k_L \rho^3} e^{ik_L \rho} + \frac{k_T}{\rho^2} e^{ik_T \rho} \right), \quad (146)$$

$$B_{1z}^L \approx \frac{\mu_0}{2\pi k_1^2} \sin \phi e^{ik_1(z+d)} \frac{k_T^2}{\rho^2} e^{ik_T \rho}. \quad (147)$$

From Eqs. (142)–(147) it may be seen that the horizontal electric-field components $E_{1\rho}^L$ and $E_{1\phi}^L$ are proportional to the horizontal magnetic-field components $B_{1\phi}^L$ and $B_{1\rho}^L$, respectively. They include terms of both electric and magnetic type. The vertical components E_{1z} and B_{1z} are much smaller than the corresponding horizontal components, and include only terms of either electric or magnetic type.

In Region 2, on the other hand, due to the boundary condition $k_1^2 E_{1z} = k_L^2 E_{2z}|_{z=0}$, the vertical component E_{2z} is much larger than the horizontal electric-field components. Therefore, the Poynting vector is essentially vertically up into the sea water, and radially outward in the rock. The electromagnetic energy travels down into the rock first. Since the rock is anisotropic, it generates waves of both electric and magnetic type that propagate in the rock along the surface, then leak vertically upward into the sea water. Because the magnetic-type wave has only horizontal electric-field components, the wave number k_T depends only on σ_T . For the electric-type wave in the rock, the vertical electric-field component is much larger than the horizontal components. For it, the wave number k_L depends only on σ_L .

In the near and intermediate distances with $|k_L \rho (k_T^2/2k_1)| < 1$, the Fresnel-integral term is small compared with the other terms, and the formulas for the lateral-wave part of the electromagnetic field can be approximated as

$$E_{1\rho}^L \approx -\frac{\omega \mu_0}{2\pi k_1^2} \cos \phi e^{ik_1(z+d)} \left[\left(\frac{ik_L k_T}{\rho} - \frac{k_T}{\rho^2} \right) e^{ik_L \rho} - \frac{i}{\rho^3} e^{ik_T \rho} \right], \quad (148)$$

$$E_{1\phi}^L \approx \frac{\omega \mu_0}{2\pi k_1^2} \sin \phi e^{ik_1(z+d)} \left[\frac{k_T}{\rho^2} e^{ik_L \rho} + \left(\frac{k_T}{\rho^2} + \frac{2i}{\rho^3} \right) e^{ik_T \rho} \right], \quad (149)$$

$$E_{1z}^L \approx \frac{i\omega\mu_0}{2\pi k_1^2} \cos \phi e^{ik_1(z+d)} \frac{k_L k_T}{k_1} \left(\frac{k_L}{\rho} + \frac{i}{\rho^2} \right) e^{ik_L \rho}, \quad (150)$$

$$B_{1\phi}^L \approx -\frac{\mu_0}{2\pi k_1} \cos \phi e^{ik_1(z+d)} \left[\left(\frac{ik_L k_T}{\rho} - \frac{k_T}{\rho^2} \right) e^{ik_L \rho} - \frac{i}{\rho^3} e^{ik_T \rho} \right], \quad (151)$$

$$B_{1\rho}^L \approx -\frac{\mu_0}{2\pi k_1} \sin \phi e^{ik_1(z+d)} \left[\frac{k_T}{\rho^2} e^{ik_L \rho} + \left(\frac{k_T}{\rho^2} + \frac{2i}{\rho^3} \right) e^{ik_T \rho} \right], \quad (152)$$

$$B_{1z}^L \approx -\frac{i\mu_0}{2\pi k_1^2} \sin \phi e^{ik_1(z+d)} \left(\frac{ik_T^2}{\rho^2} - \frac{3k_T}{\rho^3} - \frac{3i}{\rho^4} \right) e^{ik_T \rho}. \quad (153)$$

In Fig. 2 $|E_{1\rho}|$ is shown as a function of the radial distance ρ when $d = z = 1$ m, $\phi = 0$, and $\sigma_1 = 3.6$ S/m, for the frequencies $f = 1$ Hz and $f = 1$ kHz. The solid lines are for $\sigma_x = \sigma_y = 0.002$ S/m, $\sigma_z = 0.004$ S/m; the dashed lines are

for $\sigma_x = \sigma_y = 0.004$ S/m, $\sigma_z = 0.002$ S/m. The dotted and dot-dashed lines are for the isotropic rock with $\sigma_2 = 0.002$ S/m and $\sigma_2 = 0.004$ S/m, respectively. The corresponding curves for $|E_{1\phi}|$ at $\phi = \pi/2$ are shown in Fig. 3.

In Fig. 2(a), with $f = 1$ Hz, it may be seen that the solid line is very close to the dot-dashed line, and the dashed line is very close to the dotted line. This means that in this frequency and distance range, the magnetic-type wave term of $E_{1\rho}$ is not important, and the lateral wave propagates basically as in the isotropic rock with the conductivity $\sigma_2 = \sigma_L$. When the frequency is increased to 1 kHz, the dashed line in Fig. 2(b) is still very close to the dotted line, but the solid line is separated from the dot-dashed line at larger distances. This is because, when $\sigma_z > \sigma_x = \sigma_y$, the exponential factor $e^{ik_L \rho}$ of the electric-type wave term attenuates faster than the corresponding factor $e^{ik_T \rho}$ of the magnetic-type wave. Therefore,

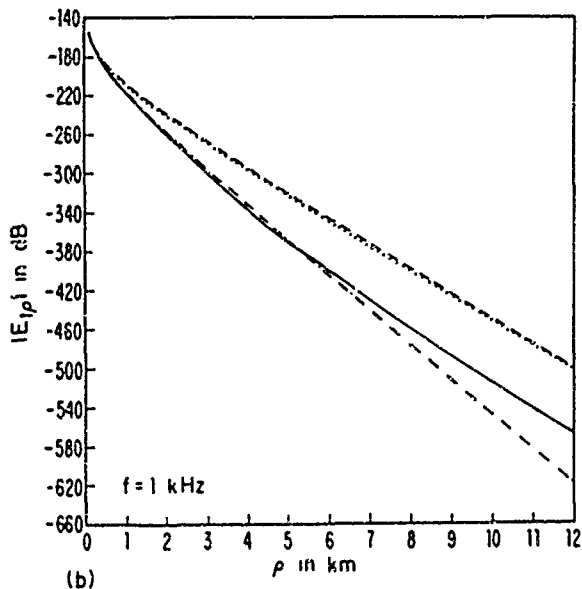
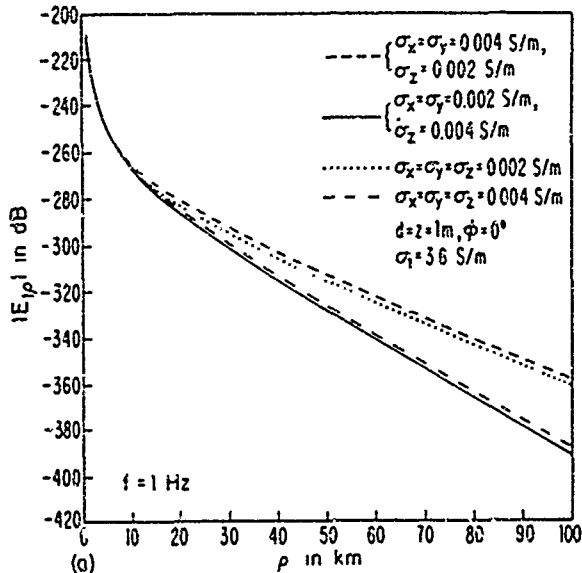


FIG. 2. $|E_{1\rho}|$ at $(\rho, 0, 1)$ m due to unit horizontal electric dipole at $(0, 0, 1)$ m in sea water (Region 1, $\sigma_1 = 3.6$ S/m) over one-dimensionally anisotropic rock (Region 2, $\sigma_x = \sigma_y = \sigma_T$, $\sigma_z = \sigma_L$). (a) $f = 1$ Hz. (b) $f = 1$ kHz.

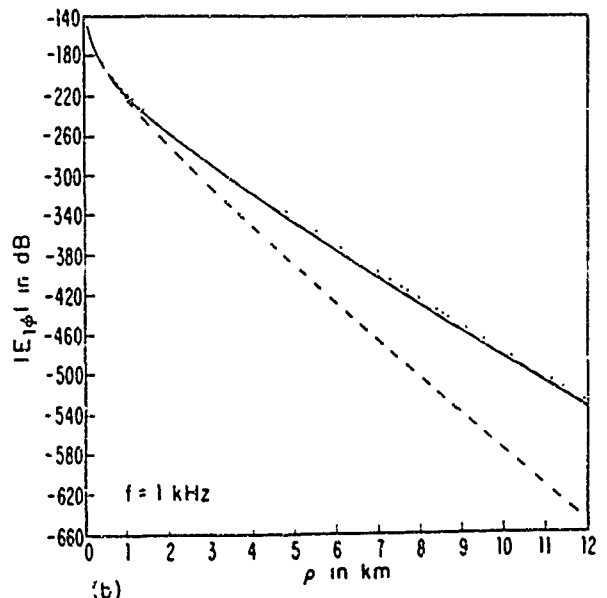
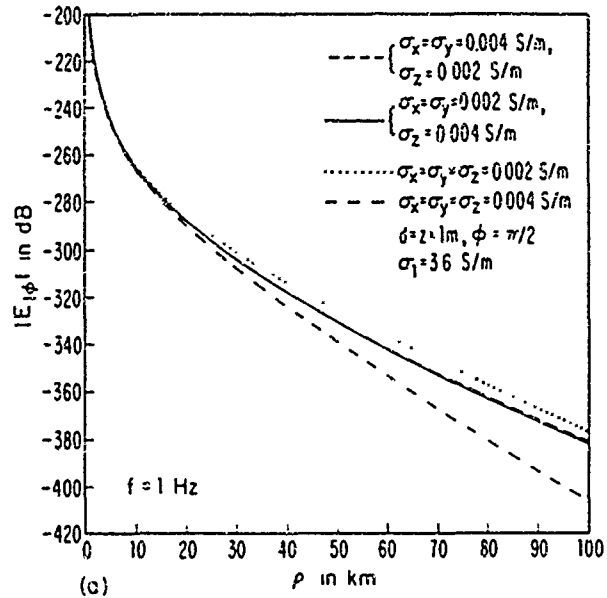


FIG. 3. $|E_{1\phi}|$ at $(\rho, \pi/2, 1)$ m due to unit horizontal electric dipole at $(0, 0, 1)$ m in sea water (Region 1, $\sigma_1 = 3.6$ S/m) over one-dimensionally anisotropic rock (Region 2, $\sigma_x = \sigma_y = \sigma_T$, $\sigma_z = \sigma_L$). (a) $f = 1$ Hz. (b) $f = 1$ kHz.

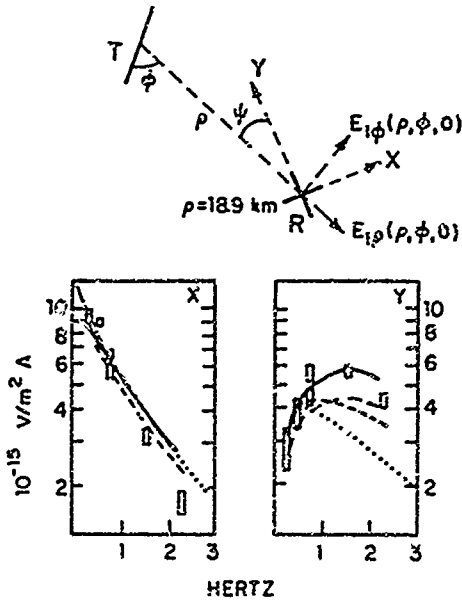


FIG. 4. Traced from Figs. 2 and 3 of Young and Cox (Ref. 3).

at large distances the magnetic-type wave is dominant, and the solid line becomes separated from the dot-dashed line and bent to be parallel with the dotted line.

In Fig. 3 for $|E_{1\phi}|$, in contrast with $|E_{1\rho}|$, the solid lines and dashed lines almost coincide and are located between the dotted and the dot-dashed lines. This is because the coefficients of the electric- and magnetic-type wave terms of the $E_{1\phi}$ component are nearly equal and in phase. Therefore, an interchange of σ_L and σ_T has almost no effect on $|E_{1\phi}|$.

In order to compare the theoretical formulas with the measurements of Young and Cox,³ their Figs. 2 and 3 are reproduced here in Fig. 4. In their experiment the insulated transmitting dipole T is located a distance $\rho = 18.9$ km along the sea floor from the crossed-dipole receiving antenna R .

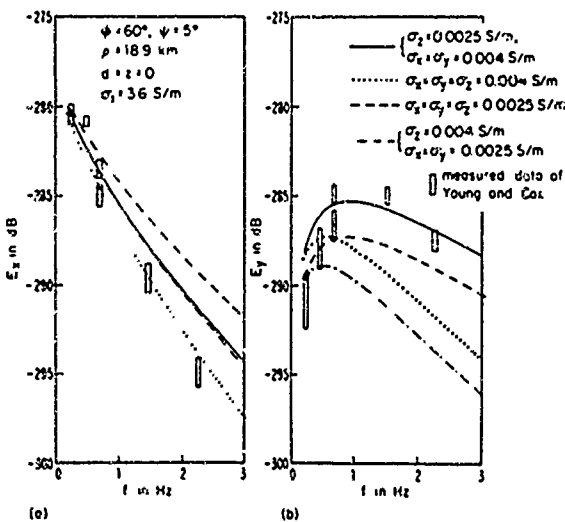


FIG. 5 Comparison of surface wave field components calculated for a one-dimensionally anisotropic rock (Region 2, $\sigma_x = \sigma_y = \sigma_T$, $\sigma_z = \sigma_L$) with sea-floor measurements by Young and Cox (Ref. 3). (a) $E_x = E_{1\rho} \sin \psi + E_{1\phi} \cos \psi$. (b) $E_y = -E_{1\rho} \cos \psi + E_{1\phi} \sin \psi$.

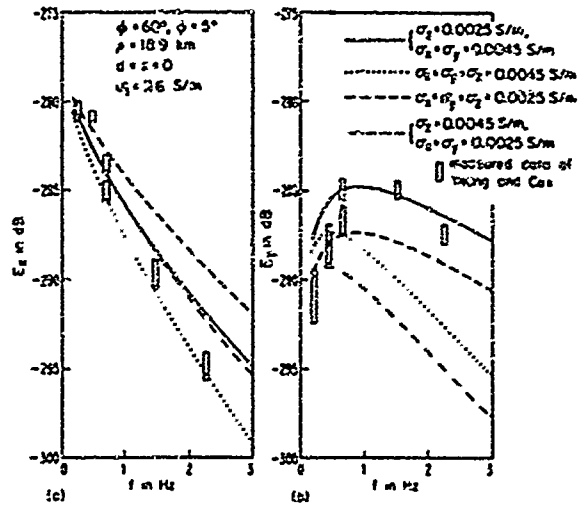


FIG. 6. Comparison of surface-wave field components calculated for a one-dimensionally anisotropic rock (Region 2, $\sigma_x = \sigma_y = \sigma_T$, $\sigma_z = \sigma_L$) with sea-floor measurements by Young and Cox (Ref. 3). (a) $E_x = E_{1\rho} \sin \psi + E_{1\phi} \cos \psi$. (b) $E_y = -E_{1\rho} \cos \psi + E_{1\phi} \sin \psi$.

The angle between the transmitting antenna and the radial line is ϕ . The height of each antenna above the sea floor is zero. Vectors to represent the components $E_{1\rho}(\rho, \phi, 0)$ and $E_{1\phi}(\rho, \phi, 0)$ at R are shown in the figure. The two arms of the crossed-dipole receiving antenna used by Young and Cox were aligned to measure the components E_x and E_y along the arbitrary x and y directions shown in the diagram, rather than $E_{1\rho}$ and $E_{1\phi}$. The angle between the y and ρ axes is ψ . The angles ϕ and ψ are not specified by Young and Cox. However, based on the figure, a reasonable range for ϕ appears to be from 45° to 60° , an estimated range for ψ is from 5° to 15° .

The components E_x and E_y can be expressed in terms of the basic horizontal components $E_{1\rho}(\rho, \phi, 0)$

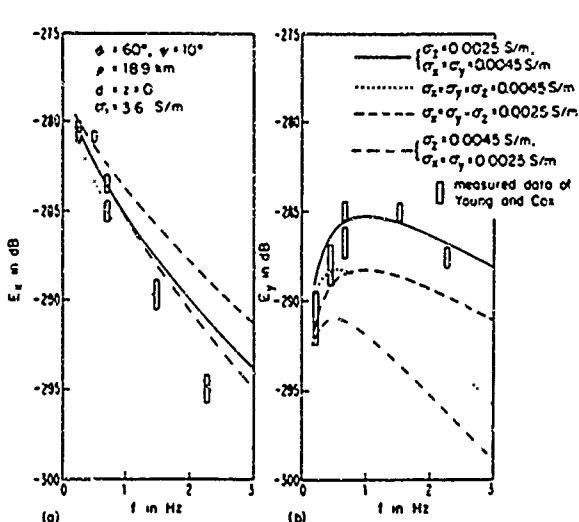


FIG. 7. Comparison of surface-wave field components calculated for a one-dimensionally anisotropic rock (Region 2, $\sigma_x = \sigma_y = \sigma_T$, $\sigma_z = \sigma_L$) with sea-floor measurements by Young and Cox (Ref. 3). (a) $E_x = E_{1\rho} \sin \psi + E_{1\phi} \cos \psi$. (b) $E_y = -E_{1\rho} \cos \psi + E_{1\phi} \sin \psi$.

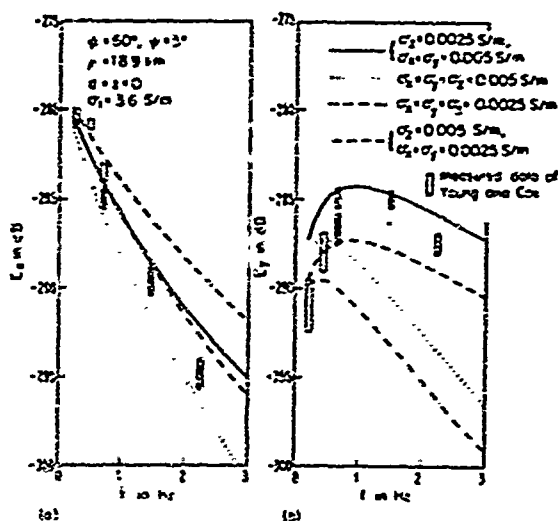


FIG. 8. Comparison of surface-wave field components calculated for a one-dimensionally anisotropic rock (Region 2, $\sigma_x = \sigma_y = \sigma_T$, $\sigma_z = \sigma_L$) with sea-floor measurements by Young and Cox (Ref. 3). (a) $E_x = E_{1p} \sin \psi + E_{1s} \cos \psi$; (b) $E_y = -E_{1p} \cos \psi + E_{1s} \sin \psi$.

$= E_{1p}(\rho, 0, 0) \cos \psi$ and $E_{1s}(\rho, \psi, 0) = E_{1s}(\rho, \pi/2, 0) \sin \psi$ as follows:

$$E_x = E_{1p}(\rho, \psi, 0) \sin \psi + E_{1s}(\rho, \psi, 0) \cos \psi, \quad (154)$$

$$E_y = -E_{1p}(\rho, \psi, 0) \cos \psi + E_{1s}(\rho, \psi, 0) \sin \psi. \quad (155)$$

With the choice $\phi = 60^\circ$, ψ from 5° to 10° , and σ_T, σ_L from 0.0025 to 0.005 S/m, E_x and E_y are plotted and compared with the measured data of Young and Cox³ in Figs. 5-8. In these figures the solid lines and dot-dashed lines represent the one-dimensionally anisotropic rock, the solid lines are for $\sigma_L < \sigma_T$, the dot-dashed lines for $\sigma_L > \sigma_T$. The dotted lines and dashed lines stand for the isotropic rock. From these figures it is seen that for E_y only the solid lines agree well with the measured data. In contrast, for E_x the solid lines and dot-dashed lines are nearly coincident and both of them agree well with the measured data. The reason why E_x is not sensitive to the two different anisotropic models is that E_x is nearly equal to E_{1s} , and for E_{1s} the coefficients of both the electric- and magnetic-type waves are approximately equal. Hence, the interchange of σ_L and σ_T has almost no effect on the total field. From a combination of the figures for E_x and E_y , it may be concluded that the conductivity of the rock where the measurements were made is one-dimensionally anisotropic, with σ_z smaller than $\sigma_x = \sigma_y$. Reasonable values of the conductivities are $\sigma_z \approx 0.0025$ S/m, $\sigma_x = \sigma_y \approx 0.004-0.005$ S/m.

V. CONCLUSION

A set of simple and accurate formulas for the surface wave in a one-dimensionally anisotropic rock along the boundary with sea water has been obtained. When $\sigma_L = \sigma_T$, the new formulas coincide exactly with the formulas of Wu and King⁹⁻¹¹ for the isotropic Region 2. When $\sigma_L \neq \sigma_T$, the lateral-wave part of the electromagnetic field in Region 2 is separated into two terms, the one of electric type with the wave number $k_2 = k_L$, the other of magnetic type with the

wave number $k_2 = k_T$. Since the new formulas are obtained by the same method and under the same conditions as those of Wu and King, it is assured that they are good approximations subject to the same conditions as before. These are $|k_1| > 3|k_T|$, $|k_1| > 3|k_L|$, $\rho > 5z$, $\rho > 5d$, $|k_1\rho| > 3$.

Their application to the measured data of Young and Cox³ provides a simple alternative to their "best fit" model based on the numerical evaluation of in-depth reflections.

ACKNOWLEDGMENTS

The author is grateful to Professor R. W. P. King for giving him many helpful instructions and for correcting the manuscript. He also wishes to thank Ms. Margaret Owens for preparing it for publication. This research was supported in part by the Joint Services Electronics Program under Contract N00014-84-K-0465 with Harvard University.

APPENDIX: THE EVALUATION OF $G(\rho)$ AND $H(\rho)$

The function $G(\rho)$ is defined in Eq. (96) as follows:

$$G(\rho) = -k_L k_T \int_0^\infty \gamma_1^2 \left(\frac{1}{k_1^2 \gamma_1^2 + k_L k_T \gamma_1} - \frac{1}{k_1^2 \gamma_1^2} \right) \times [J_0(\lambda \rho) - J_2(\lambda \rho)] \lambda d\lambda \\ = -\frac{k_L k_T}{2} \int_0^\infty \gamma_1^2 \left(\frac{1}{k_1^2 \gamma_1^2 + k_L k_T \gamma_1} - \frac{1}{k_1^2 \gamma_1^2} \right) \times [H_0^{(1)}(\lambda \rho) - H_2^{(1)}(\lambda \rho)] \lambda d\lambda. \quad (A1)$$

The integrand of Eq. (A1) has two pairs of branch points at $\lambda = \pm k_1$ and $\lambda = \pm k_L$, so that the integral contour may be changed to be along the branch cut in the upper λ plane. Because $\text{Im } k_1 > \text{Im } k_L$, only one branch cut from k_L to infinity is necessary. When $|k_L \rho| > 1$, the Hankel function may be approximated as follows:

$$H_n^{(1)}(\lambda \rho) = \left(\frac{2}{\pi \lambda \rho} \right)^{1/2} e^{i\lambda \rho - \pi/4 - n\pi/2}. \quad (A2)$$

Now let

$$\lambda = k_L(1 + i\tau), \quad d\lambda = ik_L d\tau.$$

The most important contribution to the integral is from the neighborhood of the branch point $\lambda = k_L$, so that

$$\gamma_1 \approx k_1, \quad (A3)$$

$$\gamma_1^2 \approx \pm e^{-i\pi/4} k_L \sqrt{2\tau}. \quad (A4)$$

The plus sign is for the left side of the branch cut, the minus sign for the right side. With Eqs. (A2)-(A4), Eq. (A1) may be rewritten as

$$G(\rho) = -2ik_T k_L^2 \left(\frac{2}{\pi k_L \rho} \right)^{1/2} e^{ik_L \rho} \times \int_0^\infty \left[\frac{1}{\sqrt{2\tau}} - \frac{\sqrt{2\tau}}{2(\tau - ik_T^2/2k_1^2)} \right] e^{-k_L \rho \tau} d\tau \\ = -\frac{2k_T^2 k_L^2}{k_1^2} \left(\frac{1}{\pi k_L \rho} \right)^{1/2} e^{ik_L \rho} \int_0^\infty \frac{e^{-k_L \rho \tau}}{\tau^2 - ik_T^2/2k_1^2} d\tau$$

$$\begin{aligned}
&= -e^{i\pi/4} \frac{k_T^2 k_L^2}{k_1} \left(\frac{2\pi}{k_L \rho} \right)^{1/2} e^{i k_L \rho} e^{-i k_L \rho k_T^2 / 2 k_1^2} \\
&\quad \times \operatorname{erfc} \left\{ \left[-i k_L \rho (k_T^2 / 2 k_1^2) \right]^{1/2} \right\} \\
&= -\frac{2 k_T^2 k_L^2}{k_1} \left(\frac{\pi}{k_L \rho} \right)^{1/2} e^{i k_L \rho} e^{-i k_L \rho k_T^2 / 2 k_1^2} \mathcal{F},
\end{aligned} \tag{A5}$$

where \mathcal{F} is defined in Eq. (99) in terms of the Fresnel integral $C_2(z) + iS_2(z)$ given in Eq. (100).

The function $H(\rho)$ is defined in Eq. (113) as follows:

$$\begin{aligned}
H(\rho) &= -k_L k_T \int_0^\infty \gamma_1^2 \left(\frac{1}{k_1^2 \gamma_1^2 + k_L k_T \gamma_1} - \frac{1}{k_1^2 \gamma_1^2} \right) \\
&\quad \times [J_0(\lambda \rho) + J_2(\lambda \rho)] \lambda d\lambda \\
&= -\frac{k_L k_T}{2} \int_0^\infty \gamma_1^2 \left(\frac{1}{k_1^2 \gamma_1^2 + k_L k_T \gamma_1} - \frac{1}{k_1^2 \gamma_1^2} \right) \\
&\quad \times [H_0^{(1)}(\lambda \rho) + H_2^{(1)}(\lambda \rho)] \lambda d\lambda.
\end{aligned} \tag{A6}$$

Because

$$\begin{aligned}
H_0^{(1)}(\lambda \rho) + H_2^{(1)}(\lambda \rho) &= \frac{2}{\lambda \rho} H_1^{(1)}(\lambda \rho) \\
&= \frac{2}{\lambda \rho} \left(\frac{2}{\pi \lambda \rho} \right)^{1/2} e^{i \lambda \rho - 3\pi/4},
\end{aligned} \tag{A7}$$

and with a similar procedure, $H(\rho)$ may be rewritten as

$$\begin{aligned}
H(\rho) &= -\frac{i}{k_L \rho} G(\rho) \\
&= \frac{2 i k_L^2 k_T^2}{k_1} \frac{\pi^{1/2}}{(k_L \rho)^{3/2}} e^{i k_L \rho} e^{-i k_L \rho k_T^2 / 2 k_1^2} \mathcal{F}.
\end{aligned} \tag{A8}$$

¹A. D. Chave and C. S. Cox, *J. Geophys. Res.* **87**, 5327 (1982).

²C. S. Cox and A. D. Chave, "Controlled source electromagnetic exploration of the continental shelves and oceanic lithosphere," presented at the 1983 International IEEE/AP-S Symposium, Houston, TX (1983).

³P. D. Young and C. S. Cox, *Geophys. Res. Lett.* **8**, 1043 (1981).

⁴E. I. Parkhomenko, *Electrical Properties of Rocks* (Plenum, New York, 1967), pp. 87, 134-136.

⁵R. W. P. King, *J. Appl. Phys.* **58**, 3612 (1985).

⁶R. N. Edwards, D. C. Nobes, and E. Gómez-Treviño, *Geophys.* **49**, 566 (1984).

⁷R. W. P. King, M. Owens, and T. T. Wu, *Radio Sci.* (to be published).

⁸R. W. P. King and G. S. Smith, *Antennas in Matter* (M.I.T., Cambridge, MA, 1981), Chap. 11.

⁹T. T. Wu and R. W. P. King, *Radio Sci.* **17**, 521 (1982).

¹⁰T. T. Wu and R. W. P. King, *Radio Sci.* **17**, 532 (1982); correction 19, 1422 (1984).

¹¹R. W. P. King and T. T. Wu, *J. Appl. Phys.* **54**, 507 (1983); erratum 56, 3365 (1984).

Electromagnetic Surface Waves: New Formulas and Applications

RONOLD W. P. KING, LIFE FELLOW, IEEE

Abstract—Relatively simple and accurate formulas are now available for the complete electromagnetic field generated by vertical and horizontal dipoles located on or near the boundary between two electrically different half-spaces such as air and water or rock and sea water. The principal part of the field is an outward-traveling lateral wave with useful properties. The formulas are given and their application to a variety of problems reviewed briefly. These include: radio communication over the surface of the earth or sea, the wave antenna, communication with submarines using vertical dipoles in air and horizontal dipoles in the sea, the location of buried objects using horizontal dipoles on the surface of the earth, and the measurement of the conductivity of the sea floor.

I. INTRODUCTION

THE ELECTROMAGNETIC field generated by a vertical or horizontal electric dipole on or near the boundary between electrically different regions, such as the air over the surface of the earth (soil, lake, ocean) or sea water over the ocean floor, is important in radio communication and geophysical exploration. The presence of the boundary makes the field very different from that of the same dipole in an infinite homogeneous region or of a monopole on a perfectly conducting plane. This was recognized more than 50 years ago by Sommerfeld [1], [2] who derived general complex integrals for the associated Hertz potentials from which the components of the electromagnetic field could be determined by differentiation. Since that time the problem has been treated by a great many investigators who have sought in various ways to obtain more explicit and useful expressions for the field [3]–[5]. Important comprehensive contributions are by Wait [6] and Baños [7] who obtained sets of quite simple approximate formulas valid in restricted and generally nonoverlapping ranges of the parameters and variables. These are known as the quasistatic or near field, the intermediate field, and the far or asymptotic field. Recently, explicit integrals for the several components of the electromagnetic field have been derived by King [8] for the vertical and by King and Smith [9] for the horizontal electric dipole. These have been evaluated with relatively unimportant restrictions to obtain new, relatively simple and comprehensive formulas for all of the components of the electromagnetic field [8], [10]–[12]. Each of these formulas contains all of the previously derived discrete ranges in a single continuous range that extends from points very near

the dipole to infinity. Because of the simplicity and generality of these expressions, it has been possible to use them in the solution of new problems and to gain new insights into old ones. It is perhaps well to point out that this paper is concerned only with antennas on or below the surface of the earth. Elevated antennas that generate fields incident on the earth at arbitrary angles are not treated.

It is the purpose of this paper to review the new formulas and summarize their application to the solution and new evaluation of problems of current interest.

II. THE ELECTROMAGNETIC FIELD

The rigorous general integrals for the three components of the field of a vertical electric dipole located on or near the plane boundary ($z = 0$) between region 1 ($z \geq 0$) and region 2 ($z \leq 0$) (see Fig. 1) are given by (14)–(16) in Appendix I. The corresponding integrals for the six components of the electromagnetic field of an x -directed, similarly located horizontal electric dipole are given by (35)–(40) in Appendix II. The rotationally symmetric field of the vertical dipole is represented at a point (ρ, z) , the field of the horizontal dipole at (ρ, ϕ, z) in region 1. The cylindrical coordinates ρ, ϕ, z have their origin on the boundary and the angle ϕ is measured from the positive x -axis in the Cartesian system x, y, z . The dipole in each case is located at $(0, 0, d)$ in region 1. The formulas involve the complex wavenumbers

$$k_j = \beta_j + i\alpha_j = [\omega^2 \mu_0 \epsilon_j + i\omega \mu_0 \sigma_j]^{1/2}; \quad j = 1, 2, \quad (1)$$

where ϵ_j is the real effective permittivity, σ_j the real effective conductivity of region j . The time dependence is $e^{-i\omega t}$.

The integrals have been evaluated subject to the following conditions on the wavenumbers and the distances ρ, z , and d . They are

$$|k_1| \geq 3|k_2|; |k_1\rho| \geq 3; \rho \geq 5|z|; \rho \geq 5d. \quad (2)$$

The accuracy of the representation increases with increasing values of $|k_1/k_2|$. If region 1 is the earth and region 2 the air above it, this first condition is satisfied for soil, lake or sea water, but possibly not for the very dry sand of a desert at higher frequencies when $|k_1/k_2| \sim \epsilon_1^{1/2}$. If region 1 is sea water and region 2 the sediment and rock of the sea floor, useful frequencies are usually quite low so that $|k_1/k_2| \geq 3$ reduces to $(\sigma_1/\sigma_2) \geq 9$. Since σ_1 for sea water is of the order of 4 S/m, this condition limits the representation to sediment or rock with $\sigma_2 \leq 0.44$ S/m. The second condition in (2) excludes a small range very close to the dipole. The third and fourth conditions require the radial distance ρ to be considera-

Manuscript received October 19, 1984; revised March 22, 1985. This work was supported in part by the Joint Services Electronics Program under Contract N00014-84-K-0465 and in part by the Office of Naval Research under Contract N00014-79-C-0419, both with Harvard University.

The author is with the Gordon McKay Laboratory, Harvard University, Cambridge, MA 02138.

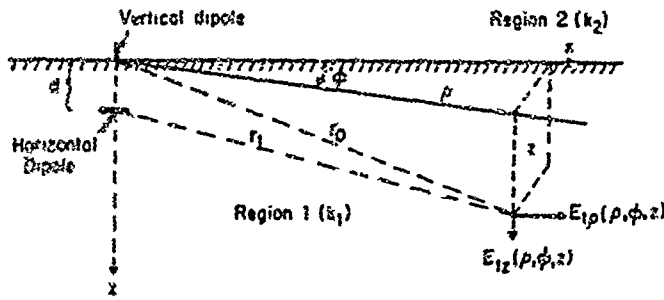


Fig. 1. Vertical dipole on boundary surface; horizontal dipole below boundary surface.

bly greater than both the depth of the dipole in region 1 and the depth of the point of observation. None of these formulas is valid on the surface of an antenna for evaluating its admittance—this has been carried out directly from the integral equations obtained from an application of the boundary conditions [9, chs. 7 and 8].

The complete set of formulas for the components of the electric and magnetic fields at an arbitrary point (ρ, ϕ, z) in region 1 due to a dipole at $(0, 0, d)$ also in region 1 are given by (20)–(22) for the vertical dipole, by (45)–(50) for the horizontal dipole. The fields are expressed as the sum of two parts in the form:

$$\vec{E}_1 = \vec{E}_1^L + \vec{E}_1^D; \quad \vec{B}_1 = \vec{B}_1^L + \vec{B}_1^D. \quad (3)$$

Here the first term with the superscript L represents the surface or lateral wave, the second term with the superscript D the sum of the direct and reflected fields. The lateral wave is identified by the exponential factors $e^{ik_2\rho}e^{ik_1(z+d)}$ which represent a plane wave traveling (1) vertically upward from the dipole in region 1 to the boundary a distance d with an exponential decrease in amplitude $e^{-\alpha_1 d}$ and phase shift $\beta_1 d$ in $e^{i\beta_1 d}$, (2) radially outward in region 2 a distance ρ with an exponential decrease in amplitude $e^{-\alpha_2 \rho}$ and a phase shift $\beta_2 \rho$ in $e^{i\beta_2 \rho}$, and (3) vertically downward a distance z to the point of observation with an exponential attenuation $e^{-\alpha_1 z}$ and phase shift $\beta_1 z$ in $e^{i\beta_1 z}$. If region 2 is air, $\alpha_2 = 0$, and the lateral wave is unattenuated along its radial path. If region 2 is the sea floor, the upward and downward directions are interchanged, $\alpha_2 \neq 0$, and there is significant attenuation along the radial path.

The terms forming the direct field are identified by the exponential factor $e^{ik_1 r_1} = e^{-\alpha_1 r_1} e^{i\beta_1 r_1}$ where $r_1 = [\rho^2 + (z - d)^2]^{1/2}$ which represents a spherical wave expanding from the source with the exponential attenuation $e^{-\alpha_1 r_1}$ and phase shift $\beta_1 r_1$ in $e^{i\beta_1 r_1}$. The terms forming the reflected field [or field from an image dipole at $(0, 0, -d)$ in region 2] are identified by the exponential factor $e^{ik_1 r_2} = e^{-\alpha_1 r_2} e^{i\beta_1 r_2}$ where $r_2 = [\rho^2 + (z + d)^2]^{1/2}$ is the distance from an image source at $(0, 0, -d)$ or the distance traveled by a once-reflected wave. The sum of the direct and reflected waves includes the factors $e^{-\alpha_1 r_1}$ and $e^{-\alpha_1 r_2}$. In most practical cases, $\alpha_1 \gg \alpha_2$ and since $r_2 > r_1 > \rho$, it follows that $e^{-\alpha_1 r_1}$ and $e^{-\alpha_1 r_2}$ are very small compared to $e^{-\alpha_2 \rho}$ when $\rho > \alpha_1^{-1}$ where, then, only the lateral wave is significant.

Also given in Appendices I and II are the components of the

field in region 1 and along the boundary surface in region 2 when the dipole is on the surface in region 2.

III. THE VERTICAL DIPOLE IN AIR ON THE SURFACE OF THE EARTH OR SEA

The electromagnetic field on the surface ($z = 0$) of the earth (region 1) due to a unit ($Ih_e = 1 \text{ A} \cdot \text{m}$) vertical antenna erected in the air (region 2) above the earth at radial distances $\rho > \alpha_1^{-1}$ is given by (32)–(34). The largest component of the electric field is (33):

$$E_{2z}^L(\rho, 0) = \frac{\omega\mu_0}{2\pi k_2} g(\rho) e^{ik_2 \rho}, \quad (4)$$

where, with $k_2 = \omega(\mu_0\epsilon_0)^{1/2}$, $(\omega\mu_0/2\pi k_2) = 60 \Omega$. In Fig. 2 graphs of $20 \log_{10} |E_{2z}(\rho, 0)|$ of the field over sea water are shown as a function of the radial distance ρ ranging from less than a meter to over 1000 km. The parameter is the frequency from 10 Hz to 1 GHz. A typical curve that exhibits all of the essential characteristics is that at $f = 10 \text{ MHz}$. It includes a near-field range from close to the antenna to $k_2 \rho \sim 1$ in which the field decreases very rapidly as ρ^{-3} , then an intermediate range between $k_2 \rho \sim 1$ and $k_2 \rho \sim |k_1/k_2|$ where the field decreases slowly as ρ^{-1} , and finally an asymptotic range with $k_2 \rho > |k_1/k_2|$ where the field decreases as ρ^{-2} . At $f = 10 \text{ Hz}$ the field in Fig. 2 is entirely in the range $|E_{2z}(\rho, 0)| \sim \rho^{-3}$; at $f = 1 \text{ GHz}$ the asymptotic range begins at $\rho \sim 1 \text{ m}$. The best frequency for $\rho = 100 \text{ km}$ is $f \sim 10 \text{ MHz}$. As demonstrated in a recent paper [13], the formula (4) and the graphs in Fig. 2 contain the Norton surface wave over the range where the latter is an adequate approximation.

The largest component of the electric field at a depth z in the sea due to the same unit vertical electric dipole in air with $d \sim 0$ is $E_{1z}(\rho, z)$ as given by (29),

$$E_{1z}^L(\rho, z) = E_{1z}^L(\rho, 0) e^{-\alpha_1 z} e^{i\beta_1 z}, \quad (5)$$

where

$$E_{1z}^L(\rho, 0) = -\frac{\omega\mu_0}{2\pi k_1} f(\rho) e^{ik_2 \rho}. \quad (6)$$

In the useful range $1 \leq k_2 \rho \leq 8|k_1/k_2|$, $f(\rho) = ik_2' \rho$. The application of this formula to communication with submarines in the frequency range 10 to 30 kHz used by the top-loaded vertical monopoles of the Cutler, ME, antenna is discussed in [13]. It is shown that, because of the factor $e^{-\alpha_1 z}$, this frequency range is useful for submarine depths up to about $z = 10 \text{ m}$ with maximum possible output from the very large antennas. For depths up to $z = 50 \text{ m}$, a frequency of the order of $f \sim 1 \text{ kHz}$ is optimum, but it would be difficult to construct an efficient vertical antenna for so low a frequency.

IV. THE HORIZONTAL ELECTRIC DIPOLE NEAR AN AIR-SEA OR AIR-EARTH BOUNDARY

The field in region 1 (sea water) of a unit horizontal electric dipole located at the air-sea water surface with $d \sim 0$ is given by (45a) to be

$$E_{1\rho}^L(\rho, \phi, z) = -\frac{\omega\mu_0 k_2}{2\pi k_1} g(\rho) e^{ik_2 \rho} e^{ik_1 z} \cos \phi. \quad (7)$$

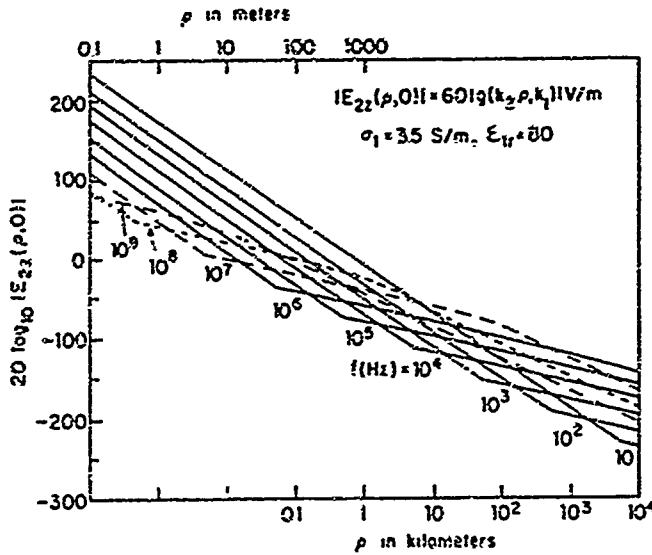


Fig. 2. Magnitude of $E_z(\rho, 0)$ due to a vertical unit electric dipole in air above the surface of sea water. $f = 10$ to 10^9 Hz.

It is smaller than the field (5) of a comparable vertical dipole in air in the direction $\phi = 0$ by a factor k_2/k_1 . However, it is possible to construct large horizontal antennas just below the surface of the sea for use at low frequencies. A properly designed long insulated traveling-wave antenna can have a large effective length so that with large currents the field of such an antenna, viz.,

$$[E_{1\rho}^L(\rho_0, \phi_0, z)]_{am} = I_x(0) h_e(\phi_0) E_{1\rho}^L(\rho_0, \phi_0, z), \quad (8)$$

can be very great compared to that of the unit dipole. This field can be further enhanced by a factor N if N such antennas are arranged side by side in an upward-directed broadside array. A subsurface array for generating lateral waves at $f = 1$ kHz for propagation in the air above sea water and then down into the sea is described in [13].

A horizontal insulated traveling-wave antenna can be laid in the air directly on the surface of the earth or sea. If the insulation is air, such an antenna consists simply of a horizontal wire located at a height d above the surface, i.e., it is a horizontal-wire antenna that generates lateral waves. If the terminating resistance at each end is connected to grounded vertical conductors, the familiar Beverage antenna is obtained. A complete analysis of the wave antenna for both the transmission and reception of lateral electromagnetic waves is in [14]. The optimum effective length for low-frequency operation requires a physically very long structure. On the other hand, at higher frequencies, and in combination with other identical elements, it provides a highly directive transmitting and receiving array, for example, for an over-the-horizon radar. The analysis [14] shows that the contributions to the field from the currents in the short vertical terminations contribute negatively but also negligibly to the field generated by the currents in the long horizontal conductor.

A quite different application of the horizontal electric dipole and the lateral-wave electromagnetic field it generates is the discovery and bounding of a buried or submerged object or a localized region with electrical properties that depart significantly from those of the surroundings. For this purpose a

simple half-wave dipole is placed horizontally just above the surface of the earth. It is center-driven by a suitable emf at a properly selected frequency. In effect, it constitutes an air-insulated horizontal electric dipole lying on the surface of the earth. A point on a buried object at a depth z and radial distance ρ from the transmitting antenna experiences the field given by (45)–(50). If the radial distance satisfies the condition $\rho > \alpha_1^{-1}$, only the lateral-wave part of the field is significant. It will have traveled radially outward a distance ρ and then vertically downward a distance z to where it encounters the buried object. This scatters a field upward which interacts with the incident field in the air above the surface to generate an interference pattern. A horizontal dipole receiving antenna (or a vertical loop) moved about on the surface can detect this pattern and with it the area under which the obstacle is located. A complete analysis of the scattering of lateral electromagnetic waves by a buried insulated conductor is in [15], [16]. Typical interference patterns are shown. A sample is shown in Fig. 3 for a submerged insulated wire. Measured interference patterns have been reported by Bansal [17].

V. THE HORIZONTAL ELECTRIC DIPOLE ON THE SEA FLOOR

An insulated horizontal electric dipole laid on the sea floor is used as a source by geophysicists for measuring the electrical conductivity beneath the oceans. This application is called a controlled or active electromagnetic source method to distinguish it from those that make use of natural electromagnetic fields generated by sources in the earth's magnetosphere and ionosphere. In recent work by Chave and Cox [18] the general integrals (35)–(40) were rederived and applied to a horizontally layered region by replacing the functions P and Q in (41) with generalized response functions and using numerical methods to evaluate the integrals. Their formulation is limited to very low frequencies for which (1) reduces to $k_j = (i\omega\mu_0\sigma_j)^{1/2}$, $j = 1, 2, \dots, n$, where region 1 is the ocean and the remaining $n - 1$ regions are horizontal layers in the lithosphere. Measurements with an insulated horizontal wire on the sea floor have been reported by Young and Cox [19] but no adequate description of the construction and properties of their antenna is provided nor is the method of calculation of the field given. In their discussion, Chave and Cox [18] state that "the mathematical complexity" of the general integral expressions for the electromagnetic field "masks their conceptual simplicity," since each component can be interpreted as the sum of two sets of terms, the one as the "primary field in the ocean," the other as the "field due to an image current induced in the earth." Significantly, no reference is made to the lateral wave that contributes the entire field along the sea floor ($z = 0$) when the lithosphere is treated as a homogeneous, isotropic half-space, and a dominant part when there are reflected fields from horizontal layers at increasing depths in the lithosphere. As seen from (45a), when both receiving and transmitting antennas are on the sea floor ($z = d = 0$), the lateral wave involves only the radial distance ρ between the two antennas in

$$E_{1\rho}^L(\rho, 0, 0) = -\frac{\omega\mu_0 k_2}{2\pi k_1^2} g(\rho) e^{i\omega t}. \quad (9)$$

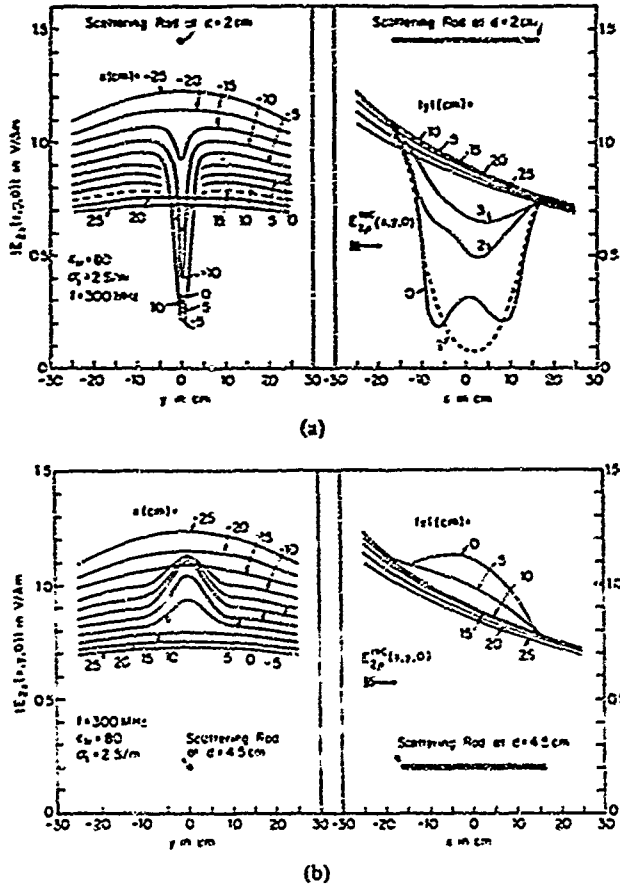


Fig. 3 Electric field in air above insulated scattering rod of length $2l = 33.4$ cm at depth d cm in salt water ($\sigma_1 = 2$ S/m). (a) $d = 2$ cm. (b) $d = 4.5$ cm

Calculations of the Poynting vector [20] show that the maximum depth of penetration of the lateral wave into region 2 is $z_m = \text{Re}(k_2/k_1)\rho/2.718$ [$\sim (\sigma_2/\sigma_1)^{1/2}\rho/2.718$ at low frequencies]. Therefore, the field observed at the radial distance ρ must be interpreted with great care when reflections from layers more or less deep in the lithosphere are superimposed on the lateral wave.

The formula (9) has interesting properties that make it useful in the measurement of the conductivity of the lithosphere below the sea floor when this can be approximated by a homogeneous half-space. The two ranges of interest are

$$E_{1\rho}^L(\rho, 0, 0) \sim \frac{i\omega\mu_0}{2\pi k_1^2 \rho^3}; \quad |k_2\rho| < 1, \quad (10a)$$

$$E_{1\rho}^L(\rho, 0, 0) \sim -\frac{i\omega\mu_0 k_2^2}{2\pi k_1^2} \frac{e^{ik_2\rho}}{\rho}; \quad 1 \leq |k_2\rho| \leq 8|k_1^2/k_2^2|. \quad (10b)$$

The very low frequency near-field formula (10a) does not involve k_2 so that it is useless in the determination of σ_2 from $k_2 \sim (i\omega\mu_0\sigma_2)^{1/2}$. On the other hand, (10b) involves $k_2 = \beta_2 + i\alpha_2$ in the exponential and this suggests interesting possibilities for measuring α_2 . Graphs of $20 \log_{10} |E_{1\rho}^L(\rho, 0, 0)|$ are shown in Fig. 4 as a function of the radial distance from $\rho = 10$ m to $\rho = 100$ km. The conductivity in the form $\sigma_2 = 4$

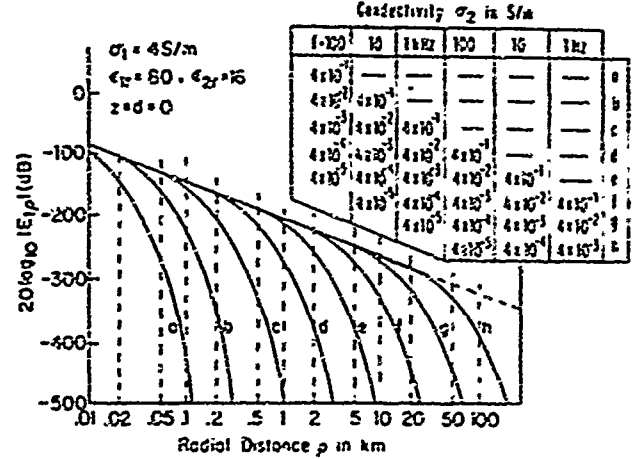


Fig. 4. Radial electric field of antenna on the bottom of the sea ($\sigma_1 = 4$ S/m, $\epsilon_1 = 80$) above rock or deep sediment ($\sigma_2, \epsilon_2 = 16$). Electric moment is 1 A·m.

$\times 10^{-N}$ S/m, $N = 1$ to 5 , and the frequency in the range from 1 Hz to 100 kHz are the parameters. It would appear that with a transmitting antenna on the sea floor, the receiving antenna could be moved radially outward in steps, and $|E_{1\rho}(\rho, 0, 0)|$ measured at each location. A measured graph of $20 \log_{10} |E_{1\rho}(\rho, 0, 0)|$ as a function of ρ should yield a curve like one of those in Fig. 4 from which σ_2 could be determined.

Actual measurements of the conductivity of the sea floor have been reported by Young and Cox [19] who located an insulated dipole transmitting antenna denoted by T (see Fig. 5) on the sea floor and a crossed-dipole receiving antenna R at $\rho \approx 18.9$ km. There was no significant sediment on the sea floor between the two antennas. The crossed dipoles measured E_X and E_Y along arbitrarily oriented X and Y axes as a function of the frequency in the very low range from $f = 0.25$ to $f = 2.25$ Hz. As shown on the upper left in Fig. 5, the X and Y axes are inclined, respectively, with respect to the directions of ρ and ϕ by the small angle ψ . The ranges of the measured values of E_X and E_Y are shown by the rectangular boxes in the lower parts of Fig. 5. Also shown are theoretical curves obtained by Young and Cox presumably by numerical integration of the general integrals. The dotted curves are for a lithosphere consisting of a homogeneous, isotropic half-space with $\sigma_2 = 0.004$ S/m. The three dashed and solid-line curves are for three horizontally layered models with eight different conductivity distributions to a depth of 33 km, as shown on the upper right in Fig. 5. It is seen that the half-space model agrees quite well with the measured values of E_X (lower left) but not with those of E_Y (lower right), while the "best fit" eight-layered model in solid lines agrees moderately well with the measured values of both E_X and E_Y .

On the basis of this agreement Young and Cox concluded that the lithosphere is laterally isotropic and horizontally stratified with a layer of low conductivity between $z = 2$ and $z = 8$ km. They do not explain why the layers reflect E_Y strongly and differently in the three layered models whereas E_X is not appreciably reflected by any of them since all three agree quite well with the half-space model. They also do not explain why E_X and E_Y behave so differently with increasing

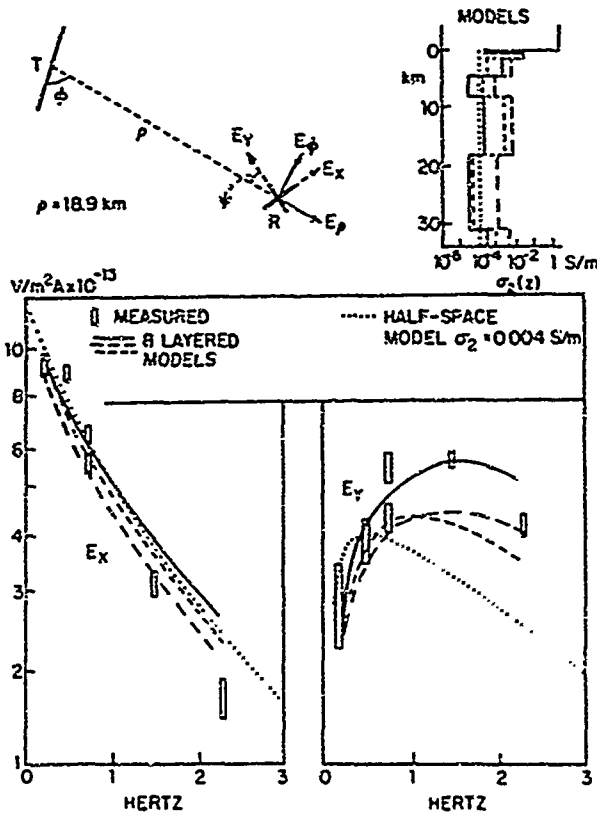


Fig. 5. Measurements and calculations of Young and Cox (1981)

frequency; E_x decreases steadily and rapidly. E_y increases to a maximum and then decreases.

The newly derived relatively simple formulas for the electromagnetic field of a horizontal electric dipole cannot, of course, be used to obtain the field at the boundary of a multilayered region since they apply specifically to two homogeneous, isotropic half-spaces. However, they can be used to explain the graphs obtained by Young and Cox, shown in dotted lines in Fig. 5, for the half-space model of the lithosphere. In the very low-frequency range $f = 0.25$ to 2.25 Hz, the simple integrated formulas for $E_{1\rho}(\rho, \phi, z)$ and $E_{1\phi}(\rho, \phi, z)$ given in (45a) and (46a) are well approximated at $\rho = 18.9$ km and $z + d = 2$ m by

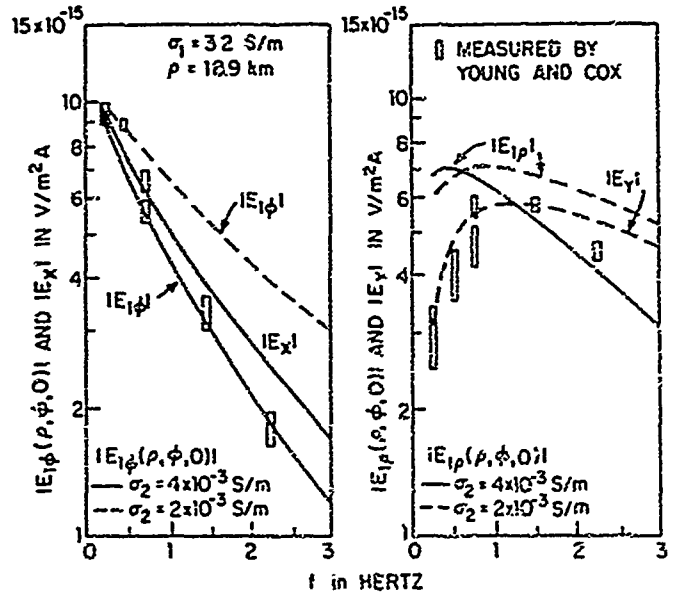
$$E_{1\rho}(\rho, \phi, z) \sim E_{1\rho}(\rho, \phi, 0)$$

$$- \frac{\omega \mu_0 k_2}{2\pi k_1^2} \left[\frac{ik_2}{\rho} - \frac{1}{\rho^2} - \frac{i}{k_2 \rho^3} \right] e^{ik_2 \rho} \cos \phi, \quad (11)$$

$$E_{1\phi}(\rho, \phi, z) \sim E_{1\phi}(\rho, \phi, 0)$$

$$- \frac{\omega \mu_0 k_2}{2\pi k_1^2} \left[\frac{2}{\rho^2} + \frac{2i}{k_2 \rho^3} \right] e^{ik_2 \rho} \sin \phi, \quad (12)$$

where $k_2 = (\omega \mu_0 \sigma_2)^{1/2} = (1 + i)\alpha_2$. It is readily shown that $E_{1\rho}(\rho, 0, 0)$ has a maximum at $\alpha_2 \rho = 1.62$ while $E_{1\phi}(\rho, \pi/2, 0)$ decreases continuously and rapidly with increasing ρ . Specifically, when $\rho = 18.9$ km and $\sigma_2 = 0.004$ S/m, the graphs for $E_{1\rho}(\rho, \phi, 0)$ and $E_{1\phi}(\rho, \phi, 0)$ as calculated from (11) and (12) are shown in solid lines in Fig. 6. The calculated maximum for $|E_{1\rho}(\rho, \phi, 0)|$ is $f = 0.46$ Hz in complete agreement with the numerically evaluated graph of Young and

Fig. 6. Fields calculated from simple formulas; $\phi = 50^\circ$ and $\psi = 10^\circ$.

Cox in Fig. 5. On the other hand, when $\sigma_2 = 0.002$ S/m, the graphs shown in dashed lines in Fig. 6 are obtained. For this conductivity, the maximum of $|E_{1\rho}(\rho, \phi, 0)|$ is at $f = 0.92$ Hz and the rate of decrease of $|E_{1\rho}(\rho, \phi, 0)|$ is reduced. When, with the choice $\phi = 50^\circ$ and $\psi = 10^\circ$,

$$E_x = E_{1\rho} \sin \psi + E_{1\phi} \cos \psi \sim E_{1\phi} \text{ for } \psi \text{ small}$$

is calculated for $\sigma_2 = 0.004$ S/m as shown on the left in Fig. 6 and

$$E_y = -E_{1\rho} \cos \psi + E_{1\phi} \sin \psi \sim -E_{1\rho} \text{ for } \psi \text{ small}$$

is calculated for $\sigma_2 = 0.002$ S/m as shown on the right in Fig. 6, the resulting curves are seen to be in good agreement with the respective measured values. This suggests that a possible model of the lithosphere as seen by the lateral waves may be a half-space which is two-dimensionally anisotropic in the conductivity with the volume density of current \vec{J}_2 given by

$$\begin{pmatrix} J_{2x} \\ J_{2y} \\ J_{2z} \end{pmatrix} = \begin{pmatrix} \sigma_{2a} & 0 & 0 \\ 0 & \sigma_{2a} & 0 \\ 0 & 0 & \sigma_{2b} \end{pmatrix} \begin{pmatrix} E_{2x} \\ E_{2y} \\ E_{2z} \end{pmatrix}, \quad (13)$$

where $\sigma_{2a} = 0.004$ S/m and $\sigma_{2b} = 0.002$ S/m. This possibility could have been tested by Young and Cox if they had oriented their antennas successively so that 1) $\psi = 0$, $\phi = 0$, and 2) $\psi = 0$, $\phi = \pi/2$. With orientation 1), the electric field at the receiving antenna is $E_{1y} = -E_{1\rho}(\rho, 0, 0)$, $E_{1x} = E_{1\phi}(\rho, 0, 0) = 0$. The field in the lithosphere below the receiving antenna has the components $E_{2\rho} = E_{1\rho}$, $E_{2z} = (k_1^2/k_2^2)E_{1z}$, and $B_{2\phi} = B_{1\phi}$. It is dominated by the large component $E_{2z} = J_{2z}/\sigma_{2b}$. This suggests that E_{2y} must depend primarily on $\sigma_{2b} = 0.002$ S/m. Similarly with orientation 2), the electric field at the receiving antenna is $E_{1y} = -E_{1\rho}(\rho, \pi/2, 0) = 0$, $E_{1x} = E_{1\phi}(\rho, \pi/2, 0)$. The associated field in the lithosphere below the receiving antenna has the components $E_{2\rho} = E_{1\rho}$, $B_{2\phi} = B_{1\phi}$, and $B_{2z} = B_{1z}$. Since $E_{2\phi} = J_{2\phi}/\sigma_{2a}$, it is to be expected that E_{2x} depends primarily on $\sigma_{2a} = 0.004$ S/m. By

determining the conductivity σ_{23} from E_{1Y} with the orientation 1) and the conductivity σ_{22} from E_{1X} with the orientation 2), the validity of the anisotropic possibility could have been determined. It is supported by the above discussion and by a complete analytical study carried out by Fan [21].

CONCLUSION

Complete, relatively simple integrated formulas for the electromagnetic fields of vertical and horizontal electric dipoles near the boundary between two electrically different half-spaces have been summarized. Unlike earlier approximate formulas, these provide a single continuous range over all distances from quite close to infinity at all useful frequencies. The near, intermediate, and asymptotic parts of this range join smoothly and continuously. Because of their simplicity, these formulas are readily applied and interpreted. These important properties have been illustrated by a variety of interesting and useful applications in communication and remote sensing.

APPENDIX I

THE VERTICAL ELECTRIC DIPOLE

The general integrals for the three components of the rotationally symmetric electromagnetic field at a point (ρ, z) in region 1 due to a vertical electric dipole with unit electric moment ($Ih_e = 1 \text{ A} \cdot \text{m}$) located at $(0, d)$ in region 1 are [8]:

$$E_{1\rho}(\rho, z) = \frac{i\omega\mu_0}{2\pi k_1^2} \int_0^\infty \left[\pm \frac{e^{\gamma_1|z-d|}}{2} - \frac{e^{\gamma_1(z+d)}}{2} + \frac{k_2^2 \gamma_1 e^{\gamma_1(z+d)}}{k_1^2 \gamma_2 + k_2^2 \gamma_1} \right] J_1(\lambda\rho) \lambda^2 d\lambda; \quad \begin{cases} z > d \\ 0 \leq z \leq d \end{cases} \quad (14)$$

$$E_{1z}(\rho, z) = -\frac{\omega\mu_0}{2\pi k_1^2} \int_0^\infty \left[\frac{e^{\gamma_1|z-d|}}{2\gamma_1} - \frac{e^{\gamma_1(z+d)}}{2\gamma_1} + \frac{k_2^2 e^{\gamma_1(z+d)}}{k_1^2 \gamma_2 + k_2^2 \gamma_1} \right] J_0(\lambda\rho) \lambda^3 d\lambda, \quad (15)$$

$$B_{1\phi}(\rho, z) = \frac{i\mu_0}{2\pi} \int_0^\infty \left[\frac{e^{\gamma_1|z-d|}}{2\gamma_1} - \frac{e^{\gamma_1(z+d)}}{2\gamma_1} + \frac{k_2^2 e^{\gamma_1(z+d)}}{k_1^2 \gamma_2 + k_2^2 \gamma_1} \right] J_1(\lambda\rho) \lambda^2 d\lambda, \quad (16)$$

where

$$\gamma_1 = (k_1^2 - \lambda^2)^{1/2}; \quad \gamma_2 = (k_2^2 - \lambda^2)^{1/2}. \quad (17)$$

Subject to the conditions

$$|k_1| \geq 3|k_2|; |k_1\rho| \geq 3; \rho \geq 5|z|; \rho \geq 5d, \quad (18)$$

the above integrals lead to

$$\begin{aligned} E_{1\rho}(\rho, z) &= E_{1\rho}^L(\rho, z) + E_{1\rho}^D(\rho, z), \\ E_{1z}(\rho, z) &= E_{1z}^L(\rho, z) + E_{1z}^D(\rho, z), \\ B_{1\phi}(\rho, z) &= B_{1\phi}^L(\rho, z) + B_{1\phi}^D(\rho, z). \end{aligned} \quad (19)$$

where

$$E_{1\rho}^L(\rho, z) = -\frac{\omega\mu_0 k_2^2}{2\pi k_1^3} f(\rho) e^{ik_2\rho} e^{ik_1(z+d)}, \quad (20a)$$

$$E_{1\rho}^D(\rho, z) = \frac{\omega\mu_0}{2\pi k_1^2} \left[\frac{ik_2^2 e^{ik_1 r_2}}{k_1 \rho^2} + \frac{1}{2} \left(\frac{z-d}{\rho} e^{ik_1 r_1} - \frac{z+d}{\rho} e^{ik_1 r_2} \right) \times \left(\frac{ik_1^2}{\rho} - \frac{3k_1}{\rho^2} - \frac{3i}{\rho^3} \right) \right], \quad (20b)$$

$$E_{1z}^L(\rho, z) = \frac{\omega\mu_0 k_2^3}{2\pi k_1^4} g(\rho) e^{ik_2\rho} e^{ik_1(z+d)}, \quad (21a)$$

$$E_{1z}^D(\rho, z) = -\frac{\omega\mu_0}{4\pi k_1} (e^{ik_1 r_1} - e^{ik_1 r_2}) \left(\frac{ik_1}{\rho} - \frac{1}{\rho^2} - \frac{i}{k_1 \rho^3} \right), \quad (21b)$$

$$B_{1\phi}^L(\rho, z) = (k_1/\omega) E_{1\rho}^L(\rho, z), \quad (22a)$$

$$B_{1\phi}^D(\rho, z) = -\frac{\mu_0}{4\pi} (e^{ik_1 r_1} - e^{ik_1 r_2}) \left(\frac{ik_1}{\rho} - \frac{1}{\rho^2} \right). \quad (22b)$$

In these formulas

$$r_1 = [\rho^2 + (z-d)^2]^{1/2}; \quad r_2 = [\rho^2 + (z+d)^2]^{1/2}, \quad (23)$$

and

$$f(\rho) - \frac{i}{k_2 \rho^3} = g(\rho) = \frac{ik_2}{\rho} - \frac{1}{\rho^2} - \frac{i}{k_2 \rho^3} - \frac{k_2^3}{k_1} \left(\frac{\pi}{k_2 \rho} \right)^{1/2} e^{-ip\mathfrak{F}(\rho)}, \quad (24)$$

where

$$p = k_2^3 \rho / 2k_1^2 \quad (25)$$

is the "numerical distance,"

$$\mathfrak{F}(\rho) = \frac{1}{2} (1+i) - C_2(p) - iS_2(p) \quad (26)$$

and

$$C_2(p) + iS_2(p) = \int_0^p (2\pi t)^{-1/2} e^{it} dt \quad (27)$$

is the Fresnel integral. For large values of $|k_2\rho|$

$$f(\rho) \sim g(\rho) \sim -k_1^2/k_2^2 \rho^2; \quad |k_2\rho| \geq 8|k_1^2/k_2^2|. \quad (28)$$

When the vertical dipole is located just across the boundary in region 2 with $d \sim 0$ and $r_1 = r_2 = r_0 = (\rho^2 + z^2)^{1/2}$, the components of the field in region 1 are:

$$E_{1\rho}(\rho, z) = -\frac{\omega\mu_0}{2\pi k_1} [f(\rho) e^{ik_2\rho} e^{ik_1 z} - i e^{ik_1 r_0} / \rho^2], \quad (29)$$

$$E_{1z}(\rho, z) = \frac{\omega\mu_0 k_2}{2\pi k_1^2} g(\rho) e^{ik_2\rho} e^{ik_1 z}, \quad (30)$$

$$B_{1\phi}(\rho, z) = -\frac{\mu_0}{2\pi} f(\rho) e^{ik_2\rho} e^{ik_1 z}. \quad (31)$$

The field in region 2 close to the boundary surface is obtained from (29)–(31) with $z \sim 0$ and the use of the boundary conditions for the electromagnetic vectors. Thus

$$E_{2\phi}(\rho, 0) = E_{1\phi}(\rho, 0) = -\frac{\omega\mu_0}{2\pi k_1} [f(\rho)e^{ik_2\rho} - ie^{ik_1\rho}/\rho^2], \quad (32)$$

$$E_{2z}(\rho, 0) = (k_1^2/k_2^2)E_{1z}(\rho, 0) = \frac{\omega\mu_0}{2\pi k_2} g(\rho)e^{ik_2\rho}, \quad (33)$$

$$B_{2\phi}(\rho, 0) = B_{1\phi}(\rho, 0) = -\frac{\mu_0}{2\pi} f(\rho)e^{ik_2\rho}. \quad (34)$$

APPENDIX II

THE HORIZONTAL ELECTRIC DIPOLE

The electromagnetic field at a point (ρ, ϕ, z) in region 1 due to a unit horizontal electric dipole located at $(0, 0, d)$ in region 1 is much more complicated than that of the corresponding vertical dipole located at the same point. Rotational symmetry does not obtain and all six components of the field are generated. Let the dipole be located at the depth d below the origin $(0, 0, 0)$ of the cylindrical coordinates ρ, ϕ, z with its axis along the x -axis from which the cylindrical coordinate ϕ is measured. The electric moment of the dipole is $|I_e h_e| = 1$ A m. The general integrals of the field as derived in King and Smith [9] are:

$$\begin{aligned} E_{1\phi}(\rho, \phi, z) &= -\frac{\omega\mu_0}{4\pi k_1^2} \cos \phi \left(\int_0^\infty \{(\gamma_1 Q/2)[J_0(\lambda\rho) - J_2(\lambda\rho)] \right. \\ &\quad - (k_1^2 P/2\gamma_1)[J_0(\lambda\rho) + J_2(\lambda\rho)]\} e^{\gamma_1(z-d)} \lambda \, d\lambda \\ &\quad + \int_0^\infty \{k_1^2 J_0(\lambda\rho) - (\lambda^2/2)[J_0(\lambda\rho) \\ &\quad \left. - J_2(\lambda\rho)]\} \gamma_1^{-1} e^{\gamma_1(z-d)} \lambda \, d\lambda \right), \quad (35) \\ E_{1\phi}(\rho, \phi, z) &= \frac{\omega\mu_0}{4\pi k_1^2} \sin \phi \left(\int_0^\infty \{(\gamma_1 Q/2)[J_0(\lambda\rho) + J_2(\lambda\rho)] \right. \\ &\quad - (k_1^2 P/2\gamma_1)[J_0(\lambda\rho) - J_2(\lambda\rho)]\} e^{\gamma_1(z-d)} \lambda \, d\lambda \\ &\quad + \int_0^\infty \{k_1^2 J_0(\lambda\rho) - (\lambda^2/2)[J_0(\lambda\rho) \\ &\quad \left. + J_2(\lambda\rho)]\} \gamma_1^{-1} e^{\gamma_1(z-d)} \lambda \, d\lambda \right), \quad (36) \end{aligned}$$

$$\begin{aligned} E_{1z}(\rho, \phi, z) &= \frac{i\omega\mu_0}{4\pi k_1^2} \cos \phi \\ &\quad \times \int_0^\infty [Qe^{\gamma_1(z+d)} \pm e^{\gamma_1(z-d)}] J_1(\lambda\rho) \lambda^2 \, d\lambda, \quad (37) \end{aligned}$$

$$\begin{aligned} B_{1\phi}(\rho, \phi, z) &= -\frac{\mu_0}{4\pi} \sin \phi \left(\int_0^\infty \{(Q/2)[J_0(\lambda\rho) + J_2(\lambda\rho)] \right. \\ &\quad - (P/2)[J_0(\lambda\rho) - J_2(\lambda\rho)]\} e^{\gamma_1(z+d)} \lambda \, d\lambda \\ &\quad \left. \pm \int_0^\infty J_0(\lambda\rho) e^{\gamma_1(z-d)} \lambda \, d\lambda \right), \quad (38) \end{aligned}$$

$$\begin{aligned} B_{1\phi}(\rho, \phi, z) &= -\frac{\mu_0}{4\pi} \cos \phi \left(\int_0^\infty \{(Q/2)[J_0(\lambda\rho) - J_2(\lambda\rho)] \right. \\ &\quad - (P/2)[J_0(\lambda\rho) + J_2(\lambda\rho)]\} e^{\gamma_1(z+d)} \lambda \, d\lambda \\ &\quad \left. \pm \int_0^\infty J_0(\lambda\rho) e^{\gamma_1(z-d)} \lambda \, d\lambda \right), \quad (39) \end{aligned}$$

$$\begin{aligned} B_{1z}(\rho, \phi, z) &= -\frac{i\mu_0}{4\pi} \sin \phi \\ &\quad \times \int_0^\infty [Pe^{\gamma_1(z+d)} - e^{\gamma_1(z-d)}] \gamma_1^{-1} J_1(\lambda\rho) \lambda^2 \, d\lambda. \quad (40) \end{aligned}$$

Where two signs appear, the upper one is for the range $d < z$, the lower sign for $0 \leq z \leq d$. When $\mu_1 = \mu_2 = \mu_0$,

$$P = (\gamma_2 - \gamma_1)/(\gamma_1 + \gamma_2), \quad Q = (k_1^2 \gamma_2 - k_2^2 \gamma_1)/(k_1^2 \gamma_2 + k_2^2 \gamma_1), \quad (41)$$

$$\gamma_1 = (k_1^2 - \lambda^2)^{1/2}, \quad \gamma_2 = (k_2^2 - \lambda^2)^{1/2}. \quad (42)$$

The time dependence is $e^{-i\omega t}$. Note that $E_{1\phi}, E_{1z}, B_{1\phi}$ constitute a field of electric type that vanishes when $\phi = \pi/2$ and is the entire field when $\phi = 0$. Similarly, the components $B_{1\phi}, B_{1z}, E_{1\phi}$ are a field of magnetic type that vanishes when $\phi = 0$ and is the entire field when $\phi = \pi/2$. These two parts of the field are not independent.

Subject to the conditions:

$$|k_1| \geq 3|k_2|; |k_1\rho| \geq 3; \rho \geq 5|z|; \rho \geq 5d, \quad (43)$$

the above integrals lead to

$$\begin{aligned} \vec{E}(\rho, \phi, z) &= \vec{E}^L(\rho, \phi, z) + \vec{E}^D(\rho, \phi, z), \\ \vec{B}(\rho, \phi, z) &= \vec{B}^L(\rho, \phi, z) + \vec{B}^D(\rho, \phi, z), \quad (44) \end{aligned}$$

where

$$\begin{aligned} E_{1\phi}^L(\rho, \phi, z) &= -\frac{\omega\mu_0 k_2}{2\pi k_1^2} g(\rho) e^{ik_2\rho} e^{ik_1(z-d)} \cos \phi \\ &= -[E_{1z}^L(\rho, z)]^v (k_1^2/k_2^2) \cos \phi, \quad (45a) \end{aligned}$$

$$E_{1\phi}^D(\rho, \phi, z) = \frac{\omega\mu_0}{2\pi k_1^2} \left[\frac{k_1}{\rho^2} + \frac{i}{\rho^3} \right] e^{ik_1\rho} \cos \phi, \quad (45b)$$

$$\begin{aligned} E_{1z}^L(\rho, \phi, z) &= \frac{\omega\mu_0}{\pi k_1^2} \left[\frac{k_2}{\rho^2} + \frac{i}{\rho^3} + \frac{ik_2^3}{2k_1\rho} \left(\frac{\pi}{k_2\rho} \right)^{1/2} e^{-i\pi/4} \mathcal{F}(\rho) \right] \\ &\quad \times e^{ik_2\rho} e^{ik_1(z-d)} \sin \phi, \quad (46a) \end{aligned}$$

$$\begin{aligned} E_{1z}^D(\rho, \phi, z) &= \frac{\omega\mu_0}{\pi k_1^2} \left\{ e^{ik_1\rho} \left[\frac{ik_1^2}{2\rho} - \frac{k_1}{\rho^2} - \frac{i}{\rho^3} \right] - \frac{1}{4} (e^{ik_1\rho_1} + e^{ik_1\rho_2}) \right. \\ &\quad \left. \times \left[\frac{ik_1^2}{\rho} - \frac{k_1}{\rho^2} - \frac{i}{\rho^3} \right] \right\} \sin \phi, \quad (46b) \end{aligned}$$

$$E_{1z}^L(\rho, \phi, z) = \frac{\omega\mu_0 k_2^2}{2\pi k_1^2} f(\rho) e^{ik_2 z} e^{ik_1(z+d)} \cos \phi$$

$$= -[E_{1z}^L(\rho, z)]^* \cos \phi, \quad (47a)$$

$$E_{1z}^D(\rho, \phi, z)$$

$$= -\frac{\omega\mu_0}{2\pi k_1^2} \left\{ \frac{ik_2^2 e^{ik_1 r_2}}{k_1 \rho^2} + \frac{1}{2} \left(\frac{z-d}{\rho} e^{ik_1 r_1} + \frac{z+d}{\rho} e^{ik_1 r_2} \right) \right.$$

$$\times \left[\frac{ik_1^2}{\rho} - \frac{3k_1}{\rho^2} - \frac{3i}{\rho^3} \right] \left. \right\} \cos \phi, \quad (47b)$$

$$B_{1z}^L(\rho, \phi, z)$$

$$= -\frac{\mu_0}{2\pi k_1} \left[\frac{2k_2}{\rho^2} + \frac{2i}{\rho^3} + \frac{ik_2^3}{k_1 \rho} \left(\frac{\pi}{k_2 \rho} \right)^{1/2} e^{-\varphi \mathcal{F}(\rho)} \right]$$

$$\times e^{ik_2 z} e^{ik_1(z+d)} \sin \phi, \quad (48a)$$

$$B_{1z}^D(\rho, \phi, z)$$

$$= -\frac{\mu_0}{2\pi k_1} \left\{ e^{ik_1 r_2} \left(\frac{z+d}{\rho} \right) \left[\frac{ik_1^2}{\rho} - \frac{2k_1}{\rho^2} - \frac{2i}{\rho^3} \right] \right.$$

$$- \frac{1}{2} \left(\frac{z-d}{\rho} e^{ik_1 r_1} + \frac{z+d}{\rho} e^{ik_1 r_2} \right)$$

$$\times \left[\frac{ik_1^2}{\rho} + \frac{2i}{\rho^3} - \frac{3}{k_1 \rho^4} \right] \left. \right\} \sin \phi, \quad (48b)$$

$$B_{1z}^L(\rho, \phi, z) = (k_1/\omega) E_{1z}^L(\rho, \phi, z), \quad (49a)$$

$$B_{1z}^D(\rho, \phi, z) = -\frac{\mu_0}{4\pi k_1} \left\{ e^{ik_1 r_2} \left[\frac{2}{\rho^3} + \frac{3i}{k_1 \rho^4} \right] \right.$$

$$+ \left(\frac{z-d}{\rho} e^{ik_1 r_1} + \frac{z+d}{\rho} e^{ik_1 r_2} \right) \left[\frac{ik_1^2}{\rho} - \frac{k_1}{\rho^2} \right] \left. \right\} \cos \phi, \quad (49b)$$

$$B_{1z}^L(\rho, \phi, z) = \frac{\mu_0}{2\pi k_1^2} \left[\frac{k_2^2}{\rho^2} + \frac{3ik_2}{\rho^3} - \frac{3}{\rho^4} \right]$$

$$\times e^{ik_2 z} e^{ik_1(z+d)} \sin \phi, \quad (50a)$$

$$B_{1z}^D(\rho, \phi, z) = -\frac{\mu_0}{2\pi k_1^2} \left\{ e^{ik_1 r_2} \left[\frac{k_1^2}{\rho^2} + \frac{3ik_1}{\rho^3} - \frac{3}{\rho^4} \right] \right.$$

$$+ \frac{1}{2} (e^{ik_1 r_1} - e^{ik_1 r_2}) \left[\frac{ik_1^3}{\rho} - \frac{k_1^2}{\rho^2} \right] \left. \right\} \sin \phi. \quad (50b)$$

In these formulas r_1 and r_2 are defined in (23), $f(\rho)$ and $g(\rho)$ in (24), p in (25), and $\mathcal{F}(\rho)$ in (26).

When the dipole is moved to the surface, the field in region 1 is given by the above formulas with $d = 0$. The field is the same whether the horizontal dipole is just above the surface in region 2 or just below the surface in region 1, so long as the unit electric moment is maintained. This will require different driving voltages in the two regions.

The field in region 2 close to the boundary surface when the dipole is on the boundary is obtained from (45a), (45b)-(50a), (50b) by setting $d = z = 0$ and making use of the boundary

conditions. Thus

$$E_{2z}(\rho, \phi, 0) = E_{1z}(\rho, \phi, 0) = -\frac{\omega\mu_0}{2\pi k_1^2}$$

$$\cdot \left\{ k_2 g(\rho) e^{ik_2 z} - \left[\frac{k_1}{\rho^2} + \frac{i}{\rho^3} \right] e^{ik_1 \rho} \right\} \cos \phi, \quad (51)$$

$$E_{2\theta}(\rho, \phi, 0) = E_{1\theta}(\rho, \phi, 0) = \frac{\omega\mu_0}{\pi k_1^2} \left\{ \left[\frac{k_2}{\rho^2} \right. \right.$$

$$+ \frac{i}{\rho^3} + \frac{ik_2^3}{2k_1 \rho} \left(\frac{\pi}{k_2 \rho} \right)^{1/2} e^{-\varphi \mathcal{F}(\rho)} \left. \right] e^{ik_2 \rho}$$

$$- \frac{1}{2} \left[\frac{k_1}{\rho^2} + \frac{i}{\rho^3} \right] e^{ik_1 \rho} \left. \right\} \sin \phi, \quad (52)$$

$$E_{2z}(\rho, \phi, 0) = (k_1^2/k_2^2) E_{1z}(\rho, \phi, 0)$$

$$= \frac{\omega\mu_0}{2\pi k_1} \left[f(\rho) e^{ik_2 z} - \frac{ie^{ik_1 \rho}}{\rho^2} \right] \cos \phi, \quad (53)$$

$$B_{2z}(\rho, \phi, 0) = B_{1z}(\rho, \phi, 0) = -\frac{\mu_0}{2\pi k_1}$$

$$\times \left\{ \left[\frac{2k_2}{\rho^2} + \frac{2i}{\rho^3} + \frac{ik_2^3}{k_1 \rho} \left(\frac{\pi}{k_2 \rho} \right)^{1/2} e^{-\varphi \mathcal{F}(\rho)} \right] \right.$$

$$\times e^{ik_2 z} + \left[\frac{ik_1^2}{\rho} - \frac{2k_1}{\rho^2} - \frac{2i}{\rho^3} \right] e^{ik_1 \rho} \left. \right\} \sin \phi, \quad (54)$$

$$B_{2\theta}(\rho, \phi, 0) = B_{1\theta}(\rho, \phi, 0)$$

$$= -\frac{\mu_0}{2\pi k_1} \left\{ k_2 g(\rho) e^{ik_2 z} + \left[\frac{1}{\rho^3} + \frac{3i}{2k_1 \rho^4} \right] e^{ik_1 \rho} \right\} \cos \phi, \quad (55)$$

$$B_{2z}(\rho, \phi, 0) = B_{1z}(\rho, \phi, 0)$$

$$= \frac{\mu_0}{2\pi k_1^2} \left\{ \left[\frac{k_2^2}{\rho^2} + \frac{3ik_2}{\rho^3} - \frac{3}{\rho^4} \right] e^{ik_2 \rho} \right.$$

$$- \left[\frac{k_1^2}{\rho^2} + \frac{3ik_1}{\rho^3} - \frac{3}{\rho^4} \right] e^{ik_1 \rho} \left. \right\} \sin \phi. \quad (56)$$

REFERENCES

- [1] A. Sommerfeld, "Propagation of waves in wireless telegraphy," *Ann. Phys.*, vol. 28, pp. 665-736, Mar. 1909.
- [2] —, "Propagation of waves in wireless telegraphy," *Ann. Phys.*, vol. 81, pp. 1135-1153, Dec. 1926.
- [3] W. H. Wise, "Asymptotic dipole radiation formulae," *Bell Syst. Tech. J.*, vol. 8, pp. 662-671, Oct. 1929.
- [4] F. H. Murray, "Asymptotic dipole expansions for small horizontal angles," *Proc. Camb. Phil. Soc.*, vol. 28, pp. 433-441, Oct. 31, 1932.
- [5] D. C. Chang and R. J. Fisher, "A unified theory on radiation of a vertical electric dipole above a dissipative earth," *Radio Sci.*, vol. 9, pp. 1129-1138, Dec. 1974.
- [6] J. R. Wait, "The electromagnetic fields of a horizontal dipole in the presence of a conducting half-space," *Can. J. Phys.*, vol. 39, pp. 1017-1028, 1961.
- [7] A. Baños, Jr., *Dipole Radiation in the Presence of a Conducting Half-Space*, Oxford, England, Pergamon, 1966.
- [8] R. W. P. King, "New formulas for the electromagnetic field of a

vertical electric dipole in a dielectric or conducting half-space near its horizontal interface." *J. Appl. Phys.*, vol. 53, pp. 8476-8482, Dec. 1982; erratum, vol. 56, p. 3366, Dec. 1984.

- [9] R. W. P. King and G. S. Smith, *Antennas in Matter*. Cambridge, MA: MIT Press, 1981.
- [10] T. T. Wu and R. W. P. King, "Lateral waves: A new formula and interference patterns," *Radio Sci.*, vol. 17, pp. 521-531, May-June 1982.
- [11] —, "Lateral waves: New formulas for E_{1a} and E_{1z} ," *Radio Sci.*, vol. 17, pp. 532-538, May-June 1982; correction, vol. 19, p. 1422, Sept.-Oct. 1984.
- [12] R. W. P. King and T. T. Wu, "Lateral waves: New formulas for the magnetic field," *J. Appl. Phys.*, vol. 54, pp. 507-514, Feb. 1983; erratum, vol. 56, p. 3365, Dec. 1984.
- [13] R. W. P. King and M. F. Brown, "Lateral electromagnetic waves along plane boundaries: A summarizing approach," *Proc. IEEE*, vol. 72, pp. 595-611, May 1984.
- [14] R. W. P. King, "The wave antenna for transmission and reception," *IEEE Trans. Antennas Propagat.*, vol. AP-31, pp. 956-965, Nov. 1983.
- [15] —, "The scattering of lateral waves by buried or submerged objects. I. The incident lateral-wave field," *J. Appl. Phys.*, vol. 57, pp. 1453-1459, Mar. 1985.
- [16] —, "The scattering of lateral waves by buried or submerged objects. II. The electric field on the surface above a buried insulated wire," *J. Appl. Phys.*, vol. 57, pp. 1460-1472, Mar. 1985.
- [17] R. Bansal, "Electromagnetic scattering from conducting objects immersed in a dissipative half space," presented at the Nat. Radio Sci. Meeting, Boston, MA, June 1984.
- [18] A. D. Chave and C. S. Cox, "Controlled electromagnetic sources for measuring electrical conductivity beneath the oceans. I. Forward problem and model study," *J. Geophys. Res.*, vol. 87, pp. 5327-5338, 1982.
- [19] P. D. Young and C. S. Cox, "Electromagnetic active source sounding

near the East Pacific Rise," *Geophys. Res. Lett.*, vol. 8, pp. 1043-1046, 1981.

- [20] R. W. P. King, M. Owens, and T. T. Wu, "Properties of lateral electromagnetic fields and their application," *Radio Sci.*, to be published.
- [21] W. -Y. Pan, "Surface wave propagation along the boundary between sea water and one-dimensionally anisotropic rock," *J. Appl. Phys.*, to be published.



Ronald W. P. King (A'30-SM'43-F'53-LF'71) was born in Williamstown, MA, on September 19, 1905. He received the B.A. and M.S. degrees in physics from the University of Rochester, Rochester, NY, in 1927 and 1929, respectively, and the Ph.D. degree from the University of Wisconsin, Madison, in 1932, after having done graduate work at the University of Munich, Munich, Germany, and at Cornell University, Ithaca, NY.

He served as a Teaching and Research Assistant at the University of Wisconsin from 1932 to 1934, and as an Instructor and Assistant Professor of Physics at Lafayette College, Easton, PA, from 1934 to 1937. During the academic year 1937-1938 he was a Guggenheim Fellow in Germany. In 1938 he joined the faculty of Harvard University, Cambridge, MA.

Dr. King has been Gordon McKay Professor of Applied Physics at Harvard from 1946 to 1972, when he became Gordon McKay Professor of Applied Physics, Emeritus. He was again a Guggenheim Fellow in 1958. He is a fellow of the American Physical Society and the American Academy of Arts and Sciences, a corresponding member of the Bavarian Academy of Sciences, and a member of the American Association for the Advancement of Science, Commission B of the International Scientific Radio Union, Phi Beta Kappa, and Sigma Xi. He is the author or coauthor of ten books, numerous articles in books and encyclopedias, and over 240 original papers in technical journals.

Shallow sounding of crustal regions using electromagnetic surface waves

M. F. Brown and R. W. P. King

Gordon McKay Laboratory, Harvard University, Cambridge, Massachusetts

(Received November 14, 1985; revised April 14, 1986; accepted April 14, 1986.)

A specific physical interpretation of the effect of relative permittivities ϵ , and conductivities σ upon the amplitude and phase of propagating electromagnetic surface waves is given, where ϵ , and σ characterize the layered material regions of a planetary lithosphere. The interpretation is made possible by the availability of simple formulas for the fields of vertical and horizontal unit electric dipoles near interfaces between regions of matter, the earth's lithosphere at its interface with salt water is used as an example. The ranges of ϵ , σ , frequency f , and radial distance ρ over which the formulas apply are shown to be quite broad. The $E_{1\rho}$ component (the radial electric field in region 1, characterized by complex wave number k_1 and adjoined at a planar interface to region 2, characterized by k_2 , where $|k_1|^2 \gg |k_2|^2$) is discussed in detail. The attenuation of $20 \log_{10} |E_{1\rho}|$ as a function of ρ and ρ/δ_2 , where δ is the skin depth, is illustrated for conductivity ratios $\sigma_2/\sigma_1 = 10^{-1}$ to 10^{-3} , over a range of f from 1 Hz to 10^5 Hz. $|E_{1\rho}|$ is shown to be significant for determining permittivities ϵ_2 at the higher frequencies in this range. The use of $|E_{1\rho}|$ to infer conductivities σ_2 at lower frequencies in shallow sounding of the earth's sea floor is discussed in terms of specific lithological and sediment-related parameters. The technology required to transmit and receive $20 \log_{10} |E_{1\rho}|$ at freshwater and saltwater interfaces with the earth's crust is addressed. A specific experiment is proposed for testing a specialized insulated antenna for seafloor use in shallow coastal waters at 1 kHz.

1. INTRODUCTION

The electromagnetic field which exists near an interface of the type depicted between regions 1 and 2 of Figure 1 includes a surface wave component. The surface wave is termed a "lateral wave"; regions 1 and 2 may consist of a diverse range of planetary constituents. Region 1 is typified by a hydrospheric liquid, for example, salt water, while region 2 may be a poorly conducting or nonconducting atmospheric gas or a range of lithospheric materials such as rock, soil, oil, or ice.

Although the surface wave does not penetrate deeply into region 2 [King *et al.*, 1981; King *et al.*, 1986] for small radial distances ρ from the source dipole, its utility in shallow crustal sounding is strongly indicated by recent theory [Wu and King, 1982a, b; King and Wu, 1983; King and Brown, 1984] and experiments [Brown *et al.*, 1982, 1984]. At large ρ the effects of penetration of electrically thin layers by the surface wave are evidenced at observation

points P near the interface; underlying basement layers are sampled.

The aforementioned theory and experiments at Harvard University have been concerned with the overall electromagnetic attributes (simple analytical formulas and measured decay rates, reflection, and scattering from obstacles) of lateral waves. A specialization to geoelectromagnetics of equations which have been experimentally verified and are perfectly general, excepting the precise constraints $|k_1| \geq 3|k_2|$, $\rho \geq 5d$, $\rho \geq 5z$, and $|k_1\rho| \geq 3$, is the objective of the present paper. Here z and d are indicated in Figure 1, k_1 and k_2 are complex wave numbers describing propagation in regions 1 and 2, respectively, and ρ is the radial distance from the radiation source.

Related theoretical work all derives from the problem described by the original Sommerfeld integrals [Sommerfeld, 1926]. This includes (1) approximations for Sommerfeld equations primarily concerned with fields in air [Norton, 1936], (2) field formulas partitioned into nonoverlapping domains of frequency and distance [Baños, 1966], and (3) purely numerical evaluations of Sommerfeld integrals [Chave and Cox, 1982].

Related experimental work includes (1) physical

Copyright 1986 by the American Geophysical Union

Paper number 6S0196.

0048-6604/86/006S-0196\$08.00

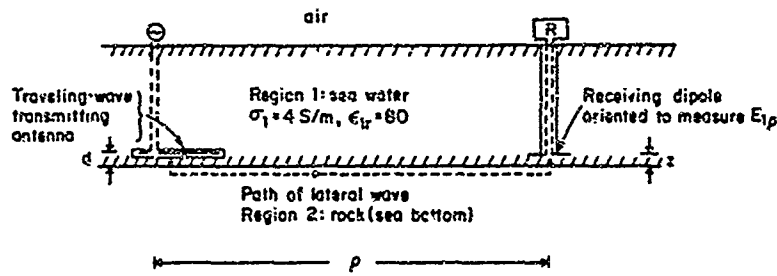


Fig. 1. Schematic diagram of directional transmitter and receiver near the bottom of the sea.

modeling of wave propagation by King and Mailey [1965] and (2) source-receiver measurements at 21°N near the East Pacific Rise by Young and Cox [1981]. The first of these investigations is concerned primarily with fields in air, the analysis of the present paper is distinguished from it by including explicit treatment of measured fields in a liquid conducting medium (salt water) as a means of determining the properties of an adjacent lithosphere. The second investigation describes an interesting experiment involving fields at the sea floor in which frequencies of 0.25–2.25 Hz are used with antenna separations of 18.9 km. At such low frequencies the electromagnetic signal is intended for deep sounding and may be characterized by a “diffusion” process. Even at the frequencies of the Young and Cox experiment, the authors describe a signal traveling “... from the transmitter to the receiver in a down-under-up path, thereby usefully sampling the electrical conductivity properties of the crustal and upper mantle rocks in the region between.” The formulas of the present paper allow a precise physical interpretation to be given for the “down-under-up” signal.

2. DERIVATION OF CYLINDRICAL FIELD COMPONENTS

The barest description of the problem to be treated is illustrated in Figure 2. The adjacent layers of matter adjoining at a plane $z = 0$ may be excited by a source dipole specified by a depth distance d . The

solution of the Maxwell equations shown on the right in the figure using boundary conditions attendant to the material layers (which may be referred to as “half-spaces”) may be made using potential functions of polarization or magnetization (Hertz potentials). Legions of such solutions have been obtained and expanded in either (1) bundles of inhomogeneous plane waves or (2) cylindrical waves, building upon the original Sommerfeld integrals [Sommerfeld, 1909, 1926]; see the list in the bibliography of the monograph by Baños [1966]. Alternatively, a direct solution may be found for which no potentials are introduced; in this way, expressions for all of the field components in both types of coordinates are given by King and Smith [1981, chap. 11] for a unit horizontal electric dipole source. When one half-space is highly conducting, for example, the sea at the earth's sea floor, the radial (E_ρ) component is the most important in that half-space (strongest in relation to the other cylindrical components). This component is dominant in magnitude along the radial line $\phi = 0$ parallel to the antenna except very near the source [King et al., 1980]. It is given by

$$E_{1\rho}(\rho, \phi, z) = -\frac{\omega\mu_0}{4\pi k_1^2} \cos \phi \left\{ \int_0^\infty \Lambda d\Lambda [k_1^2 J_0(\Lambda\rho) - (\Lambda^2/2)(J_0(\Lambda\rho) - J_2(\Lambda\rho))] \Gamma_1^{-1} e^{-\Gamma_1 |z-d|} + \int_0^\infty \Lambda d\Lambda \left[\frac{(k_1^2 - \Lambda^2)^{1/2}}{2} \frac{(\tilde{\epsilon}_1 \Gamma_2 - \tilde{\epsilon}_2 \Gamma_1)}{(\tilde{\epsilon}_1 \Gamma_2 + \tilde{\epsilon}_2 \Gamma_1)} (J_0(\Lambda\rho) - J_2(\Lambda\rho)) \right] \right\}$$

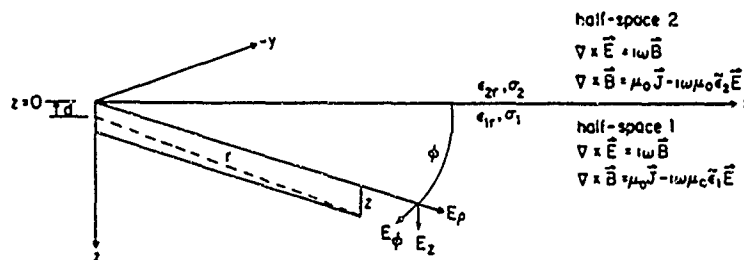


Fig. 2. Adjoining half-spaces with associated Maxwell equations.

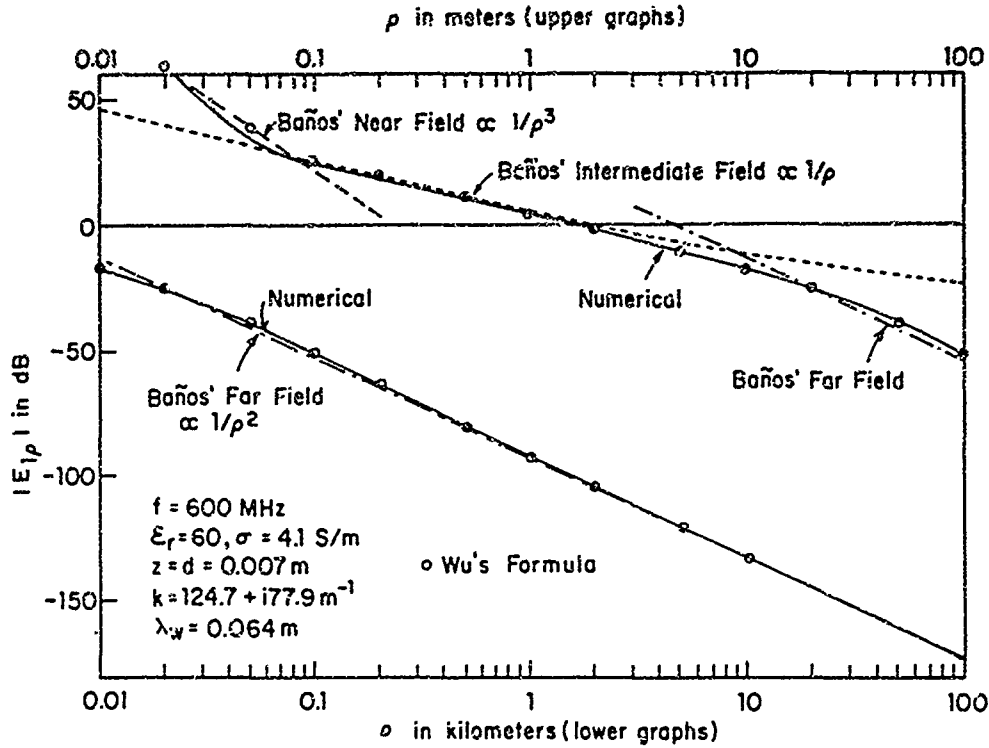


Fig. 3. Theoretical $|E_{1\rho}|$ for a lateral wave along sea water-air boundary.

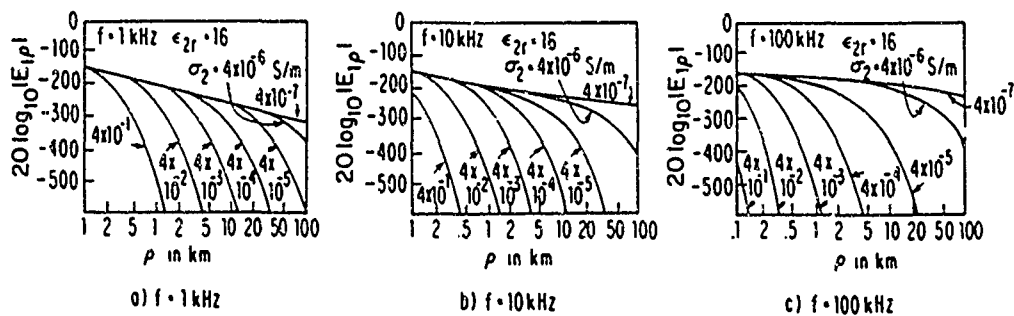
$$-\frac{k_1^2}{2\Gamma_1} \frac{(\Gamma_2 - \Gamma_1)}{(\Gamma_2 + \Gamma_1)} (J_0(\Lambda\rho) + J_2(\Lambda\rho)) \left[e^{i\Gamma_1(z-d)} \right] \quad (1)$$

Here $\bar{\epsilon}_1$ and $\bar{\epsilon}_2$ are the complex permittivities of regions 1 and 2, respectively; $\Gamma_j = (k_j^2 - \Lambda^2)^{1/2}$, where $j = 1, 2$; $k_j = \omega(\mu_j \bar{\epsilon}_j)^{1/2}$ is the complex wave number of region j , where $j = 1, 2$; Λ is an integration variable; μ_j is usually taken to be μ_0 , the permeability of free space, for nonmagnetic regions; a time dependence of $e^{-i\omega t}$ has been assumed.

An unpartitioned, highly accurate formula which is characterized by minimal approximations has recently

been derived by working directly with the general exact integral (equation (1)). It is difficult to ascribe any geophysical meaning to the strange admixture of integrals over Bessel functions, as is written in (1). The problem is improved by choosing a sum of three integrals in the most judicious way. Therefore one may write $E_{1\rho} \sim \text{const} \times \cos \phi [I^{(1)} + I^{(2)} + I^{(3)}]$, with

$$I^{(1)} = \frac{1}{2} \int_0^\infty d\Lambda \Lambda e^{i\Gamma_1(z-d)} [\Gamma_1(J_0 - J_2) + k_1^2 \Gamma_1^{-1} (J_0 + J_2)] \quad (2a)$$



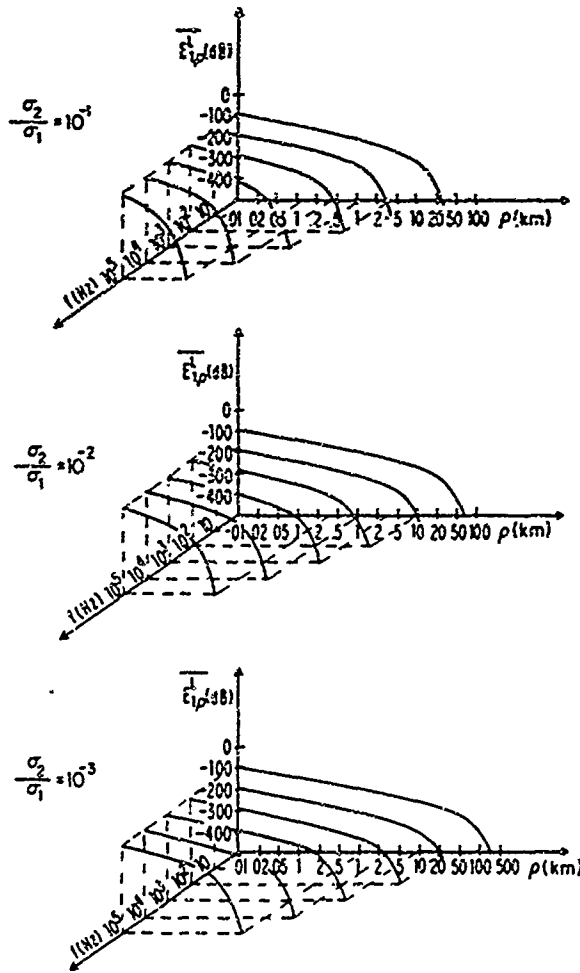


Fig. 5. Attenuation levels for $\bar{E}_{1p}^L \equiv 20 \log_{10} |E_{1p}^L(\rho, 0, 0)|$ for three ratios of conductivity. The value σ_2 parameterizes deep sediment or rock, and $\sigma_1 = 4 \text{ S/m}$; $\epsilon_2 = 16$ and $\epsilon_1 = 80$. The electric moment is 1 A m. The origin is at $(f, \rho, \bar{E}_{1p}^L) = (1 \text{ Hz}, 0.01 \text{ km}, -500 \text{ dB})$.

$$I^{(2)} = e^{i\Gamma_1(z+d)} \frac{1}{2} \int_0^\infty d\Lambda \Lambda [\Gamma_1(J_0 - J_2) + k_1^2 \Gamma_1^{-1}(J_0 + J_3)] \quad (2b)$$

$$I^{(3)} = -\bar{\epsilon}_2 \int_0^\infty d\Lambda \Lambda [\Gamma_1^{-2}(\bar{\epsilon}_2 \Gamma_1 + \bar{\epsilon}_1 \Gamma_2)](J_0 - J_2) e^{i\Gamma_1(z+d)} \\ - k_1^2 \int_0^\infty d\Lambda \Lambda \left[\frac{\Gamma_2 \Gamma_1^{-1}}{\Gamma_2 + \Gamma_1} \right] (J_0 + J_2) e^{i\Gamma_1(z+d)} \quad (2c)$$

which, upon evaluation subject to the constraints $|k_1|^2 \gg |k_2|^2$, $\rho^2 \gg z^2$, and $\rho^2 \gg d^2$ (easily satisfied in

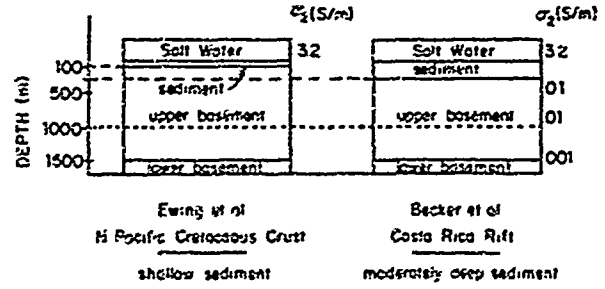


Fig. 6. Two profiles of stratification in the oceanic lithosphere.

practice), becomes

$$E_{1p}(\rho, \phi, z) = -\frac{\omega \mu_0}{2\pi k_1^2} \cos \phi \left\{ e^{i k_1 z - d} e^{i k_2 \rho} \left[\frac{i k_2^2}{\rho} - \frac{k_2}{\rho^2} - \frac{i}{\rho^3} \right. \right. \\ \left. \left. - \frac{k_2^2}{k_1} \left(\frac{\pi}{k_2 \rho} \right)^{1/2} \exp[-i k_2 \rho (k_2^2 - 2k_1^2)] \left[\frac{1}{2} - C_2(k_2 \rho (k_2^2 - 2k_1^2)) \right] \right. \right. \\ \left. \left. + i \left[\frac{1}{2} - S_2(k_2 \rho (k_2^2 - 2k_1^2)) \right] \right] \right\} \\ - \exp[i k_1(\rho^2 + (z-d)^2)^{1/2}] \left[\frac{k_1}{\rho^2} + \frac{i}{\rho^3} \right] \quad (3)$$

Here C_2 and S_2 are Fresnel integral terms as defined by Jahnke and Emde [1945]. The full derivation of this component is discussed elsewhere [Wu and King, 1982a]. The simplicity of the component may be

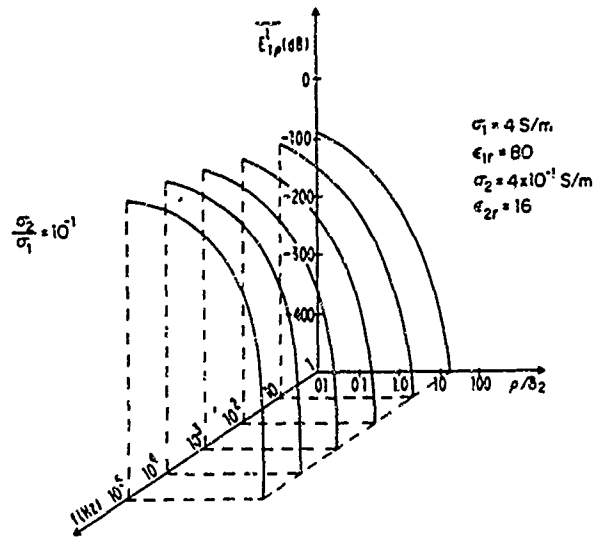


Fig. 7. Attenuation levels for $\bar{E}_{1p}^L \equiv 20 \log_{10} |E_{1p}^L(\rho, 0, 0)|$ versus ratio of antenna separation to skin depth of region 2 and frequency: $\sigma_2/\sigma_1 = 10^{-1}$. The origin is at $(f, \rho, \bar{E}_{1p}^L) = (1 \text{ Hz}, 0.01, -500 \text{ dB})$.

noted by writing the dependence of the field upon ρ and z , along a radial direction $\phi = 0$, in the form

$$E_{1\rho}(\rho, z) \sim \text{const} \times k_1^{-2} \{ e^{\alpha_1(z+d)} e^{\alpha_2 z} \zeta_1(\rho) - \exp [ik_1(\rho^2 + (z-d)^2)^{1/2}] \zeta_2(\rho) \} \quad (4)$$

where the ρ -dependent terms within the large brackets in (3) have been collected into ζ_1 and ζ_2 . Clustering terms in this way allows a physical interpretation to be given to the exponential functions of wave numbers and lengths. One may trace the wave associated with (4) from the source to the point at which it is received, as it would propagate near a pair of infinite regions described by k_1 and k_2 which adjoin in a plane. The first exponentials of (4) may be written in terms of the real and imaginary parts of k_1 and k_2 as $\exp \{ -[x_1(z+d) + z_2 \rho] \} \exp \{ i[\beta_1(z+d) + \beta_2 \rho] \}$; three phase changes and three attenuations with distance are implicit in this part of the field expression. This exponential factor describes a traveling wave that proceeds vertically from the source in the region of higher wave number ($|k_1|$) for a distance d , suffers a phase change $e^{i\beta_1 d}$ and an amplitude change $e^{-x_1 d}$, and continues along the interface in the medium of lower wave number ($|k_2|$) for a radial distance ρ with a phase change $e^{i\beta_2 \rho}$ and an amplitude change $e^{-z_2 \rho}$. The wave then proceeds vertically for a distance z to the observation point with a decrease in amplitude of $e^{-z_1 z}$ and a phase change

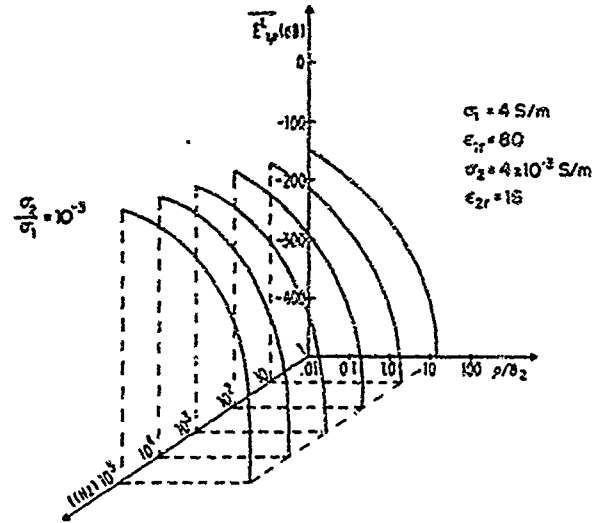


Fig. 9. Attenuation levels for $\overline{E}_{1\rho} \equiv 20 \log_{10} |E_{1\rho}(\rho, 0, 0)|$ versus ratio of antenna separation to skin depth of region 2 and frequency: $\sigma_2/\sigma_1 = 10^{-2}$. The origin is at $(f, \rho/\delta_2, \overline{E}_{1\rho}) = (1 \text{ Hz}, 0.01, -500 \text{ dB})$.

of $e^{i\beta_2 \rho}$. The exponential to the right of the minus sign in (4) describes a wave that travels in the region of higher wave number ($|k_1|$) directly from the source to the observation point, in a seawater region this contribution becomes negligible except very near the source.

The accuracy of the $E_{1\rho}$ component given by (3) has been verified by numerical evaluation of the general exact integral (equation (1)) [Wu and King, 1982a]. Equation (3) is compared with the numerical evaluation and with Baños' [1966] field regions in Figure 3, where (3) is designated as Wu's formula.

The symmetry which obtains when (3) is compared with other recently derived field components is plainly evident in radial distance behavior. Components for vertical dipoles have been derived [King, 1982] from general exact integrals which accompany (1). The components for both vertical and horizontal dipoles [Wu and King, 1982a, b; King and Wu, 1983] may be written in a form which distinguishes lateral-wave terms, $E_{1\rho}^L$, E_{1z}^L , and $B_{1\phi}^L$, from the remaining terms in the equations for $E_{1\rho}$, E_{1z} , and $B_{1\phi}$. Except very near the source the vertical-dipole components denoted by $E_{1\rho}^L$, E_{1z}^L , and $B_{1\phi}^L$, share with those of the horizontal dipole denoted by $E_{1\rho}^H$, E_{1z}^H , and $B_{1\phi}^H$, an almost pure symmetry in radial and azimuthal dependence. Only a $(\cos \phi)(k_1/k_2)$ distinguishes the two types of three lateral-wave components. Thus except near the source, along a radial

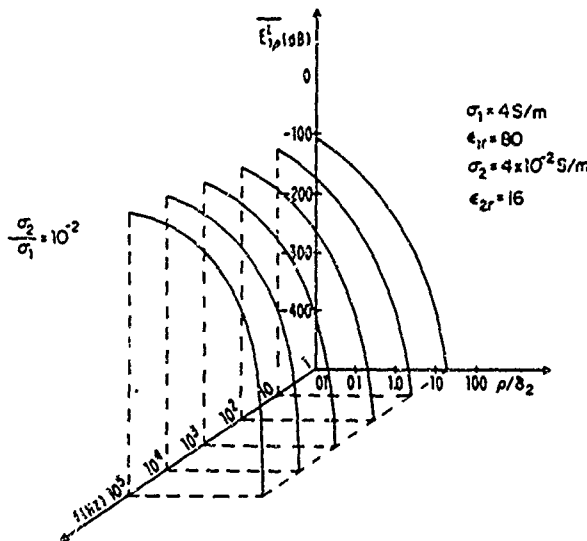


Fig. 8. Attenuation levels for $\overline{E}_{1\rho} \equiv 20 \log_{10} |E_{1\rho}(\rho, 0, 0)|$ versus ratio of antenna separation to skin depth of region 2 and frequency: $\sigma_2/\sigma_1 = 10^{-2}$. The origin is at $(f, \rho/\delta_2, \overline{E}_{1\rho}) = (1 \text{ Hz}, 0.01, -500 \text{ dB})$.

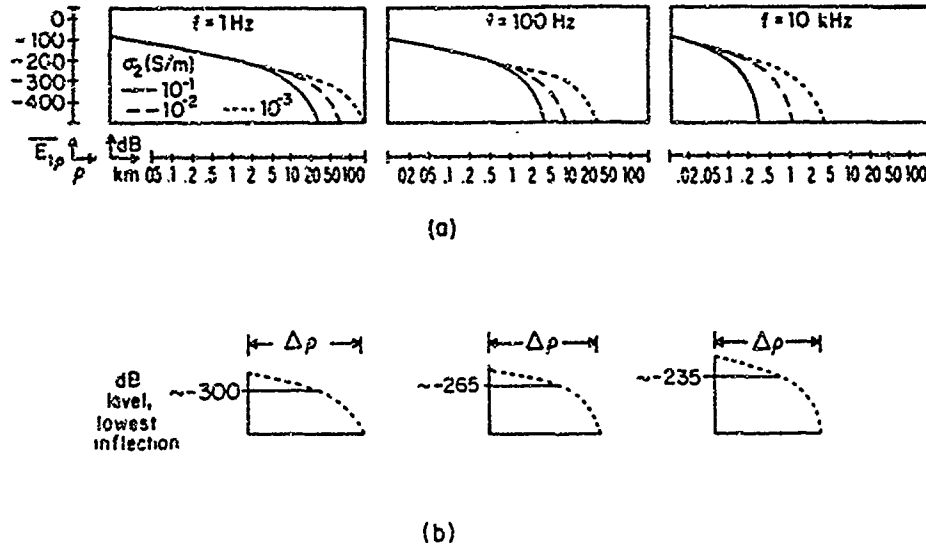


Fig. 10. (a) Attenuation levels in decibels of $E_{1\rho} \approx 20 \log_{10} |E_{1\rho}|$ for three frequencies with σ_2 ranging from 10^{-1} to 10^{-3} S m, where $\epsilon_2 = 16$ and electric moment is 1 A m. (b) Level in decibels of lowest inflection in range of σ_2 to be explored.

direction $\phi = 0$, the fields $E_{1\rho}^L$, E_{1z}^L , and $B_{1\phi}^L$ corresponding to vertical and horizontal dipoles differ only by a factor (k_1/k_2) . For a given pair of half-spaces (i.e., for a particular pair of material regions satisfying $|k_1|^2 \gg |k_2|^2$ and well approximated by a planar interface), measurements of electromagnetic field quantities along a direction $\phi = 0$ at a particular frequency satisfy the following simple linear relations:

$$\begin{aligned} E_{1\rho}^L(\rho, z) &= c E_{1\rho}^L(\rho, z) \\ E_{1z}^L(\rho, z) &= c E_{1z}^L(\rho, z) \quad |k_2 \rho| \geq 10 \\ B_{1\phi}^L(\rho, z) &= c B_{1\phi}^L(\rho, z) \end{aligned} \quad (5)$$

where the factor c is given by (k_2/k_1) .

3. DETERMINATION OF β_2 AND α_2 FROM $|E_{1\rho}|$

From the complex wave number $k_2 = \beta_2 + i\alpha_2 = [\mu_0(\omega^2 \epsilon_2 + i\omega \sigma_2)]^{1/2}$ the constitutive parameters ϵ_2 and σ_2 are given by

$$\epsilon_2 = (\beta_2^2 - \alpha_2^2 / \mu_0 \omega^2)^{-1} \quad \sigma_2 = 2\alpha_2 \beta_2 (\mu_0 \omega)^{-1} \quad (6)$$

When β_2 differs appreciably from α_2 , as at high frequencies with region 2 a poor conductor, a specific example illustrates how β_2 may be obtained using two transmitting antennas driven out of phase by a factor of π , at equal amplitudes. The antennas generate a useful standing wave when pointed at each other along a direction $\phi = 0$. The relevant terms of

the Wu formula, referred to the midpoint ρ_0 between the antennas, may be written in the region of the standing wave as [King, 1985]

$$E_{1\rho}(\rho, 0, z = \text{const}) = -\frac{\omega \mu_0 k_2}{2\pi k_1^2} e^{ik_1(z-d)} \left(\frac{e^{ik_2 \rho_0} - e^{ik_2 \rho_0^*}}{\rho_0^*} - \frac{e^{ik_2 \rho_0}}{\rho_0} \right) \quad \text{high frequency: } \alpha_2^2 \ll \beta_2^2 \quad (7)$$

where $\rho_0^* \equiv \rho_0 \pm x$, with x measured along a Cartesian axis zeroed at ρ_0 . With x small, $e^{\pm i\alpha_2 x} \approx 1$ and

$$|E_{1\rho}(\rho, 0, z = \text{const})|_{\max} \sim \frac{2}{\rho_0 [1 - (x/\rho_0)^2]} \quad (8a)$$

$$\beta_2 x = (n + \frac{1}{2})\pi$$

$$|E_{1\rho}(\rho, 0, z = \text{const})|_{\min} \sim \frac{2|x|}{\rho_0^2 [1 - (x/\rho_0)^2]} \quad (8b)$$

$$\beta_2 x = \frac{n\pi(\beta_2 \rho_0)^2}{(\beta_2 \rho_0)^2 - 1} \approx n\pi \quad (\beta_2 \rho_0)^2 \gg 1$$

where $n = 0, 1, 2, \dots$. The parameter β_2 is then found by locating ρ_0 , moving a distance x to a second minimum near $\beta_2 = \pi/x$, and checking the value at $\beta_2 = -\pi/x$. The determination of β_2 from phase changes which occur over a distance ρ , namely, $\beta_1(z+d) + \beta_2 \rho$, discussed formerly as arguments in the exponential terms of the Wu formula of section 2, is unnecessary under the conditions of low frequency and high conductivity. Under such con-

ditions relevant to seafloor studies, $\sigma_2 \gg \omega\epsilon_2$ and $\beta_2 \sim \alpha_2$ so that σ_2 is given by $2\alpha_2^2/\omega\mu_0$. The value of α_2 may be determined graphically from the fact that the measured quantity $20 \log_{10} |E_{1\rho}(\rho, \phi, z = \text{const})|$ is described along ρ by $e^{-\alpha_2 \rho}/\rho$. The fact that $|E_{1\rho}|$ is quite sensitive to frequency changes and increments of conductivity is indicated by the curves in Figure 4.

Two aspects of the resolution of the $|E_{1\rho}|$ method may be noted, one for each of the variables ρ and f . The resolving power is $R_\rho = \bar{\rho}/\Delta\rho$, where $\bar{\rho}$ is the average separation between two of a collection of measured exponential decays of $20 \log_{10} |E_{1\rho}|$ which can barely be recognized as discrete, and where $\Delta\rho$ is the actual separation difference between them. Similarly, $R_f = \bar{f}/\Delta f$ may be defined. Thus the smaller $\Delta\rho$ or Δf can be made while the other is held constant, the closer the decays associated with distinct values of σ_2 may be, and still be resolved. For example, at 10 kHz it will be easy to resolve a measured σ_2 value between 0.4 and 0.04 by fitting to the curves of Figure 4b; in order to resolve a conductivity measurement between 0.3 and 0.4, the range in ρ will need to be measured to an accuracy of ~ 0.3 of the interval from 0.4 to 1.4 km, or 300 m. The effective length of receiving antennas for use even at 1 kHz may be ~ 10 m (see section 5 and the appendix), and displacement of such an antenna over 300 m is quite feasible. The question of resolution is essentially one of accurately marking the endpoints of radially deployed transmitting and receiving antennas. In this example the frequency is assumed to be held constant: if ρ is held constant, the resolution depends on the drift in frequency of the generating instrument about a central value f_0 . Indoor measurements [Brown et al., 1984] have been made with a frequency stability of less than $\pm 1\%$ variation about $f_0 = 600$ MHz and $f_0 = 1$ GHz, lower frequencies needed for seafloor work may be generated with the same order of stability.

The effects of deviations from "flatness" of the plane surface near which $|E_{1\rho}|$ is measured are indicated by indoor experiments with discontinuities in the form of rectangular and wedge-shaped objects [Brown et al., 1982]. These studies performed at 600 MHz show that the $|E_{1\rho}|$ field is perturbed only locally in both magnitude and phase by irregularities whose dimensions may be comparable to the wavelength λ_2 associated with region 2. The effect is primarily one of increase in $|E_{1\rho}|$ directly in front of the obstacle, owing to backscattering from the obstacle. A concurrent decrease in $|E_{1\rho}|$ occurs behind (down-field from) the obstacle; the overall decay rate is es-

TABLE 1. Source and Receiver Parameters

	$f = 1$ Hz	$f = 100$ Hz	$f = 10$ kHz
Decibel level, unit dipole ($M_0 = 1$ A m)	-300	-265	-235
$M_{eff} = I_0 h_{eff} $, A m	3×10^4	3×10^3	3×10^2
$20 \log_{10} I_0 h_{eff} /M_0$, dB	89.6	109.6	129.6
Augmented decibel level	~ -210	~ -155	~ -105
Electric field strength $ E_{1\rho}(\rho, 0, 0) $, V/m	$\sim 10^{-10}$	$\sim 10^{-8}$	$\sim 10^{-5}$
Receiver sensitivity, μ V (receiver effective length is 10 m)	$\sim 10^{-3}$	$\sim 10^{-1}$	$\sim 10^2$
Receiver sensitivity, μ V (receiver effective length is 100 m)	$\sim 10^{-3}$	~ 1	$\sim 10^3$

entially unaltered. For obstacle dimensions much less than λ_2 , for example, shallow surface roughness, the perturbation in the $|E_{1\rho}|$ decay rate is quite small. Thus along a distance 300 m with $f = 10$ kHz, as cited in the above example, localized discontinuities in the sea floor will not impede the determination of σ_2 from $|E_{1\rho}|$.

4. $E_{1\rho}^L$ COMPONENT AND CRUSTAL PARAMETERS

The quasi-static range for $E_{1\rho}$ dipole fields where $|k_2 \rho| \ll 1$, as defined by Kraichman [1970, p. 3-18, Table 3.9], is readily obtained as a special case of the Wu formula. In particular,

$$|E_{1\rho}| = \omega\mu_0(2\pi)^{-1} \left| \frac{1}{k_1^2} \right| e^{-\alpha_1(z+d)} \frac{1}{\rho^3} \quad (9)$$

$$|k_2 \rho| \leq 0.1 \quad \zeta_1 \sim -i/\rho^3 \quad e^{ik_2 \rho} \sim 1$$

Since this is independent of k_2 , it is useless for determining the properties of the lithosphere (region 2). the wave is totally reflected at the sea floor. However, for $|k_2 \rho| > 1$,

$$|E_{1\rho}| = \omega\mu_0(2\pi)^{-1} \left| \frac{k_2^2}{k_1^2} \right| e^{-\alpha_1(z+d)} \frac{e^{-\alpha_2 \rho}}{\rho} \quad (10)$$

$$1 \leq |k_2 \rho| \leq 8 |k_1^2/k_2^2| \quad \zeta_1 \sim ik_2^2 \rho$$

It is the exponential decrease $e^{-\alpha_2 \rho}/\rho$ which is critically sensitive to σ_2 . The quantity $20 \log_{10} |E_{1\rho}(\rho, 0, 0)|$ is shown in Figure 4 for various conductivities. Since the lateral-wave terms in $E_{1\rho}$ dominate except very close to the source, the notation $E_{1\rho}^L$ will be used hereinafter.

The attenuation of $E_{1\rho}^L(\rho, 0, 0)$ over a range of frequencies from 1 Hz to 10^5 Hz is shown diagrammatically in Figure 5. The attenuation for given con-

ductivity ratios (σ_2 , deep sediment or rock; $\sigma_1 = 4$ S/m) is described by a family of umbrellalike surfaces.

The utility of $E_{1\rho}^L(\rho, 0, z)$ in seafloor studies must be assessed in terms of two types of parameters. The specific rock- and sediment-related parameters exemplary of the region of interest in the absence of source or receiving antennas compose one type (see this section). These crustal parameters must first be specified. A second type is associated with the technology required to transmit and receive $E_{1\rho}^L$ in a region so specified (see section 5). Before detailing the two types it is useful to note a few general aspects of Figure 5. The usual qualities of dipole fields in adjoining half-spaces are observed. The decay of $\overline{E_{1\rho}^L} \equiv 20 \log_{10} |E_{1\rho}^L|$ in decibels falls off increasingly fast with frequency. $\overline{E_{1\rho}^L}$ decays less rapidly with frequency as the lower layer (described by σ_2) becomes less conducting. Actual measurements of such decays in salt water at its interface with the earth's crust may be made as a function of the two variables f and ρ . The measured curvature may be fitted to the appropriate $f, \rho, \overline{E_{1\rho}^L}$ surface for a particular conductivity. For measurements at a particular frequency such a procedure for inferring σ_2 corresponds to interpolation between the family of curves which crosscut the type of surfaces illustrated in Figure 5.

Two important types of stratifications based upon independently reported studies are constructed in Figure 6. The aspects of the layered profiles may each be discussed in terms of its compatibility with the $E_{1\rho}^L$ measurements.

One important type of configuration for which $E_{1\rho}^L$ is expected to be particularly useful is that of a quite thin sedimentary layer or region of deep exposed rock at the sea floor. The seismic disturbance studies of Ewing *et al.* [1967] indicate extensions of clay in old Cretaceous crust where sedimentation is documented to be <100 m. A typical sedimentary conductivity reported by Shor *et al.* [1970] of 1–2 S/m is associated with a skin depth δ_2 of 0.4–0.5 km at 1.0 Hz; it is plain that at frequencies for which the sediment layer is electrically thin, the $E_{1\rho}^L$ component will effectively sample an underlying basement layer of lower conductivity.

The in situ resistivities reported by the collaboration of Becker *et al.* [1982] are shown as equivalent conductivities at depths of about 0.3, 1, and 1.5 km on the right in Figure 6. The mapping of hole 504B of the Costa Rica Rift provides an insightful view of the conductivities to be expected underlying sediment. The sediment layer is moderately deep in relation to the previous example. In such cases where the

layer is significantly greater than 100 m, ranging up to 0.5 km, frequencies may be chosen which allow the $E_{1\rho}^L$ component to sample sediment only. Varying the frequency will allow sampling of the average properties of the sediment at different depths, sediment of uniform resistivity at a given sampling depth will allow effective use of calculated $E_{1\rho}^L$ to compare with a measured exponential field decay. Where the resistivity is mildly inhomogeneous with sampling depth, the calculated $E_{1\rho}^L$ values are expected to be a good approximation to actual average properties. The resolution of $E_{1\rho}^L$ theoretical values (based upon two half-spaces) for such cases and for σ_x, σ_y , and σ_z anisotropies has been studied recently [Pan, 1985] and found to have important geologic implications.

As a precedent to discussion of specific frequencies and technology needed to measure $E_{1\rho}^L(\rho, 0, 0)$ effectively in typical stratifications, it is instructive to plot the quantity ρ/δ_2 , the ratio of antenna-receiver separation to skin depth of the lower layer, versus $20 \log_{10} |E_{1\rho}^L|$ at various orders of magnitude in frequency. These parameters are shown for 3 orders of magnitude in σ_2 in Figures 7–9. The parameter ρ/δ_2 is similar to the sea induction number θ defined by Coggon and Morrison [1970], but with σ_2 replacing the sea conductivity σ_s in the skin depth of their definition. It is noted that for a minimal decibel level of -300 associated with a unit dipole of moment 1 A m (effective moments may be made to be significantly greater, as will be shown later in this paper), useful ρ/δ_2 values are ~ 5 or less. The magnitude of $\overline{E_{1\rho}^L}$ is seen to decrease, for a given ρ/δ_2 , with orders of magnitude in σ_2/σ_1 .

5. $E_{1\rho}^L$ COMPONENT AND TECHNICAL ASPECTS OF SOURCE AND RECEIVER

The attenuation levels in decibels of $E_{1\rho}^L$ for three distinct combinations of frequency and conductivity σ_2 are shown in Figure 10a. The range in ρ over which the exponential decrease used to obtain α_2 and/or β_2 occurs is indicated in Figure 10b.

The ability to receive usable $\overline{E_{1\rho}^L}$ signal strength depends on specialized insulated antenna design. The results of a wide array of indoor and outdoor experiments obtained over many years may be brought to bear upon this problem [see King and Smith, 1981, chap. 8]. What is important here is the electric moment M of the transmitting element. M may be related to both input current I_0 and effective length h_{eff} ; h_{eff} depends on $k_2 = \beta_2 + i\alpha_2$ and k_L (see the appendix).

In order to determine the exponential decay associated with a given range in σ_2 , the decibel level identified with the lowest onset of inflection (deviation from a straight line) in the corresponding $20 \log_{10} |E_{1\rho}^L|$ curves must be measured. For the range of 10^{-1} – 10^{-3} S/m in Figure 10 this will occur for the 10^{-3} S/m curve at each of the frequencies indicated; in the wider ranges of σ_2 charted in Figure 4, it likewise occurs for the lowest conductivity. In the latter curves it is clear that the slope of these inflection points decreases with increasing frequency. The points along the 10^{-3} S/m curve at which the inflection is located are indicated in Figure 10.

The decay levels in Figure 10 are based on the unit moment $M_0 = 1$ A m; finite antennas with sizeable input currents will have an associated shift in the decay upward in relation to 1 A m by a constant factor in decibels. This upward shift is shown for different effective moments M_{eff} in Table 1. Table 1 also lists the increment in decibels over the unit dipole, the net shifted decibel level, and the signal strength of the electric field at the maximal source-receiver separation, along with the requisite receiver sensitivity. Electric moments M_{eff} of magnitude needed to produce signal levels suitable for the receiver sensitivities of Table 1 are indeed realizable. This is shown for specialized antenna designs that are quite feasible for full-scale seafloor use and related to input currents (see the appendix).

The subject of atmospheric noise has been investigated [de Bettencourt, 1984] specifically in regard to lateral waves. This study has shown that useful signal-to-noise ratios are attainable for effective moments of 10^5 A m at frequencies as high as 1 MHz and improve at lower frequencies.

6. CONCLUSIONS

The general integral expressions which implicitly contain the effects of electromagnetic surface waves have recently been reduced to a set of geophysically useful equations. The lateral-wave component $E_{1\rho}^L$ of the electric field of a horizontal dipole has been shown, under the geophysically relevant conditions $1 \leq |k_2 \rho| \leq 8 |k_2^2/k_1^2|$, to decay as $e^{-\alpha_2 \rho}/\rho$ for a region described by $k_2 = \beta_2 + i\alpha_2$ (with $|k_1| \geq 3 |k_2|$). The sensitivity of $E_{1\rho}^L$ to the conductivity σ_2 of rock or sediment underlying salt water, its decay as a function of ρ , f , and ρ/δ_2 , and the technical aspects of its transmission and reception indicate that σ_2 may be determined at high frequencies and low conductivities, while σ_1 may be determined at low frequencies and high conductivities. Electric mo-

ments needed to produce signal levels for σ_2 studies at the sea floor have been shown to be realizable. Specialized antenna designs feasible for full-scale use at the sea floor are outlined in the appendix.

APPENDIX: SPECIALIZED ANTENNA DESIGNS

The use of insulated antennas in salt water results in increased directivity in relation to bare wires. It is well known that the current flowing along bare metal wires attenuates rapidly in highly conducting earth or salt water [Shen and King, 1979]. Thus propagation experiments with both short bare dipoles and longer insulated wires have been undertaken. A plastic enclosure must be used in the latter type to prevent infiltration of salt water. A traveling wave is generated by placing a carbon resistor at approximately $\lambda_G/4$ from the end of the antenna, where $\lambda_G = 2\pi k_L^{-1}$ for the current of complex wave number k_L . The use of resilient materials to overcome the problems of thermal disruption of water-tight seals by the Joule heating which occurs in such antennas has been quite involved. An effective insulated antenna continuously sheathed with plastic is shown in Figure A1b. The number and type of antenna elements have been altered on a short time scale in the laboratory. Linear broadside arrays of insulated antennas have been studied by the present authors; these increase the directivity of the field pattern as the number of radiating broadside elements increases. The measured field patterns of a monopole and a two-element array in a dissipative saltwater medium are shown in Figure A2.

The design criteria for a large-scale seafloor antenna may be discussed concurrently with those for an antenna useful in fresh water. The attributes of seafloor and lakefloor antennas to be utilized at lower frequencies may be regarded as specializations of an insulated antenna designed for generating lateral waves at the interface between lake water and air. The dependence of the dimensions of subsurface antennas upon the complex wave number $k_L = \beta_L + i\alpha_L$ may in this way be shown for a wide range of frequencies. An insulated antenna for use in the megahertz range in fresh water may be discussed concisely in terms of a parameter which contains its important dimensions, namely,

$$F(r_{1,2,3}, l_{1,2}, s_{1,2}) = Z_c[k_L(r_1, r_2, r_3)] f_0(k_L, l_1, l_2, s_1, s_2) \quad (A1)$$

The brackets on the right side of the equation indicate that the quantity Z_c is a function of k_L , where k_L

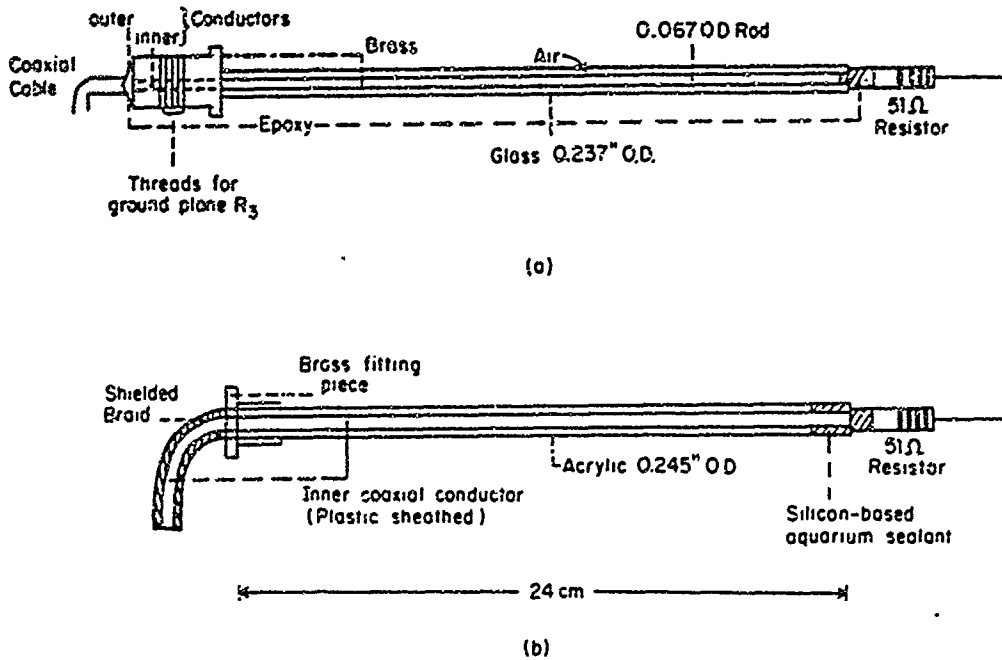


Fig. A1. (a) Glass prototype traveling-wave antenna for salt water. (b) Continuously enclosed plastic version.

depends upon the radii r_1 , r_2 , and r_3 of three cylinders associated with the insulated antenna. The three cylinders associated with (A1) and the antenna length quantities s and l are shown in Figure A3. The figure caption defines three difference equations Δ_{ij} which

measure the relative positions of the axes of the cylinders and hence the eccentricity of the inner conductor. The point of common eccentricity ζ of the cylinders is spaced at length δ from the axis $r_3 = 0$ of the outermost cylinder. The complex wave numbers k_1 through k_3 describe the dielectric or conducting media in regions 1' through 3' associated with cylinders of radii r_1 , r_2 , and r_3 , respectively, while k_4 ($=k_1$) describes the ambient medium external to the antenna. A specific choice of insulators may be made which, at a given operating frequency, satisfies the conditions $|k_4|/|k_2| \gg 1$ and $|k_2|(r_3 - \Delta_{13}) \ll 1$.

Figure A3 details the side view of an antenna much like the laboratory prototypes of Figure A1, although generalized somewhat by the displacement of the inner conductor. The antenna of Figure A3 is further generalized by the presence of two lumped impedances Z_{T1} and Z_{T2} analogous to the 51-Ω resistor of the prototype. The two generalizations permit the design of a transmitting element which is highly directive. The directivity is optimized by the proper choice of parameters which occur as arguments in F of (A1). Thus it is useful to write Z_c and f_0 entirely in terms of constant quantities and antenna dimensions. The complex wave number k_L for the antenna may be written explicitly as

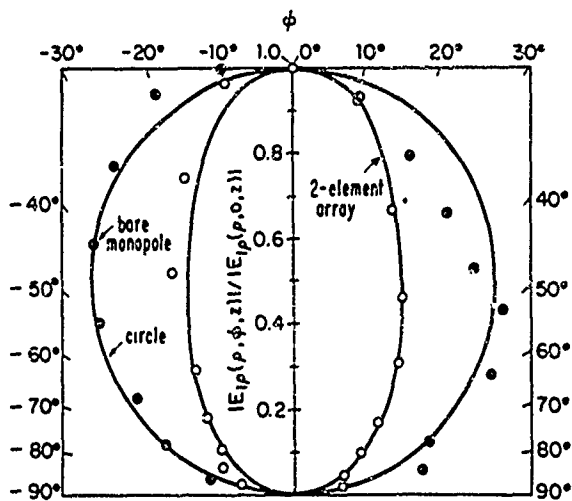


Fig. A2. Measured lateral-wave field patterns of a short bare monopole and a two-element array of insulated traveling-wave antennas; $\rho = 0.8$ m, $z = d = 0.5$ cm, and $f = 600$ MHz.

$$k_L = k'_2 \left\{ 1 + \frac{\frac{H_0^{(1)}(k'_4 r_3)}{H_1^{(1)}(k'_4 r_3)} + 2 \sum_{n=1}^{\infty} \frac{H_n^{(1)}(k'_4 r_3)}{H_{n+1}^{(1)}(k'_4 r_3)} (\Delta_{13} \delta)^n r_3^{-2n}}{k'_4 r_3 \cosh^{-1} \left(\frac{r_1^2 + r_3^2 - \Delta_{13}^2}{2r_1 r_3} \right)} \right\}^{1/2} \quad (A2)$$

$$\cdot \left\{ \frac{\cosh^{-1} \left(\frac{r_1^2 + r_3^2 - \Delta_{13}^2}{2r_1 r_3} \right)}{\left(\frac{\epsilon'_2}{\epsilon'_3} \right) \cosh^{-1} \left(\frac{r_2^2 + r_3^2 - \Delta_{23}^2}{2r_2 r_3} \right) + \cosh^{-1} \left(\frac{r_1^2 + r_2^2 - \Delta_{12}^2}{2r_1 r_2} \right)} \right\}^{1/2}$$

The quantity f_0 is given explicitly by

$$\begin{aligned} f_0 = & Z_c \sinh \{ik_L(-1)(l_1 + l_2) \\ & + \coth^{-1} [(Z_{T_1} Z_c) + \coth (ik_L(l_1 - s_1))] \\ & + \coth^{-1} [(Z_{T_2} Z_c) + \coth (ik_L(l_2 - s_2))]\} \\ & \cdot \{\sinh [ik_L(-1)l_2 + \coth^{-1} [(Z_{T_2} Z_c) \\ & + \coth (ik_L(l_2 - s_2))]] \sinh [ik_L(-1)l_1 \\ & + \coth^{-1} [(Z_{T_1} Z_c) + \coth (ik_L(l_1 - s_1))]]\}^{-1} \end{aligned} \quad (A3)$$

where the characteristic impedance Z_c is simply

$$\begin{aligned} Z_c = & \left(\frac{k_L}{2\pi\omega\epsilon'_2} \right) \left[\cosh^{-1} \left(\frac{r_1^2 + r_2^2 - \Delta_{12}^2}{2r_1 r_2} \right) \right. \\ & \left. + \cosh^{-1} \left(\frac{r_2^2 + r_3^2 - \Delta_{23}^2}{2r_2 r_3} \right) \left(\frac{\epsilon'_2}{\epsilon'_3} \right) \right] \end{aligned} \quad (A4)$$

A detailed derivation of the current distribution along the lossy transmission line associated with the above quantities as well as electric fields in regions 2' and 4' are included in recent works by *Shen and King* [1979] and *King et al.* [1981]. The use of a characteristic impedance for the freshwater antenna whose current is parameterized by $k_L = \beta_L + i\alpha_L$ shows that conventional transmission-line theory may be generalized to describe the antenna. An impedance per unit length, z_L , may be associated with the insulated metal conductor. In this way the radiation may be regarded as partitioned into units; z_L includes two effects—ohmic heat losses as well as power radiated to the ambient lake water.

In regions of the earth's crust beneath the sea water, useful frequencies extend to orders of magnitude lower than the megahertz range for which the antennas of Figures A1 and A3 (lower diagram) have been designed. The layers of insulation which improve the directionality of antennas used in the me-

gahertz range become increasingly thin electrically as operating frequencies of 1 Hz and below are approached. Such layers may be included in the design, although they will provide little improvement in directionality. The directionality and efficiency enjoyed at higher frequencies in fresh water is difficult to achieve in a seafloor version of the insulated antenna, pictured in the lower part of Figure A3, without having $S = s_1 + s_2$ be inordinately long (S is in kilometer range). What is required is a length-shrinking factor for S such that S' , the length of a specialized low-frequency antenna, will be associated with an acceptable gain level.

For effective moments M_{eff} of the magnitude chartered in Table 1, an antiresonant antenna may be designed which is essentially that pictured in the lower part of Figure A3, but with the lumped impedances Z_{T_1} and Z_{T_2} removed and the metal conductor extended without insulation (bare) into the water. These modifications, which compose only part of the required design, are shown in the upper part of Figure A3. In addition, a tubular metal sheath (which may be a metal braid) of length l_0 may be folded back upon the coaxial feedline and be insulated from its walls except at the driving point. Such a sheath essentially constitutes a folded-back ground plane for the resulting monopole.

The important quantities associated with insulated antennas are developed in *King and Smith* [1981]; antiresonant bare antennas are treated by *King* [1956]. The relevant formulas for an insulated antiresonant antenna for use at the sea floor are listed below.

The radial component of the electric field is given by

$$E_{1\rho}(\rho, 0, z) = E_{1\rho}(\rho, 0, z) \Big|_{\text{dipole}}^{\text{unit}} I_0 h_{eff} \quad (A5)$$

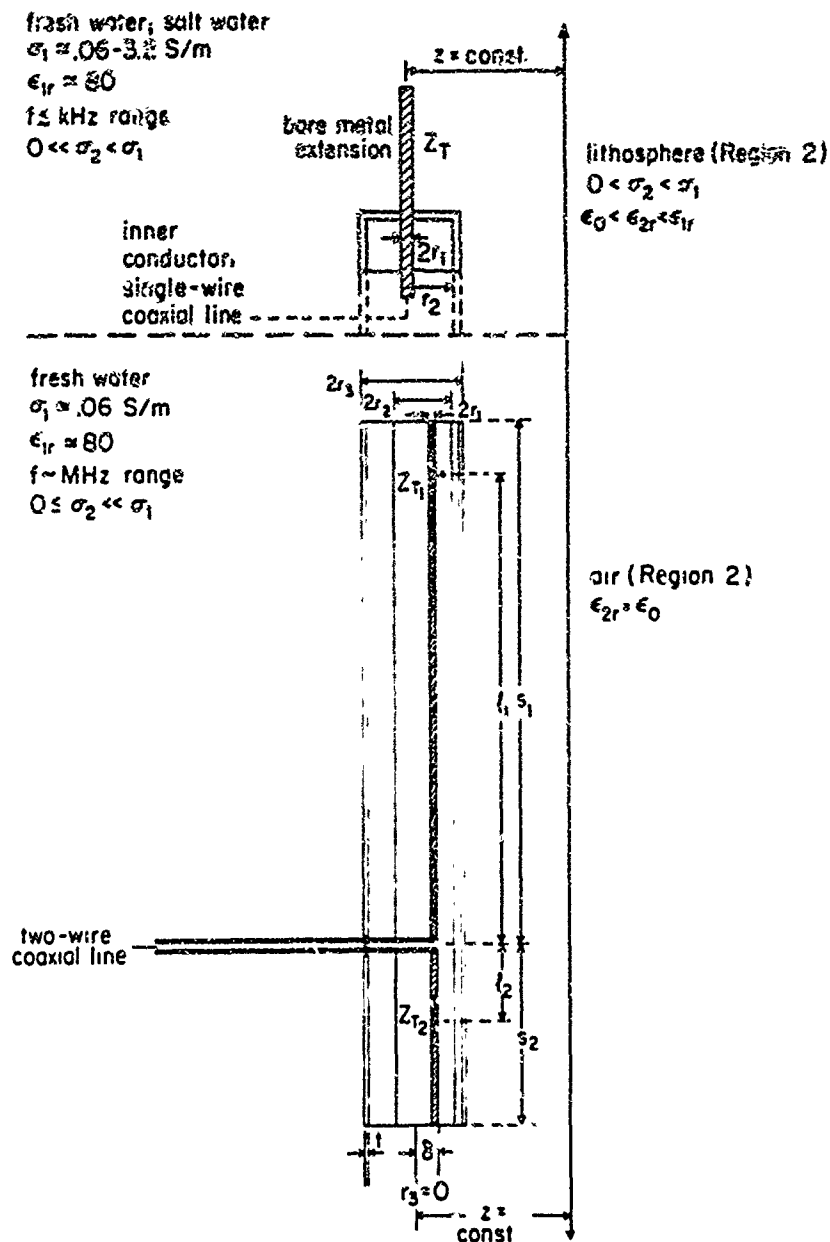


Fig. A3 Insulated antennas for freshwater and saltwater use. The lower diagram shows the directional freshwater antenna of dielectric cylinders of radii r_1 , r_2 , and r_3 . Cylindrical axes are related spatially by $\Delta_{ij} = r_j - r_i - t$, where $i < j \leq 3$. The upper diagram shows extension of the bare inner conductor to form the termination of impedance Z_T , Z_{T_1} , Z_{T_2} , and eccentricity are removed.

where I_0 is the input current and h_{eff} is given by

$$h_{eff} = \frac{k_2 e^{-ik_2 s_1} + ik_L \cos \eta \, x_L s'_1 + ik_2 \sinh x_L s'_1}{(k_L^2 - k_2^2) \sinh x_L s'_1} \quad (A6)$$

with s_1 being the length of the insulated section of the antenna between the driving point $x = 0$ (at

which the outer metal sheath is folded back by a distance l_0 and the bare metal termination. The anti-resonant antenna has an electrical length $\beta_L s'_1 \sim \pi/2$ with termination impedance $Z_T (= R_T - iX_T) \ll Z_c$, the characteristic impedance. The current along the antenna is

$$I_{\phi}(x) = \frac{I_0(0) \cos [k_L(s_1 - x') + i(R_T/R_c - iX_T/R_c)]}{\cos [k_L s_1 + i(R_T/R_c - iX_T/R_c)]} \quad (A7)$$

Using $f = 1$ kHz, $\beta_1 l_0 > \pi/2$ or $l_0 \approx 12$ m, the length of the bare wire and folded sheath sections. (To protect such sections at the sea bottom, the antenna may be enclosed with a nonmetallic rope or braid.) If #000 wire is used for the antenna, the radius r_1 of the conductor is 0.52 cm; the outer radius of the insulating sleeve may be made as small as 0.521 cm if a dielectric coating like enamel is used. With the wave number of copper $|k_c| = 688 \text{ m}^{-1}$ at 1 kHz for the conductor, the following quantities may be calculated:

$$k_L = (4.12 + i0.32) \times 10^{-3} \text{ m}^{-1} \quad Z_c = 3.44 + i0.267 \Omega$$

$$s_1 = \pi(2\beta_L)^{-1} = 381 \text{ m} \quad |h_{eff}| = 9.66 \times 10^3 \text{ m}$$

The input current I_0 required to produce an electric moment of $3 \times 10^5 \text{ A m}$ is $I_0 = 31.1 \text{ A}$. The total input power is $P_0 = |I_0|^2 R_0 = 26.5 \text{ kW}$. The ratio of the power P_C dissipated in the ohmic resistance of the insulated wire to the power P_R radiated is $P_C/P_R = 0.106$. It follows that $P_R = 23.23 \text{ kW}$ and $P_C = 2.46 \text{ kW}$. The radiating efficiency of the insulated section is $P_R/R_0 = 87.6\%$.

A simple experiment to test a higher-frequency version of the specialized antiresonant antenna may be proposed. In such an experiment the nylon-rope-enclosed insulated and bare sections of the antenna are put in place in a tidal basin (such as those that occur off the New England shoreline) at low tide and energized for measurement using a suitable receiving element (effective length may be < 10 m) at high tide. In this way the conductivity of the underlying crust may be determined independently using conductivity probes in situ, provided the water is shallow. At $f = 1$ kHz, $\delta_1 < 10$ m so that the high tide need not be deep to prevent air-water surface effects.

Acknowledgments. The authors are grateful to J. G. Heacock of the U.S. Office of Naval Research for his continued interest in this project, B. H. Sandler for carrying out the numerical calculations, and M. Owens for preparing the manuscript. This research was supported in part by the U.S. Office of Naval Research under contract N00014-79-C-0419 with Harvard University.

REFERENCES

- Baños, A., Jr., *Dipole Radiation in the Presence of a Conducting Half-Space*, Pergamon, New York, 1966.
- Becker, K., R. P. Von Herzen, T. J. G. Francis, R. N. Anderson, J. Honnorez, A. C. Adamson, J. C. Alt, R. Emmermann, P. D. Kempton, H. Kinoshita, C. Laverns, M. J. Mottl, and R. L. Newmark, In situ electrical resistivity and bulk porosity of the oceanic crust Costa Rica Rift, *Nature*, **300**, 594-598, 1982.
- Brown, M. F., R. W. P. King, and T. T. Wu, Lateral-wave studies in a model lithosphere, *J. Appl. Phys.*, **53**, 3387-3396, 1982.
- Brown, M. F., R. W. P. King, and T. T. Wu, Experiments on the reflection of lateral electromagnetic waves, *J. Appl. Phys.*, **55**, 3927-3933, 1984.
- Chave, A. D., and C. S. Cox, Controlled electromagnetic sources for measuring electrical conductivity beneath the oceans. 1. Forward problem and model study, *J. Geophys. Res.*, **87**, 5327-5338, 1982.
- Coggon, J. H., and H. F. Morrison, Electromagnetic investigation of the sea floor, *Geophysics*, **35**, 476-489, 1970.
- deBettencourt, J. T., Lateral waves near the air-sea boundary and atmospheric noise, *Proc. IEEE*, **72**, 1219-1221, 1984.
- Ewing, J., M. Ewing, T. Aiken, and W. J. Ludwig, North Pacific sediment layers measured by seismic profiling, in *The Crust and Upper Mantle of the Pacific Area*, *Geophys. Monogr. Ser.*, vol. 12, edited by L. Knopoff et al., pp. 147-175, AGU, Washington, D. C., 1967.
- Jahnke, E., and F. Emde, *Tables of Functions*, Dover, New York, 1945.
- King, R. J., and S. W. Maley, Model experiments on propagation of ground waves across an abrupt boundary at perpendicular incidence, *J. Res. Natl. Bur. Stand. Sect. D*, **69**, 1375-1382, 1965.
- King, R. W. P., *The Theory of Linear Antennas*, Harvard University Press, Cambridge, Mass., 1956.
- King, R. W. P., New formulas for the electromagnetic field of a vertical electric dipole in a dielectric or conducting half-space near its horizontal interface, *J. Appl. Phys.*, **53**, 8476-8482, 1982. (Erratum, *J. Appl. Phys.*, **56**, 3366, 1984.)
- King, R. W. P., Electromagnetic surface waves: New formulas and their application to determine the electrical properties of the sea bottom, *J. Appl. Phys.*, **58**, 3612-3624, 1985.
- King, R. W. P., and M. F. Brown, Lateral electromagnetic waves along plane boundaries. A summarizing approach, *Proc. IEEE*, **72**, 595-611, 1984.
- King, R. W. P., and G. S. Smith, *Antennas in Matter*, MIT Press, Cambridge, Mass., 1981.
- King, R. W. P., and T. T. Wu, Lateral waves: Formulas for the magnetic field, *J. Appl. Phys.*, **54**, 507-514, 1983 (Erratum, *J. Appl. Phys.*, **56**, 3365, 1984.)
- King, R. W. P., B. H. Sandler, and L. C. Shen, A comprehensive study of subsurface propagation from horizontal electric dipoles, *IEEE Trans. Geosci. Remote Sens.*, **GE-18**, 225-233, 1980.
- King, R. W. P., L. C. Shen, and T. T. Wu, Embedded insulated antennas for communication and heating, *Electromagnetics*, **1**, 51-72, 1981.
- King, R. W. P., M. Owens, and T. T. Wu, Properties of lateral electromagnetic fields and their application, *Radio Sci.*, **21**, 13-23, 1986.
- Kraichman, M. B., *Handbook of Electromagnetic Propagation in Conducting Media*, U.S. Government Printing Office, Washington, D. C., 1970.
- Norton, N. A., The propagation of radio waves over the surface of the earth and in the upper atmosphere, *Proc. IEEE*, **24**, 1367-1387, 1936.
- Pan, W.-Y., Surface-wave propagation along the boundary between sea water and one-dimensionally anisotropic rock, *J. Appl. Phys.*, **58**, 3963-3974, 1985.
- Shen, L. C., and R. W. P. King, An eccentrically insulated

- traveling-wave antenna for subsurface communication, *Proc. Inst. Electr. Eng.*, 126, 793-797, 1979.
- Shor, G. G., Jr., K. W. Menard, and R. W. Raitt, Structure of the Pacific Basin, in *The Sea*, vol. 4, edited by A. E. Maxwell, part II, chap. 1, Wiley-Interscience, New York, 1970.
- Sommerfeld, A. N., On the propagation of waves in wireless telegraphy (in German), *Ann. Phys.*, 28, 665-736, 1909.
- Sommerfeld, A. N., On the propagation of waves in wireless telegraphy (in German), *Ann. Phys.*, 81, 1135-1153, 1926.
- Wu, T. T., and R. W. P. King, Lateral waves. A new formula and interference patterns, *Radio Sci.*, 17, 521-531, 1982a.
- Wu, T. T., and R. W. P. King, Lateral waves: New formulas for $E_{1\theta}$ and $E_{1\phi}$, *Radio Sci.*, 17, 532-538, 1982b. (Correction, *Radio Sci.*, 19, 1422, 1984.)
- Young, P. D., and C. S. Cox, Electromagnetic active source sounding near the East Pacific Rise, *Geophys. Res. Lett.*, 8, 1043-1046, 1981.
-
- M. F. Brown and R. W. P. King, Gordon McKay Laboratory, Harvard University, Cambridge, MA 02138.

Properties of lateral electromagnetic fields and their application

Ronold W. P. King, Margaret Owens, and Tai Tsun Wu

Gordon McKay Laboratory, Harvard University, Cambridge, Massachusetts

(Received April 3, 1985; revised August 13, 1985; accepted August 13, 1985.)

The formulas for the complete electromagnetic field in region 1 ($z \geq 0$, k_1) due to a horizontal electric dipole also located in region 1 near its plane boundary with region 2 ($z \leq 0$, k_2 ; $|k_2|^2 \ll |k_1|^2$) are reviewed and applied to determine the moment of a magnetic dipole that effectively generates the field in region 2. Use is made of this field to determine the locus of the Poynting vector, the maximum depth of penetration into region 2 of the lateral wave part of the field, and the fraction of power associated with the lateral wave in a specified range. Application is made to the use of horizontal antennas on the seafloor for geophysical exploration of the lithosphere.

1. INTRODUCTION

Lateral electromagnetic waves are excited along a boundary between two electrically different media by vertical or horizontal electric dipoles located near or on that boundary. Specifically, when a unit ($I_x h_e = 1$ Am) horizontal x -directed electric dipole is located in region 1 ($z \geq 0$, wave number $k_1 = \beta_1 + i\alpha_1 = \omega[\mu_0(\epsilon_1 + i\sigma_1/\omega)]^{1/2}$) at a distance d from the boundary with region 2 ($z \leq 0$, wave number $k_2 = \beta_2 + i\alpha_2 = \omega[\mu_0(\epsilon_2 + i\sigma_2/\omega)]^{1/2}$) (Figure 1), the electromagnetic field in region 1 at the point ρ, ϕ, z in cylindrical coordinates consists of six components. The following three are of interest here:

$$E_{1\rho}(\rho, \phi, z) = -\frac{\omega\mu_0}{2\pi k_1^2} \cos \phi \left\{ k_2 g(k_2 \rho, k_1) e^{ik_2 \rho} e^{ik_1(z+d)} - \left[\frac{k_1}{\rho^2} + \frac{i}{\rho^3} \right] e^{ik_1 r_1} \right\} \quad (1)$$

$$E_{1z}(\rho, \phi, z) = \frac{\omega\mu_0}{2\pi k_1^2} \cos \phi \left\{ \frac{k_2^2}{k_1} \left[f(k_2 \rho, k_1) e^{ik_2 \rho} e^{ik_1(z+d)} - \frac{ie^{ik_1 r_2}}{\rho^2} \right] - \frac{1}{2} \left(\frac{z-d}{\rho} e^{ik_1 r_1} + \frac{z+d}{\rho} e^{ik_1 r_2} \right) \left[\frac{ik_1^2}{\rho} - \frac{3k_1}{\rho^2} - \frac{3i}{\rho^3} \right] \right\} \quad (2)$$

$$B_{1\phi}(\rho, \phi, z) = -\frac{\mu_0}{2\pi k_1} \cos \phi \left\{ k_2 g(k_2 \rho, k_1) e^{ik_2 \rho} e^{ik_1(z+d)} + \frac{1}{2} \left[\frac{2}{\rho^3} + \frac{3i}{k_1 \rho^4} \right] e^{ik_1 r_2} + \frac{1}{2} \left(\frac{z-d}{\rho} e^{ik_1 r_1} + \frac{z+d}{\rho} e^{ik_1 r_2} \right) \left[\frac{ik_1^2}{\rho} - \frac{k_1}{\rho^2} \right] \right\} \quad (3)$$

Formulas for the components $E_{1\phi}(\rho, \phi, z)$, $B_{1\rho}(\rho, \phi, z)$, and $B_{1z}(\rho, \phi, z)$ are given by King and Wu [1983]. In (1)-(3),

$$f(k_2 \rho, k_1) = \frac{i}{k_2 \rho^3} = g(k_2 \rho, k_1) = \frac{ik_2}{\rho} - \frac{1}{\rho^2} - \frac{i}{k_2 \rho^3} - \frac{k_2^3}{k_1} \left(\frac{\pi}{k_2 \rho} \right)^{1/2} e^{-ik_2 \rho} {}_2F_2(k_2 \rho, k_1) \quad (4)$$

with

$$\mathcal{F}(k_2 \rho, k_1) = \frac{1}{2}(1+i) - C_2(k_2^3 \rho, 2k_1^2) - iS_2(k_2^3 \rho, 2k_1^2) \quad (5)$$

and

$$C_2(u) + iS_2(u) = \int_0^u (2\pi t)^{-1/2} e^{-t} dt \quad (6)$$

The distances r_1 from the source dipole and r_2 from its image to the point of observation are

$$r_1 = [(z-d)^2 + \rho^2]^{1/2} \quad r_2 = [(z+d)^2 + \rho^2]^{1/2} \quad (7)$$

The formulas are accurate, subject to the conditions

$$|k_1| \geq 3|k_2| \quad |k_1 \rho| \geq 3 \quad \rho \geq 5|z| \quad \rho \geq 5d \quad (8)$$

They include three types of terms, namely, direct field terms with the factor $e^{ik_1 r_1}$, image field terms with the factor $e^{ik_1 r_2}$, and lateral wave terms with the factor $e^{ik_2 \rho} e^{ik_1(z+d)}$. When region 1 is the sea or earth and region 2 is air or the lithosphere at the seafloor, $\alpha_1 \gg \alpha_2$, so that $e^{-\alpha_1 \rho} \ll e^{-\alpha_2 \rho}$, the direct and image field terms decay rapidly, and only the lateral wave field remains. Its amplitude is greatest when $z+d$ is small, so that $e^{-\alpha_1(z+d)} \sim 1$. The exponentials in the lateral wave terms all indicate that the wave travels vertically a distance d from the dipole to the boundary surface in region 1, then horizontally along the boundary a distance ρ in region 2, and finally verti-

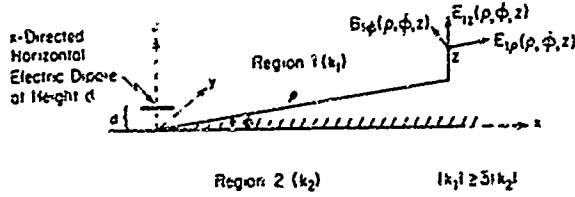


Fig. 1. Horizontal electric dipole near the boundary.

cally in region 1 to the point of observation at (ρ, ϕ, z) . The questions to be answered are: (1) What is the actual path of the lateral wave field along the boundary in region 2? (2) What is the maximum depth of penetration into region 2? (3) What fraction of the total power transferred to region 2 from the source is associated with the lateral wave? Answers to these questions require formulas for the electromagnetic field in region 2. These formulas are known along the boundary from (1)-(3) and the following boundary conditions:

$$\begin{aligned} E_{2\rho}(\rho, \phi, 0) &= E_{1\rho}(\rho, \phi, 0) \\ E_{2z}(\rho, \phi, 0) &= (k_1^2/k_2^2)E_{1z}(\rho, \phi, 0) \\ B_{2\phi}(\rho, \phi, 0) &= B_{1\phi}(\rho, \phi, 0) \end{aligned} \quad (9)$$

2. THE FIELD IN REGION 2 (AIR, OCEANIC CRUST)

In order to determine the depth of penetration of the lateral wave field into region 2 it is necessary to obtain explicit formulas for the complete field in that region. These can be derived from the incident field on the boundary $z = 0$ due to the horizontal electric dipole in region 1. The components of the field of an x-directed dipole in an infinite region with the wave number k_1 are well known. They are

$$E_x = \frac{i\omega\mu_0}{4\pi k_1^2} e^{ik_1 r_0} \left[\left(\frac{k_1^2}{r_0} + \frac{ik_1}{r_0^2} - \frac{1}{r_0^3} \right) - \frac{x^2}{r_0^2} \left(\frac{k_1^2}{r_0} + \frac{3ik_1}{r_0^2} - \frac{3}{r_0^3} \right) \right] \quad (10)$$

$$E_y = -\frac{i\omega\mu_0}{4\pi k_1^2} e^{ik_1 r_0} \frac{xy}{r_0^2} \left(\frac{k_1^2}{r_0} + \frac{3ik_1}{r_0^2} - \frac{3}{r_0^3} \right) \quad (11)$$

$$E_z = -\frac{i\omega\mu_0}{4\pi k_1^2} e^{ik_1 r_0} \frac{xz}{r_0^2} \left(\frac{k_1^2}{r_0} + \frac{3ik_1}{r_0^2} - \frac{3}{r_0^3} \right) \quad (12)$$

$$\mathbf{B} = \frac{\mu_0}{4\pi r_0} e^{ik_1 r_0} (\hat{y}z - \hat{z}y) \left(\frac{ik_1}{r_0} - \frac{1}{r_0^2} \right) \quad (13)$$

where $r_0 = (\rho^2 + z^2)^{1/2}$. The field on the plane boundary with region 2 is given by (10)-(13), with $z = d$. However, this is not the complete field because of reflection at the boundary.

The plane wave reflection coefficient R for normal incidence, as seen from region 1 (where the dipole is located), is defined by the components of the field tangent to the boundary, that is,

$$\begin{aligned} B_{tan} &= B_{tan}^{inc} e^{ik_1 z} + R e^{-ik_1 z} \\ E_{tan} &= E_{tan}^{inc} e^{ik_1 z} - R e^{-ik_1 z} \end{aligned} \quad (14)$$

at $z = 0$. In (14),

$$R = \frac{k_2 - k_1}{k_2 + k_1} \quad (15)$$

Since $|k_2|^2 \ll |k_1|^2$, it follows that

$$R \sim -1 + 2k_2/k_1 \quad (16)$$

On the boundary $z = 0$,

$$B_{tan} \sim 2(k_2/k_1)B_{tan}^{inc} \quad E_{tan} \sim 2E_{tan}^{inc}(1 - k_2/k_1) \quad (17)$$

As a first approximation, let $B_{tan} \sim 0$, $E_{tan} \sim 2E_{tan}^{inc}$. This is equivalent to an unbounded region 1 with the source dipole at $z = -d$ and an image dipole with codirectional current at $z = d$. Thus the tangential electric field on the boundary at $z = 0$ is effectively double that of the source dipole alone; the magnetic field is near zero. It follows that the tangential electric field in region 1 on the boundary plane $z = 0$ is

$$E_{1x} \sim \frac{i\omega\mu_0}{2\pi k_1^2} e^{ik_1 r_0} \left[\left(\frac{k_1^2}{r_0} + \frac{ik_1}{r_0^2} - \frac{1}{r_0^3} \right) - \frac{x^2}{r_0^2} \left(\frac{k_1^2}{r_0} + \frac{3ik_1}{r_0^2} - \frac{3}{r_0^3} \right) \right] \quad (18)$$

$$E_{1y} \sim -\frac{i\omega\mu_0}{2\pi k_1^2} e^{ik_1 r_0} \frac{xy}{r_0^2} \left(\frac{k_1^2}{r_0} + \frac{3ik_1}{r_0^2} - \frac{3}{r_0^3} \right) \quad (19)$$

This primary field is equivalent to a sheet of magnetic surface current \mathbf{K}_m in generating a field in region 2. It is defined by

$$\mathbf{K}_m = \hat{n} \times \mathbf{E}_{tan} = \hat{z} \times (\hat{x}E_{1x} + \hat{y}E_{1y}) = \hat{y}E_{1x} - \hat{x}E_{1y} \quad (20)$$

Since this current is large primarily on the parts of the surface near the dipole, its magnetic moment can be lumped at the origin for calculating the field in region 2 not too close to the origin and not too close to the boundary surface. The integrated moment is obtained from

$$m_y = \int_{-\infty}^{\infty} \int_{-\infty}^{\infty} E_x dx dy = -\frac{2\omega\mu_0}{k_1} e^{ik_1 d} \quad (21)$$

$$m_x = \int_{-\infty}^{\infty} \int_{-\infty}^{\infty} E_y dx dy = 0 \quad (22)$$

Hence the equivalent magnetic moment of a mag-

netic dipole located at the origin is $m = \hat{y}m_y$, as given by (21).

To a first approximation the field in region 2 ($z \leq 0$) not too close to the origin and not too close to the boundary surface is simply the field of a y -directed magnetic dipole at the origin (Figure 2). It is given by (A1)-(A6) in the appendix. It assumes that the tangential electric field vanishes at the boundary. This is adequate for points in region 2 not too close to the boundary. It can be improved to include the boundary by calculating higher-order approximations with $E_{1tan} = E_{2tan} = -(\omega/k_2)(\hat{z} \times B_2)$. This fairly long calculation is outlined in the appendix. It leads to the following improved formulas for the field in region 2 ($z \leq 0$) including the boundary with region 1:

$$E_{2\rho}(\rho, \phi, z) \sim -\frac{\omega\mu_0}{2\pi k_1} e^{ik_1 z} \cos \phi \left(\frac{ik_2}{r_0} - \frac{1}{r_0^2} \right) e^{ik_2 r_0} \cdot \left[\frac{z}{r_0} + \frac{k_2}{k_1} (1 + \mathcal{G}) \right] \quad (23)$$

$$E_{2\phi}(\rho, \phi, z) \sim \frac{\omega\mu_0}{2\pi k_1} e^{ik_1 z} \sin \phi \left(\frac{z}{r_0} \right) \left(\frac{ik_2}{r_0} - \frac{1}{r_0^2} \right) e^{ik_2 r_0} \quad (24)$$

$$E_{2z}(\rho, \phi, z) \sim \frac{\omega\mu_0}{2\pi k_1} e^{ik_1 z} \cos \phi \left(\frac{\rho}{r_0} \right) \left(\frac{ik_2}{r_0} - \frac{1}{r_0^2} \right) e^{ik_2 r_0} (1 + \mathcal{G}) \quad (25)$$

$$B_{2\rho}(\rho, \phi, z) \sim -\frac{\mu_0 k_2}{2\pi k_1} e^{ik_1 z} \sin \phi \cdot \left[\frac{ik_2 z^2}{r_0^3} + \frac{(2\rho^2 - z^2)}{r_0^2} \left(\frac{1}{r_0^2} + \frac{i}{k_2 r_0^3} \right) + \frac{1}{r_0^2} \mathcal{G} \right] e^{ik_2 r_0} \quad (26)$$

$$B_{2\phi}(\rho, \phi, z) \sim -\frac{\mu_0 k_2}{2\pi k_1} e^{ik_1 z} \cos \phi \cdot \left(\frac{ik_2}{r_0} - \frac{1}{r_0^2} - \frac{i}{k_2 r_0^3} \right) e^{ik_2 r_0} (1 + \mathcal{G}) \quad (27)$$

$$B_{2z}(\rho, \phi, z) \sim \frac{\mu_0 k_2}{2\pi k_1} e^{ik_1 z} \sin \phi \cdot \left(\frac{\rho z}{r_0^2} \right) \left(\frac{ik_2}{r_0} - \frac{3}{r_0^2} - \frac{3i}{k_2 r_0^3} \right) e^{ik_2 r_0} \quad (28)$$

These formulas are good approximations everywhere in region 2 except near the source, that is, $|k_1 r_0| \gg 1$. In these formulas,

$$\mathcal{G} = i(2\pi R)^{1/2} e^{-i\pi(R-Z)/2} \left\{ \frac{1}{2}(1+i) - C_2[(R-Z)/R] - iS_2[(R-Z)/R] \right\} \quad (29)$$

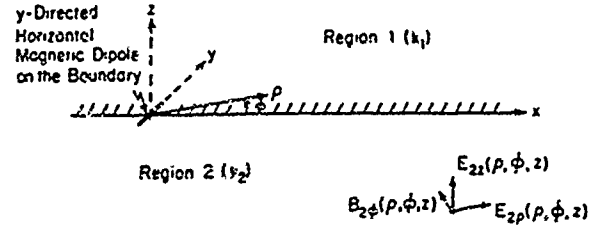


Fig. 2. Equivalent magnetic dipole on the boundary for determining field in region 2.

with $R \equiv k_2^2 \rho / 2k_1^2$ and $Z \equiv k_2^2 z / 2k_1 \leq 0$; $C_2(u)$ and $S_2(u)$ are defined in (6).

A more precise formulation of the condition $|k_1 r_0| \gg 1$ can be obtained from a comparison of (29) at $z = 0$ with (1) at $z = 0$. When $z = 0$, $r_0 \rightarrow \rho$ and

$$\mathcal{G} \rightarrow \frac{ik_2^2 \rho}{k_1} \left(\frac{\pi}{k_2 \rho} \right)^{1/2} e^{-ik_2^2 \rho / 2k_1^2} \mathcal{F}(k_2 \rho, k_1) \quad (30)$$

so that (23) becomes

$$E_{2\rho}(\rho, \phi, 0) = -\frac{\omega\mu_0 k_2}{2\pi k_1^2} e^{ik_1 z} \cos \phi \left(\frac{ik_2}{\rho} - \frac{1}{\rho^2} \right) e^{ik_2 \rho} \cdot \left[1 + \frac{ik_2^2 \rho}{k_1} \left(\frac{\pi}{k_2 \rho} \right)^{1/2} e^{-ik_2^2 \rho / 2k_1^2} \mathcal{F}(k_2 \rho, k_1) \right] \sim -\frac{\omega\mu_0 k_2}{2\pi k_1^2} e^{ik_1 z} e^{ik_2 \rho} \cos \phi \cdot \left[\frac{ik_2}{\rho} - \frac{1}{\rho^2} - \frac{k_2^2}{k_1} \left(\frac{\pi}{k_2 \rho} \right)^{1/2} e^{-ik_2^2 \rho / 2k_1^2} \mathcal{F}(k_2 \rho, k_1) \right] \quad (31)$$

where, as in (1), only ik_2/ρ is retained in $[(ik_2/\rho) - (1/\rho^2)]$ where this is a factor of the Fresnel integral, since this term is negligible when $|k_2 \rho|$ is not large. A comparison of (31) and (1) shows that the two are in agreement when $r_1 = r_0 = (\rho^2 + d^2)^{1/2}$ is sufficiently great to make the direct field negligible (i.e., $\exp(-\alpha_1 r_0) \leq 0.04$ or $\alpha_1 r_0 \geq 3$), and ρ is sufficiently large to make the term $i/k_2 \rho^3$ negligible compared with $[(ik_2/\rho) - (1/\rho^2)]$ or $|k_2^2 \rho^2|$ large compared with 1. Calculations from (23) show that actually, $E_{1\rho}(\rho, \phi, z)$ is proportional to $1/\rho$ when $|k_2 \rho| \geq 1$. It is reasonable to assume that the general expressions (23)-(29) are good approximations when $\alpha_1 r_0 \geq 3$ and $|k_2 r_0| \geq 1$.

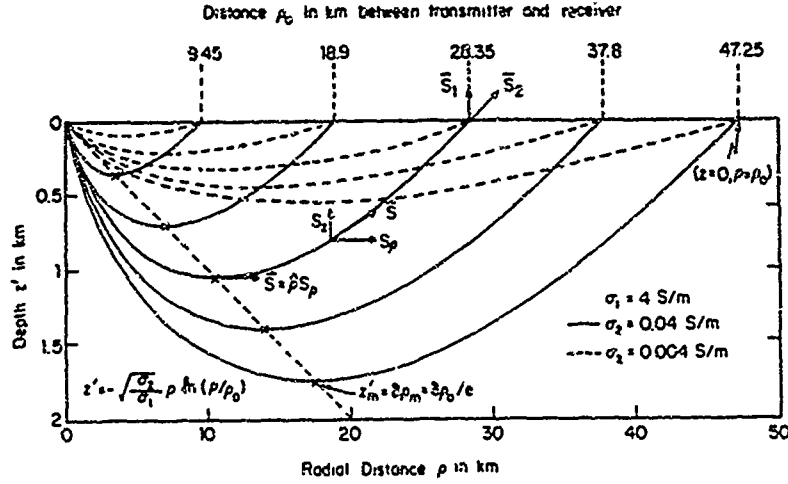


Fig. 3. Locus of Poynting vector in half-space model of lithosphere; $k_1 \sim (i\omega\mu_0\sigma_1)^{1/2}$, $k_2 \sim (i\omega\mu_0\sigma_2)^{1/2}$. At $z = 0$, $S_{1\rho} = (\sigma_2/\sigma_1)S_{2\rho}$, and $S_{1z} = S_{2z}$.

3. LOCUS OF THE POYNTING VECTOR IN REGION 2 (AIR, OCEANIC CRUST): DEPTH OF PENETRATION OF LATERAL WAVE

The complex Poynting vector in region 2 is given by

$$S_2 = \frac{1}{2\mu_0} E_2 \times B_2^* = \frac{1}{2\mu_0} [\bar{z} E_{2\rho} B_{2\phi}^* - \bar{\rho} E_{2z} B_{2\phi}^*] \quad (32)$$

In the range $|k_2\rho| \leq 4|k_1^2/k_2^2|$ the contributions from the Fresnel integral terms are negligible. In this range, with $z \leq 0$,

$$E_{2\rho}(\rho, \phi, z) \sim -\frac{\omega\mu_0}{2\pi k_1} \cos \phi e^{ik_1 z} \left(\frac{ik_2}{r_0^2} - \frac{1}{r_0^3} \right) \cdot \left(z + \frac{k_2}{k_1} r_0 \right) e^{ik_2 r_0} \quad (33)$$

$$E_{2z}(\rho, \phi, z) \sim \frac{\omega\mu_0}{2\pi k_1} \cos \phi e^{ik_1 z} \left(\frac{ik_2}{r_0^2} - \frac{1}{r_0^3} \right) \rho e^{ik_2 r_0} \quad (34)$$

$$B_{2\phi}^*(\rho, \phi, z) = -\frac{\mu_0 k_2^*}{2\pi k_1^*} \cos \phi e^{i\mu_1 z} \cdot \left(-\frac{ik_2^*}{r_0} - \frac{1}{r_0^2} + \frac{i}{k_2^* r_0^3} \right) e^{-ik_2^* r_0} \quad (35)$$

It follows that

$$S_{2z} \approx A [z + (k_2/k_1)r_0] \cos^2 \phi \quad S_{2\rho} \approx A\rho \cos^2 \phi \quad (36)$$

where

$$A = A_R + iA_I = \frac{\omega\mu_0 k_2^*}{8\pi |k_1|^2} e^{-2\alpha_1 r_0} e^{-2\alpha_2 r_0} \cdot \left(\frac{ik_2}{r_0^2} - \frac{1}{r_0^3} \right) \left(-\frac{ik_2^*}{r_0} - \frac{1}{r_0^2} + \frac{i}{k_2^* r_0^3} \right) \quad (37)$$

The real parts are

$$\text{Re } S_{2\rho} = A_R \rho \cos^2 \phi \quad \text{Re } S_{2z} \sim A_R (z + \delta r_0) \cos^2 \phi \quad (38)$$

where, with $k = \beta + i\alpha$,

$$\delta = \text{Re } (k_2/k_1) = \frac{\beta_1\beta_2 + \alpha_1\alpha_2}{\beta_1^2 + \alpha_1^2} \quad (39)$$

The two cases of interest are the air-earth or sea boundary, where $\alpha_2 = 0$, and the ocean-seafloor boundary at low frequencies at which $k = (i\omega\mu_0\sigma)^{1/2}$ in both regions. In these cases, $\delta = \beta_1\beta_2/|k_1|^2$ and $\delta = (\sigma_2/\sigma_1)^{1/2}$, respectively. With (8), δ is small, and δ^2 is negligible.

Since z is negative in region 2, it is convenient to let $z' = -z$. The slope of the locus of the Poynting vector is

$$-\frac{dz'}{d\rho} = \text{Re } \frac{S_{2z}}{S_{2\rho}} \approx \frac{-z' + \delta r_0}{\rho} \quad (40)$$

The equation for the locus of the Poynting vector in region 2 ($z \leq 0$) with $z' = -z$, is

$$\frac{dz'}{d\rho} - \frac{z'}{\rho} = -\delta(1 + z'^2/\rho^2)^{1/2} \quad (41)$$

Since δ is small and z'/ρ is small on all parts of the locus except near the origin where none of the formulas is accurate, a proper approximation over the range $\rho \geq 5z'$ is

$$\frac{dz'}{d\rho} = \frac{z'}{\rho} - \delta \quad (42)$$

This is readily solved with the substitution $z' = s\rho$, $(dz'/d\rho) = s + \rho(ds/d\rho)$, which gives

$$ds = -\delta \frac{d\rho}{\rho} \quad (43a)$$

or

$$s = -\delta \ln(\rho/\rho_0) \quad (43b)$$

Hence the equation of the locus of the Poynting vector is

$$z' = -\delta \rho \ln(\rho/\rho_0) \quad (44)$$

where $z' = 0$ at $\rho = 0$ and $\rho = \rho_0$. Typical loci are shown in Figure 3 for the lateral wave in the lithosphere below the seafloor under physical conditions characteristic of the measurements made by Young and Cox [1981] on the seafloor. Note that the scale of z' is enlarged 10 times over that of ρ . The depth of penetration of the lateral wave into region 2 depends on the radial distance ρ_0 where the field is observed. The maximum depth is at

$$z' = z'_m = \delta \rho_0 e = \delta \rho_0 2.718 = \delta \rho_m \quad (45)$$

where $e = 2.718$ is the base of the natural logarithm and

$$\rho_m = \rho_0 e = \rho_0 2.718 \quad (46)$$

On the conical surface defined by (45) the Poynting vector is purely radial, that is,

$$S_2 = \rho S_{2r}, \quad S_{2z} = 0, \quad z' = z'_m = \delta \rho_0 e \quad (47)$$

This cone has the apex half-angle Θ'_m , defined by

$$\Theta'_m = \frac{\pi}{2} - \tan^{-1} \frac{z'_m}{\rho_m} = \frac{\pi}{2} - \tan^{-1} \delta \sim \frac{\pi}{2} - \delta \quad (48)$$

4. DIVISION OF POWER BETWEEN LATERAL WAVE AND SPACE WAVE IN REGION 2

The real part of the radial spherical component S_r of the Poynting vector is given by

$$\begin{aligned} \text{Re } S_r &= \text{Re} [-S_z \cos \Theta' + S_\phi \sin \Theta'] \\ &\sim A_R \left[(z' - \delta r_0) \left(\frac{z'}{r_0} \right) + \frac{\rho^2}{r_0} \right] \cos^2 \phi \\ &\approx A_R (r_0 - \delta z') \cos^2 \phi \end{aligned}$$

or

$$\text{Re } S_r = A_R r_0 (1 - \delta \cos \Theta') \cos^2 \phi \quad (49)$$

The total power radiated by the magnetic dipole into region 2 across a hemisphere of radius r_0 is given by the integral of $\text{Re } S_r$ over the surface of that hemisphere, as shown in Figure 4. Thus with $S_{2r} = \text{Re } S_r$, as given in (49),

$$\begin{aligned} P_{2T} &= \int_0^{\pi/2} \int_0^{2\pi} r_0 d\Theta' \int_0^{2\pi} S_{2r} r_0 \sin \Theta' d\phi \\ &= \pi A_R r_0^3 (1 - \delta/2) \end{aligned} \quad (50)$$

The large fraction of this power that crosses the section of the hemisphere bounded by the circle through the points $P(\rho_m, z'_m)$ is

$$\begin{aligned} P_{2S} &= \int_0^{\Theta'_m} \int_0^{2\pi} r_0 d\Theta' \int_0^{2\pi} S_{2r} r_0 \sin \Theta' d\phi \\ &= \pi A_R r_0^3 \left(1 - \cos \Theta'_m - \frac{\delta}{2} \sin^2 \Theta'_m \right) \end{aligned} \quad (51)$$

Since the Poynting vector is always tangent to the logarithmic surfaces OQ and OR in Figure 4, the power between them is transmitted to the section of the boundary surface between Q and R where it enters region 1. If region 2 is dissipative, a part of this power appears as heat in the shaded volume. The fraction of the total power that crosses the section of the hemisphere between P and Q is readily evaluated. It is the power P_L in the lateral wave that reaches the surface between Q and R.

$$\begin{aligned} P_{2L} &= \int_{\Theta'_m}^{\pi/2} \int_0^{2\pi} r_0 d\Theta' \int_0^{2\pi} S_{2r} r_0 \sin \Theta' d\phi \\ &= \pi A_R r_0^3 \left(1 - \cos \Theta'_m - \frac{\delta}{2} \sin^2 \Theta'_m \right) \end{aligned} \quad (52)$$

If use is now made of (48) and (45), it follows that

$$\cos \Theta'_m = \frac{z'_m}{(\rho_m^2 + z_m'^2)^{1/2}} = \frac{\delta \rho_m}{\rho_m (1 + \delta^2)^{1/2}} = \frac{\delta}{(1 + \delta^2)^{1/2}} \sim \delta$$

$$\sin \Theta'_m = \frac{\rho_m}{(\rho_m^2 + z_m'^2)^{1/2}} = \frac{\rho_m}{\rho_m (1 + \delta^2)^{1/2}} \sim 1$$

With these values and neglecting $\delta^2 \ll 1$,

$$P_{2S} \sim \pi A_R r_0^3 \left(1 - \frac{3\delta}{2} \right) \quad P_{2L} \sim \pi A_R r_0^3 \delta \quad (53)$$

and

$$\frac{P_{2S}}{P_{2T}} \sim \frac{1 - 3\delta/2}{1 - \delta/2} \sim 1 - \delta \quad \frac{P_{2L}}{P_{2T}} \sim \frac{\delta}{1 - \delta/2} \sim \delta \quad (54)$$

from the source to the point of observation in the useful intermediate zone where the magnitude of the radial component of the lateral wave field is

$$|E_{1\rho}^L(\rho, 0, 0)| \approx \frac{\omega\mu_0\sigma_2}{2\pi\sigma_1} e^{-\alpha_1 D} \frac{e^{-\alpha_2 \rho}}{\rho} |\cos \phi| \quad (55)$$

This is the entire field if there are no reflections of the space wave which is given by (23)–(28) with the lateral terms omitted. In the spherical coordinates r, Θ, ϕ the space wave has the following components:

$$E_{2r}(r_0, \Theta, \phi) = 0 \quad (56)$$

$$E_{2\theta}(r_0, \Theta, \phi) = -\frac{\omega\mu_0}{2\pi k_1} e^{ik_1 D} e^{ik_2 r_0} \left(\frac{ik_2}{r_0} - \frac{1}{r_0^2} \right) \cos \phi \quad (57)$$

$$B_{2\theta}(r_0, \Theta, \phi) = -\frac{\mu_0 k_2}{2\pi k_1} e^{ik_1 D} e^{ik_2 r_0} \left(\frac{ik_2}{r_0} - \frac{1}{r_0^2} - \frac{i}{k_2 r_0^3} \right) \cos \phi \quad (58)$$

$$E_{2\phi}(r_0, \Theta, \phi) = \frac{\omega\mu_0}{2\pi k_1} e^{ik_1 D} e^{ik_2 r_0} \left(\frac{ik_2}{r_0} - \frac{1}{r_0^2} \right) \sin \phi \cos \Theta \quad (59)$$

$$B_{2r}(r_0, \Theta, \phi) = -\frac{\mu_0 k_2}{2\pi k_1} e^{ik_1 D} e^{ik_2 r_0} \left(\frac{2}{r_0^2} - \frac{2i}{k_2 r_0^3} \right) \sin \phi \sin \Theta \quad (60)$$

$$B_{2\theta}(r_0, \Theta, \phi) = -\frac{\mu_0 k_2}{2\pi k_1} e^{ik_1 D} e^{ik_2 r_0} \left(\frac{ik_2}{r_0} - \frac{1}{r_0^2} - \frac{i}{k_2 r_0^3} \right) \sin \phi \cos \Theta \quad (61)$$

Note that Θ' in the previous discussion is $\Theta' = \pi - \Theta$.

When $|k_2 r_0| > 1$, the $1/r_0$ term dominates, and the highly attenuated outward traveling spherical wave has the form $e^{ik_2 r_0}/r_0 = e^{-\alpha_2 r_0} e^{i\beta_2 r_0}/r_0$. This wave is partly of the electric type ($E_{2r} = 0, E_{2\theta}$, and $B_{2\phi}$) and partly of the magnetic type ($B_{2r} \sim$ small, $B_{2\theta}$, and $E_{2\phi}$). It is this field that is partly reflected, partly transmitted when incident on a surface of discontinuity in σ_2 . However, since the field is not a plane wave, is not normally incident on such surfaces, and is not independent of the transverse coordinates ρ and ϕ , it follows that it is not readily determined except when the reflection coefficient for plane waves is ± 1 . When this is true, and there are boundaries that approximate it quite well, the reflected field is the field of an image magnetic dipole with equal and codirectional or equal and opposite magnetic moment. If the reflecting boundary is at $z' = D$, the image is at $z' = 2D$, and the field at $\rho = \rho_0$ just below the surface in region 2 is given by (57) with r_0 re-

placed by $2r_0 = (4D^2 + \rho_0^2)^{1/2}$. When $|k_2 r_0| > 1$, this is

$$E_{2\theta}^S \sim \frac{i\omega\mu_0 k_2}{2\pi k_1} e^{ik_1 D} \frac{e^{i2k_2 r_0}}{2r_0} \quad (62)$$

The plane wave transmission coefficient for the electric field at the surface of region 1 is

$$T = \frac{2 \cos \Theta'}{\cos \Theta' + [(k_1/k_2)^2 - \sin^2 \Theta']} \sim \frac{2k_2 \cos \Theta'}{k_2 \cos \Theta' + k_1} \sim \frac{2k_2}{k_1} \cos \Theta' \quad (63)$$

The approximations on the right-hand side of (63) depend on $|k_1|^2 \gg |k_2|^2$. The field across the boundary in region 1 is approximated by

$$E_{1\rho}^S(\rho_0, \phi, 0) \sim T E_{2\theta}^S = \frac{i\omega\mu_0}{2\pi} \frac{k_2^2}{k_1^2} e^{ik_1 D} \left(\frac{D e^{i2k_2 r_0}}{r_0^2} \right) \cos \phi \quad (64)$$

With $k = (i\omega\mu_0\sigma)^{1/2}$ the magnitude is

$$|E_{1\rho}^S(\rho_0, \phi, 0)| \sim \frac{\omega\mu_0}{2\pi} \frac{\sigma_2}{\sigma_1} e^{-\alpha_1 D} \frac{D}{r_0^2} e^{-2\alpha_2 r_0} |\cos \phi| \quad (65)$$

The ratio of the reflected space wave to the lateral wave (55) at $\rho_0, \phi, 0$ is

$$\mathcal{R} = \frac{\rho_0 D}{r_0^2} e^{-\alpha_2(2r_0 - \rho_0)} \quad (66)$$

where $\alpha_2 = (\omega\mu_0\sigma_2/2)^{1/2}$. Calculations of this ratio as a function of $2D/\rho_0$ for $\sigma_1 = 4$ S/m and $\sigma_2 = 0.004, 0.01, 0.04$, and 0.1 S/m are represented graphically in Figure 5 for $f = 1$ and 2 Hz. The curves show that the field due to the reflected space wave first rises to a maximum as the depth D of the reflecting layer is increased and then decays. The initial rise is due to the increase in $E_{2\rho} \sim E_{2\theta} \cos \Theta' = E_{2\theta}(D/r_0)$ as D becomes larger; the final decay is caused by the exponential factor.

Even at its greatest value, with $\sigma_2 = 0.004$ S/m, $D \sim 0.25\rho_0 = 5$ km, and $f = 1$ Hz, the contribution by the reflected space wave to the total field observed on the seafloor is less than 40%, with the lateral wave contributing over 60%. For other depths and conductivities the lateral wave may contribute as much as 90% or more to the total field observed at $\rho_0 = 20$ km on the seafloor. Since the lateral wave penetrates only a short distance into the lithosphere, as shown in the inset in Figure 5, great care must be used in interpreting measured values of the total field. If no consideration is given to the lateral wave and the entire observed field is treated as a space

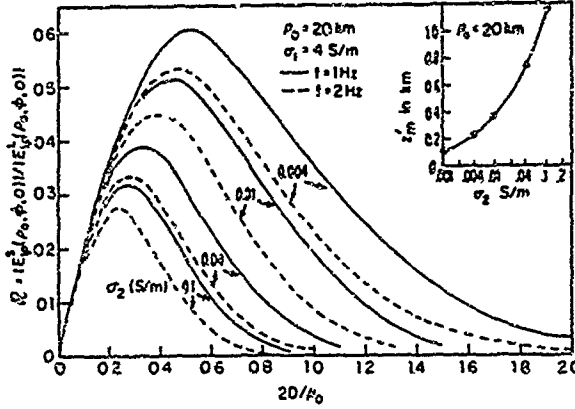


Fig. 5. Ratio of reflected space wave field to lateral wave field on seafloor; depth of penetration of lateral wave (inset).

wave into the lithosphere that has been partially reflected from the boundaries of a succession of hypothetical horizontal layers, each with its own conductivity. large errors in interpretation are inevitable. The 60-90% of the observed field that has sampled only a thin layer of the lithosphere cannot be ignored.

APPENDIX: THE FIELD IN REGION 2

The complete field in region 2 is obtained as a refinement of the field due to a y -directed magnetic dipole with the magnetic moment $(-2\omega\mu_0/k_1)e^{ik_1d}$, located on the boundary surface at the origin of the cylindrical coordinates ρ, ϕ, z , where ϕ is measured from the positive x axis. The components of the field are

$$E_{2\rho}(\rho, \phi, z) = -\frac{\omega\mu_0}{2\pi k_1} e^{ik_1d} \cos \phi \left(\frac{z}{r_0} \right) \left(\frac{ik_2}{r_0} - \frac{1}{r_0^2} \right) e^{ik_2z} \quad (A1)$$

$$E_{2\phi}(\rho, \phi, z) = \frac{\omega\mu_0}{2\pi k_1} e^{ik_1d} \sin \phi \left(\frac{z}{r_0} \right) \left(\frac{ik_2}{r_0} - \frac{1}{r_0^2} \right) e^{ik_2z} \quad (A2)$$

$$E_{2z}(\rho, \phi, z) = \frac{\omega\mu_0}{2\pi k_1} e^{ik_1d} \cos \phi \left(\frac{\rho}{r_0} \right) \left(\frac{ik_2}{r_0} - \frac{1}{r_0^2} \right) e^{ik_2z} \quad (A3)$$

$$B_{2\rho}(\rho, \phi, z) = -\frac{\mu_0 k_2}{2\pi k_1} e^{ik_1d} \sin \phi$$

$$\left[\frac{ik_2 z^2}{r_0^3} + \frac{(2\rho^2 - z^2)}{r_0^2} \left(\frac{1}{r_0^2} + \frac{i}{k_2 r_0^3} \right) \right] e^{ik_2z} \quad (A4)$$

$$B_{2\phi}(\rho, \phi, z) = -\frac{\mu_0 k_2}{2\pi k_1} e^{ik_1d} \cos \phi \left(\frac{ik_2}{r_0} - \frac{1}{r_0^2} - \frac{i}{k_2 r_0^3} \right) e^{ik_2z} \quad (A5)$$

$$B_{2z}(\rho, \phi, z) = \frac{\mu_0 k_2}{2\pi k_1} e^{ik_1d} \sin \phi \left(\frac{\rho z}{r_0^2} \right) \left(\frac{ik_2}{r_0} - \frac{3}{r_0^2} - \frac{3i}{k_2 r_0^3} \right) e^{ik_2z} \quad (A6)$$

where $r_0 = (\rho^2 + z^2)^{1/2}$. This field is consistent with the boundary condition $E_{2tan} \sim 0$, which is an approximation of the actual boundary condition, namely,

$$E_{1tan}(\rho, \phi, 0) = E_{2tan}(\rho, \phi, 0) \\ = -(\omega/k_2)\hat{z} \times \nabla_{2tan}(\rho, \phi, 0) \quad (A7)$$

where $z \leq 0$ in region 2. Use can then be made of this accurate boundary condition and the assumed inequality

$$n^2 \equiv k_2^2/k_1^2 \ll 1 \quad (A8)$$

to extend the range of (A1)-(A6) to include the region near the boundary. This is accomplished with Maxwell's equations in cylindrical coordinates, namely,

$$\frac{1}{\rho} \frac{\partial B_z}{\partial \phi} - \frac{\partial B_\phi}{\partial z} = -\frac{ik^2}{\omega} E_\rho \quad (A9)$$

$$\frac{\partial B_\rho}{\partial z} - \frac{\partial B_z}{\partial \rho} = -\frac{ik^2}{\omega} E_\phi \quad (A10)$$

$$\frac{1}{\rho} \left[\frac{\partial}{\partial \rho} (\rho B_\phi) - \frac{\partial B_\rho}{\partial \phi} \right] = -\frac{ik^2}{\omega} E_z \quad (A11)$$

$$\frac{1}{\rho} \frac{\partial E_z}{\partial \phi} - \frac{\partial E_\phi}{\partial z} = i\omega B_\rho \quad (A12)$$

$$\frac{\partial E_\rho}{\partial z} - \frac{\partial E_z}{\partial \rho} = i\omega B_\phi \quad (A13)$$

$$\frac{1}{\rho} \left[\frac{\partial}{\partial \rho} (\rho E_\phi) - \frac{\partial E_\rho}{\partial \phi} \right] = i\omega B_z \quad (A14)$$

applied to the leading terms of the field in (A1)-(A6), after the variables ρ and z have been changed according to

$$R = \rho k_2^2/2k_1^2 = n^2 k_2 \rho/2 \quad Z = z k_2^2/2k_1^2 = n k_2 z/2$$

or

$$k_2 \rho = 2R/n^2 \quad k_2 z = 2Z/n \quad (A15)$$

Note that the newly defined variable R is Sommerfeld's "numerical distance." The correction to (A1)-(A6) is to apply specifically to a region near the boundary where $\rho^2 \gg z^2$ or $r_0 = (\rho^2 + z^2)^{1/2} \sim \rho$. In order to simplify the calculation the correction term will be evaluated only for the leading terms; the other terms can be replaced after the correction terms have been added.

In terms of the new variables R and Z the leading terms in (A1)–(A6) are

$$E_{2\rho} \sim A \cos \phi e^{i2R/n^2} n \tilde{E}_{2\rho} \quad \tilde{E}_{2\rho} = -(Z/R^2) e^{iZ^2/R} \quad (\text{A16})$$

$$E_{2\phi} \sim A \sin \phi e^{i2R/n^2} n \tilde{E}_{2\phi} \quad \tilde{E}_{2\phi} = (Z/R^2) e^{iZ^2/R} \quad (\text{A17})$$

$$\tilde{E}_{2z} \sim A \cos \phi e^{i2R/n^2} \tilde{E}_{2z} \quad \tilde{E}_{2z} = (1/R) e^{iZ^2/R} \quad (\text{A18})$$

$$B_{2\rho} \sim A(k_2/\omega) \sin \phi e^{i2R/n^2} n^2 \tilde{B}_{2\rho} \quad \tilde{B}_{2\rho} = \left(\frac{1}{R^2} - \frac{Z^2}{R^3} \right) e^{iZ^2/R} \quad (\text{A19})$$

$$B_{2\phi} \sim A(k_2/\omega) \cos \phi e^{i2R/n^2} \tilde{B}_{2\phi} \quad \tilde{B}_{2\phi} = -(1/R) e^{iZ^2/R} \quad (\text{A20})$$

$$B_{2z} \sim A(k_2/\omega) \sin \phi e^{i2R/n^2} n \tilde{B}_{2z} \quad \tilde{B}_{2z} = (Z/R^2) e^{iZ^2/R} \quad (\text{A21})$$

where $A \equiv i\omega\mu_0 k_2^2 n^2 / 4\pi k_1$. If these formulas are inserted in Maxwell's equations (A9)–(A14) and the terms are arranged in order of the powers of the small quantity n , the following first-order relations are obtained. (Note that $\partial/\partial\rho \rightarrow ik_2 + \partial/\partial\rho = ik_2 + (n^2 k_2/2) \partial/\partial R$.)

$$\frac{\partial \tilde{B}_{2\phi}}{\partial Z} = 2i \tilde{E}_{2\rho} \quad \tilde{B}_{2z} = \tilde{E}_{2\phi} \quad (\text{A22})$$

$$\frac{\partial \tilde{E}_{2\phi}}{\partial Z} + \frac{\tilde{E}_{2z}}{R} = -2i \tilde{B}_{2\rho} \quad \tilde{E}_{2z} = -\tilde{B}_{2\phi} \quad (\text{A23})$$

With appropriate combination the following second-order equations are obtained:

$$\left(\frac{1}{R} \frac{\partial}{\partial R} R + \frac{\partial}{\partial R} \right) \tilde{B}_{2\phi} = -\frac{\partial \tilde{E}_{2\rho}}{\partial Z} \quad (\text{A24})$$

$$\left(\frac{1}{R} \frac{\partial}{\partial R} R + \frac{\partial}{\partial R} \right) \tilde{E}_{2\phi} + \frac{\partial \tilde{B}_{2z}}{\partial R} - \frac{\partial \tilde{B}_{2\phi}}{\partial Z} = -\frac{\tilde{E}_{2\rho}}{R} \quad (\text{A25})$$

If (A22) and (A23) are combined with these last two equations, the two equations (A26) and (A29) remain to be solved:

$$\left(\frac{1}{R} + 2 \frac{\partial}{\partial R} \right) \tilde{B}_{2\phi} - \frac{i}{2} \frac{\partial^2 \tilde{B}_{2\phi}}{\partial Z^2} = 0 \quad (\text{A26})$$

subject to the boundary condition

$$\tilde{E}_{2\rho} = \tilde{B}_{2\phi} \quad Z = 0 \quad (\text{A27})$$

and from (A16) and (A20),

$$\tilde{E}_{2\rho} = -(Z/R^2) e^{iZ^2/R} \quad \tilde{B}_{2\phi} = -(1/R) e^{iZ^2/R} \quad (\text{A28})$$

far from the boundary, and

$$\left(\frac{1}{R} + 2 \frac{\partial}{\partial R} \right) \tilde{E}_{2\phi} - \frac{\partial \tilde{B}_{2\rho}}{\partial Z} + \frac{\partial \tilde{B}_{2z}}{\partial R} = -\frac{\tilde{E}_{2\rho}}{R} \quad (\text{A29})$$

subject to the boundary condition

$$\tilde{E}_{2\phi} \sim 0 \quad Z = 0 \quad (\text{A30})$$

and from (A17)

$$\tilde{E}_{2\phi} = (Z/R^2) e^{iZ^2/R} \quad (\text{A31})$$

far from the boundary.

The solution of (A26) is carried out with the substitution

$$F = F(R, Z) = R^{1/2} \tilde{B}_{2\phi} \quad (\text{A32})$$

so that

$$\tilde{E}_{2\rho} = -\frac{i}{2} \frac{\partial \tilde{B}_{2\phi}}{\partial Z} = -\frac{i}{2} R^{-1/2} \frac{\partial F}{\partial Z} \quad (\text{A33})$$

With this substitution in (A24), (A24) becomes

$$\frac{\partial^2 F}{\partial Z^2} + 4i \frac{\partial F}{\partial R} = 0 \quad (\text{A34})$$

and with (A27), (A33) gives

$$\left[\frac{\partial F}{\partial Z} - 2iF \right]_{Z=0} = 0. \quad (\text{A35})$$

With (A28),

$$F \rightarrow -R^{-1/2} e^{iZ^2/R} \quad (\text{A36})$$

far from the boundary. The solution of (A34), subject to (A35) and (A36), is required.

Since far from the boundary $F \rightarrow -R^{-1/2} e^{iZ^2/R}$, the solution near the boundary can be obtained in the form

$$F_0 = F + R^{-1/2} e^{iZ^2/R} \quad (\text{A37})$$

where $F_0 \sim 0$ at sufficient distance from the boundary where $-R^{-1/2} e^{iZ^2/R}$ is the solution. Since $[(\partial^2/\partial Z^2) + 4i(\partial/\partial R)]R^{-1/2} e^{iZ^2/R} = 0$, it follows that

$$\frac{\partial^2 F_0}{\partial Z^2} + 4i \frac{\partial F_0}{\partial R} = 0 \quad (\text{A38})$$

Also, with (A35) it follows that

$$\left[\frac{\partial F_0}{\partial Z} - 2iF_0 \right]_{Z=0} = -2iR^{-1/2} \quad (\text{A39})$$

A solution of (A38) with (A39) can be obtained with the Fourier transform

$$F_0(\xi, Z) = \int_0^\infty F_0(R, Z) e^{-i\xi R} dR \quad (\text{A40})$$

When (A38) and (A39) are Fourier-transformed, they give

$$\frac{\partial^2 F_0}{\partial Z^2} - 4\xi F_0 = 0 \quad F_0 = A(\xi) e^{2\xi^{1/2} Z} \quad (\text{A41})$$

$$\left[\frac{\partial F_0}{\partial Z} - 2iF_0 \right]_{Z=0} = -2(\pi i)^{1/2} \xi^{-1/2} \quad (\text{A42}) \quad \text{where}$$

With (A41) in (A42),

$$A(\xi) = \frac{-(\pi i)^{1/2}}{\xi^{1/2}(\xi^{1/2} - i)} \quad (\text{A43})$$

so that

$$F_0(\xi, Z) = -\frac{(\pi i)^{1/2} e^{2\xi^{1/2} Z}}{\xi^{1/2}(\xi^{1/2} - i)} \quad (\text{A44})$$

When the inverse transform of (A44) is substituted in (A37), the solution for $F = F(R, Z)$ is

$$F(R, Z) = -R^{-1/2} e^{iZ^2 R} - \left(\frac{i}{4\pi} \right)^{1/2} \int_{-\infty}^{\infty} \frac{e^{2\xi^{1/2} Z}}{\xi^{1/2}(\xi^{1/2} - i)} e^{i\xi R} d\xi \quad (\text{A45})$$

With (A45), (A32) gives

$$\tilde{B}_{2\phi} = -\frac{e^{iZ^2 R}}{R} - \left(\frac{i}{4\pi R} \right)^{1/2} I(R, Z) \quad (\text{A46})$$

where

$$I \equiv I(R, Z) = \int_{-\infty}^{\infty} \frac{1}{\xi^{1/2}(\xi^{1/2} - i)} e^{2\xi^{1/2} Z} e^{i\xi R} d\xi \quad (\text{A47})$$

This integral can be expressed in terms of the Fresnel integral. As a first step, note that

$$\begin{aligned} \frac{1}{2} \frac{\partial}{\partial Z} (e^{-2iZ} I) &= \left(\frac{1}{2} \frac{\partial I}{\partial Z} - iI \right) e^{-2iZ} \\ &= e^{-2iZ} \int_{-\infty}^{\infty} \frac{1}{\xi^{1/2}} e^{2\xi^{1/2} Z} e^{i\xi R} d\xi \\ &= 2 \left(\frac{\pi i}{R} \right)^{1/2} e^{-2iZ} e^{iZ^2 R} \end{aligned} \quad (\text{A48})$$

Since $I(\infty) = 0$, it follows that for $z \leq 0$,

$$I = 4 \left(\frac{\pi i}{R} \right)^{1/2} e^{2iZ} \int_Z^{\infty} e^{-2iZ'} e^{iZ'^2/R} dZ' \quad (\text{A49})$$

With the change in variable $Z' = R - Z''$,

$$I = 4 \left(\frac{\pi i}{R} \right)^{1/2} e^{2iZ} e^{-iR} \int_{R-Z}^{\infty} e^{iZ'^2/R} dZ'' \quad (\text{A50})$$

Finally, let $t = Z''^2/R$. Then

$$I = 4 \left(\frac{\pi i}{R} \right)^{1/2} e^{2iZ} e^{-iR} \left(\frac{\pi R}{2} \right)^{1/2} \int_u^{\infty} \frac{e^{it}}{(2\pi t)^{1/2}} dt \quad (\text{A51})$$

where $u = (R - Z)^2/R$. Also,

$$\int_u^{\infty} \frac{e^{it}}{(2\pi t)^{1/2}} dt = \frac{1}{2} (1 + i) - C_2(u) - iS_2(u) \quad (\text{A52})$$

$$C_2(u) + iS_2(u) = \int_0^u \frac{e^{it}}{(2\pi t)^{1/2}} dt \quad (\text{A53})$$

is the Fresnel integral. Thus

$$I = 4\pi \left(\frac{i}{2} \right)^{1/2} e^{2iZ} e^{-iR} \left[\frac{1}{2} (1 + i) - C_2(u) - iS_2(u) \right] \quad (\text{A54})$$

and

$$\tilde{B}_{2\phi} = -\frac{e^{iZ^2 R}}{R} (1 + \mathcal{G}) \quad (\text{A55})$$

where

$$\mathcal{G} \equiv i(2\pi R)^{1/2} e^{-iR - Z^2 R} \mathcal{F} \quad (\text{A56})$$

and

$$\begin{aligned} \mathcal{F} &= \frac{1}{2} (1 + i) - C_2[(R - Z)^2/R] \\ &\quad - iS_2[(R - Z)^2/R] \quad z \leq 0. \end{aligned} \quad (\text{A57})$$

When (A55) is substituted in (A20), this becomes

$$B_{2\phi} \sim -A(k_2' \omega) \cos \phi e^{i2R n^2} \frac{e^{iZ^2 R}}{R} (1 + \mathcal{G}) \quad (\text{A58})$$

With (A23) and (A55),

$$\tilde{E}_{2z} \sim \frac{e^{iZ^2 R}}{R} (1 + \mathcal{G}) \quad (\text{A59})$$

so that with (A18),

$$E_{2z} \sim A \cos \phi e^{i2R n^2} \frac{e^{iZ^2 R}}{R} (1 + \mathcal{G}) \quad (\text{A60})$$

With (A33) and (A55),

$$\tilde{E}_{2\phi} = -\frac{e^{iZ^2 R}}{R} \left[\frac{Z}{R} + (1 + \mathcal{G}) \right] \quad z \leq 0 \quad (\text{A61})$$

Substituting this in (A16) gives

$$E_{2\phi} = -A \cos \phi e^{i2R n^2} e^{iZ^2 R} \frac{n}{R} \left[\frac{Z}{R} + (1 + \mathcal{G}) \right] \quad z \leq 0 \quad (\text{A62})$$

When the variables in (A62), (A60), and (A58) are changed and the terms that were omitted in these equations are reinserted, (A1), (A3), and (A5) become (23), (25), and (27), respectively.

The second equation to be solved is (A29). With (A22) it becomes

$$\left(\frac{1}{R} \frac{\partial}{\partial R} R + \frac{\partial}{\partial Z} \right) \tilde{E}_{2\phi} - \frac{\partial \tilde{B}_{2\phi}}{\partial Z} = -\frac{\tilde{E}_{2\phi}}{R} \quad (\text{A63})$$

When the two equations in (A23) are combined, the result is

$$\bar{B}_{2\rho} = \frac{i}{2} \left[\frac{\partial \bar{E}_{2\phi}}{\partial Z} - \frac{\bar{B}_{2\phi}}{R} \right] \quad (A64)$$

so that with (A22),

$$\frac{\partial \bar{B}_{2\rho}}{\partial Z} = \frac{i}{2} \left[\frac{\partial^2 \bar{E}_{2\phi}}{\partial Z^2} - \frac{\partial \bar{B}_{2\phi}}{R \partial Z} \right] = \frac{i}{2} \frac{\partial^2 \bar{E}_{2\phi}}{\partial Z^2} + \frac{1}{R} \bar{E}_{2\rho} \quad (A65)$$

When this is substituted in (A63), it reduces to

$$\left(\frac{1}{R} \frac{\partial}{\partial R} R + \frac{\partial}{\partial R} - \frac{i}{2} \frac{\partial^2}{\partial Z^2} \right) \bar{E}_{2\phi} = 0 \quad (A66)$$

which has the solution

$$\bar{E}_{2\phi} = \frac{Z}{R^2} e^{iZ^2/R} \quad (A67)$$

This satisfies the conditions (A30) and (A31). When substituted in (A17),

$$E_{2\phi} \sim A \sin \phi \frac{nZ}{R^2} e^{i2R/n^2} e^{iZ^2/R} \quad (A68)$$

With (A22) and (A21),

$$B_{2z} = A(k_2/\omega) \sin \phi \frac{nZ}{R^2} e^{i2R/n^2} e^{iZ^2/R} \quad (A69)$$

The substitution of (A67) and (A55) in (A64) gives

$$\bar{B}_{2\rho} = \left[\frac{i}{R^2} \left(1 + \frac{1}{2} \mathcal{G} \right) - \frac{Z^2}{R^3} \right] e^{iZ^2/R} \quad (A70)$$

so that with (A19),

$$B_{2\rho} \sim A(k_2/\omega) \sin \phi e^{i2R/n^2} e^{iZ^2/R} n^2 \cdot \left[\frac{i}{R^2} \left(1 + \frac{1}{2} \mathcal{G} \right) - \frac{Z^2}{R^3} \right] \quad (A71)$$

When the variables in (A68), (A69), and (A71) are changed and the terms omitted in the determination of the field along the boundary are included to form (A2), (A4), and (A6), the complete formulas given in (24), (26), and (28) are obtained.

Acknowledgments. This research was supported in part by the Joint Services Electronics Program under contract N00014-84-K-0465 with Harvard University. In addition, R.W.P.K. received support as an IBM Visiting Scholar at Northeastern University.

REFERENCES

- Chave, A. D., and C. S. Cox, Controlled electromagnetic sources for measuring electrical conductivity beneath the oceans. 1. Forward problem and model study, *J. Geophys. Res.*, 87, 5327-5338, 1982.
- King, R. W. P., and T. T. Wu, Lateral waves: Formulas for the magnetic field, *J. Appl. Phys.*, 54, 507-514, 1983. (Erratum, 56, 3365, 1984.)
- Young, P. D., and C. S. Cox, Electromagnetic active source sounding near the East Pacific Rise, *Geophys. Res. Lett.*, 8, 1043-1046, 1981.

R. W. P. King, M. Owens, and T. T. Wu, Gordon McKay Laboratory, Harvard University, 9 Oxford Street, Cambridge, MA 02138.

Properties of the Lateral Electromagnetic Field of a Vertical Dipole and Their Applications

RONOLD W. P. KING, LIFE FELLOW, IEEE

Abstract—The formulas for the electromagnetic field in Region 1 ($z \geq 0$, k_1) due to a vertical electric dipole also in Region 1 near its plane boundary with Region 2 ($z \leq 0$, k_2 ; $|k_2|^2 \ll |k_1|^2$) are reviewed. The corresponding formulas for the field in Region 2 are then determined. Use is made of this field to determine the locus of the Poynting vector and the maximum depth of penetration into Region 2 of the lateral-wave part of the field. Application is made to the use of the vertical antenna in the sea for the measurement of the conductivity of the oceanic crust.

I. INTRODUCTION

ELECTROMAGNETIC surface waves of a type known as *lateral waves* are excited along a boundary between two electrically different half-spaces by both vertical and horizontal electric dipoles located near or on that boundary. The first complete analysis of the field generated by a vertical dipole was given by Sommerfeld [1], [2] in terms of general integrals of the Hertz potential from which expressions for the components of the electromagnetic field could be obtained by differentiation. The approximate evaluation of these integrals occupied many investigators over a wide span of years. Notable in its application to radio propagation between vertical antennas on the earth or sea was the work of Norton [3], which provided extensive tables and graphs. A comprehensive summary and reanalysis of the problem are contained in the important book by Baños [4] and in a paper by Wait and Campbell [5] who obtain approximate simple formulas in three nonoverlapping ranges known as the near or quasi-static field, the intermediate field, and the far or asymptotic field. A summary and an extensive listing of formulas in these ranges are in the monograph by Kraichman [6]. Beginning with the work of Siegel and King [7]–[9], numerical methods and high-speed computers were used to evaluate the general Sommerfeld integrals and determine the electromagnetic field of horizontal electric dipoles in sea water near the air surface. This was continued in more general terms by King and Sandler [10], Bubenik [11], King, deBertencourt, and Sandler [12], King, Sandler, and Shen [13], and Rahmat-Samii, Mittra, and Parhami [14]. A comprehensive tabulation and graphical representation of numerically evaluated fields over wide

ranges of permittivity, conductivity, and frequency are in King and Smith [15].

Because neither the general integrals for the Hertz potentials nor the numerically evaluated tables and graphs for the electromagnetic field calculated from them provided adequate physical insight into the nature of the electromagnetic lateral waves—which dominate the field along boundaries—and the associated fields in the adjacent regions, exact integrals specifically for all of the components of the electric and magnetic fields were derived for the field of the horizontal dipole by King and Smith [15] and for the vertical dipole by King [16]. Similar integrals but specialized by the condition $\omega\epsilon \ll \sigma$ for geophysical applications were derived for the horizontal dipole on the sea floor by Chave and Cox [17] and for the vertical dipole by Edwards *et al.* [18], [19]. Beginning in the papers by Wu and King [20], [21] and King and Wu [22] for the horizontal dipole and by King [16] for the vertical dipole, the general integrals for the components of the electric and magnetic fields were *integrated* to obtain simple, accurate, and continuous formulas valid over radial distances from very close to the source to infinity. These apply specifically to the field in Region 1 and along the boundary in Region 2 (when the dipole is in Region 1 or on the boundary in Region 2), subject to the inequality $|k_1| \geq 3|k_2|$ where k_1 and k_2 are the wavenumbers of the two half-spaces. Applications of these formulas were made to communication with submarines by King and Brown [23], to the detection of buried objects by King [24], [25], and to measurements on the sea floor by King [26] for an isotropic oceanic crust and by Pan [27] for an anisotropic crust. The determination of integrated formulas for the field throughout Region 2 including a detailed study of the lateral waves is carried out in King, Owens, and Wu [28] for the horizontal dipole. The corresponding investigation of the fields of a vertical electric dipole is the subject of this paper.

II. ELECTROMAGNETIC FIELDS

Consider a unit ($I \cdot h_e = 1 \text{ A} \cdot \text{m}$) vertical z -directed electric dipole located in Region 1 ($z \geq 0$, wavenumber $k_1 = \beta_1 + i\alpha_1 = \omega[\mu_0(\epsilon_1 + i\sigma_1/\omega)]^{1/2}$) at a distance d from the boundary with Region 2 ($z \leq 0$, wavenumber $k_2 = \beta_2 + i\alpha_2 = \omega[\mu_0(\epsilon_2 + i\sigma_2/\omega)]^{1/2}$) (Fig. 1). The rotationally symmetric electromagnetic field in Region 1 at the point ρ, z in cylindrical coordinates consists of the

Manuscript received January 9, 1986; revised June 8, 1986. This work was supported in part by the Joint Services Electronics Program under Contract N00014-84-K-0465 with Harvard University.

The author is with the Gordon McKay Laboratory, Harvard University, Cambridge, MA 02138.

IEEE Log Number 8610357.

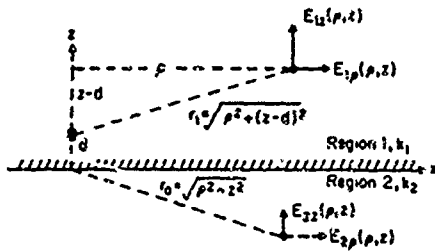


Fig. 1. Vertical dipole at (0, d) in Region 1.

three components $E_{1\rho}$, E_{1z} , and $B_{1\phi}$. Each of these is conveniently expressed as a sum of three parts, viz., the direct field, the perfect image (reflected) field, and the lateral-wave field. They are given by [16]

$$B_1(\rho, z) = B_1^d(\rho, z) + B_1^i(\rho, z) + B_1^l(\rho, z), \quad (1)$$

$$E_1(\rho, z) = E_1^d(\rho, z) + E_1^i(\rho, z) + E_1^l(\rho, z), \quad (2)$$

where, with

$$r_1 = [\rho^2 + (z - d)^2]^{1/2}$$

$$r_2 = [\rho^2 + (z + d)^2]^{1/2} \quad (3)$$

and

$$N = k_1^2 \gamma_2 + k_2^2 \gamma_1$$

$$\gamma_j = (k_j^2 - \lambda^2)^{1/2}, \quad j = 1, 2; \quad (4)$$

$$\begin{aligned} B_{1\phi}^d(\rho, z) &= \frac{i\mu_0}{4\pi} \int_0^\infty \frac{e^{i\gamma_1(z-d)}}{\gamma_1} J_1(\lambda\rho) \lambda^2 d\lambda \\ &= -\frac{\mu_0}{4\pi} e^{ik_1 r_1} \left(\frac{ik_1}{r_1} - \frac{1}{r_1^2} \right) \left(\frac{\rho}{r_1} \right) \end{aligned} \quad (5)$$

$$\begin{aligned} E_{1\rho}^d(\rho, z) &= \frac{i\omega\mu_0}{4\pi k_1^2} \int_0^\infty \pm e^{i\gamma_1(z-d)} J_1(\lambda\rho) \lambda^2 d\lambda, \\ &\begin{cases} z > d \\ 0 \leq z \leq d \end{cases} \\ &= -\frac{\omega\mu_0}{4\pi k_1^2} e^{ik_1 r_1} \left(\frac{ik_1^2}{r_1} - \frac{3k_1}{r_1^2} - \frac{3i}{r_1^3} \right) \\ &\quad \cdot \left(\frac{\rho}{r_1} \right) \left(\frac{z-d}{r_1} \right) \end{aligned} \quad (6)$$

$$\begin{aligned} E_{1z}^d(\rho, z) &= -\frac{\omega\mu_0}{4\pi k_1^2} \int_0^\infty \frac{e^{i\gamma_1(z-d)}}{\gamma_1} J_0(\lambda\rho) \lambda^3 d\lambda \\ &= \frac{\omega\mu_0}{4\pi k_1^2} e^{ik_1 r_1} \left[\left(\frac{ik_1^2}{r_1} - \frac{k_1}{r_1^2} - \frac{i}{r_1^3} \right) - \left(\frac{z-d}{r_1} \right)^2 \right. \\ &\quad \cdot \left. \left(\frac{ik_1^2}{r_1} - \frac{3k_1}{r_1^2} - \frac{3i}{r_1^3} \right) \right] \end{aligned} \quad (7)$$

$$\begin{aligned} B_{1\phi}^i(\rho, z) &= -\frac{i\mu_0}{4\pi} \int_0^\infty \frac{e^{i\gamma_1(z+d)}}{\gamma_1} J_1(\lambda\rho) \lambda^2 d\lambda \\ &= \frac{\mu_0}{4\pi} e^{ik_1 r_2} \left(\frac{ik_1}{r_2} - \frac{1}{r_2^2} \right) \left(\frac{\rho}{r_2} \right) \end{aligned} \quad (8)$$

$$\begin{aligned} E_{1\rho}^i(\rho, z) &= -\frac{i\omega\mu_0}{4\pi k_1^2} \int_0^\infty e^{i\gamma_1(z+d)} J_1(\lambda\rho) \lambda^2 d\lambda \\ &= \frac{\omega\mu_0}{4\pi k_1^2} e^{ik_1 r_2} \left(\frac{ik_1^2}{r_2} - \frac{3k_1}{r_2^2} - \frac{3i}{r_2^3} \right) \\ &\quad \cdot \left(\frac{\rho}{r_2} \right) \left(\frac{z+d}{r_2} \right) \end{aligned} \quad (9)$$

$$\begin{aligned} E_{1z}^i(\rho, z) &= \frac{\omega\mu_0}{4\pi k_1^2} \int_0^\infty \frac{e^{i\gamma_1(z+d)}}{\gamma_1} J_0(\lambda\rho) \lambda^3 d\lambda \\ &= -\frac{\omega\mu_0}{4\pi k_1^2} e^{ik_1 r_2} \left[\left(\frac{ik_1^2}{r_2} - \frac{k_1}{r_2^2} - \frac{i}{r_2^3} \right) - \left(\frac{z+d}{r_2} \right)^2 \right. \\ &\quad \cdot \left. \left(\frac{ik_1^2}{r_2} - \frac{3k_1}{r_2^2} - \frac{3i}{r_2^3} \right) \right] \end{aligned} \quad (10)$$

$$\begin{aligned} B_{1\phi}^l(\rho, z) &= \frac{i\mu_0 k_2^2}{2\pi} \int_0^\infty \frac{e^{i\gamma_1(z+d)}}{N} J_1(\lambda\rho) \lambda^2 d\lambda \\ &\quad - \frac{\mu_0 k_2^2}{2\pi k_1^2} e^{ik_1(z+d)} e^{ik_2\rho} f(k_2\rho, k_1) \end{aligned} \quad (11)$$

$$\begin{aligned} E_{1\rho}^l(\rho, z) &= \frac{i\omega\mu_0 k_2^2}{2\pi k_1^2} \int_0^\infty \frac{\gamma_1 e^{i\gamma_1(z+d)}}{N} J_1(\lambda\rho) \lambda^2 d\lambda \\ &\quad - \frac{\omega\mu_0 k_2^2}{2\pi k_1^2} \left[e^{ik_1(z+d)} e^{ik_2\rho} f(k_2\rho, k_1) - \frac{ie^{ik_1 r_2}}{r_2^2} \right] \end{aligned} \quad (12)$$

$$\begin{aligned} E_{1z}^l(\rho, z) &= -\frac{\omega\mu_0 k_2^2}{2\pi k_1^2} \int_0^\infty \frac{e^{i\gamma_1(z+d)}}{N} J_0(\lambda\rho) \lambda^3 d\lambda \\ &\quad - \frac{\omega\mu_0 k_2^2}{2\pi k_1^2} e^{ik_1(z+d)} e^{ik_2\rho} g(k_2\rho, k_1). \end{aligned} \quad (13)$$

In these formulas

$$\begin{aligned} g(k_2\rho, k_1) &= f(k_2\rho, k_1) - \frac{i}{k_2\rho^3} = \frac{ik_2}{\rho} - \frac{1}{\rho^2} - \frac{i}{k_2\rho^3} \\ &\quad - \frac{k_2^3}{k_1} \left(\frac{\pi}{k_2\rho} \right)^{1/2} e^{-ip} \mathfrak{F}(p) \end{aligned} \quad (14)$$

where $p \equiv k_2^3\rho/2k_1^2$ and

$$\mathfrak{F}(p) = \frac{1}{2} (1 + i) - C_2(p) - iS_2(p) = \int_p^\infty \frac{e^{it}}{(2\pi t)^{1/2}} dt \quad (15)$$

is the Fresnel integral. The last term in (12) with the wavenumber k_1 in the exponent is actually not a part of the lateral wave but a correction term for the image field

given in (9). For large arguments

$$f(k_2\rho, k_1) \sim g(k_2\rho, k_1) \sim -k_1^2/k_2^2\rho^2, \\ |k_2\rho| \geq 8|k_1^2/k_2^2|. \quad (16)$$

The integrated formulas for the direct and reflected fields in (5)-(10) are exact. Those for the lateral-wave field in (11)-(13) were evaluated with the approximation

$$e^{j\gamma_1(z+d)} \sim e^{j\gamma_1(z+d)} = e^{-\alpha_1(z+d)} e^{j\beta_1(z+d)} \quad (17)$$

under the conditions

$$|k_1| \geq 3|k_2| \\ \rho \geq 5z \\ \rho \geq 5d. \quad (18)$$

The first of these is essential to the integration of (11)-(13) in which $|k_2/k_1|^2$ is treated as a small quantity. The specific ratio $|k_1| \geq 3|k_2|$ is verified by the comparison of the integrated formulas with the numerical evaluation of the integrals in critical ranges. The requirement that ρ be large compared to z and d is needed only for the lateral-wave terms because of the approximation (17). Since the depth of penetration of the lateral waves is only a fraction of the radial distance, this is generally not an important restriction.

The lateral-wave electromagnetic field in Region 2 along the boundary $z = 0$ where $r_1 = r_2$ is readily obtained from the field in Region 1 with the help of the boundary conditions. Note that direct and reflected field terms in $E_{2\rho}(\rho, 0)$ are omitted. Thus

$$B_{2\phi}(\rho, 0) = B_{1\phi}(\rho, 0) = -\frac{\mu_0 k_2^2}{2\pi k_1^2} e^{j\gamma_1 d} e^{j\gamma_2 \rho} f(k_2\rho, k_1) \quad (19)$$

$$E_{2\rho}(\rho, 0) = E_{1\rho}(\rho, 0) = -\frac{\omega\mu_0 k_2^2}{2\pi k_1^2} e^{j\gamma_1 d} e^{j\gamma_2 \rho} f(k_2\rho, k_1) \quad (20)$$

$$E_{2z}(\rho, 0) = \frac{k_1^2}{k_2^2} E_{1z}(\rho, 0) = \frac{\omega\mu_0 k_2^2}{2\pi k_1^2} e^{j\gamma_1 d} e^{j\gamma_2 \rho} g(k_2\rho, k_1). \quad (21)$$

The field in Region 2 in general is given by the following exact integrals which are derived in [16]:

$$B_{2\phi}(\rho, z) = \frac{j\mu_0 k_2^2}{2\pi} \int_0^\infty \frac{e^{j\gamma_1 d} e^{-j\gamma_2 z}}{N} J_1(\lambda\rho) \lambda^2 d\lambda \quad (22)$$

$$E_{2\rho}(\rho, z) = -\frac{j\omega\mu_0}{2\pi} \int_0^\infty \frac{\gamma_2 e^{j\gamma_1 d} e^{-j\gamma_2 z}}{N} J_1(\lambda\rho) \lambda^2 d\lambda \quad (23)$$

$$E_{2z}(\rho, z) = -\frac{\omega\mu_0}{2\pi} \int_0^\infty \frac{e^{j\gamma_1 d} e^{-j\gamma_2 z}}{N} J_0(\lambda\rho) \lambda^3 d\lambda \quad (24)$$

where $N = k_1^2 \gamma_2 + k_2^2 \gamma_1$ and $\gamma_j = (k_j^2 - \lambda^2)^{1/2}$, $j = 1, 2$. The evaluation of these integrals can be carried out directly subject to certain restrictions, which it is important

to formulate for subsequent practical applications. The principal restriction is the requirement $|k_1^2| \gg |k_2^2|$ as specified on the left in (18). With this condition it is evident that the first term in N is the larger one. This permits the separation of each of the integrals into two parts by writing

$$\frac{1}{N} = \frac{1}{N_0} + \left(\frac{1}{N} - \frac{1}{N_0} \right) \quad (25)$$

where

$$N_0 = k_1^2 \gamma_2 = k_1^2 (k_1^2 - \lambda^2)^{1/2}. \quad (26)$$

The first part of the integrals is given by (22)-(24) with N_0 substituted for N . In these it is clear that the major contributions must come from the range $\lambda \sim O(k_2)$. Therefore, $\gamma_1 = (k_1^2 - \lambda^2)^{1/2} \sim k_1$ and the integrals reduce to

$$B_{2\phi}^{(0)}(\rho, z) = \frac{j\mu_0 k_2^2}{2\pi k_1^2} e^{j\gamma_1 d} \int_0^\infty \frac{e^{j\gamma_2 z}}{\gamma_2} J_1(\lambda\rho) \lambda^2 d\lambda \\ = -\frac{\mu_0 k_2^2}{2\pi k_1^2} e^{j\gamma_1 d} e^{j\gamma_2 \rho} \left(\frac{ik_2}{r_0} - \frac{i}{r_0^2} \right) \left(\frac{\rho}{r_0} \right) \quad (27)$$

$$E_{2\rho}^{(0)}(\rho, z) = -\frac{j\omega\mu_0}{2\pi k_1^2} e^{j\gamma_1 d} \int_0^\infty e^{j\gamma_2 z} J_1(\lambda\rho) \lambda^2 d\lambda \\ = -\frac{\omega\mu_0 k_2^2}{2\pi k_1^2} e^{j\gamma_1 d} e^{j\gamma_2 \rho} \left(\frac{ik_2}{r_0} - \frac{3}{r_0^2} - \frac{3i}{k_2 r_0^3} \right) \left(\frac{\rho z}{r_0^2} \right) \quad (28)$$

$$E_{2z}^{(0)}(\rho, z) = -\frac{\omega\mu_0}{2\pi k_1^2} e^{j\gamma_1 d} \int_0^\infty \frac{e^{j\gamma_2 z}}{\gamma_2} J_0(\lambda\rho) \lambda^3 d\lambda \\ = \frac{\omega\mu_0 k_2^2}{2\pi k_1^2} e^{j\gamma_1 d} e^{j\gamma_2 \rho} \left[\left(\frac{ik_2}{r_0} - \frac{1}{r_0^2} - \frac{i}{k_2 r_0^3} \right) \right. \\ \left. - \left(\frac{ik_2}{r_0} - \frac{3}{r_0^2} - \frac{3i}{k_2 r_0^3} \right) \left(\frac{z^2}{r_0^2} \right) \right] \quad (29)$$

where $r_0 = (\rho^2 + z^2)^{1/2}$. The integrals in (27)-(29) are like those in (5)-(10), but with $d = 0$ and the change $\gamma_1 \rightarrow \gamma_2$. As in (5)-(10), the integrated exact formulas are obtained from the field of the vertical electric dipole in a homogeneous infinite medium given in King [29].

In the second part of each integral the factor $1/N$ is replaced by

$$\frac{1}{N} - \frac{1}{N_0} = \frac{1}{k_1^2 \gamma_2 + k_2^2 \gamma_1} - \frac{1}{k_1^2 \gamma_2}. \quad (30)$$

Specifically

$$B_{2\phi}^{(1)}(\rho, z) = \frac{j\mu_0 k_2^2}{2\pi} e^{j\gamma_1 d} G_{2\phi}(\rho, z) \\ G_{2\phi}(\rho, z) = \int_0^\infty \left(\frac{1}{N} - \frac{1}{N_0} \right) e^{-j\gamma_2 z} J_1(\lambda\rho) \lambda^2 d\lambda, \\ z \leq 0 \quad (31)$$

$$E_{2\rho}^{(1)}(\rho, z) = -\frac{i\omega\mu_0}{2\pi} e^{ik_1 d} G_{2\rho}(\rho, z)$$

$$G_{2\rho}(\rho, z) = \int_0^\infty \left(\frac{1}{N} - \frac{1}{N_0} \right) e^{-i\gamma z} \gamma_2 J_1(\lambda \rho) \lambda^2 d\lambda, \quad z \leq 0 \quad (32)$$

$$E_{2z}^{(1)}(\rho, z) = -\frac{\omega\mu_0}{2\pi} e^{ik_1 d} G_{2z}(\rho, z)$$

$$G_{2z}(\rho, z) = \int_0^\infty \left(\frac{1}{N} - \frac{1}{N_0} \right) e^{-i\gamma z} J_0(\lambda \rho) \lambda^3 d\lambda, \quad z \leq 0. \quad (33)$$

The three functions $G_{2\rho}$, $G_{2\rho}$, and G_{2z} are evaluated in Appendix I. The results are

$$B_{2\rho}^{(1)}(\rho, z) = \frac{\mu_0 k_2^2}{2\pi k_1^3} e^{ik_1 d} e^{ik_2 \rho}$$

$$\times \left(\frac{\pi}{k_2 \rho} \right)^{1/2} e^{-i(R-2Z)} \mathcal{F}[(R-Z)^2/R], \quad z \leq 0 \quad (34)$$

$$E_{2\rho}^{(1)}(\rho, z) = -\frac{i\omega\mu_0}{2\pi} \frac{k_2^3}{k_1^3} e^{ik_1 d} e^{ik_2 \rho} \left[\frac{e^{iZ^2/R}}{\rho} \right.$$

$$\left. + \frac{ik_2^2}{k_1} \left(\frac{\pi}{k_2 \rho} \right)^{1/2} e^{-i(R-2Z)} \mathcal{F}[(R-Z)^2/R] \right], \quad z \leq 0 \quad (35)$$

$$E_{2z}^{(1)}(\rho, z) = -\frac{\omega\mu_0 k_2^4}{2\pi k_1^3} e^{ik_1 d} e^{ik_2 \rho}$$

$$\times \left(\frac{\pi}{k_2 \rho} \right)^{1/2} e^{-i(R-2Z)} \mathcal{F}[(R-Z)^2/R], \quad z \leq 0 \quad (36)$$

with $R = k_2^2 \rho / 2k_1^2$, $Z = k_2^2 z / 2k_1$ and

$$\mathcal{F}(P) = \int_P^\infty \frac{e^{it}}{(2\pi t)^{1/2}} dt = \frac{1}{2} (1 + i) - C_2(P) - iS_2(P). \quad (37)$$

The complete field is the sum of (27)-(29) and (34)-(36). The final formulas for the field in Region 2 due to a vertical electric dipole at $z = d$ in Region 1 are

$$B_{2\rho}(\rho, z) = B_{2\rho}^{(0)}(\rho, z) + B_{2\rho}^{(1)}(\rho, z)$$

$$= -\frac{\mu_0 k_2^2}{2\pi k_1^2} e^{ik_1 d} \left\{ e^{ik_2 r_0} \left(\frac{ik_2}{r_0} - \frac{1}{r_0^2} \right) \left(\frac{\rho}{r_0} \right) \right.$$

$$\left. - e^{ik_2 \rho} \frac{k_2^3}{k_1} \left(\frac{\pi}{k_2 \rho} \right)^{1/2} \cdot e^{-i(R-2Z)} \mathcal{F}[(R-Z)^2/R] \right\}, \quad z \leq 0 \quad (38)$$

$$E_{2\rho}(\rho, z) = E_{2\rho}^{(0)}(\rho, z) + E_{2\rho}^{(1)}(\rho, z)$$

$$= -\frac{\omega\mu_0 k_2}{2\pi k_1^2} e^{ik_1 d} \left\{ e^{ik_2 r_0} \left(\frac{ik_2}{r_0} - \frac{3}{r_0^2} - \frac{3i}{k_2 r_0^3} \right) \left(\frac{\rho z}{r_0^2} \right) \right.$$

$$\left. + \frac{k_2}{k_1} e^{ik_2 \rho} \left[\left(\frac{ik_2}{\rho} - \frac{1}{\rho^2} \right) e^{iZ^2/R} - \frac{k_2^3}{k_1} \left(\frac{\pi}{k_2 \rho} \right)^{1/2} e^{-i(R-2Z)} \mathcal{F}[(R-Z)^2/R] \right] \right\}, \quad z < 0 \quad (39a)$$

$$E_{2\rho}(\rho, 0) = \frac{\omega\mu_0}{2\pi k_1^2} e^{ik_1 d} \left(\frac{ik_2^2}{r_d} - \frac{3k_1}{r_d^2} - \frac{3i}{r_d^3} \right) \left(\frac{\rho d}{r_d^2} \right)$$

$$- \frac{\omega\mu_0 k_2^3}{2\pi k_1^3} \left[e^{ik_1 d} e^{ik_2 \rho} f(k_2 \rho, k_1) - \frac{ie^{ik_1 r_d}}{r_d^2} \right], \quad z = 0 \quad (39b)$$

$$E_{2z}(\rho, z) = E_{2z}^{(0)}(\rho, z) + E_{2z}^{(1)}(\rho, z)$$

$$= \frac{\omega\mu_0 k_2}{2\pi k_1^2} e^{ik_1 d} \left\{ e^{ik_2 r_0} \left[\left(\frac{ik_2}{r_0} - \frac{1}{r_0^2} - \frac{i}{k_2 r_0^3} \right) \right. \right.$$

$$\left. - \left(\frac{ik_2}{r_0} - \frac{3}{r_0^2} - \frac{3i}{k_2 r_0^3} \right) \left(\frac{z^2}{r_0^2} \right) \right]$$

$$\left. - e^{ik_2 \rho} \frac{k_2^3}{k_1} \left(\frac{\pi}{k_2 \rho} \right)^{1/2} \cdot e^{-i(R-2Z)} \mathcal{F}[(R-Z)^2/R] \right\}, \quad z \leq 0. \quad (40)$$

In (39b), $r_d = (\rho^2 + d^2)^{1/2}$ and $f(k_2 \rho, k_1)$ is defined in (14). These formulas are good approximations throughout Region 2 except near the source. They correspond for Region 2 to (11)-(13) for Region 1. The components $B_{2\rho}(\rho, z)$ and $E_{2z}(\rho, z)$ satisfy the boundary conditions: $B_{2\rho}(\rho, 0) = B_{1\rho}(\rho, 0)$ and $E_{2z}(\rho, 0) = (k_1^2/k_2^2) E_{1z}(\rho, 0)$. To satisfy the boundary condition $E_{2\rho}(\rho, 0) = E_{1\rho}(\rho, 0)$, a separate formula (39b) for $E_{2\rho}(\rho, 0)$ is required. This is derived and discussed in Appendix II. Note that in (39a) the term in $1/\rho^2$ has been added in the square bracket. The evaluation of $E_{2\rho}(\rho, z)$, $z < 0$, in Appendix I was carried out for $k_2 \rho$ not small. This restriction was not made in the evaluation of $E_{1\rho}(\rho, z)$ so this is a better approximation when $k_2 \rho$ is kept small.

III. THE LOCUS OF THE POYNTING VECTOR IN REGION 2

The formulas (38)-(40) for the field in Region 2 include a spherical wave that travels outward from the equivalent source at (0, 0) in Region 2 and a lateral wave that proceeds along the boundary. It is of interest—especially in measurements made on the sea floor—to know how deep into Region 2 the lateral wave proceeds before returning to the boundary at the point of measurement. This can be determined by following the locus of the Poynting vector.

This is defined as follows:

$$\begin{aligned} S_2(\rho, z) &= \frac{1}{2\mu_0} [E_2(\rho, z) \times B_2^*(\rho, z)] \\ &= \frac{1}{2\mu_0} [zE_{2\rho}(\rho, z) B_{2z}^*(\rho, z) \\ &\quad - \rho E_{2z}(\rho, z) B_{2\rho}^*(\rho, z)]. \end{aligned} \quad (41)$$

The asterisk indicates the complex conjugate. Since z is negative in Region 2, it is convenient to introduce $z' = -z$. The slope of the locus of the Poynting vector is

$$-\frac{dz'}{d\rho} = \operatorname{Re} \frac{S_{2z}(\rho, z)}{S_{2\rho}(\rho, z)} = \operatorname{Re} \frac{E_{2\rho}(\rho, z)}{-E_{2z}(\rho, z)}. \quad (42)$$

Evidently the locus of the Poynting vector is perpendicular to the lines of the electric field. In the range $\rho \geq 5z'$, the second term in (40), which is multiplied by z^2/r_0^2 , can be neglected compared to the first term. It follows that

$$\frac{E_{2\rho}(\rho, z)}{-E_{2z}(\rho, z)} \sim \frac{\frac{\rho z}{r_0^2} \left(\frac{ik_2}{r_0} - \frac{3}{r_0^2} - \frac{3i}{k_2 r_0^3} \right) + \frac{k_2}{k_1} \left(\frac{ik_2}{\rho} - \frac{1}{\rho^2} \right)}{\left(\frac{ik_2}{r_0} - \frac{1}{r_0^2} - \frac{i}{k_2 r_0^3} \right)} \quad (43)$$

where the Fresnel integral terms have been omitted since they are negligible when $k_2 \rho$ is not large. In the near and intermediate fields—which are the only ones of interest in low-frequency measurements on the sea floor—the following condition is valid:

$$|k_2^2 r_0^2| \sim |k_2^2 \rho^2| \ll 3 \quad \text{or} \quad |k_2 \rho| \leq 0.6. \quad (44)$$

With (44) the $1/r_0 \sim 1/\rho$ terms in (43) are negligible and

$$\frac{E_{2\rho}(\rho, z)}{-E_{2z}(\rho, z)} \sim \frac{3z\rho}{r_0^2} + \frac{k_2 r_0^2}{k_1 \rho^2} \left(\frac{k_2 r_0}{k_2 r_0 + i} \right). \quad (45)$$

At low frequencies $k_2 \sim (1+i)\beta_2$ where $\beta_2 = (\omega\mu_0\sigma_2/2)^{1/2}$. Also, $k_2/k_1 = (\sigma_2/\sigma_1)^{1/2}$. It follows that, with $r_0 = (\rho^2 + z^2)^{1/2} \sim \rho$

$$\operatorname{Re} \frac{E_{2\rho}(\rho, z)}{-E_{2z}(\rho, z)} \sim \frac{3z + \delta\beta_2 \rho^2}{\rho} \sim \frac{-3z' + \delta\beta_2 \rho^2}{\rho} \quad (46)$$

where

$$\delta = (\sigma_2/\sigma_1)^{1/2}. \quad (47)$$

When (46) is substituted in (42), this becomes

$$\frac{dz'}{d\rho} = \frac{3z'}{\rho} - \delta\beta_2 \rho. \quad (48)$$

This equation is readily solved with the substitution $z' = s\rho^2$, ($dz'/d\rho = 2\rho s + \rho^2(ds/d\rho)$). Thus

$$\frac{ds}{s - \delta\beta_2} = \frac{d\rho}{\rho} \quad (49)$$

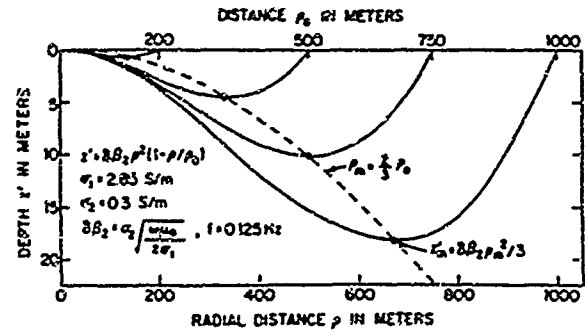


Fig. 2. Locus of Poynting vector in half-space model of the oceanic crust: $k_1 = (i\omega\mu_0\sigma_1)^{1/2}$, $k_2 = (i\omega\mu_0\sigma_2)^{1/2}$; $S_{1\rho}(\rho_0, 0) = (\sigma_2/\sigma_1)S_{2\rho}(\rho_0, 0)$, $S_{1z}(\rho_0, 0) = S_{2z}(\rho_0, 0)$.

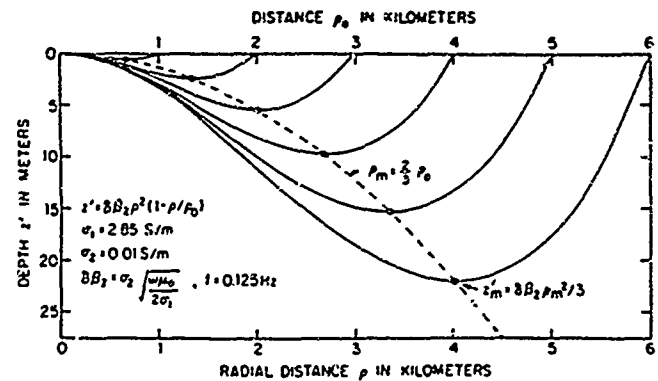


Fig. 3. Locus of Poynting vector in half-space model of the oceanic crust: $k_1 = (i\omega\mu_0\sigma_1)^{1/2}$, $k_2 = (i\omega\mu_0\sigma_2)^{1/2}$; $S_{1\rho}(\rho_0, 0) = (\sigma_2/\sigma_1)S_{2\rho}(\rho_0, 0)$, $S_{1z}(\rho_0, 0) = S_{2z}(\rho_0, 0)$.

so that

$$\ln(s - \delta\beta_2) = \ln C\rho \quad (50)$$

where C is a constant of integration. The solution with $s = z'/\rho^2$ and $C = -\delta\beta_2/\rho_0$ is

$$z' = \delta\beta_2 \rho^2 (1 - \rho/\rho_0). \quad (51)$$

This equation defines the locus of the Poynting vector between the source at $\rho = 0$, $z' = 0$ and the point of observation at $\rho = \rho_0$, $z' = 0$. The maximum depth of penetration is determined by $dz'/d\rho = 0$. With (51), the coordinates of the point of deepest penetration into Region 2 are

$$\begin{aligned} \rho &= \rho_m = \frac{2\rho_0}{3} \\ z' &= z'_m = \frac{1}{3} \delta\beta_2 \rho_m^2 = \frac{4}{27} \delta\beta_2 \rho_0^2. \end{aligned} \quad (52)$$

Note that

$$\begin{aligned} \delta\beta_2 &= \beta_2^2/\beta_1 = \sigma_2 R_s \\ R_s &= (\omega\mu_0/2\sigma_1)^{1/2}. \end{aligned} \quad (53)$$

Here R_s is the surface resistance.

Graphs of the loci defined by (51) are shown in Figs. 2 and 3 for parameters that apply to actual measurements made on the sea floor. Fig. 2 applies to the sea-sediment boundary with $\sigma_1 = 2.85$ S/m, $\sigma_2 = 0.3$ S/m, and $f =$

0.125 Hz. For a radial range of 1 km, the maximum depth of penetration is about 18 m. Fig. 3 applies to a sea-rock boundary with $\sigma_1 = 2.85$ S/m, $\sigma_2 = 0.01$ S/m, and $f = 0.125$ Hz. For a radial range of 5 km, the maximum depth of penetration of the lateral wave into the rock is only 15.3 m.

IV. THE MEASUREMENT OF THE CONDUCTIVITY OF THE OCEANIC CRUST

An interesting set of measurements has been reported by Edwards *et al.* [30] for determining the conductivity of the oceanic crust below the Bute Inlet, British Columbia, Canada. It provides a useful vehicle for the application and discussion of the theory developed in the preceding sections. The site of the measurements has the cross section sketched on the right in Fig. 4. The sea water (Region 1, $\sigma_1 = 2.85$ S/m) has a depth $D_1 = 640$ m in a channel that is almost 4 km wide at the surface and 2 km wide on the floor. Below the water is a layer of sediment (Region 2, σ_2) that fills a trough that is estimated to have a central depth near $D_2 = 600$ m. The conductivity of the sediment was estimated from measurements of the moisture content of sample cores to be between 1/11 to 1/5 that of the salt water, so that $\sigma_2 \sim 0.26$ S/m to 0.57 S/m. The country rock (Region 3, σ_3) below the sediment has a conductivity of the order of $\sigma_3 \sim 0.01$ S/m. Above the sea water is, of course, the air (Region 0).

The antenna used by Edwards *et al.* was an insulated conductor that extended from the sea floor to the air surface so that $h = D_1 = 640$ m. At each end the antenna was conductively connected to the salt water by bare metal rods. Its consecutive locations in the Bute Inlet are indicated by the numbered circles in Fig. 4. At the very low frequency of $f = 0.125$ Hz, the wavenumber of the salt water was $k_1 = (\omega\mu_0\sigma_1)^{1/2} = 1.68 \times 10^{-3} e^{i\pi/4}$ m⁻¹ and the electrical length of the antenna was $\beta_1 h = 0.76$, which is short enough so that a current with the uniform amplitude I was maintained over its entire length. The electric moment is Ih_e , where h_e is the effective length of the antenna. For an antenna of length h in an ocean with a depth D_1 that is much greater than both the skin depth and the length of the antenna, the effective length is

$$h_e = \int_0^h e^{ik_1 z} dz = ik_1^{-1}(1 - e^{ik_1 h}). \quad (54)$$

With $k_1 = 1.68 \times 10^{-3} e^{i\pi/4}$ m⁻¹ and $h = 640$ m, $h_e = 438e^{i0.335}$ m. Since the antenna extends from the sea floor to the surface with $h = D_1 = 640$ m and this is actually less than the skin depth $d_s = \alpha_1^{-1} = 847$ m, the presence of the sea-air boundary must be taken into account. This is readily done since, at the very low frequency used, the reflection coefficient at the air-sea boundary for the magnetic field of a wave incident from the sea is extremely close to -1 . It follows that the boundary surface can be approximated by a magnetic wall on which the tangential magnetic field vanishes. That is, $B_{1\phi}(\rho, h) = 0$. This means that the entire air half-space can be replaced by an

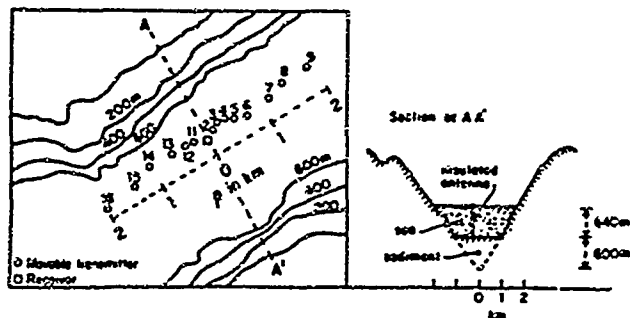


Fig. 4. Location of measurements by Edwards *et al.* [30].

inverted image of the lower half-space containing the sea and oceanic crust. The antenna thus has an image with reversed current so that the effective length becomes

$$h_e = \int_0^h e^{ik_1 z} dz - \int_h^{2h} e^{ik_1 z} dz = ik_1^{-1}(1 - e^{ik_1 h})^2. \quad (55)$$

With $k_1 = 1.68 \times 10^{-3} e^{i\pi/4}$ m⁻¹ and $h = 640$ m, this gives $h_e = 321e^{-i0.12}$ m. In order to maintain the zero value of the magnetic field at $z = h$ —now the midpoint in the ocean with image which has a combined depth of $2h$ —the lateral wave traveling in the oceanic crust at $z < 0$ must also have an image that travels along the image of the crust at $z > 2h$. The contribution of the image wave to the field at $(\rho, 0)$ on the sea floor is identical with that of the actual wave but with opposite sign and with an additional distance $2h$ of travel down in the sea water from the plane $z = 2h$ to the plane $z = 0$. The total magnetic field observed in the sea on the sea floor, that is, at $(\rho, 0)$ in Region 1, includes the lateral wave traveling vertically upward into the sea from the sediment, the image wave traveling vertically down, and multiple reflections of these. The magnetic field at any point z is given by

$$B_{1\phi}(\rho, z) = B_{1\phi}^{inc}(\rho, 0) \left[\frac{e^{ik_1 z} - e^{ik_1(2h-z)}}{1 + \Gamma_m e^{i2k_1 h}} \right] \quad (56)$$

where

$$\Gamma_m = -\frac{k_1 - k_2}{k_1 + k_2} = -\frac{\sqrt{\sigma_1} - \sqrt{\sigma_2}}{\sqrt{\sigma_1} + \sqrt{\sigma_2}} \quad (57)$$

is the reflection coefficient of magnetic type at the sea-sediment boundary. Note that $B_{1\phi}(\rho, h) = 0$ as required. With $\sigma_2 = 0.4$ S/m and $\sigma_1 = 2.85$ S/m, $\Gamma_m = -0.45$. The field on the sea floor at $z = 0$ is given by

$$B_{1\phi}(\rho, 0) = B_{1\phi}^{inc}(\rho, 0) \left[\frac{1 - e^{i2k_1 h}}{1 + \Gamma_m e^{i2k_1 h}} \right]. \quad (58)$$

The complete effective length as modified by the effect of the air-sea boundary is

$$h_e = \frac{i}{k_1} \frac{(1 - e^{i2k_1 h})^2 (1 - e^{i2k_1 h})}{1 + \Gamma_m e^{i2k_1 h}}. \quad (59)$$

With $\Gamma_m = -0.45$, $k_1 = 1.68 \times 10^{-3} e^{i\pi/4}$ m⁻¹, and $h =$

640 m

$$h_r = 326e^{-0.241} \text{ m.} \quad (60)$$

With $\Gamma_m = 0$, $h_r = 329e^{-0.241} \text{ m}$. Clearly, only the first reflection is significant.

It is to be noted that while all of the multiple reflections of the lateral waves reaching the point of observation at $(\rho, 0)$ in the sea are included, the antenna generating these waves includes only the section of length $2h$ in the sea with image and images of equal length in the oceanic crust and its image. This gives a total length of $6h$ with a uniform current that alternates in sign in successive lengths h . The effect of multiple reflections on the waves leaving the antenna are not included and cannot be provided by image antennas unless the reflection coefficient of the crust is close to ± 1 —which it is not. When σ_2 lies between 0.26 and 0.57 S/m, and $\sigma_1 = 2.85 \text{ S/m}$, the reflection coefficient, $-(\sqrt{\sigma_1} - \sqrt{\sigma_2})/(\sqrt{\sigma_1} + \sqrt{\sigma_2})$, ranges from -0.53 to -0.38 . The formula (59) is evidently accurate so long as contributions from image antennas beyond $4k_1 h$ are negligible. That is, it is necessary that $|e^{i4k_1 h}| = e^{-4\alpha_1 h} \ll 1$. With $\alpha_1 = 1.188 \times 10^{-3} \text{ m}^{-1}$ and $h = 640 \text{ m}$, $e^{-4\alpha_1 h} = 0.02$. It follows that the magnitude of the lateral wave and its image should be correct within 2 percent when (59) is used. Note, however, that (59) is not useful in the limit of zero frequency. An alternative formula that has application in this limit is given and discussed in Appendix III.

Measurements of the horizontal magnetic field on the sea floor were made by Edwards *et al.* with the transmitting antenna at the numbered locations relative to the stationary receiving antenna (magnetometer), as shown on the left in Fig. 4. The measured field is shown by the numbered crosses in Fig. 5 as a function of the radial distance from the base of the transmitting antenna.

The values of the wavenumbers k_j , $j = 0, 1, 2, 3$, for the air ($\sigma_0 = 0$), sea water ($\sigma_1 = 2.85 \text{ S/m}$), sediment ($\sigma_2 = 0.26, 0.3, 0.4$, and 0.57 S/m), and rock ($\sigma_3 = 0.01 \text{ S/m}$) are listed in Table I together with the ratio $\delta = (\sigma_2/\sigma_1)^{1/2}$, the range of electrical distance $|k_2 \rho|$ that corresponds to the actual range $0.1 \leq \rho \leq 2 \text{ km}$, the maximum allowable range of ρ to satisfy the condition for the neglect of the far-field terms, and the associated maximum depths of penetration of the Poynting vector.

In general, the electromagnetic field in a four-layered region cannot be determined from formulas for the field in a two-layered region. In the case at hand, the properties of the layers at the very low frequency and the locations of the transmitting antenna and the magnetometer provide a special situation which makes the two-layer theory useful for determining the conductivity of the layer of sediment from measurements of the magnetic field on the sea floor. However, the idealization that all boundaries are parallel plane surfaces is required.

The measured field is in the sea water (Region 1) at its boundary with the sediment (Region 2). Theory shows that, if the sea were unbounded upward and the sediment unbounded downward, the direct and reflected fields of

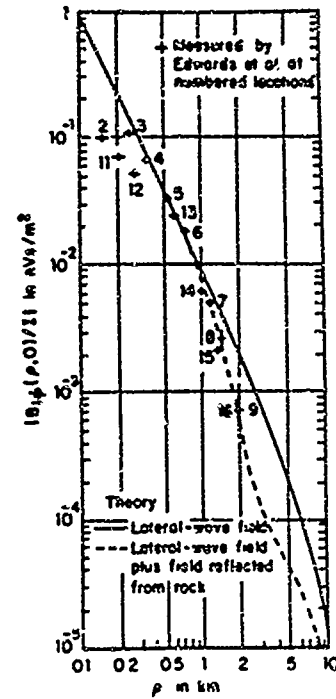


Fig. 5. Magnetic field measured by Edwards *et al.* [30] and field calculated from (62) and (70). $f = 0.125 \text{ Hz}$, $\sigma_1 = 2.85 \text{ S/m}$, $\sigma_2 = 0.4 \text{ S/m}$, $\sigma_3 = 0.01 \text{ S/m}$; $D_1 = 640 \text{ m}$, $D_2 = 600 \text{ m}$.

the vertical antenna cancel so that the entire magnetic field on the boundary is the lateral-wave field. However, theory also shows that for the radial distances involved in the measurements the maximum depth of penetration of the lateral wave into the sediment is a small fraction of the depth D_2 of that sediment. This means that the lateral-wave field $B_{10}^l(\rho, 0)$ is the same when $D_2 \gg z_m$ as when $D_2 = \infty$. But it may not be the entire field. There may be a significant reflected field from the sediment-rock boundary that travels upward in the sediment to the point of observation in the sea. Furthermore, since the vertical antenna extends to the air-sea surface, its currents also generate a lateral wave that propagates along that boundary and down in the sea to the point of measurement on the sea floor. Thus

$$B_{10}(\rho, 0) = B_{10}^l(\rho, 0) + B_{10}^r(\rho, 0) + B_{10}^T(\rho, 0) \quad (61)$$

where

$$B_{10}^l(\rho, 0) = -\frac{\mu_0 k_2^2}{2\pi k_1^2} I h_r e^{i k_2 \rho} \left(\frac{i k_2}{\rho} - \frac{1}{\rho^2} \right) \quad (62)$$

is the lateral wave along the sediment-sea boundary, as given by (11). The Fresnel integral term is negligible over the distances involved. The second term in (61)

$$B_{10}^r(\rho, 0) = -\frac{\mu_0 k_2^2}{2\pi k_1^2} I h_r e^{i k_1 D_1} e^{i k_2 \rho} \left(\frac{i k_2}{\rho} - \frac{1}{\rho^2} \right) \quad (63)$$

is the lateral wave that travels along the air-sea boundary a radial distance ρ and then proceeds vertically down the depth D_1 of the sea to the point of measurement on the sea floor. $B_{10}^T(\rho, 0)$ is the field that propagates down in

TABLE I
NUMERICAL VALUES OF PARAMETERS

$f = 0.125 \text{ Hz}, \quad k_0 = 0.25 \times 10^{-6} \text{ m}^{-1}; \quad \sigma_2 = 0.01 \text{ S/m}, \quad k_2 = 0.99 \times 10^{-4} e^{i\pi/4} \text{ m}^{-1};$ $\sigma_1 = 2.85 \text{ S/m}, \quad k_1 = 1.88 \times 10^{-3} e^{i\pi/4} \text{ m}^{-1}; \quad h = 640 \text{ m}, \quad h_e = 320 e^{-i0.241} \text{ m}$				
σ_2 in S/m	0.28	0.3	0.4	0.57
k_2 in m^{-1}	$5.06 \times 10^{-4} e^{i\pi/4}$	$5.44 \times 10^{-4} e^{i\pi/4}$	$6.44 \times 10^{-4} e^{i\pi/4}$	$7.50 \times 10^{-4} e^{i\pi/4}$
$\delta = (\sigma_2/\sigma_1)^{1/2}$	0.30	0.324	0.375	0.45
Range $0.1 \leq \rho \leq 2 \text{ km}$	$0.05 \leq k_2 \rho \leq 1$	$0.054 \leq k_2 \rho \leq 1.09$	$0.064 \leq k_2 \rho \leq 1.28$	$0.075 \leq k_2 \rho \leq 1.5$
Near field $\rho \leq 0.6 k_2^{-1} $	1.19 km	1.10 km	0.93 km	0.80 km
$z_m = 0.15 \delta \rho^2$	23.7 m	22.6 m	22.5 m	22.9 m

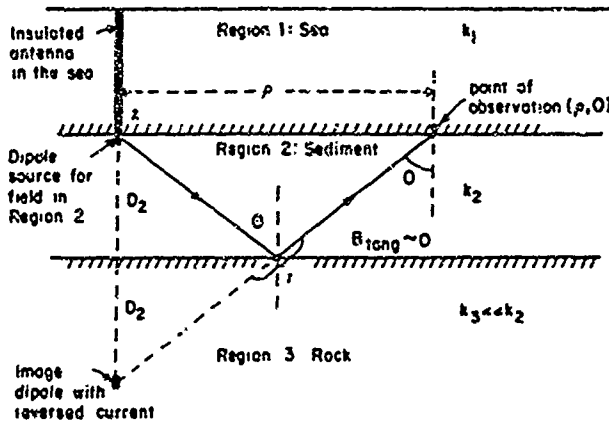


Fig. 6. Schematic diagram locating the equivalent source dipole for the field in Region 2 at $(0, 0)$, its image with reversed current at $(0, -2D_2)$, and the point of observation in Region 1 at $(\rho, 0)$

the sediment as a spherical wave given by (27), is partially reflected at the rock boundary, and then travels upward to the sediment-sea boundary where it is partly reflected, partly transmitted to the point of observation in the sea. This is shown schematically in Fig. 6.

It is readily shown that $B_{10}^T(\rho, 0)$ is negligible compared to $B_{10}^L(\rho, 0)$. The ratio $B_{10}^T(\rho, 0)/B_{10}^L(\rho, 0)$ is dominated by the ratio $k_0^2/k_2^2 = \omega^2 \mu_0 \epsilon_0 / i \omega \mu_0 \sigma_2 = -i 1.74 \times 10^{-11}$ when $f = 0.125 \text{ Hz}$ and $\sigma_2 = 0.4 \text{ S/m}$. This is so small that $B_{10}^T(\rho, 0)$ can be neglected. It follows that

$$B_{10}(\rho, 0) = B_{10}^L(\rho, 0) [1 + B_{10}^T(\rho, 0)/B_{10}^L(\rho, 0)]. \quad (64)$$

The field $B_{10}^T(\rho, 0)$ can be determined in a step-by-step manner. Consider first the spherical wave traveling downward in the sediment from the equivalent vertical dipole at $(0, 0)$ in the sediment. This is incident on the sediment-rock boundary. If on this surface it is treated as a locally plane wave, the reflection coefficient is

$$f_{rr} = \frac{(\sigma_3/\sigma_2) \cos \Theta - \sqrt{(\sigma_3/\sigma_2) - \sin^2 \Theta}}{(\sigma_3/\sigma_2) \cos \Theta + \sqrt{(\sigma_3/\sigma_2) - \sin^2 \Theta}} \quad (65)$$

where the angle of incidence is Θ and $\cos \Theta = D_2 / \sqrt{D_2^2 + (\rho/2)^2}$. With $\sigma_3 = 0.01 \text{ S/m}$ and $\sigma_2 = 0.4 \text{ S/m}$, the quantity $\sigma_3/\sigma_2 \sim 0.024$ is very small. It follows

that, except for very small angles, $\sin^2 \Theta$ is significantly greater than σ_3/σ_2 and $f_{rr} \sim -1$. This value is independent of the precise value of σ_3/σ_2 so long as this is small. With $f_{rr} \sim -1$, the reflected field is the same as the field of an image of the source dipole and located at $(0, -2D_2)$ but with reversed electric moment, i.e., with the moment $-lh_e$. The magnetic field of this image dipole incident on the sea floor from below, i.e., from the sediment, is

$$B_{20}^R(\rho, 0) = \frac{\mu_0 k_2^2}{2\pi k_1^2} lh_e e^{ik_2 r} \left(\frac{ik_2}{r} - \frac{1}{r^2} \right) \left(\frac{\rho}{r} \right) \quad (66)$$

where $r = (4D_2^2 + \rho^2)^{1/2}$ is the distance from the image dipole at $(0, -2D_2)$ to the point $(\rho, 0)$ on the boundary but in the sediment. The point of observation is at $(\rho, 0)$ in the sea. The field at this point is given in (66) multiplied by the transmission coefficient. That is

$$B_{10}^T(\rho, 0) = B_{20}^R(\rho, 0) f_{tr} \quad (67)$$

where f_{tr} is the transmission coefficient for $B_{20}^R(\rho, 0)$ which is transverse to the plane of incidence. It is given by

$$f_{tr} = \frac{2k_1^2 \cos \Theta}{k_1^2 \cos \Theta + k_2 \sqrt{k_1^2 - k_2^2 \sin^2 \Theta}} = \frac{2(\sigma_1/\sigma_2) \cos \Theta}{(\sigma_1/\sigma_2) \cos \Theta + \sqrt{(\sigma_1/\sigma_2) - \sin^2 \Theta}} \quad (68)$$

Since $k_2^2/k_1^2 = \sigma_2/\sigma_1 = 0.4/2.85 = 0.14$ is quite small and significant reflections occur only when $\rho > 2D_2$ and ρ/r is not a small fraction, a satisfactory approximation is

$$f_{tr} \sim \frac{\cos \Theta}{\cos \Theta + (\sigma_2/\sigma_1)^{1/2}} = \frac{4D_2}{2D_2 + r(\sigma_2/\sigma_1)^{1/2}} \quad (69)$$

since $\cos \Theta = 2D_2/r$. The Brewster angle at which the entire field is transmitted into the sea occurs with $\rho = 3 \text{ km}$ when $D_2 = 600 \text{ m}$. It follows with (64), (66), and (67) that

$$B_{10}(\rho, 0) = B_{10}^L(\rho, 0) \left[1 - e^{ik_2(r-\rho)} \left(\frac{ik_2 r - 1}{ik_2 \rho - 1} \right) \left(\frac{\rho}{r} \right)^3 \cdot \left(\frac{4D_2}{2D_2 + r(\sigma_2/\sigma_1)^{1/2}} \right) \right] \quad (70)$$

where $r = (4D_2^2 + \rho^2)^{1/2}$. This is the total magnetic field at the point of observation $(\rho, 0)$ on the sea floor due to the lateral wave traveling in the sediment along a locus like those shown in Fig. 2 and the reflection from the rock layer at the depth D_2 .

The magnitude of the lateral-wave magnetic field given by (62) has been calculated with $\sigma_1 = 2.85$ S/m, $D_1 = 640$ m, $\sigma_2 = 0.4$ S/m, $D_2 = 600$ m, and $\sigma_3 = 0.01$ S/m over a radial range from $\rho = 0.1$ to $\rho = 10$ km. It is shown in Fig. 5. The complete magnetic field including the reflection from the rock layer as calculated from (70) is shown in broken line in Fig. 5. The reflected field is seen to produce a significant decrease in the field due to the lateral wave in a range centered around $\rho = 3.5$ km. At this distance, the angle of incidence on the sediment-sea boundary of the diagonally upward-traveling reflected field from the rock-sediment boundary is the Brewster angle of $\Theta = 71^\circ$ (see Fig. 6).

When compared with the magnetic field measured by Edwards *et al.* in the Bute Inlet at the numbered locations shown in Fig. 4, the theoretical curve is seen to be in excellent agreement over the entire range. This indicates that the conductivity of the sediment must have an average value very near $\sigma_2 = 0.4$ S/m. This value differs from $\sigma_2 = 0.52$ S/m calculated by Edwards *et al.* from the same data by a method that is not given in detail. However, with $\omega\epsilon_2 = 0$ and $k_2 = (i\omega\mu_0\sigma_2)^{1/2}$, the formula in Edwards *et al.* [19, eq. (20)] is essentially the same as (62).

V. CONCLUSION

The complete field in Region 2 has been derived to supplement the already available field in Region 1 due to a vertical electric dipole at a distance d in Region 1 from the boundary between the two regions for which $|k_1| \geq 3|k_2|$. The new formulas are applied to determine the properties of the field in Region 2, including the locus of the Poynting vector of the lateral-wave part of the field and its maximum depth of penetration. Direct application to measurements on the sea floor show excellent agreement with measurements when appropriate values of conductivity and depth are selected.

APPENDIX I

EVALUATION OF THE INTEGRALS $G_2(\rho, z)$

The integrals to be evaluated are

$$G_{2\phi}(\rho, z) = \int_0^\infty \left(\frac{1}{N} - \frac{1}{N_0} \right) e^{-\gamma_2 z} J_1(\lambda\rho) \lambda^2 d\lambda \quad (A1)$$

$$G_{2\rho}(\rho, z) = \int_0^\infty \left(\frac{1}{N} - \frac{1}{N_0} \right) e^{-\gamma_2 z} \gamma_2 J_1(\lambda\rho) \lambda^2 d\lambda \quad (A2)$$

$$G_{2z}(\rho, z) = \int_0^\infty \left(\frac{1}{N} - \frac{1}{N_0} \right) e^{-\gamma_2 z} J_0(\lambda\rho) \lambda^3 d\lambda \quad (A3)$$

where

$$\gamma_2 = (k_2^2 - \lambda^2)^{1/2} \quad (A4)$$

and

$$\frac{1}{N} - \frac{1}{N_0} = \frac{1}{k_1^2(k_2^2 - \lambda^2)^{1/2} + k_2^2(k_1^2 - \lambda^2)^{1/2}} - \frac{1}{k_1^2(k_2^2 - \lambda^2)^{1/2}} \quad (A5)$$

Except for small arguments, the Bessel functions in (A1)-(A3) are well approximated by

$$J_0(\lambda\rho) \sim \frac{1}{(2\pi\lambda\rho)^{1/2}} [e^{i(\lambda\rho - \pi/4)} + e^{-i(\lambda\rho - \pi/4)}] \quad (A6)$$

$$J_1(\lambda\rho) \sim \frac{1}{(2\pi\lambda\rho)^{1/2}} [e^{i(\lambda\rho - 3\pi/4)} + e^{-i(\lambda\rho - 3\pi/4)}] \quad (A7)$$

so that (A1)-(A3) each becomes the sum of two integrals. With

$$F(\lambda^2) = \left(\frac{1}{N} - \frac{1}{N_0} \right) e^{-\gamma_2 z} \lambda^2 \quad (A8)$$

$$\begin{aligned} G_{2\phi}(\rho, z) &\sim \int_0^\infty F(\lambda^2) J_1(\lambda\rho) d\lambda \\ &= \int_0^\infty F(\lambda^2) \frac{e^{i(\lambda\rho - 3\pi/4)}}{(2\pi\lambda\rho)^{1/2}} d\lambda \\ &\quad + \int_0^\infty F(\lambda^2) \frac{e^{-i(\lambda\rho - 3\pi/4)}}{(2\pi\lambda\rho)^{1/2}} d\lambda \quad (A9) \end{aligned}$$

$$\begin{aligned} G_{2z}(\rho, z) &\sim \int_0^\infty F(\lambda^2) J_0(\lambda\rho) \lambda d\lambda \\ &= \int_0^\infty F(\lambda^2) \frac{e^{i(\lambda\rho - \pi/4)}}{(2\pi\lambda\rho)^{1/2}} \lambda d\lambda \\ &\quad + \int_0^\infty F(\lambda^2) \frac{e^{-i(\lambda\rho - \pi/4)}}{(2\pi\lambda\rho)^{1/2}} \lambda d\lambda. \quad (A10) \end{aligned}$$

With $F_p(\lambda^2) = \gamma_2 F(\lambda^2)$ substituted for $F(\lambda^2)$ in (A9), this gives $G_{2\rho}(\rho, z)$.

Let the variable in the second integral in (A9) and (A10) be changed to $\lambda' = -\lambda$, $d\lambda' = -d\lambda$, $\lambda = \infty \rightarrow \lambda' = -\infty$. Thus, the second integral in (A9) becomes

$$\begin{aligned} &= \int_0^{-\infty} F(\lambda'^2) \frac{e^{i(\lambda'\rho + 3\pi/4)}}{i(2\pi\lambda'\rho)^{1/2}} d\lambda' \\ &= \int_0^{-\infty} F(\lambda'^2) \frac{e^{i(\lambda'\rho - 3\pi/4)}}{(2\pi\lambda'\rho)^{1/2}} d\lambda'. \quad (A11) \end{aligned}$$

The second integral in (A10) becomes

$$\begin{aligned} &= \int_0^{-\infty} F(\lambda'^2) \frac{e^{i(\lambda'\rho + \pi/4)}}{i(2\pi\lambda'\rho)^{1/2}} \lambda' d\lambda' \\ &= \int_0^{-\infty} F(\lambda'^2) \frac{e^{i(\lambda'\rho - \pi/4)}}{(2\pi\lambda'\rho)^{1/2}} \lambda' d\lambda'. \quad (A12) \end{aligned}$$

Thus, the integrals in (A1)-(A3) are

$$G_{20}(\rho, z) = \left(\int_0^\infty + \int_0^{-\infty} \right) \left(\frac{1}{N} - \frac{1}{N_0} \right) \cdot e^{-i\gamma_2 z} \frac{e^{i(\lambda\rho - 3\pi/4)}}{(2\pi\lambda\rho)^{1/2}} \lambda^2 d\lambda \quad (\text{A13})$$

$$G_{2p}(\rho, z) = \left(\int_0^\infty + \int_0^{-\infty} \right) \left(\frac{1}{N} - \frac{1}{N_0} \right) \cdot e^{-i\gamma_2 z} \frac{e^{i(\lambda\rho - 3\pi/4)}}{(2\pi\lambda\rho)^{1/2}} \lambda^2 d\lambda \quad (\text{A14})$$

$$G_{2z}(\rho, z) = \left(\int_0^\infty + \int_0^{-\infty} \right) \left(\frac{1}{N} - \frac{1}{N_0} \right) \cdot e^{-i\gamma_2 z} \frac{e^{i(\lambda\rho - \pi/4)}}{(2\pi\lambda\rho)^{1/2}} \lambda^3 d\lambda. \quad (\text{A15})$$

It is evident from the form of (A5) that the principal contributions to the integrals must come only when λ is near k_2 . This means that λ^2 can be neglected compared with k_1^2 since $|k_1|^2 \gg |k_2|^2$. It is readily shown that the zero of N in (A5) occurs at $\lambda = k_1 k_2 / (k_1^2 + k_2^2)^{1/2} = k_2 - k_2^3 / 2k_1^2$. This suggests a change of variable of the form

$$\lambda = k_2(1 + m\tau) \\ d\lambda = k_2 m d\tau \quad (\text{A16})$$

where

$$m = k_2^3 / 2k_1^2, \quad |m| \ll 1. \quad (\text{A17})$$

In (A16), τ is the dimensionless variable of integration. It follows that

$$\lambda^2 \sim k_2^2(1 + 2m\tau) \\ \gamma_2 = (k_2^2 - \lambda^2)^{1/2} \sim k_2(-2m\tau)^{1/2} = ik_2^3\tau^{1/2}/k_1. \quad (\text{A18})$$

In amplitudes

$$\lambda \sim k_2 \\ \lambda^2 \sim k_2^2 \\ \lambda^3 \sim k_2^3. \quad (\text{A19})$$

With these values

$$\frac{1}{N} - \frac{1}{N_0} \sim \frac{1}{k_2^3 k_1} \left| \frac{1}{i\sqrt{\tau} + 1} - \frac{1}{i\sqrt{\tau}} \right| \\ = \frac{1}{k_2^3 k_1} \left| \frac{1}{\sqrt{\tau}(\sqrt{\tau} - i)} \right|. \quad (\text{A20})$$

The lower limit, $\lambda = 0$, in the integrals (A13)–(A15) becomes $\tau = -1/m = -2k_1^2/k_2^2$ where $[2k_1^2/k_2^2] \gg 1$. It follows that the very large lower limit can be approximated by $-\infty$. This means that the second integrals in (A13)–(A15) become vanishingly small. When (A16)–(A20) are used in (A13), this becomes

$$G_{20}(\rho, z) = -\frac{ik_2^3}{4k_1^3} \left(\frac{2}{\pi k_2 \rho} \right)^{1/2} e^{i(k_2 \rho - \pi/4)} I_0 \quad (\text{A21})$$

where

$$I_0 = \int_{-\infty}^\infty \frac{e^{2Z\sqrt{\tau}}}{\sqrt{\tau}(\sqrt{\tau} - i)} e^{iR\tau} d\tau \quad (\text{A22})$$

and

$$Z = k_2^2 z / 2k_1 \\ R = k_2^3 \rho / 2k_1^2. \quad (\text{A23})$$

The integral I_0 can be expressed in terms of the Fresnel integral. As a first step, note that

$$\frac{1}{2} \frac{\partial}{\partial Z} (e^{-2iZ} I_0) \\ = \left(\frac{1}{2} \frac{\partial I_0}{\partial Z} - iI_0 \right) e^{-2iZ} \\ = e^{-2iZ} \int_{-\infty}^\infty \left| \frac{1}{\sqrt{\tau} - i} - \frac{i}{\sqrt{\tau}(\sqrt{\tau} - i)} \right| e^{2Z\sqrt{\tau}} e^{iR\tau} d\tau \\ = e^{-2iZ} \int_{-\infty}^\infty \frac{1}{\sqrt{\tau}} e^{2Z\sqrt{\tau}} e^{iR\tau} d\tau. \quad (\text{A24a})$$

This integral can be evaluated with the substitution $x^2 = \tau$, $2x dx = d\tau$. Also, $iR\tau + 2Z\sqrt{\tau} = iRx^2 + 2Zx = (\sqrt{iR}x + Z/\sqrt{iR})^2 - Z^2/iR$, so that

$$e^{-2iZ} \int_{-\infty}^\infty \frac{1}{\sqrt{\tau}} e^{2Z\sqrt{\tau}} e^{iR\tau} d\tau \\ = 2e^{-2iZ} e^{iZ^2/iR} \int_{-\infty}^\infty e^{i(\sqrt{iR}x + Z/\sqrt{iR})^2} dx. \quad (\text{A24b})$$

With the substitutions

$$iy = (\sqrt{iR}x + Z/\sqrt{iR}) \\ -y^2 = (\sqrt{iR}x + Z/\sqrt{iR})^2 \\ i dy = \sqrt{iR} dx \quad (\text{A25a})$$

the integral becomes

$$\frac{2i}{\sqrt{iR}} e^{-2iZ} e^{iZ^2/iR} \int_{-\infty}^\infty e^{-y^2} dy \\ = 2 \left(\frac{\pi i}{R} \right)^{1/2} e^{-2iZ} e^{iZ^2/iR}. \quad (\text{A25b})$$

It follows that

$$\frac{1}{2} \frac{\partial}{\partial Z} (e^{-2iZ} I_0) = 2 \left(\frac{\pi i}{R} \right)^{1/2} e^{-2iZ} e^{iZ^2/iR}. \quad (\text{A26})$$

This gives for $Z \leq 0$

$$I_0 = 4 \left(\frac{\pi i}{R} \right)^{1/2} e^{2iZ} \int_{-\infty}^Z e^{-2iZ'} e^{iZ'^2/iR} dZ'. \quad (\text{A27})$$

The evaluation of (A27) is carried out with the change of variable $Z' = R - Z''$, $dZ' = -dZ''$. Thus, with $I_0(\infty) = 0$

$$I_0 = 4 \left(\frac{\pi i}{R} \right)^{1/2} e^{2iZ} e^{-iR} \int_{R-Z}^\infty e^{iZ''^2/iR} dZ''. \quad (\text{A28})$$

Finally, let $t = Z^2/R$, $dZ = \frac{1}{2} \sqrt{R/t} dt$, so that

$$I_\phi = 4 \left(\frac{\pi i}{R} \right)^{1/2} e^{2iZ} e^{-iR} \left(\frac{\pi R}{2} \right)^{1/2} \int_P^\infty \frac{e^{it}}{(2\pi t)^{1/2}} dt \quad (A29)$$

where $P = (R - Z)^2/R$ with $Z \leq 0$. The integral can be expanded as follows:

$$\begin{aligned} \mathfrak{F}(P) &= \int_P^\infty \frac{e^{it}}{(2\pi t)^{1/2}} dt \\ &= \frac{1}{2} (1 + i) - C_2(P) - iS_2(P) \end{aligned} \quad (A30)$$

where

$$C_2(P) + iS_2(P) = \int_0^P \frac{e^{it}}{(2\pi t)^{1/2}} dt \quad (A31)$$

is the well-known Fresnel integral. In this notation

$$I_\phi = 4\pi \left(\frac{i}{2} \right)^{1/2} e^{2iZ} e^{-iR} \mathfrak{F}(P), \quad Z \leq 0. \quad (A32)$$

With (A21) and (A32)

$$\begin{aligned} G_{2\phi}(\rho, z) &= -\frac{ik_2^3}{k_1^3} \left(\frac{\pi}{k_2\rho} \right)^{1/2} e^{ik_2\rho} e^{2iZ} e^{-iR} \mathfrak{F}[(R - Z)^2/R], \\ &Z \leq 0. \end{aligned} \quad (A33)$$

The second integral (A14) for $G_{2\rho}(\rho, z)$ differs from the integral for $G_{2\phi}(\rho, z)$ only in the additional factor $\gamma_2 = (k_2^2 - \lambda^2)^{1/2} \sim ik_2^2 \tau^{1/2}/k_1$. Hence, with (A21) and (A22)

$$G_{2\rho}(\rho, z) = \frac{k_2^5}{4k_1^4} \left(\frac{2}{\pi k_2\rho} \right)^{1/2} e^{i(k_2\rho - \pi/4)} I_\rho \quad (A34)$$

where

$$I_\rho = \int_{-\infty}^\infty \frac{e^{2Z\sqrt{\tau}}}{\sqrt{\tau} - i} e^{iR\tau} d\tau. \quad (A35a)$$

This integral can be evaluated in the manner used for (A22). Thus

$$\begin{aligned} \frac{1}{2} \frac{\partial}{\partial Z} (e^{-2iZ} I_\rho) &= \left(\frac{1}{2} \frac{\partial I_\rho}{\partial Z} - iI_\rho \right) e^{-2iZ} \\ &= e^{-2iZ} \int_{-\infty}^\infty \left[\frac{\sqrt{\tau}}{\sqrt{\tau} - i} - \frac{i}{\sqrt{\tau} - i} \right] e^{2Z\sqrt{\tau}} e^{iR\tau} d\tau \\ &= e^{-2iZ} \int_{-\infty}^\infty e^{2Z\sqrt{\tau}} e^{iR\tau} d\tau. \end{aligned} \quad (A35b)$$

This integral can be evaluated with $\tau = x^2$, $d\tau = 2x dx$. The integral is

$$2e^{-2iZ} e^{iZ^2/R} \int_{-\infty}^\infty e^{(\sqrt{R}x + Z/\sqrt{R})^2} x dx.$$

The variable is changed to

$$\begin{aligned} iy &= \sqrt{iR}x + Z/\sqrt{iR} \\ i dy &= \sqrt{iR} dx \end{aligned}$$

with

$$x = \frac{iy}{\sqrt{iR}} - \frac{Z}{iR}$$

so that

$$\begin{aligned} \frac{1}{2} \frac{\partial}{\partial Z} (e^{-2iZ} I_\rho) &= \frac{2i}{\sqrt{iR}} e^{-2iZ} e^{iZ^2/R} \left\{ \frac{i}{\sqrt{iR}} \int_{-\infty}^\infty e^{-y^2} dy \right. \\ &\quad \left. - \frac{Z}{iR} \int_{-\infty}^\infty e^{-y^2} dy \right\}. \end{aligned} \quad (A36a)$$

Here the first integral vanishes; the second is like that in (A25b) and equal to $\sqrt{\pi}$. Thus

$$\frac{1}{2} \frac{\partial}{\partial Z} (e^{-2iZ} I_\rho) = \frac{2iZ}{R} \left(\frac{\pi i}{R} \right)^{1/2} e^{-2iZ} e^{iZ^2/R}. \quad (A36b)$$

The integration of both sides with $Z \leq 0$ gives

$$I_\rho = \frac{4i}{R} \left(\frac{\pi i}{R} \right)^{1/2} e^{2iZ} \int_{-\infty}^Z e^{-2iZ'} e^{iZ'^2/R} dZ'. \quad (A37)$$

This can be integrated with the substitution $Z' = R - Z''$ to obtain

$$I_\rho = 4i\pi \left(\frac{i}{2} \right)^{1/2} e^{2iZ} e^{-iR} \mathfrak{F}(P) + 2 \left(\frac{\pi i}{R} \right)^{1/2} e^{iZ^2/R}. \quad (A38)$$

When (A38) is substituted in (A34), this becomes

$$\begin{aligned} G_{2\rho}(\rho, z) &= \frac{k_2^5}{k_1^4} e^{ik_2\rho} \left\{ \frac{k_1 e^{iZ^2/R}}{k_2^2\rho} + i \left(\frac{\pi}{k_2\rho} \right)^{1/2} \right. \\ &\quad \left. \cdot e^{2iZ} e^{-iR} \mathfrak{F}[(R - Z)^2/R] \right\}, \quad Z \leq 0. \end{aligned} \quad (A39)$$

The integral for $G_{2z}(\rho, z)$ in (A15) differs from the integral for $G_{2\phi}(\rho, z)$ in the factor $\lambda e^{i\pi/2} \sim ik_2$. Thus, with (A33)

$$\begin{aligned} G_{2z}(\rho, z) &= \frac{k_2^4}{k_1^3} \left(\frac{\pi}{k_2\rho} \right)^{1/2} e^{ik_2\rho} e^{2iZ} e^{-iR} \mathfrak{F}[(R - Z)^2/R], \\ &Z \leq 0. \end{aligned} \quad (A40)$$

APPENDIX II

THE RADIAL ELECTRIC FIELD ALONG THE BOUNDARY

When the source dipole is in Region 1 ($|k_1|^2 \gg |k_2|^2$), the field in Region 2 is transmitted vertically in a narrow cone across the boundary. This cone is bounded by the critical angle for total internal reflection. When the dipole is horizontal, this cone is in the direction of maximum radiation; when the dipole is vertical, the radiation along the axis of the cone is zero. This leads to special complications with the approximation (17) in determining the radial electric field near the boundary close to a vertical dipole when this is at a distance d from the surface, and

makes (39a) invalid at the surface $z = 0$. The formulas (6), (9), and (12) in (2) with the boundary condition $E_{2\rho}(\rho, 0) = E_{1\rho}(\rho, 0)$ give the correct value at $z = 0$. The appropriate formula (39b) can be derived directly from the integral (23) with $z = 0$. Thus

$$\begin{aligned} E_{2\rho}(\rho, 0) &= -\frac{i\omega\mu_0}{2\pi k_1^2} \int_0^\infty \frac{k_1^2 \gamma_2 e^{i\gamma_1 d}}{N} J_1(\lambda\rho) \lambda^2 d\lambda \\ &= -\frac{i\omega\mu_0}{2\pi k_1^2} \left\{ \int_0^\infty e^{i\gamma_1 d} J_1(\lambda\rho) \lambda^2 d\lambda \right. \\ &\quad \left. - \int_0^\infty \frac{k_1^2 \gamma_1 e^{i\gamma_1 d}}{N} J_1(\lambda\rho) \lambda^2 d\lambda \right\} \\ &= \frac{\omega\mu_0}{2\pi k_1^2} e^{ik_1 r_d} \left(\frac{ik_1^2}{r_d} - \frac{3k_1}{r_d^2} - \frac{3i}{r_d^3} \right) \left(\frac{\rho d}{r_d^2} \right) \\ &\quad + \frac{i\omega\mu_0 k_1^2}{2\pi k_1^2} \int_0^\infty \frac{\gamma_1 e^{i\gamma_1 d}}{N} J_1(\lambda\rho) \lambda^2 d\lambda. \quad (A41) \end{aligned}$$

The final integral in (A41) can be separated into two integrals with (25) and (26). These are

$$\begin{aligned} &\int_0^\infty \frac{\gamma_1 e^{i\gamma_1 d}}{N} J_1(\lambda\rho) \lambda^2 d\lambda \\ &= \frac{1}{k_1^2} \int_0^\infty \frac{\gamma_1 e^{i\gamma_1 d}}{\gamma_2} J_1(\lambda\rho) \lambda^2 d\lambda + k_1 e^{ik_1 d} G_{20}(\rho, 0) \end{aligned} \quad (A42)$$

where $G_{20}(\rho, 0)$ is obtained from (A33) with $Z = 0$. The first integral is evaluated in the manner of [16, Appendix A, eq. (A3)]. The result is

$$\begin{aligned} &\int_0^\infty \frac{\gamma_1 e^{i\gamma_1 d}}{\gamma_2} J_1(\lambda\rho) \lambda^2 d\lambda \\ &= k_1 \left| \frac{e^{ik_1 r_d}}{r_d^2} - \left(\frac{k_2}{\rho} + \frac{i}{\rho^2} \right) e^{ik_2 \rho} e^{ik_1 d} \right|. \quad (A43) \end{aligned}$$

When (A43) is substituted in (A42) and this is inserted in (A41), the final formula is (39b).

APPENDIX III

THE EFFECTIVE LENGTH OF THE ANTENNA

The formula (62) for the magnetic field on the sea floor corresponds to the formula (20) given by Edwards *et al.* [19] but their effective length is

$$h_e = \frac{i}{k_1} \left| \frac{1 - 2e^{ik_1 h} + e^{i2k_1 h}}{1 - e^{i2k_1 h}} \right| = \frac{i}{k_1} \left| \frac{1 - e^{ik_1 h}}{1 + e^{ik_1 h}} \right|. \quad (A44)$$

Their formula is obtained from the exact integral in the low-frequency limit, $\omega \rightarrow 0$, with the condition that the reflection coefficient of the crust be close to -1 .

It is interesting to note that (A44) is exactly the effective length of a *semi-infinite* array of images extending from the sea-air boundary to $+\infty$, with the reflection coefficient of all *images* of the sea-crust boundary set equal to -1 . No reflections from the actual sea-crust boundary at $z = 0$ are included, only reflections from its images in

the sea-air boundary. That is

$$\begin{aligned} h_e &= \left(\int_0^h - \int_h^{2h} + \int_{2h}^{3h} - \int_{3h}^{4h} + \dots \right) e^{ik_1 z} dz \\ &= \frac{i}{k_1} (1 - e^{ik_1 h})(1 - e^{ik_1 h} + e^{i2k_1 h} - e^{i3k_1 h} + \dots) \end{aligned}$$

or

$$h_e = \frac{i}{k_1} \left| \frac{1 - e^{ik_1 h}}{1 + e^{ik_1 h}} \right|. \quad (A45)$$

This is exactly (A44). The field generated by this array violates the boundary condition that $B_{1\phi}(\rho, z) = 0$ when $z = h, 3h, 5h, \dots$, i.e., on the sea-air boundary and its images, yet assumes the reflection coefficient for each of these boundaries to be -1 . The lateral wave along the actual sea crust boundary is preserved because the reflection coefficient for it has its true value and is not set equal to -1 as for all images of the same boundary. However, the lateral waves along the image boundaries are all cancelled. If the contribution from the image lateral wave in (59) is set equal to zero (the term $e^{i2k_1 h}$ in the numerator) and Γ_m is set equal to -1 , (59) is identically (A44).

So long as $e^{-4\pi i h} \ll 1$, the formula (59) should be more accurate than (A44). However, in the limit $\omega \rightarrow 0$, (59) has no application and (A44) reduces to $h/2$. With $k_1 = 1.68 \times 10^{-3} e^{i\pi/4} \text{ m}^{-1}$ and $h = 640 \text{ m}$, (A44) gives

$$h_e = 318 e^{i1.0}. \quad (A46)$$

This differs from $h_e = 326$ given by (59) by 2.5 percent. Since the first reflection from the sea-air boundary makes the only really significant contribution, the treatment of higher order reflections is largely irrelevant.

REFERENCES

- [1] A. Sommerfeld, "Ueber die Ausbreitung der Wellen in der drahtlosen telegraphie," *Ann. Phys.*, vol. 28, pp. 665-736, 1909; *Ann. Phys.*, vol. 81, pp. 1135-1153, 1926.
- [2] —, in *Die Differential u. Integralgleichungen der Mechanik u. Physik*, vol. II, P. Frank and R. von Mises, Eds., Braunschweig, Germany: F. Vieweg, 1935, pp. 919-941, ch. 23.
- [3] K. A. Norton, "The propagation of radio waves over the surface of the earth and in the upper atmosphere," *Proc. IRE*, vol. 24, pp. 1367-1387, 1936.
- [4] A. Baños, Jr., *Dipole Radiation in the Presence of a Conducting Half-Space*, Oxford, England: Pergamon, 1966.
- [5] J. R. Wait and L. L. Campbell, "The fields of an electric dipole in a semi-infinite conducting medium," *J. Geophys. Res.*, vol. 58, pp. 21-28, 1953.
- [6] M. B. Kraichman, *Handbook of Electromagnetic Propagation in Conducting Media*, Washington, DC: Superintendent of Documents, U.S. Government Printing Office, 1970.
- [7] M. Siegel and R. W. P. King, "Electromagnetic fields in a dissipative half-space: A numerical approach," *J. Appl. Phys.*, vol. 41, pp. 2415-2423, 1970.
- [8] —, "Radiation from linear antennas in a dissipative half-space," *IEEE Trans. Antennas Propagat.*, vol. AP-19, pp. 477-485, 1971.
- [9] —, "Electromagnetic propagation between antennas submerged in the ocean," *IEEE Trans. Antennas Propagat.*, vol. AP-21, pp. 507-513, 1973.
- [10] R. W. P. King and B. Sandler, "Subsurface communication between dipoles in general media," *IEEE Trans. Antennas Propagat.*, vol. AP-25, pp. 770-775, 1977.
- [11] D. M. Bubenik, "A practical method for the numerical evaluation of

- Sommerfeld integrals," *IEEE Trans. Antennas Propagat.*, vol. AP-25, pp. 904-906, 1977.
- [12] R. W. P. King, J. T. deBettencourt, and B. H. Sandler, "Lateral-wave propagation of electromagnetic waves in the lithosphere," *IEEE Trans. Geosci. Electron.*, vol. GE-17, pp. 86-92, 1979.
- [13] R. W. P. King, B. H. Sandler, and L. C. Shen, "A comprehensive study of subsurface propagation from horizontal electric dipoles," *IEEE Trans. Geosci. Remote Sensing*, vol. GE-18, pp. 225-233, 1980.
- [14] Y. Rahmat-Saini, R. Mittra, and P. Parhami, "Evaluation of Sommerfeld integrals for lossy-half-space problems," *Electromagnetics*, vol. 1, pp. 1-28, 1981.
- [15] R. W. P. King and G. S. Smith, *Antennas in Matter*. Cambridge, MA: M.I.T. Press, 1981, ch. 11.
- [16] R. W. P. King, "New formulas for the electromagnetic field of a vertical electric dipole in a dielectric or conducting half-space near its horizontal interface," *J. Appl. Phys.*, vol. 53, pp. 8476-8482, Dec. 1982; erratum, vol. 56, p. 3366, Dec. 1984.
- [17] A. D. Chave and C. S. Cox, "Controlled electromagnetic sources for measuring electrical conductivity beneath the oceans. I. Forward problem and model study," *J. Geophys. Res.*, vol. 87, pp. 5327-5338, July 1982.
- [18] R. N. Edwards, L. K. Law, and J. M. DeLaurier, "On measuring the electrical conductivity of the oceanic crust by a modified magnetometric resistivity method," *J. Geophys. Res.*, vol. 86, pp. 11 609-11 615, Dec. 1981.
- [19] R. N. Edwards, D. C. Nobes, and E. Gomez-Treviño, "Offshore electrical exploration of sedimentary basins. The effects of anisotropy in horizontally isotropic, layered media," *Geophysics*, vol. 49, pp. 566-576, May 1984.
- [20] T. T. Wu and R. W. P. King, "Lateral waves. A new formula and interference patterns," *Radio Sci.*, vol. 17, pp. 521-531, May-June 1982.
- [21] —, "Lateral waves: New formulas for E_{10} and E_{11} ," *Radio Sci.*, vol. 17, pp. 532-538, May-June 1982; correction, vol. 19, p. 1422, Sept.-Oct. 1984.
- [22] R. W. P. King and T. T. Wu, "Lateral waves. Formulas for the magnetic field," *J. Appl. Phys.*, vol. 54, pp. 507-514, Feb. 1983; erratum, vol. 56, p. 3365, Dec. 1984.
- [23] R. W. P. King and M. F. Brown, "Lateral electromagnetic waves along plane boundaries: A summarizing approach," *Proc. IEEE*, vol. 72, pp. 595-611, May 1984.
- [24] R. W. P. King, "Scattering of lateral waves by buried or submerged objects. I. The incident lateral-wave field," *J. Appl. Phys.*, vol. 57, pp. 1453-1459, Mar. 1985.
- [25] —, "Scattering of lateral waves by buried or submerged objects. II. The electric field on the surface above a buried insulated wire," *J. Appl. Phys.*, vol. 57, pp. 1460-1472, Mar. 1985.
- [26] —, "Electromagnetic surface waves. New formulas and their application to determine the electrical properties of the sea bottom," *J. Appl. Phys.*, vol. 58, pp. 3612-3624, Nov. 1985.
- [27] W.-Y. Pan, "Surface-wave propagation along the boundary between sea water and one-dimensionally anisotropic rock," *J. Appl. Phys.*, vol. 58, pp. 3963-3974, Dec. 1985.
- [28] R. W. P. King, M. Owens, and T. T. Wu, "Properties of lateral electromagnetic fields and their application," *Radio Sci.*, vol. 21, pp. 13-23, Jan.-Feb. 1986.
- [29] R. W. P. King, *Theory of Linear Antennas*. Cambridge, MA: Harvard University Press, 1956, ch. 7.
- [30] R. N. Edwards, L. K. Law, P. A. Wolfgram, D. C. Nobes, M. N. Bone, D. F. Triggs, and J. M. DeLaurier, "First results of Moses experiment: Sea-sediment conductivity and thickness determination. Bute Inlet, British Columbia, by magnetometric offshore electrical sounding," *Geophysics*, vol. 50, pp. 153-160, 1985.

Ronald W. P. King (A'30-SM'43-F'53-LF'71) was born in Williamstown, MA, on September 19, 1905. He received the B.A. and M.S. degrees in physics from the University of Rochester, Rochester, NY, in 1927 and 1929, respectively, and the Ph.D. degree from the University of Wisconsin, Madison, in 1932, after having done graduate work at the University of Munich, Munich, Germany, and at Cornell University, Ithaca, NY.

He served as a Teaching and Research Assistant at the University of Wisconsin from 1932 to 1934, and as an Instructor and Assistant Professor of Physics at Lafayette College, Easton, PA, from 1934 to 1937. During the academic year 1937-1938 he was a Guggenheim Fellow in Germany. In 1938 he joined the faculty of Harvard University, Cambridge, MA. He has been Gordon McKay Professor of Applied Physics at Harvard from 1946 to 1972, when he became Gordon McKay Professor of Applied Physics, Emeritus. He was again a Guggenheim Fellow in 1958. He is the author or coauthor of ten books, numerous articles in books and encyclopedias, and over 240 original papers in technical journals.

Dr. King is a fellow of the American Physical Society and the American Academy of Arts and Sciences, a corresponding member of the Bavarian Academy of Sciences, and a member of the American Association for the Advancement of Science, Commission B of the International Scientific Radio Union, Phi Beta Kappa, and Sigma Xi.

floor carefully designed for different frequencies or distances, these formulas may be used to diagnose the electrical properties of the rock. When the rock is made up of many layers or there is a layer of sediment above the rock, the problem is more complicated. The work of Dunn [5]–[7] provides generalized formulas for lateral waves generated by a horizontal electric dipole with unit moment in sea water near its boundary with a medium of arbitrary thickness and electrical properties intermediate to those of the sea water and the rock (the three-layer problem). Experiments corresponding to this configuration have been performed in the laboratory using a water tank.

II. THEORETICAL FORMULAS

The assumed model of the earth's crust consists of a layer of sediment (region 2) over a half-space of rock (region 3) and beneath a half-space of sea water (region 1). The source antennas are in the sea water near the sea floor. The geometry is shown in Fig. 1. When the wavenumbers of the three regions satisfy $|k_1|^2 \gg |k_2|^2 \gg |k_3|^2$ (which is adequately satisfied when $|k_1| \geq 3|k_2| \geq 3|k_3|$), and the horizontal distance ρ between the horizontal transmitting and receiving antennas is sufficiently large, the field at the receiving antenna is that of a lateral wave. This is generated by the transmitting antenna and travels first down through the sediment (when this is not too thick) into the rock and then radially outward in the rock, and finally proceeds back through the sediment into the sea water and to the receiving antenna. The most useful components of the field are $E_{1\rho}$ and $E_{1\phi}$. They are expressed approximately as [5]:

$$E_{1\rho} = -iE_0 \cos \phi \left(\frac{k_3^2}{\rho} + \frac{ik_3}{\rho^2} - \frac{1}{\rho^3} \right) (1 + F_1), \quad (1)$$

$$E_{1\phi} = iE_0 \sin \phi \left(-\frac{2ik_3}{\rho^2} + \frac{2}{\rho^3} - \frac{ik_3}{\rho^2} F_1 \right), \quad (2)$$

where

$$E_0 = \frac{\omega\mu_0}{2\pi k_1^2} \frac{1}{(\cos k_2 l - i\alpha \sin k_2 l)^2} \exp [ik_1(z+d) + ik_3 \rho], \quad (3)$$

$$F_1 = \exp (i3\pi/4) \sqrt{k_3 \rho v^2/2}$$

$$\cdot \operatorname{erfc} (\sqrt{-ik_3 \rho v^2/2}) \exp (-ik_3 \rho v^2/2), \quad (4)$$

where l is the thickness of the intermediate layer of sediment (region 2) and ν is the equivalent normalized surface impedance in region 3, given by

$$\nu = \delta \frac{i\alpha \cos k_2 l + \sin k_2 l}{i \cos k_2 l + \alpha \sin k_2 l}, \quad (5)$$

with

$$\delta = k_3/k_2; \quad \alpha = k_2/k_1. \quad (6)$$

A comparison of (1) and (2) with the corresponding formulas for the two-layer problem [3], [4] shows the following differences.

1) For all of the components, there is an extra factor $G = (\cos k_2 l - i\alpha \sin k_2 l)^{-2}$ that depends on the thickness and electrical properties of the middle layer, but does not involve the horizontal distance ρ .

2) The equivalent normalized surface impedance α of the two-layer problem is replaced by ν in the three-layer case.

Measurement of Lateral Waves Along a Three-Layered Medium

WEI-YAN PAN

Abstract—An indoor experiment to simulate lateral waves propagating along the sea floor when this consists of a layer of sediment over rock has been carried out. The measurements are compared with theory.

I. INTRODUCTION

Lateral waves propagating along the sea floor may be used to explore the electrical properties of the continental shelves and oceanic lithosphere [1], [2]. When the sea floor is uniform rock, a set of accurate, very general and simple formulas for the surface-wave field of horizontal antennas near a boundary surface (the two-layer problem) has been derived [3], [4]. With measurements on the sea

Manuscript received August 22, 1985, revised September 25, 1985. This work was supported in part by the Joint Services Electronics Program under Contract N00014-84-K-0465 with Harvard University.

The author was a Visiting Scholar from the People's Republic of China at the Gordon McKay Laboratory, Harvard University, Cambridge, MA 02138. He is now with the China Research Institute of Radio Wave Propagation, Xin Xiang, Henan Province, People's Republic of China.

IEEE Log Number 8406399.

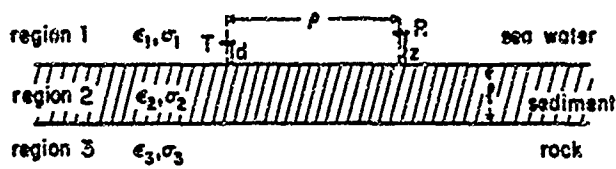


Fig. 1. Geometry of the problem.

3) The wavenumber k_2 in the two-layer problem is replaced by k_3 . When $l = 0$, (1) and (2) are identical to the corresponding formulas for the two-layer problem except that k_2 is replaced by k_3 .

III. APPARATUS AND MEASUREMENTS

The experiment was conducted in the laboratory. The apparatus included a model tank, generator, vector voltmeter, transmitting antenna, and automated movable receiving antenna. The octagonal tank measures 8.5 ft in diameter, 2.5 ft in height. Schematic diagrams of the experimental setup are in Figs. 2 and 3. The transmitting antenna is located at the center of the tank; the receiving antenna can move radially outward from the transmitter on a track. Both of the antennas are horizontal insulated linear dipoles, oriented in the radial direction. The depths of the dipoles from the water surface are $d = 2$ cm for the transmitter and $z = 1.7$ cm for the receiver. In order to have the radial range extend a few wavelengths, the frequency was chosen to be 1.503 GHz. The tank is filled with distilled water. Due to relaxation, the effective conductivity of distilled water at a frequency of 1.5 GHz is approximately 0.49 S/m. The relative dielectric constant ϵ_r is 80.0, virtually the same as the static value. Because the decay length in the water at this frequency is only 9.6 cm, the depth of the water, viz., 46 cm, is about five decay lengths. It follows that the bottom of the tank will not affect the field patterns.

On the water surface there is a slab supported by four plastic columns. This slab is also octagonal and a little smaller than the tank in size. It consists of one or more sheets of homosote adhered to a slab of styrofoam, 16 cm thick. The layers are held together by plastic bolts and nuts to assure flatness. Initially the composite slab was wrapped with very thin plastic film to keep the homosote dry. After the field had been measured with the dry homosote, the plastic film was removed and the homosote was lowered into the water for three days to absorb water. In the process, the thickness of each sheet of homosote increased from 1.35 cm to 1.6 cm. By weighing a small sample of the homosote, it was estimated that the completely wet homosote slab included 18 percent water. Since the conductivity and relative dielectric constant of the styrofoam are nearly the same as those of air, it is unnecessary to distinguish the styrofoam from the air. The electrical properties of the homosote were not measured directly. Since the homosote material is made of paper, its relative dielectric constant ϵ_2 , and the loss tangent $p_2 = \sigma_2 / \omega \epsilon_2 \epsilon_0$ when dry at 1.5 GHz may be estimated as [8]: $\epsilon_2^{\text{dry}} \approx 2.7$, $p_2^{\text{dry}} \approx 0.06$ and $\sigma_2^{\text{dry}} \approx 0.01352$ S/m. For the wet homosote, the corresponding parameters are estimated to be

$$\epsilon_2^{\text{wet}} = 2.7 \times 0.82 + 80 \times 0.18 = 16.61, \quad (7)$$

$$\sigma_2^{\text{wet}} = 0.01352 \times 0.82 + 0.49 \times 0.18 = 0.0993 \text{ S/m}. \quad (8)$$

When the homosote is wet, the electrical properties in the three regions approximately satisfy the condition $|k_1| \geq 3|k_2| \geq 3|k_3|$, as required by the real problem shown in Fig. 1.

The radial electric-field component $E_{1\rho}$ was measured with one, two, and four sheets of homosote in both the dry and wet states. The measurements are shown in Figs. 4 and 5.

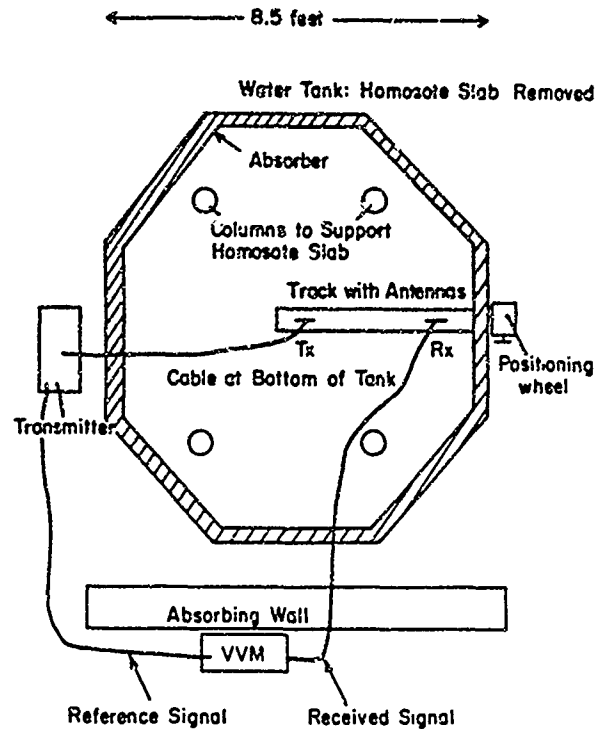


Fig. 2. Schematic of laboratory setup.

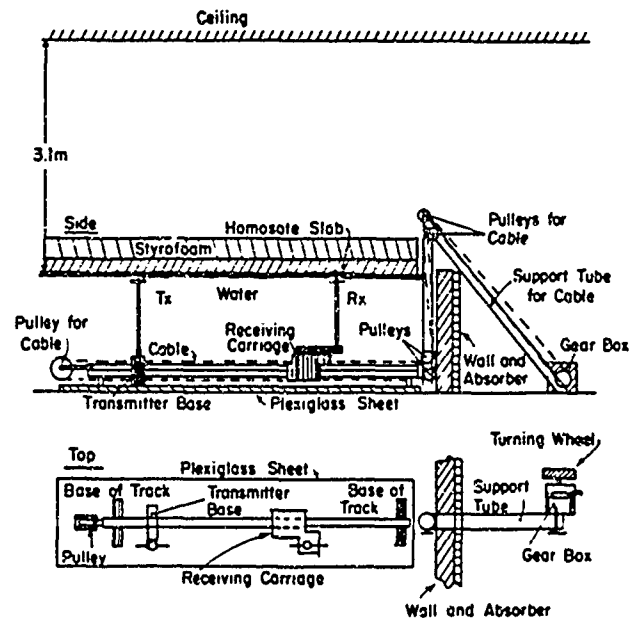


Fig. 3. Schematic of track in tank.

IV. DISCUSSION

In Fig. 4 the amplitude and phase of $E_{1\rho}$, as measured with the dry homosote on the water surface, are plotted. The dotted lines, dashed lines, and dot-dashed lines represent, respectively, measurements with one, two, and four sheets of dry homosote ($l = 1.35, 2.7$ and 5.4 cm). The solid lines apply with the homosote absent. From Fig 4(a) it may be seen that when the horizontal distance ρ is smaller than 0.25 m, the amplitude curves are oscillatory. The distance between two adjacent minima is 2 to 3 cm. On the other hand, the wavelength in the water for $f = 1.5$ GHz is $\lambda_1 = 2.2$ cm, and in the distance range $1\text{m} (k_1\rho) \leq 2.5$, the direct wave in the water is not small. It

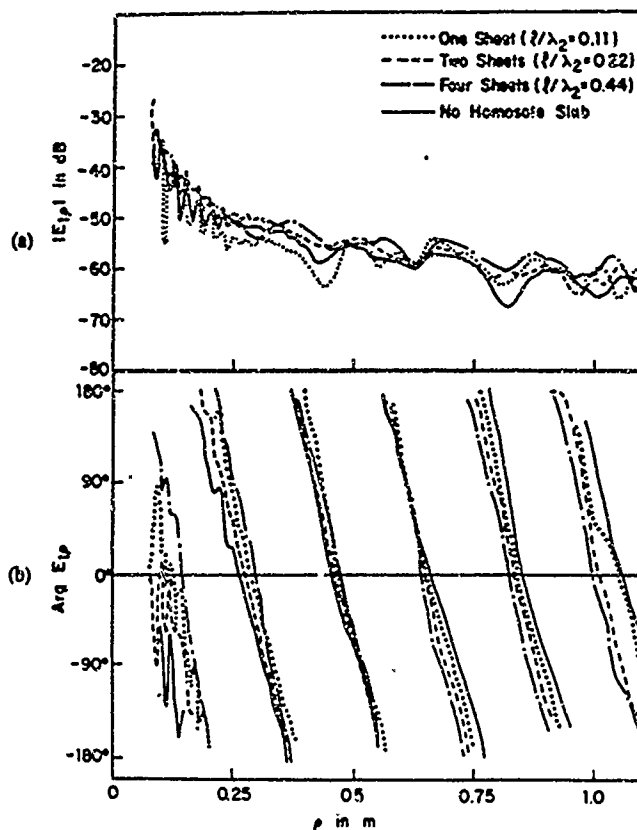


Fig. 4. Measured radial electric field E_r in water (region 1) near boundary with dry homosote slab (region 2) beneath air (region 3); $d = 2.0$ cm, $z = 1.7$ cm, $f = 1.503$ GHz, $\lambda_2 = 12.2$ cm. (a) Amplitude. (b) Phase.

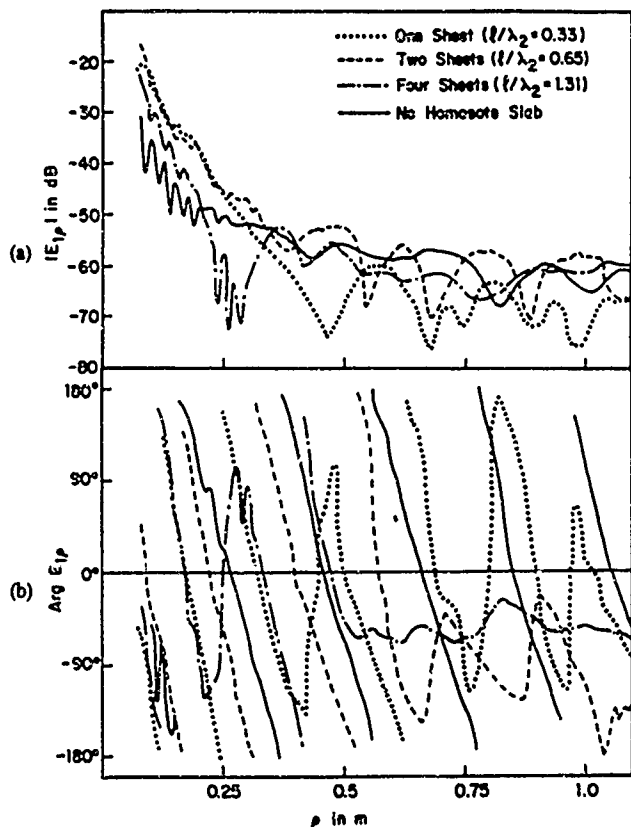


Fig. 5. Measured radial electric field E_r in water (region 1) near boundary with wet homosote slab (region 2) beneath air (region 3); $d = 2.0$ cm, $z = 1.7$ cm, $f = 1.503$ GHz, $\lambda_2 = 4.9$ cm. (a) Amplitude. (b) Phase.

interferes with the lateral wave so that the total field is oscillatory with an interference distance of 2.2 cm. When $\rho \geq 0.25$ m, the amplitude curves decrease smoothly with an interference distance of about 20 cm. This is caused by reflections from the ceiling which is 3.1 m above the water surface. The effects of the ceiling were noted and analyzed previously in conjunction with the experiment by Brown *et al.* [9]. All four amplitude curves are very close. When $\rho < 0.45$ m, the dashed line is about 5 dB higher than the dotted line, and the solid and dot-dashed lines are in between. When $\rho \geq 0.45$ m, these four curves have different interference patterns but are not significantly different in terms of an average field. The corresponding phase curves are plotted in Fig. 4(b). They show that when $\rho \geq 0.2$ m, all four phase curves are essentially straight lines and so represent outward traveling waves with a wavelength of 20 cm. Therefore, the waves propagate through the air. When $\rho < 0.2$ m, the interference with the direct wave causes the phase curves to vary rapidly and in a complicated manner.

The measured fields with the wet homosote slab are plotted in Fig. 5. From the curves in Fig. 5(a), it may be seen that when $\rho \leq 0.2$ m, the amplitudes of the fields with the wet homosote slab are much larger than with it absent. The interference with the direct wave is almost invisible with one and two sheets of homosote, and not significant with four sheets. This means that, for the three-layer problem with the wet homosote layer, the lateral wave has increased significantly in this distance range, while the direct wave in the water is about the same as for the two-layer problem. Therefore, the amplitude curves of the total field are higher than the corresponding curves for the two-layer problem and have smaller oscillation.

In the range from $\rho = 22$ cm to 32 cm, the amplitude curve for the four-sheet case has a deep minimum with an interference distance of about 5 cm. In this case the wavelength in the middle layer is $\lambda_2 = 4.9$ cm. The combined thickness of the four sheets of wet homosote is 6.4 cm, which is more than a wavelength in the medium. Since the loss tangent of the middle medium is only 0.067, $\text{Im}(k_2\rho)$ is smaller than 1.4 in this distance range. Hence, the deep minimum reveals that there is a wave propagating in the middle layer that interferes with the lateral wave propagating in the air. Corresponding deep minima do not appear in the curves for the one- and two-sheet cases. The reason for this is probably that the thickness of one and two sheets of wet homosote is less than the cutoff wavelength in the waveguide of the middle layer. Therefore, there is no propagating wave in the middle layer.

When $\rho \geq 0.4$ m, the amplitude curves with wet homosote are oscillatory with an interference distance of about 20 cm. For the one- and two-sheet cases, the difference in magnitude between each adjacent maximum and minimum is more than 10 dB—much larger than the corresponding value for dry homosote. On the other hand, the associated phase curves for this distance range are not straight lines. This means that the reflected waves from the ceiling have increased to be comparable with the lateral wave propagating along the surface of the wet homosote. The total field is characterized by standing waves. The reflected wave from the ceiling should be about the same for both the two- and three-layer problems. For the former, the lateral wave is larger than the reflected wave so that the lateral wave will decrease with distance faster along the wet homosote than in its absence, i.e., in the two-layer problem. In the range $\rho > 0.4$ m, the dot-dashed line of Fig. 5(a) is also oscillatory, but the variation of its amplitude is smaller than for the dotted and dashed lines. The dot-dashed line in Fig. 5(b) shows that the phase of the total field for four sheets of wet homosote has no significant variation in the range $\rho \geq 0.5$ m. This means that the reflected wave from the ceiling is larger than the lateral wave propagating along the layer of four wet sheets. Therefore, the lateral wave along this four-sheet layer decreases

faster with distance than that along the one- and two-sheet layers. The oscillation of the curves in Fig. 5(a) notwithstanding, in the range of $\rho \geq 0.4$ m the dashed line is about 5 dB higher than the dotted line and the solid line is in between.

The curves of the field E_1 , calculated from (1) are plotted in Fig. 6. Fig. 6(a) is for the dry homosote case, Fig. 6(b) for the wet case. The electrical parameters of the middle medium are taken to be $\epsilon_2^{dy} = 2.7$, $\sigma_2^{dy} = 0.0135$ S/m and $\epsilon_2^{wt} = 16.61$, $\sigma_2^{wt} = 0.0993$ S/m. The thickness of each homosote sheet in the composite slabs is 1.35 cm for dry homosote and 1.6 cm for wet. From Fig. 6(b) it may be seen that, in the range $\rho \geq 0.4$ m, the dashed line is from about 3 to 5 dB higher than the dotted line, with the solid line in between. This agrees with the measured curves of Fig. 5(a). The oscillation caused by the interference of the reflections from the ceiling are, of course, not present in the theoretical curves. The dot-dashed line in Fig. 6(b) is the lowest among all the four curves. Considering the fact that in this range of distance the reflected wave is larger than the lateral wave along the slab of four sheets of wet homosote, the calculated curves of the lateral waves are reasonable. In the near range $\rho \leq 0.2$ m, the theoretical formula (1) shows that the lateral wave of the three-layer problem may be approximated by

$$E_{1\rho} \approx -\frac{i\omega\mu_0 \cos \phi}{2\pi k_1^2} \frac{i}{(\cos k_2 l - i\alpha \sin k_2 l)^2} \cdot \left(\frac{k_3^2}{\rho} + \frac{ik_3}{\rho^2} - \frac{1}{\rho^3} \right) \exp [ik_1(z+d) + ik_3\rho]. \quad (9)$$

A comparison of (9) with the corresponding formula for the two-layer problem shows that the only difference is the extra factor $G = (\cos k_2 l - i\alpha \sin k_2 l)^{-2}$. The factor G is plotted in Fig. 7 as a function of the thickness l of the middle layer. From this figure it may be seen that $|G|$ is usually larger than one. Therefore, in the near range, the lateral wave along the wet homosote slab should be larger than the corresponding value for the two-layer case. The measured curves in Fig. 5(a) show that the fields with the slab of wet homosote are significantly larger than the field with no homosote slab. But the differences among the four curves in Fig. 5(a) are larger than those in Fig. 6(b). The calculated curves do not quantitatively agree well with the measured data. The probable reason for this is the effect of the wave propagating in the middle layer.

Fig. 6(a) shows that the amplitude differences of the field for the different thicknesses of dry homosote are expected to be from about 10 to 15 dB. However, the corresponding measured curves in Fig. 4(a) show relatively little difference. The reason why the calculated curves for the dry case do not agree with the measurements is that the expression (1) is a good approximation only when $|k_1|^2 \gg |k_2|^2 \gg |k_3|^2$ and all three parameters α , δ , and ν are small. The equivalent normalized surface impedance ν of the slab is plotted in Fig. 8 as a function of the thickness of the middle layer. From this figure it may be seen that the factor ν will be larger than one in the dry case. Therefore, formula (1) is not a good approximation. Since the electrical properties of the dry homosote are near those of air, the measured field with dry homosote is similar to the case of no middle layer.

V. CONCLUSION

In summary, the following conclusions may be drawn.

1) The measurements for the wet slab agree quite well with the results calculated from (1). The field at the receiving antenna is a lateral wave which is generated by the transmitting antenna, travels up through the middle layer of homosote, then radially forward in the air, and finally down through the middle layer into the water and to the receiving antenna.

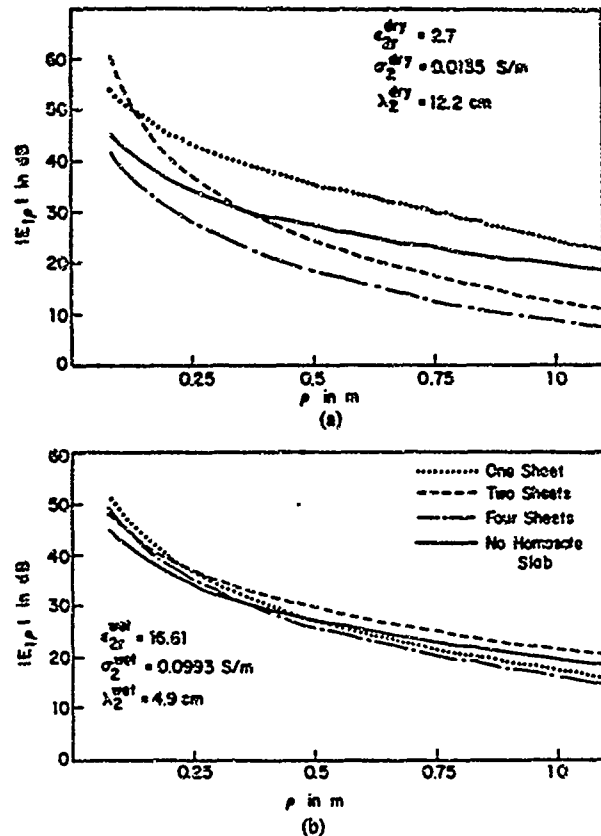


Fig. 6. Calculated amplitude curves of the lateral-wave part of E_1 for a three-layered medium with region 2 a layer of (a) dry homosote, and (b) wet homosote; $d = 2.0$ cm, $z = 1.7$ cm, $f = 1.5$ GHz.

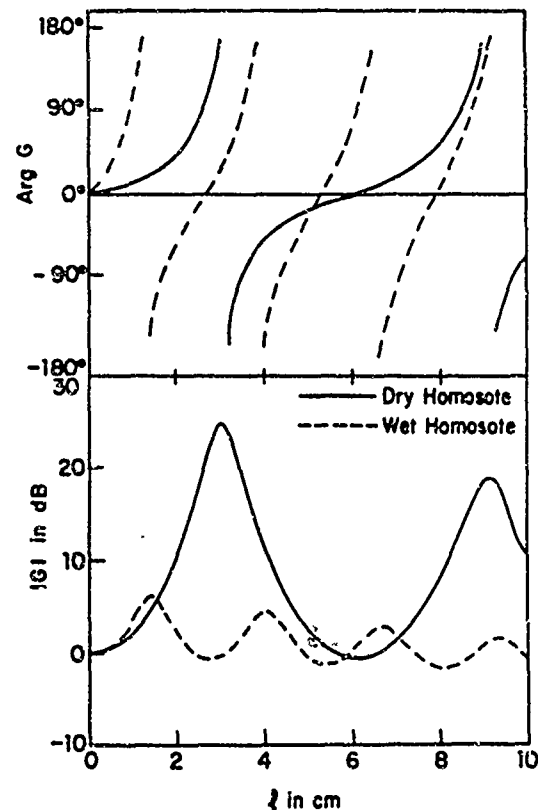


Fig. 7. Magnitude and phase of factor $G = (\cos k_2 l - i\alpha \sin k_2 l)^{-2}$ as a function of l ; $f = 1.5$ GHz.

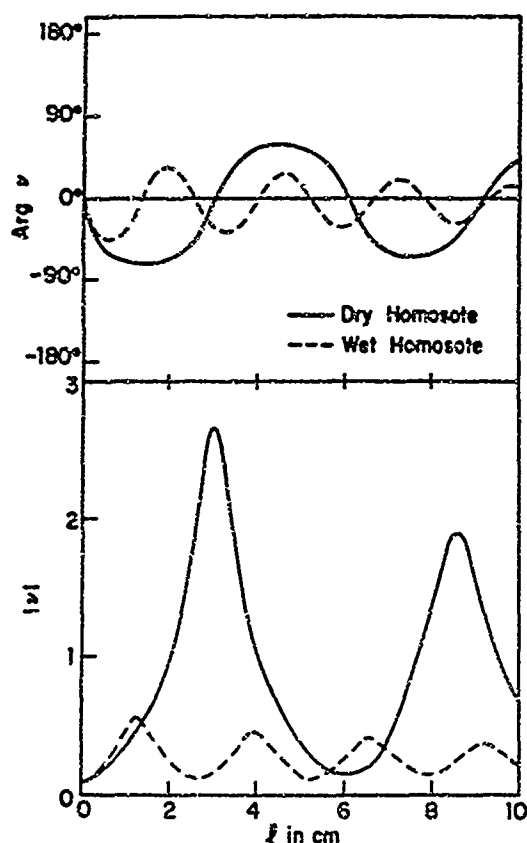


Fig. 8. Magnitude and phase of v , the equivalent normalized surface impedance in region 3, as a function of l ; $f = 1.5$ GHz.

2) In the near range, the field with the wet homosote slab will be larger than the corresponding value without the middle layer.

3) If the thickness of the middle layer is greater than one wavelength in the medium, the amplitude of the wave propagating in the middle layer is not small and the wave will interfere with the lateral wave propagating in the air in a range of distance.

4) When the electrical properties of the middle layer are not very different from those of air (as is the case for dry homosote), the field is similar to that of the two-layer problem.

ACKNOWLEDGMENT

The author is grateful to Professor Ronald W. P. King and Mrs. Margaret Owens for correcting the manuscript.

REFERENCES

- [1] R. W. P. King, "Electromagnetic surface waves: New formulas and their application to determine the electrical properties of the sea bottom," *J. Appl. Phys.*, p. 3612-3624, Nov. 1985.
- [2] C. S. Cox and A. D. ..., "Controlled source electromagnetic exploration of the continental shelves and oceanic lithosphere," presented at the 1983 Int. IEEE/Antennas Propagat. Soc. Symp., Houston, TX, May 1983.
- [3] T. T. Wu and R. W. P. King, "Lateral waves: A new formula and interference patterns," *Radio Sci.*, vol. 17, pp. 521-531, May-June 1982.
- [4] —, "Lateral waves: New formulas for $E_{1\theta}$ and $E_{1\phi}$," *Radio Sci.*, vol. 17, pp. 532-538, May-June 1982; correction, vol. 19, p. 1422, Sept.-Oct. 1984.
- [5] J. M. Dunn, "Electromagnetic lateral waves in layered media," Ph.D. dissertation, Harvard Univ., Cambridge, MA, 1984.
- [6] —, "Lateral waves in three-layered media," presented at the 1984 Int. IEEE/Antennas Propagat. Soc. Symp., Boston, MA, June 1984.

- [7] —, "Lateral wave propagation in a three-layered medium," in preparation.
- [8] A. R. Von Hippel, Ed., *Dielectric Materials and Applications*. Cambridge, MA: M.I.T. Press, 1984.
- [9] M. F. Brown, R. W. P. King, and T. T. Wu, "Experiments on the reflection of lateral electromagnetic waves," *J. Appl. Phys.*, vol. 55, pp. 3927-3933, June 1984.

Antennas in Material Media Near Boundaries with Application to Communication and Geophysical Exploration, Part I: The Bare Metal Dipole

RONOLD W. P. KING, LIFE FELLOW, IEEE

Abstract—The properties of the bare metal dipole embedded in a dissipative medium near a boundary are examined. These include the distribution of current, the driving-point admittance and impedance, and the effective length, with particular reference to antennas in the earth near the air surface at frequencies in the range from 30 to 300 kHz and antennas on the sea floor at frequencies in the range from 0.3 to 3 Hz. The effects of the internal impedance of the copper conductor are included at the low frequencies where they are important.

I. INTRODUCTION

ANTENNAS ARE LOCATED on or near the boundary between two electrically different media for many purposes including communication, remote sensing, and geophysical exploration. Their properties and the fields they generate are strongly influenced by the proximity of the boundary. Some of the effects of a boundary are conveniently represented in terms of a suitable image. Others, like the lateral-wave fields, are in addition to image effects. Notably, the reflected field attributed to the image cancels the direct field along the boundary, so that the lateral-wave field is the only and entire field. This is well understood for vertical antennas erected over the earth or sea [1], and for horizontal wave antennas [2] which are actually eccentrically air-insulated antennas on the surface of the earth. Completely insulated and end-terminated horizontal transmitting and receiving antennas on the surface of the earth are also useful in the discovery and location of buried or submerged objects [3], [4] or electrically different regions in the earth, e.g., reservoirs of oil or deposits of ore. The primary agents of remote sensing in this case are lateral waves. The properties of a buried insulated scattering antenna have been determined [4]. Antennas located on, in or below the surface of the arctic ice are prospective tools in the study of the properties of surface layers of ice and of the ocean below. On a much smaller scale, the properties of transponder antennas embedded under the skin of living organisms depend on the location in the layered region of skin, fat, and muscle [5]. Finally, antennas are used on the sea floor for geophysical studies of the oceanic crust, notably its conductivity [6]–[9]. Measurements for this pur-

pose are usually made at very low frequencies at which the properties of insulated antennas are very different from those at higher frequencies.

This paper is concerned with the properties of antennas embedded in a medium like soil, sand, ice, fresh or salt water near its boundary with air and with similar antennas located in the salt water near the oceanic crust under the sea floor. In all cases and as shown in Fig. 1, the transmitting and receiving antennas under study are located in region 1, $z \geq 0$, with the complex wavenumber $k_1 = \beta_1 + i\alpha_1 = \omega[\mu_0(\epsilon_1 + i\sigma_1/\omega)]^{1/2}$ where β_1 is the phase constant and α_1 the attenuation constant. The wavenumber in the adjacent region 2, $z \leq 0$, is $k_2 = \beta_2 + i\alpha_2 = \omega[\mu_0(\epsilon_2 + i\sigma_2/\omega)]^{1/2}$. The two regions are characterized by their respective permittivities ϵ_j , conductivities σ_j , and permeabilities μ_j , $j = 1, 2$. For all media considered here, it is assumed that $\mu_1 = \mu_2 = \mu_0$ for air. In either region the wavelength is $\lambda_j = 2\pi/\beta_j$, the skin depth $d_{sj} = 1/\alpha_j$. The wave impedance is $\zeta_j = \omega\mu_0/k_j$ and the normalizing factor $\Delta_j = \zeta_0\beta_j/\omega\mu_0$ where $\zeta_0 = (\mu_0/\epsilon_0)^{1/2} = 120\pi$ ohms. When region 2 is air, $\sigma_2 = 0$, $\epsilon_2 = \epsilon_0$, and $k_2 = \beta_2 = \omega(\mu_0\epsilon_0)^{1/2}$; $\alpha_2 = 0$. When the frequency is sufficiently low so that $\epsilon_j \ll \sigma_j/\omega$, $k_j = (i\omega\mu_0\sigma_j)^{1/2} = (1+i)(\omega\mu_0\sigma_j/2)^{1/2}$ and $\beta_j = \alpha_j$. Numerical values for many of these quantities are listed in Table I for two sets of frequencies, viz., $f = 0.3, 1$ and 3 Hz when region 1 is sea water with $\sigma_1 = 4$ S/m, $\epsilon_{1r} = 80$; and $f = 0.3 \times 10^5, 10^5$ and 3×10^5 Hz when region 1 is moist earth with $\sigma_1 = 10^{-3}$ S/m, $\epsilon_{1r} = 8$.

Also listed in Table I is the electrical radius $|k_c a|$ of the copper conductor forming the antenna with $|k_c| = (\omega\mu_0\sigma_c)^{1/2}$ and $\sigma_c = 5.65 \times 10^7$ S/m.

II. THE BARE CYLINDRICAL ANTENNA IN A DISSIPATIVE MEDIUM

For some applications and as terminations for insulated antennas in the earth or ocean, the bare metal cylinder is useful. Complete general formulas for the current distribution in and the admittance of such an antenna are available [10] as a function of the half-length h and the radius a when located in an infinite homogeneous and isotropic medium with arbitrary values of permittivity and conductivity. The formulas assume that the very large but finite conductivity of copper ($\sigma_c = 5.65 \times 10^7$ S/m) or other metals is well approximated by $\sigma_c \sim \infty$. This is true at all but the very lowest frequencies. The normalized admittance $Y/\Delta_1 = (G - iB)/\Delta_1$ and impedance $Z\Delta_1 = (R - iX)\Delta_1$ as computed with these formulas for antennas in the two frequency ranges and in the two media

Manuscript received August 28, 1985. This work was supported in part by the Joint Services Electronics Program under Contract N00014-84-K-0465 with Harvard University.

R. W. P. King is with the Gordon McKay Laboratory, Harvard University, Cambridge, MA 02138. During the preparation of this manuscript he served as IBM Visiting Distinguished Scholar at Northeastern University.

IEEE Log Number 8407358.

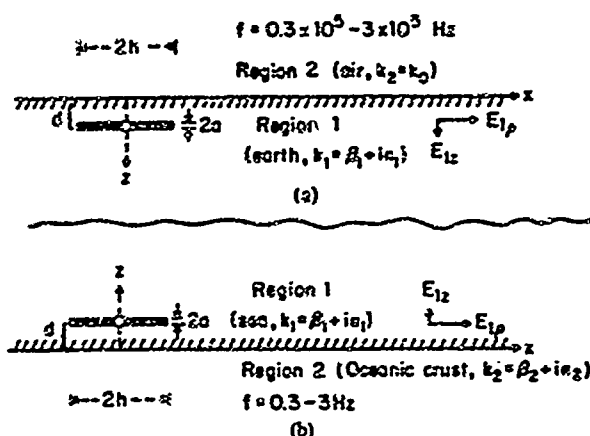


Fig. 1. Bare copper antenna. (a) In earth near air surface. (b) In sea near sea floor.

TABLE I
QUANTITIES USEFUL FOR ANTENNAS IN A DISSIPATIVE REGION

Sea Water: $\epsilon_1 = 80$, $\sigma_1 = 4$ S/m			
f (Hz)	0.3	1	3
β_1 (m ⁻¹)	2.18×10^{-3}	3.97×10^{-3}	6.83×10^{-3}
α_1 (m ⁻¹)	2.18×10^{-3}	3.97×10^{-3}	6.83×10^{-3}
β_1^{-1} (m)	458.7	251.9	145.3
λ_1 (m)	2884	1893	913
a (mm)	5.2	5.2	5.2
a/λ_1	1.8×10^{-6}	2.3×10^{-6}	5.7×10^{-6}
$ k_c a $	0.03	0.12	0.19
r' (N/m)	2.08×10^{-4}	2.08×10^{-4}	2.08×10^{-4}
$2\pi r'/\omega\mu_0$	391.7	135.2	65.2
Δ_1	3.45×10^5	1.90×10^5	1.094×10^5

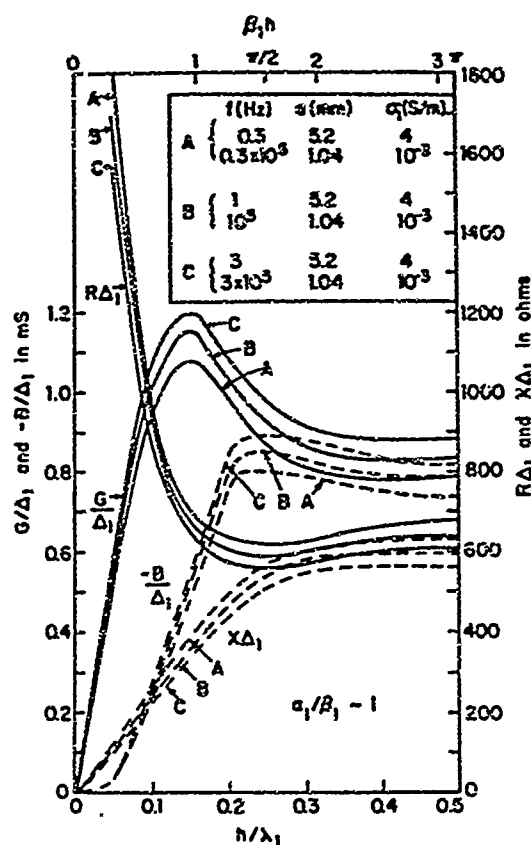
Moist Earth: $\epsilon_1 = 8$, $\sigma_1 = 10^{-3}$ S/m			
f (Hz)	3×10^4	10^5	3×10^5
β_1 (m ⁻¹)	1.09×10^{-3}	2.03×10^{-3}	3.97×10^{-3}
α_1 (m ⁻¹)	1.07×10^{-3}	1.94×10^{-3}	3.21×10^{-3}
β_1^{-1} (m)	91.7	49.5	27.2
λ_1 (m)	878	311	171.2
a (mm)	1.04	1.04	1.04
a/λ_1	1.8×10^{-6}	2.3×10^{-6}	6.1×10^{-6}
$ k_c a $	3.8	6.94	12.02
r' (N/m)	0.73×10^{-3}	1.23×10^{-3}	2.23×10^{-3}
$2\pi r'/\omega\mu_0$	0.195	0.101	0.059
Δ_1	17.34	9.67	5.84

$$k_1 = \beta_1 + i\alpha_1 = \omega(\mu_0\epsilon_1)^{1/2}(1 + i\sigma_1/\omega\epsilon_1)^{1/2}; \quad \lambda_1 = 2\pi/\beta_1; \quad \Delta_1 = (i\omega\mu_0\sigma_1)^{1/2};$$

$$\Delta_1 = \omega\beta_1/\omega\mu_0 = \beta_1/\beta_0; \quad r' = r' - i\sigma' = r_0 \frac{k_c a}{2} \frac{J_0(k_c a)}{J_1(k_c a)};$$

$$r' - r_0 = 1/\pi a^2 \sigma_1, \quad |k_c a| \leq 2; \quad r' \sim -ik_c/3\pi\sigma_1, \quad |k_c a| \geq 5.$$

listed in Table I are shown in Fig. 2 as functions of h/λ_1 where $\lambda_1 = 2\pi/\beta_1$. These graphs apply specifically to bare antennas with radius $a = 1.04$ mm (5.2 mm) in moist earth (sea water) at $f = 0.3 \times 10^5$ to 3×10^5 Hz (0.3 to 3 Hz). They show that the conductance rises from zero to a maximum near $h/\lambda_1 \sim 0.15$ or $\beta_1 h \sim 1$ and then decreases to an approximately constant value beyond $h/\lambda_1 \sim 0.25$ or $\beta_1 h \sim \pi/2$. Similarly,

Fig. 2. Normalized admittance $Y/\Delta_1 = (G - iB)/\Delta_1$ and impedance $Z\Delta_1 = (R - iX)\Delta_1$ of bare, perfectly conducting antenna.

the resistance decreases from large values to a minimum near $h/\lambda_1 \sim 0.25$ or $\beta_1 h \sim \pi/2$, beyond which it remains sensibly constant. These values suggest that when $\alpha_1/\beta_1 \sim 1$, the maximum useful length of a bare antenna is $h \sim \lambda_1/4$ or $\beta_1 h \sim \pi/2$. This is a consequence of the fact that the current in the antenna decays to virtually zero beyond $x \sim \lambda_1/4$ when $h \geq \lambda_1/4$. Similar graphs for a range of values of α_1/β_1 are shown in Fig. 3 for the admittance and in Fig. 4 for the impedance. It is seen that as α_1/β_1 is reduced, the useful length of the antenna increases.

In order to investigate the effect of the finite conductivity of the metal conductor, it is necessary to reformulate and resolve the integral equation for the current with the actual internal impedance per unit length of the conductor. This is

$$z' = r' - iX' = r_0 \frac{k_c a}{2} \frac{J_0(k_c a)}{J_1(k_c a)}; \quad r_0 = (\pi a^2 \sigma_c)^{-1}. \quad (1)$$

Important limiting forms are

$$|k_c a| \leq 2: \quad r' \sim r_0; \quad X' = \omega l' \sim \frac{\omega\mu_c}{8\pi}, \quad (2a)$$

$$|k_c a| \geq 5: \quad r' \sim X' \sim \frac{1}{2\pi a} \left(\frac{\omega\mu_c}{2\sigma_c} \right)^{1/2}. \quad (2b)$$

This has been carried out [11] and the following expression for

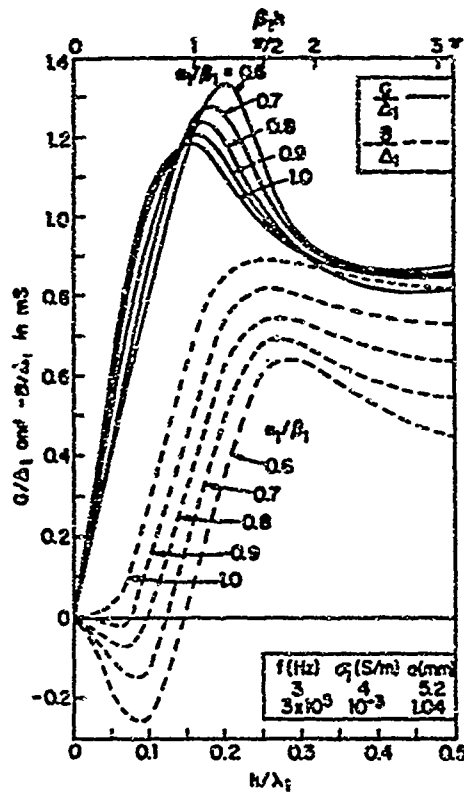


Fig. 3. Normalized admittance $Y/\Delta_1 = (G - jB)/\Delta_1$ of bare, perfectly conducting antenna with α_1/β_1 as parameter.

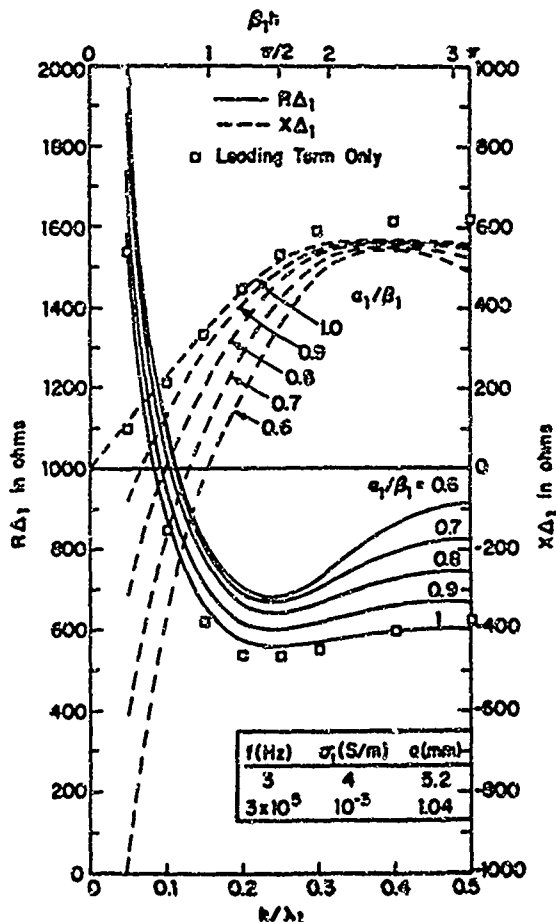


Fig. 4. Normalized impedance $Z\Delta_1 = (R - jX)\Delta_1$ of bare, perfectly conducting antenna with α_1/β_1 as parameter.

the current obtained:

$$I_x(x) = -\frac{i2\pi k_1^2 V_0^e}{\omega\mu_0 k_1 \Psi \cos k_1 h} \left[\sin k_1(h-|x|) + T_U(\cos k_1 x - \cos k_1 h) + T_D \left(\cos \frac{1}{2} k_1 x - \cos \frac{1}{2} k_1 h \right) \right], \quad (3)$$

where

$$k_1 = \beta_1 + i\alpha_1 = k_1 \left(1 + \frac{i4\pi z^1}{\omega\mu_0 \Psi} \right)^{1/2} \quad (4)$$

is the complex wavenumber of the current in the antenna. Formulas for T_U and T_D are given in [11]. Note that the wavenumber appearing in the coefficient of T_D is k_1 and not k_2 . When $|k_2|$ is significantly greater than $|k_1|$, the contribution to the current by the third term in (3) will decay more slowly than the contributions by the other two. This can have only a negligible effect on the current near the driving point. Its contribution to the current elsewhere is also relatively small when $\beta_1 \sim \alpha_1$. In this case the leading first term in (3) is a generally adequate approximation. That is,

$$I_x(x) \sim V_0^e Y \frac{\sin k_1(h-|x|)}{\sin k_1 h}; \quad Y = -\frac{i2\pi k_1^2 \tan k_1 h}{\omega\mu_0 \Psi k_1}, \quad (5)$$

where

$$\Psi = 2 \ln(h/a) - 2. \quad (6)$$

It is seen from (5) that $I_x(x)$ and Y depend only on k_1 and not on k_2 when $|k_1 h|^2 \ll 3$. Note that $|k_1 h| < |k_2 h|$.

The formula (4) for k_1 permits the definition of the low-frequency range in which the internal impedance is significant as distinct from higher frequencies for which the copper conductor can be approximated by a perfect conductor. Specifically, let the higher frequencies be defined by

$$(\omega\mu_0)^2 \gg \left(\frac{4\pi r^1}{\Psi} \right)^2 \quad \text{or} \quad \omega\mu_0 \gg 4\pi r^1, \quad (7)$$

since $\Psi \sim 20$. With $r^1 \sim 1/\pi a^2 \sigma_c$ and $\sigma_c = 5.65 \times 10^7$ S/m,

$$f \geq \frac{r^1 \times 10^7}{2\pi} \approx \frac{10^7}{2\pi^2 a^2 \sigma_c} \approx \frac{10^{-2}}{a^2} = \begin{cases} 400 \text{ Hz, } a = 5.2 \text{ mm} \\ 10^4 \text{ Hz, } a = 1.04 \text{ mm.} \end{cases} \quad (8)$$

Thus, the dividing line is between $f = 400$ Hz and 10 kHz depending on the cross-sectional size of the copper conductor. In the following analysis, antennas in the earth will be considered with $f \sim 10^5$ Hz and $a \sim 1$ mm so that the conductor can be treated as if perfect. Also considered are antennas on the sea floor with $a = 5.2$ mm when $f \sim 1$ Hz and $f \sim 1$ kHz (in Part II of this paper). For the latter the internal impedance is negligibly small, for the former it is dominant. For earth with $\sigma_1 \sim 10^{-3}$ S/m, $\epsilon_1 \sim 8$ and $f \leq 10^6$ Hz and for

sea water with $\sigma_1 \sim 4 \text{ S/m}$, $\epsilon_1 \sim 80$ and $f \leq 10 \text{ Hz}$, $\omega\epsilon_1/\sigma_1$ is sufficiently small to permit the approximation $k_1^2 \sim i\omega\mu_0\sigma_1$. This simplifies (5) since now

$$Y = G - iB = \frac{2\pi\sigma_1 \tan k_1 h}{\Psi} = Z^{-1}. \quad (9)$$

The driving-point impedance is

$$Z = R - iX = \frac{\Psi}{2\pi\sigma_1} k_1 \cot k_1 h. \quad (10)$$

In (9) and (10),

$$k_1 = \beta_1 + i\alpha_1 = [i\omega\mu_0\sigma_1 - 4\pi z_1'/\Psi]^{1/2}. \quad (11)$$

Explicit formulas for β_1 and α_1 can be written down, but they are quite long and not actually required since all desired numerical values are easily computed from (11). With (10) and the relation

$$\cot k_1 h = \frac{\sin 2\beta_1 h - i \sinh 2\alpha_1 h}{\cosh 2\alpha_1 h - \cos 2\beta_1 h}, \quad (12)$$

it follows that

$$R = \frac{\Psi}{2\pi\sigma_1} \left[\frac{\beta_1 \sin 2\beta_1 h + \alpha_1 \sinh 2\alpha_1 h}{\cosh 2\alpha_1 h - \cos 2\beta_1 h} \right], \quad (13)$$

$$X = \frac{\Psi}{2\pi\sigma_1} \left[\frac{\beta_1 \sinh 2\alpha_1 h - \alpha_1 \sin 2\beta_1 h}{\cosh 2\alpha_1 h - \cos 2\beta_1 h} \right]. \quad (14)$$

The resistance R in (13) consists of two parts in the form $R = R^i + R^e$ where R^i is associated with the power dissipated in heating the conductor and R^e with the power transferred to the ambient medium. The former is readily evaluated as follows.

$$I_x(0)I_x^*(0)R^i = r^i \int_{-h}^h I_x(x)I_x^*(x) dx, \quad (15)$$

where $I_x(x)$ is given by (5). The result is

$$R^i = \frac{r^i}{\alpha_1 \beta_1} \left[\frac{\beta_1 \sinh 2\alpha_1 h - \alpha_1 \sin 2\beta_1 h}{\cosh 2\alpha_1 h - \cos 2\beta_1 h} \right]. \quad (16)$$

It follows that

$$R^e = R - R^i. \quad (17)$$

The corresponding formulas for the electrically short antenna are of particular interest and clarity. Subject to

$$\beta_1 h < \alpha_1 h < 1, \quad (18)$$

the expansion in series of the trigonometric and hyperbolic functions leads to

$$R \sim \frac{\Psi}{2\pi\sigma_1 h} \left[1 + \frac{1}{3} h^2 (\alpha_1^2 - \beta_1^2) \right] = \frac{\Psi}{2\pi\sigma_1 h} + \frac{2}{3} h r^i, \quad (19)$$

where the last step follows from (11) which gives $\alpha_1^2 - \beta_1^2 =$

$$X \sim \frac{\alpha_1 \beta_1 h \Psi}{3\pi\sigma_1} = \frac{\omega\mu_0 \Psi h}{6\pi}, \quad (20)$$

where the last step follows from (11) which gives $2\alpha_1 \beta_1 \sim \omega\mu_0 \sigma_1$. Also, from (16) and (17),

$$R^i \sim \frac{2}{3} h r^i; \quad R^e = R - R^i \sim \frac{\Psi}{2\pi\sigma_1 h}. \quad (21)$$

The resistances R , R^i , and R^e are shown in Fig. 5 as a function of h/λ_1 for a copper conductor with radius $a = 5.2 \text{ mm}$ in sea water ($\sigma_1 = 4 \text{ S/m}$) at $f = 3 \text{ Hz}$. A scale is also given for the normalized resistances $R\Delta_1$, $R^i\Delta_1$, and $R^e\Delta_1$ to permit direct comparison with Fig. 4 (curve with $\alpha_1/\beta_1 = 1$) which applies when $r^i = 0$. In this case, $R = R^e$ since $R^i = 0$. Note that the curve for $R = R^e$ in Fig. 4 is similar to that for R^e in Fig. 5 but not the same. This is because the current distribution changes from $\sin k_1(h - |x|)$ when r^i is significant to $\sin k_1(h - |x|)$ when $r^i = 0$. It is seen from Fig. 5 that the contribution to the total resistance by the internal resistance is insignificant for sufficiently short antennas and becomes comparable and somewhat greater when $h > 0.1 \lambda_1$. The constancy of all resistances and the reactance when $h \geq 0.25 \lambda_1$ indicates that the current on the conductor is reduced to near zero for $x \geq 0.25 \lambda_1$ for all lengths $h > 0.25 \lambda_1$.

III. EFFECTIVE LENGTH AND FIGURE OF MERIT OF BARE ANTENNA

The purpose of a transmitting antenna is to generate a useful electromagnetic field at a distance. The magnitude of such a field is determined by the electric moment of the antenna. When the antenna is in region 1 (with wavenumber $k_1 = \beta_1 + i\alpha_1$) near a boundary with region 2 ($k_2 = \beta_2 + i\alpha_2$) and $|k_1|^2 \gg |k_2|^2$, the only significant field along the boundary surface in either region is due to the lateral wave which travels along the boundary in region 2 with the wavenumber k_2 . Thus, the effective half-length for a dipole of length $2h$ as obtained from the first term in (5) is

$$h_e(\phi_0) = \int_0^h \frac{\sin k_1(h-x)}{\sin k_1 h} e^{-ik_2 x \cos \phi_0} dx, \quad (22)$$

where ϕ_0 is the angle between the antenna and the direction of observation. The direction of maximum field is $\phi_0 = 0$ and the associated maximum effective length is

$$h_e(0) = h_e = \int_0^h \frac{\sin k_1(h-x)}{\sin k_1 h} e^{-ik_2 x} dx. \quad (23a)$$

This integrates into

$$h_e = \frac{k_1}{k_1^2 - k_2^2} \frac{\cos k_2 h - \cos k_1 h}{\sin k_1 h}. \quad (23b)$$

For the electrically short antenna with $\beta_1 h < \alpha_1 h < 1$,

$$|h_e| = h/2. \quad (24)$$

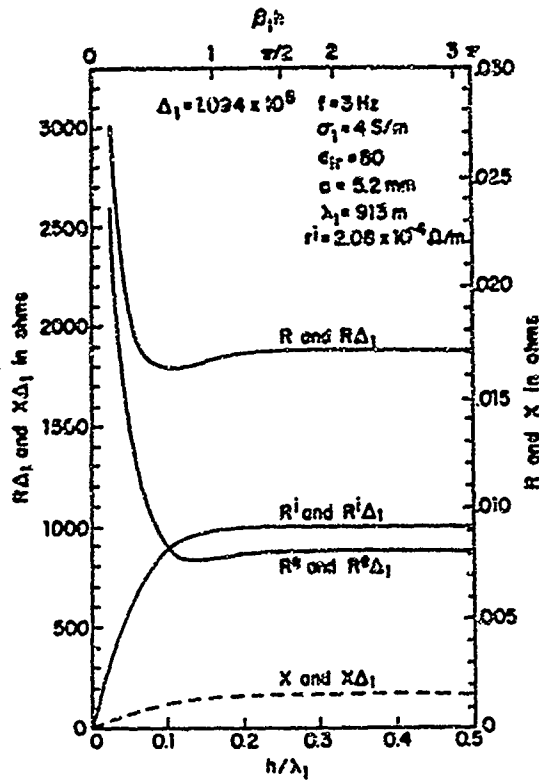


Fig. 5. Impedance $Z = R - iX$ of bare, imperfectly conducting antenna.

Since $|k_2|^2 \ll |k_1|^2 \leq |k_l|^2$, it is usually adequate to approximate $\cos k_2 h \sim 1$ so that

$$|h_e| = \frac{1}{k_l} \tan(k_l h/2) \\ = \frac{1}{(\beta_l^2 + \alpha_l^2)^{1/2}} \left[\frac{\cosh \alpha_l h - \cos \beta_l h}{\cosh \alpha_l h + \cos \beta_l h} \right]^{1/2} \quad (25)$$

When $k_l \sim k_1 = \beta_1(1 + i)$, the useful range is when $|k_l h| \leq 2$, so that $|h_e| \sim h/2$. Alternatively, at very low frequencies, $\beta_l \ll \alpha_l$ and $|h_e| \sim (1/\alpha_l) \tanh(\alpha_l h/2)$.

The quantity $|h_e|/h$ is shown graphically in Fig. 6 (dashed lines) for the bare dipole in the two ranges of interest. These are $f \sim 10^5$ Hz with $\sigma_1 = 10^{-3}$ S/m, $a = 1.04$ mm, where the internal impedance is of no significance, and $f \sim 1$ Hz with $\sigma_1 = 4$ S/m, $a = 5.2$ mm, where the internal impedance is dominant. It is seen that when the internal impedance is negligible, $|h_e|/h$ remains close to 0.5 up to $h/\lambda_1 \sim 0.25$, but decreases very rapidly from 0.5 when, at sufficiently low frequencies, r^i is dominant.

In order to generate a large electric moment, it is possible to increase the current to compensate for a small effective length, but only up to the current-carrying capacity of the conductor and the available power. It is evidently desirable to have as large an effective length as possible and use a minimum of power. Accordingly the ratio $[2|h_e J_x(0)|/|J_x^2(0)|R]$ is to be as large as possible. A related useful figure of merit is defined for unit current in terms of the electrical effective length in the ambient medium, $\beta_1 |h_e|$, and the normalized resistance, $R\Delta_1$,

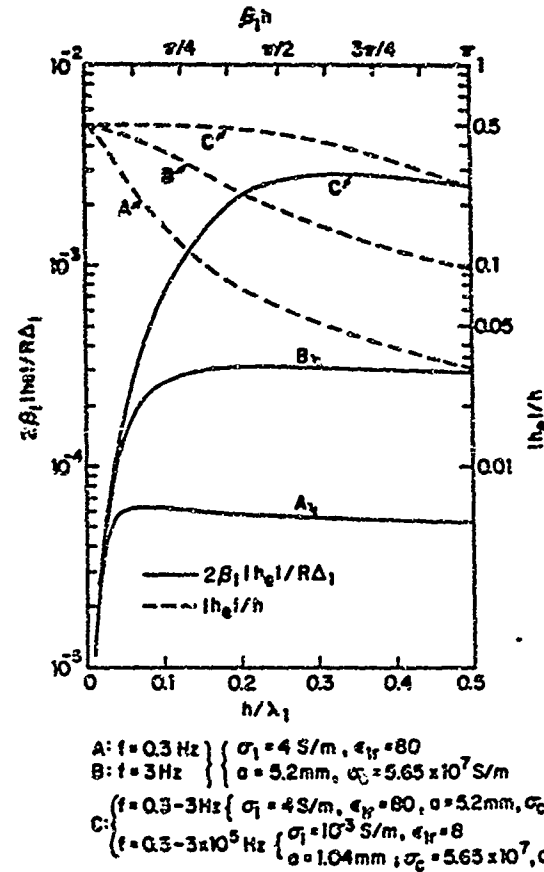


Fig. 6. Ratio of electrical effective length to normalized resistance and ratio of effective length to actual length for bare antenna in dissipative medium.

where $\Delta_1 = \beta_1 \zeta_0 / \omega \mu_0 = \beta_1 / \beta_0$. It is

$$F = \frac{2\beta_1 |h_e|}{R\Delta_1} \quad (26)$$

This quantity is also shown in Fig. 6 (in solid lines) specifically for antennas in sea water at $f = 0.3$ and 3 Hz for which the internal impedance is important and for antennas in earth at $f = 0.3 \times 10^5$ and $f = 3 \times 10^5$ Hz where the internal impedance contributes negligibly and the antennas behave like perfect conductors. It is seen that in this last case the ratio has a maximum near $h/\lambda_1 \sim 0.3$ where $|h_e|/h \sim 0.42$. At $f = 3$ Hz, the maximum of F is at $h/\lambda_1 \sim 0.2$ where $|h_e|/h \sim 0.23$; at $f = 0.3$ Hz, F_{\max} is at $h/\lambda_1 \sim 0.075$ where $|h_e|/h \sim 0.2$.

IV. THE BARE CYLINDRICAL ANTENNA IN A DISSIPATIVE MEDIUM NEAR A BOUNDARY

In the applications to be studied, the antenna is located in a dissipative medium region 1 ($z \geq 0$, k_1 ; earth, sea water) at a small distance d from its boundary ($z = 0$) with a region 2 ($z \leq 0$, k_2 ; air, sea floor); $|k_1|^2 \gg |k_2|^2$. Since $|k_1 d| \ll 1$, the antenna in region 1 is strongly affected by the adjacent, quite different region 2. Since $|k_1|^2 \gg |k_2|^2$, the reflection coefficient seen by the antenna is $(k_1 - k_2)/(k_1 + k_2) \sim 1$. This means that the reflected electric field is almost equal to and in phase with the incident electric field, the reflected magnetic field almost equal to and in phase opposition to the

incident magnetic field. This condition is approximated by an image antenna at $z = -d$ with current and voltage in phase with those in the actual antenna, as shown in Fig. 7. Since $|2k_1 d| \ll 1$, the two antennas behave like a single one at $z = 0$ with effective radius $a_e = (2ad)^{1/2}$. Hence, (6) becomes

$$\Psi_e = \frac{1}{2} \ln(h/a_e) - 2. \quad (27)$$

Since only half the current is in the antenna, this is obtained from (5) with (9) and (27). Thus

$$I_{1x}(x) = \frac{V_1^e Y_e \sin k_1(h - |x|)}{2 \sin k_1 h}; \quad Y_e = \frac{2\pi\sigma_1 \tan k_1 h}{\Psi_e \cdot k_1}, \quad (28)$$

where Y_e is obtained from (9). The driving-point admittance Y_1 and impedance Z_1 are

$$Y_1 = \frac{Y_e}{2} = \frac{Y\Psi}{2\Psi_e}; \quad Z_1 = 2Z_e = \frac{2Z\Psi_e}{\Psi}, \quad (29)$$

where Y and Z are the quantities for the antenna when far from the boundary.

The internal resistance $R_1^i = R^i$ is unaffected by the boundary if this is not so close as to cause a proximity effect. The external resistance R_1^e is approximately double R^e . Graphs of R_1^i , R_1^e and R_1^t are shown in Fig. 8 as functions of h/λ_1 for both $f = 3$ Hz and $f = 0.3$ Hz with $d = 10.4$ cm. For the higher frequencies at which the internal impedance is negligible, the admittance or impedance of an antenna at a small distance d from a boundary is readily obtained from Fig. 3 or Fig. 4 with (29), (6) and (27). In Table II of the next section, $d = 50$ cm for $f = 30$ and 300 kHz.

V. SUMMARY AND CONCLUSION

The theory of the bare metal dipole antenna has been developed in terms of two specific applications. These are the subsurface antenna for communication between two points below the surface of the earth and the sea-floor antenna for use in studies of the conductivity of the oceanic crust. For the former the frequency range from 30 to 300 kHz is useful, for the latter very low frequencies in the range from 0.3 to 3 Hz are needed to penetrate sufficiently deeply into the lithosphere. In both locations the transmitting antenna is in a region of large wavenumber (region 1), adjacent to a region with a much smaller wavenumber (region 2). Furthermore, since the receiving antenna is in a similar location at a more or less distant point along the boundary, the received electromagnetic field is a surface or lateral wave that travels along the boundary in the region of smaller wavenumber—air for antennas near the surface of the earth, the crustal rock for antennas near the sea floor. Since the lateral wave must travel approximately vertically in region 1 from the transmitting antenna to the boundary, then radially in region 2 along the boundary, and finally vertically in region 1 to the receiving antenna, horizontal antennas parallel to the boundary are superior to vertical ones.

The principal differences between the antennas near the air

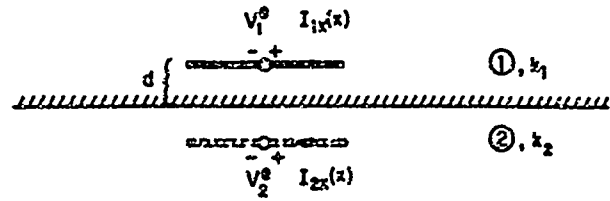


Fig. 7. Horizontal antenna near boundary with image; $V_2^e = V_1^e$, $I_2(x) = I_1(x)$.

surface and those near the sea floor are a consequence of the large difference in frequency. At the very low frequencies used on the sea floor the internal impedance of the copper conductor is important, whereas it is negligible at the higher frequencies used near the air surface. This means that whereas the bare metal antenna is highly efficient in transferring power from the antenna to the exterior media (regions 1 and 2) at the higher frequencies, it is subject to an unavoidable large internal power loss in heating the antenna at the low frequencies.

The properties of bare copper antennas in the two applications are summarized in Table II where columns 2 and 3 apply to a region 1 of sea water over rock, columns 4 and 5 to moist earth under air. The corresponding frequencies are $f = 0.3$ and 3 Hz, and $f = 0.3 \times 10^5$ and 3×10^5 Hz, with copper antennas respectively with radii $a = 5.2$ mm and 1.04 mm. The maximum figure of merit occurs with antennas of half length h_m obtained from Fig. 6. Also obtained from this figure is the effective length $|h_e|$ corresponding to this length. The associated driving-point impedances Z for the antenna far from the boundary and Z_1 at the distance d from the boundary are obtained from Figs. 2, 4, 5 and 8 or the formulas from which these were calculated.

The maximum currents for the copper conductors are those suggested for insulated wire with the specified radii. Bare conductors in contact with an ambient medium like the earth or sea can handle considerably more current without overheating. The dipole moments for the specified maximum currents and effective lengths are seen to be quite large at the low frequencies because the conductor is much thicker and can handle much more current. This is necessary in salt water and for the transmission in the crustal rock or sediment which at these low frequencies behaves like a conductor with an exponential attenuation with distance. The total power supplied with the specified maximum currents is also listed. Because of the extremely low resistances of the thick low frequency antennas in the highly conducting salt water, the power supplied at the low frequencies is much less than at the higher frequencies and about half of this is actually dissipated by the axial current in heating the conductor. The antennas in the relatively poorly conducting earth at the higher frequencies transfer all of the input power to the ambient earth, partly by means of the radial current, partly in radiation by the axial current.

The use of the bare antenna as a termination for an insulated antenna is considered in Part II of this paper.

TABLE II
EFFECTIVE LENGTHS, IMPEDANCES, AND ELECTRIC MOMENTS

f (Hz)	Dry Water $\sigma_1 = 4 \text{ S/m}; \epsilon = 8.2 \text{ mm}$		Moist Earth $\sigma_1 = 10^{-3} \text{ S/m}; \epsilon = 1.04 \text{ mm}$	
	0.3	3	0.3×10^3	3×10^3
λ_1 (meters)	2894	913	573	171.3
Δ_0/λ_1	0.075	0.3	0.3	0.3
k_{eff} (meters)	216.3	182.6	172.5	51.2
$ k_0 /k_{\text{eff}}$	0.21	0.33	0.62	0.62
$ k_0 $ (meters)	48.4	62.0	72.6	21.6
ϵ_1/β_1	1	1	0.08	0.07
Δ_1	2.45×10^3	1.094×10^3	17.24	5.64
$Z\Delta_1 = R\Delta_1 - iX\Delta_1$	6153 - i35	1800 - i100	630 - i200	570 - i360
$Z = R - iX (\Omega)$	$(17.9 - i0.16) \times 10^{-3}$	$(1.7 - i0.16) \times 10^{-3}$	$35.8 - i34.6$	$97.6 - i94.2$
δ (cm)	10.4	10.4	50	50
$S_1 = R_1 - iX_1 (\Omega)$	$(2.94 - i0.023) \times 10^{-3}$	$(2.74 - i0.25) \times 10^{-3}$	$69.3 - i47.6$	$126.9 - i132.5$
I_{max} (A)	325	325	20	20
$2I_{\text{max}} k_0 $ (A-m)	29,510	27,200	2804	354
$ I_{\text{max}} ^2 R$ (W)	1.01	1.80	14.2	39.0
$ I_{\text{max}} ^2 R_1$ (kW)	1.64	2.89	19.7	50.8

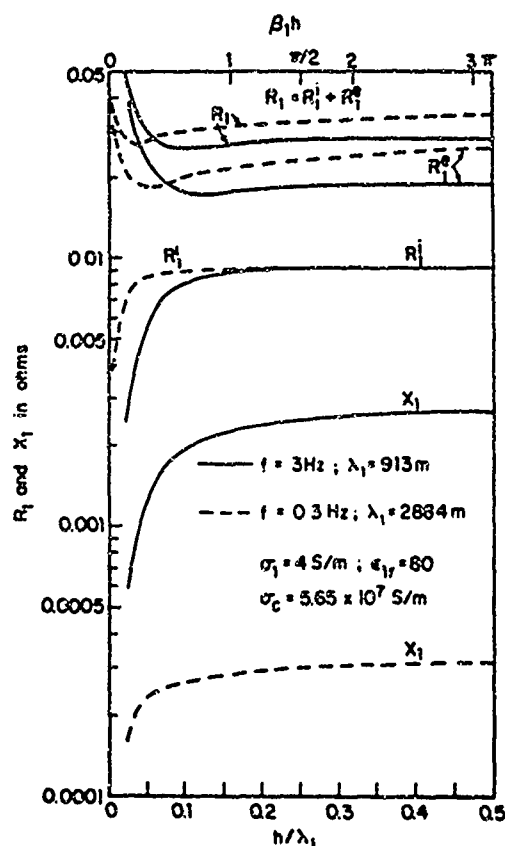


Fig. 8. Impedance $Z_1 = R_1 - iX_1$ of bare copper dipole (radius $a = 5.2$ mm; half-length h) at $d = 10.4$ cm above the sea floor.

REFERENCES

- [1] R. W. P. King and M. F. Brown, "Lateral electromagnetic waves along plane boundaries: A summarizing approach," *Proc. IEEE*, vol. 72, pp. 595-611, May 1984.

- [2] R. W. P. King, "The wave antenna for transmission and reception," *IEEE Trans. Antennas Propagat.*, vol. AP-31, pp. 956-965, Nov. 1983.
- [3] —, "Scattering of lateral waves by buried or submerged objects. I. The incident lateral-wave field," *J. Appl. Phys.*, vol. 57, pp. 1453-1459, Mar. 1985.
- [4] —, "Scattering of lateral waves by buried or submerged objects. II. The electric field on the surface above a buried insulated wire," *J. Appl. Phys.*, vol. 57, pp. 1460-1472, Mar. 1985.
- [5] R. W. P. King, S. Prasad, and B. H. Sandler, "Transponder antennas in and near a three-layered body," *IEEE Trans. Microwave Theory Tech.*, vol. MTT-28, pp. 586-596, June 1980.
- [6] P. D. Young and C. S. Cox, "Electromagnetic active source sounding near the East Pacific Rise," *Geophys. Res. Lett.*, vol. 8, pp. 1043-1046, 1981.
- [7] R. N. Edwards, L. K. Law, and J. M. DeLaurier, "On measuring the electrical conductivity of the oceanic crust by a modified magnetometric resistivity method," *J. Geophys. Res.*, vol. 86, pp. 11609-11615, Dec. 1981.
- [8] R. N. Edwards, D. C. Nobes, and E. Gómez-Treviño, "Offshore electrical exploration of sedimentary basins: The effects of anisotropy in horizontally layered media," *Geophys.*, vol. 49, pp. 566-576, May 1984.
- [9] R. N. Edwards, L. K. Law, P. A. Wolfgram, D. C. Nobes, M. N. Bone, D. F. Trigg, and J. M. DeLaurier, "First results of the MOSES experiment: Sea sediment conductivity and thickness determination, Bute Inlet, British Columbia, by magnetometric offshore electrical sounding," *Geophys.*, vol. 50, pp. 153-161, Jan. 1985.
- [10] R. W. P. King, B. Sandler, and T. T. Wu, "Cylindrical antennas immersed in arbitrary homogeneous isotropic media," *J. Appl. Phys.*, vol. 40, pp. 5049-5065, Dec. 1969. (Correction, vol. 41, p. 3559, 1970.)
- [11] R. W. P. King, "Cylindrical antennas and arrays," in *Antenna Theory, Part I*, R. E. Collin and F. J. Zucker, Eds. New York: McGraw-Hill, 1969, ch. 9.

Ronald W. P. King (A'30-SM'43-F'53-LF'71), for a photograph and biography please see page 1212 of the November 1985 issue of this TRANSACTIONS.

Antennas in Material Media Near Boundaries with Application to Communication and Geophysical Exploration, Part II: The Terminated Insulated Antenna

RONOLD W. P. KING, LIFE FELLOW, IEEE

Abstract—The properties of the insulated antenna in a dissipative medium near a boundary are reviewed. The important effects on antennas of being embedded in media with different properties over a wide range of frequencies are treated specifically in terms of three examples. These are: 1) a traveling-wave antenna in the earth below air at $f \sim 0.1$ MHz for subsurface communication; 2) an antiresonant antenna on the sea floor at $f \sim 1$ kHz and 3) an electrically short antenna on the sea floor at $f \sim 1$ Hz—both for geophysical measurements. In each case the current distribution, impedance, input power, effective length, and electric field in the range of interest are determined.

I. CIRCUIT PROPERTIES OF INSULATED ANTENNA

WHEN THE AMBIENT medium in which a bare metal antenna is embedded is conducting, radial currents from the antenna into the medium decrease the axial current. This means that often only electrically relatively short antennas are useful with correspondingly small effective lengths. Radial currents can obviously be eliminated by enclosing the metal cylinder (radius a , conductivity σ_c , internal impedance per unit length z^i) in a dielectric sheath (outer radius b , wavenumber $k_d = \omega[\mu_0(\epsilon_d + i\sigma_d/\omega)]^{1/2}$, $\sigma_d \sim 0$), as shown in Fig. 1. This greatly changes the properties of the antenna. In particular, the wavenumber of the current is no longer the wavenumber $k_1 = k_1[1 + (i4\pi z^i/\omega\mu_0)]^{1/2}$ as given by (4) in Part I—which reduces simply to the wavenumber $k_1 = \omega[\mu_0(\epsilon_1 + i\sigma_1/\omega)]^{1/2}$ of the ambient medium except at very low frequencies.

The insulated antenna behaves like a generalized transmission line with the wavenumber k_L and characteristic impedance Z_c given by the conventional formulas [1]:

$$k_L = (-z_L y_L)^{1/2}; \quad Z_c = (z_L / y_L)^{1/2}, \quad (1)$$

with

$$z_L = z^i - i\omega l + z^e + z_{12}; \quad y_L = g_L - i\omega c_L. \quad (2)$$

Here z^i is the internal impedance per unit length defined in (1) of Part I;

$$l = \frac{\mu_0}{2\pi} \ln \frac{b}{a} \quad (3)$$

Manuscript received August 28, 1985. This work was supported in part by the Joint Services Electronics Program under Contract N00014-84-K-0465 with Harvard University.

R. W. P. King is with the Gordon McKay Laboratory, Harvard University, Cambridge, MA 02138. During the preparation of this manuscript he served as IBM Visiting Distinguished Scholar at Northeastern University.

IEEE Log Number 8407357.

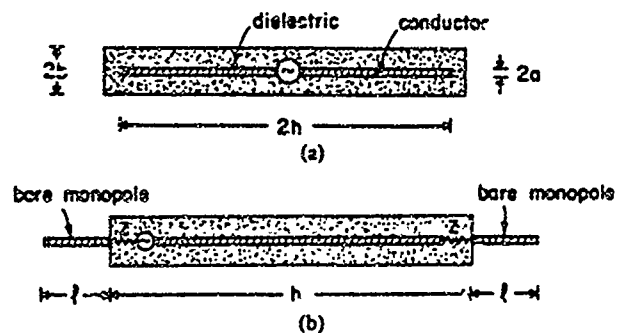


Fig. 1. Insulated antennas. (a) Completely insulated dipole. (b) Terminated insulated antenna. Ambient medium: earth, sea water.

is the series inductance per unit length;

$$z^e = r^e - ix^e = -\frac{i\omega\mu_0}{2\pi} \left[\frac{H_0^{(1)}(k_1 b)}{k_1 b H_1^{(1)}(k_1 b)} \right] \quad (4)$$

is the series external impedance per unit length; and

$$z_{12} = r_{12} - ix_{12} = -\frac{i\omega\mu_0}{2\pi} \left[\frac{H_0^{(1)}(2k_1 d)}{k_1 b H_1^{(1)}(k_1 b)} \right] \quad (5)$$

is the series mutual impedance per unit length due to an image with codirectional currents (to take account of the effect of the boundary with region 2 at the distance d). When the internal impedance is negligible, $z^i \sim 0$; when the antenna is far from the boundary, $z_{12} = 0$. The shunt admittance y_L is defined as follows:

$$y_L = -\frac{i2\pi k_d^2}{\omega\mu_0 \ln(b/a)} = \frac{2\pi\sigma_d}{\ln(b/a)} - i\omega \frac{2\pi\epsilon_d}{\ln(b/a)} = g_L - i\omega c_L. \quad (6)$$

The current in the insulated conductor is distributed like that in a transmission line [2] but with k_L and Z_c the generalized quantities defined in (1) with (2)–(6). The general formula for a center-driven, end-loaded, insulated antenna with half-length h is

$$I_x(x) = -\frac{iV_0^e \sin[k_L(h - |x|) + i\theta_A]}{2Z_c \cos(k_L h + i\theta_A)} = V_0^e Y \frac{\sin[k_L(h - |x|) + i\theta_A]}{\sin(k_L h + i\theta_A)}, \quad (7)$$

where the admittance Y and impedance $Z = 1/Y$ are

$$Y = G - iB = -\frac{i}{2Z_c} \tan(k_L h + i\theta_h), \quad (8a)$$

$$Z = R - iX = i2Z_c \cot(k_L h + i\theta_h). \quad (8b)$$

The antenna is terminated at each end in an arbitrary impedance Z_h which is contained in the terminal function θ_h as follows:

$$\theta_h = \rho_h - i\Phi_h = \coth^{-1}(Z_h/Z_c). \quad (9)$$

Note that

$$\coth(\rho_h - i\Phi_h) = r_h - ix_h = \operatorname{Re}(Z_h/Z_c) - i \operatorname{Im}(Z_h/Z_c), \quad (10a)$$

with

$$r_h = \frac{\sinh 2\rho_h}{\cosh 2\rho_h - \cos 2\Phi_h}; \quad x_h = \frac{-\sin 2\Phi_h}{\cosh 2\rho_h - \cos 2\Phi_h} \quad (10b)$$

or

$$\rho_h = \frac{1}{2} \tanh^{-1} \frac{2r_h}{r_h^2 + x_h^2 + 1}; \quad \Phi_h = \frac{1}{2} \tan^{-1} \frac{-2x_h}{r_h^2 + x_h^2 - 1}. \quad (10c)$$

For a low-impedance termination, $|Z_h/Z_c| \ll 1$ and $\rho_h \sim r_h$, $\Phi_h \sim \pi/2 + x_h$; for an insulated end, $|Z_h/Z_c| \rightarrow \infty$ and $\rho_h = 0$, $\Phi_h = 0$ or π ; for a matched load defined by $Z_h/Z_c = 1$, $r_h = 1$ and $\rho_h = \infty$. For the end-driven insulated antenna with the terminating impedance Z_0 at the generator end and Z_h at the load end, the formulas (7) and (8a), (8b) apply when $2Z_c$ is replaced by $Z_0 + Z_c$.

For applications at frequencies that are not too high and when the cross-sectional size of the antenna is electrically small in the ambient region 1 so that $|k_1 b| < 1$, the small-argument approximations of the Hankel functions can be used. That is, $H_0^{(1)}(z) \sim 1 + (2i/\pi)[0.5772 + \ln(z/2)]$ and $z H_1^{(1)}(z) \sim -2i/\pi$; also, $k_1 \sim (i\omega\mu_0\sigma_1)^{1/2} = (\omega\mu_0\sigma_1)^{1/2} e^{i\pi/4}$. With these approximations,

$$z' = r' - i\omega l' - r_0 - \frac{i\omega\mu_0}{8\pi}; \quad r_0 = (\pi a^2 \sigma_c)^{-1}, \quad (11)$$

$$z'' = r'' - ix'' - \frac{\omega\mu_0}{8} - \frac{i\omega\mu_0}{2\pi} \left(\ln \frac{2}{|k_1 b|} - 0.5772 \right), \quad (12)$$

$$z_{12} = r_{12} - ix_{12} - \frac{\omega\mu_0}{8} - \frac{i\omega\mu_0}{2\pi} \left(\ln \frac{1}{|k_1 d|} - 0.5772 \right), \quad (13)$$

so that

$$z_L = r_L - ix_L = r_0 + \frac{\omega\mu_0}{4} - \frac{i\omega\mu_0}{2\pi} \left(\ln \frac{b}{a} + \ln \frac{2}{|k_1 b|} + \ln \frac{1}{|k_1 d|} - 0.90 \right). \quad (14)$$

With a good dielectric, $\sigma_d \sim 0$ and

$$y_L \sim -i\omega c_L \quad \text{with} \quad c_L = \frac{2\pi\epsilon_d}{\ln(b/a)}. \quad (15)$$

In (14), r_0 is the internal resistance per unit length of the conductor associated with the heat dissipated in the conductor, $\omega\mu_0/4$ is the external resistance per unit length associated with energy transferred to the ambient medium (when the antenna is far from the boundary this reduces to $\omega\mu_0/8$). With (14) and (15) the explicit expressions for the wavenumber k_L and characteristic impedance Z_c are

$$k_L = k_d \left\{ 1 + \frac{1}{\ln(b/a)} \left[i \left(\frac{2\pi r_0}{\omega\mu_0} + \frac{\pi}{2} \right) + \ln \frac{2}{|k_1 b|} + \ln \frac{1}{|k_1 d|} - 0.90 \right] \right\}^{1/2}, \quad (16)$$

$$Z_c = \frac{\omega\mu_0 k_L}{2\pi k_d^2} \ln \frac{b}{a}. \quad (17)$$

At very low frequencies the leading terms reduce to

$$k_L = (-z_L y_L)^{1/2} \sim (i\omega c_L r_0)^{1/2} = (1 + i)(\omega c_L r_0/2)^{1/2}, \quad (18)$$

$$Z_c = (z_L/y_L)^{1/2} \sim (ir_0/\omega c_L)^{1/2} = (1 + i)(r_0/2\omega c_L)^{1/2}. \quad (19)$$

These are identically the formulas for a so-called ocean cable which is defined in conventional coaxial-line theory by $r/\omega l \gg 1$, $g/\omega c \ll 1$. All of the power supplied to the insulated conductor is transferred to the loads at the ends or dissipated as heat in the conductor itself. The structure acts like a lossy transmission line for transferring power to a load, not like an antenna that transfers power directly as radiation.

The impedance of the insulated conductor at very low frequencies is given by (8b) with (16) and (17). With a low-impedance termination, $\theta_h = r_h - i(\pi/2 + x_h)$ and

$$Z = i2Z_c \cot(k_L h + ir_h + \pi/2 + x_h) = -i2Z_c \tan(k_L h + ir_h + x_h). \quad (20)$$

With $|k_L h + ir_h + x_h| < 1$, the impedance of the insulated dipole with half-length h and identical low-impedance terminations at both ends is

$$Z = -i2Z_c(k_L h + ir_h + x_h) = 2(r_0 h + R_h - iX_h). \quad (21)$$

Note that low-impedance terminations must be used if significant currents are desired. If the ends are insulated ($Z_h = \infty$), $I(0) \sim 0$ and, hence, $I(z) \sim 0$. The terminations as defined in (10a) are expressed in the following normalized form:

$$r_h - ix_h = \frac{R_h - iX_h}{R_c - iX_c} = \frac{R_h R_c + X_h X_c}{R_c^2 + X_c^2} - i \frac{X_h R_c - R_h X_c}{R_c^2 + X_c^2}. \quad (22)$$

II. THE EFFECTIVE LENGTH

The insulated antenna has numerous parameters that can be adjusted to change its properties. These include the length h , the terminating impedance Z_h , the ratio b/a of the radius of the insulation to the radius of the conductor, and the electrical radius of the insulation $\beta_1 b$ in $k_1 b$. When $|k_1 b|$ is not too small, the conductor can be located eccentrically in the insulating sleeve to provide a significant transverse directional effect. Insulated antennas with parameters suitably adjusted for many special applications have been described [1], [3]. In this paper, attention is directed particularly to applications that require frequencies that are in the range from a fraction of a Hertz to near a megahertz. These have not been treated before.

One of the most important qualities of the insulated antenna is its electric moment. This depends on the effective length h_e , which, in turn, is determined by the current distribution and the actual length h . For the applications to be discussed, a maximum current is maintained along the insulated antenna when it is terminated either in a low impedance or in its characteristic impedance. The relevant current distributions are, for the antiresonant antenna,

$$I_x(x) = I_x(0) \frac{\cos [k_L(h-x) + i\theta_h]}{\cos (k_L h + i\theta_h)}, \quad (23)$$

where $\theta_h = r_h - i(x_h + \pi/2)$ with $r_h \ll 1$ and $|x_h| \ll 1$. In determining the effective length, it is adequate to neglect the effect of the low-impedance termination on the current. For the antenna with matched load ($r_h = 1$) with $\theta_h = \infty$,

$$I_x(x) = I_x(0) e^{ik_L x}. \quad (24)$$

Since the wavenumber for these currents is different from k , for the lateral electromagnetic waves they generate along the boundary in region 2, the phase relations among the successive elements of current and the outward traveling field are important in the definition of the effective electric moment $I_x(0)h_e(\phi_0)$. Note that the effective length $h_e(\phi_0)$ involves the angle ϕ_0 between the direction of propagation along the antenna and the point of observation. The effective length associated with the current (23) is

$$h_e(\phi_0) = \int_0^h \frac{\cos k_L(h-x')}{\cos k_L h} e^{-ik_2 x' \cos \phi_0} dx'. \quad (25)$$

In the direction $\phi_0 = 0$ of maximum field, this gives

$$h_e(0) = h_e = \frac{-ik_2 e^{-ik_2 h} + ik_2 \cos k_L h + k_L \sin k_L h}{(k_L^2 - k_2^2) \cos k_L h}. \quad (26)$$

Similarly, with the current (24),

$$h_e(\phi_0) = \int_0^h e^{ik_L x'} e^{-ik_2 x' \cos \phi_0} dx', \quad (27)$$

and, for $\phi_0 = 0$,

$$h_e(0) = h_e = \frac{i[1 - e^{i(k_L - k_2)h}]}{k_L - k_2}. \quad (28)$$

The maximum magnitude of the effective lengths with respect to the actual lengths h occurs in (26) near the minimum of the denominator, $\cos k_L h$. This is near

$$\beta_L h = \pi/2 \quad \text{or} \quad h = \pi/2\beta_L, \quad (29)$$

for which $\cos k_L h = -i \sinh \alpha_L h$, $\sin k_L h = \cosh \alpha_L h$, so that

$$|h_{em}| = \left| \frac{k_2 e^{-ik_2 h} + ik_2 \sinh \alpha_L h + ik_L \cosh \alpha_L h}{(k_L^2 - k_2^2) \sinh \alpha_L h} \right|, \quad (30)$$

where $k_2 = \beta_2 + i\alpha_2$, $k_L = \beta_L + i\alpha_L$, and h is given by (29).

The maximum magnitude of h_e in (28) occurs near

$$(\beta_L - \beta_2)h = \pi \quad \text{or} \quad h = \pi/(\beta_L - \beta_2), \quad (31)$$

where

$$|h_e| = \left| \frac{i[1 - e^{-(\alpha_L - \alpha_2)h}]}{k_L - k_2} \right|, \quad (32)$$

and h is given by (31).

When the insulated antenna is terminated either in a low impedance or its characteristic impedance, the terminations often consist of bare monopoles of length l . The effective length of these has been determined in Part I, but the effective length of the terminated antenna is not just the sum of the effective lengths of the parts since the relative phases make a significant difference. It is possible to evaluate the complete effective length. It has the form:

$$h_e = \frac{\tan(k_1 l/2)}{k_1} (1 + e^{ik_L h}) + \frac{i}{k_L - k_2} [1 - e^{i(k_L - k_2)h}]. \quad (33)$$

At all but the very low frequencies, the internal impedance of the bare sections is negligible and, over the lengths of interest, $k_1^{-1} \tan(k_1 l/2) \sim l/2$. At the low frequencies where the internal impedance dominates, $k_1^{-1} \tan(k_1 l/2) \sim \alpha_1^{-1} \tanh(\alpha_1 l/2)$. Even with these simplifications, the magnitude $|h_e|$ is not a simple formula. For most applications the contribution to the effective length by the relatively short terminations is relatively small and can be ignored. For any particular case, it can be evaluated from (33).

III. ANTENNAS FOR SPECIAL PURPOSES

Three potentially useful antennas are treated in the following. These include:

- 1) a terminated traveling-wave antenna in the earth parallel to its surface with air in a frequency range centered near 0.1 MHz;
- 2) an antiresonant insulated antenna on the sea floor in a frequency range centered near 1 kHz; and
- 3) an electrically short insulated antenna on the sea floor in a frequency range near 1 Hz.

A. An Underground Antenna

A useful subsurface antenna for communicating from a point at a depth d below the surface of the earth to a point below, on, or above the surface at a radial distance ρ is the

insulated traveling-wave antenna. As shown in Fig. 2, this consists of a conductor (radius a , resistance per unit length r') enclosed in an insulating sheath (radius b , permittivity ϵ_d) of length h . It is terminated at $x = h$ in a lumped impedance Z in series with a bare metal antenna (length l , input impedance Z_l); the generator (emf V_0) is connected in series with the insulated conductor at $x = 0$ and a second bare metal antenna (length l , input impedance Z_l).

The current in the antenna is

$$I_x(x) = I_x(0) e^{ik_L x} = \frac{V_0}{Z_m} e^{ik_L x}, \quad Z_m = Z_l + Z_c, \quad (34)$$

where Z_c is given by (17) and k_L by (16). It is required that, at $x = h$, Z is adjusted so that

$$Z_h = Z_l + Z = Z_c. \quad (35)$$

The input power to the antenna is

$$P_m = |I_x(0)|^2 (R_c + R_l). \quad (36)$$

The bare metal terminations are monopoles with length l . The normalized input impedance is half the impedance of a dipole, as given in Fig. 4 of Part I. For moist earth ($\sigma_1 \sim 10^{-3}$ S/m, $\epsilon_1 = 8$) at $f = 3 \times 10^5$ Hz, the normalizing factor is $\Delta_1 = 5.84$ so that the impedance of a bare monopole with radius $a = 1.04$ mm and length $l = \lambda_1/4 \sim 42$ m, as obtained from Table II of Part I, is $Z_l = Z_1/2 = 63.9 - i50.0 \Omega$. This value assumes the antenna is at a depth $d = 50$ cm.

The insulated conductor consists of the copper wire with radius $a = 1.04$ mm. In order to have the wavenumber k_L for the current close to that for the lateral waves in air, the insulation should be styrofoam. Also, as seen from (16), b/a should be large. Accordingly, the choice $b = 1.04$ cm is made. With data obtained from Tables I and II in Part I for $f = 3 \times 10^5$ Hz, it follows from (16) and (17) that

$$k_L = k_d(2.36 + i0.141) \\ = (1.48 + i0.088) \times 10^{-2} \text{ m}^{-1} = \beta_L + i\alpha_L. \quad (37)$$

With styrofoam insulation, $k_d = k_2 = \omega/c = 2\pi \times 10^{-3} \text{ m}^{-1}$. Also,

$$Z_c = 325 + i19.3 \Omega. \quad (38)$$

The terminating impedance is $Z_h = Z_l + Z$, where Z is to be adjusted to make $Z_h = Z_c$. Therefore,

$$Z = Z_c - Z_l = 325 + i19.3 - 63.9 + i50 = 261.1 + i69.3 \Omega. \quad (39)$$

The optimum length of the insulated antenna is obtained from (31) to be

$$h = \pi/(\beta_L - k_2) \sim 369 \text{ m}. \quad (40)$$

The associated effective length given by (32) is

$$|h_e| \sim 201 \text{ m}. \quad (41)$$

(Note that h and $|h_e|$ can be increased by reducing β_L by

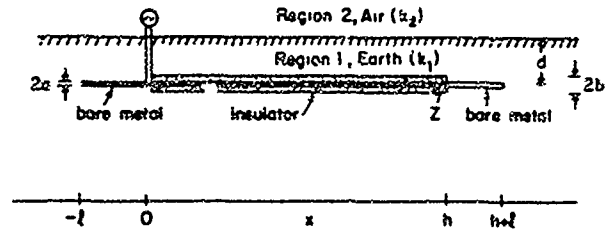


Fig. 2. Terminated insulated antenna at depth d in earth.

increasing b/a .) The input power per unit current is obtained from (36). It is

$$P_m/|I_x(0)|^2 = R_c + R_l = 325 + 63.9 = 389 \Omega. \quad (42a)$$

With $|I_x(0)| = 25$ A,

$$P_m = 243 \text{ kW}. \quad (42b)$$

The radial electric field at the surface at a distance of 500 km is readily evaluated. At this distance, $\rho > 4|k_1^2/k_2^2| = 4[(4.88)^2 \times 10^{-4}/(2\pi)^3 \times 10^{-9}] = 38.4$ km, so that the point of observation is in the far field where [4]

$$|E_{1r}(\rho, 0, 0)| = |I_x(0)h_e| \frac{\omega\mu_0}{2\pi k_2} \frac{1}{\rho^2} = |I_x(0)| \times 0.48 \times 10^{-7}. \quad (43)$$

With $|I_x(0)| = 25$ A, the field is

$$|E_{1r}(\rho, 0, 0)| \sim 1.2 \mu\text{V/m},$$

which is easily measurable.

B. An Antenna for the Sea Floor at $f = 1$ kHz

Terminated insulated antennas can be used on the sea floor to measure the conductivity of the oceanic crust. In one arrangement the antenna is laid horizontally in the sea water (region 1, $\sigma_1 = 4$ S/m, $k_1 = (i\omega\mu_0\sigma_1)^{1/2}$) at a small height d over the crust (Region 2, $\sigma_2 = 10^{-4}$ to 10^{-1} S/m, $k_2 = (i\omega\mu_0\sigma_2)^{1/2}$). The field generated by the antenna is measured at successive radial distances ρ in the sea water just above the crust. Except very close to the antenna, this field is entirely a lateral-wave field if there are no reflecting layers at moderate distances in the crust. But even if such layers are present, the lateral-wave field which samples only a relatively shallow depth is from 60 to 90 percent of the observed field [5]. In the most useful range of measurement, $1 \leq |k_2\rho| \leq 4|k_1^2/k_2^2|$, the magnitude of the dominant radial component has the following simple form in the direction along the axis of the antenna [6], [7]:

$$|E_{1r}(\rho, 0, 0)| = |I_x(0)h_e| \frac{\omega\mu_0 k_2^2}{2\pi k_1^2} \frac{e^{-\alpha_2 \rho}}{\rho} \\ = |I_x(0)h_e| \frac{\omega\mu_0 \sigma_2}{2\pi \sigma_1} \frac{e^{-\alpha_2 \rho}}{\rho}, \quad (44)$$

where $\alpha_2 = (\omega\mu_0\sigma_2/2)^{1/2}$. The behavior of this field as a function of the radial distance is shown in Fig 3 for σ_2 ranging

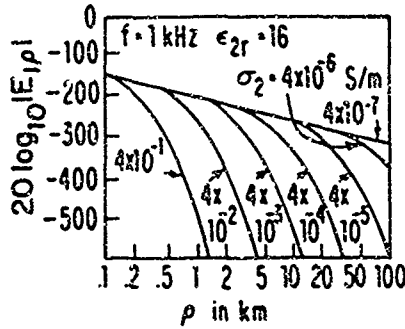


Fig. 3. Radial electric field at $z = 15$ cm in sea water ($\sigma_1 = 4$ S/m, $\epsilon_1 = 80$) above rock or deep sediment ($\sigma_2, \epsilon_2 = 16$) as a function of the radial distance ρ from a unit horizontal dipole at height $d = 15$ cm above sea bottom; $f = 1$ kHz.

from 4×10^{-1} to 4×10^{-7} S/m. By measuring the radial field at successive distances, an observed graph of $20 \log_{10} |E_{\rho}(\rho, 0, 0)|$ can be compared with theoretical ones and σ_2 obtained by interpolation. The rapid exponential decrease at locations that depend on σ_2 assures reasonable accuracy.

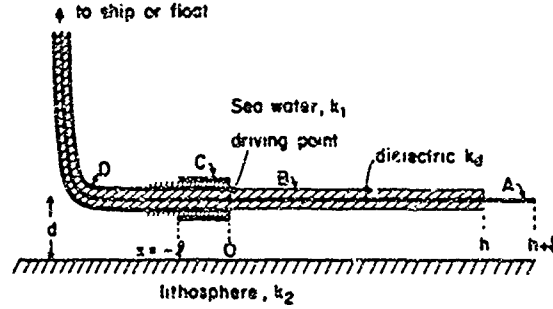
Let the transmitting antenna be designed for use at $f = 1$ kHz (Fig. 4). It consists of an insulated main section B with the conductor radius a and insulation radius b that extends from $x = 0$ to $x = h$. The conductor with the insulation removed continues from $x = h$ to $x = h + l$ as a bare monopole A terminating the insulated section. At the driving point ($x = 0$), the insulated conductor is connected to the inner conductor of the feeding coaxial line D from the ship or float. Since this is quite long, efficient power transmission requires the characteristic resistance of the line to be equal to the input resistance of the antenna. As shown in Fig. 2, the insulated terminated monopole is driven against a bare monopole that consists of a metal sleeve C that extends from $x = 0$ to $x = -l$. The sleeve is insulated from the metal walls of the coaxial line except at $x = 0$ where it is conductively connected.

The lengths l of the two bare sections are chosen so that $\beta_1 l > \pi/2$ or $l \sim 12$ m at $f = 1$ kHz. The input impedance of each monopole is of the order $Z_i \sim 0.0135 - i0.0065 \Omega$. The dimensions of the main insulated section are $a = 0.52$ cm, $b = 0.521$ cm. The insulation is chosen very thin so that k_L is not too different from k_2 . It may be neoprene with $\epsilon_{dr} = 6.6$ (or any other dielectric including enamel). At $f = 1$ kHz, $k_2 = \omega(\mu_0 \epsilon_d)^{1/2} = 5.38 \times 10^{-3} \text{ m}^{-1}$. With the antenna at a mean height $d = 5$ cm above the sea bottom, (16) gives

$$\begin{aligned} k_L &= k_d \{1 + 520.5[i(0.166 + \pi/2) + 11.25]\}^{1/2} \\ &= k_d(76.7 + i5.88) = (4.12 + i0.32) \times 10^{-3} \text{ m}^{-1} \\ &= \beta_L + i\alpha_L, \end{aligned} \quad (45)$$

$$Z_c = 3.44 + i0.267 \Omega. \quad (46)$$

The normalized resistance and reactance of the terminations are obtained from (22) to be $r_h = 3.9 \times 10^{-3} \Omega$, $x_h = 2.2 \times 10^{-3} \Omega$ —very small quantities. The length h of the insulated section when this is antiresonant is given by (29), the



- A Bare metal monopole of length $l \sim 12$ m
- B Insulated antenna of length $h \sim 381$ m
- C Sleeve monopole folded back on coaxial line: length $l \sim 12$ m
- D Coaxial line to ship, preferably insulated to avoid corrosion

Fig. 4. Terminated insulated antenna for use on the sea floor at $f = 1$ kHz. Transverse dimensions are not to scale.

associated effective length by (30). They are

$$h = \pi/2\beta_L = 381 \text{ m}; \quad |h_e| = 9.66 \text{ km}. \quad (47)$$

The effective length is greater than the actual length because it is referred to the driving-point current $I_x(0)$, which is the minimum current; the current increases to the maximum at $x = h$. Thus,

$$I_x(h) = \frac{I_x(0)}{\sinh(\alpha_L h + r_h)}. \quad (48)$$

The driving-point impedance of the antenna when $\beta_L h = \pi/2 + x_h \sim \pi/2$ is:

$$Z_{in} = R_{in} = R_c \coth(\alpha_L h + r_h) = 27.45 \Omega. \quad (49)$$

The power input to the antenna is $|I_x(0)|^2 R_{in}$. The power in the two bare terminations is insignificant as is their contribution to the effective length. The fraction of the power dissipated in the internal resistance of the insulated copper conductor is proportional to the contribution to α_L by the internal impedance. It is seen from (44) that this is $0.166/(0.166 + \pi/2) = 0.096$ —a relatively small amount.

The field to be generated is given by (44) and represented in Fig. 3 for unit electric moment. It is seen that measurements over a useful range of σ_2 are possible if they can be made down to $20 \log_{10} |E_{\rho}(\rho, 0, 0)| = -250$ dB per unit electric moment. With a transmitting antenna that provides an effective electric moment $|I_x(0)h_e| \sim 3 \times 10^5 \text{ A} \cdot \text{m}$, the minimum level of -250 dB is raised to -140 dB. The corresponding smallest electric field that must be measured is $|E_{\rho}(\rho, 0, 0)| \sim 0.1 \mu\text{V/m}$. If the receiving antenna has an effective length of only 10 m, the required sensitivity is $1 \mu\text{V/m}$.

With the effective length given in (47), the required input current is $|I_x(0)| = 31.1 \text{ A}$. With (49), the input power is $P_{in} = (31.1)^2 \times 27.45 = 26.5 \text{ kW}$.

C. An Antenna for the Sea Floor at Very Low Frequencies

Geophysicists use antennas on the sea floor at frequencies so low that the internal resistance of the copper conductor—

which plays a negligible role when $f > 100$ Hz—becomes a dominant factor. This is true of both bare and insulated antennas. In the frequency range from 0.3 to 3 Hz, the magnitude of the complete radial electric field in the sea water near the oceanic crust at a radial distance ρ from a unit horizontal dipole is given by [8]

$$|E_{1\rho}(\rho, 0, 0)| = \left| \frac{e^{ik_2\rho}}{2\pi\sigma} \left(\frac{1}{\rho^3} - \frac{ik_2}{\rho^2} - \frac{k_2^2}{\rho} \right) \right| = \frac{e^{-\alpha_2\rho}}{2\pi\sigma_1\rho^3} (1 + 2\alpha_2\rho + 2\alpha_2^2\rho^2 + 4\alpha_2^3\rho^3 + 4\alpha_2^4\rho^4)^{1/2}. \quad (50)$$

This formula assumes the oceanic crust to be a homogeneous isotropic half-space with wavenumber $k_2 = \beta_2 + i\alpha_2$ and $\beta_2 = \alpha_2 = (\omega\mu_0\sigma_2/2)^{1/2}$. At $f = 3$ Hz and with $\sigma_2 = 4 \times 10^{-3}$ S/m, $\sigma_1 = 4$ S/m, and $\rho = 18.9$ km,

$$20 \log_{10} |E_{1\rho}(\rho, 0, 0)| = -288 \text{ dB}. \quad (51)$$

If it is assumed that a receiver is sensitive to $0.1 \mu\text{V/m}$ and is connected to a receiving antenna with an effective length of the order of 80 m, the transmitting antenna must raise the signal level by 110 dB to -178 dB. This requires an electric moment

$$|I_x(0)h_e| \sim 3.25 \times 10^5 \text{ A}\cdot\text{m}. \quad (52)$$

It is seen from Fig. 6 in Part I that a bare termination should be of the order of $0.15 \lambda_1$ in length or, at $f = 3$ Hz, $l \sim 0.15 \times 913 = 137$ m for which $l_e = 0.295 \times 137 = 40$ m. From Fig. 8 in Part I the impedance of a bare monopole at a height $d = 10.4$ cm from the sea floor is

$$Z_l = 0.013 - i0.0011 \Omega. \quad (53)$$

The wavenumber of an insulated section of length h , terminated in Z_l is obtained from (18). For a conductor with radius $a = 5.2$ mm and an insulator with radius $b = 8$ mm and relative permittivity $\epsilon_d = 6.6$ (for neoprene), (18) gives $k_L = 1.29 \times 10^{-6}(1 + i) \text{ m}^{-1}$. For an electrically short antenna with $|k_L h| \leq 1$,

$$Z_m \sim -iZ_c k_L h = r_0 h + 2Z_l. \quad (54)$$

The effective length of an electrically short insulated antenna terminated in a very low impedance is the actual length since $I_x(x) \sim I_x(0)$ for all values of x . The maximum current for the insulated conductor is 325 A, so that the electric moment is $325|h_e| \text{ A}\cdot\text{m}$. For the required value of $|I_x(0)h_e| = 3.25 \times 10^5 \text{ A}\cdot\text{m}$, it is necessary that $|h_e| = h = 1$ km. With the two bare terminations, the total length is

$$h + 2l = 1274 \text{ m}. \quad (55)$$

The contribution to the effective length by the terminations is small and has not been included.

With this length the impedance of the antenna is

$$Z_m = 2.08 \times 10^{-4} \times 1000 + 0.026 - i0.002 = 0.23 - i0.002 \Omega. \quad (56)$$

The input power is

$$P_m = |I_x(0)|^2 R_m = 24.3 \text{ kW}. \quad (57)$$

The insulated terminated antenna described above is quite similar to an antenna actually used by Young and Cox [9] for measurements on the sea floor in the frequency range $f = 0.25$ to 2.25 Hz. The insulated part was 800 m long with a conductor radius of $a = 3.5$ mm. It had a resistance $r_0 h = 5.13 \times 10^{-4} \times 800 = 0.41 \Omega$. Each of the two bare terminations had lengths $l = 15$ m and input resistances of 0.07Ω when at a height $d \sim 10.4$ cm above the sea floor. Thus, the total resistance was $R_m = r_0 h + 2R_l = 0.55 \Omega$ and, with $|I_x(0)| = 70$ A, $P_m = 2.7$ kW. Since the bare terminations were short and oriented so that their currents were oppositely directed, their contributions to the field and the effective length cancelled. The effective length of the insulated section was $h_e = 800$ m and, with a current of 70 A, the electric moment was $5.6 \times 10^4 \text{ A}\cdot\text{m}$ so that the field at $\rho = 18.9$ km was raised by 95 dB from -288 dB for the unit dipole to -193 dB or $|E_{1\rho}(\rho, 0, 0)| = 2.2 \times 10^{-10} \text{ V/m}$. The bare receiving dipole had a length of 9 m and an effective length of 4.5 m, so that the voltage across the load was $V_L \sim 10^{-9} \text{ V}$. This is so low that noise was a serious problem and required a receiver with a sensitivity higher than $0.001 \mu\text{V}$.

IV. CONCLUSION

The insulated conductor with its various possible terminations (including especially bare monopoles) is a highly effective antenna when embedded in a general dielectric or conducting region with a wavenumber that is much larger in magnitude than the wavenumber of the insulating sleeve. Depending on the ratio b/a of the radius of the insulating sleeve to that of the conductor, the insulated conductor acts more like an antenna for transferring power to the ambient medium ($b/a \sim 1$) or a transmission line for supplying power to the terminations ($b/a \geq 10$). At frequencies of 1 kHz and higher, the power loss in the internal resistance of the conductor is negligible and all power is either radiated or transferred to the terminations without loss. At frequencies below 100 Hz, the power loss in the internal resistance becomes dominant and the radiated power transferred directly to the ambient medium negligibly small. In this case, the insulated conductor is a highly inefficient transmission line feeding the terminations.

When located in region 1 (k_1) near a boundary with a half space (region 2, k_2) with $|k_1| \geq 3|k_2|$, the insulated conductor is effective as a generator of electromagnetic surface waves that travel close to the boundary in region 2. They are responsible for the entire field in region 1 at even moderate distances from the source. If region 2 is not a homogeneous half-space but is horizontally layered, there may be reflections from these layers. When this is true, the reflected field reaching a receiver in region 1 is necessarily much smaller than the surface-wave field [5]. The latter penetrates region 2 only to a depth that is a small fraction of the radial distance from the source to the point of observation in region 1 near the boundary [5].

REFERENCES

- [1] R. W. P. King and G. S. Smith, *Antennas in Matter*. Cambridge, MA: M.I.T. Press, 1981, chs. 1 and 8.
- [2] R. W. P. King, *Transmission-Line Theory*, 2nd ed. New York: Dover, 1965, ch. 4.
- [3] —, "The many faces of the insulated antenna," *Proc. IEEE*, vol. 64, pp. 228-238, Feb. 1976.
- [4] R. W. P. King and M. F. Brown, "Lateral electromagnetic waves along plane boundaries: A summarizing approach," *Proc. IEEE*, vol. 72, pp. 595-611, May 1984.
- [5] R. W. P. King, M. Owens, and T. T. Wu, "Properties of lateral electromagnetic fields and their application," *Radio Sci.*, vol. 21, pp. 13-23, Jan.-Feb. 1986.
- [6] T. T. Wu and R. W. P. King, "Lateral waves: A new formula and interference patterns," *Radio Sci.*, vol. 17, pp. 521-531, May-June 1982.
- [7] R. W. P. King, "Electromagnetic surface waves: New formulas and applications," *IEEE Antennas and Propagat.*, vol. AP-33, no. 11, pp. 1704-1212, Nov. 1985.
- [8] —, "Electromagnetic surface waves: New formulas and their application to determine the electrical properties of the sea bottom," *J. Appl. Phys.*, vol. 58, pp. 3612-3624, Nov. 1985.
- [9] P. D. Young and C. S. Cox, "Electromagnetic active source sounding near the East Pacific Rise," *Geophys. Res. Lett.*, vol. 8, pp. 1043-1046, 1981.

Revised W. P. King (A'30-SM'43-F'53-LF'71), for a photograph and biography please see page 1212 of the November 1985 issue of this TRANSACTIONS.

Lateral electromagnetic pulses generated by a vertical dipole on the boundary between two dielectrics

Tai T. Wu and Ronald W. P. King

Gordon McKay Laboratory, Harvard University, Cambridge, Massachusetts 02138

(Received 1 June 1987; accepted for publication 20 August 1987)

An exact solution in terms of elementary functions is obtained in the time domain for the vertical electric field $E_z(\rho, t)$ and the transverse magnetic field $B_\phi(\rho, t)$ of a dipole located on the plane boundary $z = 0$ between air (region 2, $z < 0$) and a perfect dielectric (region 1, $z > 0$) when the dipole is excited by a single delta-function current pulse. The vertical electric field on the boundary consists of a delta-function pulse that travels in the air with the velocity c , an oppositely directed delta-function pulse that travels in the dielectric with the smaller velocity $c/\epsilon^{1/2}$, an amplitude structure that varies in time between the two pulses, and a final static electric field due to the charges left on the dipole. The horizontal magnetic field is similar. For comparison, the vertical electric field in the equatorial plane of the same dipole in a homogeneous dielectric is also derived. The comparison indicates that the field along the boundary is a surface-wave or lateral pulse.

I. INTRODUCTION: THE FIELD OF THE ISOLATED DIPOLE

The properties in the frequency domain of lateral electromagnetic waves generated by horizontal and vertical electric dipoles located on or near the plane boundary between two electrically different media like the air and earth or air and ocean have been summarized in a recent paper¹ and related to several applications.²⁻⁴ Also of interest are the properties and possible applications of lateral pulses generated by dipoles in the time domain. An important introduction to the transient field generated by a vertical electric dipole on the plane boundary between half-spaces of air and a perfect dielectric was given by Van der Poel⁵ who determined the Hertz potential when the dipole is excited by a step function in charge (or a delta-function current). He used a Laplace transformation of Sommerfeld's solution in the frequency domain. At any radial distance ρ from the source the observed potential was shown to have the temporal behavior typical of a surface wave. The electromagnetic field associated with the Hertz potential was not evaluated. The same problem was studied in greater detail entirely in the time domain by Bremmer.⁶ It was also investigated by Haddad and Chang⁷ in the more difficult generalization of a vertical dipole over a dissipative earth rather than a perfect dielectric. They transformed the double infinite integrals in the frequency domain to approximate single finite integrals that were evaluated numerically. The problem of the transient field of a vertical dipole with a ramp-function excitation over both a plane and a spherical earth has been treated variously by Wait.⁸⁻¹⁰ The formulas he obtained involve certain "key approximations."

The analysis carried out in this paper determines the exact transient field of a vertical dipole on the boundary between two perfect dielectrics. Instead of continuous-wave excitation at an angular frequency with the electric moment

$$I(t)h_e = \text{Re } I(0)h_e e^{-i\omega t}, \quad (1)$$

a single pulse (or sequence of such pulses) is applied. If this is a delta function, the electric moment is

$$I(t)h_e = I(0)h_e \delta(t), \quad (2)$$

where the delta function is defined by the Fourier integral

$$\delta(t) = \frac{1}{2\pi} \int_{-\infty}^{\infty} e^{-i\omega t} d\omega. \quad (3)$$

Before pulse excitation is studied for a dipole on the plane boundary between two electrically different half-spaces, it is useful for the later interpretation of the transient field to consider the isolated dipole in an infinite homogeneous dielectric with the relative permittivity $\epsilon_r = \epsilon$ that is independent of the frequency. Although this problem is most easily solved by treating directly the time-dependent Maxwell's equations, this approach is difficult to generalize to apply to a planar boundary between electrically different half-spaces. Therefore, the dipole in an infinite homogeneous dielectric is treated by applying the Fourier transform to the frequency-dependent field. For E_z in the equatorial plane, $z = 0$,

$$\begin{aligned} \bar{E}_z(\rho, \omega) &= -\frac{\omega\mu_0}{4\pi} \int_0^\infty \frac{J_0(\lambda\rho)\lambda^3 d\lambda}{k^2(k^2 - \lambda^2)^{1/2}} \\ &= \frac{\omega\mu_0}{4\pi} e^{ik\rho} \left(\frac{i}{\rho} - \frac{1}{k\rho^2} - \frac{i}{k^2\rho^3} \right), \end{aligned} \quad (4)$$

where $k^2 = k_0^2\epsilon = \omega^2\epsilon/c^2$. With $\lambda' = c\lambda$, $\rho' = \rho/c$, the integral form of (4) becomes

$$\bar{E}_z(\rho', \omega) = -\frac{\omega\mu_0}{4\pi c\epsilon} \int_0^\infty \frac{J_0(\lambda'\rho')\lambda'^3 d\lambda'}{\omega^2(\omega^2\epsilon - \lambda'^2)^{1/2}}, \quad (5)$$

with the branch cut and contour of integration shown in Fig. 1. With a delta-function current with unit moment, i.e., $I(t)h_e = I(0)h_e \delta(t)$ with $I(0)h_e = 1 \text{ A m}$, the time-dependent field is

$$\begin{aligned} E_z(\rho', t) &= \frac{1}{\pi} \text{Re} \int_0^\infty d\omega e^{-i\omega t} \bar{E}_z(\rho', \omega) \\ &= -\frac{\mu_0}{4\pi^2 c\epsilon} \text{Re} \int_0^\infty d\omega e^{-i\omega t} \omega^2 \\ &\quad \times \int_0^\infty \frac{J_0(\omega\xi\rho')\xi^3 d\xi}{(\epsilon - \xi^2)^{1/2}}, \end{aligned} \quad (6)$$

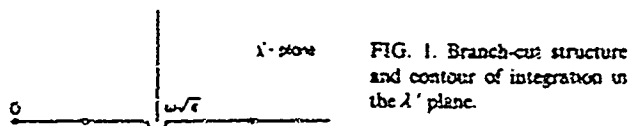


FIG. 1. Branch-cut structure and contour of integration in the λ' plane.

where the change in variable $\xi = \lambda' / \omega$ has been made. This is equivalent to

$$E_z(\rho', t) = \frac{\mu_0}{4\pi^2 c \epsilon} \frac{\partial^2}{\partial t^2} \operatorname{Re} \int_0^\infty d\xi \frac{\xi^3}{(\epsilon - \xi^2)^{1/2}} \times \int_0^\infty J_0(\omega \xi \rho') e^{-i\omega t} d\omega. \quad (7)$$

The integral with respect to ω can be carried out with formula (6.611-1) on p. 707 of Gradshteyn and Ryzhik.¹¹ For $t > \xi \rho'$, this gives

$$\int_0^\infty J_0(\omega \xi \rho') e^{-i\omega t} d\omega = -i(t^2 - \xi^2 \rho'^2)^{-1/2}, \quad (8)$$

so that

$$E_z(\rho', t) = -\frac{\mu_0}{4\pi^2 c \rho' \epsilon} \frac{\partial^2}{\partial t^2} \left(\int_{\epsilon^{1/2}}^{t/\rho'} \frac{\xi^3 d\xi}{(\xi^2 - \epsilon)^{1/2} (t^2/\rho'^2 - \xi^2)^{1/2}} - \int_{t/\rho'}^\infty \frac{\xi^3 d\xi}{(\xi^2 - \epsilon)^{1/2} [-(t^2/\rho'^2 - \xi^2)^{1/2}]} \right) \\ = -\frac{\mu_0}{2\pi^2 c \rho' \epsilon} \frac{\partial^2}{\partial t^2} \int_{\epsilon^{1/2}}^{t/\rho'} \frac{\xi^3 d\xi}{(\xi^2 - \epsilon)^{1/2} (t^2/\rho'^2 - \xi^2)^{1/2}}. \quad (11)$$

The integral is elementary. Let $x = \xi^2$. Then

$$E_z(\rho', t) = -\frac{\mu_0}{4\pi^2 c \rho' \epsilon} \frac{\partial^2}{\partial t^2} f\left(\frac{t}{\rho'}\right), \quad (12)$$

where

$$f\left(\frac{t}{\rho'}\right) = \int_{\epsilon^{1/2}}^{t/\rho'} \frac{x dx}{\sqrt{X}} \\ = -\sqrt{X} \Big|_{\epsilon^{1/2}}^{t/\rho'} + \frac{1}{2} \left(\epsilon + \frac{t^2}{\rho'^2} \right) \int_{\epsilon^{1/2}}^{t/\rho'} \frac{dx}{\sqrt{X}}, \quad (13)$$

where

$$X = (x - \epsilon)(t^2/\rho'^2 - x) \\ = -\epsilon t^2/\rho'^2 + (\epsilon + t^2/\rho'^2)x - x^2 \\ = a + bx + cx^2,$$

with $a = -\epsilon t^2/\rho'^2$, $b = (\epsilon + t^2/\rho'^2)$, and $c = -1$. The second integral gives

$$\int \frac{dx}{\sqrt{X}} = -\frac{1}{\sqrt{-c}} \sin^{-1} \frac{2cx + b}{\sqrt{-q}}, \quad (14)$$

where $q = 4ac - b^2 = -(t^2/\rho'^2 - \epsilon)^2$. The substitution of the limits shows that the first term on the right in (13) is zero and the arcsines have the arguments -1 and $+1$, so that

$$f(t/\rho') = \frac{1}{2} \pi (t^2/\rho'^2 + \epsilon). \quad (15)$$

The differentiation of this function must be carried out with care, since it and its derivatives have discontinuous behaviors at $t/\rho' = \epsilon^{1/2}$. Thus, since $E_z(\rho', t)$ and $f(t/\rho')$ are zero when $t/\rho' < \epsilon^{1/2}$ so that $f(\epsilon^{1/2} -) = 0$, whereas $f(\epsilon^{1/2} +) = \pi\epsilon$, there is a step increase in $f(t/\rho')$ as t/ρ'

$$E_z(\rho', t) = \frac{\mu_0}{4\pi^2 c \rho' \epsilon} \frac{\partial^2}{\partial t^2} \times \operatorname{Im} \int_0^\infty \frac{\xi^3 d\xi}{(\epsilon - \xi^2)^{1/2} (t^2/\rho'^2 - \xi^2)^{1/2}}. \quad (9)$$

Now let the contour of integration be chosen as shown in Fig. 2. When $t/\rho' < \epsilon^{1/2}$, the integrand in (9) is real so that there is no contribution to the relevant imaginary part of the integral. When $\epsilon^{1/2} < t/\rho'$, the integral becomes

$$E_z(\rho', t) = \frac{\mu_0}{4\pi^2 c \rho' \epsilon} \frac{\partial^2}{\partial t^2} \times \operatorname{Im} \int_0^\infty \frac{\xi^3 d\xi}{i(\xi^2 - \epsilon)^{1/2} (t^2/\rho'^2 - \xi^2)^{1/2}}. \quad (10)$$

Along the indicated contours, the only contribution is

increases across $t/\rho' = \epsilon^{1/2}$. When $t/\rho' > \epsilon^{1/2}$, $f(t/\rho') = \frac{1}{2} \pi (t^2/\rho'^2 + \epsilon)$. Now let $f'(t/\rho') = \partial f(t/\rho') / \partial t$. When $t/\rho' < \epsilon^{1/2}$, $f'(t/\rho') = 0$; when $t/\rho' > \epsilon^{1/2}$, $f'(t/\rho') = \pi t / \rho'^2$. Thus

$$f'\left(\frac{t}{\rho'}\right) = \pi \epsilon \delta(t - \epsilon^{1/2} \rho') + \begin{cases} 0, & t/\rho' < \epsilon^{1/2}, \\ \pi t / \rho'^2, & t/\rho' > \epsilon^{1/2}. \end{cases} \quad (16)$$

Evidently, there is a step increase by $(\pi t / \rho'^2)$ at $t/\rho' = \epsilon^{1/2}$. Let $f''(t/\rho') = \partial f'(t/\rho') / \partial t$. When $t/\rho' < \epsilon^{1/2}$, $f''(t/\rho') = 0$; when $t/\rho' > \epsilon^{1/2}$, $f''(t/\rho') = \pi / \rho'^2$. Hence

$$f''\left(\frac{t}{\rho'}\right) = \pi \epsilon \delta'(t - \epsilon^{1/2} \rho') + \frac{\pi t}{\rho'^2} \delta(t - \epsilon^{1/2} \rho') + \begin{cases} 0, & t/\rho' < \epsilon^{1/2}, \\ \pi / \rho'^2, & t/\rho' > \epsilon^{1/2}. \end{cases} \quad (17)$$

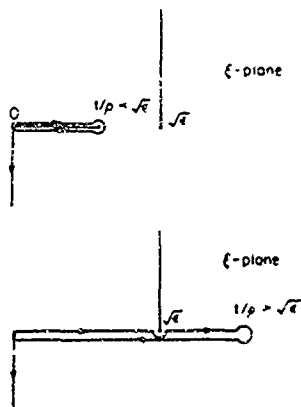


FIG. 2. Branch-cut structure and contour of integration in the ξ plane.

However,

$$(t/\rho')\delta(t - \epsilon^{1/2}\rho') = \epsilon^{1/2}\delta(t - \epsilon^{1/2}\rho').$$

Hence, with $\rho' = \rho/c$ and $c^2 = (\mu_0\epsilon_0)^{-1}$,

$$E_z(\rho, t) = -\frac{\mu_0}{4\pi\rho}\delta\left(t - \frac{\epsilon^{1/2}\rho}{c}\right) - \frac{\zeta_s}{4\pi\rho^2}\delta\left(t - \frac{\epsilon^{1/2}\rho}{c}\right) - \frac{1}{4\pi\epsilon\epsilon_0\rho^3}\begin{cases} 0, & ct/\rho < \epsilon^{1/2} \\ 1, & ct/\rho > \epsilon^{1/2} \end{cases} \quad (18)$$

where $\zeta_s = (\mu_0/\epsilon\epsilon_0)^{1/2}$. An alternative form makes use of the relation $t\delta'(t) = -\delta(t)$ so that

$$\delta\left(t - \frac{\epsilon^{1/2}\rho}{c}\right) = -\frac{\delta(t - \epsilon^{1/2}\rho/c)}{(t - \epsilon^{1/2}\rho/c)}. \quad (19)$$

Formula (18) indicates that, in the equatorial plane of the dipole, pulses of the form $\delta'(t - \epsilon^{1/2}\rho/c)$ and $\delta(t - \epsilon^{1/2}\rho/c)$ travel radially outward with the velocity $v = c/\epsilon^{1/2}$, with the amplitude factors $\mu_0/4\pi\rho$ and $\zeta_s/4\pi\rho^2$, respectively. The δ' pulse corresponds to the far-field term $(i\omega\mu_0/4\pi\rho)e^{i(k_2\rho - \omega t)}$, and the δ pulse corresponds to the term $(-\zeta_s/4\pi\rho^2)e^{i(k_2\rho - \omega t)}$ in the steady-state field (4). After the pulses have passed any radial distance ρ , a static electric field with magnitude $1/4\pi\epsilon\epsilon_0\rho^3$ remains. This is due to the charge that remains separated on the dipole after the current pulses have occurred. The corresponding term in the steady-state formula (4) is the quasistatic term $(-i\omega\mu_0/4\pi k^2\rho^3)e^{i(k_2\rho - \omega t)} \equiv (-1/4\pi\omega\epsilon\epsilon_0\rho^3)e^{i(k_2\rho - \omega t)}$.

II. TIME-INDEPENDENT FIELD OF A UNIT VERTICAL ELECTRIC DIPOLE ON THE BOUNDARY BETWEEN ELECTRICALLY DIFFERENT HALF-SPACES

Consider next a vertical dipole in region 1 (lake water, $z > 0$) on the boundary, i.e., at $d = 0$, between region 1 and region 2 (air, $z < 0$). The wave numbers of these regions are $k_1 = \epsilon_1^{1/2}\omega/c$ and $k_2 = \omega/c$, where $\epsilon_1 = \epsilon_1/\epsilon_0$ is the real permittivity of region 1. The components of the electromagnetic field on the boundary $z = 0$ in region 2 are given elsewhere¹² with $z = d = 0$. They are

$$\bar{B}_\theta(\rho, \omega) = \frac{\mu_0 k_1^2}{2\pi} \int_0^\infty N^{-1} J_1(\lambda\rho) \lambda^2 d\lambda, \quad (20)$$

$$\bar{E}_\rho(\rho, \omega) = -\frac{i\omega\mu_0}{2\pi} \int_0^\infty \gamma_2 N^{-1} J_1(\lambda\rho) \lambda^2 d\lambda, \quad (21)$$

$$\begin{aligned} (\epsilon_1/\epsilon_0)\bar{E}_z(\rho, \omega) &= \bar{E}_z(\rho, \omega) \\ &= -\frac{\omega\mu_0}{2\pi} \int_0^\infty N^{-1} J_0(\lambda\rho) \lambda^2 d\lambda, \end{aligned} \quad (22)$$

where

$$N = k_1^2 \gamma_2 + k_2^2 \gamma_1, \quad \gamma_j = (k^2 - \lambda^2)^{1/2}, \quad j = 1, 2 \quad (23)$$

These are the time-independent field components generated by a current varying periodically at the angular frequency ω



FIG. 3 λ plane and the path of integration along the real axis

and with a unit electric moment, i.e., $I(t)h_s = I(0)h_s e^{-i\omega t}$ with $I(0)h_s = 1$ A m. They are the Fourier transforms of the time-dependent components $B_\theta(\rho, t)$, $E_\rho(\rho, t)$, and $E_z(\rho, t)$, which are to be determined.

III. TIME-DEPENDENT COMPONENT $\bar{E}_z(\rho, t)$ WITH A DELTA-FUNCTION EXCITATION

The integral for $\bar{E}_z(\rho, \omega)$ in explicit form is

$$\begin{aligned} \bar{E}_z(\rho, \omega) &= -\frac{\omega\mu_0}{2\pi} \int_0^\infty \\ &\times \frac{\lambda^3 J_0(\lambda\rho)}{k_1^2(k_1^2 - \lambda^2)^{1/2} + k_2^2(k_1^2 - \lambda^2)^{1/2}} d\lambda \end{aligned} \quad (24)$$

It is convenient to express this in terms of ω instead of the wave numbers. Thus, with $k_1^2 = \omega^2\epsilon/c^2$ and $k_2^2 = \omega^2/c^2$, where $c = (\mu_0\epsilon_0)^{-1/2}$ is the velocity of light and $\epsilon = \epsilon_1/\epsilon_0 = \epsilon_1/\epsilon_0$,

$$\begin{aligned} \bar{E}_z(\rho, \omega) &= -\frac{\omega\mu_0}{2\pi c} \int_0^\infty \\ &\times \frac{\lambda^3 J_0(\lambda\rho)}{\omega^2\epsilon(\omega^2 - \lambda^2)^{1/2} + \omega^2(\omega^2\epsilon - \lambda^2)^{1/2}} d\lambda \end{aligned} \quad (25)$$

In this formula, $\lambda = c\lambda'$ and $\rho' = \rho/c$. The path of integration in the λ plane is shown in Fig. 3. The integral in (25) is analytic in the upper half of the ω plane. This follows since in moving from the positive real axis to the upper half-plane as shown in Fig. 4, there is no need at all to deform the contour. Furthermore, since $\bar{E}_z(\rho, \omega)$ as defined in (25) is the Fourier transform of the real time-dependent component $E_z(\rho, t)$, it follows that

$$\bar{E}_z(\rho', \omega) = \bar{E}_z^*(\rho, \omega), \quad (26)$$

where the asterisk denotes the complex conjugate.

Let the vertical dipole be excited by a unit moment that is a delta-function pulse in time, i.e., $I(t)h_s = I(0)h_s \delta(t)$ with $I(0)h_s = 1$ A m. In order to carry out the Fourier transform explicitly in a way similar to that of Sec. I, the assumption, or approximation, is made that the relative dielectric constant ϵ , is independent of frequency. The real electric field is then given by the Fourier transform

$$E_z(\rho, t) = \frac{1}{\pi} \text{Re} \int_0^\infty e^{-i\omega t} \bar{E}_z(\rho', \omega) d\omega \quad (27)$$

With (25), this becomes

$$E_z(\rho, t) = -\frac{\mu_0}{2\pi^2 c} \text{Re} \int_0^\infty d\omega e^{-i\omega t} \omega \int_0^\infty d\lambda \frac{\lambda^3 J_0(\lambda\rho)}{\omega^2[\epsilon(\omega^2 - \lambda^2)^{1/2} + (\omega^2\epsilon - \lambda^2)^{1/2}]} \quad (28)$$

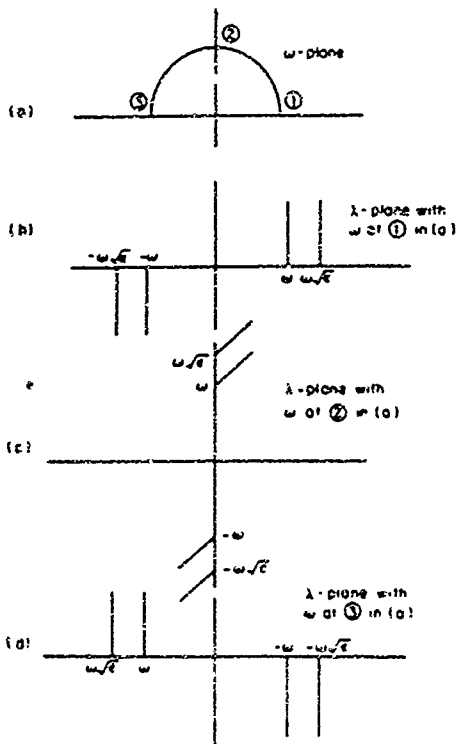


FIG 4 ω plane and λ plane for three locations of ω

Now let the variable be changed to ξ with $\lambda' = \omega\xi$, $d\lambda' = \omega d\xi$. The result is

$$E_{2z}(\rho', t) = -\frac{\mu_0}{2\pi^2 c} \operatorname{Re} \int_0^\infty d\omega e^{-i\omega t} \omega \times \int_0^\infty d\xi \frac{\xi^3 J_0(\omega\xi\rho')}{\epsilon(1-\xi^2)^{1/2} + (\epsilon - \xi^2)^{1/2}} \quad (29)$$

This integral is equal to the following:

$$E_{2z}(\rho', t) = \frac{\mu_0}{2\pi^2 c} \frac{\partial^2}{\partial t^2} \operatorname{Re} \times \int_0^\infty d\xi \frac{\xi^3}{\epsilon(1-\xi^2)^{1/2} + (\epsilon - \xi^2)^{1/2}} \times \int_0^\infty d\omega e^{-i\omega t} J_0(\omega\xi\rho'). \quad (30)$$

The integration with respect to ω can be carried out with formula (6.61'-1) on p. 707 of Gradshteyn and Ryzhik.¹¹ With $t > 0$, the integral is

$$\int_0^\infty d\omega e^{-i\omega t} J_0(\omega\xi\rho') = \begin{cases} -i(t^2 - \xi^2\rho'^2)^{-1/2}, & \xi\rho' < t, \\ (\xi^2\rho'^2 - t^2)^{-1/2}, & \xi\rho' > t, \end{cases} \quad (31)$$

so that, with $t > \xi\rho'$,

$$E_{2z}(\rho', t) = \frac{\mu_0}{2\pi^2 c} \frac{\partial^2}{\partial t^2} \operatorname{Im} \int_0^\infty d\xi \frac{\xi^3}{[\epsilon(1-\xi^2)^{1/2} + (\epsilon - \xi^2)^{1/2}](t^2/\rho'^2 - \xi^2)^{1/2}}, \quad (32)$$

with the branch-cut structure shown in Fig 5. In (32), ξ has been taken to be real. It is now convenient to let ξ be complex and to deform the contour of integration from the real axis to that shown in Fig. 6. Since the integrand is real on the vertical piece of the contour, integration along it yields zero. For $t < \rho'$, the integrand also remains real along the rest of the contour. Hence

$$E_{2z}(\rho', t) = 0, \quad t/\rho' < 1 \quad (33)$$

When $1 < t/\rho' < \epsilon^{1/2}$, there is a contribution to the integral. Thus

$$E_{2z}(\rho', t) = \frac{\mu_0}{2\pi^2 c} \frac{\partial^2}{\partial t^2} \operatorname{Im} \left[\int_0^1 d\xi \xi^3 \left(\frac{1}{[\epsilon(1-\xi^2)^{1/2} + (\epsilon - \xi^2)^{1/2}](t^2/\rho'^2 - \xi^2)^{1/2}} - \frac{1}{[\epsilon(1-\xi^2)^{1/2} + (\epsilon - \xi^2)^{1/2}](t^2/\rho'^2 - \xi^2)^{1/2}} \right) + \int_1^{t/\rho'} d\xi \xi^3 \left(\frac{1}{[i\epsilon(\xi^2 - 1)^{1/2} + (\epsilon - \xi^2)^{1/2}](t^2/\rho'^2 - \xi^2)^{1/2}} - \frac{1}{[i\epsilon(\xi^2 - 1)^{1/2} + (\epsilon - \xi^2)^{1/2}](t^2/\rho'^2 - \xi^2)^{1/2}} \right) \right] \quad (34)$$

The integrand of the first integral is real, so that there is no contribution to the imaginary part. The integrand in the second integral is complex so that

$$E_{2z}(\rho', t) = \frac{\mu_0}{\pi^2 c} \frac{\partial^2}{\partial t^2} \operatorname{Im} \int_1^{t/\rho'} d\xi \xi^3 \frac{1}{[i\epsilon(\xi^2 - 1)^{1/2} + (\epsilon - \xi^2)^{1/2}](t^2/\rho'^2 - \xi^2)^{1/2}} \quad (35)$$

The real and imaginary parts are readily separated and only the relevant imaginary part retained. This leaves

$$E_{2z}(\rho', t) = \frac{\mu_0}{\pi^2 c} \frac{\partial^2}{\partial t^2} \int_1^{t/\rho'} d\xi \xi^3 \frac{-\epsilon(\xi^2 - 1)^{1/2}}{(\epsilon - 1)[(\epsilon + 1)\xi^2 - \epsilon](t^2/\rho'^2 - \xi^2)^{1/2}}. \quad (36)$$

It is now convenient to change the variable to $\zeta = \xi^2$, $d\zeta = 2\xi d\xi$, and obtain

$$E_{2z}(\rho', t) = -\frac{\epsilon}{\epsilon-1} \frac{\mu_0}{2\pi^2 \rho' c} \frac{\partial^2}{\partial t^2} \int_1^{t/\rho'} \frac{(\xi-1)^{1/2} \xi d\xi}{[(\epsilon+1)\xi-\epsilon](t^2/\rho'^2-\xi^2)^{1/2}}, \quad 1 < \frac{t}{\rho'} < \epsilon^{1/2}. \quad (37)$$

The expression corresponding to (35) for the range $t/\rho' > \epsilon^{1/2}$ is

$$E_{2z}(\rho', t) = \frac{\mu_0}{\pi^2 \rho' c} \frac{\partial^2}{\partial t^2} \text{Im} \left(\int_1^{t/\rho'} \frac{\xi^3 d\xi}{[i\epsilon(\xi^2-1)^{1/2} + (\epsilon-\xi^2)^{1/2}](t^2/\rho'^2-\xi^2)^{1/2}} + \int_{t/\rho'}^{\epsilon^{1/2}} \frac{\xi^3 d\xi}{[i\epsilon(\xi^2-1)^{1/2} + i(\xi^2-\epsilon)^{1/2}](t^2/\rho'^2-\xi^2)^{1/2}} \right). \quad (38)$$

The imaginary part is

$$E_{2z}(\rho', t) = -\frac{\mu_0}{\pi^2 \rho' c} \frac{\partial^2}{\partial t^2} \left(\int_1^{t/\rho'} \frac{-\epsilon(\xi^2-1)^{1/2} \xi^3 d\xi}{(\epsilon-1)[(\epsilon+1)\xi^2-\epsilon](t^2/\rho'^2-\xi^2)^{1/2}} + \int_{t/\rho'}^{\epsilon^{1/2}} \frac{[-\epsilon(\xi^2-1)^{1/2} + (\xi^2-\epsilon)^{1/2}] \xi^3 d\xi}{(\epsilon-1)[(\epsilon+1)\xi^2-\epsilon](t^2/\rho'^2-\xi^2)^{1/2}} \right). \quad (39)$$

The first part of the second integral can be combined with the first integral to obtain

$$E_{2z}(\rho', t) = -\frac{1}{\epsilon-1} \frac{\mu_0}{\pi^2 \rho' c} \frac{\partial^2}{\partial t^2} \left(\epsilon \int_1^{t/\rho'} \frac{(\xi^2-1)^{1/2} \xi^3 d\xi}{[(\epsilon+1)\xi^2-\epsilon](t^2/\rho'^2-\xi^2)^{1/2}} - \int_{t/\rho'}^{\epsilon^{1/2}} \frac{(\xi^2-\epsilon)^{1/2} \xi^3 d\xi}{[(\epsilon+1)\xi^2-\epsilon](t^2/\rho'^2-\xi^2)^{1/2}} \right). \quad (40)$$

In terms of the variable $\xi = \xi^2$, this becomes

$$E_{2z}(\rho', t) = -\frac{1}{\epsilon-1} \frac{\mu_0}{2\pi^2 \rho' c} \frac{\partial^2}{\partial t^2} \left(\epsilon \int_1^{t/\rho'} \frac{(\xi-1)^{1/2} \xi d\xi}{[(\epsilon+1)\xi-\epsilon](t^2/\rho'^2-\xi)^{1/2}} - \int_{t/\rho'}^{\epsilon^{1/2}} \frac{(\xi-\epsilon)^{1/2} \xi d\xi}{[(\epsilon+1)\xi-\epsilon](t^2/\rho'^2-\xi)^{1/2}} \right), \quad \frac{t}{\rho'} > \epsilon^{1/2}. \quad (41)$$

IV. EVALUATION OF THE INTEGRALS FOR $E_{2z}(\rho, t)$

Expressions (37) and (41) are more convenient for integration with the notation

$$T_0 = (t^2/\rho'^2) - 1, \quad T_\epsilon = (t^2/\rho'^2) - \epsilon, \quad (42)$$

and the change in variables $x' = \xi - 1$, $y' = \xi - \epsilon$. Thus, by using ϑ_0 and ϑ_ϵ to denote the integrals that appear in (37) and (41),

$$\begin{aligned} \vartheta_0 &= \int_1^{t/\rho'} \frac{(\xi-1)^{1/2} \xi d\xi}{[(\epsilon+1)\xi-\epsilon](t^2/\rho'^2-\xi^2)^{1/2}} \\ &= \int_1^{T_0+1} \frac{(\xi-1)^{1/2} \xi d\xi}{[(\epsilon+1)\xi-\epsilon][T_0-(\xi-1)]^{1/2}} \\ &= \int_0^{T_0} \frac{x'(x'+1) dx'}{[(\epsilon+1)(x'+1)-\epsilon][(T_0-x')x']^{1/2}}, \end{aligned} \quad (43)$$

$$\vartheta_\epsilon = \int_{t/\rho'}^{\epsilon^{1/2}} \frac{(\xi-\epsilon)^{1/2} \xi d\xi}{[(\epsilon+1)\xi-\epsilon](t^2/\rho'^2-\xi^2)^{1/2}}$$

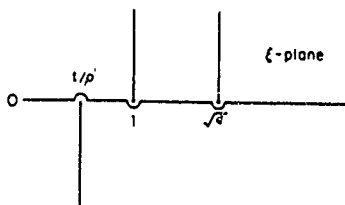


FIG 5. Branch-cut structure for the integral in (32).

$$\begin{aligned} &= \int_{t/\rho'}^{T_\epsilon+\epsilon} \frac{(\xi-\epsilon)^{1/2} \xi d\xi}{[(\epsilon+1)\xi-\epsilon][T_\epsilon-(\xi-\epsilon)]^{1/2}} \\ &= \int_0^{T_\epsilon} \frac{y'(y'+\epsilon) dy'}{[(\epsilon+1)(y'+\epsilon)-\epsilon][(T_\epsilon-y')y']^{1/2}} \end{aligned} \quad (44)$$

As a temporary shorthand, let $E_0 = 1/(\epsilon+1)$, $E_\epsilon = \epsilon^2/(\epsilon+1)$; also, introduce $x = x' + E_0$ and $y = y' + E_\epsilon$. The integrals now become

$$\vartheta_0 = \frac{1}{\epsilon+1} \int_{E_0}^{T_0+E_0} \frac{(x+1-E_0)(x-E_0) dx}{x[(T_0+E_0-x)(x-E_0)]^{1/2}}, \quad (45)$$

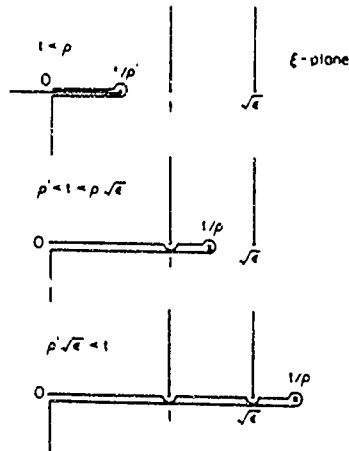


FIG 6. Contours of integration for (32)

$$\vartheta_e = \frac{1}{\epsilon + 1} \int_{E_e}^{T_e + E_e} \frac{(y + \epsilon - E_e)(y - E_e) dy}{y[(T_e + E_e - y)(y - E_e)]^{1/2}}. \quad (46)$$

These can be reduced to standard form. Let

$$\begin{aligned} X &= (T + E - x)(x - E) \\ &= -E(T + E) + (T + 2E)x - x^2 \\ &= a + bx + cx^2, \end{aligned} \quad (47)$$

where T stands for T_0 or T_e , E for E_0 or E_e , and x for x or y . Note that $q = 4ac - b^2 = -T^2$ so that $\sqrt{-q} = T$. With this notation

$$\begin{aligned} \vartheta &= \frac{1}{\epsilon + 1} \left(\int_E^{T+E} \frac{x dx}{\sqrt{X}} + (1 - 2E) \int_E^{T+E} \frac{dx}{\sqrt{X}} \right. \\ &\quad \left. - E(1 - E) \int_E^{T+E} \frac{dx}{x\sqrt{X}} \right). \end{aligned} \quad (48)$$

These are tabulated integrals. When the limits are inserted in the integrated expressions, the first integral vanishes, and

the second and third integrals yield arcsines with arguments ± 1 . The final integrated formula is

$$\vartheta = \frac{\pi}{2(\epsilon + 1)} \left(T - 2(E - 1) + \frac{2(E - 1)E}{[E(T + E)]^{1/2}} \right) \quad (49)$$

The substitutions T_0 and T_e for T , E_0 and E_e for E , and 1 and ϵ for 1 in $(E - 1)$ can now be made, followed by the substitution. $T_0 = (t^2/\rho'^2) - 1$, $T_e = (t^2/\rho'^2) - \epsilon$, $E_0 = (\epsilon + 1)^{-1}$, and $E_e = \epsilon^2(\epsilon + 1)^{-1}$. The resulting formulas are

$$\begin{aligned} \vartheta_0 &= \frac{\pi}{2(\epsilon + 1)} \left[\frac{t^2}{\rho'^2} - 1 + \frac{2\epsilon}{\epsilon + 1} \right. \\ &\quad \left. - \frac{2\epsilon}{\epsilon + 1} \left((\epsilon + 1) \frac{t^2}{\rho'^2} - \epsilon \right)^{-1/2} \right], \end{aligned} \quad (50)$$

$$\begin{aligned} \vartheta_e &= \frac{\pi}{2(\epsilon + 1)} \left[\frac{t^2}{\rho'^2} - \epsilon + \frac{2\epsilon}{\epsilon + 1} \right. \\ &\quad \left. - \frac{2\epsilon^2}{\epsilon + 1} \left((\epsilon + 1) \frac{t^2}{\rho'^2} - \epsilon \right)^{-1/2} \right]. \end{aligned} \quad (51)$$

V. EVALUATION OF $E_{2z}(\rho, t)$

With the integrated values (50) and (51), the expressions (37) and (41) for $E_{2z}(\rho', t)$ become

$$E_{2z}(\rho', t) = -\frac{\epsilon}{\epsilon^2 - 1} \frac{\mu_0}{4\pi\rho'c} \frac{\partial^2}{\partial t^2} \left[\frac{t^2}{\rho'^2} - 1 + \frac{2\epsilon}{\epsilon + 1} - \frac{2\epsilon}{\epsilon + 1} \left((\epsilon + 1) \frac{t^2}{\rho'^2} - \epsilon \right)^{-1/2} \right], \quad 1 < \frac{t}{\rho'} < \epsilon^{1/2}, \quad (52)$$

$$\begin{aligned} E_{2z}(\rho', t) &= -\frac{\epsilon}{\epsilon^2 - 1} \frac{\mu_0}{4\pi\rho'c} \frac{\partial^2}{\partial t^2} \left[\frac{t^2}{\rho'^2} - 1 + \frac{2\epsilon}{\epsilon + 1} - \frac{2\epsilon}{\epsilon + 1} \left((\epsilon + 1) \frac{t^2}{\rho'^2} - \epsilon \right)^{-1/2} \right] \\ &\quad + \frac{1}{\epsilon^2 - 1} \frac{\mu_0}{4\pi\rho'c} \frac{\partial^2}{\partial t^2} \left[\frac{t^2}{\rho'^2} - \epsilon + \frac{2\epsilon}{\epsilon + 1} - \frac{2\epsilon^2}{\epsilon + 1} \left((\epsilon + 1) \frac{t^2}{\rho'^2} - \epsilon \right)^{-1/2} \right], \quad \frac{t}{\rho'} > \epsilon^{1/2}. \end{aligned} \quad (53)$$

The second formula reduces to

$$E_{2z}(\rho', t) = -\frac{1}{\epsilon + 1} \frac{\mu_0}{4\pi\rho'c} \frac{\partial^2}{\partial t^2} \left(\frac{t^2}{\rho'^2} + \frac{2\epsilon}{\epsilon + 1} \right), \quad \frac{t}{\rho'} > \epsilon^{1/2}. \quad (54)$$

Similar to the case of the infinite homogeneous dielectric of Sec. I, the differentiation of (52) and (54) must be carried out with care, owing to the presence of discontinuities at $t/\rho' = 1$ and $\epsilon^{1/2}$. Thus, with

$$f(t/\rho') \equiv \begin{cases} 0, & t/\rho' < 1, \\ \frac{\epsilon}{\epsilon^2 - 1} \left[\frac{t^2}{\rho'^2} - 1 + \frac{2\epsilon}{\epsilon + 1} - \frac{2\epsilon}{\epsilon + 1} \left((\epsilon + 1) \frac{t^2}{\rho'^2} - \epsilon \right)^{-1/2} \right], & 1 < \frac{t}{\rho'} < \epsilon^{1/2}, \\ \frac{1}{\epsilon + 1} \left(\frac{t^2}{\rho'^2} + \frac{2\epsilon}{\epsilon + 1} \right), & \epsilon^{1/2} < \frac{t}{\rho'}, \end{cases} \quad (55)$$

$$\frac{\epsilon}{\epsilon^2 - 1} \left[\frac{t^2}{\rho'^2} - 1 + \frac{2\epsilon}{\epsilon + 1} - \frac{2\epsilon}{\epsilon + 1} \left((\epsilon + 1) \frac{t^2}{\rho'^2} - \epsilon \right)^{-1/2} \right], \quad 1 < \frac{t}{\rho'} < \epsilon^{1/2}, \quad (56)$$

$$\frac{1}{\epsilon + 1} \left(\frac{t^2}{\rho'^2} + \frac{2\epsilon}{\epsilon + 1} \right), \quad \epsilon^{1/2} < \frac{t}{\rho'}, \quad (57)$$

it follows that

$$E_{2z}(\rho', t) = -\frac{\mu_0}{4\pi\rho'c} \frac{\partial^2}{\partial t^2} f\left(\frac{t}{\rho'}\right). \quad (58)$$

Consider first the continuity of $f(t/\rho')$ at $t/\rho' = 1$ and $\epsilon^{1/2}$. From (55) and (56),

$$f(1-) = f(1+) = 0. \quad (59)$$

Similarly, from (56) and (57),

$$f(\epsilon^{1/2}-) = f(\epsilon^{1/2}+) = \frac{\epsilon(\epsilon + 3)}{(\epsilon + 1)^2}. \quad (60)$$

It follows that $f(t/\rho')$ is everywhere continuous. Consider next the behavior of $\partial f(t/\rho')/\partial t$. Let $f'(t/\rho') = \partial f(t/\rho')/\partial t$. Then

$$f'(t/\rho') = \begin{cases} 0, & t/\rho' < 1, \\ \frac{\epsilon}{\epsilon^2 - 1} \frac{2t}{\rho'^2} \left[1 + \epsilon \left((\epsilon + 1) \frac{t^2}{\rho'^2} - \epsilon \right)^{-3/2} \right], & 1 < \frac{t}{\rho'} < \epsilon^{1/2}, \\ \frac{1}{\epsilon + 1} \frac{2t}{\rho'^2}, & \epsilon^{1/2} < \frac{t}{\rho'}. \end{cases} \quad (61)$$

$$f'(t/\rho') = \begin{cases} 0, & t/\rho' < 1, \\ \frac{\epsilon}{\epsilon^2 - 1} \frac{2t}{\rho'^2} \left[1 + \epsilon \left((\epsilon + 1) \frac{t^2}{\rho'^2} - \epsilon \right)^{-3/2} \right], & 1 < \frac{t}{\rho'} < \epsilon^{1/2}, \\ \frac{1}{\epsilon + 1} \frac{2t}{\rho'^2}, & \epsilon^{1/2} < \frac{t}{\rho'}. \end{cases} \quad (62)$$

$$f'(t/\rho') = \begin{cases} 0, & t/\rho' < 1, \\ \frac{\epsilon}{\epsilon^2 - 1} \frac{2t}{\rho'^2} \left[1 + \epsilon \left((\epsilon + 1) \frac{t^2}{\rho'^2} - \epsilon \right)^{-3/2} \right], & 1 < \frac{t}{\rho'} < \epsilon^{1/2}, \\ \frac{1}{\epsilon + 1} \frac{2t}{\rho'^2}, & \epsilon^{1/2} < \frac{t}{\rho'}. \end{cases} \quad (63)$$

At $t/\rho' = 1$ and $\epsilon^{1/2}$, $f'(t/\rho')$ has the following behavior:

$$f'(1-) = 0, \quad f'(1+) = [\epsilon/(\epsilon - 1)](2/\rho'). \quad (64)$$

Hence there is a step discontinuity of $2\epsilon/(\epsilon - 1)\rho'$ in $f'(t/\rho')$ at $t/\rho' = 1$. Similarly,

$$f'(\epsilon^{1/2}-) = \frac{\epsilon}{\epsilon^2 - 1} \frac{2\epsilon^{1/2}}{\rho'} (1 + \epsilon^{-2}) = \frac{\epsilon^2 + 1}{\epsilon^{1/2}(\epsilon^2 - 1)} \frac{2}{\rho'}, \quad (65)$$

$$f'(\epsilon^{1/2}+) = \frac{\epsilon^{1/2}}{\epsilon + 1} \frac{2}{\rho'}. \quad (66)$$

There is a step discontinuity of

$$\left(\frac{\epsilon^{1/2}}{\epsilon + 1} - \frac{\epsilon^2 + 1}{\epsilon^{1/2}(\epsilon^2 - 1)} \right) \frac{2}{\rho'} = -\frac{1}{\epsilon^{1/2}(\epsilon - 1)} \frac{2}{\rho'}$$

at $t/\rho' = \epsilon^{1/2}$. Now, let $f''(t/\rho') = \partial f'(t/\rho')/\partial t$. Its behavior is

$$f''(t/\rho') = \begin{cases} 0, & t/\rho' < 1, \\ \frac{\epsilon}{\epsilon^2 - 1} \frac{2}{\rho'^2} \left[1 - \frac{\epsilon}{(\epsilon + 1)^{3/2}} \left(\frac{2t^2}{\rho'^2} + \frac{\epsilon}{\epsilon + 1} \right) \left(\frac{t^2}{\rho'^2} - \frac{\epsilon}{\epsilon + 1} \right)^{-5/2} \right], & 1 < \frac{t}{\rho'} < \epsilon^{1/2}, \\ \frac{1}{\epsilon + 1} \frac{2}{\rho'^2}, & \epsilon^{1/2} < \frac{t}{\rho'}. \end{cases} \quad (67)$$

$$f''(t/\rho') = \begin{cases} 0, & t/\rho' < 1, \\ \frac{\epsilon}{\epsilon^2 - 1} \frac{2}{\rho'^2} \left[1 - \frac{\epsilon}{(\epsilon + 1)^{3/2}} \left(\frac{2t^2}{\rho'^2} + \frac{\epsilon}{\epsilon + 1} \right) \left(\frac{t^2}{\rho'^2} - \frac{\epsilon}{\epsilon + 1} \right)^{-5/2} \right], & 1 < \frac{t}{\rho'} < \epsilon^{1/2}, \\ \frac{1}{\epsilon + 1} \frac{2}{\rho'^2}, & \epsilon^{1/2} < \frac{t}{\rho'}. \end{cases} \quad (68)$$

$$f''(t/\rho') = \begin{cases} 0, & t/\rho' < 1, \\ \frac{\epsilon}{\epsilon^2 - 1} \frac{2}{\rho'^2} \left[1 - \frac{\epsilon}{(\epsilon + 1)^{3/2}} \left(\frac{2t^2}{\rho'^2} + \frac{\epsilon}{\epsilon + 1} \right) \left(\frac{t^2}{\rho'^2} - \frac{\epsilon}{\epsilon + 1} \right)^{-5/2} \right], & 1 < \frac{t}{\rho'} < \epsilon^{1/2}, \\ \frac{1}{\epsilon + 1} \frac{2}{\rho'^2}, & \epsilon^{1/2} < \frac{t}{\rho'}. \end{cases} \quad (69)$$

In view of the discontinuities of $f''(t/\rho')$ at 1 and $\epsilon^{1/2}$, it follows that, with $\rho' = \rho/c$ and $\mu_0 c^2 = \epsilon_0^{-1}$, the complete final expression for

$$E_{2z}(\rho, t) = -(\mu_0/4\pi\rho) f''(t/\rho)$$

is

$$E_{2z}(\rho, t) = -\frac{1}{2\pi\epsilon_0\rho^3 c(\epsilon - 1)} [\epsilon\delta(t - \rho/c) - \epsilon^{-1/2}\delta(t - \epsilon^{1/2}\rho/c)]$$

$$-\frac{1}{2\pi\epsilon_0\rho^3(\epsilon + 1)} \left\{ \begin{aligned} &0, \quad ct/\rho < 1 \\ &\frac{\epsilon}{\epsilon - 1} \left[1 - \frac{\epsilon}{(\epsilon + 1)^{3/2}} \left(\frac{2c^2t^2}{\rho^2} + \frac{\epsilon}{\epsilon + 1} \right) \left(\frac{c^2t^2}{\rho^2} - \frac{\epsilon}{\epsilon + 1} \right)^{-5/2} \right], & 1 < \frac{ct}{\rho} < \epsilon^{1/2} \\ &1, & \epsilon^{1/2} < ct/\rho \end{aligned} \right\}. \quad (70)$$

This is the vertical electric field in region 2 just above the boundary. The field in region 1 just below the boundary is obtained from the boundary condition. It is

$$E_{1z}(\rho, t) = \epsilon^{-1} E_{2z}(\rho, t), \quad (71)$$

where $\epsilon \equiv \epsilon_{12}$. Note that the dipole source is located on the boundary in region 1. At any radial distance ρ , the electric field is initially zero until the instant $t = \rho/c$ when a downward-directed electric field arrives in the form of a delta-function pulse. That is, the magnitude of the field increases momentarily to infinity and decreases to the value

$$E_{2z}\left(\rho, \frac{\rho}{c}\right) = -\frac{1}{2\pi\epsilon_0\rho^3} \frac{\epsilon(1 - 3\epsilon^2 - 2\epsilon)}{\epsilon^2 - 1}. \quad (72)$$

This pulse has traveled along the boundary in region 2 (air) with the velocity c . The field then rises gradually with time according to

$$E_{2z}(\rho, t) = -\frac{1}{2\pi\epsilon_0\rho^3} \frac{\epsilon}{\epsilon^2 - 1}$$

$$\times \left[1 - \frac{\epsilon}{(\epsilon + 1)^{3/2}} \left(\frac{2c^2t^2}{\rho^2} + \frac{\epsilon}{\epsilon + 1} \right) \left(\frac{c^2t^2}{\rho^2} - \frac{\epsilon}{\epsilon + 1} \right)^{-5/2} \right]$$

$$\times \left(\frac{c^2t^2}{\rho^2} - \frac{\epsilon}{\epsilon + 1} \right)^{-3/2}, \quad (73)$$

until $t = \epsilon^{1/2}\rho/c$, when it has the value

$$E_{2z}\left(\rho, \frac{\epsilon^{1/2}\rho}{c}\right) = -\frac{1}{2\pi\epsilon_0\rho^3} \frac{\epsilon^3 - 2\epsilon - 3}{\epsilon^2(\epsilon^2 - 1)}. \quad (74)$$

At this instant an upward-directed delta function rises momentarily in magnitude to infinity and decreases to

$$E_{2z}(\rho, t) = -1/2\pi\epsilon_0\rho^3(\epsilon + 1). \quad (75)$$

The second pulse that arrives at $t = \epsilon^{1/2}\rho/c$ has traveled

along the boundary in region 1 (the dielectric) with the velocity $c/\epsilon^{1/2}$. When it has passed, the field drops to the static value due to the charged infinitesimal dipole. Note that the electric field (70) is always directed downward except during the instant when the second delta-function pulse passes, when it is directed upward.

It is of interest to note that for the first pulse, traveling in air, the adjacent boundary with the dielectric acts approximately like an electric wall so that the vertically directed current is approximately doubled in amplitude along the boundary surface. On the other hand, for the second pulse, traveling in the dielectric, the adjacent boundary with air acts approximately like a magnetic wall so that the vertically directed reflected field is almost canceled by the direct field along the boundary. In the two cases the doubling is exact and the cancellation complete when the permittivity of the dielectric half-space is infinite, i.e., $\epsilon \rightarrow \infty$. Specifically, when $\epsilon < \infty$, the amplitude for the pulse in air is not exactly 2 but given by

$$2\epsilon/(\epsilon - 1) = 1 + (\epsilon + 1)/(\epsilon - 1) \rightarrow 2$$

when $\epsilon \rightarrow \infty$; similarly, the cancellation in the dielectric is

not complete and the difference between the direct and reflected fields is the quantity

$$-1/(\epsilon - 1) \approx 1 - \epsilon/(\epsilon - 1) \rightarrow 0$$

when $\epsilon \rightarrow \infty$. Evidently, when ϵ is large but finite, the positive contribution to the field in the air from the imperfect image is slightly greater than the direct field, so that the total field is positive and slightly more than doubled; similarly, the negative contribution to the field in the dielectric by the imperfect image is slightly greater than the direct field, so that the total field in this case is small and negative.

It is significant to note that the amplitude of the delta-function pulses in (70) includes the factor $1/\rho^2$. This is also the radial dependence in the far field of the frequency-dependent field and consists entirely of the lateral wave. Since the spectrum of the delta function is dominated by high frequencies, this behavior is readily understood. Note that the pulse of the dipole in a homogeneous single medium also follows the far-field behavior of the steady state, but this is the direct field with $1/\rho$ decrease. When the dipole is on the boundary, the far field is entirely due to lateral waves or a lateral pulse with $1/\rho^2$ decrease with distance.

VI. TIME-DEPENDENT COMPONENT $B_{2\phi}(\rho, t)$ WITH A DELTA-FUNCTION EXCITATION

The integral for $\tilde{B}_{2\phi}(\rho, \omega)$ in explicit form is

$$\tilde{B}_{2\phi}(\rho', \omega) = \frac{i\mu_0\omega^2}{2\pi c^2} \int_0^\infty \frac{J_1(\lambda' \rho') \lambda'^2 d\lambda'}{\omega^2 \epsilon (\omega^2 - \lambda'^2)^{1/2} + \omega^2 (\omega^2 \epsilon - \lambda'^2)^{1/2}}, \quad (76)$$

where $\lambda' = c\lambda$ and $\rho' = \rho/c$. The corresponding time-dependent component for the excitation (2) is

$$\begin{aligned} B_{2\phi}(\rho', t) &= \frac{1}{\pi} \operatorname{Re} \int_0^\infty e^{-i\omega t} \tilde{B}_{2\phi}(\rho', \omega) d\omega \\ &= \operatorname{Re} \frac{i\mu_0}{2\pi^2 c^2} \int_0^\infty d\omega e^{-i\omega t} \omega^2 \int_0^\infty \frac{J_1(\lambda' \rho') \lambda'^2 d\lambda'}{\omega^2 [\epsilon (\omega^2 - \lambda'^2)^{1/2} + (\omega^2 \epsilon - \lambda'^2)^{1/2}]} \end{aligned} \quad (77)$$

Now let the variable be changed to ξ with the substitution $\lambda' = \omega\xi$, $d\lambda' = \omega d\xi$. The result is

$$\begin{aligned} B_{2\phi}(\rho', t) &= \frac{\mu_0}{2\pi^2 c^2} \int_0^\infty d\xi \int_0^\infty d\omega \operatorname{Re} i\omega^2 e^{-i\omega t} \frac{\xi^2 J_1(\omega\xi\rho')}{\epsilon(1 - \xi^2)^{1/2} + (\epsilon - \xi^2)^{1/2}} \\ &= \frac{\mu_0}{2\pi^2 c^2} \frac{\partial^2}{\partial t^2} \int_0^\infty d\xi \operatorname{Im} \frac{\xi^2}{\epsilon(1 - \xi^2)^{1/2} + (\epsilon - \xi^2)^{1/2}} \int_0^\infty d\omega e^{-i\omega t} J_1(\omega\xi\rho'). \end{aligned} \quad (78)$$

The integration with respect to ω can be carried out with formula (6.611-1) on p. 707 of Gradshteyn and Ryzhik.¹¹ The result is

$$B_{2\phi}(\rho', t) = \frac{\mu_0}{2\pi^2 c^2} \frac{\partial^2}{\partial t^2} \operatorname{Im} \int_0^\infty \frac{\xi^2}{\epsilon(1 - \xi^2)^{1/2} + (\epsilon - \xi^2)^{1/2}} \left(1 - \frac{t}{(t^2 - \xi^2 \rho'^2)^{1/2}}\right) \frac{d\xi}{\xi \rho'}. \quad (79)$$

This integral can be separated into two parts as follows:

$$\begin{aligned} B_{2\phi}(\rho', t) &= \frac{\mu_0}{2\pi^2 c^2 \rho'} \frac{\partial^2}{\partial t^2} \operatorname{Im} \left(\int_0^\infty \frac{\xi d\xi}{\epsilon(1 - \xi^2)^{1/2} + (\epsilon - \xi^2)^{1/2}} \right. \\ &\quad \left. - \frac{t}{\rho'} \int_0^\infty \frac{\xi d\xi}{[\epsilon(1 - \xi^2)^{1/2} + (\epsilon - \xi^2)^{1/2}](t^2/\rho'^2 - \xi^2)^{1/2}} \right). \end{aligned} \quad (80)$$

With the branch-cut structure in Fig. 5, it follows that

$$B_{2\phi}(\rho', t) = 0, \quad t/\rho' < 1, \quad (81)$$

$$\begin{aligned} B_{2\phi}(\rho', t) &= \frac{\mu_0}{2\pi^2 c^2 \rho'} \frac{\partial^2}{\partial t^2} \operatorname{Im} \left(\int_0^\infty \frac{\xi d\xi}{i\epsilon(\xi^2 - 1)^{1/2} + (\epsilon - \xi^2)^{1/2}} \right. \\ &\quad \left. - \frac{t}{\rho'} \int_0^\infty \frac{\xi d\xi}{[i\epsilon(\xi^2 - 1)^{1/2} + (\epsilon - \xi^2)^{1/2}](t^2/\rho'^2 - \xi^2)^{1/2}} \right), \quad 1 < \frac{t}{\rho'} < \epsilon^{1/2}. \end{aligned} \quad (82)$$

The real and imaginary parts are readily separated and only the imaginary part retained. The result is

$$B_{2a}(\rho', t) = -\frac{\epsilon}{\epsilon-1} \frac{\mu_0}{2\pi^2 c^2 \rho'} \frac{\partial^2}{\partial t^2} \left(\int_0^\infty \frac{(\xi^2-1)^{1/2} \xi d\xi}{(\epsilon+1)\xi^2-\epsilon} - \frac{t}{\rho'} \int_0^\infty \frac{(\xi^2-1)^{1/2} \xi d\xi}{[(\epsilon+1)\xi^2-\epsilon](t^2/\rho'^2-\xi^2)^{1/2}} \right) \quad (83)$$

With the contour in Fig. 6, this becomes

$$\begin{aligned} B_{2a}(\rho', t) &= -\frac{\epsilon}{\epsilon-1} \frac{\mu_0}{2\pi^2 c^2 \rho'} \frac{\partial^2}{\partial t^2} \left(\int_1^{t/\rho'} \frac{(\xi^2-1)^{1/2} \xi d\xi}{(\epsilon+1)\xi^2-\epsilon} \right. \\ &\quad - \frac{t}{\rho'} \int_1^{t/\rho'} \frac{(\xi^2-1)^{1/2} \xi d\xi}{[(\epsilon+1)\xi^2-\epsilon](t^2/\rho'^2-\xi^2)^{1/2}} - \int_1^{t/\rho'} \frac{(\xi^2-1)^{1/2} \xi d\xi}{(\epsilon+1)\xi^2-\epsilon} \\ &\quad \left. + \frac{t}{\rho'} \int_1^{t/\rho'} \frac{(\xi^2-1)^{1/2} \xi d\xi}{[(\epsilon+1)\xi^2-\epsilon](-t^2/\rho'^2-\xi^2)^{1/2}} \right) \\ &= \frac{\epsilon}{\epsilon-1} \frac{\mu_0}{\pi^2 c^2 \rho'} \frac{\partial^2}{\partial t^2} \left(\frac{t}{\rho'} \int_1^{t/\rho'} \frac{(\xi^2-1)^{1/2} \xi d\xi}{[(\epsilon+1)\xi^2-\epsilon](t^2/\rho'^2-\xi^2)^{1/2}} \right) \end{aligned} \quad (84)$$

With $\xi = \xi^2$,

$$B_{2a}(\rho', t) = \frac{\epsilon}{\epsilon-1} \frac{\mu_0}{2\pi^2 c^2 \rho'} \frac{\partial^2}{\partial t^2} \left(\frac{t}{\rho'} \int_1^{t/\rho'} \frac{(\xi-1)^{1/2} d\xi}{[(\epsilon+1)\xi-\epsilon](t^2/\rho'^2-\xi)^{1/2}} \right), \quad 1 < \frac{t}{\rho'} < \epsilon^{1/2} \quad (85)$$

Let $T_0 = t^2/\rho'^2 - 1$, $x' = \xi - 1$. Then

$$B_{2a}(\rho', t) = \frac{\epsilon}{\epsilon-1} \frac{\mu_0}{2\pi^2 c^2 \rho'} \frac{\partial^2}{\partial t^2} \left(\frac{t}{\rho'} \int_0^{T_0} \frac{x' dx'}{[(\epsilon+1)(x'+1)-\epsilon][(T_0-x')x']^{1/2}} \right) \quad (86)$$

Finally, with $x = x' + E_0$ and $E_0 = 1/(\epsilon+1)$,

$$B_{2a}(\rho', t) = \frac{\epsilon}{\epsilon^2-1} \frac{\mu_0}{2\pi^2 c^2 \rho'} \frac{\partial^2}{\partial t^2} \left[\frac{t}{\rho'} \left(\int_{E_0}^{T_0+E_0} \frac{dx}{\sqrt{X_0}} - E_0 \int_{E_0}^{T_0+E_0} \frac{dx}{x\sqrt{X_0}} \right) \right], \quad (87)$$

where $X_0 = a_0 + b_0 x + c_0 x^2$ with $a_0 = -E_0(T_0 + E_0)$, $b_0 = T_0 + 2E_0$, and $c_0 = -1$. These integrals are like those in (48). They give

$$B_{2a}(\rho', t) = \frac{\epsilon}{\epsilon^2-1} \frac{\mu_0}{2\pi^2 c^2 \rho'} \frac{\partial^2}{\partial t^2} \left[\frac{t}{\rho'} \left[1 - \left((\epsilon+1) \frac{t^2}{\rho'^2} - \epsilon \right)^{-1/2} \right] \right], \quad 1 < \frac{t}{\rho'} < \epsilon^{1/2} \quad (88)$$

In the remaining range, $t/\rho' > \epsilon^{1/2}$,

$$\begin{aligned} B_{2a}(\rho', t) &= \frac{\mu_0}{2\pi^2 c^2 \rho'} \frac{\partial^2}{\partial t^2} \operatorname{Im} \left(\int_0^\infty \frac{\xi d\xi}{i\epsilon(\xi^2-1)^{1/2} + (\epsilon-\xi^2)^{1/2}} \right. \\ &\quad - \frac{t}{\rho'} \int_0^\infty \frac{\xi d\xi}{[i\epsilon(\xi^2-1)^{1/2} + (\epsilon-\xi^2)^{1/2}](t^2/\rho'^2-\xi^2)^{1/2}} \\ &\quad \left. + \int_{t/\rho'}^\infty \frac{\xi d\xi}{i\epsilon(\xi^2-1)^{1/2} + i(\xi^2-\epsilon)^{1/2}} - \frac{t}{\rho'} \int_{t/\rho'}^\infty \frac{\xi d\xi}{[i\epsilon(\xi^2-1)^{1/2} + i(\xi^2-\epsilon)^{1/2}](t^2/\rho'^2-\xi^2)^{1/2}} \right) \end{aligned} \quad (89)$$

The contributing imaginary part of the integrals is

$$\begin{aligned} B_{2a}(\rho', t) &= -\frac{1}{\epsilon-1} \frac{\mu_0}{2\pi^2 c^2 \rho'} \frac{\partial^2}{\partial t^2} \left(\epsilon \int_0^{t/\rho'} \frac{(\xi^2-1)^{1/2} \xi d\xi}{(\epsilon+1)\xi^2-\epsilon} - \frac{\epsilon t}{\rho'} \int_0^{t/\rho'} \frac{(\xi^2-1)^{1/2} \xi d\xi}{[(\epsilon+1)\xi^2-\epsilon](t^2/\rho'^2-\xi^2)^{1/2}} \right. \\ &\quad \left. - \int_{t/\rho'}^\infty \frac{[-\epsilon(\xi^2-1)^{1/2} + (\xi^2-\epsilon)^{1/2}] \xi d\xi}{(\epsilon+1)\xi^2-\epsilon} + \frac{t}{\rho'} \int_{t/\rho'}^\infty \frac{[-\epsilon(\xi^2-1)^{1/2} + (\xi^2-\epsilon)^{1/2}] \xi d\xi}{[(\epsilon+1)\xi^2-\epsilon](t^2/\rho'^2-\xi^2)^{1/2}} \right) \end{aligned} \quad (90)$$

The integrands of the first terms in the third and fourth integrals are, respectively, the same as the integrands in the first and second integrals, so that they can be combined to give

$$\begin{aligned} B_{2a}(\rho', t) &= -\frac{1}{\epsilon-1} \frac{\mu_0}{2\pi^2 c^2 \rho'} \frac{\partial^2}{\partial t^2} \left(\epsilon \int_0^\infty \frac{(\xi^2-1)^{1/2} \xi d\xi}{(\epsilon+1)\xi^2-\epsilon} - \frac{\epsilon t}{\rho'} \int_0^\infty \frac{(\xi^2-1)^{1/2} \xi d\xi}{[(\epsilon+1)\xi^2-\epsilon](t^2/\rho'^2-\xi^2)^{1/2}} \right. \\ &\quad \left. - \int_{t/\rho'}^\infty \frac{(\xi^2-\epsilon)^{1/2} \xi d\xi}{(\epsilon+1)\xi^2-\epsilon} + \frac{t}{\rho'} \int_{t/\rho'}^\infty \frac{(\xi^2-\epsilon)^{1/2} \xi d\xi}{[(\epsilon+1)\xi^2-\epsilon](t^2/\rho'^2-\xi^2)^{1/2}} \right). \end{aligned} \quad (91)$$

When the contour of integration is changed to that in Fig. 6 and the variable to $\xi = \xi^2$, the contributing integrals are

$$\begin{aligned} B_{2a}(\rho', t) &= -\frac{1}{\epsilon-1} \frac{\mu_0}{2\pi^2 c^2 \rho'} \frac{\partial^2}{\partial t^2} \left[\frac{t}{\rho'} \left(-\epsilon \int_1^{t/\rho'} \frac{(\xi-1)^{1/2} d\xi}{[(\epsilon+1)\xi-\epsilon](t^2/\rho'^2-\xi)^{1/2}} \right. \right. \\ &\quad \left. \left. + \int_{t/\rho'}^\infty \frac{(\xi-\epsilon)^{1/2} d\xi}{[(\epsilon+1)\xi-\epsilon](t^2/\rho'^2-\xi)^{1/2}} \right) \right]. \end{aligned} \quad (92)$$

The first integral is the same as the integral in (85). The second integral can be treated in the same manner with the substitutions $x = \xi - \epsilon$ and $T_2 = t^2/\rho'^2 - \epsilon$. These lead to the integral

$$I_2 = \int_0^{T_2} \frac{x' dx'}{[(\epsilon + 1)x + \epsilon^2] \{(T_2 - x')x'\}^{1/2}} \quad (93)$$

in which the substitution $x = x' + E_2$ and $E_2 = \epsilon^2/(\epsilon + 1)$ gives

$$I_2 = \frac{1}{\epsilon + 1} \left(\int_{E_2}^{T_2 + E_2} \frac{dx}{\sqrt{X_2}} - E_2 \int_{E_2}^{T_2 + E_2} \frac{dx}{x\sqrt{X_2}} \right) \quad (94)$$

where $X_2 = a_2 + b_2 x + c_2 x^2$ with $a_2 = -E_2(T_2 + E_2)$, $b_2 = T_2 + 2E_2$, and $c_2 = -1$. The integrals in (94) integrate into arcsines, and the substitution of the limits reduces their arguments to ± 1 . Hence

$$f\left(\frac{t}{\rho'}\right) = \begin{cases} 0, & t/\rho' < 1, \\ \frac{\epsilon}{\epsilon^2 - 1} \frac{t}{\rho'} \left[1 - \left((\epsilon + 1) \frac{t^2}{\rho'^2} - \epsilon \right)^{-1/2} \right], & 1 < \frac{t}{\rho'} < \epsilon^{1/2}, \\ \frac{1}{\epsilon + 1} \frac{t}{\rho'}, & \epsilon^{1/2} < \frac{t}{\rho'} \end{cases} \quad (97)$$

Then

$$B_{2a}(\rho', t) = \frac{\mu_0}{2\pi c^2 \rho'} \frac{\partial^2}{\partial t^2} f\left(\frac{t}{\rho'}\right) \quad (98)$$

Since

$$f(1-) = f(1+) = 0, \quad f(\epsilon^{1/2}-) = f(\epsilon^{1/2}+) = \epsilon^{1/2}/(\epsilon + 1),$$

$f(t/\rho')$ is everywhere continuous. But with $f'(t/\rho') = \partial f(t/\rho')/\partial t$,

$$f'\left(\frac{t}{\rho'}\right) = \begin{cases} 0, & t/\rho' < 1, \\ \frac{\epsilon}{\epsilon^2 - 1} \frac{1}{\rho'} \left[1 - \left((\epsilon + 1) \frac{t^2}{\rho'^2} - \epsilon \right)^{-1/2} + \frac{t^2}{\rho'^2} (\epsilon + 1) \left((\epsilon + 1) \frac{t^2}{\rho'^2} - \epsilon \right)^{-3/2} \right], & 1 < \frac{t}{\rho'} < \epsilon^{1/2}, \\ \frac{1}{\epsilon + 1} \frac{1}{\rho'}, & \epsilon^{1/2} < \frac{t}{\rho'} \end{cases} \quad (99)$$

it follows that $f'(1-) = 0$, $f'(1+) = \epsilon/(\epsilon - 1)\rho'$. Thus $f'(t/\rho')$ has a step discontinuity of $\epsilon/(\epsilon - 1)\rho'$ at $t/\rho' = 1$. Similarly,

$$f'(\epsilon^{1/2}-) = (\epsilon^2 + 1)/\epsilon(\epsilon^2 - 1)\rho', \quad f'(\epsilon^{1/2}+) = 1/(\epsilon + 1)\rho'.$$

This is a step of $-1/\epsilon(\epsilon - 1)\rho'$.

With $f''(t/\rho') = \partial f'(t/\rho')/\partial t$,

$$f''\left(\frac{t}{\rho'}\right) = \begin{cases} 0, & t/\rho' < 1, \\ -\frac{3\epsilon^2}{(\epsilon - 1)} \frac{1}{\rho'^2} \frac{t}{\rho'} \left((\epsilon + 1) \frac{t^2}{\rho'^2} - \epsilon \right)^{-5/2}, & 1 < \frac{t}{\rho'} < \epsilon^{1/2}, \\ 0, & \epsilon^{1/2} < t/\rho'. \end{cases} \quad (100)$$

When these results are combined with (98) and $\rho' = \rho/c$, the final formula for the magnetic field is

$$B_{1a}(\rho, t) = B_{2a}(\rho, t) = \frac{\mu_0}{2\pi \rho^2} \frac{1}{\epsilon - 1} \left[\epsilon \delta\left(t - \frac{\rho}{c}\right) - \epsilon^{-1} \delta\left(t - \frac{\epsilon^{1/2} \rho}{c}\right) \right] \\ - \frac{\mu_0 c}{2\pi \rho^3} \frac{\epsilon^2}{\epsilon - 1} \begin{cases} 0, & ct/\rho < 1 \\ \frac{3ct}{\rho} \left((\epsilon + 1) \frac{c^2 t^2}{\rho^2} - \epsilon \right)^{-5/2}, & 1 < \frac{ct}{\rho} < \epsilon^{1/2} \\ 0, & \epsilon^{1/2} < ct/\rho \end{cases} \quad (101)$$

$$I_1 = \frac{\pi}{\epsilon + 1} \left[1 - \epsilon \left((\epsilon + 1) \frac{t^2}{\rho'^2} - \epsilon \right)^{-1/2} \right] \quad (95)$$

When this is substituted for the second integral in (92) and the value of the first integral is obtained from (88), the result is

$$B_{2a}(\rho', t) = \frac{1}{\epsilon^2 - 1} \frac{\mu_0}{2\pi c^2 \rho'} \frac{\partial^2}{\partial t^2} \\ \times \left(\frac{t}{\rho'} \left\{ \epsilon \left[1 - \left((\epsilon + 1) \frac{t^2}{\rho'^2} - \epsilon \right)^{-1/2} \right] \right. \right. \\ \left. \left. - \left[1 - \epsilon \left((\epsilon + 1) \frac{t^2}{\rho'^2} - \epsilon \right)^{-1/2} \right] \right\} \right) \\ = \frac{1}{\epsilon + 1} \frac{\mu_0}{2\pi c^2 \rho'} \frac{\partial^2}{\partial t^2} \frac{t}{\rho'}, \quad \epsilon^{1/2} < \frac{t}{\rho'} \quad (96)$$

The magnetic field in the three ranges (81), (88), and (96) is summarized as follows. Let

VII. TIME-DEPENDENT COMPONENT $E_{2p}(\rho, t)$ WITH A DELTA-FUNCTION EXCITATION

The integral for $\tilde{E}_{2p}(\rho, \omega)$ in explicit form is

$$\tilde{E}_{2p}(\rho', \omega) = -\frac{i\omega\mu_0}{2\pi c} \int_0^\infty \frac{(\omega^2 - \lambda'^2)^{1/2} \lambda'^2 J_1(\lambda' \rho') d\lambda'}{\omega^2 \epsilon (\omega^2 - \lambda'^2)^{1/2} + \omega^2 (\omega^2 \epsilon - \lambda'^2)^{1/2}}, \quad (102)$$

where $\lambda' = c\lambda$ and $\rho' = \rho/c$. The time-dependent component is

$$\begin{aligned} E_{2p}(\rho', t) &= \frac{1}{\pi} \operatorname{Re} \int_0^\infty e^{-i\omega t} \tilde{E}_{2p}(\rho', \omega) d\omega \\ &= -\operatorname{Re} \frac{\mu_0}{2\pi^2 c} \int_0^\infty d\omega e^{-i\omega t} \int_0^\infty \frac{(\omega^2 - \lambda'^2)^{1/2} J_1(\lambda' \rho') \lambda'^2 d\lambda'}{\omega^2 [\epsilon (\omega^2 - \lambda'^2)^{1/2} + (\omega^2 \epsilon - \lambda'^2)^{1/2}]} \end{aligned} \quad (103)$$

With the change in variable $\lambda' = \omega \xi$,

$$\begin{aligned} E_{2p}(\rho', t) &= -\frac{\mu_0}{2\pi^2 c} \int_0^\infty d\xi \int_0^\infty d\omega \operatorname{Re} i\omega^2 \frac{(1 - \xi^2)^{1/2} \xi^2 J_1(\omega \xi \rho')}{\epsilon (1 - \xi^2)^{1/2} + (\epsilon - \xi^2)^{1/2}} \\ &= -\frac{\mu_0}{2\pi^2 c} \frac{\partial^2}{\partial t^2} \int_0^\infty d\xi \operatorname{Im} \frac{(1 - \xi^2)^{1/2} \xi^2}{\epsilon (1 - \xi^2)^{1/2} + (\epsilon - \xi^2)^{1/2}} \int_0^\infty d\omega e^{-i\omega t} J_1(\omega \xi \rho'). \end{aligned} \quad (104)$$

The integration with respect to ω is the same as in (78). The result is

$$E_{2p}(\rho', t) = -\frac{\mu_0}{2\pi^2 c} \frac{\partial^2}{\partial t^2} \operatorname{Im} \int_0^\infty \frac{\xi^2 (1 - \xi^2)^{1/2}}{\epsilon (1 - \xi^2)^{1/2} + (\epsilon - \xi^2)^{1/2}} \left(1 - \frac{t}{(t^2 - \xi^2 \rho'^2)^{1/2}}\right) \frac{d\xi}{\xi \rho'}. \quad (105)$$

This gives the following two integrals:

$$\begin{aligned} E_{2p}(\rho', t) &= -\frac{\mu_0}{2\pi^2 c \rho'} \frac{\partial^2}{\partial t^2} \operatorname{Im} \left(\int_0^\infty \frac{\xi (1 - \xi^2)^{1/2} d\xi}{\epsilon (1 - \xi^2)^{1/2} + (\epsilon - \xi^2)^{1/2}} \right. \\ &\quad \left. - \frac{t}{\rho'} \int_0^\infty \frac{\xi (1 - \xi^2)^{1/2} d\xi}{[\epsilon (1 - \xi^2)^{1/2} + (\epsilon - \xi^2)^{1/2}] (t^2/\rho'^2 - \xi^2)^{1/2}} \right). \end{aligned} \quad (106)$$

They lead to some elliptic integrals and hence are not expressible in terms of elementary functions.

VIII. CONCLUSION

The exact formulas for the vertical electric and horizontal magnetic components of the transient electromagnetic field generated by a delta-function current in a vertical electric dipole on the boundary between air and a perfect dielectric are illuminating. The appearance of two successive pulses with opposite signs and with one traveling in each medium is consistent with the corresponding observation by Van der Pol³ for the step-function-generated Hertz potential. The structure of the electromagnetic field between the two delta functions is, of course, quite different from that of the Hertz potential between two step functions. The surface-wave nature of the entire field of the delta function is inferred from a comparison with the corresponding field of the same dipole in a single medium with no boundary. Instead of a $1/\rho$ amplitude factor, which is characteristic of propagation in an unbounded region, the amplitude factor of the pulsed field along the boundary is $1/\rho^2$, which is characteristic of the surface wave.

ACKNOWLEDGMENTS

This work was supported in part by the Joint Services Electronics Program under Contract No. N00014-84-K-0465 with Harvard University.

- ¹R. W. P. King, *Proc. IEEE* **72**, 595 (1984).
- ²R. W. P. King, *IEEE Trans. Antennas Propag.* **AP-33**, 1204 (1985).
- ³R. W. P. King, M. Owens, and T. T. Wu, *Radio Sci.* **21**, 13 (1986).
- ⁴R. W. P. King, *IEEE Trans. Geosci. Remote Sensing* **GE-24**, 813 (1986).
- ⁵B. Van der Pol, *IRE Trans. Antennas Propag.* **AP-4**, 288 (1956).
- ⁶H. Bremmer, in *Electromagnetic Waves*, edited by R. E. Langer (University of Wisconsin Press, Madison, WI, 1962), pp. 39-64.
- ⁷H. Haddad and D. C. Chang, *Radio Sci.* **16**, 165 (1981).
- ⁸J. R. Wait, *IRE Trans. Antennas Propag.* **AP-5**, 198 (1957).
- ⁹J. R. Wait, *Wave Propagation Theory* (Pergamon, New York, 1981), Chap. 12.
- ¹⁰J. R. Wait, *Proc. IEEE* **74**, 1173 (1986).
- ¹¹I. S. Gradshteyn and I. M. Ryzhik, *Table of Integrals, Series, and Products* (Academic, New York, 1980).
- ¹²R. W. P. King, *J. Appl. Phys.* **53**, 8476 (1982), **56**, 3366 (1984).

Wave packets of lateral waves due to a vertical monopole: Experiment and theory

M. F. Brown

Gordon McKay Laboratory, Harvard University, Cambridge, Massachusetts

(Received January 16, 1987; revised June 10, 1987; accepted June 10, 1987.)

A wave packet or pulse comprised of a distribution of single-frequency lateral waves due to a vertical monopole is analyzed. The Fresnel-integral terms in the Fourier transform of a general formula for $E_{zz}(\rho, z, \omega)$, the vertical electric-field component in air, are represented using confluent hypergeometric functions. A wave packet of lateral waves is calculated for a pulsed short bare monopole at the boundary between a pair of Earth's material regions and compared with experimental measurements.

1 INTRODUCTION

Electromagnetic surface waves (lateral waves) due to a dipole source operating at a single frequency (CW operation) have unusual and important properties [King and Brown, 1984]. In addition to the CW mode, a dipole driven by a pulse of wide bandwidth may be used to generate lateral waves.

The signal due to a pulsed dipole near the interface between two regions of matter forms a wave packet of lateral waves. Such a wave packet or pulse comprised of a distribution of single-frequency lateral waves is analyzed in sections 2 and 3 to follow. The wave packet is calculated for an indoor model of a pair of Earth's material regions and compared with experimental measurements.

For source S and receiver R both vertical monopoles, a qualitative picture of the involvement of a pulsed lateral wave in geoelectromagnetic sounding of the earth's crust is indicated in Figure 1. In order to resolve the complicated effects of the superimposed single-frequency surface waves at various radial distances, the transient radiated waveform may be visualized in terms of the three distinct paths indicated in the figure. Paths 1 and 2 involve the surface waves and will be addressed first.

Path 1 describes a signal which proceeds from the source S 's driving point along the interface which separates region 1 (e.g., moist earth, conductivity $\sigma_1 > 0$) from region 2 (e.g., air, $\sigma_2 = 0$). While propagating along the interface, some of the field energy in

the signal travels downward. Although path 1 is drawn parallel to the boundary between the two material regions, the individual wavefronts which may be resolved from the signal have a slight tilt relative to this boundary since the surface waves are elliptically polarized. Part of the energy which propagates along path 1 may proceed to a local region at some distance from the interface in region 1. This local region may consist of any object or layer having constitutive parameters σ_l, ϵ_l which differ significantly from σ_1, ϵ_1 associated with region 1. After interacting with the local region of (σ_l, ϵ_l) , the energy is typically scattered in many directions; some of it may return to the interface where it proceeds as a surface-wave signal to the receiver R .

Path 2 represents a class of paths which originate at the end point of S and proceed to various radial distances between S and R along the interface. The signals associated with these paths give rise to surface waves, some of the energy of which may travel downward to a local region. Part of this energy may, in turn, be reflected back to the interface where it proceeds as a surface-wave signal to R .

The signal associated with path 3 does not involve a surface wave; it proceeds directly from S to R in region 2. Nonetheless, its relation to the signals in path 1 and path 2 points up an important distinguishing factor between CW and transient surface-wave sources, the notion of a delay time Δt .

A set of distinct delay times $\Delta t_1, \Delta t_2$ and Δt_3 is associated with the signals radiated from S to R along paths 1, 2 and 3 of Figure 1, respectively. An initial delay between the signal radiated along path 1 and that radiated along path 2 or 3 is due to the time

Copyright 1987 by the American Geophysical Union

Paper number 750524
0048-6604/87/0075-0524\$08.00

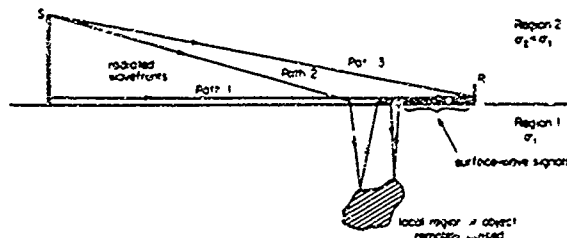


Fig. 1. Simplified picture of paths of wave fronts for surface waves and waves incident upon and reflected from local region or object, remotely sensed. S and R denote vertical monopole source and vertical monopole receiver respectively.

required for the pulse to travel from the driving point to the end point of the linear antenna of finite length. In addition, the lengths of the paths differ, the velocities of the wavefronts differ in the two material regions. In the limit of high frequencies, one may use optical terms the difference in index of refraction between the regions results in different optical path lengths.

The delay times are of critical importance in yielding information not available in the CW case to be used in remote sensing of a local region at various depths. For example, the remotely sensed region may be a layer of Earth's crust at a distinct depth d , having a characteristic conductivity σ_1 . Each such layer σ_1 may be characterized by a time delay Δt_1 required for a signal to proceed along a path of the type denoted by path 1 in Figure 1. Each layer is also characterized by a time delay $\Delta t_2 > \Delta t_1$ required for a signal to proceed along a path 2, etc. Replacing a continuous train of waves in the CW case is a wave packet localized in time which undergoes deformation and attenuation as it propagates: replacing a measurement of the total field (incident plus scattered fields) at some distance from a local region illuminated by a surface wave is the measurement of a distinct incident reference pulse which may be compared to a distinct scattered pulse. Thus there is much fine structure in the signal in terms of its temporal information.

The type of surface-wave signals depicted in Figure 1 may be studied using either a vertical or horizontal dipole for various pairs of regions 1 and 2 satisfying $|k_1| > 3|k_2|$, where $k = [\omega^2 \mu_0 (\epsilon + i\sigma/\omega)]^{1/2}$ specifies a complex wave number. Thus the regions may consist of the earth's lithosphere at its interface with seawater. The details of seafloor sounding including specific antenna effective lengths, field strengths, and receiver sensitivities, have been analyzed [Brown and King, 1986] for distinct frequencies $f_0 = 1$ Hz, 100 Hz, and 10 kHz.

A useful and versatile pair of materials which accommodates a diverse range of studies indoors is salt water at ocean conductivity and permittivity ($\sigma_1 \sim 3.5$ S/m, $\epsilon_{1r} = \epsilon_1/\epsilon_0 \sim 80$) for region 1, and air ($\sigma_2 = 0$, $\epsilon_{2r} = 1$) for region 2. A region of salt water having a plane interface with air may be formed for the indoor modeling of pulsed surface waves using a semicircular wading pool. Such a pool is pictured in Figure 2. The surface wave associated with a CW source driven at $f_0 = 600$ MHz has been formerly observed in detail using such a model [Brown et al., 1982]. The reflections of lateral waves at discontinuities and boundaries have been measured at 644 MHz and 1.5 GHz, bounding the perimeter of the model in seven distinct ways [Brown et al., 1984].

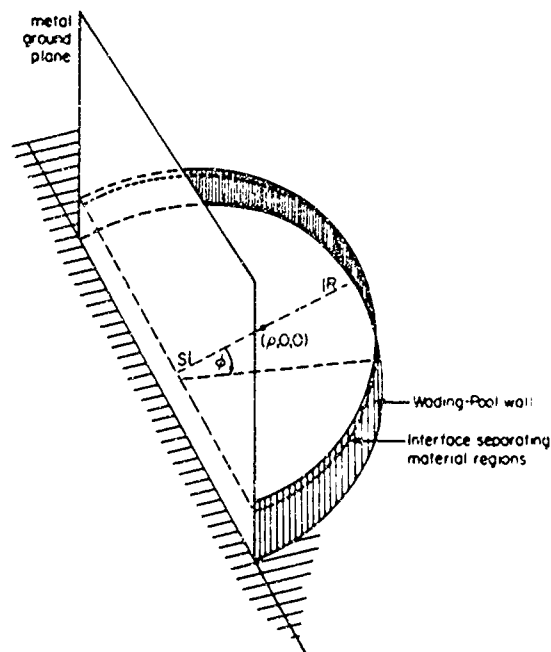


Fig. 2. Sketch of semicircular wading pool S denotes vertical source monopole, R denotes configuration of vertical receiving monopoles at $\phi = 0$. Coaxial input and output lines to S and R, respectively, not shown.

A vertical monopole source S and receiver R having lengths short compared to the width of the driving pulse have been used just above the surface of the aforementioned pool. In this way essentially all signals received at R are associated with path 1 of Figure 1. The scope of the present paper is focused upon the pulsed signals associated with path 1 at or near the interface of Figure 1; treatment of the scattered fields due to a local region or object submerged in region 1 is not addressed. The use of a vertical source in air versus a horizontal one in salt water is more fundamental in an initial study of wave packets. The transient response of a linear source antenna in air is less complicated, since the insulating sheath(s) and terminating resistor needed for the efficient operation of a source in salt water are absent. Studies of the former provide a sound basis for studies of the latter.

A single-frequency component of the electromagnetic surface-wave pulse which travels along the paths of Figure 1 may be described theoretically in cylindrical coordinates. Regions 1 and 2 of Figure 1 may be termed "half-spaces." The fields in each of these half-spaces have been expressed in many ways over 7 decades since the original Sommerfeld solution [Sommerfeld, 1909, 1926], see bibliography in the important monograph due to Baños [1966]. A set of 18 newly derived equations for the field components due to infinitesimal (Hertzian) horizontal and vertical electric unit dipoles (CW case) has been obtained as original Wu formulas extended by King [1985a]. These relations are highly accurate over an entire spectrum of distinct f_0 values and unified in their ranges of applicability, i.e., the formulas maintain accuracy over a broad continuous range in $k\rho$, where k is the wave number and ρ the radial distance from the source. The formulas are important in subsurface communications [King and Brown, 1984] as well as exploration geophysics [King, 1985b].

The Wu-King formula relevant to the present paper is that for a CW field component $E_{2z}(\rho, z)$ due to an infinitesimal vertical diode in the upper half-space (region 2, air) of Figure 1. This $E_{2z}(\rho, z)$ field excites a current on a vertical monopole probe also in the upper half-space; the subscript 2 denotes a field radiated into region 2 and z locates the radiated field along the vertical cylindrical coordinate. At the interface ($z = 0$) the field is

$$E_{2z}(\rho, 0) = \frac{\omega\mu_0}{2\pi k_2} e^{ik_2 z} \left[\frac{ik_2}{\rho} - \frac{1}{\rho^2} - \frac{1}{k_2 \rho^3} - \frac{k_2^3}{k_1} \right]$$

$$\cdot \left(\frac{\pi}{k_2 \rho} \right)^{1/2} e^{-ik_2 \rho} \mathcal{F} \quad (1)$$

where \mathcal{F} is defined in terms of Fresnel integrals C_2 and S_2 as

$$\mathcal{F}(k_2^3 \rho / 2k_1^2) = \frac{1}{2}(1 + i) - C_2(k_2^3 \rho / 2k_1^2) - iS_2(k_2^3 \rho / 2k_1^2) \quad (2)$$

A harmonic time dependence $e^{-i2\pi f_0 t}$ for operating frequency $f_0 = \omega/2\pi$ is assumed in (1). In (2) the argument of C_2 and S_2 which involves the wave numbers k_1 and k_2 , when multiplied by i , may be referred to as a Sommerfeld numerical distance.

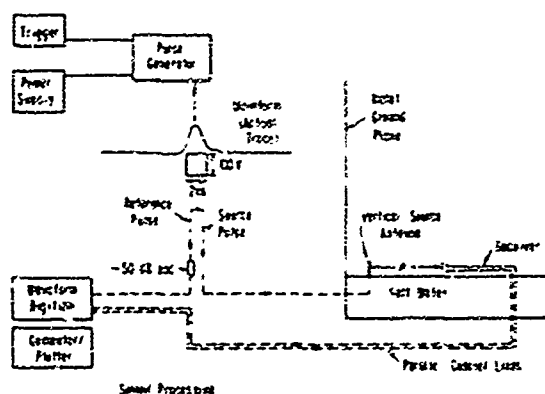
Some observations, of which the author is aware, that pertain to sounding using transient fields include the works of Azad [1977], Antonov and Manshtein [1979], and Morozova [1979]. Important related theoretical work includes the comparison of flat-Earth and spherical-Earth models using a ramp current as a standard source [Wait [1986]; see bibliography therein].

2. EXPERIMENT

The semicircular wading pool cited in the introduction and sketched in Figure 2 constitutes a salt-water basin used for experimental observations. The radius of the pool is 185.4 cm (6 ft, 1 in.), while its depth is 30.5 cm. The vertical metal ground plane extends to 1.1 m.

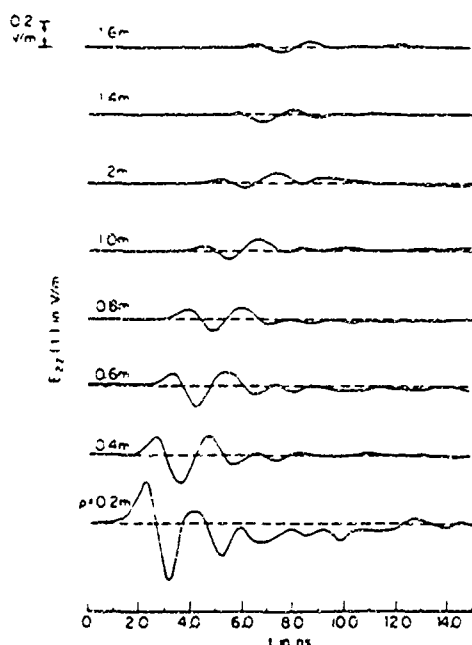
A Gaussian-shaped pulse of amplitude 120 V and width at half-amplitude of 2 ns is used as a source of wave packets to be propagated over the saltwater basin. A trace of the actual waveform is shown in Figure 3. The Fourier transform of the waveform is a Gaussian distribution in frequency having a bandwidth with appreciable amplitudes to 500 MHz. The tail of the distribution extends to ~ 1 GHz. Thus although large radial distances are needed to be in the far field of the very low frequency components of the radiated pulse, the intermediate and far fields of many of the frequencies are contained within the radius of the semicircular region of Figure 2.

The source S of Figure 2 (fed by a coaxial line not indicated in the figure) is a short ($h = 4.0$ cm) vertical monopole. The monopole is a 1/4 in. diameter stainless-steel rod. A small circular disk (4.0 cm in diameter) is used as a conducting plate in contact with the outer conductor of the coaxial feedline at the base of the antenna where it contacts the salt water. The support of the conducting plate is by vertical rods extending to the floor of the wading pool; these rods produce a negligible effect upon the field



measured in the air by the vertical monopole receiver. All submerged parts are of 316 steel impervious to corrosion in salt water. The origin of the radial coordinate ($\rho = 0$) is centered upon the axis of the source S .

The receiving system denoted by R consists of two short ($h = 2.5$ cm) monopoles, oriented such that one points toward the saltwater region and one points away from it. This rotatable configuration of probes involves two separately wired brass rods, each 1/4 in. in diameter. It is designed to utilize a special dual-measuring procedure formerly developed for EMP



simulation studies at Harvard [Shen *et al.*, 1984]. The procedure subtracts out the induced-noise currents which arise in the cabling of the receiving system. The system is suspended by nylon thread with the lower tip of the bottom monopole just above the level of the salt water.

The dual inputs from the receiver *R* may be connected to a data acquisition system (Tektronix WP2110 with 7912AD programmable digitizer) which displays the input voltage in the time domain, digitizes it, and utilizes a computer program to Fourier-transform, plot, introduce scale factors, etc. A schematic diagram of the interconnections involved in the processing of signals associated with the experiment is drawn in Figure 3. A high-power attenuator of very good quality must be used for the reference pulse input to the digitizer; the peak power of the 2 ns pulse may be quite high (kilowatt range), since the time intervals for transient peaks are so narrow.

The measured $E_{\Sigma}(\rho, 0, t)$ field for radial distances $\rho = 0.2$ m to $\rho = 1.6$ m is shown in Figure 4. Note that a slanted line may be drawn with a straight edge from the lower left to upper right through the crest of the first peak in amplitude for seven of the curves ($\rho = 0.4$ m to $\rho = 1.2$ m) and $\Delta\rho/\Delta t \sim (1.6 - 0.4)/(6.6 - 2.6)$ m/ns $= 3.0 \times 10^8$ m/s. The

$\rho = 0.2$ m curve is offset from the rest; however, S and R are so close at this point that some coupling between them is expected.

In Figure 5, the waveforms of Figure 4 are shown for longer times in altered scale. The trailing peaks associated with each waveform have two main sources, both of which are intrinsic to the transmission system. Let the two maxima of highest amplitude in each curve be defined as the primary waveform (the causes of these peaks will be addressed in section 3 to follow). There are three significant smaller maxima to the right of the primary waveform which may be resolved in the $\rho = 0.4$ m to $\rho = 1.6$ m curves. (The $\rho = 0.2$ m $E_{2z}(\rho, 0, t)$ field is, as formerly mentioned, offset from the progression in time of the other seven fields and is associated with a very short interantenna spacing between S and R .) The first two small maxima may be clearly seen at the right of the primary waveform in the $\rho = 1.6$ m curve. This pair may be similarly identified in the curves for earlier times (albeit in the 1.2 m curve the pair seems to have coalesced). The source of these first trailing peaks cannot be reflections from the edge of the semicircular water region since they always maintain the same spacing (~ 2 ns downfield) relative to the second major peak of the primary waveform. These first two trailing peaks have been found to be due to a small degree of impedance mismatch between the 50- Ω output line of the pulse generator and the vertical source monopole. A small bump is always associated with the older (i.e., right) edge of the output Gaussian pulse (see the trace of the actual waveform in Figure 3), impedance mismatches notwithstanding. Similarly, the third small maximum to the right of the primary waveform of the $\rho = 1.6$ m curve, like its appearance in the earlier curves (starting at ~ 16.5 ns in the $\rho = 0.4$ m curve), travels along with the primary waveform and cannot be due to a reflection from the pool wall. This third small maximum has been found to be a reflection from the vertical monopole back to the pulse generator. The cable length along this path is 160 cm (each way) while the spacing between the right edge of the primary waveform and the third small maximum is ~ 10.7 ns or $(10.7 \text{ ns}) \times (30 \text{ cm/ns}) = 321 \text{ cm}$.

3. THEORY

Infinitesimal dipole in free space. The formula introduced in (1) for the $E_{2z}(\rho, 0)$ component in air due to an infinitesimal dipole in air above salt water may be written

$$E_{2z}(\rho, 0, \omega) = \frac{\omega \mu_0}{2\pi} e^{ik_2 \rho} \left[\frac{1}{\rho} - \frac{1}{k_2 \rho^2} - \frac{1}{k_2^2 \rho^3} - \frac{k_2^2}{k_1} \left(\frac{\pi}{k_2 \rho} \right)^{1/2} e^{-i\theta} \mathcal{F}(\theta) \right] \quad (3)$$

where

$$\mathcal{F}(\theta) = \frac{1}{2}(1 + i) - [C_2(\theta) + iS_2(\theta)] \quad (4)$$

with

$$C_2(\theta) + iS_2(\theta) = \int_0^\theta \frac{e^{i\zeta}}{(2\zeta)^{1/2}} d\zeta \quad (5)$$

Equation (5) specifies the Fresnel integrals C_2 and S_2 in the notation of Abramowitz and Stegun [1972]. The quantity $i\theta$ is the Sommerfeld numerical distance $ik_2^2 \rho^2 / 2k_1^2$. Hereafter, the shortened notation $(\frac{1}{2}, \frac{1}{2}) - (C_2(\theta), S_2(\theta))$ will be used for $\mathcal{F}(\theta)$ in (4).

Let the purely free-space terms in (3), which involve region 2 (and hence k_2) only, be regarded as a source of wave packets. A Fourier integral may be written for these terms. That is,

$$E_{2z}(\rho, 0, t) = \frac{\mu_0}{2\pi} \int_{-\infty}^{\infty} e^{ik_2 \rho} \left(\frac{1}{\rho} - \frac{1}{k_2 \rho^2} - \frac{1}{k_2^2 \rho^3} \right) \omega \hat{f}(\omega) e^{-i\omega t} d\omega \quad (6)$$

where $\hat{f}(\omega)$ is the inverse transform of a source pulse in time, which will be taken to be of Gaussian shape. Thus

$$\hat{f}(\omega) = \frac{1}{2\pi} \int_{-\infty}^{\infty} dt f(t) e^{i\omega t} \quad (7)$$

where

$$f(t) = A e^{-t^2/\Delta^2} \quad (8)$$

with A the amplitude of the Gaussian function and Δ the half-width (full width is defined as the distance between inflection points). Therefore

$$\hat{f}(\omega) = \frac{A}{2} \pi^{-1/2} \Delta e^{-\Delta^2 \omega^2 / 4} \quad (9)$$

and

$$E_{2z}(\rho, 0, t) = \frac{\mu_0 A \Delta}{4\pi^{3/2}} \int_{-\infty}^{\infty} e^{ik_2 \rho} \left(\frac{1}{\rho} - \frac{1}{k_2 \rho^2} - \frac{1}{k_2^2 \rho^3} \right) \omega e^{-\Delta^2 \omega^2 / 4} e^{-i\omega t} d\omega \quad (10)$$

The integral in (10) may be written

$$I = \left(\frac{1}{\rho}\right) I_1 - \left(\frac{1}{\rho^2}\right) I_2 - \left(\frac{1}{\rho^3}\right) I_3 \quad (11)$$

where

$$I_1 = \int_{-\infty}^{\infty} e^{i(\omega - \mu c t - \Delta^2 \omega^2 / 2)} d\omega \quad (12)$$

$$I_2 = \int_{-\infty}^{\infty} e^{i(\omega - \mu c t - \Delta^2 \omega^2 / 2)} \omega d\omega \quad (13)$$

$$I_3 = \int_{-\infty}^{\infty} e^{i(\omega - \mu c t - \Delta^2 \omega^2 / 2)} \omega^2 d\omega \quad (14)$$

The k_2 value ωc for free space has been written explicitly in (12)–(14). Note that the first and third integrands differ from the second by factors of ω and ω^2 , respectively.

The integrals in (12)–(14) are evaluated in the appendix. The evaluations yield

$$I_1 = -\frac{i\Delta\pi^{1/2}}{\Delta^2} T e^{-T^2/\Delta^2} \quad (15)$$

$$I_2 = \frac{2\pi^{1/2}}{\Delta} e^{-T^2/\Delta^2} \quad (16)$$

$$I_3 = -i\pi \operatorname{erfi}(T/\Delta) \quad (\text{principal value}) \quad (17)$$

where $T \equiv (t - \mu z)$ is a retarded time; erf denotes the error function of a real argument.

Equation (10) is thus

$$E_{z, \rho=0}(t) = \frac{\mu_0 A}{\pi} \left\{ \left(\frac{1}{\rho}\right) \frac{T}{\Delta^2} e^{-T^2/\Delta^2} - \left(\frac{1}{\rho^2}\right) \frac{2}{\Delta} e^{-T^2/\Delta^2} - \left(\frac{1}{\rho^3}\right) \frac{\pi^{1/2} c^2 \Delta}{4} \operatorname{erfi}\left(\frac{T}{\Delta}\right) \right\} \quad (18)$$

The first term in (18) contains the derivative of a Gaussian function, the second contains a Gaussian function, and the third contains a steplike function. The coefficients of the terms involve ρ , Δ , and constants. Plainly, very close to the source (small ρ), the $1/\rho^3$ term (steplike function) will predominate, at distances much further from the source (large ρ), the $1/\rho$ term (derivative of a Gaussian) will predominate. The $1/\rho^2$ term (Gaussian) will be important in the transition between these two regimes.

The infinitesimal dipole with its triangular CW current distribution [King, 1956, section II.31] is primarily useful as an elementary source which forms the basis for more complicated situations which occur in practice. In the CW case, one such situation

is the definition of an effective moment \mathcal{M}_{eff} which includes a specific current distribution along a particular effective length h_{eff} associated with a finite antenna.

The infinitesimal dipole whose pulsed field in time is given by (18) above has been treated as the most elementary source of wave packets in that no differentiations of the Gaussian moment pulse are present. This is somewhat unphysical, as evidenced by the singularity in (14) evaluated in the appendix. In the laboratory, a short finite dipole is used. Such a dipole has a more complicated train of radiated wave packets.

Finite dipole in free space A theory for the measured fields of the foregoing section 2 must include the effects of the finite length of the short monopole denoted by S . A second-derivative operator with a proportionality constant may be used to link the input to S (voltage) to the output from S (radiated field). The validity conditions for the differentiation effect are (1) $k_2 h \ll 1$ for the frequencies in the input pulse having appreciable amplitudes, where h is the length of the antenna, (2) $|Z_p(f)| \ll |Z_0(f)|$, where Z_0 and Z_p are the antenna input impedance and internal driving system impedance, respectively. The driving system consists of the pulse generator and its coaxial line. The aforementioned proportionality constant is $(h/c)^2$. These conditions are stated in terms of the notation used in a systematic analysis of pulsed cylindrical antennas above a metal ground plane carried out by Schmitt *et al.* [1966].

The condition $k_2 h \ll 1$ is well satisfied by a significant bandwidth of frequencies within the distribution which results from the Fourier transform of the 2-n source pulse. This distribution is itself a Gaussian (peak amplitudes ~ 500 MHz $\rightarrow k_2 h = 0.4$). The condition $|Z_p(f)| \ll |Z_0(f)| \ll |Z_0(f)|$ is satisfied for S of section 2, since $Z_0(f) \propto (k_2 h)^{-1}$, and $Z_p(f)$ is not strongly capacitive.

The following relation between such a derivative and its inverse Fourier transform is useful

$$\frac{d^n f(t)}{dt^n} \rightarrow (i\omega)^n \hat{f}(\omega) \quad (19)$$

Using this relation with (9),

$$\frac{d^2 f(t)}{dt^2} \rightarrow -\frac{\hat{A}}{2} \pi^{-1/2} \Delta \omega^2 e^{-\Delta^2 \omega^2 / 2} \quad \hat{A} = (h/c)^2 A \quad (20)$$

The evaluation of the time transform of (3) to correspond to the experimental configuration of section 2

consists of two parts. Let these be denoted by $E_{2z}^{(1)}(\rho, 0, t)$ and $E_{2z}^{(2)}(\rho, 0, t)$. The first part is associated with the free-space terms (those involving k_2 only) in (3), using the time transform to the right of the arrow in (20). This is evaluated in this subsection in the equations immediately following. The second part in (3) involving the Fresnel-integral term will be calculated in the next subsection, whose subject is the finite monopole over an imperfectly conducting salt water.

Replacing (9) with (20) and using the free-space terms in (3), one obtains

$$E_{2z}^{(1)}(\rho, 0, t) = \frac{\mu_0 \hat{A} \Delta}{4\pi^{3/2}} \int_{-\infty}^{\infty} e^{i\omega t} \left(-\frac{1}{\rho} + \frac{1}{k_2 \rho^2} + \frac{1}{k_2^2 \rho^3} \right) \omega^3 e^{-\Delta^2 \omega^2 / 4} e^{-i\omega t} d\omega \quad (21)$$

The integral in (21) may be written

$$I = -\left(\frac{1}{\rho}\right) I_4 + \left(\frac{1}{\rho^2}\right) I_5 + \left(\frac{1}{\rho^3}\right) I_6 \quad (22)$$

where

$$I_4 = \int_{-\infty}^{\infty} e^{i\omega t} e^{-\Delta^2 \omega^2 / 4} \omega^3 d\omega \quad (23)$$

$$I_5 = \int_{-\infty}^{\infty} e^{i\omega t} e^{-\Delta^2 \omega^2 / 4} \omega^3 d\omega \quad (24)$$

$$I_6 = \int_{-\infty}^{\infty} e^{i\omega t} e^{-\Delta^2 \omega^2 / 4} \omega^3 d\omega \quad (25)$$

The integrals (23) and (24) are evaluated in the appendix. I_6 is the same as I_1 . Therefore the above three equations lead to

$$I_4 = -\frac{1}{\Delta^3} \left(24T - \frac{16T^3}{\Delta^2} \right) e^{-(T/\Delta)^2} \quad (26)$$

$$I_5 = \frac{4}{\Delta^3} \left[1 - 2\left(\frac{T}{\Delta}\right)^2 \right] e^{-(T/\Delta)^2} \quad (27)$$

$$I_6 = -\frac{16\pi^{1/2}}{\Delta^3} T e^{-(T/\Delta)^2} \quad (28)$$

Equation (21) then becomes

$$E_{2z}^{(1)}(\rho, 0, t) = \frac{\mu_0 \hat{A}}{\pi \Delta^2} \left\{ -\left(\frac{1}{\rho}\right) \left[\frac{6T}{\Delta^2} - \frac{4T^3}{\Delta^4} \right] e^{-(T/\Delta)^2} + \left(\frac{1}{\rho^2}\right) \left[1 - \frac{2T^2}{\Delta^2} \right] e^{-(T/\Delta)^2} + \left(\frac{1}{\rho^3}\right) c^2 T e^{-(T/\Delta)^2} \right\} \quad (29)$$

The field in (29) plainly involves more differentiations than that of (18). The T , T^2 , and T^3 terms in (29) are

associated with the first, second, and third derivatives, respectively, of the Gaussian function $e^{-(T/\Delta)^2}$. The error function in (18) associated with the $(1/\rho^3)$ term is no longer present.

Finite dipole at air-water interface. The evaluation for a finite dipole of the second part of the time transform of (3) follows. This part is denoted by $E_{2z}^{(2)}(\rho, 0, t)$. Unlike $E_{2z}^{(1)}(\rho, 0, t)$, it contains $k_1 = [\omega^2 \mu_0 (\epsilon_1 + i\sigma_1/\omega)]^{1/2}$ and hence the electrical properties of region 1. In particular,

$$E_{2z}^{(2)}(\rho, 0, t) = \frac{\mu_0}{2\pi} \int_{-\infty}^{\infty} e^{i\omega t} \left[-\frac{k_2^2}{k_1} \left(\frac{\pi}{k_2 \rho} \right)^{1/2} e^{-i\theta} \left(\frac{1}{2}, \frac{1}{2} \right) - (C_2(\theta), S_2(\theta)) \right] \times \omega^2(t) e^{-i\omega t} d\omega \quad (30)$$

By using (20),

$$E_{2z}^{(2)}(\rho, 0, t) = \frac{\mu_0 \hat{A} \Delta}{4\pi \rho^{1/2}} \int_{-\infty}^{\infty} e^{i\omega t} \left[\frac{k_2^{3/2}}{k_1} e^{-i\theta} \left(\frac{1}{2}, \frac{1}{2} \right) - (C_2(\theta), S_2(\theta)) \right] \times e^{-\Delta^2 \omega^2 / 4} \omega^3 e^{-i\omega t} d\omega \quad (31)$$

The Fresnel integrals C_2 and S_2 have an equivalent representation in terms of C and S :

$$[C_2(\theta), S_2(\theta)] = [C(\sqrt{2\theta/\pi}), S(\sqrt{2\theta/\pi})] \quad (32)$$

where C and S may be written in terms of a confluent hypergeometric function M as

$$[C(\sqrt{2\theta/\pi}), S(\sqrt{2\theta/\pi})] = \sqrt{2\theta/\pi} M\left(\frac{1}{2}, \frac{3}{2}, i\theta\right) \quad (33)$$

The function M is represented by the Kummer series

$$M(a, b, z) = 1 + \frac{az}{b} + \frac{(a)_2 z^2}{(b)_2 2!} + \cdots + \frac{(a)_N z^N}{(b)_N N!} + \cdots \quad (34)$$

where $(a)_N = a(a+1)(a+2)\cdots(a+N-1)$, $a_0 \equiv 1$. The notation of (32)–(34) is that of Abramowitz and Stegun [1972, sections 7.3 and 13.1]; M may be calculated over a wide range in $|z|$. Hence

$$(C_2(\theta), S_2(\theta)) = \sqrt{2\theta/\pi} \{ 1 + \frac{1}{2}i\theta - \frac{1}{16}\theta^2 + \cdots \} \quad (35)$$

That is,

$$e^{-i\theta} (C_2(\theta), S_2(\theta)) = (1 - i\theta - \theta^2/2! + \cdots) \sqrt{2/\pi} \theta^{1/2} + i\sqrt{2/9\pi} \theta^{3/2} - \sqrt{1/50\pi} \theta^{5/2} + \cdots \quad (36)$$

$$= \sqrt{2/\pi} \theta^{1/2} - i\sqrt{2/\pi} \theta^{3/2} + i\sqrt{2/9\pi} \theta^{3/2} + O(\frac{1}{2}) + O(\frac{1}{2}) + O(\frac{1}{2}) + \cdots \quad (37)$$

TABLE 1. Frequency f and Parameter θ

f , Hz	k_1 , m^{-1}	$ \theta = k_1^2 \rho / 2k_1^2 $
1	$(3.7 + i3.7) \times 10^{-3}$	2.7×10^{-19}
10	$(1.2 + i1.2) \times 10^{-2}$	2.7×10^{-17}
100	$(3.7 + i3.7) \times 10^{-2}$	2.7×10^{-15}
10^3	$(1.2 + i1.2) \times 10^{-1}$	2.7×10^{-13}
10^4	$(3.7 + i3.7) \times 10^{-1}$	2.7×10^{-11}
10^5	$1.2 + i1.2$	2.7×10^{-9}
10^6	$3.7 + i3.7$	2.7×10^{-7}
10^7	$(1.2 + i1.2) \times 10^1$	2.7×10^{-5}
10^8	$(4.0 + i3.5) \times 10^1$	2.6×10^{-3}
10^9	$(2.0 + i0.7) \times 10^2$	1.6×10^{-1}

$$\rho = 1.6 \text{ m}; \epsilon_1 = 80, \sigma_1 = 3.5 \text{ S/m}, \epsilon_2 = 1, \sigma_2 = 0.$$

where O indicates the order of the exponent in θ .

For the θ magnitudes associated with the experiment of section 2 ($\theta < 0.1$, see Table 1), one is interested in the terms of lowest order in (37). Also, noting that

$$e^{-i\theta(\frac{1}{2}, \frac{1}{2})} \sim \frac{1}{2} + \frac{i}{2} - \frac{i\theta}{2} + \frac{\theta}{2} + O(2) + \dots \quad (38)$$

(31) may be written

$$E_{2z}^{(2)}(\rho, 0, t) = \frac{\mu_0 \hat{A} \Delta}{4\pi \rho^{1/2}} \int_{-\infty}^{\infty} e^{ik_1 \rho} \left[\frac{k_1^{3/2}}{k_1} \left\{ \frac{1}{2}(1+i) - \sqrt{2/\pi} \theta^{1/2} \right\} \right] e^{-\Delta^2 \omega^2 / 4} \omega^3 e^{-i\omega t} d\omega \quad (39)$$

to leading order in θ .

The first term in (39) is

$$[E_{2z}^{(2)}(\rho, 0, t)]^{(1)} = \frac{\mu_0 \hat{A} c^{-3/2} \Delta}{8\pi \rho^{1/2}} \int_{-\infty}^{\infty} \frac{(1+i)e^{i(1-i)\rho c\omega - \Delta^2 \omega^2 / 4} \omega^9}{\sqrt{\omega^2 \mu_0 (\epsilon_1 + i\sigma_1/\omega)}} d\omega \quad (40)$$

$$= \left(\frac{1}{\rho^{1/2}} \right) \frac{\mu_0 \hat{A} c^{-3/2} \Delta}{8\pi} \int_{-\infty}^{\infty} \frac{(\mu_0 \epsilon_1)^{-1/2} F(\omega)}{\sqrt{1 + i\sigma_1/\omega \epsilon_1}} d\omega \quad (41)$$

where

$$F(\omega) = (1+i)(\cos T\omega - i \sin T\omega) e^{-\Delta^2 \omega^2 / 4} \omega^{7/2} \quad (42)$$

$$T \equiv (t - \rho/c)$$

An upper bound on $[E_{2z}^{(2)}(\rho, 0, t)]^{(1)}$ may be specified in terms of a band of constant field amplitude since

$$\left| \int_{-\infty}^{\infty} \frac{F(\omega)}{\sqrt{1 + i\sigma_1/\omega \epsilon_1}} d\omega \right| \leq \int_{-\infty}^{\infty} |F(\omega)| d\omega \quad (43)$$

Within this band, $[E_{2z}^{(2)}(\rho, 0, t)]^{(1)}|_{\sigma_1=0}$ yields an upper bound on the amplitude of each of the oscillations of

$[E_{2z}^{(2)}(\rho, 0, t)]^{(1)}$. It is useful to note that

$$\int_{-\infty}^{\infty} F^*(\omega) d\omega = \int_{-\infty}^{\infty} F(-\omega) d\omega \quad (44)$$

since $[E_{2z}^{(2)}(\rho, 0, t)]^{(1)}$ is real, so that

$$\int_{-\infty}^{\infty} F(\omega) d\omega = 2 \operatorname{Re} \int_0^{\infty} F(\omega) d\omega \quad (45)$$

$$= 2 \operatorname{Re} \int_0^{\infty} (1+i)(\cos T\omega - i \sin T\omega) e^{-\Delta^2 \omega^2 / 4} \omega^{7/2} d\omega \quad (46)$$

$$= 2 \int_0^{\infty} \cos T\omega e^{-\Delta^2 \omega^2 / 4} \omega^{7/2} d\omega + 2 \int_0^{\infty} \sin T\omega e^{-\Delta^2 \omega^2 / 4} \omega^{7/2} d\omega \quad (47)$$

The integrals in (47) are, using *Gradshteyn and Ryzhik* [1980, equations 3.952.7 and 3.952.8],

$$\int_0^{\infty} \omega^{7/2} e^{-\Delta^2 \omega^2 / 4} \cos T\omega d\omega = \frac{\Gamma(9/4)}{2(\Delta^2/4)^{9/4}} M\left(\frac{9}{2}, \frac{1}{2}, -T^2/\Delta^2\right) \quad (48)$$

and

$$\int_0^{\infty} \omega^{7/2} e^{-\Delta^2 \omega^2 / 4} \sin T\omega d\omega = \frac{T e^{-(T/\Delta)^2} \Gamma(\frac{11}{4})}{2(\Delta^2/4)^{11/4}} M\left(-\frac{1}{2}, \frac{3}{2}, T^2/\Delta^2\right) \quad (49)$$

where Γ is the gamma function and M is another instance of the confluent hypergeometric function defined in (34) and denoted as ${}_1F_1$ by *Gradshteyn and Ryzhik* [1980]. The right sides of (48) and (49) are, respectively,

$$\frac{12.82}{\Delta^{9/2}} \left[1 - 4.50(T/\Delta)^2 + 4.87(T/\Delta)^4 - 2.76(T/\Delta)^6 + \dots + \frac{(9/4)_N (-T^2/\Delta^2)^N}{(1/2)_N N!} + \dots \right] \quad (50)$$

and

$$\frac{36.39 T e^{-(T/\Delta)^2}}{\Delta^{11/2}} \left[1 - 0.833(T/\Delta)^2 + 0.042(T/\Delta)^4 + 0.0030(T/\Delta)^6 + \dots + \frac{(-5/4)_N (T^2/\Delta^2)^N}{(3/2)_N N!} + \dots \right] \quad (51)$$

where $(a)_N$ is as in (34).

For small T/Δ , the series in brackets in (50) and (51) converge after very few terms. For example,

BROWN: WAVE PACKETS OF LATERAL WAVES

841

TABLE 2. Properties of Series in Equations (50) and (51)

Series in Brackets in (50)			Series in Brackets in (51)		
N	$\frac{(a)_N(-T/\Delta)^{2N}}{(b)_N N!}$	S_N	N	$\frac{(a)_N(T/\Delta)^{2N}}{(b)_N N!}$	S_N
1	$-0.112\ 50 \times 10^1$	$-0.125\ 00$	1	$-0.208\ 33$	$0.791\ 67$
2	$0.304\ 69$	$0.179\ 69$	2	$0.260\ 42 \times 10^{-2}$	$0.794\ 27$
3	$-0.431\ 64 \times 10^{-1}$	$0.136\ 52$	3	$0.465\ 03 \times 10^{-4}$	$0.794\ 32$
4	$0.404\ 66 \times 10^{-2}$	$0.140\ 57$	4	$0.113\ 03 \times 10^{-5}$	$0.794\ 32$
5	$-0.281\ 02 \times 10^{-3}$	$0.140\ 29$	5	$0.282\ 57 \times 10^{-7}$	$0.794\ 32$
6	$0.154\ 35 \times 10^{-4}$	$0.140\ 30$	6	$0.679\ 26 \times 10^{-9}$...
7	$-0.699\ 64 \times 10^{-6}$	$0.140\ 30$	7	$0.153\ 64 \times 10^{-10}$...
8	$0.269\ 65 \times 10^{-7}$	$0.140\ 30$	8	$0.324\ 79 \times 10^{-12}$...
9	$-0.903\ 26 \times 10^{-9}$...	9	$0.641\ 04 \times 10^{-14}$...
10	$0.267\ 41 \times 10^{-10}$...	10	$0.118\ 25 \times 10^{-15}$...
11	$-0.709\ 04 \times 10^{-11}$...	11	$0.204\ 55 \times 10^{-17}$...
12	$0.170\ 20 \times 10^{-13}$...	12	$0.332\ 39 \times 10^{-19}$...
13	$-0.373\ 12 \times 10^{-15}$...	13	$0.509\ 00 \times 10^{-21}$...
14	$0.732\ 66 \times 10^{-17}$...	14	$0.736\ 55 \times 10^{-23}$...
15	$-0.140\ 58 \times 10^{-18}$...	15	$0.100\ 98 \times 10^{-24}$...
16	$0.244\ 46 \times 10^{-20}$...	16	$0.131\ 48 \times 10^{-26}$...
17	$-0.397\ 63 \times 10^{-22}$...	17	$0.162\ 97 \times 10^{-28}$...
18	$0.607\ 49 \times 10^{-24}$...	18	$0.192\ 70 \times 10^{-30}$...
19	$-0.874\ 95 \times 10^{-26}$...	19	$0.217\ 80 \times 10^{-32}$...
20	$0.119\ 18 \times 10^{-27}$	$0.140\ 30$	20	$0.235\ 73 \times 10^{-34}$	$0.794\ 32$

N = number of terms, S_N = partial sum, $(a)_N$ and $(b)_N$ in recurring terms are defined as in (34) $T/\Delta = \pm 0.5$

using $T/\Delta = \pm 0.5$, the partial sums S_N to 5 decimal places for increasing numbers of terms are shown in Table 2. For intermediate and large T/Δ , the series converges nicely when more of its terms are included. The relevant range in $T \equiv t - c/c$ for the measured pulses of section 2 is $-3.7\text{ ns} \leq T \leq 3.7\text{ ns}$. The negative retarded time occurs, since for $\rho = 0$ the Gaussian waveform $f(t)$ is centered on the origin at $t = 0\text{ ns}$. The half-width Δ of the pulse is 1 ns ; therefore $(T/\Delta)^2 \leq (\pm 3.7)^2$. For $T/\Delta = \pm 3.7$, the greatest number of terms in (50) and (51) need to be included. For $T/\Delta = \pm 3.7$, the partial sums to 5 decimal places for selected increasing terms in the two series are shown in Table 3.

Coalescing (45)-(51),

$$\int_{-\infty}^{\infty} F(\omega) d\omega = \frac{25.63}{\Delta^{9/2}} \left[1 - 4.50(T/\Delta)^2 + 4.87(T/\Delta)^4 - 2.76(T/\Delta)^6 + \dots + \frac{(9/4)_N(-T^3/\Delta^2)^N}{(1/2)_N N!} + \dots \right]$$

$$+ \frac{72.78 T e^{-(T/\Delta)^2}}{\Delta^{11/3}} \left[1 - 0.833(T/\Delta)^2 + 0.042(T/\Delta)^4 + 0.0030(T/\Delta)^6 + \dots + \frac{(-5/4)_N(T^2/\Delta^2)^N}{(3/2)_N N!} + \dots \right] \quad (52)$$

and therefore

$$[E_{2r}^{(2)}(\rho, 0, t)]^{(1)} \leq \left(\frac{1}{\rho^{1/2}} \right) \frac{\mu_0^{1/2} \hat{A}}{\epsilon_1^{1/2} c^{3/2} \pi} \left[\frac{3.20}{\Delta^{7/2}} \sum_1 + \frac{9.10 T e^{-(T/\Delta)^2}}{\Delta^{9/2}} \sum_2 \right] \quad (53)$$

where the series terms in the first pair of brackets in (52) are denoted by \sum_1 , and those in the second are denoted by \sum_2 . The inequality sign in (53) refers specifically to amplitudes of oscillation, comparing successively each local maximum of the function on its left with the corresponding local maximum of the function on its right.

TABLE 3. Properties of Series in Equations (50) and (51)

Series in Brackets in (50)			Series in Brackets in (51)		
N	$\frac{(a)_N(-T/\Delta)^{2N}}{(b)_N N!}$	S_N	N	$\frac{(a)_N(T/\Delta)^{2N}}{(b)_N N!}$	S_N
1	$-0.616\ 05 \times 10^2$	$-0.607\ 05 \times 10^2$	1	$-0.114\ 08 \times 10^2$	$-0.104\ 08 \times 10^2$
5	$-0.138\ 37 \times 10^4$	$-0.108\ 22 \times 10^4$	5	$0.139\ 14 \times 10^2$	$0.291\ 14 \times 10^3$
10	$0.648\ 36 \times 10^7$	$0.593\ 95 \times 10^7$	10	$0.286\ 79 \times 10^2$	$0.153\ 44 \times 10^3$
15	$-0.167\ 84 \times 10^9$	$-0.832\ 99 \times 10^7$	15	$0.120\ 55 \times 10^2$	$0.253\ 14 \times 10^3$
20	$0.700\ 62 \times 10^7$	$0.293\ 97 \times 10^7$	20	$0.138\ 57 \times 10^1$	$0.275\ 07 \times 10^3$
25	$-0.769\ 53 \times 10^6$	$-0.279\ 71 \times 10^6$	21	$0.787\ 82$	$0.275\ 86 \times 10^3$
30	$0.294\ 80 \times 10^5$	$0.545\ 32 \times 10^4$	22	$0.430\ 32$	$0.276\ 29 \times 10^3$
35	$-0.473\ 22 \times 10^3$	$-0.135\ 77 \times 10^3$	23	$0.226\ 16$	$0.276\ 52 \times 10^3$
40	$0.362\ 12 \times 10^1$	$0.943\ 54$	24	$0.114\ 53$	$0.276\ 63 \times 10^3$
42	$0.428\ 48$	$0.110\ 65$	25	$0.559\ 51 \times 10^{-1}$	$0.276\ 69 \times 10^3$
44	$0.459\ 70 \times 10^{-1}$	$0.145\ 91 \times 10^{-1}$	26	$0.264\ 03 \times 10^{-1}$	$0.276\ 71 \times 10^3$
46	$0.449\ 21 \times 10^{-2}$	$0.454\ 80 \times 10^{-2}$	27	$0.120\ 49 \times 10^{-1}$	$0.276\ 72 \times 10^3$
48	$0.401\ 49 \times 10^{-3}$	$0.359\ 18 \times 10^{-2}$	28	$0.532\ 25 \times 10^{-2}$	$0.276\ 73 \times 10^3$
50	$0.329\ 46 \times 10^{-4}$	$0.350\ 85 \times 10^{-2}$	29	$0.227\ 84 \times 10^{-2}$	$0.276\ 73 \times 10^3$
52	$0.249\ 08 \times 10^{-5}$	$0.350\ 19 \times 10^{-2}$	30	$0.945\ 95 \times 10^{-3}$	$0.276\ 73 \times 10^3$
54	$0.174\ 06 \times 10^{-6}$	$0.350\ 14 \times 10^{-2}$	31	$0.381\ 27 \times 10^{-3}$	
56	$0.112\ 76 \times 10^{-7}$	$0.350\ 14 \times 10^{-2}$	32	$0.149\ 31 \times 10^{-3}$	
58	$0.679\ 10 \times 10^{-9}$	$0.350\ 14 \times 10^{-2}$	33	$0.568\ 57 \times 10^{-4}$	
60	$0.381\ 18 \times 10^{-10}$...	34	$0.210\ 68 \times 10^{-4}$	
62	$0.119\ 89 \times 10^{-11}$	$0.350\ 14 \times 10^{-2}$	35	$0.760\ 24 \times 10^{-5}$	$0.276\ 73 \times 10^3$

N = number of terms; S_N = partial sum, $(a)_N$ and $(b)_N$ in recurring terms are defined as in (34). $T/\Delta = \pm 3.7$

The second term in (39) is

$$[E_{2z}^{(2)}(\rho, 0, t)]^{(2)} = -\frac{\mu_0 \hat{A} c^{-3} \Delta}{4\pi^{3/2}}$$

$$\int_{-\infty}^{\infty} \frac{e^{i-1(1-\rho c t)\omega - \Delta^2 \omega^2/4}}{\mu_0(\varepsilon_1 + i\sigma_1/\omega)} d\omega \quad (54)$$

$$= -\frac{\mu_0 \hat{A} c^{-3} \Delta}{4\pi^{3/2}} \int_{-\infty}^{\infty} \frac{(\mu_0 \varepsilon_1)^{-1} \hat{F}(\omega)}{1 + i\sigma_1/\omega \varepsilon_1} d\omega \quad (55)$$

where

$$\hat{F}(\omega) = (\cos T\omega - i \sin T\omega) e^{-\Delta^2 \omega^2/4} \quad (56)$$

with T as in (42). An upper bound on $[E_{2z}^{(2)}(\rho, 0, t)]^{(2)}$ may be specified in terms of a band of constant field amplitude, since

$$\left| \int_{-\infty}^{\infty} \frac{\hat{F}(\omega)}{1 + i\sigma_1/\omega \varepsilon_1} d\omega \right| \leq \int_{-\infty}^{\infty} |\hat{F}(\omega)| d\omega \quad (57)$$

Within this band, $[E_{2z}^{(2)}(\rho, 0, t)]^{(2)}|_{\sigma_1=0}$ yields an upper bound on the amplitude of each of the oscillations of $[E_{2z}^{(2)}(\rho, 0, t)]^{(2)}$. Using symmetry and asymmetry properties of the integrand about the origin, the integral of (56) over all ω is [Gradshteyn and Ryzhik, 1980, equation 3.952.8]:

$$\int_{-\infty}^{\infty} \hat{F}(\omega) d\omega = 2 \int_0^{\infty} \omega^4 e^{-\Delta^2 \omega^2/4} \cos T\omega d\omega$$

$$= \frac{\Gamma(5/2)}{(\Delta^2/4)^{5/2}} M\left(\frac{1}{2}, \frac{1}{2}, -T^2 \Delta^2\right) \quad (58)$$

$$= \frac{42.54}{\Delta^5} \left[1 - 5.00(T/\Delta)^2 + 5.83(T/\Delta)^4 - 3.50(T/\Delta)^6 + \frac{(5/2)_N (-T^2/\Delta^2)^N}{(1/2)_N N!} + \dots \right] \quad (59)$$

so that

$$[E_{2z}^{(2)}(\rho, 0, t)]^{(2)} \leq -\frac{10.63 \hat{A} \sum_3}{\pi^{3/2} c^3 \varepsilon_1 \Delta^4} \quad (60)$$

which leads to

$$E_{2z}^{(2)}(\rho, 0, t) = \{[E_{2z}^{(2)}(\rho, 0, t)]^{(1)} + [E_{2z}^{(2)}(\rho, 0, t)]^{(2)}\} \leq \frac{\hat{A}}{\pi c \varepsilon_1} \left\{ \left(\frac{\mu_0 \varepsilon_1}{c \rho} \right)^{1/2} \left[\frac{3.20}{\Delta^{7/2}} \sum_1 + \frac{9.10 T e^{-(T/\Delta)^2}}{\Delta^{9/2}} \sum_2 \right] - \frac{10.63}{\pi^{1/2} c^3 \Delta^4} \sum_3 \right\} \quad (61)$$

where the series terms in square brackets in (59) are denoted by \sum_3 , and the inequality sign applies as in (53). Note that the magnitude of (61) is proportional to significant inverse powers of Δ , the pulse half-width. Thus for a very narrow Gaussian pulse the

TABLE 4 Comparison of $E_{2z}(\rho, 0, t) = E_{2z}^{(1)}(\rho, 0, t) + E_{2z}^{(2)}(\rho, 0, t)$ Field Magnitudes

$t - \rho/c$ ns	$E_{2z}^{(1)}(\rho, 0, t)$ V/m	$E_{2z}^{(2)}(\rho, 0, t)$ V/m	$E_{2z}(\rho, 0, t)$ V/m
$\rho = 0.40$ m			
-2.7	6.4×10^{-3}	-9.0×10^{-4}	5.5×10^{-3}
-1.7	1.1×10^{-1}	-5.6×10^{-3}	1.0×10^{-1}
-0.7	-1.3×10^{-1}	2.8×10^{-2}	-1.0×10^{-1}
0.7	1.2×10^{-1}	-1.1×10^{-2}	1.1×10^{-1}
1.7	-3.3×10^{-2}	8.1×10^{-3}	-2.5×10^{-2}
2.7	-3.6×10^{-3}	-1.1×10^{-3}	-4.7×10^{-3}
$\rho = 1.0$ m			
-2.7	9.6×10^{-4}	-2.5×10^{-4}	7.1×10^{-4}
-1.7	1.4×10^{-2}	-1.5×10^{-3}	1.3×10^{-2}
-0.7	-3.2×10^{-2}	7.6×10^{-3}	-2.4×10^{-2}
0.7	3.2×10^{-2}	-3.1×10^{-3}	2.9×10^{-2}
1.7	-7.8×10^{-3}	2.2×10^{-3}	-5.6×10^{-3}
2.7	-7.5×10^{-4}	-3.1×10^{-4}	-1.1×10^{-3}
$\rho = 1.6$ m			
-2.7	3.7×10^{-4}	-1.2×10^{-4}	2.5×10^{-4}
-1.7	5.0×10^{-3}	-7.8×10^{-4}	4.2×10^{-3}
-	-1.3×10^{-2}	3.8×10^{-3}	-9.2×10^{-3}
0.7	1.3×10^{-2}	-1.6×10^{-3}	1.1×10^{-2}
1.7	-3.5×10^{-3}	1.1×10^{-3}	-2.4×10^{-3}
2.7	-3.1×10^{-4}	-1.5×10^{-4}	-4.6×10^{-4}

$E_{2z}(\rho, 0, t)$ maximum amplitude scaled to 1 V/m

Fresnel term becomes quite large. This result is consistent with the analysis of a delta function (or infinitely narrow Gaussian) pulse using the general Sommerfeld integrals (T. T. Wu and R. W. P. King, unpublished manuscript, 1987), wherein it is demonstrated that for such a pulse the Fresnel term is the only term

4 DISCUSSION

The fields $E_{2z}^{(1)}(\rho, 0, t)$ given by (29), $E_{2z}^{(2)}(\rho, 0, t)$ given by (61) (upper bound), and their sum $E_{2z}(\rho, 0, t) = E_{2z}^{(1)}(\rho, 0, t) + E_{2z}^{(2)}(\rho, 0, t)$ (upper bound) are shown for three values of radial distance ρ in Table 4. The effect of the image source opposite S due to the ground plane of Figure 2 is included in this calculated field. The range of retarded times, -2.7 ns $\leq t - \rho/c \leq 2.7$ ns, is one for which the total field $E_{2z}(\rho, 0, t)$ is of appreciable magnitude; outside this range the total field falls to less than $(1/1000)A_0$, where A_0 is its maximum amplitude at $\rho = 0.20$ m. It is seen that quite close to the source ($\rho = 0.40$ m in

Table 4), $E_{2z}^{(2)}(\rho, 0, t)$ has the smallest relative correction to $E_{2z}^{(1)}(\rho, 0, t)$, i.e., the smallest fraction or proportion of $E_{2z}^{(1)}(\rho, 0, t)$. This correction becomes more significant, i.e., a greater fraction or proportion of $E_{2z}^{(1)}(\rho, 0, t)$, with increasing ρ in Table 4.

An alternative way of viewing the smallness of $E_{2z}^{(2)}(\rho, 0, t)$ mentioned above is to note that the Fresnel integrals, and hence the wave number k_1 associated with the salt-water half-space, are barely felt by the total $E_{2z}(\rho, 0, t)$ field for small ρ . Hence for the ρ values of Table 4, the salt water may be interpreted as highly but not perfectly reflective, so much so as to function essentially as a metal ground plane.

A more complete indication of the theoretical $E_{2z}^{(1)}(\rho, 0, t)$, $E_{2z}^{(2)}(\rho, 0, t)$ and $E_{2z}(\rho, 0, t)$ fields given by (29), (41), and (55) (numerically calculated) for a 0.20-m-incremented range in ρ is shown in Figures 6 and 7. It is seen that each of the waveforms for $\rho = 0.20$ m has great relative height; for the ρ values increasing from $\rho = 0.40$ m, the waveforms undergo spreading and deformation with a gradual decrease in amplitude. The k_1 correction term (shown in broken line in Figure 6) undergoes a decrement with increasing ρ although its relative contribution to the total field amplitude increases with increasing ρ .

In Figure 7 the total theoretical field $E_{2z}(\rho, 0, t)$ is plotted in solid line and compared therein to experimental data (broken line). Except in the immediate

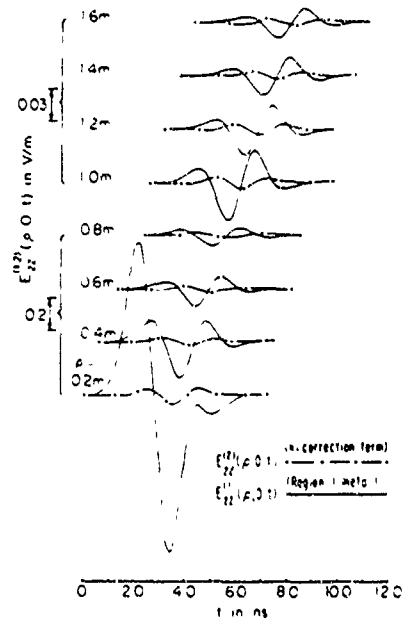


Fig. 6. Theoretical relative amplitudes of $E_{2z}^{(1)}(\rho, 0, t)$ and $E_{2z}^{(2)}(\rho, 0, t)$ versus t to 12 ns for eight successive ρ values

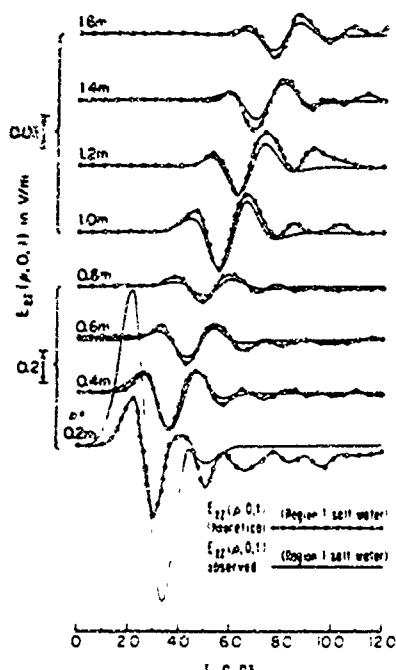


Fig. 7 Relative amplitudes of $E_z(\rho, 0, t)$ versus t to 12 ns for eight successive ρ values

radial vicinity of the source monopole, the agreement between calculated and observed fields is quite good ($\rho = 0.40$ – 1.6 m curves in Figure 7). As the receiving system R closely approaches the source monopole S so that, for most of the single frequencies having significant amplitudes in the pulse, R is in the very near field of S , complicated effects occur. These effects result in the deviation of calculated and observed fields for $\rho \leq 0.25$ m. The curves for $\rho = 0.20$ m have been included to show this deviation.

It is important to note that the theory developed in the foregoing section 3 is quite general. Although it has been shown to coincide closely with observed fields at radial distances attainable in an indoor experiment, its applicability extends to much greater ρ values. Such values are associated with greater Sommerfeld numerical distances $i\theta$, which in turn may be used to compute the $E_{2z}(\rho, 0, t)$ field when higher-order terms in (36) and (37) are included

5 CONCLUSIONS

The theory of wave packets proposed in section 3 yields a precise quantitative correction to the effect of a metal ground plane underlying a pulsed short vertical monopole (i.e., pulsed short vertical dipole in free space in the absence of a metal image plane). This

correction for replacement of the ground plane by a region of salt water involves Fresnel-integral terms which may be represented using a confluent hypergeometric function M . The influence of imperfectly conducting salt water with its associated complex wave numbers k_1 for the range of frequencies in a broadband Gaussian pulse provides a resolvable correction to the monopole field over metal even at distances $\rho \leq 1.0$ m from the source (see Table 4). This correction becomes more significant with increasing radial distance.

Except for a narrow region in the very close vicinity of the vertical source monopole, the theoretical prediction of monopole fields to $\rho = 1.6$ m is followed closely by the experimental observations of the fields (section 2).

APPENDIX EVALUATION OF INTEGRALS

The integral I_1 in (12) is

$$I_1 = \int_{-\infty}^{\infty} e^{i(-1)(1-\rho c)\omega - \Delta^2 \omega^2 / 4} \omega d\omega \quad (A1)$$

$$= \int_{-\infty}^{\infty} (\cos T\omega - i \sin T\omega) e^{-\Delta^2 \omega^2 / 4} \omega d\omega \quad (A2)$$

with $T \equiv (t - \rho c)$ defined as a retarded time. Using symmetry and asymmetry properties of the integrand about the origin, (A2) is given by

$$I_1 = -2i \int_0^{\infty} (\sin T\omega) e^{-\Delta^2 \omega^2 / 4} \omega d\omega \quad (A3)$$

Integrating by parts,

$$I_1 = -\frac{4i}{\Delta^2} \left[(\sin T\omega) e^{-\Delta^2 \omega^2 / 4} \right]_0^{\infty} + T \int_0^{\infty} (\cos T\omega) e^{-\Delta^2 \omega^2 / 4} d\omega \quad (A4)$$

or

$$I_1 = -\frac{i4\pi^{1/2}}{\Delta^3} T e^{-(T\Delta)^2} \quad (A5)$$

The integral I_2 in (13) is elementary:

$$I_2 = \int_{-\infty}^{\infty} e^{i(-1)(1-\rho c)\omega - \Delta^2 \omega^2 / 4} d\omega \quad (A6)$$

This is given by the same integral as that on the right side of (A4), so that [Gradshteyn and Ryzhik, 1980,

equation 3.896.4]

$$I_2 = 2 \int_0^\infty (\cos T\omega) e^{-\Delta^2 \omega^2 / 4} d\omega = \frac{2\pi^{1/2}}{\Delta} e^{-(T/\Delta)^2} \quad (A7)$$

The integral I_3 in (14) is given by

$$I_3 = \int_{-\infty}^\infty e^{i[(1-\rho/c)\omega - \Delta^2 \omega^2 / 4]} \omega^{-1} d\omega \quad (A8)$$

By using the principal value of (A8), the singularity at $\omega = 0$ does not interfere with the asymmetry of the integrand, so that

$$I_3 = -2i \int_0^\infty (\sin T\omega) e^{-\Delta^2 \omega^2 / 4} \omega^{-1} d\omega \quad (A9)$$

Defining the variables $u = \omega\Delta/2$ and $q = 2T/\Delta$, (A9) becomes

$$I_3 = -2i \int_0^\infty e^{-u^2} \frac{\sin qu}{u} du \quad (A10)$$

while

$$\frac{dI_3}{dq} = -2i \int_0^\infty e^{-u^2} \cos qu du = -i\sqrt{\pi} e^{-q^2/4} \quad (A11)$$

It follows that

$$I_3 = -i\sqrt{\pi} \int_0^q e^{-q'^2/4} dq' \quad (A12)$$

$$I_3 = -i\pi \operatorname{erf}\left(\frac{q}{2}\right) = -i\pi \operatorname{erf}\left(\frac{T}{\Delta}\right) \quad (\text{principal value}) \quad (A13)$$

In (A13), erf denotes the error function of a real argument. $\operatorname{erf}(q)$ has the series expansion [Abramowitz and Stegun, 1972].

$$\operatorname{erf}(q) = \frac{2}{\sqrt{\pi}} \left(q - \frac{1}{3}q^3 + \frac{1}{105}q^5 - \dots \right) \quad (A14)$$

so that the leading term in I_3 is $I_3^{(1)} = -i2\pi^{1/2}q$

The integrals I_4 in (23) and I_5 in (24) are

$$I_4 = \int_{-\infty}^\infty e^{i[(1-\rho/c)\omega - \Delta^2 \omega^2 / 4]} \omega^3 d\omega \quad (A15)$$

and

$$I_5 = \int_{-\infty}^\infty e^{i[(1-\rho/c)\omega - \Delta^2 \omega^2 / 4]} \omega^2 d\omega \quad (A16)$$

respectively. These may be evaluated using integration by parts and symmetry and asymmetry properties of integrands about the origin as in the foregoing

three integrations I_1 , I_2 and I_3 . In this way the $\omega^3 \cos T\omega$ term is eliminated in I_4 , the $\omega^2 \sin T\omega$ term in I_5 . Thus

$$I_4 = -2i \int_0^\infty (\sin T\omega) e^{-\Delta^2 \omega^2 / 4} \omega^3 d\omega \quad (A17)$$

$$I_4 = -\frac{i\sqrt{\pi}}{\Delta^3} \left(24T - \frac{16T^3}{\Delta^2} \right) e^{-(T/\Delta)^2} \quad (A18)$$

and

$$I_5 = 2 \int_0^\infty (\cos T\omega) e^{-\Delta^2 \omega^2 / 4} \omega^2 d\omega \quad (A19)$$

$$I_5 = \frac{4\sqrt{\pi}}{\Delta^3} \left[1 - 2\left(\frac{T}{\Delta}\right)^2 \right] e^{-(T/\Delta)^2} \quad (A20)$$

Acknowledgments The author is grateful to John G. Heacock of the U.S. Office of Naval Research for his continued interest in this project, to T. T. Wu for clarifications in mathematical physics, and to Margaret Owens for preparing and checking the manuscript. The author would also like to thank John M. Myers of the Harvard Antenna Group for moral support and guidance.

REFERENCES

- Abramowitz, M., and I. Stegun, *Handbook of Mathematical Functions*, Dover, New York, 1972.
- Antonov, Yu. N., and A. K. Manshtein, Development of equipment for depth sounding with transient fields in the near zone. *Akad. Nauk SSSR Novosibirsk*, 1, 18-26, 1979.
- Azad, J., Mapping stratigraphic traps with electrical transients. *Bull. Can. Pet. Geol.*, 25, 996-1036, 1977.
- Baños, A., Jr., *Dipole Radiation in the Presence of a Conducting Half-Space*, Pergamon, New York, 1966.
- Brown, M. F., and R. W. P. King, Shallow sounding of crustal regions using electromagnetic surface waves, *Radio Sci.*, 21, 831-844, 1986.
- Brown, M. F., R. W. P. King, and T. T. Wu, Lateral-wave studies in a model lithosphere, *J. Appl. Phys.*, 53, 3387-3396, 1982.
- Brown, M. F., R. W. P. King, and T. T. Wu, Experiments on the reflection of lateral electromagnetic waves, *J. Appl. Phys.*, 55, 3927-3933, 1984.
- Gradshteyn, I. S., and I. M. Ryzhik, *Table of Integrals, Series, and Products*, Academic, Orlando, Fla., 1980.
- King, R. W. P., *Theory of Linear Antennas*, Harvard University Press, Cambridge, Mass., 1956.
- King, R. W. P., Electromagnetic surface waves: New formulas and applications, *IEEE Trans. Antennas Propag.*, AP-33, 1204-1212, 1985a.
- King, R. W. P., Electromagnetic surface waves: New formulas and their application to determine the electrical properties of the sea bottom, *J. Appl. Phys.*, 58, 3612-3624, 1985b.
- King, R. W. P., and M. F. Brown, Lateral electromagnetic waves along plane boundaries: A summarizing approach, *Proc. IEEE*, 72, 595-611, 1984.

- Morozova, G. M., Method of sounding with transient fields in the near zone in deep investigations. *Akad. Nauk. SSSR Novosibirsk*, 1, 26-39, 1979
- Schmitt, H. J., C. W. Harrison, Jr., and C. S. Williams, Calculated and experimental response of thin cylindrical antennas to pulse excitation. *IEEE Trans. Antennas Propag.*, AP-14, 120-127, 1966
- Shen, H. M., R. W. P. King, and T. T. Wu, The dual-measurement procedure for eliminating systematic interference, *IEEE Trans. Electromagn. Compat.*, EMC-26, 14-18, 1984
- Sommerfeld, A. N., On the propagation of waves in wireless telegraphy (in German), *Ann. Phys.*, 28, 665-736, 1909
- Sommerfeld, A. N., On the propagation of waves in wireless telegraphy (in German), *Ann. Phys.*, 81, 1135-1153, 1926
- Wait, J. R., Propagation effects for electromagnetic pulse transmission, *Proc. IEEE*, 74, 1173-1181, 1986
-
- M. F. Brown, Gordon McKay Laboratory, Harvard University,
9 Oxford Street, Cambridge, MA 02138

LATERAL ELECTROMAGNETIC SURFACE WAVES AND PULSES

Ronold W. P. King

Gordon McKay Laboratory, Harvard University, Cambridge, Massachusetts 02138, U.S.A.

Abstract—The electromagnetic field generated by a vertical electric dipole on or near the surface of the earth or in the earth is studied for both continuous-wave and pulse excitation. The analytical foundation established by Sommerfeld and developed by many others is reviewed and simple explicit new formulas are derived for the three components of the electromagnetic field. Some of the interesting properties of the lateral waves and pulses—which constitute the entire field along the surface—are shown in conjunction with important applications to communications and geophysical exploration.

1. Introduction

Less than a decade after Heinrich Hertz, in a brilliant series of experiments, demonstrated the existence and many of the properties of electromagnetic waves, Marconi introduced the world to their most important application: long range wireless communication. But the waves that propagate along the surface of the earth are not the same as those that travel in free space. The boundary between two electrically quite different media like air and earth (fresh water, salt water, rock, sand, ice) greatly alters the nature of the electromagnetic waves traveling outward from an electric dipole located near the surface. This was shown analytically by Sommerfeld in a series of papers and articles [1]–[3] that has served as the foundation for related investigations by many others up to the present time. The solution obtained by Sommerfeld was for the Hertz potential for the two-half-space model of the earth with an oscillating vertical electric dipole on the boundary as the source. The effects of the earth's curvature and reflection from the ionosphere—which further complicate the actual propagation over the surface of the earth—are not included. The associated components of the electric and magnetic field are determined by differentiation. A disadvantage with this form of solution is the fact that the Hertz potential is represented by complex integral transforms that are difficult both to interpret physically and to apply meaningfully. Attempts to eliminate this important obstacle have been numerous and include especially the work of Norton [4], [5] in representing the surface-wave term, and of Baños [6] and Wait and Campbell [7] in developing explicit approximate formulas for the components of the electromagnetic field. These are quite simple but are limited to restricted, nonoverlapping near-, intermediate-, and far-field ranges. This limitation was removed by King [8] who derived a single set of simple formulas valid everywhere in the earth and on the boundary when the dipole is also on the boundary in either region or at depth d in the earth, subject only to the conditions:

$$|k_1^2| \gg |k_2^2| \quad \text{or} \quad |k_1| \geq 3|k_2|; \quad \text{and} \quad \rho^2 \gg |z|^2; \quad \rho^2 \gg d^2, \quad (1.1)$$

where

$$k_1 = \beta_1 + i\alpha_1 = \omega[\mu_0(\epsilon_1 + i\sigma_1/\omega)]^{1/2}; \quad k_2 = \omega(\mu_0\epsilon_0)^{1/2} = \omega/c \quad (1.2)$$

are the wave numbers of the two half-spaces, earth (Region 1, $z > 0$) and air (Region 2, $z < 0$). In (1.1), ρ is the radial distance from the source at $(0, d)$ to the point of observation at (ρ, z) , as shown in Fig. 1 for a dipole at depth d in the earth and with the point of observation at the depth z in the earth. When $d = z = 0$, the dipole and point of observation are both on the boundary.

The final generalization—to be carried out in this paper—is the derivation of simple formulas for the components of the electromagnetic field at any point $z' = -z$ in the air when the dipole is at $(0, -d)$ also in the air.

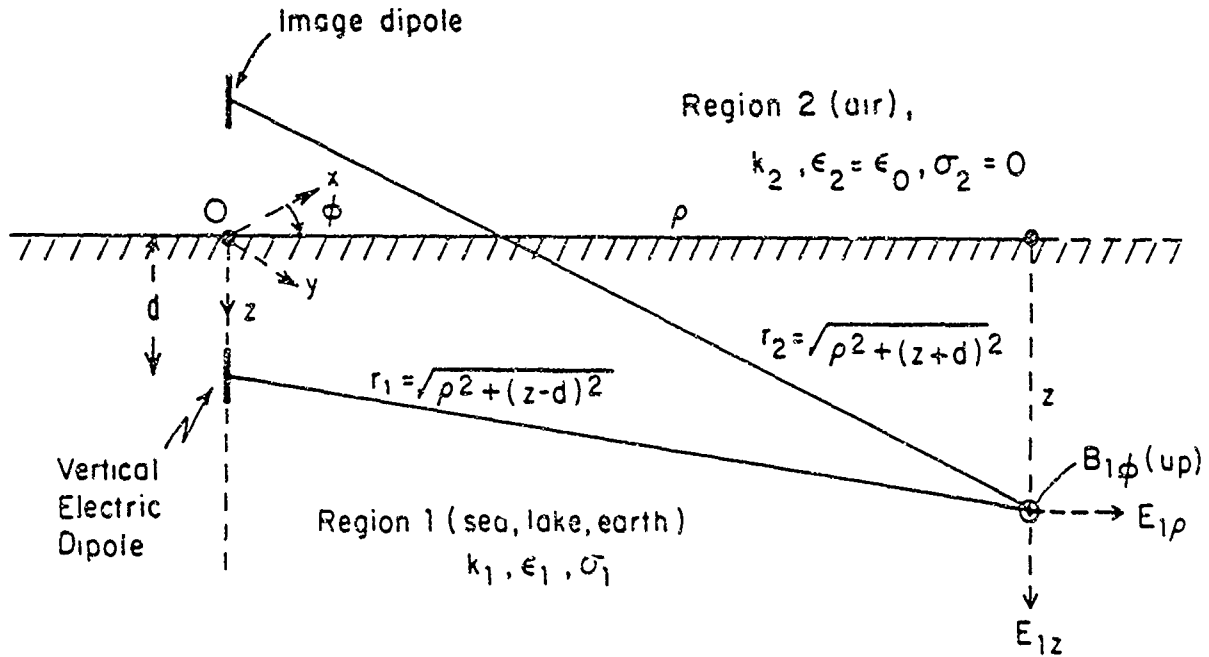


Fig. 1. Vertical electric dipole at depth d in Region 1. Electromagnetic field calculated at (ρ, z) .

2. Electromagnetic Field in Air Due to a Vertical Electric Dipole at Height d in Air

The integrals of the three components $B_{2\phi}(\rho, z')$, $E_{2\rho}(\rho, z')$, and $E_{2z}(\rho, z')$ of the electromagnetic field at (ρ, z') in the air ($z' \geq 0$) when the vertical dipole is at $(0, -d)$ in the air are readily obtained from analogous formulas in [8]. With $z' = -z$ and $\phi' = -\phi$, they are:

$$B_{2\phi}(\rho, z') = \frac{i\mu_0}{2\pi} \int_0^\infty \left[\frac{e^{i\gamma_2|x'-d|}}{2\gamma_2} - \frac{e^{i\gamma_2(x'+d)}}{2\gamma_2} + \frac{k_1^2 e^{i\gamma_2(x'+d)}}{N} \right] J_1(\lambda\rho) \lambda^2 d\lambda, \quad (2.1)$$

$$E_{2\rho}(\rho, z') = \frac{i\omega\mu_0}{2\pi k_2^2} \int_0^\infty \left[\pm \frac{e^{i\gamma_2|x'-d|}}{2} - \frac{e^{i\gamma_2(x'+d)}}{2} + \frac{k_1^2 \gamma_2 e^{i\gamma_2(x'+d)}}{N} \right] J_1(\lambda\rho) \lambda^2 d\lambda; \quad \begin{cases} z' > d \\ 0 \leq z' \leq d \end{cases}, \quad (2.2)$$

$$E_{2z'}(\rho, z') = -\frac{\omega\mu_0}{2\pi k_2^2} \int_0^\infty \left[\frac{e^{i\gamma_2|z'-d|}}{2\gamma_2} - \frac{e^{i\gamma_2(z'+d)}}{2\gamma_2} + \frac{k_1^2 e^{i\gamma_2(z'+d)}}{N} \right] J_0(\lambda\rho) \lambda^3 d\lambda, \quad (2.3)$$

where

$$N \equiv k_1^2 \gamma_2 + k_2^2 \gamma_1; \quad \gamma_j = (k_j^2 - \lambda^2)^{1/2}, \quad j = 1, 2. \quad (2.4)$$

The first two terms in (2.1)-(2.3) are, respectively, the direct field and the image field. Thus, with

$$E_2(\rho, z') = E_2^d(\rho, z') + E_2^i(\rho, z') + E_2^L(\rho, z') + E_2^c(\rho, z'), \quad (2.5)$$

$$B_2(\rho, z') = B_2^d(\rho, z') + B_2^i(\rho, z') + B_2^L(\rho, z') + B_2^c(\rho, z'), \quad (2.6)$$

the direct-field components are

$$B_{2\phi'}^d(\rho, z') = \frac{i\mu_0}{4\pi} \int_0^\infty \frac{e^{i\gamma_2|z'-d|}}{\gamma_2} J_1(\lambda\rho) \lambda^2 d\lambda = -\frac{\mu_0}{4\pi} e^{ik_2 r_1} \left(\frac{ik_2}{r_1} - \frac{1}{r_1^2} \right) \left(\frac{\rho}{r_1} \right), \quad (2.7)$$

$$E_{2\rho}^d(\rho, z') = \frac{i\omega\mu_0}{4\pi k_2^2} \int_0^\infty \pm e^{i\gamma_2|z'-d|} J_1(\lambda\rho) \lambda^2 d\lambda; \quad \begin{cases} z' > d \\ 0 \leq z' \leq d \end{cases}$$

$$= -\frac{\omega\mu_0}{4\pi k_2^2} e^{ik_2 r_1} \left(\frac{ik_2^2}{r_1} - \frac{3k_2}{r_1^2} - \frac{3i}{r_1^3} \right) \left(\frac{\rho}{r_1} \right) \left(\frac{z'-d}{r_1} \right), \quad (2.8)$$

$$E_{2z'}^d(\rho, z') = -\frac{\omega\mu_0}{4\pi k_2^2} \int_0^\infty \frac{e^{i\gamma_2|z'-d|}}{\gamma_2} J_0(\lambda\rho) \lambda^3 d\lambda$$

$$= \frac{\omega\mu_0}{4\pi k_2^2} e^{ik_2 r_1} \left[\left(\frac{ik_2^2}{r_1} - \frac{k_2}{r_1^2} - \frac{i}{r_1^3} \right) - \left(\frac{z'-d}{r_1} \right)^2 \left(\frac{ik_2^2}{r_1} - \frac{3k_2}{r_1^2} - \frac{3i}{r_1^3} \right) \right], \quad (2.9)$$

where $r_1 = [\rho^2 + (z'-d)^2]^{1/2}$. The image fields are

$$B_{2\phi'}^i(\rho, z') = -\frac{i\mu_0}{4\pi} \int_0^\infty \frac{e^{i\gamma_2(z'+d)}}{\gamma_2} J_1(\lambda\rho) \lambda^2 d\lambda = \frac{\mu_0}{4\pi} e^{ik_2 r_2} \left(\frac{ik_2}{r_2} - \frac{1}{r_2^2} \right) \left(\frac{\rho}{r_2} \right), \quad (2.10)$$

$$E_{2\rho}^i(\rho, z') = -\frac{i\omega\mu_0}{4\pi k_2^2} \int_0^\infty e^{i\gamma_2(z'+d)} J_1(\lambda\rho) \lambda^2 d\lambda$$

$$= \frac{\omega\mu_0}{4\pi k_2^2} e^{ik_2 r_2} \left(\frac{ik_2^2}{r_2} - \frac{3k_2}{r_2^2} - \frac{3i}{r_2^3} \right) \left(\frac{\rho}{r_2} \right) \left(\frac{z'+d}{r_2} \right), \quad (2.11)$$

$$E_{2z'}^i(\rho, z') = \frac{\omega\mu_0}{4\pi k_2^2} \int_0^\infty \frac{e^{i\gamma_2(z'+d)}}{\gamma_2} J_0(\lambda\rho) \lambda^3 d\lambda$$

$$= -\frac{\omega\mu_0}{4\pi k_2^2} e^{ik_2 r_2} \left[\left(\frac{ik_2^2}{r_2} - \frac{k_2}{r_2^2} - \frac{i}{r_2^3} \right) - \left(\frac{z'+d}{r_2} \right)^2 \left(\frac{ik_2^2}{r_2} - \frac{3k_2}{r_2^2} - \frac{3i}{r_2^3} \right) \right], \quad (2.12)$$

where $r_2 = [\rho^2 + (z'+d)^2]^{1/2}$. The rest of the field consists of the lateral-wave part and a correction to the image field, viz.,

$$B_{2\phi'}^L(\rho, z') + B_{2\phi'}^c(\rho, z') = \frac{i\mu_0 k_1^2}{2\pi} \int_0^\infty \frac{e^{i\gamma_2(z'+d)}}{N} J_1(\lambda\rho) \lambda^2 d\lambda, \quad (2.13)$$

$$E_{2\rho}^L(\rho, z') + E_{2\rho}^c(\rho, z') = \frac{i\omega\mu_0 k_1^2}{2\pi k_2^2} \int_0^\infty \frac{\gamma_2 e^{i\gamma_2(z'+d)}}{N} J_1(\lambda\rho) \lambda^2 d\lambda, \quad (2.14)$$

$$E_{2z'}^L(\rho, z') + E_{2z'}^c(\rho, z') = -\frac{\omega\mu_0 k_1^2}{2\pi k_2^2} \int_0^\infty \frac{e^{i\gamma_2(z'+d)}}{N} J_0(\lambda\rho) \lambda^3 d\lambda. \quad (2.15)$$

These integrals can be evaluated if use is made of the inequality $|k_1|^2 \gg |k_2|^2$. With this condition, the first term in $N = k_1^2 \gamma_2 + k_2^2 \gamma_1$ is the larger one. Let

$$\frac{1}{N} = \frac{1}{N_0} + \left(\frac{1}{N} - \frac{1}{N_0} \right); \quad N_0 = k_1^2 \gamma_2 = k_1^2 (k_2^2 - \lambda^2)^{1/2}. \quad (2.16)$$

The first part of the integrals is the correction for the reflected field. It is given by (2.13)–(2.15) with N_0 substituted for N . The integrals so obtained are the same as (2.10)–(2.12). Thus,

$$B_{2\phi'}^c(\rho, z') = \frac{i\mu_0}{2\pi} \int_0^\infty \frac{e^{i\gamma_2(z'+d)}}{\gamma_2} J_1(\lambda\rho) \lambda^2 d\lambda = -\frac{\mu_0}{2\pi} e^{ik_2 r_2} \left(\frac{ik_2}{r_2} - \frac{1}{r_2^2} \right) \left(\frac{\rho}{r_2} \right), \quad (2.17)$$

$$\begin{aligned} E_{2\rho}^c(\rho, z') &= \frac{i\omega\mu_0}{2\pi k_2^2} \int_0^\infty e^{i\gamma_2(z'+d)} J_1(\lambda\rho) \lambda^2 d\lambda \\ &= -\frac{\omega\mu_0}{2\pi k_2^2} e^{ik_2 r_2} \left(\frac{ik_2^2}{r_2} - \frac{3k_2}{r_2^2} - \frac{3i}{r_2^3} \right) \left(\frac{\rho}{r_2} \right) \left(\frac{z'+d}{r_2} \right), \end{aligned} \quad (2.18)$$

$$\begin{aligned} E_{2z'}^c(\rho, z') &= -\frac{\omega\mu_0}{2\pi k_2^2} \int_0^\infty \frac{e^{i\gamma_2(z'+d)}}{\gamma_2} J_0(\lambda\rho) \lambda^3 d\lambda \\ &= \frac{\omega\mu_0}{2\pi k_2^2} e^{ik_2 r_2} \left[\left(\frac{ik_2^2}{r_2} - \frac{k_2}{r_2^2} - \frac{i}{r_2^3} \right) - \left(\frac{z'+d}{r_2} \right)^2 \left(\frac{ik_2^2}{r_2} - \frac{3k_2}{r_2^2} - \frac{3i}{r_2^3} \right) \right]. \end{aligned} \quad (2.19)$$

In the second part of each integral, the factor $1/N$ is replaced by

$$\frac{1}{N} - \frac{1}{N_0} = \frac{1}{k_1^2 \gamma_2 + k_2^2 \gamma_1} - \frac{1}{k_1^2 \gamma_2}. \quad (2.20)$$

Specifically, the lateral-wave terms are

$$B_{2\phi'}^L(\rho, z') = \frac{i\mu_0 k_1^2}{2\pi} \int_0^\infty \left(\frac{1}{N} - \frac{1}{N_0} \right) e^{i\gamma_2(z'+d)} J_1(\lambda\rho) \lambda^2 d\lambda, \quad (2.21)$$

$$E_{2\rho}^L(\rho, z') = \frac{i\omega\mu_0 k_1^2}{2\pi k_2^2} \int_0^\infty \left(\frac{1}{N} - \frac{1}{N_0} \right) \gamma_2 e^{i\gamma_2(z'+d)} J_1(\lambda\rho) \lambda^2 d\lambda, \quad (2.22)$$

$$E_{2z'}^L(\rho, z') = -\frac{\omega\mu_0 k_1^2}{2\pi k_2^2} \int_0^\infty \left(\frac{1}{N} - \frac{1}{N_0} \right) e^{i\gamma_2(z'+d)} J_0(\lambda\rho) \lambda^3 d\lambda. \quad (2.23)$$

These integrals are readily evaluated with some manipulation and standard formulas. The results are

$$B_{2\phi'}^L(\rho, z') = \frac{\mu_0 k_2^3}{2\pi k_1} e^{ik_2 \rho} e^{ik_2(z'+d)^2/2\rho} \left(\frac{\pi}{k_2 \rho} \right)^{1/2} e^{-iP_d} \mathcal{F}(P_d), \quad (2.24)$$

$$E_{2\rho}^L(\rho, z') = \frac{\omega \mu_0}{2\pi k_1} e^{ik_2 \rho} e^{ik_2(z'+d)^2/2\rho} \left[\frac{ik_2}{\rho} - \frac{1}{\rho^2} - \frac{k_2^3}{k_1} \left(\frac{\pi}{k_2 \rho} \right)^{1/2} e^{-iP_d} \mathcal{F}(P_d) \right], \quad (2.25)$$

$$E_{2z'}^L(\rho, z') = -\frac{\omega \mu_0 k_2^2}{2\pi k_1} e^{ik_2 \rho} e^{ik_2(z'+d)^2/2\rho} \left(\frac{\pi}{k_2 \rho} \right)^{1/2} e^{-iP_d} \mathcal{F}(P_d), \quad (2.26)$$

where

$$P_d = (R + Z' + D)^2/R; \quad R = k_2^3 \rho / 2k_1^2, \quad Z' = k_2^2 z' / 2k_1, \quad D = k_2^2 d / 2k_1, \quad (2.27)$$

and

$$\mathcal{F}(P_d) = \int_{P_d}^{\infty} \frac{e^{it}}{(2\pi i)^{1/2}} dt = \frac{1}{2}(1+i) - C_2(P_d) - iS_2(P_d), \quad (2.28)$$

where $C_2(P_d) + iS_2(P_d)$ is the Fresnel integral. The complete field in Region 2 is the sum of the direct, reflected, correction and lateral-wave parts as defined in (2.5). Note that the sum of the reflected and correction terms is simply the reflected field with reversed sign. This corresponds to a codirectional instead of oppositely directed image. The complete field is:

$$B_{2\phi'}(\rho, z') = -\frac{\mu_0}{2\pi} \left[\frac{e^{ik_2 r_1}}{2} \left(\frac{\rho}{r_1} \right) \left(\frac{ik_2}{r_1} - \frac{1}{r_1^2} \right) + \frac{e^{ik_2 r_2}}{2} \left(\frac{\rho}{r_2} \right) \left(\frac{ik_2}{r_2} - \frac{1}{r_2^2} \right) - e^{ik_2 \rho} e^{ik_2(z'+d)^2/2\rho} \frac{k_2^3}{k_1} \left(\frac{\pi}{k_2 \rho} \right)^{1/2} e^{-iP_d} \mathcal{F}(P_d) \right], \quad (2.29)$$

$$E_{2\rho}(\rho, z') = -\frac{\omega \mu_0}{2\pi k_2} \left\{ \frac{e^{ik_2 r_1}}{2} \left(\frac{\rho}{r_1} \right) \left(\frac{z'-d}{r_1} \right) \left(\frac{ik_2}{r_1} - \frac{3}{r_1^2} - \frac{3i}{k_2 r_1^3} \right) + \frac{e^{ik_2 r_2}}{2} \left(\frac{\rho}{r_2} \right) \left(\frac{z'+d}{r_2} \right) \left(\frac{ik_2}{r_2} - \frac{3}{r_2^2} - \frac{3i}{k_2 r_2^3} \right) - \frac{k_2}{k_1} e^{ik_2 \rho} e^{ik_2(z'+d)^2/2\rho} \left[\frac{ik_2}{\rho} - \frac{1}{\rho^2} - \frac{k_2^3}{k_1} \left(\frac{\pi}{k_2 \rho} \right)^{1/2} e^{-iP_d} \mathcal{F}(P_d) \right] \right\}, \quad (2.30)$$

$$E_{2z'}(\rho, z') = \frac{\omega \mu_0}{2\pi k_2} \left\{ \frac{e^{ik_2 r_1}}{2} \left[\left(\frac{ik_2}{r_1} - \frac{1}{r_1^2} - \frac{i}{k_2 r_1^3} \right) - \left(\frac{z'-d}{r_1} \right)^2 \left(\frac{ik_2}{r_1} - \frac{3}{r_1^2} - \frac{3i}{k_2 r_1^3} \right) \right] + \frac{e^{ik_2 r_2}}{2} \left[\left(\frac{ik_2}{r_2} - \frac{1}{r_2^2} - \frac{i}{k_2 r_2^3} \right) - \left(\frac{z'+d}{r_2} \right)^2 \left(\frac{ik_2}{r_2} - \frac{3}{r_2^2} - \frac{3i}{k_2 r_2^3} \right) \right] - e^{ik_2 \rho} e^{ik_2(z'+d)^2/2\rho} \frac{k_2^3}{k_1} \left(\frac{\pi}{k_2 \rho} \right)^{1/2} e^{-iP_d} \mathcal{F}(P_d) \right\}, \quad (2.31)$$

where $r_1 = [\rho^2 + (z'-d)^2]^{1/2}$, $r_2 = [\rho^2 + (z'+d)^2]^{1/2}$. Note that when Region 1 is a perfect conductor, $\sigma_1 \rightarrow \infty$ and $k_1 \rightarrow \infty$, so that the surface-wave terms with k_1 in the denominator vanish and the entire field is given by the direct and image terms.

The field on the boundary where $z' = 0$ is:

$$B_{2\phi}(\rho, 0) = -\frac{\mu_0}{2\pi} \left[ik_2 r_d \left(\frac{\rho}{r_d} \right) \left(\frac{ik_2}{r_d} - \frac{1}{r_d^2} \right) - e^{ik_2 \rho} e^{ik_2 d^2/2\rho} \frac{k_2^3}{k_1} \left(\frac{\pi}{k_2 \rho} \right)^{1/2} e^{-iP_0} \mathcal{F}(P_0) \right], \quad (2.32)$$

$$E_{2\rho}(\rho, 0) = \frac{\omega\mu_0}{2\pi k_1} e^{ik_2 \rho} e^{ik_2 d^2/2\rho} \left[\frac{ik_2}{\rho} - \frac{1}{\rho^2} - \frac{k_2^3}{k_1} \left(\frac{\pi}{k_2 \rho} \right)^{1/2} e^{-iP_0} \mathcal{F}(P_0) \right], \quad (2.33)$$

$$E_{2z}(\rho, 0) = \frac{\omega\mu_0}{2\pi k_2} \left\{ e^{ik_2 r_d} \left[\left(\frac{ik_2}{r_d} - \frac{1}{r_d^2} - \frac{i}{k_2 r_d^3} \right) - \frac{d^2}{r_d^2} \left(\frac{ik_2}{r_d} - \frac{3}{r_d^2} - \frac{3i}{k_2 r_d^3} \right) \right] - e^{ik_2 \rho} e^{ik_2 d^2/2\rho} \frac{k_2^3}{k_1} \left(\frac{\pi}{k_2 \rho} \right)^{1/2} e^{-iP_0} \mathcal{F}(P_0) \right\}, \quad (2.34)$$

where $r_d = (\rho^2 + d^2)^{1/2}$ and $P_0 = (R + D)^2/R$.

Of particular interest is the field at any point in Region 2 (air) when the dipole is on the surface of Region 1 (earth or sea). The determination of this field was the original purpose of the many investigations in the period from Sommerfeld to Norton. This field is completely and accurately given by (2.29)–(2.31) with $d = 0$. It is usually convenient in the spherical coordinates r_0, Θ, Φ . With the formulas $E_{2r}(r_0, \Theta) = E_{2\rho}(\rho, z') \sin \Theta + E_{2z}(\rho, z') \cos \Theta$, $E_{2\theta}(r_0, \Theta) = E_{2\rho}(\rho, z') \cos \Theta - E_{2z}(\rho, z') \sin \Theta$, and $B_{2\phi}(r_0, \Theta) = B_{2\phi}(\rho, z')$, together with $\sin \Theta = \rho/r_0$ and $\cos \Theta = z'/r_0$, the components of the field are:

$$B_{2\phi}(r_0, \Theta) = -\frac{\mu_0}{2\pi} \left[\sin \Theta e^{ik_2 r_0} \left(\frac{ik_2}{r_0} - \frac{1}{r_0^2} \right) - e^{ik_2 \rho} e^{ik_2 z'^2/2\rho} \frac{k_2^3}{k_1} \left(\frac{\pi}{k_2 \rho} \right)^{1/2} e^{-iP_z} \mathcal{F}(P_z) \right], \quad (2.35)$$

$$E_{2r}(r_0, \Theta) = \frac{\omega\mu_0}{2\pi k_2} \left\{ \cos \Theta \left[e^{ik_2 r_0} \left(\frac{2}{r_0^2} + \frac{2i}{k_2 r_0^3} \right) - e^{ik_2 \rho} e^{ik_2 z'^2/2\rho} \frac{k_2^3}{k_1} \left(\frac{\pi}{k_2 \rho} \right)^{1/2} e^{-iP_z} \mathcal{F}(P_z) \right] + \sin \Theta e^{ik_2 \rho} e^{ik_2 z'^2/2\rho} \frac{k_2}{k_1} \left[\frac{ik_2}{\rho} - \frac{1}{\rho^2} - \frac{k_2^3}{k_1} \left(\frac{\pi}{k_2 \rho} \right)^{1/2} e^{-iP_z} \mathcal{F}(P_z) \right] \right\}, \quad (2.36)$$

$$E_{2\theta}(r_0, \Theta) = -\frac{\omega\mu_0}{2\pi k_2} \left\{ \sin \Theta \left[e^{ik_2 r_0} \left(\frac{ik_2}{r_0} - \frac{1}{r_0^2} - \frac{i}{k_2 r_0^3} \right) - e^{ik_2 \rho} e^{ik_2 z'^2/2\rho} \frac{k_2^3}{k_1} \left(\frac{\pi}{k_2 \rho} \right)^{1/2} e^{-iP_z} \mathcal{F}(P_z) \right] - \cos \Theta e^{ik_2 \rho} e^{ik_2 z'^2/2\rho} \frac{k_2}{k_1} \left[\frac{ik_2}{\rho} - \frac{1}{\rho^2} - \frac{k_2^3}{k_1} \left(\frac{\pi}{k_2 \rho} \right)^{1/2} e^{-iP_z} \mathcal{F}(P_z) \right] \right\}, \quad (2.37)$$

where $P_z = (R + Z')^2/R$. At the boundary where $Z' = 0$ and $\Theta = \pi/2$, these formulas reduce to:

$$-\frac{\omega}{k_1} B_{2\Phi}(r_0, \pi/2) = E_{2r}(r_0, \pi/2) = \frac{\omega\mu_0}{2\pi k_1} e^{ik_2\rho} f(k_2\rho, k_1), \quad (2.38)$$

$$E_{2\Theta}(r_0, \pi/2) = -\frac{\omega\mu_0}{2\pi k_2} e^{ik_2\rho} g(k_2\rho, k_1), \quad (2.39)$$

where

$$g(k_2\rho, k_1) = f(k_2\rho, k_1) - \frac{i}{k_2\rho^3} = \frac{ik_2}{\rho} - \frac{1}{\rho^2} - \frac{i}{k_2\rho^3} - \frac{k_2^3}{k_1} \left(\frac{\pi}{k_2\rho}\right)^{1/2} e^{-iR} \mathcal{F}(R), \quad (2.40)$$

and $R = k_2^3\rho/2k_1^2$. Note that at sufficient distance where

$$k_2\rho \geq 8|k_1^2|/k_2^2 \quad \text{or} \quad |R| \geq 4, \quad (2.41)$$

the Fresnel-integral term becomes

$$-\frac{k_2^3}{k_1} \left(\frac{\pi}{k_2\rho}\right)^{1/2} e^{-iR} \mathcal{F}(R) \rightarrow -\frac{ik_2}{\rho} - \frac{k_1^2}{k_2^2\rho^2}, \quad (2.42)$$

so that

$$g(k_2\rho, k_1) \sim f(k_2\rho, k_1) = -\frac{1}{\rho^2} \left(\frac{k_1^2}{k_2^2} + 1\right) \sim -\frac{k_1^2}{k_2^2\rho^2}. \quad (2.43)$$

Evidently, the Fresnel-integral term cancels the ik_2/ρ term and leaves the term $-k_1^2/k_2^2\rho^2$. The entire far field along the boundary is given by (2.38) and (2.39) with $g(k_2\rho, k_1)$ and $f(k_2\rho, k_1)$ replaced by $-k_1^2/k_2^2\rho^2$. That is,

$$\frac{\omega}{k_2} B_{2\Phi}^r(r_0, \pi/2) = -\frac{k_1}{k_2} E_{2r}^r(r_0, \pi/2) = E_{2\Theta}^r(r_0, \pi/2) = \frac{\omega\mu_0 k_1^2}{2\pi k_2^3} \frac{e^{ik_2\rho}}{\rho^2}. \quad (2.44)$$

The large-argument approximation of the Fresnel-integral terms in (2.35)-(2.37) can also be used. This is

$$T \equiv \frac{k_2^3}{k_1} \left(\frac{\pi}{k_2\rho}\right)^{1/2} e^{-iP_z} \mathcal{F}(P_z) \rightarrow \frac{k_2^3}{k_1} \left(\frac{\pi}{k_2\rho}\right)^{1/2} \frac{1}{(2\pi P_z)^{1/2}} \left(\frac{1}{2P_z} + i\right), \quad (2.45)$$

when $|P_z| \geq 4$. With $P_z = (R + Z')^2/R$, this becomes

$$T \rightarrow \frac{k_2^4}{2k_1^2} \left[\frac{R}{2(R + Z')^3} + \frac{i}{R + Z'} \right] = \frac{k_1^2}{k_2^2\rho^2 \left(1 + \frac{k_1 z'}{k_2\rho}\right)^3} + \frac{ik_2}{\rho \left(1 + \frac{k_1 z'}{k_2\rho}\right)}. \quad (2.46)$$

In spherical coordinates with $\rho = r_0 \sin \Theta$ and $z' = r_0 \cos \Theta$,

$$T(r_0, \Theta) = \frac{k_2}{k_1} \left[\frac{\sin \Theta}{r_0^2 \left(\frac{k_2}{k_1} \sin \Theta + \cos \Theta \right)^3} + \frac{ik_2}{r_0 \left(\frac{k_2}{k_1} \sin \Theta + \cos \Theta \right)} \right]. \quad (2.47)$$

Also,

$$e^{ik_2(\rho+z'/2\rho)} = e^{ik_2 r_0 \psi(\Theta)}, \quad (2.48)$$

where $\psi(\Theta) = \frac{1}{2}(\sin \Theta + \csc \Theta)$. Note that when $\Theta = \pi/2$,

$$T(r_0, \pi/2) = \frac{k_1^2}{k_2^2 r_0^2} + \frac{ik_2}{r_0}; \quad r_0 = \rho, \quad (2.49)$$

$$\psi(\pi/2) = 1; \quad e^{ik_2 r_0 \psi(\pi/2)} = e^{ik_2 r_0}; \quad r_0 = \rho. \quad (2.50)$$

With these formulas the far-field expressions for the electromagnetic field of a unit vertical dipole on the surface of Region 2 are

$$B_{2\phi}(r_0, \Theta) = -\frac{\mu_0}{2\pi} \left[\frac{ik_2}{r_0} e^{ik_2 r_0} \sin \Theta - T(r_0, \Theta) e^{ik_2 r_0 \psi(\Theta)} \right], \quad (2.51)$$

$$E_{2r}(r_0, \Theta) = -\frac{\omega\mu_0}{2\pi k_2} \left\{ \cos \Theta T(r_0, \Theta) e^{ik_2 r_0 \psi(\Theta)} - \sin \Theta e^{ik_2 r_0 \psi(\Theta)} \frac{k_2}{k_1} \left[\frac{ik_2}{r_0 \sin \Theta} - T(r_0, \Theta) \right] \right\}, \quad (2.52)$$

$$E_{2\Theta}(r_0, \Theta) = -\frac{\omega\mu_0}{2\pi k_2} \left\{ \sin \Theta \left[\frac{ik_2}{r_0} e^{ik_2 r_0} - T(r_0, \Theta) e^{ik_2 r_0 \psi(\Theta)} \right] - \cos \Theta e^{ik_2 r_0 \psi(\Theta)} \frac{k_2}{k_1} \left[\frac{ik_2}{r_0 \sin \Theta} - T(r_0, \Theta) \right] \right\}. \quad (2.53)$$

These expressions give the complete far field of the unit vertical dipole.

Graphs of the magnitude of $E_{2\Theta}(r_0, \Theta)$ for a unit vertical dipole as calculated from (2.37) are shown in Fig. 2 for four different Regions 1. These are (a) salt water with $\sigma_1 = 4$ S/m, $\epsilon_{1r} = 80$; (b) wet earth with $\sigma_1 = 0.4$ S/m, $\epsilon_{1r} = 12$; (c) dry earth with $\sigma_1 = 0.04$ S/m, $\epsilon_{1r} = 8$; and (d) lake water with $\sigma_1 = 0.004$ S/m, $\epsilon_{1r} = 80$. The frequency is $f = 10$ MHz and the radial distance is $r_0 = 500$ km. The oscillations in the field patterns are due to interference between the direct field and that reflected from the imperfectly conducting Region 1. The oscillations decrease in amplitude with increasing σ_1 ; they disappear when Region 1 is a perfect conductor with $\sigma_1 = \infty$. The magnitude of $E_{2\Theta}(r_0, \pi/2)$ is due entirely to the lateral wave. The numerical values of the first maximum and of the field with $\Theta = \pi/2$ are given on the diagrams. The loci of the minima are shown together in Fig. 3. These constitute the effective far-field patterns.

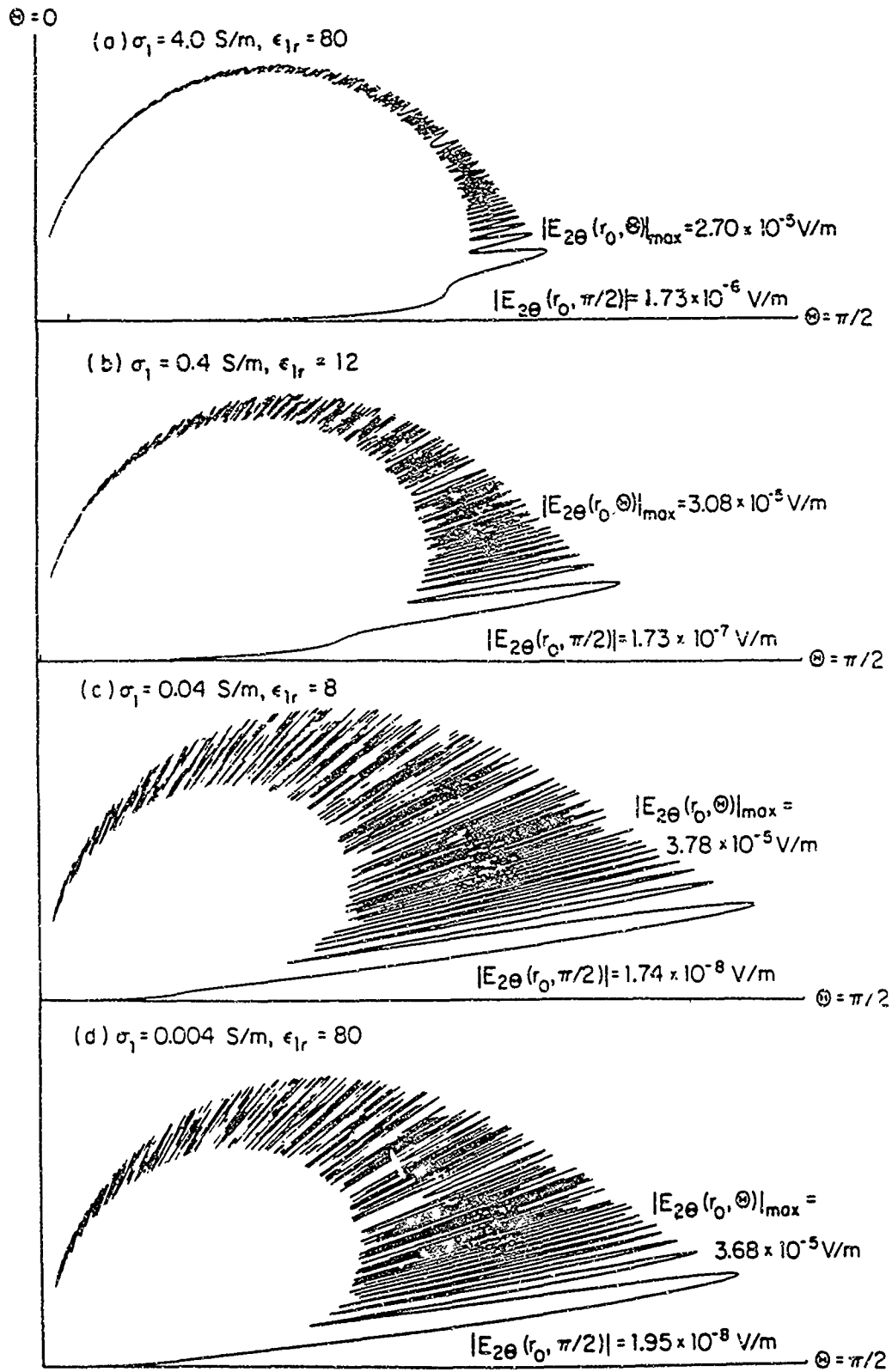


Fig. 2. Field pattern of $|E_{2\theta}(r_0, \Theta)|$ for vertical dipole on boundary between air and (a) sea water, (b) wet earth, (c) dry earth, and (d) lake water. Frequency $f = 10 \text{ MHz}$, radial distance $r_0 = 500 \text{ km}$.

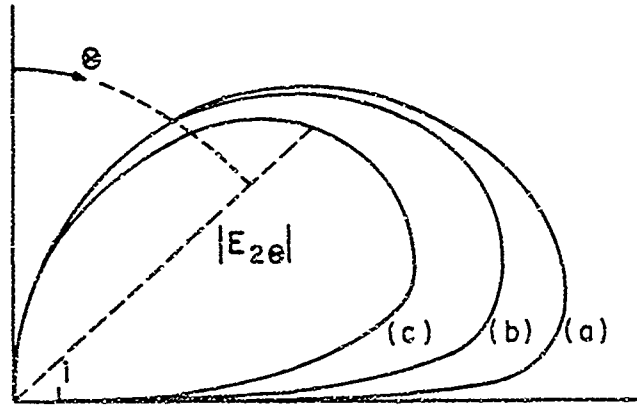


Fig. 3. Far-field pattern of vertical dipole on boundary between air and (a) sea water ($\sigma_1 = 4 \text{ S/m}$, $\epsilon_{1r} = 80$), (b) wet earth ($\sigma_1 = 0.4 \text{ S/m}$, $\epsilon_{1r} = 12$), and (c) dry earth ($\sigma_1 = 0.04 \text{ S/m}$, $\epsilon_{1r} = 8$). (Loci of minima of oscillations in Fig. 2a-c.)

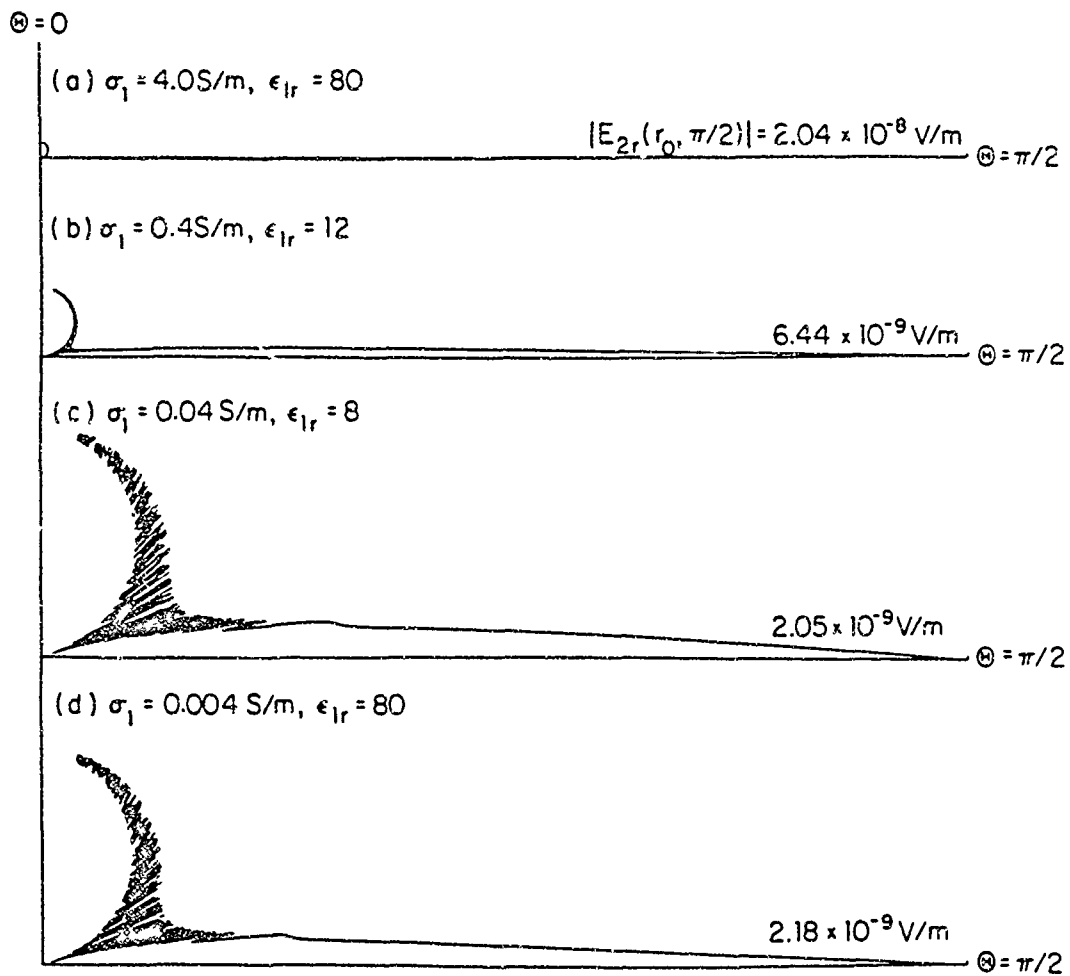


Fig. 4. Field pattern of $|E_{2r}(r_0, \Theta)|$ for vertical dipole on boundary between air and (a) sea water, (b) wet earth, (c) dry earth, and (d) lake water. Frequency $f = 10 \text{ MHz}$, radial distance $r_0 = 500 \text{ km}$.

Graphs of the magnitude of $E_{2r}(r_0, \Theta)$ are shown in Fig. 4 for the same four different Regions 1. The scales for the four regions are adjusted so that the lateral-wave values at $\Theta = \pi/2$ are equal. The actual numerical values are given on the graphs. For convenient comparison, the magnitudes of $E_{2\Theta}(r_0, \Theta)$ maximum, $E_{2\Theta}(r_0, \pi/2)$, and $E_{2r}(r_0, \pi/2)$ are listed in Table 1.

Table 1. Relative Magnitudes of $E_{2\Theta}(r_0, \Theta)$ and $E_{2r}(r_0, \Theta)$

σ_1 S/m	ϵ_{1r}	$E_{2\Theta}(r_0, \Theta)_{\max}$ V/m	$E_{2\Theta}(r_0, \pi/2)$ V/m	$E_{2r}(r_0, \pi/2)$ V/m
4.0	80	2.70×10^{-5}	1.73×10^{-6}	2.04×10^{-8}
0.4	12	3.08×10^{-5}	1.73×10^{-7}	6.44×10^{-9}
0.04	8	3.78×10^{-5}	1.74×10^{-8}	2.05×10^{-9}
0.004	80	3.68×10^{-5}	1.95×10^{-8}	2.18×10^{-9}

3. Communication with Submarines

The field at radial distances ρ and depth z in the ocean (Region 1, $z \geq 0$) due to a vertical dipole in the air on the surface of the earth or sea is of importance in communicating with submerged submarines. For this purpose the radial component of the electric field is most useful. It is given by (2.30) with $z' = d = 0$ multiplied by $\exp(ik_1 z)$, viz.,

$$E_{1\rho}(\rho, z) = -\frac{\omega\mu_0}{2\pi k_1} e^{ik_1 z} e^{ik_2 \rho} f(k_2 \rho, k_1), \quad (3.1)$$

where $f(k_2 \rho, k_1)$ is defined in (2.40). Since the far-field form of the Fresnel integral given by (2.42) applies when $R \geq 4$ and since with it $E_{1\rho}(\rho, z)$ decreases as $1/\rho^2$, it is advantageous to select a frequency for which the desired range of ρ is in the intermediate zone in which the Fresnel-integral term is small and the $1/\rho$ term in $f(k_2 \rho, k_1)$ dominates. This occurs when

$$1 \leq k_2 \rho \leq |k_1^2/k_2^2|. \quad (3.2)$$

The quantity $20 \log_{10} |E_{1\rho}(\rho, z)|$ in this range with $\rho = 5,000$ km is shown in Fig. 5. For each depth in the ocean there is an optimum frequency for a maximum received signal. This decreases as the depth increases. In the frequency range from 20 to 30 kHz—used by the U.S. Navy transmitter at Cutler, Maine—the optimum depth is seen to be in the range from $z = 10$ m to $z = 20$ m. As the depth increases further, the magnitude of the electric field decreases very rapidly. In order to communicate with submarines at greater depths, lower frequencies must be used. This is not practical using vertical dipoles.

4. Vertical Dipole in the Sea; Conductivity of the Earth's Crust

An interesting application of the vertical dipole near a boundary and the lateral waves it generates is to the measurement of the conductivity of the oceanic crust (Region 2, $z \leq 0$). For this purpose the dipole is located in the sea (Region 1, $z \geq 0$) at a small height d above the sea floor or it is extended from this all the way to the surface of the sea [9]. Measurements are made on or at a small height z above the sea floor. The preferred quantity to be measured

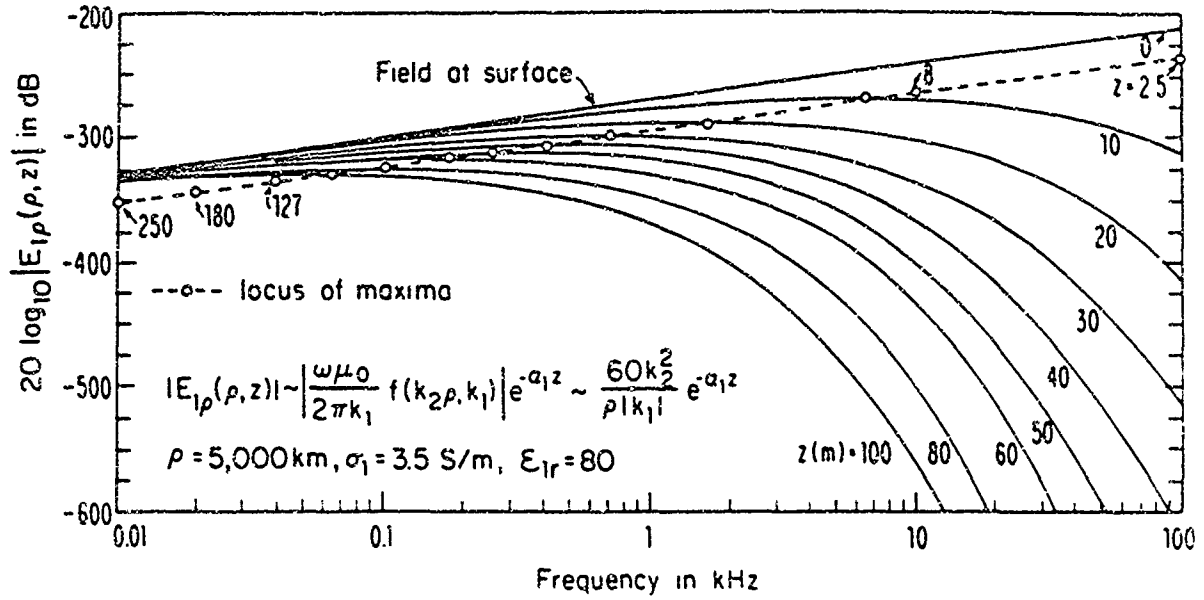


Fig. 5. Radial electric field at depth z and $\rho = 5,000$ km due to vertical electric dipole in air on surface of sea water as function of frequency with z as parameter.

is the magnetic field at very low frequencies. This is given by an integral similar to (2.1). It has the following integrated form:

$$B_{1\phi}(\rho, z) = B_{1\phi}^d(\rho, z) + B_{1\phi}^i(\rho, z) + B_{1\phi}^L(\rho, z), \quad (4.1)$$

with

$$B_{1\phi}^d(\rho, z) = -\frac{\mu_0}{4\pi} e^{ik_1 r_1} \left(\frac{ik_1}{r_1} - \frac{1}{r_1^2} \right) \left(\frac{\rho}{r_1} \right), \quad (4.2)$$

$$B_{1\phi}^i(\rho, z) = \frac{\mu_0}{4\pi} e^{ik_1 r_2} \left(\frac{ik_1}{r_2} - \frac{1}{r_2^2} \right) \left(\frac{\rho}{r_2} \right), \quad (4.3)$$

$$B_{1\phi}^L(\rho, z) = -\frac{\mu_0 k_2^2}{2\pi k_1^2} e^{ik_1(z+d)} e^{ik_2 \rho} f(k_2 \rho, k_1), \quad (4.4)$$

where $r_1 = [\rho^2 + (z-d)^2]^{1/2}$, $r_2 = [\rho^2 + (z+d)^2]^{1/2}$, and $f(k_2 \rho, k_1)$ is defined in (2.40). The direct field of the dipole is given by (4.2), the field of the image dipole is given by (4.3), and the lateral wave by (4.4). Note that when the source dipole is in the denser Region 1 and the point of observation is on the boundary surface $z = 0$, the image field is the negative of the direct field, so that the lateral-wave field $B_{1\phi}^L(\rho, 0)$ is the entire field.

In practice, measurements are made at extremely low frequencies and within relatively small radial distances where the Fresnel-integral term is negligibly small and the significant magnetic field is

$$B_{1\phi}(\rho, 0) = B_{1\phi}^L(\rho, 0) \sim -\frac{\mu_0 \sigma_2}{2\pi \sigma_1} \left(\frac{ik_2}{\rho} - \frac{1}{\rho^2} \right) e^{ik_2 \rho} e^{ik_1 d}. \quad (4.5)$$

The application of this formula [10] to actual measurements made on the sea floor [9] is illustrated in Fig. 6. The dipole extended from the surface to the floor of the sea—a distance of 640 m. The sea floor consisted of a layer of sediment 600 m thick over rock. The conductivity of the sea water was known to be 2.85 S/m; the conductivities of the sediment, $\sigma_2 = 0.4$ S/m, and the rock, $\sigma_3 = 0.01$ S/m, were determined by fitting the theory to the measured points.

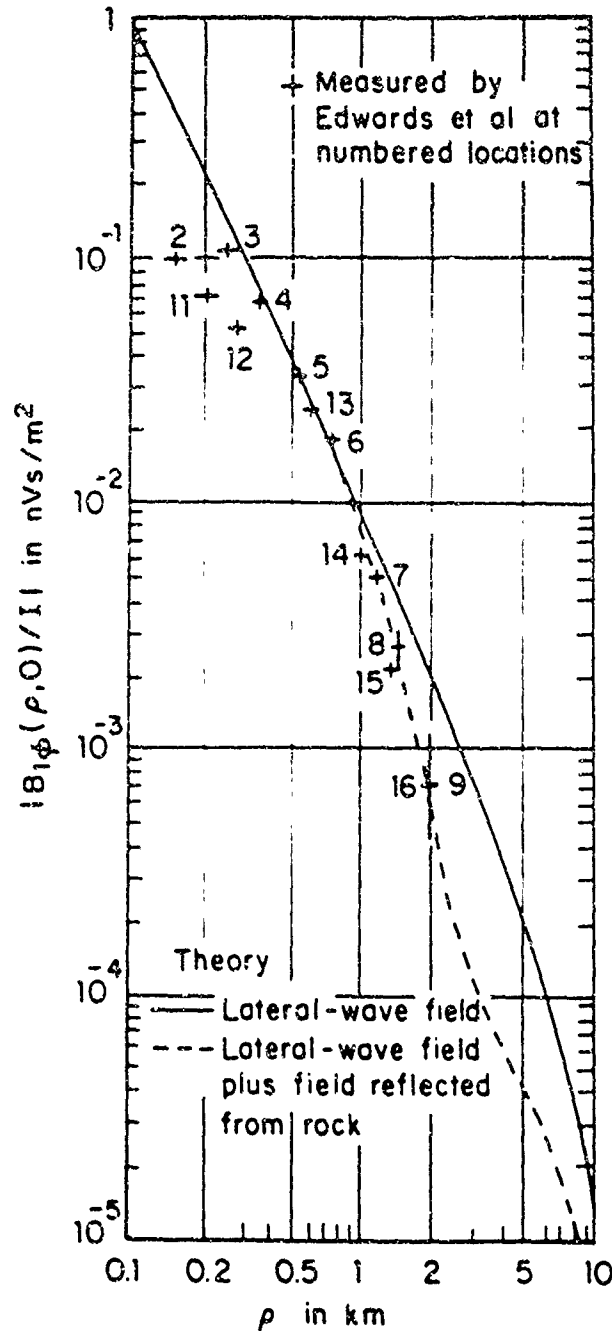


Fig. 6. Magnetic field measured by Edwards et al. [9] and field calculated from lateral-wave formula [10]; dashed curve includes correction for reflection from rock layer below. $f = 0.125$ Hz; $\sigma_1 = 2.85$ S/m, $\sigma_2 = 0.4$ S/m, $\sigma_3 = 0.01$ S/m; $D_1 = 640$ m, $D_2 = 600$ m.

5. Lateral Electromagnetic Pulses—Delta Function

The theory and applications described up to this point apply to the electromagnetic field generated by a vertical electric dipole near or on the air-earth boundary when excited by a periodic oscillation of current at any single frequency. Specifically, $I(t)h_e = \text{Re } I(0)h_e e^{-i\omega t}$ with $I(0)h_e = 1 \text{ Am}$. It is of interest and of practical importance to examine the electromagnetic field especially along the air-earth boundary under transient instead of continuous-wave conditions. This is conveniently carried out by exciting the dipole with a single current pulse. Useful and analytically tractable pulses are the delta-function and the Gaussian defined with $I(t)h_e = I(0)h_e f(t)$, $I(0)h_e = 1 \text{ Am}$ where, for the delta-function,

$$f(t) = \delta(t) = \frac{1}{2\pi} \int_{-\infty}^{\infty} e^{-i\omega t} d\omega, \quad (5.1)$$

and, for the Gaussian normalized to reduce to the delta-function when its width $2t_1 \rightarrow 0$,

$$f(t) = e^{-t^2/t_1^2}/t_1\sqrt{\pi}. \quad (5.2)$$

The Fourier transforms of the two functions are

$$\tilde{f}(\omega) = \int_{-\infty}^{\infty} \delta(t) e^{-i\omega t} dt = 1; \quad \tilde{f}(\omega) = \int_{-\infty}^{\infty} \frac{e^{-t^2/t_1^2} e^{-i\omega t}}{t_1\sqrt{\pi}} dt = e^{-\omega^2 t_1^2/4}. \quad (5.3)$$

The spectrum of the delta function includes all frequencies to the very highest, the spectrum of the Gaussian cuts off frequencies above $\omega \sim 2/t_1$.

The essential characteristics of the field along the boundary $z = 0$ are studied here with the vertical dipole source on the boundary in the earth and only for those parts of the earth's surface which are good dielectrics, e.g., lake water and dry rock. With $\sigma_1 \sim 0$, $k_1 = \omega(\mu_0\epsilon_1)^{1/2} = \epsilon_1^{1/2}\omega/c$. Let the relative permittivity of the earth be $\epsilon_{1r} = \epsilon$. Under these conditions the frequency-dependent components of the field are:

$$B_{2\phi}(\rho', \omega) = -\frac{\mu_0}{2\pi\epsilon z^2} e^{i\omega\rho'} f(\rho'), \quad (5.4)$$

$$E_{2\rho}(\rho', \omega) = -\frac{\mu_0}{2\pi\epsilon^{3/2}z} \left[e^{i\omega\rho'} f(\rho') - \frac{i e^{i\omega\epsilon^{1/2}\rho'}}{\rho'^2} \right], \quad (5.5)$$

$$E_{2z}(\rho', \omega) = \frac{\mu_0}{2\pi\epsilon c} e^{i\omega\rho'} \left[f(\rho') - \frac{i}{\omega\rho'^3} \right], \quad (5.6)$$

where $\rho' = \rho/c$ and

$$f(\rho') = \frac{i\omega}{\rho'} - \frac{1}{\rho'^2} - \omega^{3/2} \left(\frac{\pi}{\epsilon\rho'} \right)^{1/2} e^{-ip} \mathcal{F}(p), \quad (5.7)$$

with

$$\mathcal{F}(p) = \frac{1}{2}(1+i) - \int_0^p \frac{e^{it}}{\sqrt{2\pi t}} dt = \int_p^\infty \frac{e^{it}}{\sqrt{2\pi t}} dt; \quad p = \omega\rho'/2\epsilon. \quad (5.8)$$

The real time-dependent field with delta-function excitation is

$$E_{2z}(\rho', t) = \frac{1}{\pi} \operatorname{Re} \int_0^\infty e^{-i\omega t} E_{2z}(\rho', \omega) d\omega. \quad (5.9)$$

The expressions for $B_{2\phi}(\rho', \omega)$ and $E_{2\rho}(\rho', \omega)$ are similar. With (5.6), this becomes

$$E_{2z}(\rho', t) = \frac{\mu_0}{2\pi\epsilon c} \left[\frac{I_1}{\rho'} - \frac{I_2}{\rho'^2} - \frac{I_3}{\rho'^3} + \frac{I_4}{\sqrt{\pi\epsilon\rho'}} \right]. \quad (5.10)$$

The four integrals with their integrated values are:

$$I_1 = \operatorname{Re} \frac{1}{\pi} \int_0^\infty i\omega e^{-i\omega(t-\rho')} d\omega = -\delta'(t-\rho'), \quad (5.11)$$

$$I_2 = \operatorname{Re} \frac{1}{\pi} \int_0^\infty e^{-i\omega(t-\rho')} d\omega = \delta(t-\rho'), \quad (5.12)$$

$$I_3 = \operatorname{Re} \frac{1}{\pi} \int_0^\infty \frac{i}{\omega} e^{-i\omega(t-\rho')} d\omega = U(t-\rho'), \quad (5.13)$$

$$I_4 = -\operatorname{Re} \int_0^\infty \omega^{3/2} e^{-i\omega(t-\rho'+\rho'/2\epsilon)} \left[\frac{1}{2}(1+i) - \int_0^{\omega\rho'/2\epsilon} \frac{e^{i\tau}}{\sqrt{2\pi\tau}} d\tau \right] d\omega, \quad (5.14)$$

$$\frac{I_4}{\sqrt{\pi\epsilon\rho'}} = \frac{\delta'(t-\rho')}{\rho'} - \frac{\epsilon\delta(t-\rho')}{\rho'^2} + \frac{3}{4} \frac{1}{\sqrt{2\epsilon\rho'}} (t-\rho'+\rho'/2\epsilon)^{-5/2} U(t-\rho'). \quad (5.15)$$

In (5.13)–(5.15), $U(x) = 0$ for $x < 0$; $U(x) = 1$ for $x > 0$ is the Heaviside or step function. When (5.11)–(5.15) are substituted in (5.10) with $\rho' = \rho/c$, the result is

$$E_{2z}(\rho, t) = -\frac{\epsilon+1}{2\pi\epsilon_0\epsilon c\rho^2} \delta(t-\rho/c) - \frac{1}{2\pi\epsilon_0\epsilon\rho^3} \left\{ \begin{array}{ll} 0; & t < \rho/c \\ 1 - 3\epsilon^2 \left[2\epsilon \left(\frac{ct}{\rho} - 1 \right) + 1 \right]^{-5/2}; & t > \rho/c \end{array} \right\}. \quad (5.16)$$

(The corresponding formula for the Hertz potential was obtained by van der Pol [11].) The associated expressions for the other components are:

$$B_{2\phi}(\rho, t) = \frac{\mu_0(\epsilon+1)}{2\pi\epsilon\rho^2} \delta(t-\rho/c) - \frac{\mu_0 c}{2\pi\rho^3} \left\{ \begin{array}{ll} 0; & t < \rho/c \\ 3\epsilon \left[2\epsilon \left(\frac{ct}{\rho} - 1 \right) + 1 \right]^{-5/2}; & t > \rho/c \end{array} \right\}, \quad (5.17)$$

$$E_{2\rho}(\rho, t) = \frac{c}{\sqrt{\epsilon}} B_{2\phi}(\rho, t). \quad (5.18)$$

(Note that the second exponential term in (5.5) contributes nothing to $E_{2\rho}(\rho, t)$ because the real part of the associated integral is zero.) It is interesting to note that the Fresnel-integral term in I_4 contributes the term $\delta'(t-\rho')/\rho'$, which exactly cancels the I_1 term, and the term $\epsilon\delta(t-\rho')/\rho'^2$ which combines with the I_2 term. This corresponds exactly to the

steady-state behavior in the far field where the Fresnel-integral term cancels the $1/\rho$ term and adds the dominant part of the $1/\rho^2$ term—which thus becomes the far field. Evidently, the high-frequency content of the delta-function spectrum dominates so that the field at all distances has the properties of the far field.

Since the expressions (5.16)–(5.18) are Fourier transforms of approximate steady-state formulas which are derived subject to the inequalities (1.1), they are necessarily also approximate. Fortunately, (5.16) and (5.17) can be compared with exact expressions obtained from the Fourier transforms of the integrals [12]. This shows that the omission of terms smaller than $k_2^2/k_1^2 = \epsilon^{-1}$ is responsible for the nonappearance in (5.16) and (5.17) of a second delta-function term, $\delta(t - \rho\epsilon^{1/2}/c)$, which has an amplitude factor that is significantly smaller even than ϵ^{-1} times the amplitude factor of $\delta(t - \rho/c)$. Except for a delta function with its infinite amplitude, the omission of a second very much smaller pulse that arrives at $t = \rho\epsilon^{1/2}/c$ would usually be of negligible importance. The exact solution also shows that the condition $\rho/c < t$, which appears in (5.16) and (5.17), should be $\rho/c < t < \rho\epsilon^{1/2}/c$ and that, for $\rho\epsilon^{1/2}/c < t$, $E_{2x}(\rho, t) = -1/2\pi\epsilon_0\epsilon\rho^3$ and $B_{2\phi}(\rho, t) = 0$ —the static values due to the charges left on the ends of the dipole by the current pulse.

6. Lateral Electromagnetic Pulses—Gaussian Function

When a Gaussian pulse (Fig. 7) excites the vertical dipole, $E_{2x}(\rho', t)$ is again given by (5.10) but the four integrals now have the forms:

$$I_1 = \text{Re} \frac{1}{2\pi} \int_{-\infty}^{\infty} i\omega e^{-\omega^2 t_1^2/4} e^{-i\omega(t-\rho')} d\omega = \frac{2\tau'}{\pi^{1/2} t_1^2} e^{-\tau'^2}, \quad (6.1)$$

$$I_2 = \text{Re} \frac{1}{2\pi} \int_{-\infty}^{\infty} e^{-\omega^2 t_1^2/4} e^{-i\omega(t-\rho')} d\omega = \frac{1}{\pi^{1/2} t_1} e^{-\tau'^2}, \quad (6.2)$$

$$I_3 = \text{Re} \frac{1}{2\pi} \int_{-\infty}^{\infty} \frac{i}{\omega} e^{-\omega^2 t_1^2/4} e^{-i\omega(t-\rho')} d\omega = \frac{1}{2} (1 + \text{erf } \tau'), \quad (6.3)$$

$$I_4 = -\text{Re} \frac{1}{2} \int_{-\infty}^{\infty} \omega^{3/2} e^{-\omega^2 t_1^2/4} e^{-i\omega(t-\rho'+\rho'/2\epsilon)} \left[\frac{1}{2}(1+i) - \int_0^{\omega\rho'/2\epsilon} \frac{e^{i\tau}}{\sqrt{2\pi\tau}} d\tau \right] d\omega, \quad (6.4)$$

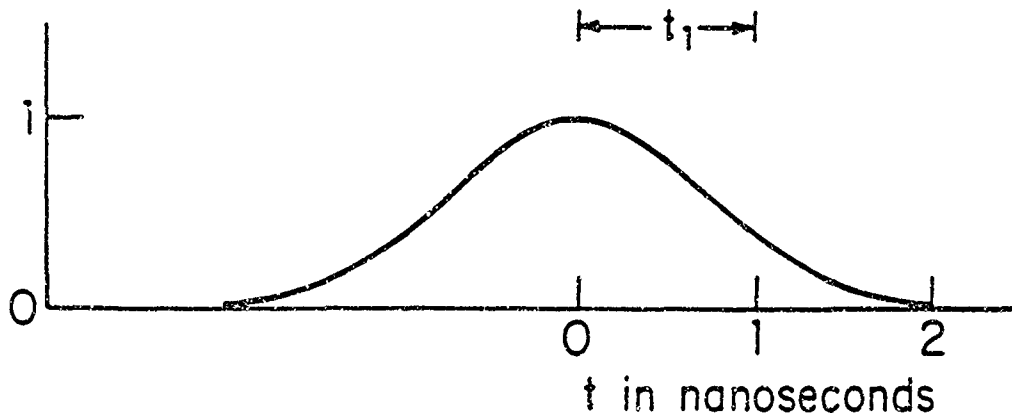


Fig. 7. Gaussian pulse with unit amplitude and half-width $t_1 = 1$ nanosecond.

where $\tau' = (t - \rho')/t_1$. With the parabolic cylinder functions $V(0, x)$, $V(-1, x)$ and $U(0, x)$, $U(-1, x)$ in Abramowitz and Stegun [13], the following approximate result for I_4 is obtained [14]:

$$\frac{I_4}{\sqrt{\pi\epsilon\rho'}} \sim -\frac{e^{-T^2/2t_1^2}}{\sqrt{\pi\epsilon\rho'}t_1^{5/2}} \left\{ \begin{array}{ll} 1.87 V\left(0, \frac{\sqrt{2}T}{t_1}\right) - 2.64 \frac{T}{t_1} V\left(-1, \frac{\sqrt{2}T}{t_1}\right); & \frac{T}{t_1} \geq 0 \\ 1.05 U\left(0, \frac{-\sqrt{2}T}{t_1}\right) + 2.90 \frac{T}{t_1} U\left(-1, \frac{-\sqrt{2}T}{t_1}\right); & \frac{T}{t_1} \leq 0 \end{array} \right\}, \quad (6.5)$$

where $T \equiv t - \rho' + \rho'/2\epsilon$. With these four integrals and the introduction of the dimensionless parameters $T' = T/t_1$ and $\rho_1 \equiv \rho'/t_1 = \rho/ct_1$,

$$E_{2z}(\rho, t) = -\frac{1}{2\pi\epsilon_0\epsilon} \frac{\pi^{-1/2}}{c^3 t_1^3} \left\{ \left[-\frac{2\tau'}{\rho_1} + \frac{1}{\rho_1^2} \right] e^{-\tau'^2} + \frac{\pi^{1/2}}{2\rho_1^3} (\text{erf } \tau' + 1) \right. \\ \left. + \frac{e^{-T'^2/2}}{\sqrt{\epsilon\rho_1}} \left[\begin{array}{ll} 1.87 V(0, \sqrt{2}T') - 2.64T' V(-1, \sqrt{2}T'); & T' \geq 0 \\ 1.05 U(0, -\sqrt{2}T') + 2.90T' U(-1, -\sqrt{2}T'); & T' \leq 0 \end{array} \right] \right\}. \quad (6.6)$$

The associated time-dependent formulas for the other two components of the field are:

$$B_{2\phi}(\rho, t) = \frac{\mu_0}{2\pi\epsilon c} \frac{\pi^{-1/2}}{c^3 t_1^3} \left\{ \left[-\frac{2\tau'}{\rho_1} + \frac{1}{\rho_1^2} \right] e^{-\tau'^2} \right. \\ \left. + \frac{e^{-T'^2/2}}{\sqrt{\epsilon\rho_1}} \left[\begin{array}{ll} 1.87 V(0, \sqrt{2}T') - 2.64T' V(-1, \sqrt{2}T'); & T' \geq 0 \\ 1.05 U(0, -\sqrt{2}T') + 2.90T' U(-1, -\sqrt{2}T'); & T' \leq 0 \end{array} \right] \right\}, \quad (6.7)$$

$$E_{2\rho}(\rho, t) = \frac{c}{\sqrt{\epsilon}} B_{2\phi}(\rho, t). \quad (6.8)$$

A graphical representation of the expression in braces in (6.6) is shown in Fig. 8 when the exciting Gaussian pulse has a half-width $t_1 = 1$ nanosecond and $\epsilon = 80$. Note that $ct_1 = 0.3$ m, so that the actual radial distance is $\rho = \rho_1 ct_1 = 0.3\rho_1$. The several curves in Fig. 8 show the vertical electric field as a function of the time at five radial distances ranging from $\rho = 0.45$ m to $\rho = 1.5$ m. Similar graphs with a different amplitude scale are in Fig. 9 at $\rho = 4.8$ m and $\rho = 7.5$ m. The shape of the pulse at any given radial distance ρ is determined by the relative contributions by the four terms in (6.6) with their very different dependences on both the radial distance and the time.

The third term represents the rapid increase in the vertical electric field as the pulse passes to leave the final electrostatic field of the charged infinitesimal dipole. This field decreases rapidly as $1/\rho^3$ with distance. The second term is a true Gaussian pulse like that in Fig. 7. It travels with the velocity of light and its amplitude decreases with distance as $1/\rho^2$. The first term, the derivative of the Gaussian pulse, travels with the Gaussian. It decreases as

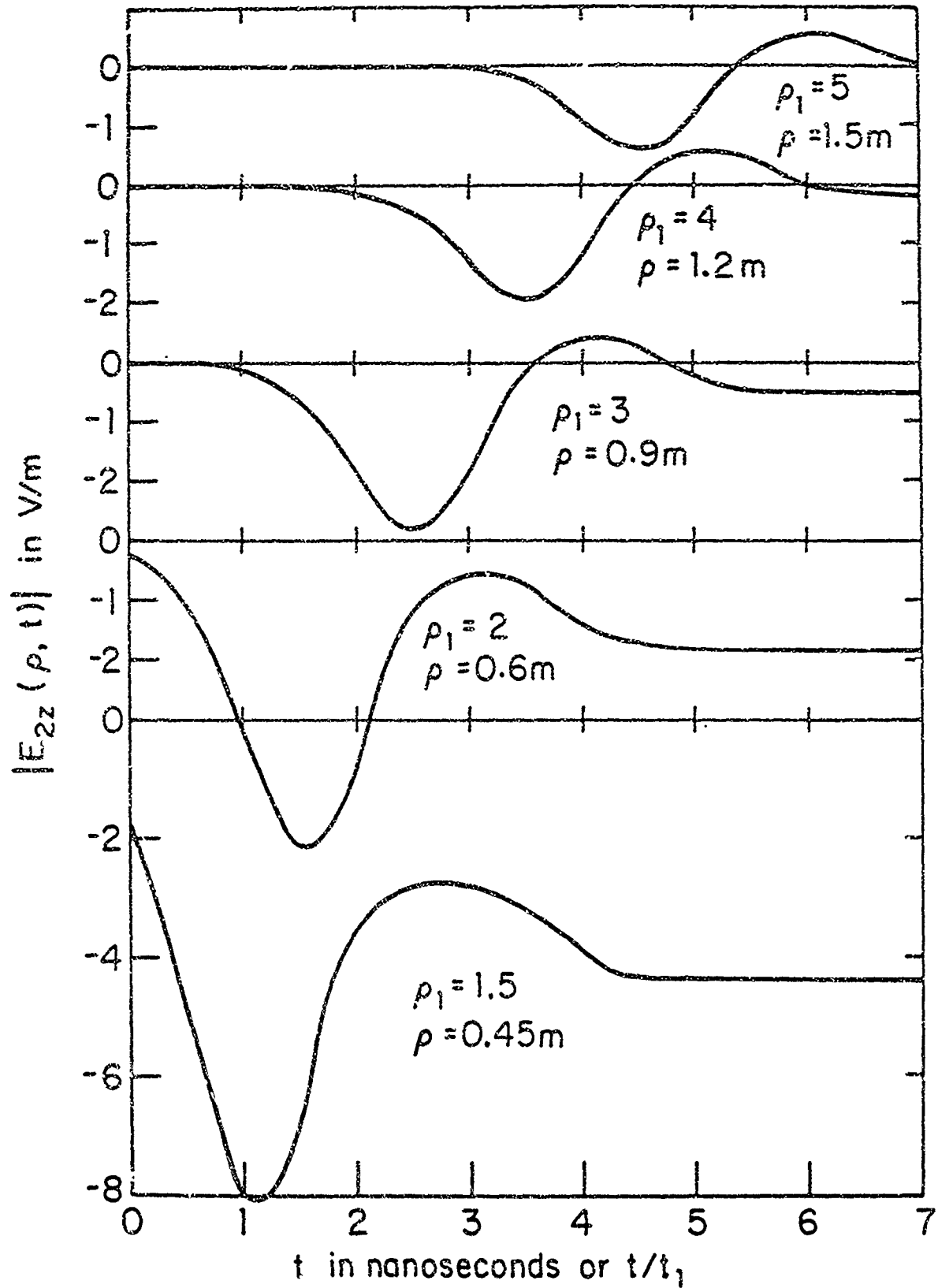


Fig. 8. Vertical electric field on the boundary in air due to a vertical electric dipole on the boundary in a perfect dielectric with relative permittivity $\epsilon = 80$. The dipole is excited by a unit Gaussian pulse with $t_1 = 1$ nanosecond.

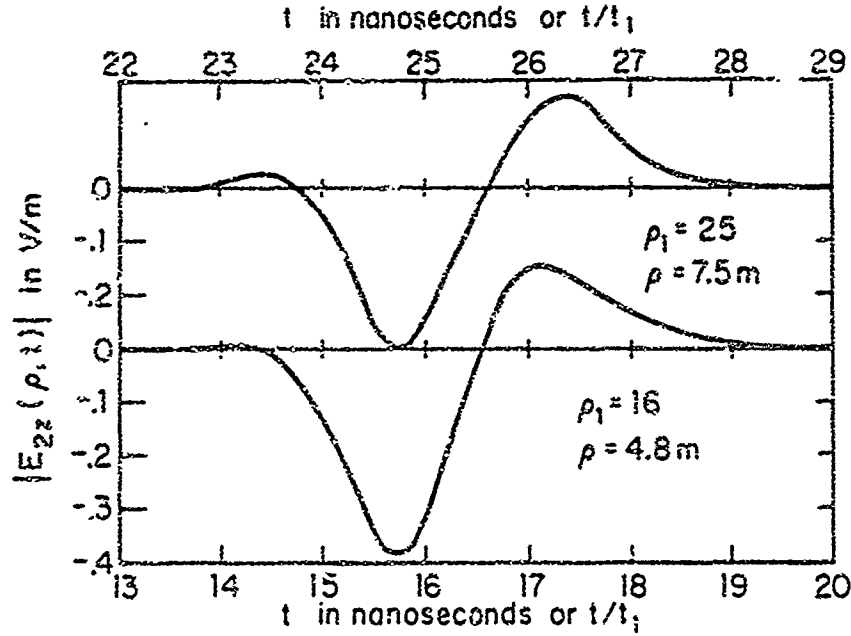


Fig. 9. Like Fig. 8 but for larger values of radial distance ρ .

$1/\rho$ so that it persists for much greater distances than the $1/\rho^2$ term. Unlike the field with the delta-function pulse or the steady-state field, the fourth term due to the Fresnel integral does not completely cancel the $1/\rho$ term. Its behavior is similar to a negative derivative of the Gaussian pulse. It cancels only a part of the first integral. The amplitudes of the first and fourth terms are approximately equal when $\rho \sim 4.8$ m; the fourth term dominates when ρ is as large as 7.5 m, as shown in Fig. 9.

Just as for the delta-function pulse, it is to be expected that the omission of terms smaller than $k_2^2/k_1^2 = \epsilon^{-1}$ in the steady-state formulas has caused the nonappearance of a second Gaussian pulse at time $t = \rho\epsilon^{1/2}/c$ which has a very small amplitude factor compared to the pulse at $t = \rho/c$ and is, therefore, generally unimportant. It may also be presumed that the transient terms for $T' \geq 0$ are in some manner limited by

$$\rho_1/2\epsilon < T' < \rho_1[\epsilon^{1/2} - 1 + (2\epsilon)^{-1}],$$

so that, as $r' = (t - \rho')/t_1 \rightarrow \infty$ and with $\rho_1 \equiv \rho/ct_1$ and $\text{erf } \infty = 1$,

$$E_{2x}(\rho, t) \rightarrow -\frac{1}{2\pi\epsilon_0\epsilon} \frac{1}{c^3 t_1^3} \frac{1}{2\rho_1^3} (\text{erf } r' + 1) \rightarrow -\frac{1}{2\pi\epsilon_0\epsilon\rho^3}; \quad B_{2\phi}(\rho, t) \rightarrow 0,$$

which is the static field maintained by the charges left at the ends of the dipole by the current pulse. Because the Gaussian pulse has no sharp cutoff, the accurate formulation must await the evaluation of exact time-dependent formulas for the Gaussian pulse corresponding to those determined for the delta-function pulse [12]. Note, however, that the ranges shown in Figs. 8 and 9 are for times before the possible arrival of the second pulse at $t = \rho\epsilon^{1/2}/c$.

Since with the Gaussian pulse the $1/\rho$ term is not completely cancelled by the Fresnel-integral term (as it is with the delta-function pulse and in the far field for the steady

state), it may be presumed that the Gaussian pulse decreases more slowly in amplitude with increasing radial distances than the steady-state field. The degree of cancellation of the $1/\rho$ term must increase as the pulse width $2t_1$ is made smaller, decrease as it is made larger. That is, the greater the low-frequency content of the Gaussian pulse, the slower is its decrease in amplitude at large radial distances.

7. Conclusion

Beginning with the predictions of Maxwell's theory, Hertz demonstrated many of the properties of electromagnetic waves in free space. These were then applied by Marconi to practical wireless communication. In the same spirit this paper begins with formulas derived from Maxwell's equations, determines many of the properties of lateral electromagnetic waves and pulses, and makes specific applications to subsurface communication and geophysical exploration. As with the pioneer work of Hertz, it leaves many questions unanswered as continuing challenges for new and imaginative research.

Acknowledgment. The author is indebted to Tai T. Wu for his many contributions and suggestions, to M. Owens for her help in correcting the manuscript and preparing it for publication, and to B. H. Sandler for carrying out many of the numerical calculations. This research was supported in part by the Joint Services Electronics Program under Contract N00014-84-K-0465 with Harvard University.

References

- [1] A. Sommerfeld, Ann. Physik 28, 665 (1909).
- [2] A. Sommerfeld, Ann. Physik 81, 1135 (1926).
- [3] A. Sommerfeld, Chapter 23 in Die Differential u. Integralgleichungen der Mechanik u. Physik, vol. II, P. Frank and R. v. Mises, eds., F. Vieweg and Son, Braunschweig (1935).
- [4] K. A. Norton, Proc. IRE 24, 1367 (1936).
- [5] K. A. Norton, Proc. IRE 29, 623 (1941).
- [6] A. Baños, Jr., Dipole Radiation in the Presence of a Conducting Half-Space, Pergamon Press, Oxford, England (1966).
- [7] J. R. Wait and L. L. Campbell, J. Geophys. Res. 58, 21 (1953).
- [8] R. W. P. King, J. Appl. Phys. 53, 8476 (1982); Erratum 56, 3366 (1984).
- [9] R. N. Edwards, L. K. Law, P. A. Wolfgram, D. C. Nobes, M. N. Bone, D. F. Triggs, and J. M. DeLaurier, Geophys. 50, 153 (1985).
- [10] R. W. P. King, IEEE Trans. Geosci. & Remote Sens. GE-24, 813 (1986).
- [11] B. van der Pol, IRE Trans. Ant. & Prop. AP-4, 288 (1956).
- [12] T. T. Wu and R. W. P. King, J. Appl. Phys., accepted for publication (1987).
- [13] M. Abramowitz and I. A. Stegun, eds., Handbook of Mathematical Functions, Dover Publications, New York (1972).
- [14] R. W. P. King, J. Electrom. Waves & Applications, invited paper, submitted for publication (1987).

LATERAL ELECTROMAGNETIC PULSES GENERATED BY A VERTICAL DIPOLE
ON A PLANE BOUNDARY BETWEEN DIELECTRICS

Ronold W. P. King
Gordon McKay Laboratory
Harvard University
Cambridge, MA 02138

Running Head: Lateral Electromagnetic Pulses

Address Correspondence to: Ronold W. P. King
Gordon McKay Laboratory
Harvard University
Cambridge, MA 02138

ABSTRACT

Approximate, quite simple formulas are derived for the transient field generated by a vertical electric dipole on the boundary between two dielectric half-spaces when the permittivity of one of these is much greater than that of the other. The three components of the field are determined for both delta-function and Gaussian-pulse excitation. The field of the former is compared with the corresponding exact expressions with generally good agreement and some interesting, readily explained differences.

Keywords: Vertical electric dipole, Dielectric half-spaces, Transient excitation,
Delta-function pulse, Gaussian pulse, Approximate formulas,
Electromagnetic field.

1. Introduction

Lateral electromagnetic waves generated by a vertical electric dipole near the plane boundary between two electrically different media like air and earth have been the subject of investigation for many years beginning with the work of Sommerfeld. This is summarized in a new approach which provides quite accurate approximate formulas in simple form.¹ The related subject of lateral electromagnetic pulses has been summarized and treated rigorously by Wu and King² for delta-function excitation when the two half-spaces are perfect dielectrics and both the dipole and the point of observation are on the boundary. In this paper the investigation of lateral pulses is extended to Gaussian pulse excitation.

The steady-state properties of lateral electromagnetic waves that travel along the boundary between electrically different half-spaces when generated by a vertical electric dipole have been determined in quite simple and accurate form.¹ The two half-spaces are Region 1 ($z > 0$, wave number $k_1 = \beta_1 + i\alpha_1 = \omega[\mu_0(\epsilon_1 + i\sigma_1/\omega)]^{1/2}$) and Region 2 ($z < 0$, wave number $k_2 = \beta_2 + i\alpha_2 = \omega[\mu_0(\epsilon_2 + i\sigma_2/\omega)]^{1/2}$). When the inequalities

$$|k_1|^2 \geq 9|k_2|^2; \quad |k_1\rho| \geq 3|k_2\rho| \geq 3, \quad (1)$$

are satisfied, the exact integral representations of the field on the boundary, $z = 0$, are well approximated by the following formulas. The unit vertical electric dipole is on the boundary in Region 1, as shown in Fig. 1 when $d = 0$. The unit electric dipole moment is $I(0)h_e = 1$ Am, where $I(0)$ is the current at the center of the dipole and h_e is its effective length.

$$\tilde{B}_{1\phi}(\rho, 0) = \tilde{B}_{2\phi}(\rho, 0) = \frac{i\mu_0 k_2^2}{2\pi} \int_0^\infty N^{-1} J_1(\lambda\rho) \lambda^2 d\lambda, \quad (2a)$$

$$\sim -\frac{\mu_0 k_2^2}{2\pi k_1^2} f(k_2\rho, k_1) e^{ik_2\rho}, \quad (2b)$$

$$\tilde{E}_{1\rho}(\rho, 0) = \tilde{E}_{2\rho}(\rho, 0) = -\frac{i\omega\mu_0}{2\pi} \int_0^\infty \gamma_2 N^{-1} J_1(\lambda\rho) \lambda^2 d\lambda, \quad (3a)$$

$$\sim -\frac{\omega\mu_0 k_2^2}{2\pi k_1^3} \left[f(k_2\rho, k_1) e^{ik_2\rho} - \frac{ie^{ik_1\rho}}{\rho^2} \right], \quad (3b)$$

$$\frac{k_1^2}{k_2^2} \tilde{E}_{1z}(\rho, 0) = \tilde{E}_{2z}(\rho, 0) = -\frac{\omega\mu_0}{2\pi} \int_0^\infty N^{-1} J_0(\lambda\rho) \lambda^3 d\lambda, \quad (4a)$$

$$\sim \frac{\omega\mu_0 k_2}{2\pi k_1^2} g(k_2\rho, k_1) e^{ik_2\rho}, \quad (4b)$$

where

$$N = k_1^2 \gamma_2 + k_2^2 \gamma_1; \quad \gamma_j = (k_j^2 - \lambda^2)^{1/2}, \quad j = 1, 2, \quad (5)$$

and

$$g(k_2\rho, k_1) = f(k_2\rho, k_1) - \frac{i}{k_2\rho^3} = \frac{ik_2}{\rho} - \frac{1}{\rho^2} - \frac{i}{k_2\rho^3} - \frac{k_2^3}{k_1} \left(\frac{\pi}{k_2\rho} \right)^{1/2} e^{-ip} \mathcal{F}(p). \quad (6)$$

Here

$$p = k_2^3\rho/2k_1^2; \quad \mathcal{F}(p) = \frac{1}{2}(1+i) - \int_0^p \frac{e^{it}}{\sqrt{2\pi t}} dt. \quad (7)$$

At values of the argument that satisfy the inequality

$$|p| \geq 4 \quad \text{or} \quad |k_2\rho| \geq 8|k_1^2/k_2^2|, \quad (8)$$

the Fresnel integral $\mathcal{F}(p)$ effectively cancels both the exponential factor and the square root preceding it in (6) and the remaining expression includes the term $-ik_2/\rho$ which exactly cancels the term ik_2/ρ in (6). The result is

$$f(k_2\rho, k_1) \sim g(k_2\rho, k_1) \sim -\frac{1}{\rho^2} \left(\frac{k_1^2}{k_2^2} + 1 \right) \sim -\frac{k_1^2}{k_2^2\rho^2}. \quad (9)$$

In the steady state, the far field decreases along the boundary as $1/\rho^2$ instead of as $1/r$ as in directions away from the boundary or in free space.

When the unit dipole is moved across the boundary from $d = 0$ in Region 1 to $d = 0$ in Region 2, the field is given by (2a,b) through (4a,b) multiplied by k_1^2/k_2^2 .

When the two regions are dielectrics with negligible conductivity (e.g., air and lake water, or air and dry rock), $\sigma_1 \sim \sigma_2 \sim 0$ so that

$$k_j = \omega(\mu_0\epsilon_j)^{1/2} = (\omega/c)\epsilon_{jr}^{1/2}, \quad j = 1, 2. \quad (10)$$

Without loss in generality, let $\epsilon_{2r} = 1$, $\epsilon_{1r} = \epsilon$, so that

$$k_1 = k_2 \epsilon^{1/2}; \quad k_2 = \omega/c, \quad (11)$$

where $c = (\mu_0 \epsilon_0)^{-1/2} = 3 \times 10^8$ m/sec.

With $\rho' = \rho/c$ and $\lambda' = \lambda c$, (2a), (3a) and (4a) become:

$$\tilde{E}_{2\phi}(\rho', 0) = \frac{i\mu_0 \omega^2}{2\pi c^2} \int_0^\infty \frac{J_1(\lambda' \rho') \lambda'^2 d\lambda'}{\omega^2 \epsilon (\omega^2 - \lambda'^2)^{1/2} + \omega^2 (\omega^2 \epsilon - \lambda'^2)^{1/2}}, \quad (12)$$

$$\tilde{E}_{2\rho}(\rho', 0) = -\frac{i\omega \mu_0}{2\pi c} \int_0^\infty \frac{(\omega^2 - \lambda'^2)^{1/2} J_1(\lambda' \rho') \lambda'^2 d\lambda'}{\omega^2 \epsilon (\omega^2 - \lambda'^2)^{1/2} + \omega^2 (\omega^2 \epsilon - \lambda'^2)^{1/2}}, \quad (13)$$

and

$$\tilde{E}_{2z}(\rho', 0) = -\frac{\omega \mu_0}{2\pi c} \int_0^\infty \frac{J_0(\lambda' \rho') \lambda'^3 d\lambda'}{\omega^2 \epsilon (\omega^2 - \lambda'^2)^{1/2} + \omega^2 (\omega^2 \epsilon - \lambda'^2)^{1/2}}. \quad (14)$$

Since the field components defined in (12)–(14) are the Fourier transforms of the real time-dependent components, $B_{2\phi}(\rho', 0; t)$, $E_{2\rho}(\rho', 0; t)$, and $E_{2z}(\rho', 0; t)$, it follows that

$$\tilde{B}_{2\phi}(\rho', 0) = \tilde{B}_{2\phi}^*(\rho', 0); \quad \tilde{E}_{2\rho}(\rho', 0) = \tilde{E}_{2\rho}^*(\rho', 0); \quad \tilde{E}_{2z}(\rho', 0) = \tilde{E}_{2z}^*(\rho', 0), \quad (15)$$

where the asterisk denotes the complex conjugate.

Let the dipole be excited by a time-dependent voltage that maintains the current $I(0, t) = I(0)f(t)$ at its center. The Fourier transform of $f(t)$ is

$$\tilde{f}(\omega) = \int_{-\infty}^{\infty} f(t) e^{i\omega t} dt. \quad (16)$$

The time-dependent components of the field are:

$$B_{2\phi}(\rho', 0; t) = \frac{1}{2\pi} \operatorname{Re} \int_{-\infty}^{\infty} \tilde{B}_{2\phi}(\rho', 0) \tilde{f}(\omega) e^{-i\omega t} d\omega, \quad (17)$$

$$E_{2\rho}(\rho', 0; t) = \frac{1}{2\pi} \operatorname{Re} \int_{-\infty}^{\infty} \tilde{E}_{2\rho}(\rho', 0) \tilde{f}(\omega) e^{-i\omega t} d\omega, \quad (18)$$

$$E_{2z}(\rho', 0; t) = \frac{1}{2\pi} \operatorname{Re} \int_{-\infty}^{\infty} \tilde{E}_{2z}(\rho', 0) \tilde{f}(\omega) e^{-i\omega t} d\omega, \quad (19)$$

where $\tilde{E}_{2\phi}(\rho', 0)$, $\tilde{E}_{2\rho}(\rho', 0)$, and $\tilde{E}_{2z}(\rho', 0)$ are given by (12)-(14).

2. The Exact Transient Field When the Dipole is Excited by a Delta-Function Current

When $f(t)$ is the delta function, i.e.,

$$f(t) = \delta(t) = \frac{1}{2\pi} \int_{-\infty}^{\infty} e^{-i\omega t} d\omega, \quad (20)$$

$$\tilde{f}(\omega) = \int_{-\infty}^{\infty} \delta(t) e^{i\omega t} dt = 1, \quad (21)$$

the integral formulas (17) and (19) can be evaluated exactly. The details are given by Wu and King.² The related formula for the Hertz potential was evaluated by Van der Pol.³ The results from Wu and King² are:

$$\begin{aligned} B_{1\phi}(\rho, 0; t) &= B_{2\phi}(\rho, 0; t) \\ &= \frac{\mu_0}{2\pi(\epsilon - 1)\rho^2} [\epsilon \delta(t - \rho/c) - \epsilon^{-1} \delta(t - \rho\epsilon^{1/2}/c)] \\ &\quad - \frac{\mu_0 c}{2\pi\rho^3} \frac{\epsilon^2}{\epsilon - 1} \left\{ \begin{array}{c} 0 \\ \frac{3ct}{\rho} \left[(\epsilon + 1) \frac{c^2 t^2}{\rho^2} - \epsilon \right]^{-5/2} \\ 0 \end{array} \right\}; \end{aligned}$$

$$\left\{ \begin{array}{l} ct/\rho < 1 \\ 1 < ct/\rho < \epsilon^{1/2} \\ \epsilon^{1/2} < ct/\rho \end{array} \right., \quad (22)$$

$$\begin{aligned} \epsilon E_{1z}(\rho, 0; t) &= E_{2z}(\rho, 0; t) \\ &= -\frac{1}{2\pi\epsilon_0(\epsilon - 1)c\rho^2} [\epsilon \delta(t - \rho/c) - \epsilon^{-1/2} \delta(t - \rho\epsilon^{1/2}/c)] \end{aligned}$$

$$-\frac{1}{2\pi\epsilon_0(\epsilon+1)\rho^3} \left\{ \begin{array}{l} 0 \\ \frac{\epsilon}{\epsilon-1} \left[1 - \frac{\epsilon}{(\epsilon+1)^{3/2}} \left(\frac{2c^2t^2}{\rho^2} + \frac{\epsilon}{\epsilon+1} \right) \right. \\ \quad \left. \times \left(\frac{c^2t^2}{\rho^2} - \frac{\epsilon}{\epsilon+1} \right)^{-5/2} \right] \\ 1 \end{array} \right\};$$

$$\left\{ \begin{array}{l} ct/\rho < 1 \\ 1 < ct/\rho < \epsilon^{1/2} \\ \epsilon^{1/2} < ct/\rho \end{array} \right. \quad (23)$$

Significant features of these formulas are:

(1) The transient field at any radial distance ρ consists of two delta-function pulses that travel with the velocities c and $c\epsilon^{-1/2}$ and arrive at the times $t = \rho/c$ and $t = \rho\epsilon^{1/2}/c$. The field varies in a complicated manner in the interval between the pulses with a radial dependence of $\rho^{-1/2}$. After the second pulse has passed, the magnetic field drops abruptly to zero, the electric field to the static value due to the oppositely charged ends of the dipole.

(2) Both pulses have the amplitude factor ρ^{-2} . The transient field at *all* radial distances has the same radial dependence as the far field along the boundary in the steady state.

(3) Since the amplitude of the first pulse includes the factor ϵ , that of the second pulse the factor ϵ^{-1} , it follows that when the condition (1) for perfect dielectrics obtains, i.e.,

$$\epsilon \geq 9 \quad \text{or} \quad \epsilon^2 \geq 81, \quad (24)$$

the amplitude factor of the second pulse is very small compared to that of the first pulse. For example with fresh water, $\epsilon = 81$ so that $\epsilon^{-2} = 1.5 \times 10^{-4}$. Since the delta-function pulses have infinite amplitude and zero width, this is of no consequence for them. However, it is an indication of what to expect with finite pulses.

3. The Approximate Transient Field When the Dipole is Excited by a Delta-Function Current

The exact evaluation of the transient field by the Fourier transformation of the general integrals has been achieved only for the components B_ϕ and E_z generated by a delta-function current in a vertical dipole on the boundary between two dielectrics. It is of interest to reevaluate these components from the approximate, relatively simple forms in (2b) and (4b) for comparison with (22) and (23). If the approximate formulas are adequate for B_ϕ and E_z , they can also be used to evaluate E_ρ for the vertical dipole and all six of the more complicated components of the horizontal electric dipole. They can also be used to evaluate the fields with transients other than the delta function.

For dielectrics with the wave numbers expressed in terms of ω , (2b), (3b) and (4b) become:

$$\tilde{B}_{2\phi}(\rho', 0) \sim -\frac{\mu_0}{2\pi\epsilon c^2} e^{i\omega\rho'} \left[\frac{i\omega}{\rho'} - \frac{1}{\rho'^2} - \omega^{3/2} \left(\frac{\pi}{\epsilon\rho'} \right)^{1/2} e^{-ip} \mathcal{F}(p) \right], \quad (25)$$

$$\begin{aligned} \tilde{E}_{2\rho}(\rho', 0) \sim -\frac{\mu_0}{2\pi\epsilon^{3/2}c} \left\{ e^{i\omega\rho'} \left[\frac{i\omega}{\rho'} - \frac{1}{\rho'^2} - \omega^{3/2} \left(\frac{\pi}{\epsilon\rho'} \right)^{1/2} e^{-ip} \mathcal{F}(p) \right] \right. \\ \left. - \frac{ie^{i\omega\epsilon^{1/2}\rho'}}{\rho'^2} \right\}, \end{aligned} \quad (26)$$

$$\tilde{E}_{2z}(\rho', 0) \sim \frac{\mu_0}{2\pi\epsilon c} e^{i\omega\rho'} \left[\frac{i\omega}{\rho'} - \frac{1}{\rho'^2} - \frac{i}{\omega\rho'^3} - \omega^{3/2} \left(\frac{\pi}{\epsilon\rho'} \right)^{1/2} e^{-ip} \mathcal{F}(p) \right], \quad (27)$$

where

$$p = \omega\rho'/2\epsilon; \quad \mathcal{F}(p) = \frac{1}{2}(1+i) - \int_0^p \frac{e^{i\tau}}{\sqrt{2\pi\tau}} d\tau. \quad (28)$$

When these formulas are substituted in (17)-(19) with $\tilde{f}(\omega) = 1$ for the delta function, they yield the following formulas:

$$B_{2\phi}(\rho', 0; t) = -\frac{\mu_0}{2\pi\epsilon c^2} \left[\frac{I_1}{\rho'} - \frac{I_2}{\rho'^2} + \frac{I_4}{\sqrt{\pi\epsilon\rho'}} \right], \quad (29)$$

$$E_{2\rho}(\rho', 0; t) = -\frac{\mu_0}{2\pi\epsilon^{3/2}c} \left[\frac{I_1}{\rho'} - \frac{I_2}{\rho'^2} + \frac{I_4}{\sqrt{\pi\epsilon\rho'}} - \frac{I_{2\epsilon}}{\rho'^2} \right], \quad (30)$$

$$E_{2z}(\rho', 0; t) = \frac{\mu_0}{2\pi\epsilon c} \left[\frac{I_1}{\rho'} - \frac{I_2}{\rho'^2} - \frac{I_3}{\rho'^3} + \frac{I_4}{\sqrt{\pi\epsilon\rho'}} \right]. \quad (31)$$

Since the time functions on the left are real, the integrals are:

$$I_1 = \text{Re} \frac{1}{\pi} \int_0^\infty i\omega e^{-i\omega(t-\rho')} d\omega, \quad (32)$$

$$I_2 = \text{Re} \frac{1}{\pi} \int_0^\infty e^{-i\omega(t-\rho')} d\omega; \quad I_{2\epsilon} = \text{Re} \frac{i}{\pi} \int_0^\infty e^{-i\omega(t-\epsilon^{1/2}\rho')} d\omega, \quad (33)$$

$$I_3 = \text{Re} \frac{1}{\pi} \int_0^\infty \frac{i}{\omega} e^{-i\omega(t-\rho')} d\omega, \quad (34)$$

$$I_4 = -\text{Re} \int_0^\infty \omega^{3/2} e^{-i\omega(t-\rho'+\rho'/2\epsilon)} \left[\frac{1}{2}(1+i) - \int_0^{\omega\rho'/2\epsilon} \frac{e^{i\tau}}{\sqrt{2\pi\tau}} d\tau \right] d\omega. \quad (35)$$

The first three integrals are elementary and give:

$$I_1 = -\frac{\partial}{\partial t} \left[\frac{1}{\pi} \int_0^\infty e^{-i\omega(t-\rho')} d\omega \right] = -\frac{\partial}{\partial t} \delta(t-\rho') = -\delta'(t-\rho'), \quad (36)$$

$$I_2 = \delta(t-\rho'); \quad I_{2\epsilon} = 0, \quad (37)$$

$$I_3 = U(t-\rho'), \quad (38)$$

where $U(x)$ is the Heaviside or step function defined by $U(x) = 0, x < 0; U(x) = 1, x > 0$.

The fourth integral is complicated. It is evaluated in the Appendix with the result:

$$\frac{I_4}{\sqrt{\pi\epsilon\rho'}} = \frac{\delta'(t-\rho')}{\rho'} - \frac{\epsilon\delta(t-\rho')}{\rho'^2} + \frac{3}{4} \frac{1}{\sqrt{2\epsilon\rho'}} (t-\rho'+\rho'/2\epsilon)^{-5/2} U(t-\rho'). \quad (39)$$

When the four integrals are substituted in (29)-(31) and ρ' is replaced by ρ/c , the final approximate formulas are:

$$B_{2\phi}(\rho, 0; t) = \frac{\mu_0(\epsilon+1)}{2\pi\epsilon\rho^2} \delta(t-\rho/c) - \frac{\mu_0 c}{2\pi\rho^3} \left\{ \begin{array}{l} 0 \\ 3\epsilon \left[2\epsilon \left(\frac{ct}{\rho} - 1 \right) + 1 \right]^{-5/2} \end{array} \right\}; \quad (40)$$

$$\left\{ \begin{array}{l} t < \rho/c \\ t > \rho/c \end{array} \right.,$$

$$E_{2\rho}(\rho, 0; t) = \frac{\epsilon + 1}{2\pi\epsilon_0\epsilon^{3/2}c\rho^2} \delta(t - \rho/c) - \frac{1}{2\pi\epsilon_0\rho^3} \left\{ \begin{array}{l} 0 \\ 3\epsilon^{1/2} \left[2\epsilon \left(\frac{ct}{\rho} - 1 \right) + 1 \right]^{-5/2} \end{array} \right\};$$

$$\left\{ \begin{array}{l} t < \rho/c \\ t > \rho/c \end{array} \right., \quad (41)$$

$$E_{2z}(\rho, 0; t) = -\frac{\epsilon + 1}{2\pi\epsilon_0\epsilon c\rho^2} \delta(t - \rho/c) - \frac{1}{2\pi\epsilon_0\epsilon\rho^3} \left\{ \begin{array}{l} 0 \\ 1 - 3\epsilon^2 \left[2\epsilon \left(\frac{ct}{\rho} - 1 \right) + 1 \right]^{-5/2} \end{array} \right\};$$

$$\left\{ \begin{array}{l} t < \rho/c \\ t > \rho/c \end{array} \right. \quad (42)$$

It is interesting to note that in the time-domain components derived from the approximate frequency-domain formulas, the Fresnel-integral terms exactly cancel the $\delta'(t - \rho/c)$ pulse with its ρ^{-1} amplitude factor, so that only lateral pulses with the radial dependence ρ^{-2} remain.

4. Comparison of Exact and Approximate Formulas

The components (40)-(42) are derived from formulas obtained from the exact integrals subject to the inequalities (1) which, for dielectrics, include (24). The significance of this condition in the time domain is of interest. Note that $\epsilon \geq 9$ means that, in the derivation of the steady-state formulas, terms that are of the order ϵ^{-2} have been neglected by omission where convenient. The consequences of this approximation are:

(1) The coefficients of the pulse $\delta(t - \rho/c)$ are essentially the same since, with $\epsilon \geq 9$, it follows that $(\epsilon + 1)/\epsilon = (\epsilon^2 - 1)/\epsilon(\epsilon - 1) \sim \epsilon/(\epsilon - 1)$.

(2) The second pulse $\delta(t - \rho\epsilon^{1/2}/c)$ is absent in the approximate formulas. The ratio of its amplitude coefficient to that of the first pulse $\delta(t - \rho/c)$ is ϵ^{-2} or $\epsilon^{-3/2}$, both of which are very small when $\epsilon \geq 9$. The terms from which this pulse was derived are clearly negligible in the steady-state formulas but their omission leads to the nonappearance of the second pulse.

(3) The third range, $t > \rho\epsilon^{1/2}/c$, which follows the arrival of the second pulse is not specified in the approximate formulas, so that the static limits— $B_{2\phi}(\rho, 0; t) = 0$ and $E_{2z}(\rho, 0, t) = -1/2\pi\epsilon_0(\epsilon + 1)\rho^3$ —which apply when $t > \rho\epsilon^{1/2}/c$ in the exact formulas are reached only as $t \rightarrow \infty$ in the approximate formulas. These latter are quite accurate up to time $t = \rho\epsilon^{1/2}/c$, but of questionable significance after that time.

(4) The exact and the approximate formulas are not readily compared in a quantitative sense in the range $\rho/c < t < \rho\epsilon^{1/2}/c$ between the successive arrival of the two pulses except by direct numerical evaluation for specific values of ϵ . Such a calculation has been made for $\epsilon = 80$ and $\epsilon = 10$. The results are listed in Table 1 where $\tau = ct/\rho$. The quite remarkable agreement between the two superficially quite different formulas is best seen from a comparison of the corresponding numerical values over their very wide range of magnitudes. A graph of $E_{2z}(\rho, 0; t)$ with $\epsilon = 80$ is shown in Fig. 2. Clearly the approximate formulas are excellent approximations even to the point of closely approximating the exact static values at $t \geq \rho\epsilon^{1/2}/c$. The only property that is missing is the delta-function pulse at $t = \rho\epsilon^{1/2}/c$. For a pulse with finite width and extremely small amplitude, this would be of little consequence in most cases.

5. The Approximate Transient Field When the Dipole is Excited by a Gaussian Pulse

An important alternative to the delta function is the Gaussian pulse with its finite amplitude and adjustable width. Except for its infinite tail, its shape is readily adapted to approximate physically realizable pulses. In a normalized form, it is

$$f(t) = \frac{e^{-t^2/t_1^2}}{t_1\sqrt{\pi}}, \quad (43)$$

where t_1 is the half-width or time in which the pulse is reduced to $e^{-1} = 0.367$ of its maximum at $t = 0$. The Fourier transform of (43) is

$$\tilde{f}(\omega) = \int_{-\infty}^{\infty} f(t)e^{i\omega t} dt = e^{-\omega^2 t_1^2/4}. \quad (44)$$

The normalized form (43) is chosen for the Gaussian pulse so that, when $t_1 \rightarrow 0$, $f(t) \rightarrow \delta(t)$, the delta function, and $\tilde{f}(\omega) \rightarrow 1$, the transform of the delta function.

When (44) is used with (25)–(27) to obtain the time-dependent formulas, these have the forms (29)–(31) with the integrals I given by:

$$I_1 = \operatorname{Re} \frac{1}{2\pi} \int_{-\infty}^{\infty} i\omega e^{-\omega^2 t_1^2/4} e^{-i\omega(t-\rho')} d\omega, \quad (45)$$

$$I_2 = \operatorname{Re} \frac{1}{2\pi} \int_{-\infty}^{\infty} e^{-\omega^2 t_1^2/4} e^{-i\omega(t-\rho')} d\omega, \quad (46)$$

$$I_3 = \operatorname{Re} \frac{1}{2\pi} \int_{-\infty}^{\infty} \frac{i}{\omega} e^{-\omega^2 t_1^2/4} e^{-i\omega(t-\rho')} d\omega, \quad (47)$$

$$I_4 = -\operatorname{Re} \frac{1}{2} \int_{-\infty}^{\infty} \omega^{3/2} e^{-\omega^2 t_1^2/4} e^{-i\omega(t-\rho')} e^{-ip\mathcal{F}(p)} d\omega. \quad (48)$$

The first three integrals (45)–(47) can be evaluated together since

$$I_1 = -\frac{\partial I_2}{\partial t}; \quad \frac{\partial I_3}{\partial t} = I_2. \quad (49)$$

With the notation

$$\tau = t - \rho' = t - \rho/c, \quad (50)$$

and with formula 3.896-4 on pg. 480 of Gradshteyn and Ryzhik,⁴

$$I_2 = \frac{1}{\sqrt{\pi}t_1} e^{-\tau^2/t_1^2}. \quad (51)$$

Since $\partial/\partial t = \partial/\partial \tau$, it follows that

$$I_1 = -\frac{\partial I_2}{\partial \tau} = \frac{2\tau}{\sqrt{\pi}t_1^3} e^{-\tau^2/t_1^2}. \quad (52)$$

Also, with (49),

$$\frac{\partial I_3}{\partial \tau} = I_2 = \frac{1}{\sqrt{\pi}t_1} e^{-\tau^2/t_1^2}, \quad (53)$$

$$I_3 = \frac{1}{\sqrt{\pi}t_1} \int_{-\infty}^{\tau} e^{-r^2/t_1^2} d\tau = \frac{1}{\sqrt{\pi}} \left[\int_0^{\tau/t_1} e^{-u^2} du + \int_0^{\infty} e^{-u^2} du \right], \quad (54)$$

where $u = \tau/t_1$. The definition of the error function is:

$$\operatorname{erf} z = \frac{2}{\sqrt{\pi}} \int_0^z e^{-u^2} du; \quad \frac{2}{\sqrt{\pi}} \int_0^\infty e^{-u^2} du = 1, \quad (55)$$

so that

$$I_3 = \frac{1}{2} [1 + \operatorname{erf}(\tau/t_1)]. \quad (56)$$

The evaluation of the fourth integral (48) is carried out in the Appendix. The result is:

$$\frac{I_4}{\sqrt{\pi \epsilon \rho'}} \sim -\frac{e^{-T^2/2t_1^2}}{\sqrt{\pi \epsilon \rho'} t_1^{5/2}} \left\{ \begin{array}{l} 1.87 V(0, \sqrt{2} T/t_1) - 2.64 \frac{T}{t_1} V(-1, \sqrt{2} T/t_1) \\ 1.05 U(0, -\sqrt{2} T/t_1) + 2.90 \frac{T}{t_1} U(-1, -\sqrt{2} T/t_1) \end{array} \right\}; \quad (57)$$

$$\left\{ \begin{array}{l} T/t_1 \geq 0 \\ T/t_1 \leq 0 \end{array} \right.,$$

where $V(0, x)$, $V(-1, x)$ and $U(0, x)$, $U(-1, x)$ are parabolic cylinder functions⁶ and

$$T \equiv t - \rho' + \rho'/2\epsilon; \quad \rho' = \rho/c. \quad (58)$$

When (51), (52), (56) and (57) are substituted in (29)-(31) with the following new notation introducing dimensionless variables,

$$\rho_1 \equiv \rho'/t_1 = \rho/ct_1; \quad t' \equiv t/t_1; \quad \tau' \equiv \tau/t_1 = t' - \rho_1, \quad (59)$$

$$T' \equiv T/t_1 = t' - \rho_1 \left(1 - \frac{1}{2\epsilon}\right), \quad (60)$$

the results are:

$$B_{2\phi}(\rho, 0; t) = \frac{\mu_0}{2\pi\epsilon c} \frac{\pi^{-1/2}}{c^3 t_1^3} \left\{ \left[-\frac{2\tau'}{\rho_1} + \frac{1}{\rho_1^2} \right] e^{-\tau'^2} \right. \\ \left. + \frac{e^{-T'^2/2}}{\sqrt{\epsilon \rho_1}} \left[\begin{array}{l} 1.87 V(0, \sqrt{2} T') - 2.64 T' V(-1, \sqrt{2} T') \\ 1.05 U(0, -\sqrt{2} T') + 2.90 T' U(-1, -\sqrt{2} T') \end{array} \right] \right\};$$

$$\begin{cases} T' \geq 0 \\ T' \leq 0 \end{cases}, \quad (61)$$

$$E_{2\rho}(\rho, 0; t) = \frac{c}{\epsilon^{1/2}} B_{2\phi}(\rho, 0; t), \quad (62)$$

$$E_{2z}(\rho, 0; t) = -\frac{1}{2\pi\epsilon_0\epsilon} \frac{\pi^{-1/2}}{c^3 t_1^3} \left\{ \left[-\frac{2\tau'}{\rho_1} + \frac{1}{\rho_1^2} \right] e^{-\tau'^2} + \frac{\pi^{1/2}}{2\rho_1^3} [\operatorname{erf} \tau' + 1] \right. \\ \left. + \frac{e^{-T'^2/2}}{\sqrt{\epsilon\rho_1}} \begin{bmatrix} 1.87 V(0, \sqrt{2} T') - 2.64 T' V(-1, \sqrt{2} T') \\ 1.05 U(0, -\sqrt{2} T') + 2.90 T' U(-1, -\sqrt{2} T') \end{bmatrix} \right\}; \quad (63)$$

$$\begin{cases} T' \geq 0 \\ T' \leq 0 \end{cases}.$$

As with the delta-function pulse, the omission of small terms with magnitudes smaller than ϵ^{-1} in the frequency-domain formulas must lead to the nonappearance of a second pulse of the form $\exp(-\tau'^2)/\rho_1^2$ where $\tau'_\epsilon = t' - \rho_1 \epsilon^{1/2}$. Its amplitude is very much smaller than that of the pulse $\exp(-\tau'^2)/\rho_1^2$ because it is multiplied by a factor of the order ϵ^{-2} ; it travels with the phase velocity $c/\epsilon^{1/2}$ instead of $c = 3 \times 10^8$ m/sec; and it arrives at any radial distance $\rho = \rho_1 c t_1$ at a time $\Delta t = (\rho/c)(\epsilon^{1/2} - 1)$ after the first pulse. The formulas (61)–(63) can be expected to be quite accurate before the second pulse arrives, i.e., when $t' < \rho_1 \epsilon^{1/2}$ or $T' < \rho_1 [\epsilon^{1/2} - 1 + (2\epsilon)^{-1}]$; they also give the correct static values as $\tau' \rightarrow \infty$, viz., $B_{2\phi}(\rho, 0; t) = 0$ and, since $\operatorname{erf} \infty = 1$ and $ct_1 \rho_1 = \rho$, $E_{2z}(\rho, 0; t) = -1/2\pi\epsilon_0\epsilon\rho^3$. However, there is no assurance that the form of (61)–(63) is correct when $t > \rho\epsilon^{1/2}/c$ or $T > [\epsilon^{1/2} - 1 + (2\epsilon)^{-1}]\rho/c$. Indeed, if the corresponding formulas for the delta-function pulse—for which exact formulas are available—are a guide, there is no $\rho^{-1/2}$ dependence when $t > \rho\epsilon^{1/2}/c$.

A graphical representation of the expression in braces in (63) is shown in Fig. 3 when the exciting Gaussian pulse has a half-width $t_1 = 1$ nanosecond and $\epsilon = 80$. The several curves show the vertical electric field as a function of the time at five radial distances from $\rho = 0.45$ m to $\rho = 1.5$ m. Similar graphs with a different amplitude scale are in Fig. 4 for

$\rho = 4.8$ m and $\rho = 7.5$ m. The shape of the pulse as a function of the time at any given radial distance ρ is determined by the relative contributions from the four terms in (63) with their very different dependences on the radial distance and the time.

The third term represents the rapid increase in the vertical electric field as the pulse passes and leaves the final electrostatic field of the charged infinitesimal dipole. This part of the field decreases as $1/\rho^3$ with distance. The second term is a Gaussian electric-field pulse that travels with the phase velocity c and with a decrease in amplitude $1/\rho^2$. The first term is the time derivative of the Gaussian pulse. It travels with the Gaussian pulse but decreases with distance only as $1/\rho$ so that it persists for much greater distances than does the $1/\rho^2$ term. The fourth term is due to the Fresnel integral. With the delta-function pulse and the steady-state far field, it contributed a term which exactly cancelled the $1/\rho$ term and added a dominant contribution to the $1/\rho^2$ term. With the Gaussian pulse, the cancellation of the $1/\rho$ term is only partial. Furthermore, the terms which tend to reduce the $1/\rho$ term and increase the $1/\rho^2$ term decrease only as $\rho^{-1/2}$. It must be remembered that these formulas cannot be expected to be good approximations for $t > \rho\epsilon^{1/2}/c$ where the field presumably is not characterized by $\rho^{-1/2}$.

The graphs in Figs. 3 and 4 indicate that the time-derivative terms dominate both near and far, so that there is little change in the shape of the outward-traveling pulses in the range $t < \rho\epsilon^{1/2}/c$. This is evident especially from Fig. 4. The amplitudes of the first and fourth terms in (63) are approximately equal when $\rho = 4.8$ m; the fourth term dominates when $\rho = 7.5$ m.

In Figs. 3 and 4, the second pulse should arrive at $t_2 = \rho\epsilon^{1/2}/c = 9\rho/(3 \times 10^8) = 30\rho$ nanoseconds when ρ is in meters. At $\rho = 0.45$ m, $t_2 = 13.5$ nanoseconds; at $\rho = 7.5$ m, $t_2 = 225$ nanoseconds. These times are off the scales in Figs. 3 and 4.

6. Conclusion

The electromagnetic field generated by a vertical electric dipole on the boundary between electrically different dielectric half-spaces is derived for transient excitation by delta-function and Gaussian pulses. The validity of determining the fields in the time

domain from Fourier transformations of the approximate formulas for the frequency domain is established together with its limitations from direct comparisons with exact formulas where these are available. Similar limitations and comparable accuracy can be assumed for the approximate formulas of the components for which exact formulas are not available. An extension of the approximate formulas to $z \neq 0$ can be carried out. An analysis when one region is an imperfect dielectric is in ref. 6.

Acknowledgment. The author is indebted to Tai T. Wu for his many contributions and suggestions, and to M. Owens for her help in correcting the manuscript and preparing it for publication. This work was supported in part by the Joint Services Electronics Program under Contract N00014-84-K-0465 with Harvard University.

APPENDIX: EVALUATION OF THE INTEGRALS

A1. Delta-Function Excitation

The integral I_4 with delta-function excitation is:

$$I_4 = -\text{Re} \int_0^\infty \omega^{3/2} e^{-i\omega(t-\rho'+\rho'/2\epsilon)} \left[\frac{1}{2}(1+i) - \int_0^p \frac{e^{i\tau}}{\sqrt{2\pi\tau}} d\tau \right] d\omega. \quad (\text{A1})$$

This is equivalent to

$$I_4 = \text{Re} \frac{\partial^2}{\partial t^2} \left\{ \frac{1}{2}(1+i) \int_0^\infty e^{-i\omega(t-\bar{\alpha})} \frac{d\omega}{\sqrt{\omega}} - \frac{1}{\sqrt{2\pi}} \int_0^\infty e^{-i\omega(t-\bar{\alpha})} \frac{d\omega}{\sqrt{\omega}} \int_0^p \frac{e^{i\tau}}{\sqrt{\tau}} d\tau \right\}, \quad (\text{A2})$$

where $\bar{\alpha} = \rho'[1 - (2\epsilon)^{-1}] = \rho' - \beta$ with $\beta = \rho'/2\epsilon$, $p = \omega\rho'/2\epsilon = \omega\beta$. Let

$$\alpha = \frac{t - \bar{\alpha}}{\beta}; \quad \omega = p/\beta. \quad (\text{A3})$$

Then

$$I_4 = \text{Re} \frac{\partial^2}{\partial t^2} \left\{ \frac{1+i}{2\sqrt{\beta}} \int_0^\infty e^{-ip\alpha} \frac{dp}{\sqrt{p}} - \frac{1}{\sqrt{2\pi\beta}} \int_0^\infty e^{-ip\alpha} \frac{dp}{\sqrt{p}} \int_0^p \frac{e^{i\tau}}{\sqrt{\tau}} d\tau \right\}. \quad (\text{A4})$$

With $x = \alpha p$, the first integral is

$$\vartheta_1 = \frac{1}{\sqrt{\alpha}} \int_0^\infty \frac{\cos x}{\sqrt{x}} dx - \frac{i}{\sqrt{\alpha}} \int_0^\infty \frac{\sin x}{\sqrt{x}} dx = \left(\frac{\pi}{2\alpha} \right)^{1/2} (1-i). \quad (\text{A5})$$

With $p = \xi^2/\alpha$ and $\tau = \zeta^2$, the second integral is

$$\vartheta_2 = \frac{4}{\sqrt{\alpha}} \int_0^\infty e^{-i\xi^2} d\xi \int_0^{\xi/\sqrt{\alpha}} e^{i\zeta^2} d\zeta = \frac{4}{\sqrt{\alpha}} \int_0^\infty e^{-i\rho^2} \rho d\rho \int_0^{\tanh^{-1}(1/\sqrt{\alpha})} d\theta, \quad (\text{A6})$$

where the cylindrical coordinates ρ, θ have been introduced with $\xi = \rho \sinh \theta$, $\zeta = \rho \cosh \theta$, and with

$$d\xi d\zeta = J \left(\frac{\xi, \zeta}{\rho, \theta} \right) d\rho d\theta = \begin{bmatrix} \cosh \theta & \sinh \theta \\ \rho \sinh \theta & \rho \cosh \theta \end{bmatrix} d\rho d\theta = \rho d\rho d\theta. \quad (\text{A7})$$

This integrates into

$$\vartheta_2 = \frac{4}{\sqrt{\alpha}} \tanh^{-1} \frac{1}{\sqrt{\alpha}} \int_0^\infty e^{-i\rho^2} \rho d\rho = -\frac{2i}{\sqrt{\alpha}} \tanh^{-1} \frac{1}{\sqrt{\alpha}}. \quad (\text{A8})$$

When (A5) and (A8) are substituted in (A4), the result is

$$I_4 = \text{Re} \frac{\partial^2}{\partial t^2} \left[\left(\frac{\pi}{2\alpha\beta} \right)^{1/2} + \frac{2i}{\sqrt{2\pi\alpha\beta}} \tanh^{-1} \frac{1}{\sqrt{\alpha}} \right]. \quad (\text{A9})$$

Here the second term is a pure imaginary so that it contributes nothing to I_4 . With $\alpha\beta = t - \bar{\alpha} = t - \rho' + \rho'/2\epsilon$, and since I_4 must be real and the pulse cannot arrive at ρ' before $t = \rho' = \rho/c$,

$$I_4 = \left(\frac{\pi}{2} \right)^{1/2} \frac{\partial^2}{\partial t^2} (t - \rho' + \rho'/2\epsilon)^{-1/2} U(t - \rho'), \quad (\text{A10})$$

where $U(x) = 0, x < 0$; $U(x) = 1, x > 0$ is the Heaviside or step function. The differentiation leads to:

$$I_4 = \left(\frac{\pi}{2} \right)^{1/2} \left[\left(\frac{2\epsilon}{\rho'} \right)^{1/2} \delta'(t - \rho') - \frac{1}{2} \left(\frac{2\epsilon}{\rho'} \right)^{3/2} \delta(t - \rho') + \frac{3}{4} (t - \rho' + \rho'/2\epsilon)^{-5/2} U(t - \rho') \right]. \quad (\text{A11})$$

A2. Gaussian-Pulse Excitation

The integral I_4 with Gaussian-pulse excitation is

$$I_4 = -\text{Re} \frac{1}{2} \int_{-\infty}^{\infty} \omega^{3/2} e^{-\omega^2 t_1^2/4} e^{-i\omega(t-\rho'+\rho'/2\epsilon)} \left[\frac{1}{2}(1+i) - \int_0^p \frac{e^{i\tau}}{\sqrt{2\pi\tau}} d\tau \right] d\omega. \quad (\text{A12})$$

This integral differs from (A1) only in the additional factor $e^{-\omega^2 t_1^2/4}$. Hence the double integral is like the corresponding integral in (A4) but with the added factor $e^{-\omega^2 t_1^2/4} = e^{-\rho^2 t_1^2/4\beta^2}$. With it, the integral in (A6) becomes:

$$\vartheta_2 = \frac{4}{\sqrt{\alpha}} \int_0^\infty e^{-i\rho^2} \rho d\rho \int_0^{\tanh^{-1}(1/\sqrt{\alpha})} e^{-(\rho^4 t_1^2/4\alpha^2\beta^2) \cosh^2 \theta} d\theta. \quad (\text{A13})$$

This is not readily integrated. However, the range of θ is small since $\alpha = 2\epsilon[(ct/\rho) - 1] - 1$ and $\epsilon \geq 9$. With $\tanh^{-1}(1/\sqrt{\alpha}) \sim 1/\sqrt{\alpha}$, $0 \leq \theta \leq 1/\sqrt{\alpha}$; also with $\coth^4 \theta \sim 1 + 2\theta^2$, the condition $2\theta^2 \ll 1$ is adequately satisfied when $\theta \leq 0.3$. Hence, $\alpha^{-1} \leq 0.09$ or $\alpha \geq 11$. This is true when $2\epsilon[(ct/\rho) - 1] - 1 \geq 11$ or $ct/\rho \geq 1 + (6/\epsilon) \geq 1.66$. Since $ct/\rho = 1$ is the center of the pulse, this is not a severe restriction on the useful range. With it, the integral ϑ_2 is the same as (A6) and yields a pure imaginary that contributes nothing to I_4 in (A12). Hence, with $T \equiv t - \rho' + \rho'/2\epsilon$,

$$I_4 = \frac{\partial^2}{\partial t^2} \operatorname{Re} \frac{1}{4}(1+i) \int_{-\infty}^{\infty} \omega^{-1/2} e^{-\omega^2 t_1^2/4} e^{-i\omega T} d\omega. \quad (\text{A14})$$

Let $\omega = \sqrt{2}\tau/t_1$ and $z = \sqrt{2}T/t_1$. Then

$$I_4 = \operatorname{Re} \frac{1}{4}(1+i) 2^{1/4} t_1^{-1/2} \frac{\partial^2}{\partial t^2} \vartheta_0 = \operatorname{Re} \frac{e^{i\pi/4} 2^{1/4}}{2\sqrt{2}t_1} \frac{\partial^2}{\partial t^2} \vartheta_0, \quad (\text{A15})$$

where

$$\begin{aligned} \vartheta_0 &= \int_{-\infty}^{\infty} \tau^{-1/2} e^{-\tau^2/2 - iz\tau} d\tau \\ &= \int_0^{\infty} \tau^{-1/2} e^{-\tau^2/2 - iz\tau} d\tau - i \int_0^{\infty} \tau^{-1/2} e^{-\tau^2/2 + iz\tau} d\tau. \end{aligned} \quad (\text{A16})$$

The two integrals on the right are related to the parabolic cylinder functions $U(0, x) \equiv D_{-1/2}(x)$ which have the following integral representation and relation to the Bessel functions (see formula 3 on pg. 19 of Erdelyi⁷ and formula 19.15.9 on pg. 692 of Abramowitz and Stegun⁵):

$$\begin{aligned} D_{-1/2}(x) &\equiv U(0, x) = \pi^{-1/2} \left(\frac{1}{2}x\right)^{1/2} K_{1/4}\left(\frac{1}{4}x^2\right) \\ &= \pi^{-1/2} e^{-x^2/4} \int_0^{\infty} e^{-xt - t^2/2} t^{-1/2} dt. \end{aligned} \quad (\text{A17})$$

[The notation $U(0, x)$ —which is not related to the step function $U(x)$ —is that used by Abramowitz and Stegun.] With $y = U(0, x)$, this function satisfies the following equation (see formula 19.1.2 on pg. 686 of Abramowitz and Stegun⁵):

$$\frac{d^2 y}{dx^2} - \frac{1}{4}x^2 y = 0. \quad (\text{A18})$$

With $x = \pm iz = ze^{\pm i\pi/2}$, the two integrals in (A16) become:

$$\int_0^\infty \tau^{-1/2} e^{-\tau^2/2 \mp i\tau} d\tau = \left(\frac{1}{2}ze^{\pm i\pi/2}\right)^{1/2} e^{-z^2/4} K_{1/4}\left(\frac{1}{4}z^2 e^{\pm i\pi}\right). \quad (\text{A19})$$

With formula 45 on pg. 80 of Erdelyi,⁷ the two Bessel functions with imaginary argument can be expanded as follows:

$$K_{1/4}(xe^{\pm i\pi}) = e^{\mp i\pi/4} K_{1/4}(x) \mp i\pi I_{1/4}(x). \quad (\text{A20})$$

With (A20) and $x = \frac{1}{4}z^2$, (A19) becomes:

$$\int_0^\infty \tau^{-1/2} e^{-\tau^2/2 \mp i\tau} d\tau = \left(\frac{1}{2}z\right)^{1/2} e^{-z^2/4} [K_{1/4}\left(\frac{1}{4}z^2\right) \mp i\pi e^{\pm i\pi/4} I_{1/4}\left(\frac{1}{4}z^2\right)]. \quad (\text{A21})$$

These expressions can now be substituted in (A16) to give:

$$\vartheta_0 = \left(\frac{1}{2}z\right)^{1/2} e^{-z^2/4} e^{-i\pi/4} f\left(\frac{1}{4}z^2\right); \quad f\left(\frac{1}{4}z^2\right) \equiv \sqrt{2} K_{1/4}\left(\frac{1}{4}z^2\right) + 2\pi I_{1/4}\left(\frac{1}{4}z^2\right). \quad (\text{A22})$$

The next step is to evaluate

$$\frac{\partial^2 \vartheta_0}{\partial t^2} = \frac{\partial^2 \vartheta_0}{\partial T^2} = \frac{2}{t_1^2} \frac{\partial^2 \vartheta_0}{\partial z^2}. \quad (\text{A23})$$

It is readily verified with (A18) that

$$\frac{\partial^2 \vartheta_0}{\partial t^2} = -\frac{2e^{-i\pi/4}}{t_1^2} \left[\frac{1}{2}(1-z^2)y + z \frac{dy}{dz} \right] e^{-z^2/4}. \quad (\text{A24})$$

With the tabulated parabolic cylinder functions $U(a, z)$ and $V(a, z)$ defined on page 687 and with formulas 19.15.1, 19.15.2, 19.15.13 and 19.15.19 in Abramowitz and Stegun,⁵

$$K_{1/4}\left(\frac{1}{4}z^2\right) = \pi^{1/2} \left(\frac{1}{2}z\right)^{-1/2} U(0, z), \quad (\text{A25})$$

$$I_{1/4}\left(\frac{1}{4}z^2\right) = z^{-1/2} V(0, z) - (\pi z)^{-1/2} U(0, z), \quad (\text{A26})$$

and

$$y = (\tfrac{1}{2}z)^{1/2} f(\tfrac{1}{4}z^2) = \frac{2\pi}{\sqrt{2}} V(0, z), \quad (\text{A27})$$

$$\frac{dy}{dz} = \frac{2\pi}{\sqrt{2}} V'(0, z) = \frac{2\pi}{\sqrt{2}} [\tfrac{1}{2}zV(0, z) - \tfrac{1}{2}V(-1, z)], \quad (\text{A28})$$

where $V'(0, z)$ is obtained with formula 19.6.5 on page 688 of Abramowitz and Stegun⁵ with $a = 0$. When y and dy/dz are substituted in (A24), the result is:

$$\frac{\partial^2 \vartheta_0}{\partial t^2} = -\frac{2\pi}{\sqrt{2}} \frac{e^{-i\pi/4} e^{-z^2/4}}{t_1^2} [V(0, z) - zV(-1, z)]; \quad z \geq 0. \quad (\text{A29})$$

For negative values of z , it is convenient to use formula 19.4.2 on page 687 of Abramowitz and Stegun⁵ with $a = 0$ and $a = -1$. This gives:

$$V(0, z) = \frac{\Gamma(\frac{1}{2})}{\pi} U(0, -z); \quad V(-1, z) = \frac{\Gamma(-\frac{1}{2})}{\pi} U(-1, -z), \quad (\text{A30})$$

where $U(0, x)$ is given by (A17) and $\Gamma(\frac{1}{2}) = \sqrt{\pi}$, $\Gamma(-\frac{1}{2}) = -3.449$. With these values,

$$\frac{\partial^2 \vartheta_0}{\partial t^2} = -\frac{2\pi}{\sqrt{2}} \frac{e^{-i\pi/4} e^{-z^2/4}}{t_1^2} [\sqrt{\pi} U(0, -z) + 1.098z U(-1, -z)]; \quad z \leq 0. \quad (\text{A31})$$

With (A29) and (A31) substituted in (A15),

$$I_4 = -\frac{\pi}{2} \frac{2^{1/4}}{t_1^{5/2}} e^{-z^2/4} \left\{ \begin{array}{ll} V(0, z) - zV(-1, z); & z \geq 0 \\ \pi^{-1/2} U(0, -z) + 1.098z U(-1, -z); & z \leq 0 \end{array} \right\}. \quad (\text{A32})$$

With $z = \sqrt{2}T/t_1$, where $T = t - \rho' + \rho'/2\epsilon$, this becomes:

$$I_4 = -\frac{e^{-T^2/2t_1^2}}{t_1^{5/2}} \left\{ \begin{array}{l} 1.87 V(0, \sqrt{2}T/t_1) - 2.64 \frac{T}{t_1} V(-1, \sqrt{2}T/t_1) \\ 1.05 U(0, -\sqrt{2}T/t_1) + 2.90 \frac{T}{t_1} U(-1, -\sqrt{2}T/t_1) \end{array} \right\}; \quad \left\{ \begin{array}{l} T/t_1 \geq 0 \\ T/t_1 \leq 0 \end{array} \right\}. \quad (\text{A33})$$

REFERENCES

1. King, R. W. P., "New formulas for the electromagnetic field of a vertical electric dipole in a dielectric or conducting half-space near its horizontal interface," *J. Appl. Phys.*, Vol. 53, 8476-8482, 1982; Erratum, Vol. 56, 3366, 1984.
2. Wu, T. T., and R. W. P. King, "Lateral electromagnetic pulses generated by a vertical dipole on the boundary between two dielectrics," *J. Appl. Phys.*, Vol. 62, 4345-4355, 1987.
3. Van der Pol, B., "On discontinuous electromagnetic waves and the occurrence of a surface wave," *IRE Trans. Antennas Propagat.*, Vol. AP-4, 288-293, 1956.
4. Gradshteyn, I. S., and I. M. Ryzhik, *Table of Integrals, Series, and Products*, Academic Press, New York, 1980.
5. Abramowitz, M., and I. A. Stegun, Eds., *Handbook of Mathematical Functions*, Dover Publications, New York, 1972.
6. Brown, M. F., "Wave packets of lateral waves due to a vertical monopole: Experiment and theory," *Radio Sci.*, Vol. 22, 833-846, 1987.
7. Erdelyi, A., Ed., *Higher Transcendental Functions, Vol. II*, Bateman Manuscript Project, McGraw-Hill Book Co., New York, 1953.

TABLE 1

Comparison of Exact and Approximate Formulas for $B_{2\phi}(\rho, \tau)$ and $E_{2z}(\rho, \tau)$
with Delta-Function Excitation; $\tau = ct/\rho \geq 1$

$(-2\pi\rho^3/\mu_0 c) B_{2\phi}(\rho, \tau)$				
Approximate			Exact	
$\frac{3\epsilon}{[2\epsilon(\tau-1)+1]^{5/2}}$			$\frac{3\epsilon^2\tau}{(\epsilon-1)[(\epsilon+1)\tau^2-\epsilon]^{5/2}}$	
τ	$\epsilon = 80$	$\epsilon = 10$	$\epsilon = 80$	$\epsilon = 10$
1.0	240	30.0	243	33.3
1.01	22.0	19.0	21.9	25.4
1.05	0.987	5.30	0.967	5.30
1.1	0.201	1.92	0.194	1.84
1.2	0.0384	0.536	0.0359	0.485
1.5	0.406×10^{-2}	0.0748	0.345×10^{-2}	0.0598
2.0	0.73×10^{-3}	0.0148	0.52×10^{-3}	0.0099
3.0	0.13×10^{-3}	0.00279	0.068×10^{-3}	0.00134
$\epsilon^{1/2}$	0.416×10^{-5}	0.00230	0.066×10^{-5}	0.00105

$-2\pi\epsilon_0\epsilon\rho^3 E_{2z}(\rho, \tau)$				
Approximate			Exact	
$1 - \frac{3\epsilon^2}{[2\epsilon(\tau-1)+1]^{5/2}}$			$\frac{\epsilon^2}{\epsilon^2-1} \left\{ 1 - \frac{\epsilon[2(c+1)\tau^2+\epsilon]}{[(\epsilon+1)\tau^2-\epsilon]^{5/2}} \right\}$	
τ	$\epsilon = 80$	$\epsilon = 10$	$\epsilon = 80$	$\epsilon = 10$
1.0	-19,200	-299	-19,400	-322
1.01	-1,760	-189	-1,750	-198
1.05	-78.0	-52.0	-77.4	-51.4
1.1	-15.1	-18.2	-15.0	-17.5
1.2	-2.07	-4.37	-2.08	-4.10
1.3	-0.142	-1.31	-0.159	-1.19
1.32	0.025	-1.01	0.008	-0.91
2.0	0.942	0.85	0.937	0.86
3.0	0.9896	0.97	0.9887	0.98
$\epsilon^{1/2}$	0.99967	0.977	0.99984	0.987

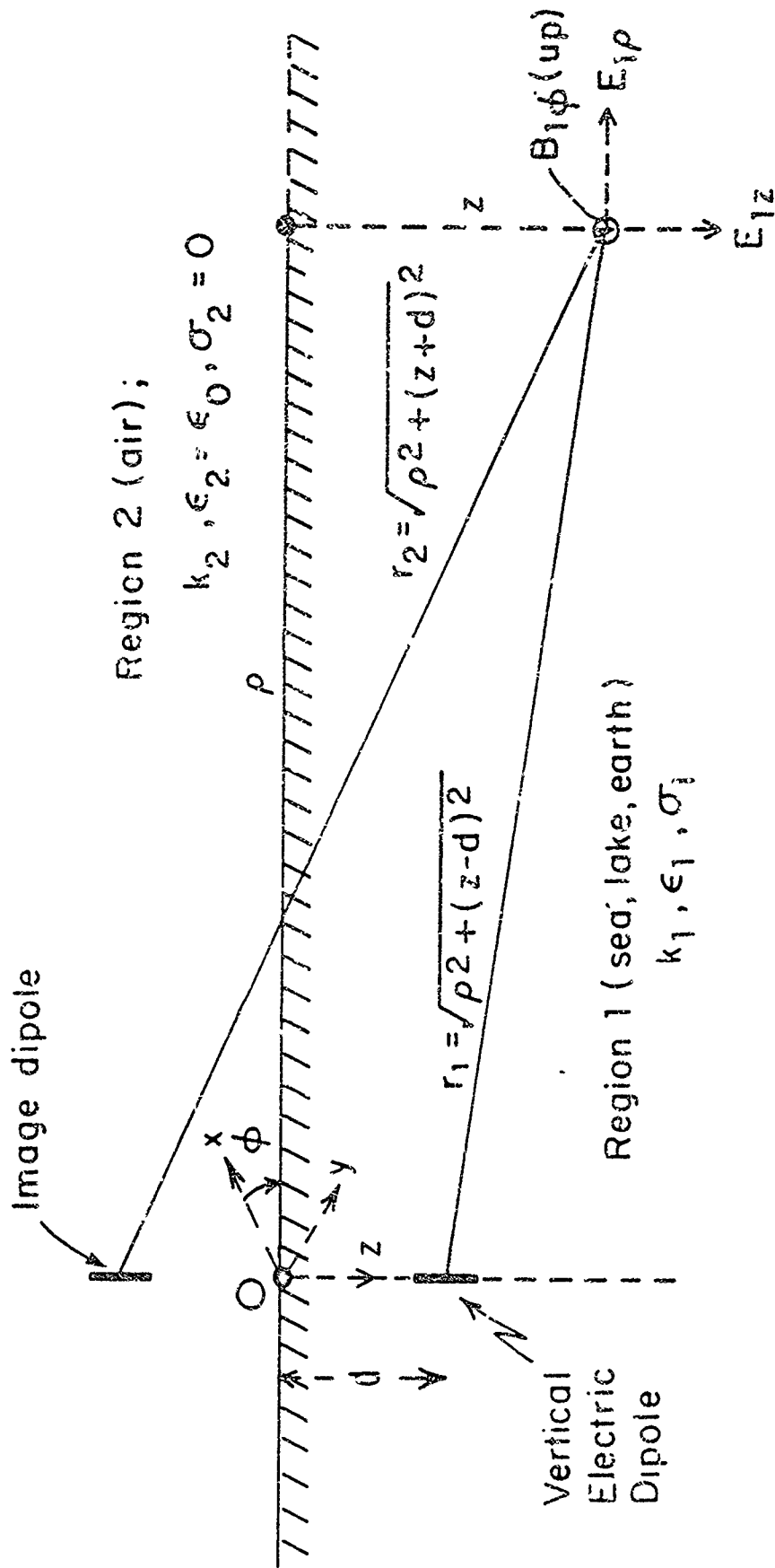


Fig. 1. Vertical electric dipole at depth d in Region 1. Electromagnetic field calculated at (ρ, z) .

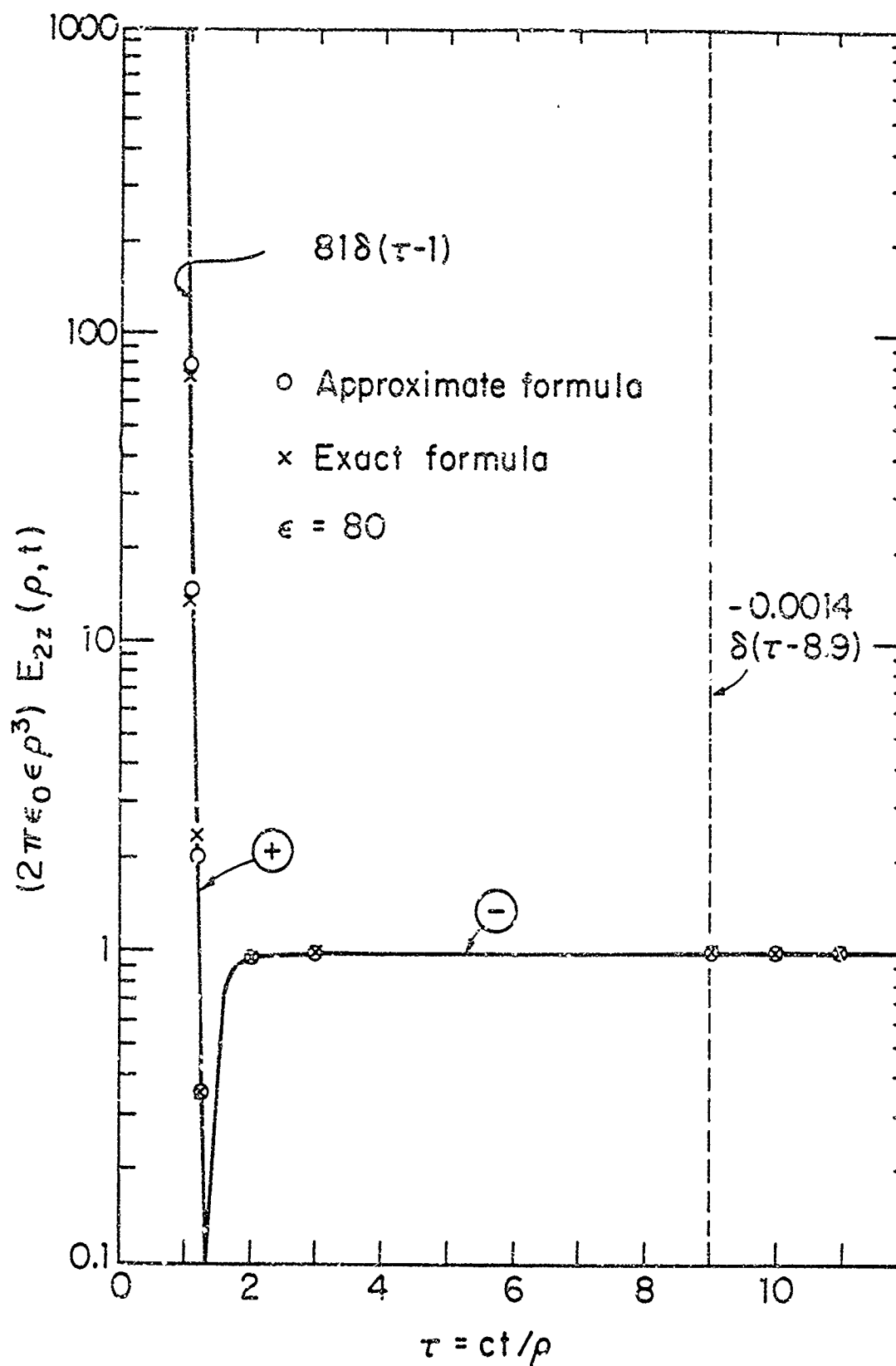


Fig. 2. Comparison of the approximate and exact formulas for $E_{2z}(\rho, t)$ with $\epsilon = 80$; delta-function excitation. Graphs of Table 1, columns for $\epsilon = 80$ and $\tau > 1$.

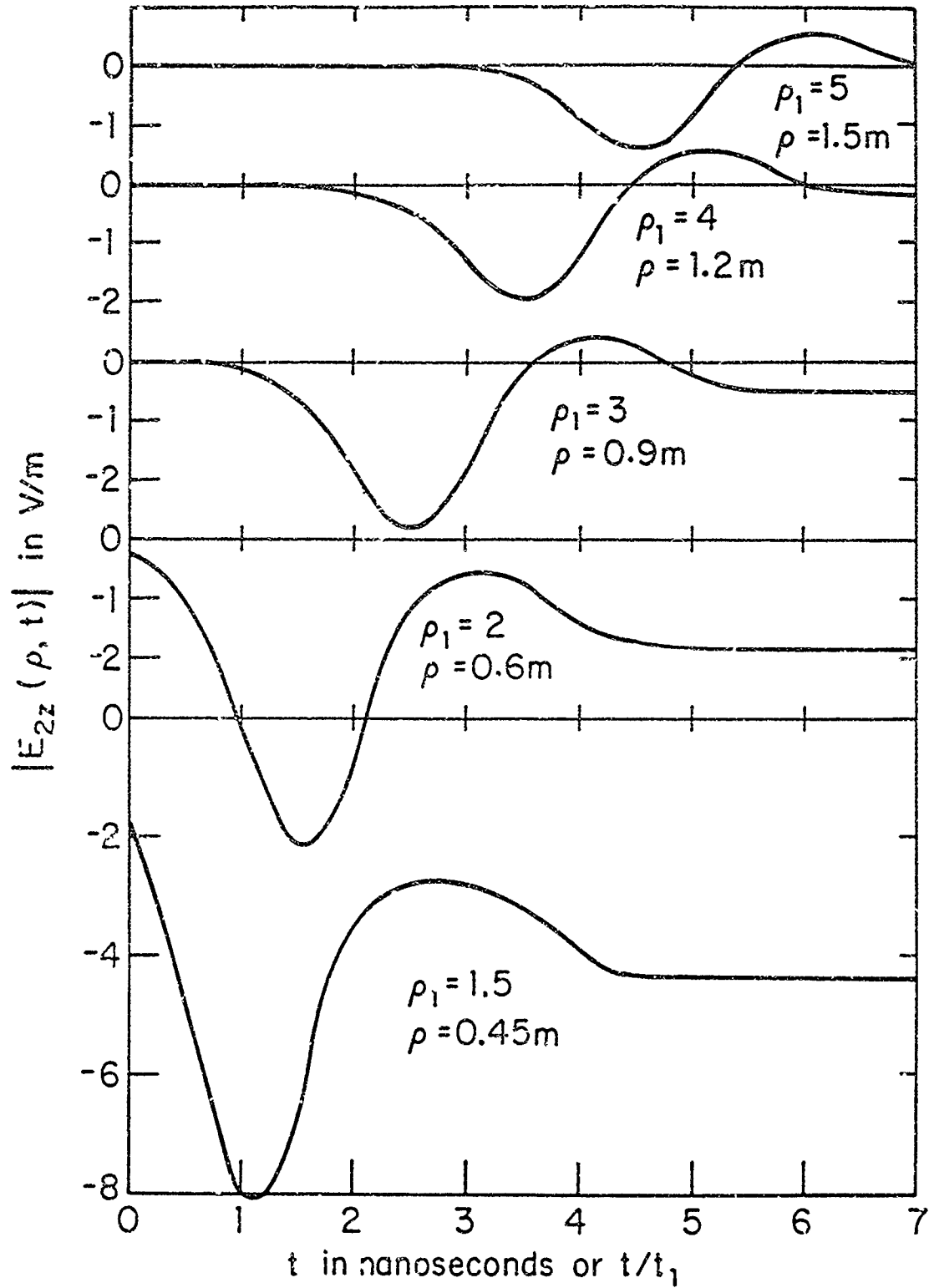


Fig. 3. Approximate vertical electric field on the boundary in air due to a vertical electric dipole on the boundary in a perfect dielectric with relative permittivity $\epsilon = 80$. The dipole is excited by a Gaussian pulse with $t_1 = 1$ nanosecond.

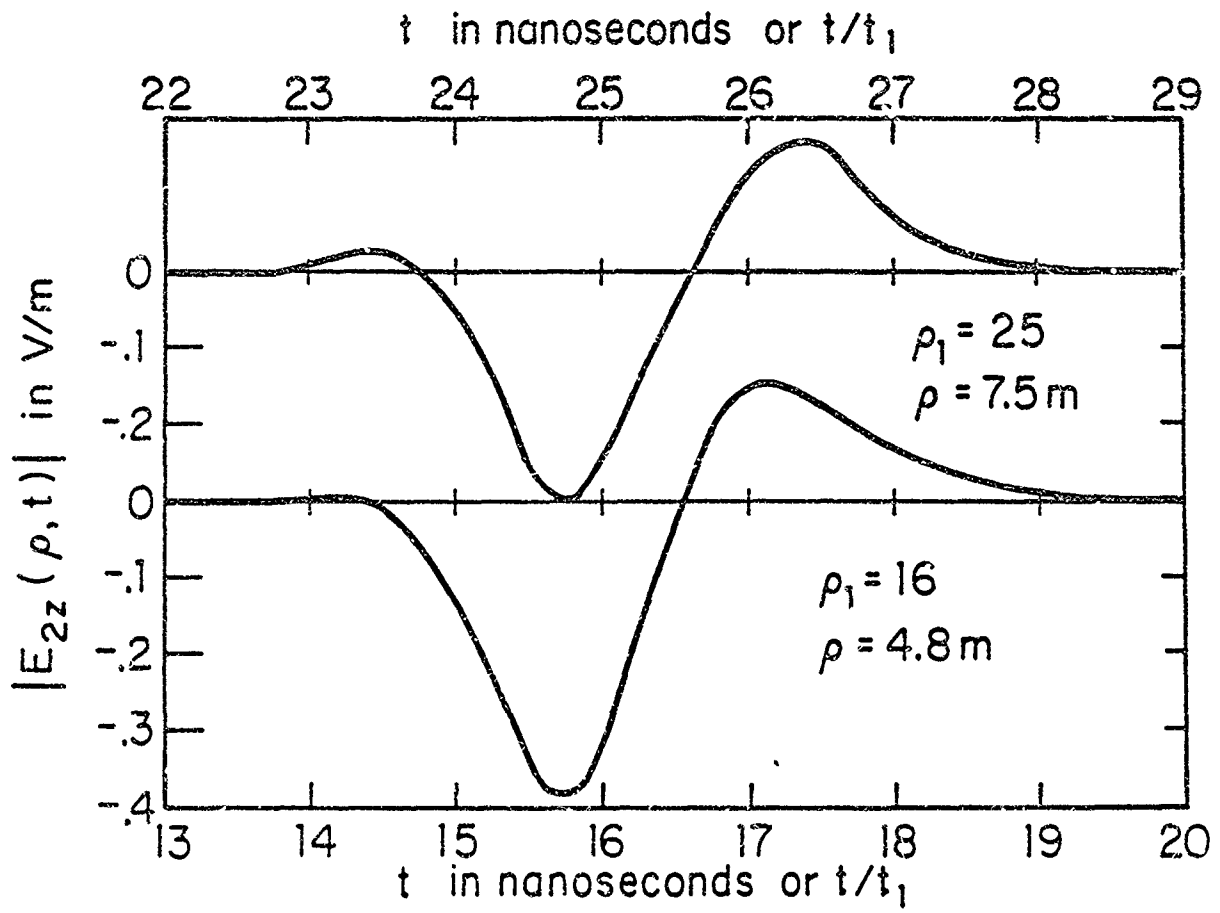


Fig. 4. Like Fig. 3 but for larger values of radial distance ρ .